Rotordynamics Prediction in Engineering

Second Edition

Michel Lalanne
and Guy Ferraris

Preface

In the design of rotating machinery it is necessary to predict the dynamic behavior of rotors in bending and in torsion. These predictions are as follows:

1. The static and dynamic behavior in torsion is performed. The natural frequencies which give the critical speeds must be determined. In addition, when electric motors or generators are present, the dynamic behavior during start-up or under short-circuit conditions must be predicted.
2. The dynamic behavior in bending is performed last. The natural frequencies as a function of the speed of rotation, which give the critical speeds, and possible instabilities must be determined. Then, the effect of forces of excitation is calculated, mass unbalance being the most important of these.

This book mainly focuses on the influence of bending; the influence of torsion, which in general is easy to predict, is dealt with in Chapter 9.

Equations are obtained systematically in the following way. First the expressions for the kinetic and strain energies of the rotor elements and the virtual work of external forces are calculated. A numerical method is then used and Lagrange's equations are applied. The Rayleigh–Ritz method gives simple models for understanding the basic phenomena, and the finite element method is convenient for industrial problems.

The authors have adopted a systematic but practical approach in order to make the book concise and useful. Particular care has been taken to make the presentation easy to read and understand. It is, however, necessary to have some background knowledge of rigid body mechanics, strength of materials, matrix calculations, differential equations and mechanical vibrations: see, for example, [37] or [39].

This book is for engineers, and undergraduate and graduate students, concerned with predictions in rotordynamics. Part of the material presented has been used by the authors for courses at INSA, Lyon, at INPG, Grenoble, at the CISM, Udine, and at the University of Campinas, Brazil.

Chapter 1 looks at the characteristics of rotor elements: disk kinetic energy, shaft kinetic and strain energies, virtual work of the forces created by bearings and mass unbalance kinetic energy.

Chapter 2 considers simple monorotor models and shows basic phenomena with equations which, when damping is not present, can be easily obtained and solved by hand calculations. In the two cases of symmetric and asymmetric rotors, the following aspects are presented: the Campbell diagram (natural frequencies as a function of the speed of rotation), the responses to mass unbalance, and an asynchronous force and a harmonic force fixed in space. Instability problems are also considered. Finally, the influence of bearing damping is shown.

Chapter 3 considers simple coaxial multirotor models and shows basic phenomena with equations which, when damping is not present, can be easily obtained and solved by hand calculations. In the two cases of symmetric and asymmetric rotors, the following aspects are presented: the Campbell diagram and the responses to mass unbalances. Finally, the influence of bearing damping is shown.

Chapter 4 introduces the finite elements to be used and the main general equations. First, the finite elements of rotors are given, followed by the equations for monorotor and coaxial multirotors. The methods used by the authors for solving these equations are examined: a direct method which does not reduce the number of degrees of freedom, and a pseudo-modal method which allows considerable saving of computer time and core memory.

Chapter 5 is devoted to the description of an industrial computer program, SYSROTOR, of which a reduced version can be obtained freely on the Internet. After presenting the program, a data set is presented and explained, and results on an industrial application are given.

Chapter 6 links the simple models of Chapters 2 and 3 to the industrial applications of Chapter 7. Among the topics presented are a test on the accuracy of the pseudo-modal method, several comments on transmissibility to the foundations, and shaft, disk and bearing modeling.

Chapter 7 deals with several industrial applications: a hybrid turbomolecular pump, a turbocharger, a centrifugal compressor, a steam

turbine, a centrifugal compressor fitted with active magnetic bearings, a propfan and an air turbine starter.

Chapter 8 deals with transient motions and passing through critical speeds.

Chapter 9 is devoted to torsion: determination of minimum shaft radius, critical speeds of branched systems, and transient motions due to start-up torque and short-circuits in electric motors or generators. An industrial electric-motor/centrifugal-compressor unit is examined.

Chapter 10 looks briefly at several miscellaneous topics: the asymmetric shaft, equations with periodic coefficients, and the influence of axial torque.

This book is not concerned with the determination of bearing characteristics, or with balancing and fluid influence as in pumps. SI units are used, and when calculations are performed, as in Chapter 2, at least eight digits are used for all the calculations; in most cases the results shown are rounded off to four significant figures.

We would like to thank Dr Ronald Eshleman, President of the Vibration Institute, who first encouraged us to write on rotordynamics when he was visiting professor at INSA and who was in favor of a new edition including a computer program. We also thank our friends and colleagues at INSA, including A. Berlioz and A. Thivillier who have implemented the computer program on the Internet.

Michel Lalanne
Guy Ferraris

Acknowledgements

Study and development of the methods presented in this book have been aided to a great extent by contracts from companies (SNECMA, SNIAS, Framatome Thermodyn, Microturbo, Metravib, Graffenstaden, Technofan, Fives Cail Babcock, Allied Signal, Alcatel-Alsthom, Spretec, ELF, Vibratech, Petrobras) and state organizations (DRET, MRT, Ecan Indret) over a period of nearly twenty years. We thank them for their financial support and, along with the Société de Mécanique Magnétique, we wish to thank them for their permission to publish some of the results featured in this volume.

We are very grateful to Jean-Marc Pugnet, Head of the Research and Development Department at Framatome Thermodyn, who has provided information on several industrial applications and with whom we have had many fruitful discussions on practical rotordynamics over the years.

Sections 1.1 and 1.2 of this book have been published previously by John Wiley [37]; Section 10.2 was published by the American Society of Mechanical Engineers [29]; Section 3.3 was published by Gauthier Villars [3]; parts of Chapter 3 were published by the Vibration Institute [41] and the Journal of Sound and Vibration [19]; application 7.2 was published by NAFEMS [24]; and parts of Chapters 3 and 6, and applications 7.2, 7.3, 7.4 and 7.6, were published by the Techniques de l'Ingénieur [42]. We are also grateful for their kind permission to use this material freely. We thank Dutch Airbus, DLR, Aérospatiale, Technofan and all the European partners involved in the DUPRIN project (Ducted Propfan Investigation) for their permission to publish the results on the propfan and ALCATEL-CIT for the permission to publish the results on the hybrid turbomolecular pump. Applications on monorotors (7.1, 7.2, 7.3, 7.4 and 7.5) were performed using the computer program SYSROTOR (licence CNRS-INSA de Lyon, Laboratoire de Mécanique des Structures).

1

Characteristics of Rotor Elements

The basic elements of a rotor are the disk, the shaft, the bearings and the seals [2, 37]. The mass unbalances which cannot be completely avoided must also be considered. Kinetic energy expressions are necessary to characterize the disk, shaft and mass unbalances. Strain energy is necessary to characterize the shaft. The forces due to bearings or seals are used to calculate their virtual work, and then the corresponding forces acting on the shaft are obtained. The general rotor equations are provided by means of the following steps:

- The kinetic energy T, the strain energy U and the virtual work δW of external forces are calculated for the elements of the system.
- A numerical method is chosen: The Rayleigh–Ritz method for a very small number of degrees of freedom, and the finite element method for engineering applications.
- Lagrange's equations are applied in the following form:

$$\frac{\mathrm{d}}{\mathrm{d}t}\left(\frac{\partial T}{\partial \dot{q}_i}\right) - \frac{\partial T}{\partial q_i} + \frac{\partial U}{\partial q_i} = Fq_i \tag{1.1}$$

where $N(1 \leqslant i \leqslant N)$ is the number of degrees of freedom, q_i are generalized independent coordinates, Fq_i are generalized forces, and $\cdot$ denotes differentiation with respect to time t.

1.1 THE DISK

The disk is assumed to be rigid and is then characterized solely by its kinetic energy. $R_0(XYZ)$ is an inertial frame and $R(x, y, z)$ is fixed to the disk (Figure 1.1). The xyz coordinate system is related to the XYZ coordinate system through a set of three angles ψ, θ and ϕ. To achieve the orientation of the disk one first rotates it by an amount ψ around the Z axis; then by an amount θ around the new x axis, denoted by x_1; and lastly by an amount ϕ around the final y axis. The instantaneous angular velocity vector of the xyz frame is

$$\omega_{R/R_0} = \dot{\psi}Z + \dot{\theta}x_1 + \dot{\phi}y \tag{1.2}$$

where Z, x_1 and y are unit vectors along the axes Z, x_1 and y. The kinetic energy of the disk about its center of mass O is calculated using the frame R. In this system the angular velocity vector becomes

$$\omega^R_{R/R_0} = \begin{bmatrix} \omega_x \\ \omega_y \\ \omega_z \end{bmatrix} = \begin{bmatrix} -\dot{\psi}\cos\theta\sin\phi + \dot{\theta}\cos\phi \\ \dot{\phi} + \dot{\psi}\sin\theta \\ \dot{\psi}\cos\theta\cos\phi + \dot{\theta}\sin\phi \end{bmatrix} \tag{1.3}$$

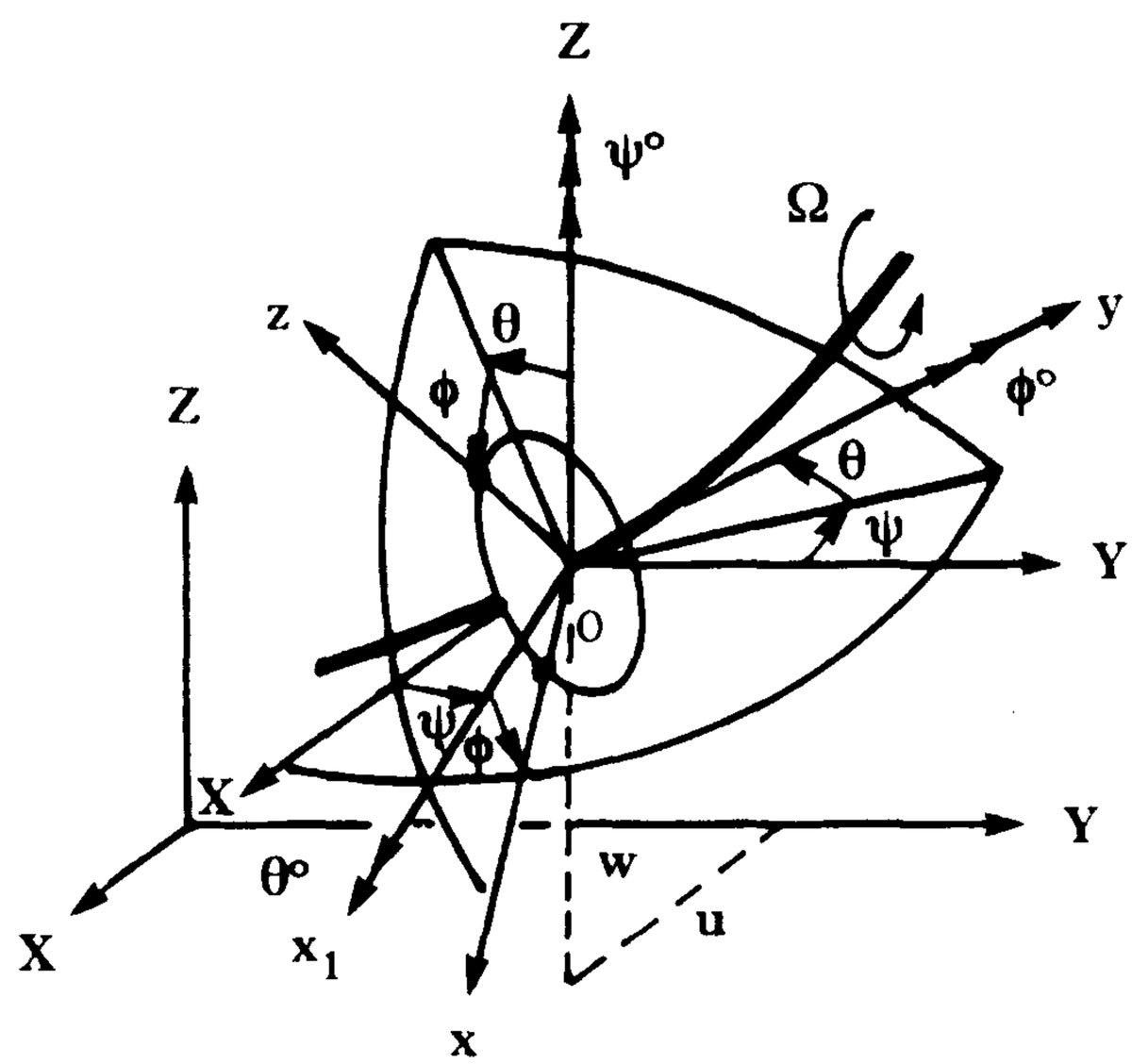

Figure 1.1. Reference frames for a disk on a rotating flexible shaft

Let u and w designate the coordinates of O in R_0, the coordinate along Y being constant. In addition, the mass of the disk is M_D and its tensor of inertia in O as xyz are principal directions of inertia is

$$I_{/0} = \begin{bmatrix} I_{Dx} & 0 & 0 \\ 0 & I_{Dy} & 0 \\ 0 & 0 & I_{Dz} \end{bmatrix} \tag{1.4}$$

The expression for the kinetic energy of the disk is

$$T_D = \tfrac{1}{2} M_D(\dot{u}^2 + \dot{w}^2) + \tfrac{1}{2}(I_{Dx}\,\omega_x^2 + I_{Dy}\,\omega_y^2 + I_{Dz}\,\omega_z^2) \tag{1.5}$$

which can be simplified here as the disk is symmetric ($I_{Dx} = I_{Dz}$), the angles θ and ψ are small, and the angular velocity is constant; that is, $\dot{\phi} = \Omega$. Equation (1.5) becomes

$$T_D = \tfrac{1}{2} M_D(\dot{u}^2 + \dot{w}^2) + \tfrac{1}{2} I_{Dx}(\dot{\theta}^2 + \dot{\psi}^2) + \tfrac{1}{2} I_{Dy}(\Omega^2 + 2\Omega\dot{\psi}\theta) \tag{1.6}$$

where the term $\frac{1}{2}\, I_{Dy}\Omega^2$, which is a constant, has no influence in the equations and represents the energy of the disk rotating at Ω, all the other displacements being zero. The last term, $I_{Dy}\Omega\dot{\psi}\theta$, represents the gyroscopic (Coriolis) effect.

1.2 THE SHAFT

The shaft is represented as a beam with a circular cross-section, and is characterized by strain and kinetic energies.

1.2.1 Kinetic energy

The general formulation of the kinetic energy of the shaft comes from an extension of the disk equation (1.6). For an element of length L, the expression for the kinetic energy is

$$\begin{aligned} T_S = {} & \frac{\rho S}{2}\int_0^L (\dot{u}^2 + \dot{w}^2)\mathrm{d}y + \frac{\rho I}{2}\int_0^L (\dot{\psi}^2 + \dot{\theta}^2)\mathrm{d}y \\ & + \rho I L\Omega^2 + 2\rho I\Omega\int_0^L \dot{\psi}\theta\,\mathrm{d}y \end{aligned} \tag{1.7}$$

where ρ is the mass per unit volume, S is the cross-sectional area of the beam, supposed to be constant, and I is the area moment of inertia of the beam cross-section about the neutral axis, also supposed to be constant.

The first integral of (1.7) is the classical expression for the kinetic energy of a beam in bending; the second integral is the secondary effect of rotatory inertia (Timoshenko beam); the term $\rho I L \Omega^2$ is a constant and has no influence on the equations; and the last integral represents the gyroscopic effect.

1.2.2 Strain energy

The following notation is used (refer to Figure 1.2): C is the geometric center of the beam, B(x, z) is a typical point on the cross-section, E is the Young's modulus of the material, ε and σ are strains and stresses, and u^* and w^* are displacements of the geometric center with respect to the x, z axis.

If second-order terms are included, the longitudinal strain of point B can be shown to be

$$\varepsilon = -x \frac{\partial^2 u^*}{\partial y^2} - z \frac{\partial^2 w^*}{\partial y^2} + \frac{1}{2}\left(\frac{\partial u^*}{\partial y}\right)^2 + \frac{1}{2}\left(\frac{\partial w^*}{\partial y}\right)^2 \tag{1.8}$$

or

$$\varepsilon = \varepsilon_l + \varepsilon_{nl} \tag{1.9}$$

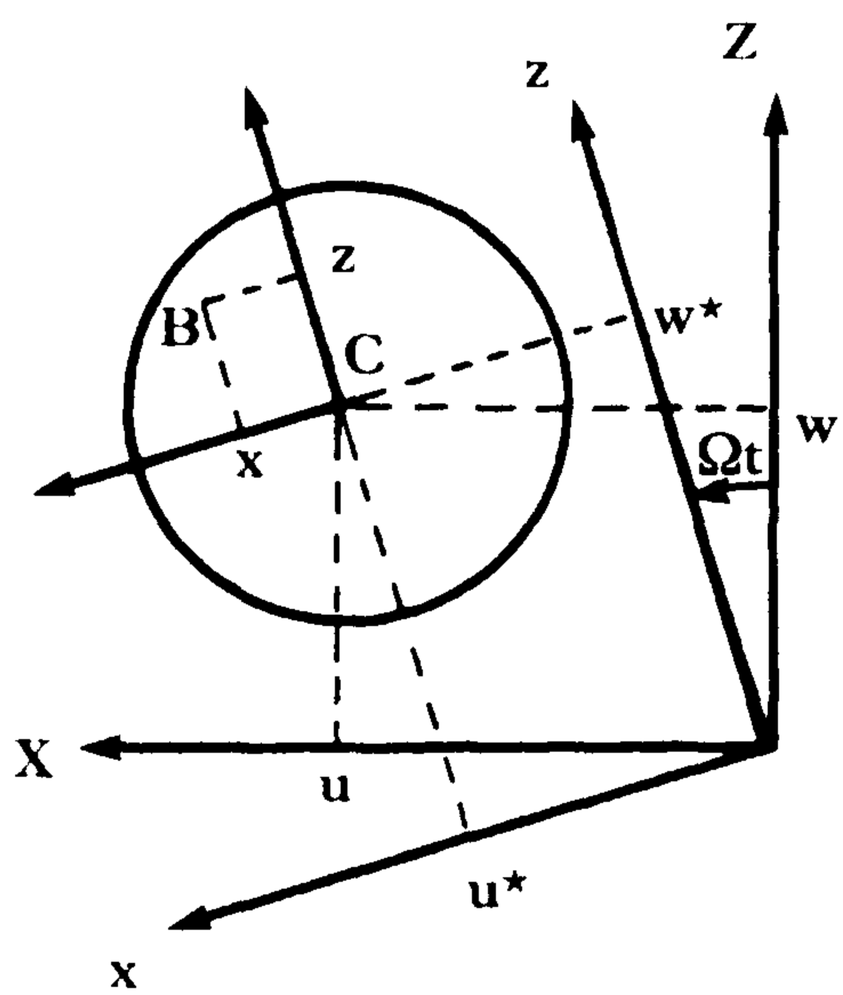

Figure 1.2. Coordinates of the geometric center C and an arbitrary point B on the shaft

where ε_l contains the linear terms and ε_{nl} the nonlinear terms. The strain energy is

$$U_l = \frac{1}{2}\int_\tau \varepsilon^T \sigma \mathrm{d}\tau \tag{1.10}$$

where "T" is the matrix transposition symbol. The relationship between stresses and strains is

$$\sigma = E\varepsilon \tag{1.11}$$

Then

$$U_l = \frac{E}{2}\int_\tau (\varepsilon_l^2 + 2\varepsilon_l\varepsilon_{nl} + \varepsilon_{nl}^2)\,\mathrm{d}\tau \tag{1.12}$$

The symmetry of the beam cross-section with respect to x and z results in

$$\int_\tau \varepsilon_{nl}\,\varepsilon_l\,\mathrm{d}\tau = 0 \tag{1.13}$$

and the third term under the integral in (1.12) is a second-order term and is neglected. The strain energy is

$$U_l = \frac{E}{2}\int_0^L \int_S \left(-x\frac{\partial^2 u^*}{\partial y^2} - z\frac{\partial^2 w^*}{\partial y^2}\right)^2 \mathrm{d}S\,\mathrm{d}y \tag{1.14}$$

$$= \frac{E}{2}\int_0^L \int_S \left[x^2\left(\frac{\partial^2 u^*}{\partial y^2}\right)^2 + z^2\left(\frac{\partial^2 w^*}{\partial y^2}\right)^2 + 2xz\frac{\partial^2 u^*}{\partial y^2}\frac{\partial^2 w^*}{\partial y^2}\right]\mathrm{d}S\,\mathrm{d}y \tag{1.15}$$

Because of symmetry, the integral which corresponds to the third term in (1.15) is nil.

Introducing the diametral cross-section of inertia with respect to x and z we have

$$I_x = \int_S z^2\,\mathrm{d}S \tag{1.16}$$

$$I_z = \int_S x^2\,\mathrm{d}S \tag{1.17}$$

The strain energy expression is thus

$$U_1 = \frac{E}{2}\int_0^L \left[I_z \left(\frac{\partial^2 u^*}{\partial y^2}\right)^2 + I_x \left(\frac{\partial^2 w^*}{\partial y^2}\right)^2 \right] \mathrm{d}y \tag{1.18}$$

If the shaft is subjected to a constant axial force F_0, there is a second contribution to the strain energy of the shaft given by

$$U_2 = \int_0^L \frac{F_0}{S}(\varepsilon_1 + \varepsilon_{\mathrm{nl}})\,\mathrm{d}\tau \tag{1.19}$$

Owing to symmetry, the first term under the integral will vanish over the cross-sectional area; and so, using (1.8) and (1.9), (1.19) becomes

$$U_2 = \frac{F_0}{2}\int_0^L \left[\left(\frac{\partial u^*}{\partial y}\right)^2 + \left(\frac{\partial w^*}{\partial y}\right)^2 \right] \mathrm{d}y \tag{1.20}$$

The combined strain energy, $U_1 + U_2$, is then

$$\begin{aligned} U_{\mathrm{S}} = {} & \frac{E}{2}\int_0^L \left[I_z \left(\frac{\partial^2 u^*}{\partial y^2}\right)^2 + I_x \left(\frac{\partial^2 w^*}{\partial y^2}\right)^2 \right] \mathrm{d}y \\ & + \frac{F_0}{2}\int_0^L \left[\left(\frac{\partial u^*}{\partial y}\right)^2 + \left(\frac{\partial w^*}{\partial y}\right)^2 \right] \mathrm{d}y \end{aligned} \tag{1.21}$$

To avoid periodic terms explicitly function of time, it is necessary, because of the bearing properties (1.3), to express the strain energy as a function of u and w, components of the displacement in R_0. Using

$$u^* = u\cos\Omega t - w\sin\Omega t \tag{1.22}$$

$$w^* = u\sin\Omega t + w\cos\Omega t \tag{1.23}$$

which can be deduced from the Figure 1.2, Equation (1.21) is written as

$$\begin{aligned} U_{\mathrm{S}} = {} & \frac{E}{2}\int_0^L \left[I_z \left(\cos\Omega t\,\frac{\partial^2 u}{\partial y^2} - \sin\Omega t\,\frac{\partial^2 w}{\partial y^2}\right)^2 \right. \\ & \left. + I_x \left(\sin\Omega t\,\frac{\partial^2 u}{\partial y^2} + \cos\Omega t\,\frac{\partial^2 w}{\partial y^2}\right)^2 \right] \mathrm{d}y \\ & + \frac{F_0}{2}\int_0^L \left[\left(\frac{\partial u}{\partial y}\right)^2 + \left(\frac{\partial w}{\partial y}\right)^2 \right] \mathrm{d}y \end{aligned} \tag{1.24}$$

Finally, for the most common case of a symmetric shaft (i.e. $I_x = I_z = I$), the strain energy becomes

$$U_S = \frac{EI}{2}\int_0^L \left[\left(\frac{\partial^2 u}{\partial y^2}\right)^2 + \left(\frac{\partial^2 w}{\partial y^2}\right)^2\right] \mathrm{d}y + \frac{F_0}{2}\int_0^L \left[\left(\frac{\partial u}{\partial y}\right)^2 + \left(\frac{\partial w}{\partial y}\right)^2\right] \mathrm{d}y \tag{1.25}$$

1.3 BEARINGS AND SEALS

The stiffness and viscous damping terms are assumed to be known, and the bending influence can in general be neglected (Figure 1.3). The virtual work δW of the forces acting on the shaft can be written as

$$\begin{aligned}\delta W = &- k_{xx}\, u\delta u - k_{xz}\, w\delta u - k_{zz}\, w\delta w - k_{zx}\, u\delta w \\ &- c_{xx}\, \dot{u}\delta u - c_{xz}\, \dot{w}\delta u - c_{zz}\, \dot{w}\delta w - c_{zx}\, \dot{u}\delta w\end{aligned} \tag{1.26}$$

or

$$\delta W = F_u \delta_u + F_w \delta w \tag{1.27}$$

where F_u and F_w are the components of the generalized force. In matrix form, Equations (1.26) and (1.27) give

$$\begin{bmatrix} F_u \\ F_w \end{bmatrix} = -\begin{bmatrix} k_{xx} & k_{xz} \\ k_{zx} & k_{zz} \end{bmatrix}\begin{bmatrix} u \\ w \end{bmatrix} - \begin{bmatrix} c_{xx} & c_{xz} \\ c_{zx} & c_{zz} \end{bmatrix}\begin{bmatrix} \dot{u} \\ \dot{w} \end{bmatrix} \tag{1.28}$$

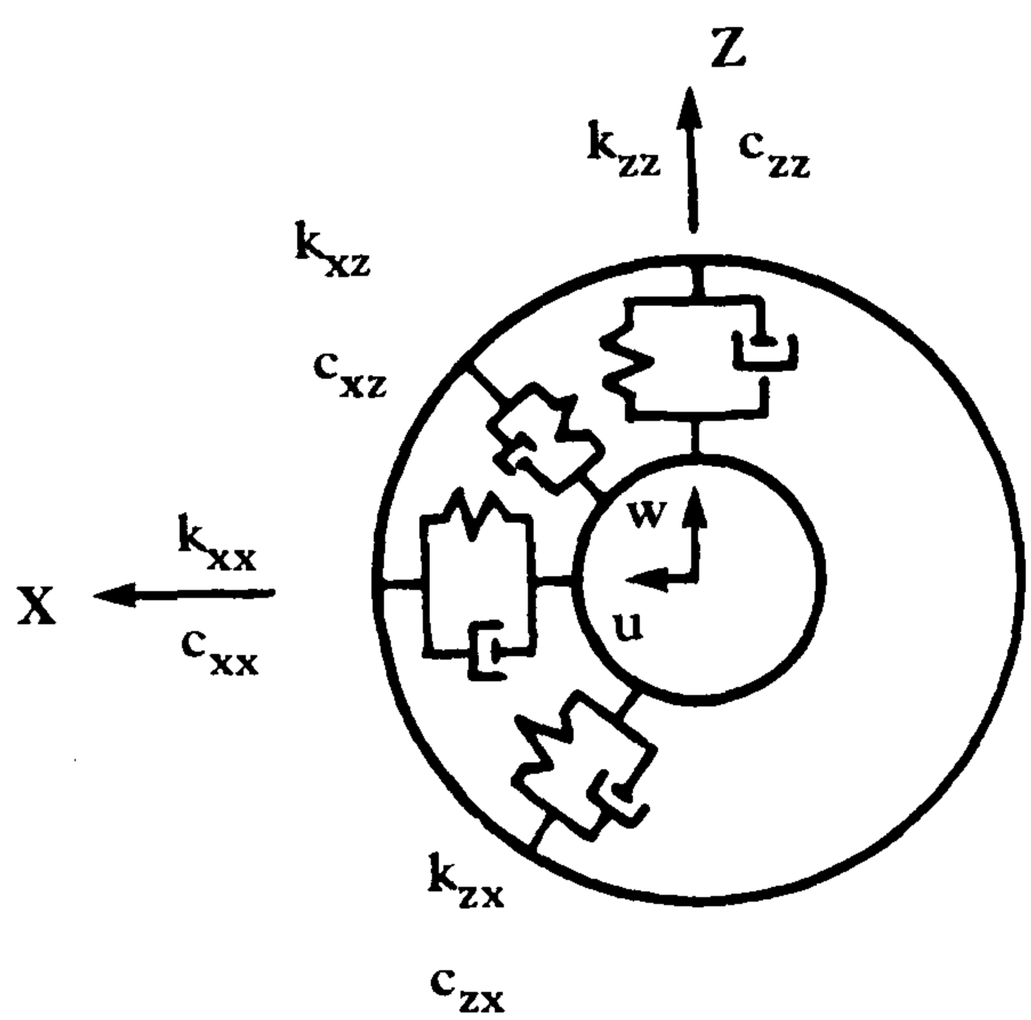

Figure 1.3. Bearing stiffness and damping

Frequently $k_{xx} \neq k_{zz}$ and $c_{xx} \neq c_{zz}$, and in addition it is very common that $k_{xz} \neq k_{zx}$ and $c_{xz} \neq c_{zx}$.

Let us now consider the case when the equations are expressed using the displacement components in R, and supposing that only k_{xx} and k_{zz} are non-zero. The expression for the virtual work is then

$$\begin{aligned}\delta W = &- k_{xx}(u^* \cos \Omega t + w^* \sin \Omega t)(\delta u^* \cos \Omega t + \delta w^* \sin \Omega t) \\ &- k_{zz}(-u^* \sin \Omega t + w^* \cos \Omega t)(-\delta u^* \sin \Omega t + \delta w^* \cos \Omega t)\end{aligned} \tag{1.29}$$

or

$$\begin{aligned}\delta W = &- \left[(k_{xx} \cos^2 \Omega t + k_{zz} \sin^2 \Omega t)u^* + \frac{\sin 2\Omega t}{2}(k_{xx} - k_{zz})w^*\right] \delta u^* \\ &- \left[(k_{xx} \sin^2 \Omega t + k_{zz} \cos^2 \Omega t)w^* + \frac{\sin 2\Omega t}{2}(k_{xx} - k_{zz})u^*\right] \delta w^*\end{aligned} \tag{1.30}$$

Equation (1.30) shows that, if $k_{xx} \neq k_{zz}$, terms coming from the bearing will contain explicitly the time in the rotating frame R. This leads to extreme difficulties in solving the equations (see Chapter 10). Then the rotor equations have to be written in the inertial reference frame R_0.

1.4 MASS UNBALANCE

The unbalance is defined by a mass m_u situated at a distance d from the geometric center of the shaft; its kinetic energy T_u has to be calculated. The mass remains in a plane perpendicular to the y axis and its coordinate along the y axis is a constant (Figure 1.4).

In R_0 the coordinates of the mass are

$$\mathbf{OD} = \begin{vmatrix} u + d \sin \Omega t \\ \text{constant} \\ w + d \cos \Omega t \end{vmatrix} \tag{1.31}$$

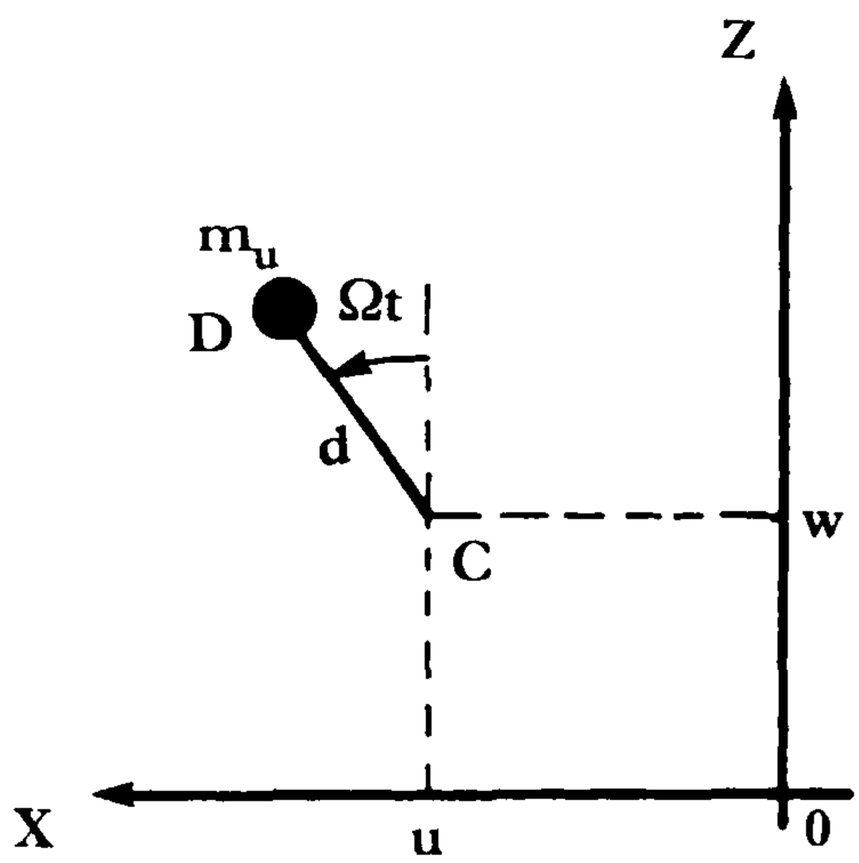

Figure 1.4. Mass unbalance

Then

$$V = \frac{\mathrm{d}\mathbf{OD}}{\mathrm{d}t} = \begin{vmatrix} \dot{u} + d\Omega\cos\Omega t \\ 0 \\ \dot{w} - d\Omega\sin\Omega t \end{vmatrix} \tag{1.32}$$

and the kinetic energy of the mass is

$$T_{\mathrm{u}} = \frac{m_{\mathrm{u}}}{2}\left(\dot{u}^2 + \dot{w}^2 + \Omega^2 d^2 + 2\Omega d\dot{u}\cos\Omega t - 2\Omega\dot{w}d\sin\Omega t\right) \tag{1.33}$$

The term $m_{\mathrm{u}}\Omega^2 d^2/2$ is a constant and has no influence on the equations. The mass m_u is much smaller then the mass of the rotor, so the expression for the kinetic energy can be written as

$$T_{\mathrm{u}} \simeq m_{\mathrm{u}}\Omega d\dot{u}\left(\cos\Omega t - \dot{w}\sin\Omega t\right) \tag{1.34}$$

Application of Lagrange's equations will give the so-called centrifugal force vector.

2

Monorotors: Simple Models, Basic Phenomena

The aim of this chapter is to show the main basic phenomena occurring in rotordynamics by using a simple but realistic example modeled by equations that are easy to solve by hand calculations. The numerical method chosen here is that of Rayleigh–Ritz, and to start with two rotors are studied: the first one is symmetric, the second is asymmetric as the behavior of symmetric and asymmetric rotors is different. Then the instability effect is shown, and lastly the influence of damping on the bahaviour of rotors is briefly presented.

The main basic phenomena are:

- natural frequencies as a function of the speed of rotation, the Campbell diagram, and instability;
- the effects of forces of excitation: mass unbalance, an asynchronous force, and a harmonic force fixed in space.

2.1 DETERMINATION OF THE MODEL

$R_0(XYZ)$ is the inertial frame, the rotor axis is along the Y axis, and the speed of rotation Ω is constant (Figure 2.1). In order to make hand calculations, only one degree of freedom is used for the displacements in the X and the Z directions. The rotor is then supposed to be simply supported at both ends. It consists of

- a symmetric shaft of length L;
- a symmetric disk with a mass unbalance, both situated at $y = l_1$;
- a bearing situated at $y = l_2$.

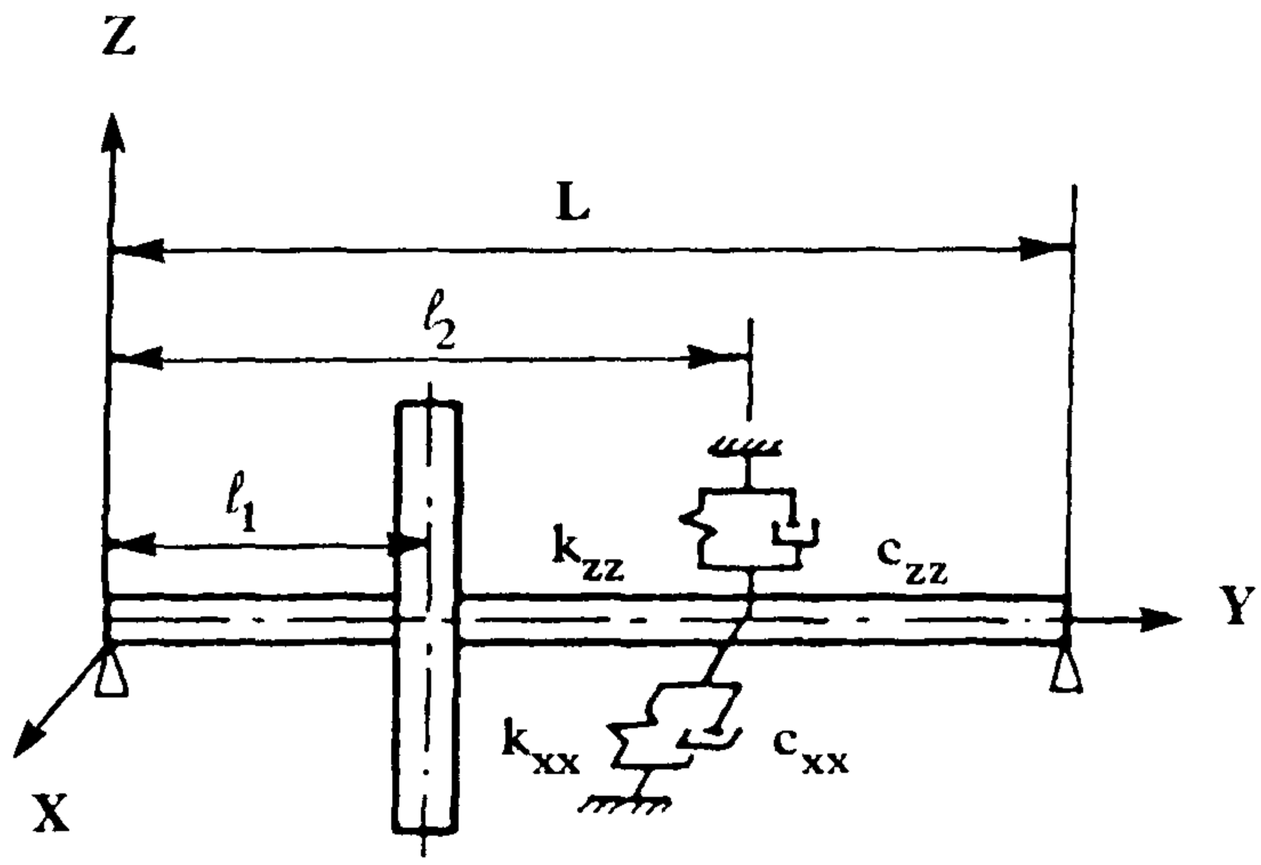

Figure 2.1. Model of the rotor

Depending on the characteristics used for the bearing, the rotor will be said to be symmetric or asymmetric. In addition, forces are supposed to exist at $y = l_3$. The expressions for kinetic energy, strain energy and virtual work given in Chapter 1 are used for each element of the rotor, and the constant term appearing in the expression for the kinetic energy is systematically canceled as its contribution to the equations is nil. The expressions for the displacements in the x and z directions are respectively

$$u(y, t) = f(y)q_1(t) = f(y)q_1 \tag{2.1}$$

$$w(y, t) = f(y)q_2(t) = f(y)q_2 \tag{2.2}$$

where q_1 and q_2 are generalized independent coordinates. As the angular displacements ψ and θ (Figure 2.2) are small, they are

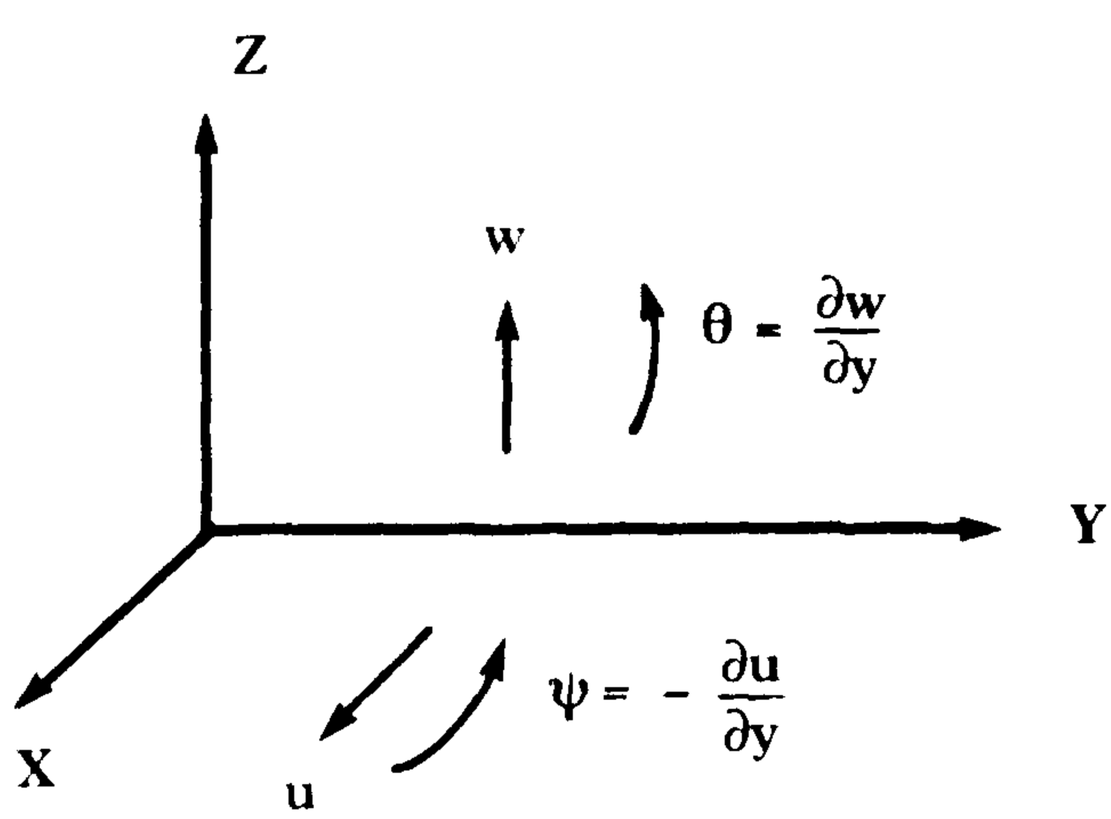

Figure 2.2. Coordinates

approximated by

$$\theta = \frac{\partial w}{\partial y} = \frac{\mathrm{d} f(y)}{\mathrm{d} y} q_2 = g(y) q_2 \tag{2.3}$$

and

$$\psi = -\frac{\partial u}{\partial y} = -\frac{\mathrm{d} f(y)}{\mathrm{d} y} q_1 = -g(y) q_1 \tag{2.4}$$

The second-order derivatives of u and w are necessary to express the strain energy; their expressions are

$$\frac{\partial^2 u}{\partial y^2} = \frac{\mathrm{d}^2 f(y)}{\mathrm{d} y^2} q_1 = h(y) q_1 \tag{2.5}$$

$$\frac{\partial^2 w}{\partial y^2} = \frac{\mathrm{d}^2 f(y)}{\mathrm{d} y^2} q_2 = h(y) q_2 \tag{2.6}$$

2.1.1 The disk

The kinetic energy T_{D} of the disk comes from Equations (2.1)–(2.4) above and Equation (1.6) in Chapter 1:

$$\begin{aligned} T_{\mathrm{D}} = & \tfrac{1}{2} M_{\mathrm{D}} f^2(l_1)\,(\dot{q}_1^2 + \dot{q}_2^2) + \tfrac{1}{2} I_{\mathrm{D}x}\, g^2(l_1)(\dot{q}_1^2 + \dot{q}_2^2) \\ & - I_{\mathrm{D}y}\, \Omega g^2(l_1) \dot{q}_1 q_2 \end{aligned} \tag{2.7}$$

which can be written as

$$T_{\mathrm{D}} = \tfrac{1}{2}\left[M_{\mathrm{D}} f^2(l_1) + I_{\mathrm{D}x}\, g^2(l_1)\right](\dot{q}_1^2 + \dot{q}_2^2) - I_{\mathrm{D}y}\, \Omega g^2(l_1) \dot{q}_1 q_2 \tag{2.8}$$

2.1.2 The shaft

The kinetic energy T_{S} of the shaft comes from Equations (2.1)–(2.4) above and Equation (1.7) in Chapter 1:

$$\begin{aligned} T_{\mathrm{S}} = & \frac{\rho S}{2} \int_0^L f^2(y)\,\mathrm{d}y\,(\dot{q}_1^2 + \dot{q}_2^2) + \frac{\rho I}{2} \int_0^L g^2(y)\,\mathrm{d}y(\dot{q}_1^2 + \dot{q}_2^2) \\ & - 2\rho I \Omega \int_0^L g^2(y)\,\mathrm{d}y\, \dot{q}_1 q_2 \end{aligned} \tag{2.9}$$

and

$$T_S = \tfrac{1}{2}\left[\rho S \int_0^L f^2(y)\,\mathrm{d}y + \rho I \int_0^L g^2(y)\,\mathrm{d}y\right](\dot{q}_1^2 + \dot{q}_2^2) - 2\rho I\Omega \int_0^L g^2(y)\,\mathrm{d}y\,\dot{q}_1 q_2 \tag{2.10}$$

Hence the kinetic energy T of the disk–shaft assembly is

$$T = T_D + T_S \tag{2.11}$$

that is

$$T = \tfrac{1}{2}\left[M_D f^2(l_1) + I_{Dx} g^2(l_1) + \rho S \int_0^L f^2(y)\mathrm{d}y + \rho I \int_0^L g^2(y)\mathrm{d}y\right](\dot{q}_1^2 + \dot{q}_2^2) - \Omega\left[I_{Dy} g^2(l_1) + 2\rho I \int_0^L g^2(y)\mathrm{d}y\right]\dot{q}_1 q_2 \tag{2.12}$$

Equation (2.12) can be written in a more compact form as

$$T = \tfrac{1}{2} m\,(\dot{q}_1^2 + \dot{q}_2^2) - \Omega a \dot{q}_1 q_2 \tag{2.13}$$

The strain energy of the shaft, U_S, comes from Equations (2.5) and (2.6) above and Equation (1.25) in Chapter 1. Then, if the axial force is nil,

$$U_S = \frac{EI}{2}\int_0^L h^2(y)\mathrm{d}y\,(q_1^2 + q_2^2) \tag{2.14}$$

Equation (2.14) can be written in a more compact form as

$$U_S = \tfrac{1}{2} k\,(q_1^2 + q_2^2) \tag{2.15}$$

2.1.3 The bearing

The virtual work done by the forces due to the bearing acting on the shaft is given by Equation (1.26) in Chapter 1. Hence

$$\begin{aligned}\delta W = &- k_{xx} u(l_2)\delta u(l_2) - k_{xz}\, w(l_2)\delta u(l_2) - k_{zz}\, w(l_2)\delta w(l_2)\\ &- k_{zx} u(l_2)\delta w(l_2) - c_{xx}\dot{u}\,(l_2)\delta u(l_2) - c_{xz}\dot{w}(l_2)\delta u(l_2)\\ &- c_{zz}\dot{w}(l_2)\delta w(l_2) - c_{zx}\dot{u}(l_2)\delta w(l_2)\end{aligned} \tag{2.16}$$

Using Equations (2.1) and (2.2), (2.16) becomes

$$\begin{aligned}\delta W = &- k_{xx} f^2(l_2) q_1 \delta q_1 - k_{xz} f^2(l_2) q_2 \delta q_1 - k_{zz} f^2(l_2) q_2 \delta q_2 \\ &- k_{zx} f^2(l_2) q_1 \delta q_2 - c_{xx} f^2(l_2) \dot{q}_1 \delta q_1 - c_{xz} f^2(l_2) \dot{q}_2 \delta q_1 \\ &- c_{zz} f^2(l_2) \dot{q}_2 \delta q_2 - c_{zx} f^2(l_2) \dot{q}_1 \delta q_2\end{aligned} \tag{2.17}$$

As

$$\delta W = F q_1 \delta q_1 + F q_2 \delta q_2 \tag{2.18}$$

a simple identification of the expressions (2.17) and (2.18) gives the two components Fq_1 and Fq_2 of the generalized force acting on the shaft.

2.1.4 Mass unbalance

From Equations (2.1) and (2.2) and Equation (1.34) in Chapter 1, the kinetic energy of the mass unbalance is

$$T_{\mathrm{u}} = m_{\mathrm{u}} \Omega d f(l_1)(\dot{q}_1 \cos \Omega t - \dot{q}_2 \sin \Omega t) \tag{2.19}$$

2.1.5 Forces

The two components of the forces are supposed to be

$$F_{\mathrm{u}} = F_1(t) \tag{2.20}$$

$$F_w = F_2(t) \tag{2.21}$$

and, as their action is supposed to act at $y = l_3$,

$$\delta W = F_1(t) \delta u(l_3) + F_2(t) \delta w(l_3) \tag{2.22}$$

which can be written as

$$\delta W = F_1(t) f(l_3) \delta q_1 + F_2(t) f(l_3) \delta q_2 \tag{2.23}$$

a simple identification of expression (2.23) with (2.18) shows that the two components of the force are

$$Fq_1 = F_1(t)\ f(l_3) \tag{2.24}$$

$$Fq_2 = F_2(t)\ f(l_3) \tag{2.25}$$

2.1.6 Numerical data

Basic data for the disk

Inner radius $R_1 = 0.01\,\mathrm{m}$
Outer radius $R_2 = 0.15\,\mathrm{m}$
Thickness $h = 0.03\,\mathrm{m}$
$\rho = 7800\,\mathrm{kg/m^3}$
$l_1 = L/3$

Then $M_\mathrm{D}, I_{\mathrm{D}x} = I_{\mathrm{D}z}$, and $I_{\mathrm{D}y}$ are obtained. These quantities are

$$M_\mathrm{D} = \pi\,(R_2^2 - R_1^2)h\rho = 16.47\,\mathrm{kg} \tag{2.26}$$

$$\begin{aligned} I_{\mathrm{D}x} = I_{\mathrm{D}z} &= \frac{M_\mathrm{D}}{12}\,(3R_1^2 + 3R_2^2 + h^2) \\ &= 9.427 \times 10^{-2}\,\mathrm{kg\,m^2} \end{aligned} \tag{2.27}$$

$$I_{\mathrm{D}y} = \frac{M_\mathrm{D}}{2}\,(R_1^2 + R_2^2) = 0.1861\,\mathrm{kg\,m^2} \tag{2.28}$$

Basic data for the shaft

Length $L = 0.4\,\mathrm{m}$
Cross-sectional radius $R_1 = 0.01\,\mathrm{m}$
$\rho = 7800\,\mathrm{kg/m^3}$
$E = 2 \times 10^{11}\,\mathrm{N/m^2}$

Then S and I are obtained as

$$S = \pi R_1^2 = 3.142 \times 10^{-4}\,\mathrm{m^2} \tag{2.29}$$

$$I = \frac{\pi R_1^4}{4} = 7.854 \times 10^{-9}\,\mathrm{m^4} \tag{2.30}$$

Basic data for mass unbalance

Mass $m_u = 10^{-4}$ kg
Distance $d = R_2 = 0.15$ m

Basic data for the bearing

In the first rotor which will be studied below there is no bearing influence and the rotor is said to be symmetric. In the second rotor the stiffness k_{zz} acts and the rotor is said to be asymmetric. This rotor can be built easily; a spring acts on the outer ring of a roller bearing, the mass of which is neglected in our calculations. The spring is situated at $l_2 = 2L/3$, its stiffness is $k_{zz} = 5 \times 10^5$N/m, and (2.17) gives

$$\delta W = -5 \times 10^5 \, f^2(2L/3) q_2 \delta q_2 \tag{2.31}$$

Displacement function

The displacement chosen is the exact first mode shape of a beam with constant cross-section in bending, simply supported at both ends; i.e.

$$f(y) = \sin \frac{\pi y}{L} = \sin \frac{\pi y}{0.4} \tag{2.32}$$

Then

$$g(y) = \frac{\pi}{L} \cos \frac{\pi y}{L} = \frac{\pi}{0.4} \cos \frac{\pi y}{0.4} \tag{2.33}$$

$$h(y) = -\left(\frac{\pi}{L}\right)^2 \sin \frac{\pi y}{L} = -\left(\frac{\pi}{0.4}\right)^2 \sin \frac{\pi y}{0.4} \tag{2.34}$$

Kinetic energy

The kinetic energy of the disk, T_D, is given by (2.7):

$$T_D = 6.175(\dot{q}_1^2 + \dot{q}_2^2) + 0.7269(\dot{q}_1^2 + \dot{q}_2^2) - 2.870\Omega \dot{q}_1 q_2 \tag{2.35}$$

Then

$$T_{\mathrm{D}} = 6.902(\dot{q}_1^2 + \dot{q}_2^2) - 2.870\,\Omega\dot{q}_1 q_2 \tag{2.36}$$

The kinetic energy of the shaft, T_{S}, is given by (2.9) and at first two integrals have to be calculated:

$$\int_0^L f^2(y)\mathrm{d}y = \int_0^{0.4} \sin^2 \frac{\pi y}{0.4}\,\mathrm{d}y = 0.2\,\mathrm{m} \tag{2.37}$$

and

$$\int_0^L g^2(y)\,\mathrm{d}y = \left(\frac{\pi}{0.4}\right)^2 \int_0^{0.4} \cos^2 \frac{\pi y}{0.4}\,\mathrm{d}y = 12.34\,\mathrm{m}^{-1} \tag{2.38}$$

Then

$$\begin{aligned} T_{\mathrm{S}} =& 0.2450(\dot{q}_1^2 + \dot{q}_2^2) + 3.779 \times 10^{-4}(\dot{q}_1^2 + \dot{q}_2^2) \\ & - 1.512 \times 10^{-3}\,\Omega\dot{q}_1 q_2 \end{aligned} \tag{2.39}$$

which becomes

$$T_{\mathrm{S}} = 0.2454(\dot{q}_1^2 + \dot{q}_2^2) - 1.512 \times 10^{-3}\,\Omega\dot{q}_1 q_2 \tag{2.40}$$

The kinetic energy of the mass unbalance, T_{u}, is given by (2.19), and

$$T_{\mathrm{u}} = 1.299 \times 10^{-5}\,\Omega(\cos\Omega t\dot{q}_1 - \sin\Omega t\dot{q}_2) \tag{2.41}$$

The kinetic energy of the system is then

$$T = T_{\mathrm{D}} + T_{\mathrm{S}} + T_{\mathrm{u}} \tag{2.42}$$

$$= 7.147(\dot{q}_1^2 + \dot{q}_2^2) - 2.871\,\Omega\dot{q}_1 q_2$$

$$+ 1.299 \times 10^{-5}\,\Omega(\cos\Omega t\dot{q}_1 - \sin\Omega t\dot{q}_2) \tag{2.43}$$

Strain energy

The strain energy is given by Equation (2.14) as

$$\int_0^L h^2(y)\,\mathrm{d}y = \int_0^{0.4} \left(\frac{\pi}{0.4}\right)^4 \sin^2 \frac{\pi y}{0.4}\,\mathrm{d}y = 7.610 \times 10^2\,\mathrm{m}^{-3} \tag{2.44}$$

Then

$$U_S = 5.977 \times 10^5 \left(q_1^2 + q_2^2\right) \tag{2.45}$$

Forces due to the stiffness k_{zz}

The expression (2.31) becomes

$$\delta W = -3.75 \times 10^5 \, q_2 \, \delta q_2 \tag{2.46}$$

and from (2.18) we have

$$Fq_1 = 0 \tag{2.47}$$

$$Fq_2 = -3.75 \times 10^5 \, q_2 \tag{2.48}$$

Equations of the rotor

The two rotor equations come from

$$\frac{\mathrm{d}}{\mathrm{d}t}\left(\frac{\partial T}{\partial \dot{q}_1}\right) - \frac{\partial T}{\partial q_1} + \frac{\partial U}{\partial q_1} = Fq_1 \tag{2.49}$$

and

$$\frac{\mathrm{d}}{\mathrm{d}t}\left(\frac{\partial T}{\partial \dot{q}_2}\right) - \frac{\partial T}{\partial q_2} + \frac{\partial U}{\partial q_2} = Fq_2 \tag{2.50}$$

2.2 SYMMETRIC ROTOR

The application of Equations (2.49) and (2.50), with the kinetic energy given by the addition of (2.13) and (2.19), the strain energy given by (2.15), and no bearing influence, gives the equations

$$m\ddot{q}_1 - a\Omega\dot{q}_2 + kq_1 = m_u d\Omega^2 f(l_1)\sin\Omega t \tag{2.51}$$

$$m\ddot{q}_2 + a\Omega\dot{q}_1 + kq_2 = m_u d\Omega^2 f(l_1)\cos\Omega t \tag{2.52}$$

The application of (2.49) and (2.50), with the kinetic energy given by (2.43), the strain energy given by (2.45), and no bearing influence, gives the equations

$$14.29\ddot{q}_1 - 2.871\Omega\dot{q}_2 + 1.195 \times 10^6 q_1 = 1.299 \times 10^{-5}\Omega^2 \sin\Omega t \tag{2.53}$$

$$14.29\ddot{q}_2 + 2.871\Omega\dot{q}_1 + 1.195 \times 10^6 q_2 = 1.299 \times 10^{-5}\Omega^2 \cos\Omega t \tag{2.54}$$

2.2.1 Natural frequencies as a function of the speed of rotation: the Campbell diagram

At first, the rotor is studied in free motion. Then Equations (2.51) and (2.52) become

$$m\ddot{q}_1 - a\Omega\dot{q}_2 + kq_1 = 0 \tag{2.55}$$

$$m\ddot{q}_2 + a\Omega\dot{q}_1 + kq_2 = 0 \tag{2.56}$$

These equations can be written in the following matrix form:

$$\begin{bmatrix} m & 0 \\ 0 & m \end{bmatrix}\begin{bmatrix} \ddot{q}_1 \\ \ddot{q}_2 \end{bmatrix} + \Omega\begin{bmatrix} 0 & -a \\ a & 0 \end{bmatrix}\begin{bmatrix} \dot{q}_1 \\ \dot{q}_2 \end{bmatrix} + \begin{bmatrix} k & 0 \\ 0 & k \end{bmatrix}\begin{bmatrix} q_1 \\ q_2 \end{bmatrix} = 0 \tag{2.57}$$

The middle 2×2 matrix multiplied by Ω gives the gyroscopic (Coriolis) effect. The other two 2×2 matrices are respectively the mass and stiffness matrices.

The solutions of (2.57) have to be sought in the form

$$q_1 = Q_1 e^{rt} \tag{2.58}$$

$$q_2 = Q_2 e^{rt} \tag{2.59}$$

Substituting (2.58) and (2.59) in (2.57) gives the homogeneous set of equations

$$\begin{bmatrix} k + mr^2 & -a\Omega r \\ a\Omega r & k + mr^2 \end{bmatrix}\begin{bmatrix} Q_1 \\ Q_2 \end{bmatrix} = 0 \tag{2.60}$$

The trivial solution, $Q_1 = Q_2 = 0$, is of no interest. The non-trivial solutions are associated with the values which bring to zero the value of the determinant of the matrix. The expansion of the determinant gives the characteristic equation

$$(k + mr^2)^2 + a^2\Omega^2 r^2 = 0 \tag{2.61}$$

which can be written as

$$m^2 r^4 + (2km + a^2\Omega^2)r^2 + k^2 = 0 \tag{2.62}$$

At rest ($\Omega = 0$) the roots of (2.62) are

$$r_{10}^2 = r_{20}^2 = j^2\omega_{10}^2 = j^2\omega_{20}^2 = -\tfrac{k}{m} \tag{2.63}$$

and the angular frequencies at rest are

$$\omega_{10} = \omega_{20} = \sqrt{\tfrac{k}{m}} \tag{2.64}$$

Under rotating conditions ($\Omega \neq 0$) the roots of (2.62) are r_1 and r_2 and the corresponding angular frequencies are ω_1 and ω_2. The expression of the first root is

$$r_1^2 = -\left[\omega_{10}^2 + \frac{a^2\Omega^2}{2m^2}\left(1 - \sqrt{1 + \frac{4m^2\omega_{10}^2}{a^2\Omega^2}}\right)\right] \tag{2.65}$$

Hence

$$r_1 = \pm j\omega_1 \tag{2.66}$$

Then

$$\omega_1 = \sqrt{\omega_{10}^2 + \frac{a^2\Omega^2}{2m^2}\left(1 - \sqrt{1 + \frac{4m^2\omega_{10}^2}{a^2\Omega^2}}\right)} \tag{2.67}$$

The expression of the second root is

$$r_2^2 = -\left[\omega_{10}^2 + \frac{a^2\Omega^2}{2m^2}\left(1 + \sqrt{1 + \frac{4m^2\omega_{10}^2}{a^2\Omega^2}}\right)\right] \tag{2.68}$$

Hence

$$r_2 = \pm j\omega_2 \tag{2.69}$$

Then

$$\omega_2 = \sqrt{\omega_{10}^2 + \frac{a^2\Omega^2}{2m^2}\left(1 + \sqrt{1 + \frac{4m^2\omega_{10}^2}{a^2\Omega^2}}\right)} \tag{2.70}$$

From (2.67) and (2.70) it can be observed that

$$\omega_1 < \omega_{10} = \omega_{20} < \omega_2 \tag{2.71}$$

In addition, Equations (2.65) and (2.68) show that r_1^2 and r_2^2 are negative quantities, so that r_1 and r_2 are imaginary quantities and the general solution of the motion given in (2.58) and (2.59) stays limited in time: the rotor is stable. The representation of the angular frequencies as a function of the speed of rotation, $\omega_1 = \omega_1(\Omega)$ and $\omega_2 = \omega_2(\Omega)$, is the Campbell diagram. In general the diagram shows

$$F_1 = \omega_1/2\pi \tag{2.72}$$

$$F_2 = \omega_2/2\pi \tag{2.73}$$

as a function of the speed of rotation N given in revolutions per minute (rpm), which is related to Ω (rad/s) by

$$N = 30\,\Omega/\pi \tag{2.74}$$

Here ω and Ω are angular frequencies and F the frequency. In all that follows this distinction in terminology will be dropped and all three will be called frequencies. Which frequency is intended will be clear from the symbol used or the units required.

The mode shapes (in general called modes) have to be considered now. The first equation in (2.60) gives

$$Q_1 = \frac{a\Omega r Q_2}{k + mr^2} \tag{2.75}$$

The modes corresponding to (2.66) (i.e. to $\pm j\omega_1$) are, if (2.60) is used,

$$Q_1(j\omega_1) = jQ_2(j\omega_1) \tag{2.76}$$

$$Q_1(-j\omega_1) = -jQ_2(-j\omega_1) \tag{2.77}$$

The modes corresponding to (2.69) (i.e. to $\pm j\omega_2$) are, if (2.60) is used,

$$Q_1(j\omega_2) = -jQ_2(j\omega_2) \tag{2.78}$$

$$Q_1(-j\omega_2) = jQ_2(-j\omega_2) \tag{2.79}$$

The general expression of the free motion of the system can now be written. Using (2.58), (2.59) and (2.76)–(2.79):

$$q_1 = jA_1\, e^{j\omega_1 t} - jB_1\, e^{-j\omega_1 t} - jA_2\, e^{j\omega_2 t} + jB_2\, e^{-j\omega_2 t} \tag{2.80}$$

$$q_2 = A_1\, e^{j\omega_1 t} + B_1\, e^{-j\omega_1 t} + A_2\, e^{j\omega_2 t} + B_2\, e^{-j\omega_2 t} \tag{2.81}$$

The four constants A_1, B_1, A_2 and B_2 are determined by the initial conditions.

Let us first choose a set of initial conditions which shows only the frequency ω_1. At $t_0 = 0$:

$$q_1 = 0 \tag{2.82}$$

$$q_2 = q_{20} \tag{2.83}$$

$$\dot{q}_1 = -\omega_1 q_{20} \tag{2.84}$$

$$\dot{q}_2 = 0 \tag{2.85}$$

Then

$$0 = A_1 - B_1 - A_2 + B_2 \tag{2.86}$$

$$q_{20} = A_1 + B_1 + A_2 + B_2 \tag{2.87}$$

$$-\omega_1 q_{20} = -A_1\omega_1 - B_1\omega_1 + A_2\omega_2 + B_2\omega_2 \tag{2.88}$$

$$0 = A_1\omega_1 - B_1\omega_1 + A_2\omega_2 - B_2\omega_2 \tag{2.89}$$

and

$$A_2 = B_2 = 0 \tag{2.90}$$

$$A_1 = q_{20}/2 \tag{2.91}$$

$$B_1 = q_{20}/2 \tag{2.92}$$

Equations (2.80) and (2.81) become

$$q_1 = \frac{q_{20}}{2}\left(je^{j\omega_1 t} - je^{-j\omega_1 t}\right) \tag{2.93}$$

$$q_2 = \frac{q_{20}}{2}\left(e^{j\omega_1 t} + e^{-j\omega_1 t}\right) \tag{2.94}$$

and as

$$e^{\pm j\omega_1 t} = \cos\omega_1 t \pm j\sin\omega_1 t \tag{2.95}$$

the expressions for q_1 and q_2 are

$$q_1 = -q_{20}\sin\omega_1 t \tag{2.96}$$

$$q_2 = q_{20}\cos\omega_1 t \tag{2.97}$$

The displacements u and w of a point situated at $y = l$ of the axis of the rotor are given by (2.1), (2.2) and the expressions for q_1 and q_2; then

$$u(l, t) = -q_{20}\sin\frac{\pi l}{L}\sin\omega_1 t = -R\sin\omega_1 t \tag{2.98}$$

$$w(l, t) = q_{20}\sin\frac{\pi l}{L}\cos\omega_1 t = R\cos\omega_1 t \tag{2.99}$$

These two expressions give

$$R = \sqrt{u^2(l,t) + w^2(l,t)} = q_{20}\sin\frac{\pi l}{L} \tag{2.100}$$

Hence the points situated on the axis of the rotor remain on circles. With the set of initial conditions chosen, the orbit is described (Figure 2.3) in a sense opposite to the sense of rotation Ω; the rotor is in the situation of backward whirl (BW).

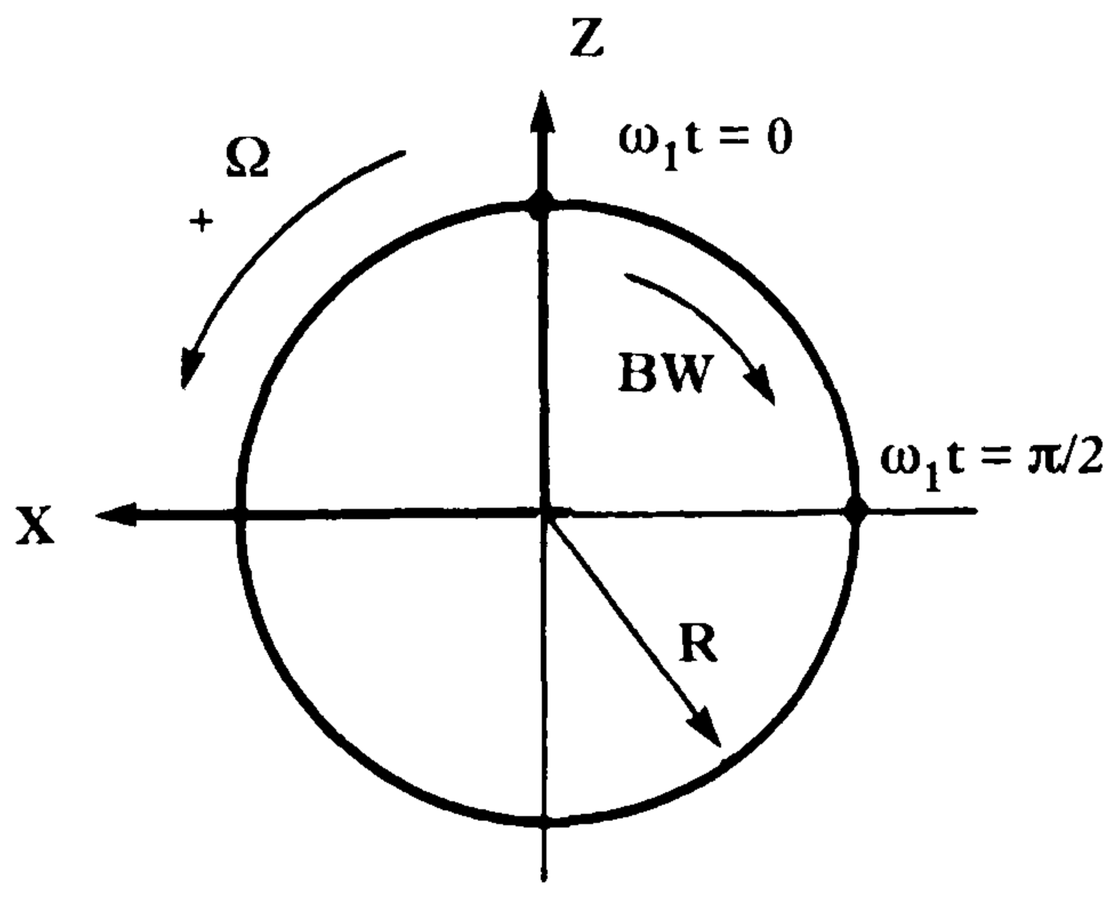

Figure 2.3. Rotor orbit: backward whirl

Let us now choose another set of initial conditions which show only the frequency ω_2. At $t_0 = 0$:

$$q_1 = q_{10} \tag{1.101}$$

$$q_2 = 0 \tag{2.102}$$

$$\dot{q}_1 = 0 \tag{2.103}$$

$$\dot{q}_2 = -\omega_2 q_{10} \tag{2.104}$$

This set of initial conditions leads to

$$q_1 = q_{10} \cos \omega_2 t \tag{2.105}$$

$$q_2 = -q_{10} \sin \omega_2 t \tag{2.106}$$

Then

$$u(l, t) = q_{10} \sin \frac{\pi l}{L} \cos \omega_2 t = R \cos \omega_2 t \tag{2.107}$$

$$w(l, t) = -q_{10} \sin \frac{\pi l}{L} \sin \omega_2 t = -R \sin \omega_2 t \tag{2.108}$$

The points situated on the rotor axis remain on circles. Here the orbit is described (Figure 2.4) in the same sense as that of the rotation Ω; the rotor is in the situation of forward whirl (FW).

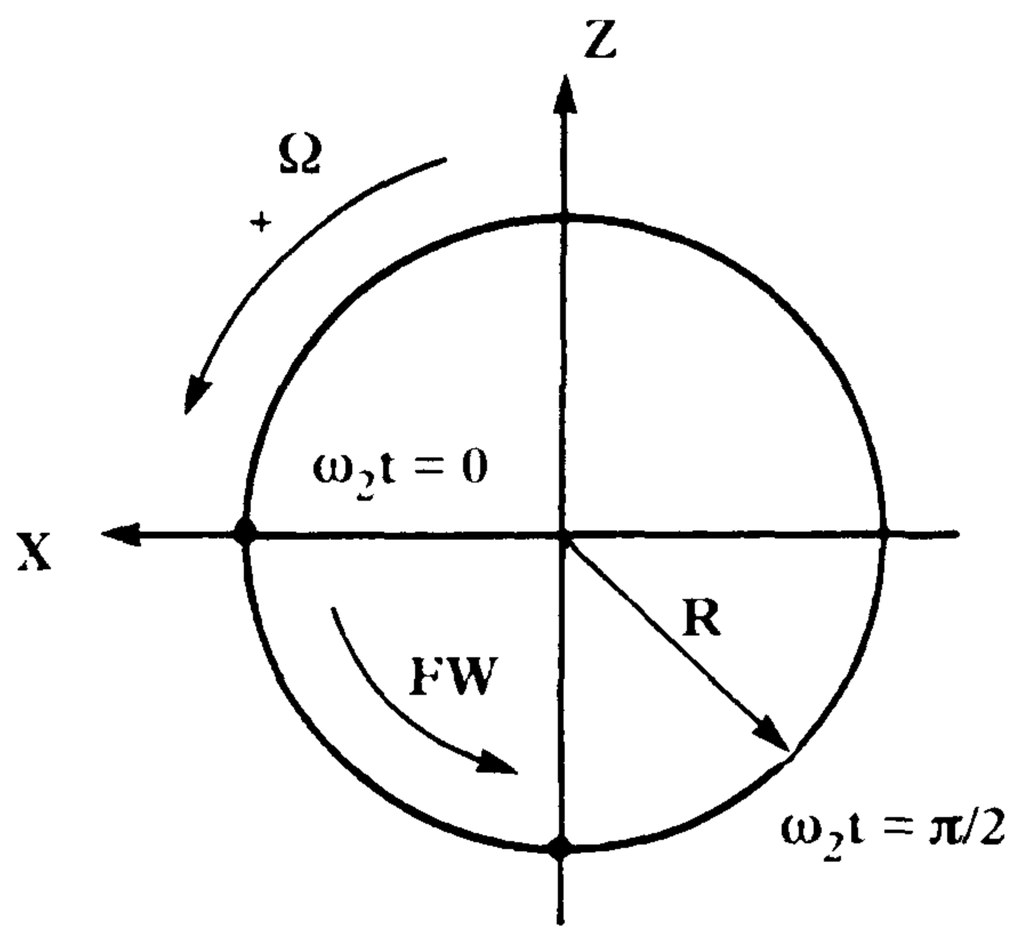

Figure 2.4. Rotor orbit: forward whirl

Let us now look at the rotor defined by (2.53) and (2.54). The characteristic equation of the free motion is

$$r^4 + (1.672 \times 10^5 + 4.034 \times 10^{-2}\Omega^2)r^2 + 6.993 \times 10^9 = 0 \quad (2.109)$$

and the frequencies at rest are

$$F_{10} = \frac{\omega_{10}}{2\pi} = F_{20} = \frac{\omega_{20}}{2\pi} = 46.02\,\text{Hz} \quad (2.110)$$

The frequencies in rotation are

$$F_1 = \frac{\omega_1}{2\pi} = \frac{1}{2\pi}\sqrt{8.362\times 10^4 + 2.017\times 10^{-2}\Omega^2\left(1-\sqrt{1+\frac{8.292\times 10^6}{\Omega^2}}\right)} \quad (2.111)$$

$$F_2 = \frac{\omega_2}{2\pi} = \frac{1}{2\pi}\sqrt{8.362\times 10^4 + 2.017\times 10^{-2}\Omega^2\left(1+\sqrt{1+\frac{8.292\times 10^6}{\Omega^2}}\right)} \quad (2.112)$$

The Campbell diagram for $F_1 = F_1(N)$ and $F_2 = F_2(N)$ is shown in Figure 2.5, where the intersections of $F_1(N)$ and $F_2(N)$ with two straight

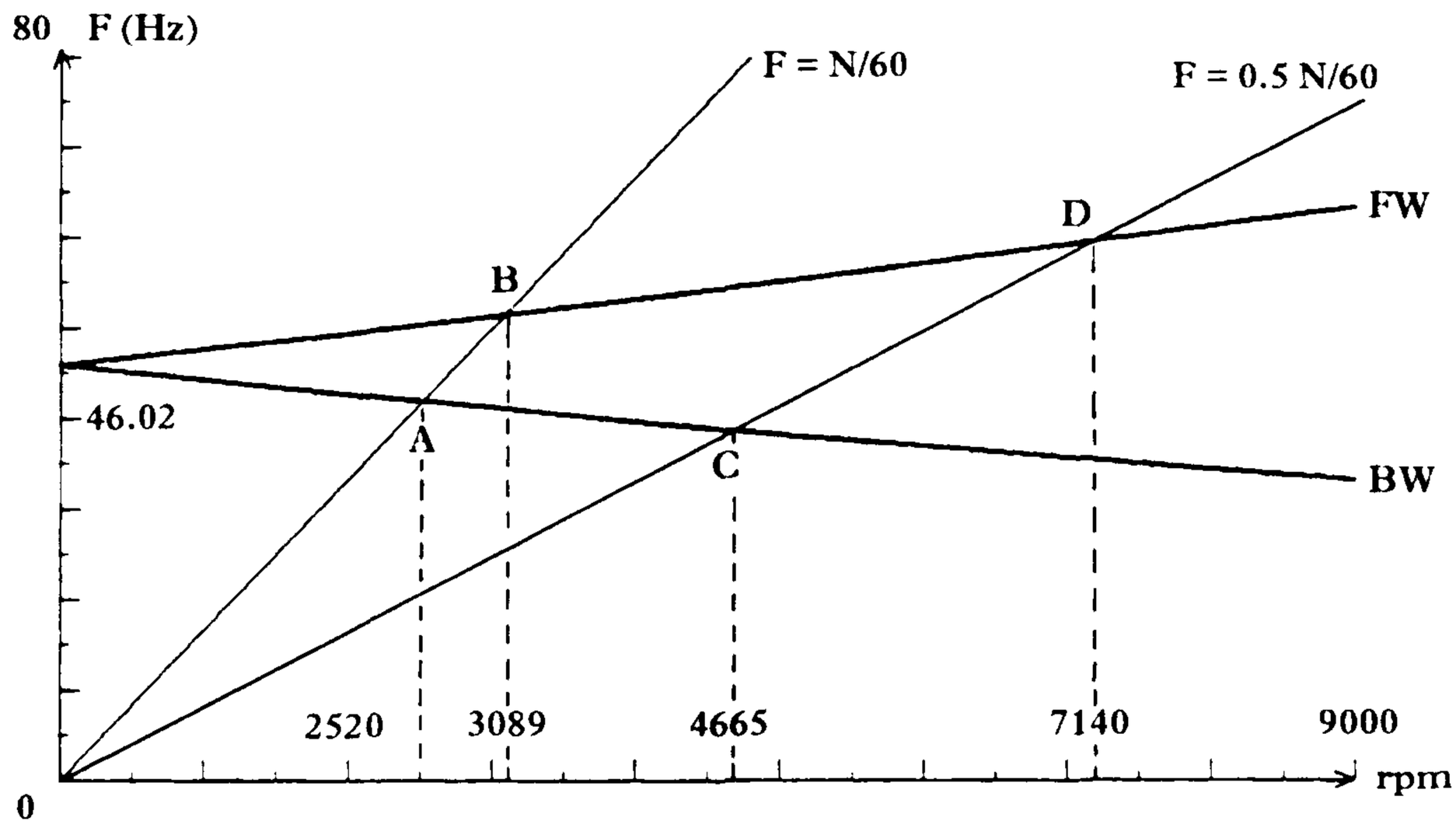

Figure 2.5. Campbell diagram

lines are shown. Points A and B correspond to the intersection with $F = N/60$; at the corresponding points a frequency of the rotor equals the frequency of the rotation. Points C and D correspond to the intersections with $F = 0.5\,N/60$; at the corresponding points, a frequency of the rotor equals half of the frequency of rotation.

It is of interest to get a general expression for the frequencies corresponding to points A, B, C and D. The general relationship between ω and Ω is

$$\omega = s\Omega \tag{2.113}$$

where $s = 1$ in A and B, and $s = 0.5$ in C and D. Expressions (2.66) and (2.69) give

$$r = \pm j\omega = \pm js\Omega \tag{2.114}$$

which, substituted in (2.62), leads to

$$s^4 m^2 \Omega^4 - (2km + a^2\Omega^2)s^2\Omega^2 + k^2 = 0 \tag{2.115}$$

and

$$s^2(s^2 m^2 - a^2)\Omega^4 - 2kms^2\Omega^2 + k^2 = 0 \tag{2.116}$$

The solutions of (2.116) are

$$\Omega_1 = \sqrt{\frac{k}{s(sm + a)}} \tag{2.117}$$

$$\Omega_2 = \sqrt{\frac{k}{s(sm - a)}} \tag{2.118}$$

and, from (2.113),

$$\omega_1 = s\sqrt{\frac{k}{s(sm + a)}} \tag{2.119}$$

which corresponds to points A ($s = 1$) and C ($s = 0.5$), and

$$\omega_2 = s\sqrt{\frac{k}{s(sm - a)}} \tag{2.120}$$

which corresponds to points B ($s = 1$) and D ($s = 0.5$).

For the application considered here:

$$\text{in A, } F_1 = 42.00\,\text{Hz}, N = 2520\,\text{rpm} \tag{2.121}$$

$$\text{in B, } F_2 = 51.48\,\text{Hz}, N = 3089\,\text{rpm} \tag{2.122}$$

$$\text{in C, } F_1 = 38.87\,\text{Hz}, N = 4665\,\text{rpm} \tag{2.123}$$

$$\text{in D, } F_2 = 59.50\,\text{Hz}, N = 7140\,\text{rpm} \tag{2.124}$$

2.2.2 Response to forces of excitation

Here only the steady-state response is calculated. The general solution of Equation (2.55) and (2.56) is not considered.

Mass unbalance

Equations (2.51) and (2.52), with $m^* = m_u f(l_1)$, become

$$m\ddot{q}_1 - a\Omega\dot{q}_2 + kq_1 = m^* d\Omega^2 \sin\Omega t \tag{2.125}$$

$$m\ddot{q}_2 + a\Omega\dot{q}_1 + kq_2 = m^* d\Omega^2 \cos\Omega t \tag{2.126}$$

As there is no damping, solutions can be sought in the form

$$q_1 = Q_1 \sin \Omega t \tag{2.127}$$

$$q_2 = Q_2 \cos \Omega t \tag{2.128}$$

Substituting (2.127) and (2.128) in (2.125) and (2.126) gives

$$-m\Omega^2 Q_1 + a\Omega^2 Q_2 + kQ_1 = m^* d\Omega^2 \tag{2.129}$$

$$-m\Omega^2 Q_2 + a\Omega^2 Q_1 + kQ_2 = m^* d\Omega^2 \tag{2.130}$$

Then

$$Q_1 = Q_2 = \frac{m^* d\Omega^2}{k + (a - m)\Omega^2} \tag{2.131}$$

The critical speed Ω_c, due to the mass unbalance, corresponds to the value which makes the displacement infinite. For the denominator of (2.131) to vanish,

$$\Omega_c = \sqrt{\frac{k}{m - a}} \tag{2.132}$$

The result shows only one critical speed which corresponds to the value of Ω_2 given in (2.118) when $s = 1$. The corresponding value is that of point B in Figure 2.5. As $Q_1 = Q_2$ the orbits described by the rotor axis are circles, and the whirl, as can be seen from the equations, is a forward whirl (FW). The position of the mass unbalance is shown in Figure 2.6.

Let us now look at the rotor defined by Equations (2.53) and (2.54). The displacements due to unbalance are

$$Q_1 = Q_2 = \frac{1.299 \times 10^{-5}\Omega^2}{1.195 \times 10^6 - 11.42\Omega^2} \tag{2.133}$$

and the critical speed corresponds to $\Omega_c/2\pi = 51.48\,\text{Hz}$; that is, $N = 3089\,\text{rpm}$. The result is that observed in free motion (Equation (2.122)). It is noted from (2.131) that, when Ω grows, the limiting value

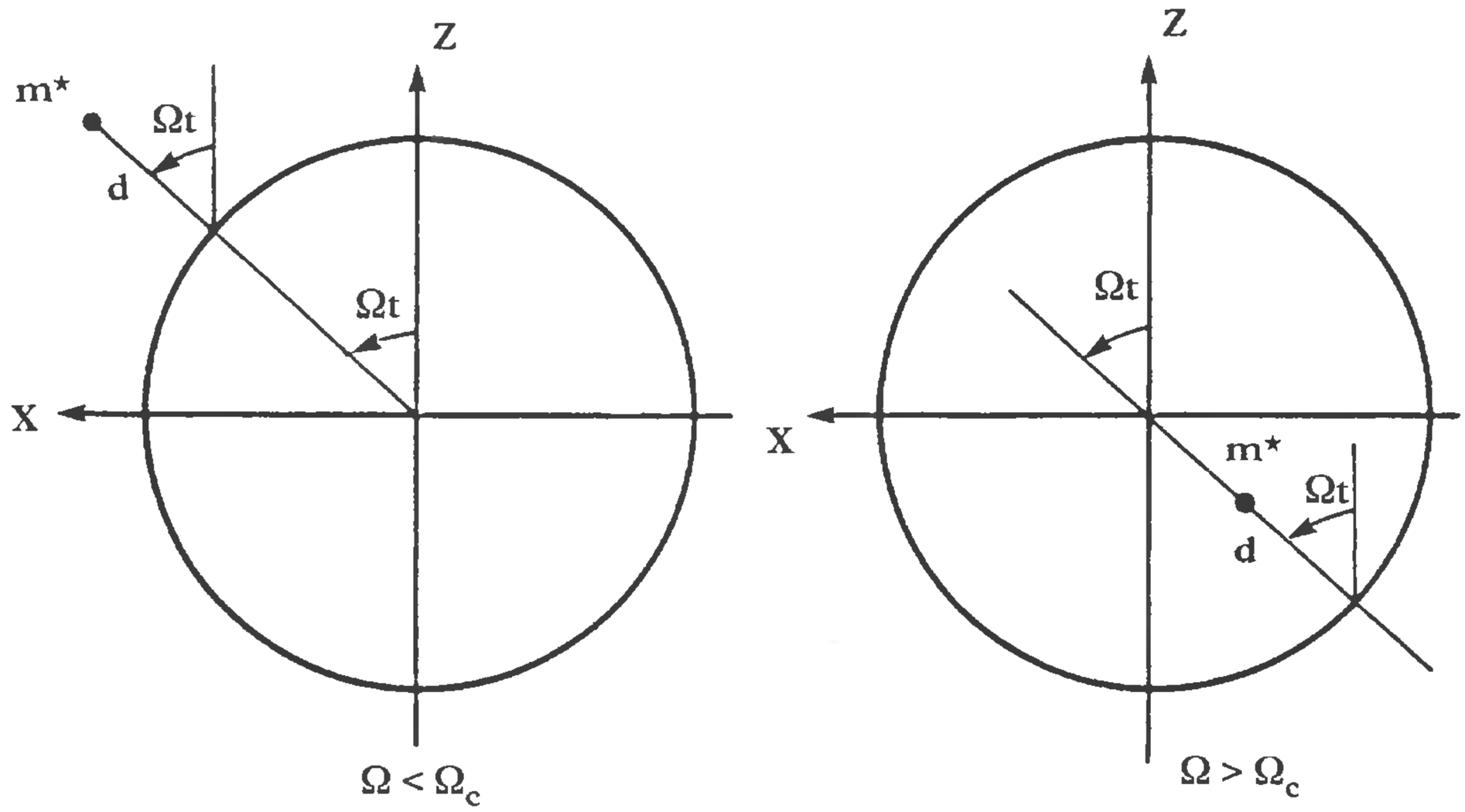

Figure 2.6. Position of the mass unbalance

of the displacement is

$$|Q_1| = |Q_2| = \left|\frac{m^* d}{a - m}\right| \tag{2.134}$$

which gives, for the rotor considered here,

$$|Q_1| = |Q_2| = 1.137 \times 10^{-6}\,\mathrm{m}$$

The amplitude of the response Q_1 is presented in Figure 2.7.

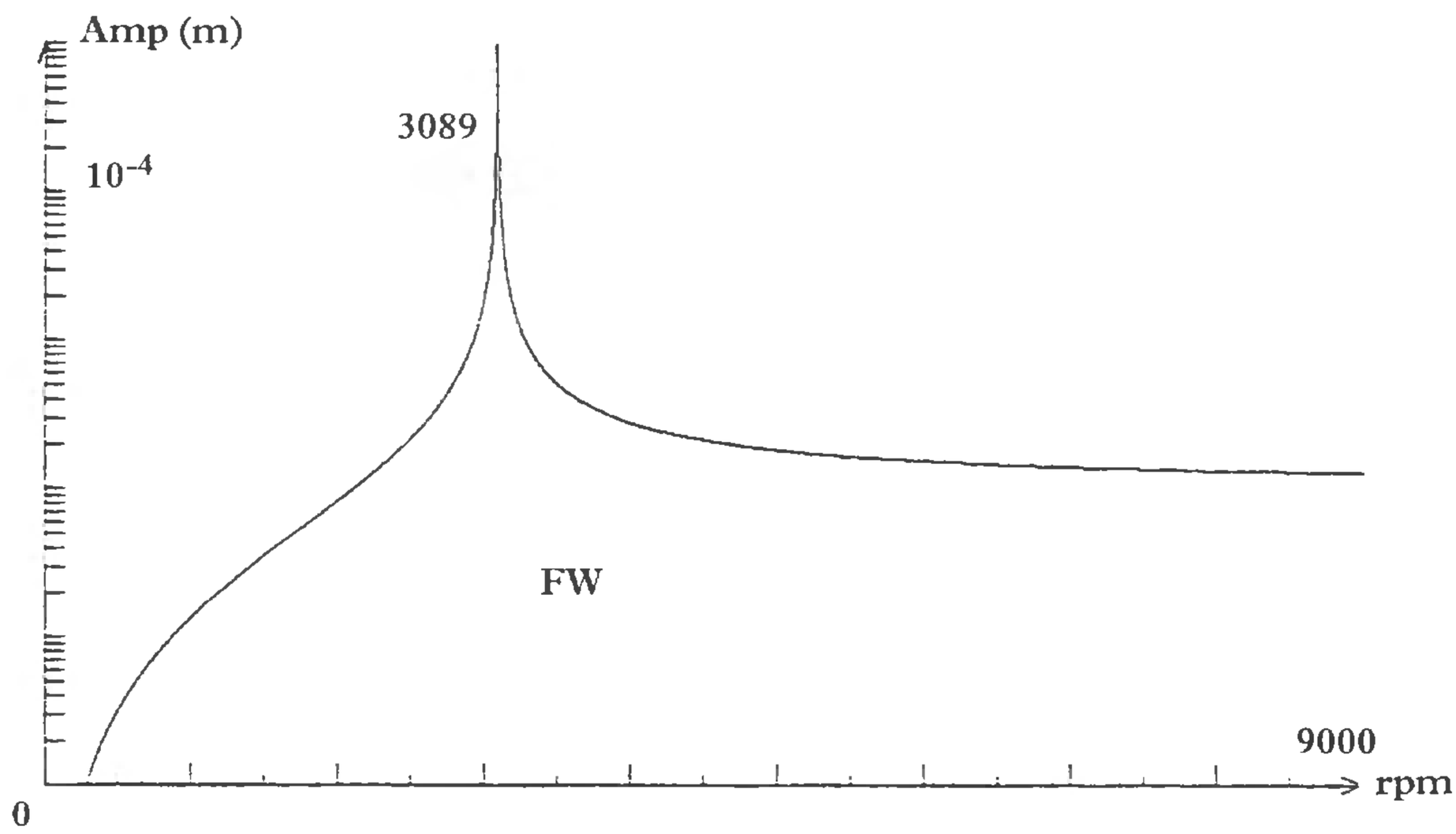

Figure 2.7. Mass unbalance response

Asynchronous force

Under operating conditions a rotor can be excited by asynchronous rotating forces. Let us suppose that the components of the force acting on the rotor are

$$Fq_1 = F_0 \sin s\Omega t\, f(l_3) = F \sin s\Omega t \tag{2.135}$$

$$Fq_2 = F_0 \cos s\Omega t\, f(l_3) = F \cos s\Omega t \tag{2.136}$$

The equations to be solved are then

$$m\ddot{q}_1 - a\Omega\dot{q}_2 + kq_1 = F \sin s\Omega t \tag{2.137}$$

$$m\ddot{q}_2 + a\Omega\dot{q}_1 + kq_2 = F \cos s\Omega t \tag{2.138}$$

Here, too, solutions can be sought as

$$q_1 = Q_1 \sin s\Omega t \tag{2.139}$$

$$q_2 = Q_2 \cos s\Omega t \tag{2.140}$$

and the solutions are

$$Q_1 = Q_2 = \frac{F}{k + (as - ms^2)\Omega^2} \tag{2.141}$$

The critical speed Ω_c, due to the asynchronous force, corresponds to the value which makes the displacement infinite. For the denominator of (2.141) to vanish,

$$\Omega_c = \sqrt{\frac{k}{s(ms - a)}} \tag{2.142}$$

The result shows only one critical speed which corresponds to the value of Ω_2 given in (2.118). As $Q_1 = Q_2$ the orbits described are circles and the whirl is always forward (FW). For the rotor defined in (2.53) and (2.54) with $s = 0.5$,

$$Q_1 = Q_2 = \frac{F}{1.195 \times 10^6 - 2.138\Omega^2} \tag{2.143}$$

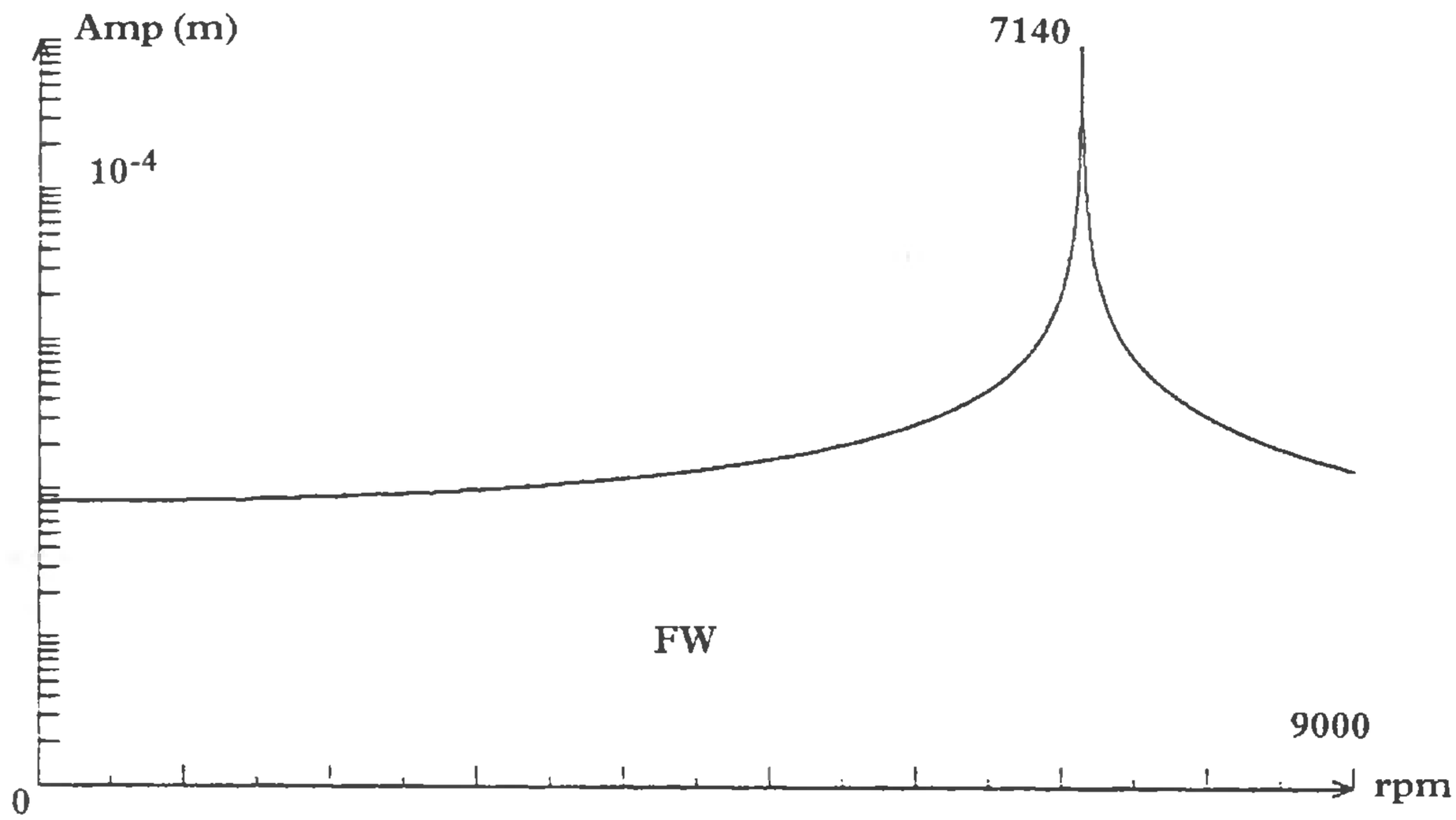

Figure 2.8. Asynchronous force response

and the critical speed corresponds to $\Omega_c/2\pi = 59.50\,\text{Hz}$; that is $N = 7140\text{rpm}$. The amplitude of the response $Q_1 = Q_2$ is presented in Figure 2.8, with $F = 1N$.

Harmonic force fixed in space

The force is assumed to act only along the x direction at $y = l_3 = 2L/3$. Then, using (2.24) and (2.25), its components are

$$Fq_1 = F_0 \sin\omega t\, f(l_3) = F \sin\omega t \tag{2.144}$$

$$Fq_2 = 0 \tag{2.145}$$

The equations to be solved are then

$$m\ddot{q}_1 - a\Omega\dot{q}_2 + kq_1 = F\sin\omega t \tag{2.146}$$

$$m\ddot{q}_2 + a\Omega\dot{q}_1 + kq_2 = 0 \tag{2.147}$$

Here too, as there is no damping, solutions can be sought as

$$q_1 = Q_1 \sin\omega t \tag{2.148}$$

$$q_2 = Q_2 \cos\omega t \tag{2.149}$$

and the result is

$$Q_1 = \frac{(k - m\omega^2)F}{(k - m\omega^2)^2 - a^2\Omega^2\omega^2} \tag{2.150}$$

$$Q_2 = \frac{-a\Omega\omega F}{(k - m\omega^2)^2 - a^2\Omega^2\omega^2} \tag{2.151}$$

The critical frequencies correspond to the value of ω which makes the denominator of (2.150) and (2.151) vanish; that is

$$m^2\omega^4 - (2km + a^2\Omega^2)\omega^2 + k^2 = 0 \tag{2.152}$$

Equation (2.152) is the same equation as (2.62) with $r = \pm j\omega$, and the two critical frequencies can also be obtained directly from the Campbell diagram. As $Q_1 \neq Q_2$ the orbits described are ellipses. When $\omega < \omega_{10}$ the whirl is backward (BW); when $\omega_{10} < \omega$ the whirl is forward (FW). In laboratory tests these excitation forms can be reproduced and used to draw the Campbell diagram from experiments. At a given speed Ω, the frequencies $\omega_1(\Omega)$ and $\omega_2(\Omega)$ are obtained by exciting the rotor with an electromagnetic shaker through the external ring of a roller bearing.

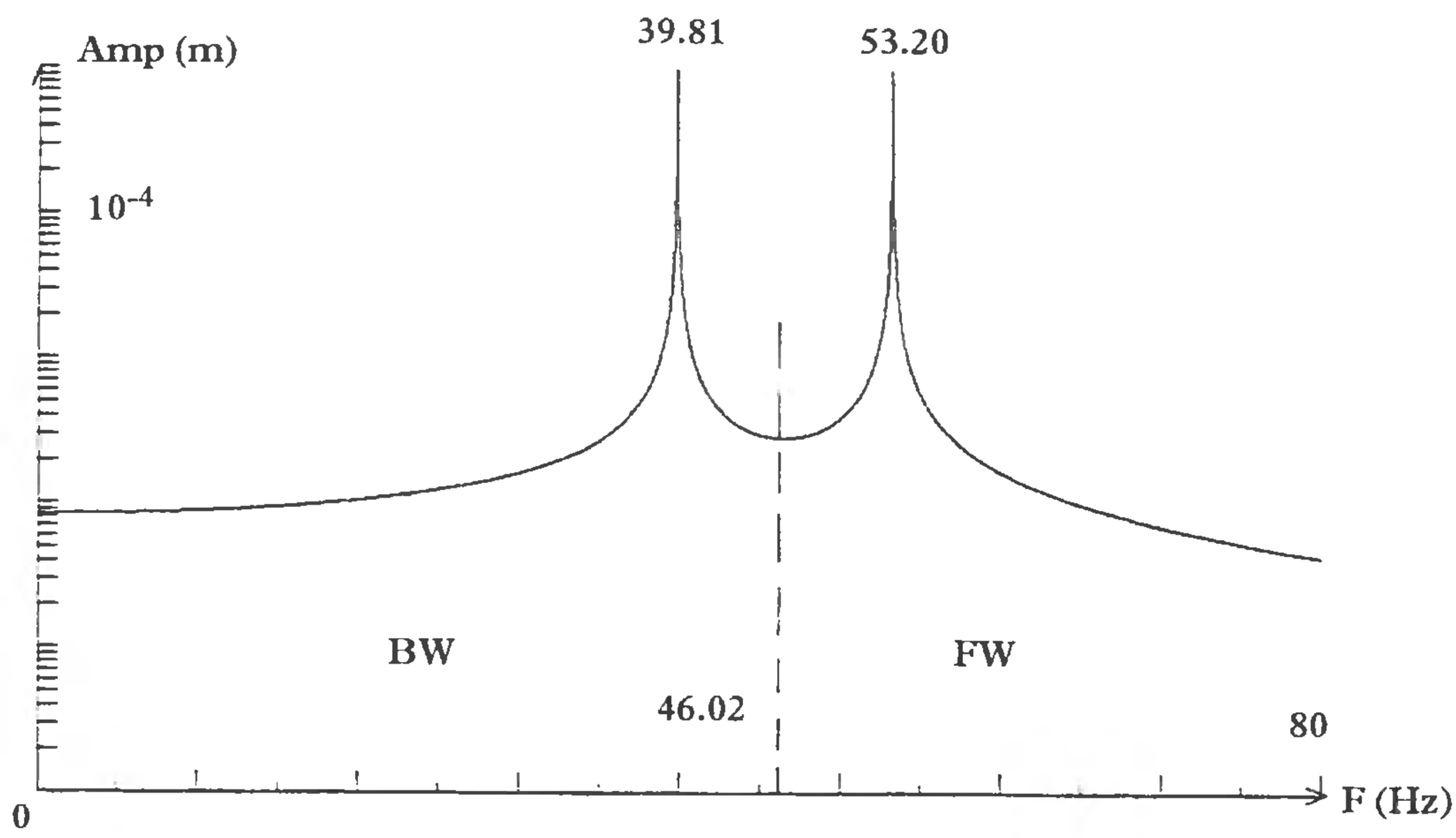

Figure 2.9. Harmonic force fixed in space response

For the rotor previously defined in (2.53) and (2.54):

$$Q_1 = \frac{(1.195 \times 10^6 - 14.29\omega^2)F}{(1.195 \times 10^6 - 14.29\omega^2)^2 - 8.243\Omega^2\omega^2} \tag{2.153}$$

$$Q_2 = \frac{-2.871\omega F}{(1.195 \times 10^6 - 14.29\omega^2)^2 - 8.243\Omega^2\omega^2} \tag{2.154}$$

The maximum amplitude of the response, Amp (that is, $|Q_1|$ or $|Q_2|$), has been calculated for $N = 4000$rpm and presented in Figure 2.9, with $F = 1N$.

2.3 ASYMMETRIC ROTOR

The asymmetry is introduced by a spring k_{zz} as shown in Equations (2.17), (2.18), (2.47) and (2.48). Then

$$k_1 = k \tag{2.155}$$

$$k_2 = k + k_{zz} f^2(l_2) \tag{2.156}$$

Equations (2.51) and (2.52) become

$$m\ddot{q}_1 - a\Omega\dot{q}_2 + k_1 q_1 = m^* d\Omega^2 \sin\Omega t \tag{2.157}$$

$$m\ddot{q}_2 + a\Omega\dot{q}_1 + k_2 q_2 = m^* d\Omega^2 \cos\Omega t \tag{2.158}$$

Equations (2.53) and (2.54) become

$$14.29\ddot{q}_1 - 2.871\Omega\dot{q}_2 + 1.195 \times 10^6 q_1 = 1.299 \times 10^{-5}\Omega^2 \sin\Omega t \tag{2.159}$$

$$14.29\ddot{q}_2 + 2.871\Omega\dot{q}_1 + 1.570 \times 10^6 q_2 = 1.299 \times 10^{-5}\Omega^2 \cos\Omega t \tag{2.160}$$

2.3.1 Natural frequencies as a function of the speed of rotation: the Campbell diagram

Again the rotor is studied in free motion. Equations (2.157) and (2.158) become

$$m\ddot{q}_1 - a\Omega\dot{q}_2 + k_1 q_1 = 0 \tag{2.161}$$

$$m\ddot{q}_2 + a\Omega\dot{q}_1 + k_2 q_2 = 0 \tag{2.162}$$

Solutions have to be sought in the form of (2.58) and (2.59) which, substituted in Equations (2.161) and (2.162), give a homogeneous set of equations in Q_1 and Q_2:

$$\begin{bmatrix} k_1 + mr^2 & -a\Omega r \\ a\Omega r & k_2 + mr^2 \end{bmatrix} \begin{bmatrix} Q_1 \\ Q_2 \end{bmatrix} = 0 \tag{2.163}$$

The non-trivial solutions come from the values of r which bring to zero the value of the determinant of the matrix. The expansion of the determinant gives the characteristic equation

$$m^2 r^4 + (k_1 m + k_2 m + a^2\Omega^2) r^2 + k_1 k_2 = 0 \tag{2.164}$$

At rest ($\Omega = 0$), the two roots of (2.164) are

$$r_{10}^2 = j^2 \omega_{10}^2 = -\frac{k_1}{m} \tag{2.165}$$

$$r_{20}^2 = j^2 \omega_{20}^2 = -\frac{k_2}{m} \tag{2.166}$$

Hence

$$\omega_{10} = \sqrt{\frac{k_1}{m}} \tag{2.167}$$

$$\omega_{20} = \sqrt{\frac{k_2}{m}} \tag{2.168}$$

Under rotating conditions ($\Omega \neq 0$):

$$r_1 = \pm j\omega_1 \tag{2.169}$$

$$r_2 = \pm j\omega_2 \tag{2.170}$$

with

$$\omega_1 = \sqrt{\frac{\omega_{10}^2}{2} + \frac{\omega_{20}^2}{2} + \frac{a^2\Omega^2}{2m^2} - \sqrt{\left(\frac{\omega_{10}^2}{2} + \frac{\omega_{20}^2}{2} + \frac{a^2\Omega^2}{2m^2}\right)^2 - \omega_{10}^2\omega_{20}^2}} \tag{2.171}$$

$$\omega_2 = \sqrt{\frac{\omega_{10}^2}{2} + \frac{\omega_{20}^2}{2} + \frac{a^2\Omega^2}{2m^2} + \sqrt{\left(\frac{\omega_{10}^2}{2} + \frac{\omega_{20}^2}{2} + \frac{a^2\Omega^2}{2m^2}\right)^2 - \omega_{10}^2\omega_{20}^2}} \tag{2.172}$$

The expressions $d\omega_1/d\Omega$ and $d\omega_2/d\Omega$ can be calculated, and they show respectively that:

$$\text{if } \frac{d\omega_1}{d\Omega} < 0, \quad \text{then } \omega_1 < \omega_{10}$$

$$\text{if } \frac{d\omega_2}{d\Omega} > 0, \quad \text{then } \omega_{20} < \omega_2$$

Hence

$$\omega_1 < \omega_{10} < \omega_{20} < \omega_2 \tag{2.173}$$

Equations (2.171) and (2.172) show that ω_1 and ω_2 are real quantities; so r_1 and r_2 are imaginary quantities and the rotor is stable. The mode shapes have also to be considered. The first equation in (2.163) gives

$$Q_1 = \frac{a\Omega r Q_2}{k_1 + mr^2} \tag{2.174}$$

The calculations corresponding to free motion are not given here as they are much more complex than those for the symmetric rotor. It is easy to observe that $Q_1 \neq Q_2$; the orbits described by the rotor axis are ellipses.

The characteristic equation of the rotor defined by (2.159) and (2.160) is

$$r^4 + (1.935 \times 10^5 + 4.034 \times 10^{-2}\Omega^2)r^2 + 9.187 \times 10^9 = 0 \tag{2.175}$$

and the frequencies at rest are

$$F_{10} = \frac{\omega_{10}}{2\pi} = 46.02\,\text{Hz} \tag{2.176}$$

$$F_{20} = \frac{\omega_{20}}{2\pi} = 52.75\,\text{Hz} \tag{2.177}$$

The Campbell diagram for $F_1 = F_1(N)$ and $F_2 = F_2(N)$ is shown in Figure 2.10, where the intersections with $F = N/60$ and $F = 0.5N/60$ are shown. Points A and B correspond to $F = N/60$ and points C and D to $F = 0.5\,N/60$.

The general equation which gives the values of the frequencies at points A, B, C and D can be obtained from (2.114) and (2.164).

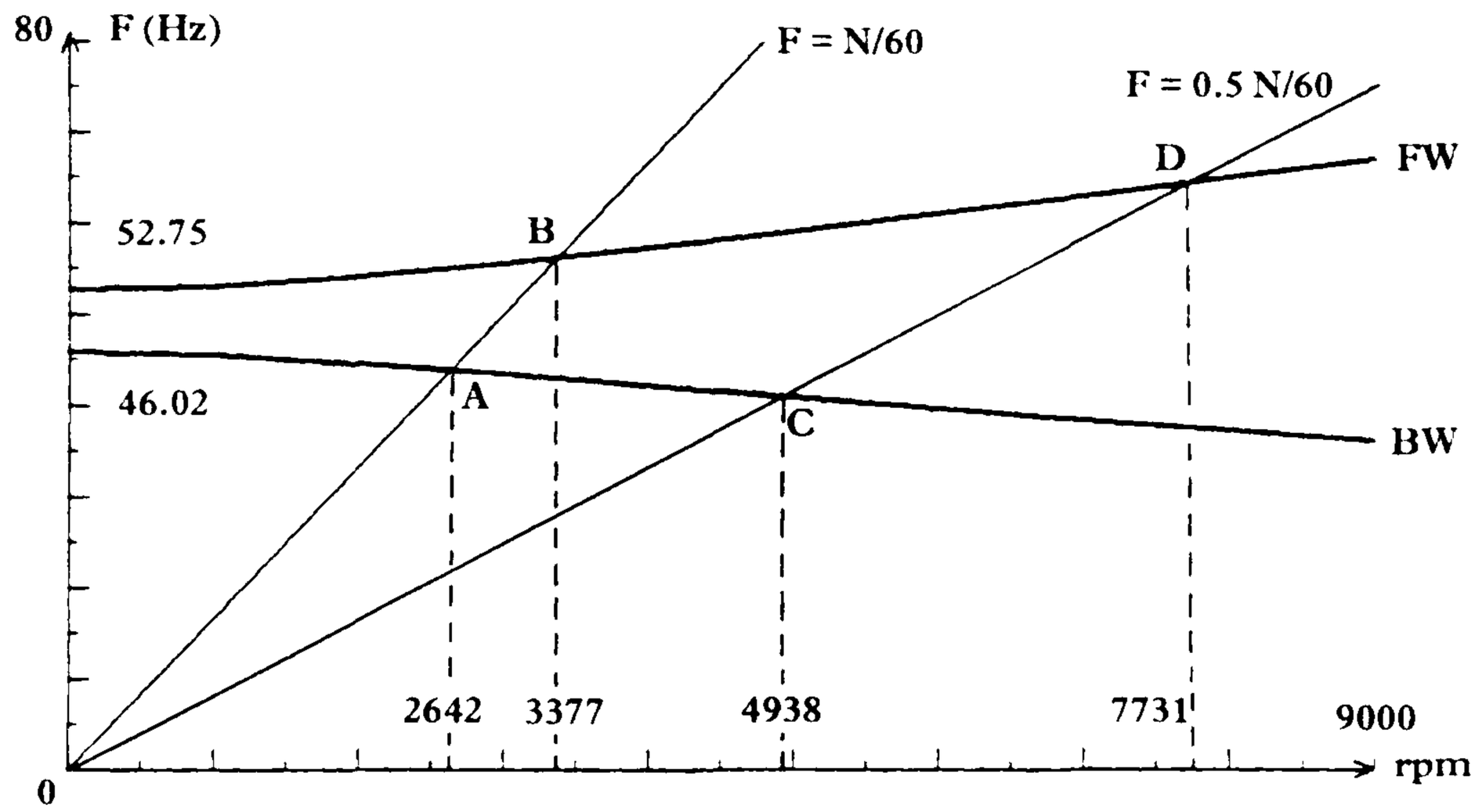

Figure 2.10. Campbell diagram

These give

$$s^4 m^2 \Omega^4 - (k_1 m + k_2 m + a^2 \Omega^2) s^2 \Omega^2 + k_1 k_2 = 0 \tag{2.178}$$

that is

$$s^2 (s^2 m^2 - a^2) \Omega^4 - m(k_1 + k_2) s^2 \Omega^2 + k_1 k_2 = 0 \tag{2.179}$$

For the example considered here:

$$\text{in A, } F_1 = 44.03\,\text{Hz}, N = 2642\,\text{rpm} \tag{2.180}$$
$$\text{in B, } F_2 = 56.29\,\text{Hz}, N = 3377\,\text{rpm} \tag{2.181}$$
$$\text{in C, } F_1 = 41.15\,\text{Hz}, N = 4938\,\text{rpm} \tag{2.182}$$
$$\text{in D, } F_2 = 64.42\,\text{Hz}, N = 7731\,\text{rpm} \tag{2.183}$$

2.3.2 Response to forces of excitation

Here, too, only the steady-state response is calculated. The general solution of (2.161) and (2.162) is not considered.

Mass unbalance

The equations to be solved are (2.157) and (2.158) and the solutions can be sought as in (2.127) and (2.128). The results are

$$Q_1 = \frac{(k_2 - (m+a)\Omega^2)m^* d\Omega^2}{(k_1 - m\Omega^2)(k_2 - m\Omega^2) - a^2\Omega^4} \tag{2.184}$$

$$Q_2 = \frac{(k_1 - (m+a)\Omega^2)m^* d\Omega^2}{(k_1 - m\Omega^2)(k_2 - m\Omega^2) - a^2\Omega^4} \tag{2.185}$$

The critical speeds due to mass unbalance are then given by

$$(k_1 - m\Omega^2)(k_2 - m\Omega^2) - a^2\Omega^4 = 0 \tag{2.186}$$

that is

$$(m^2 - a^2)\Omega^4 - m(k_1 + k_2)\Omega^2 + k_1 k_2 = 0 \tag{2.187}$$

Equation (2.187) is the same as Equation (2.179) when $s = 1$. Hence the two speeds of rotation appearing in (2.180) and (2.181) are critical speeds. The orbits described by the rotor axis are ellipses as $|Q_1| \neq |Q_2|$, and the sense of the whirl is of significant interest. Let us suppose (Figure 2.11) that at instant t the rotor axis is in A. The cross product $\mathbf{OA} \wedge d\mathbf{OA}$ gives the sense of the whirl. The components of OA are

$$\mathbf{OA} = \begin{bmatrix} Q_1 \sin \Omega t \\ 0 \\ Q_2 \cos \Omega t \end{bmatrix} \tag{2.188}$$

Then

$$d\mathbf{OA} = \begin{bmatrix} Q_1 \Omega \cos \Omega t \, \mathrm{d}t \\ 0 \\ -Q_2 \Omega \sin \Omega t \, \mathrm{d}t \end{bmatrix} \tag{2.189}$$

and

$$\mathbf{OA} \wedge \mathbf{dOA} = \begin{bmatrix} 0 \\ Q_1 Q_2 \Omega \, \mathrm{d}t \\ 0 \end{bmatrix} \tag{2.190}$$

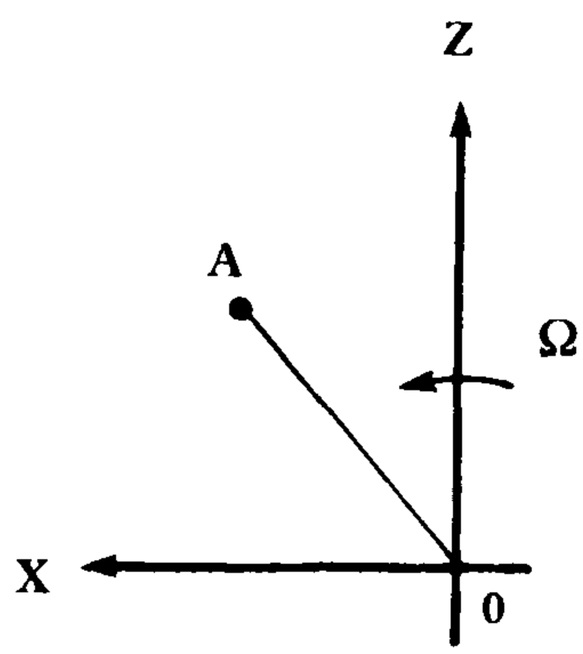

Figure 2.11. Sense of the whirl

Then if $0 < Q_1 Q_2$, the whirl is forward (FW), and if $Q_1 Q_2 < 0$ the whirl is backward (BW). Equations (2.184) and (2.185) show that the sign of $Q_1 Q_2$ is that of the expression

$$E(\Omega^2) = (k_1 - (m+a)\Omega^2)\,(k_2 - (m+a)\Omega^2) \tag{2.191}$$

Then, as $k_1 < k_2$:

$$\text{if } \Omega < \sqrt{\frac{k_1}{m+a}} \qquad \text{FW} \tag{2.192}$$

$$\text{if } \sqrt{\frac{k_1}{m+a}} < \Omega < \sqrt{\frac{k_2}{m+a}} \qquad \text{BW} \tag{2.193}$$

$$\text{if } \sqrt{\frac{k_2}{m+a}} < \Omega \qquad \text{FW} \tag{2.194}$$

If addition, it is of particular interest to know what happens at the critical speeds ω_1 and ω_2. These frequencies are solutions (2.187), and the sign of

$$F(\omega^2) = (m^2 - a^2)\omega^4 - (k_1 m + k_2 m)\omega^2 + k_1 k_2 \tag{2.195}$$

has to be considered. This expression is obviously a negative quantity when $\omega_1 < \omega < \omega_2$; otherwise it is easy to show that

$$F\left(\frac{k_1}{m+a}\right) = \frac{ak_1(k_2 - k_1)}{m+a} > 0 \tag{2.196}$$

$$F\left(\frac{k_2}{m+a}\right) = \frac{ak_2(k_1 - k_2)}{m+a} < 0 \tag{2.197}$$

Then

$$\omega_1 < \sqrt{\frac{k_2}{m+a}} < \omega_2 \tag{2.198}$$

and

$$\sqrt{\frac{k_1}{m+a}} < \omega_1 \tag{2.199}$$

Using (2.192), (2.193), (2.194), (2.198) and (2.199) gives the sense of the whirl, which is summarized in Figure 2.12.

For the rotor defined in (2.159) and (2.160):

$$Q_1 = \frac{(1.570 \times 10^6 - 17.17\Omega^2)\, 1.299 \times 10^{-5}\Omega^2}{196.1\Omega^4 - 3.954 \times 10^7\Omega^2 + 1.877 \times 10^{12}} \tag{2.200}$$

$$Q_2 = \frac{(1.195 \times 10^6 - 17.17\Omega^2) 1.299 \times 10^{-5}\Omega^2}{196.1\Omega^4 - 3.954 \times 10^7\Omega^2 + 1.877 \times 10^{12}} \tag{2.201}$$

When $\omega_2 \ll \Omega$, Q_1 and Q_2 are such that $|Q_1| = |Q_2| = 1.13 \times 10^{-6}$ m. The maximum amplitude (that is, $|Q_1|$ or $|Q_2|$) of the response is presented in Figure 2.13.

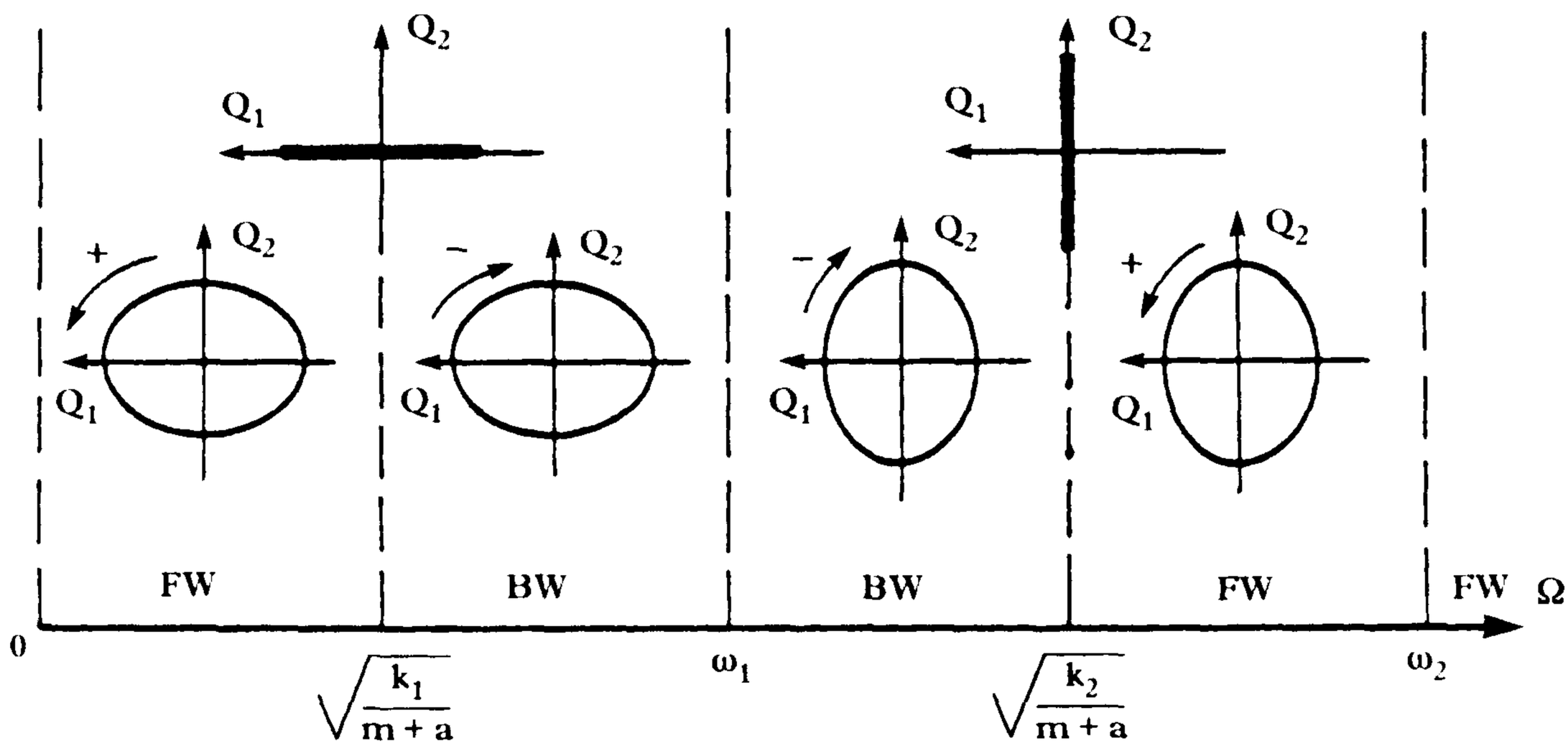

Figure 2.12. Variation of the sense of the whirl

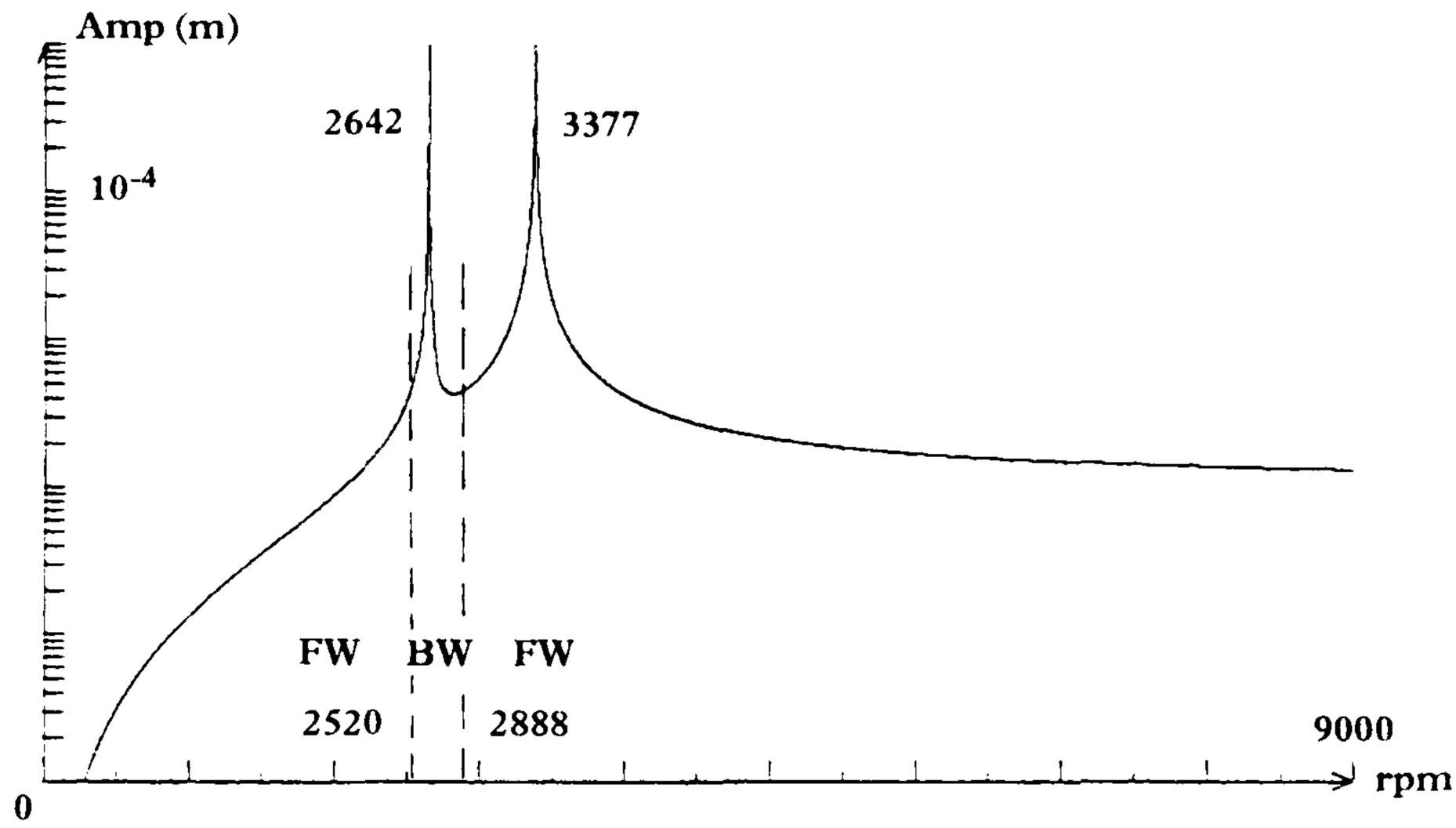

Figure 2.13. Mass unbalanse response

Asynchronous force

The force is the same as for the symmetric rotor case, and so the equations to be solved are

$$m\ddot{q}_1 - a\Omega\dot{q}_2 + k_1 q_1 = F\sin s\Omega t \tag{2.202}$$

$$m\ddot{q}_2 + a\Omega\dot{q}_1 + k_2 q_2 = F\cos s\Omega t \tag{2.203}$$

Solutions are sought as for (2.139) and (2.140), and hence

$$Q_1 = \frac{[k_2 - (ms^2 + as)\Omega^2]F}{s^2(s^2m^2 - a^2)\Omega^4 - m(k_1 + k_2)s^2\Omega^2 + k_1 k_2} \tag{2.204}$$

$$Q_2 = \frac{[k_1 - (ms^2 + as)\Omega^2]F}{s^2(s^2m^2 - a^2)\Omega^4 - m(k_1 + k_2)s^2\Omega^2 + k_1 k_2} \tag{2.205}$$

The critical speeds are given by the same equations as (2.179), the orbits are elliptical, and it can be shown that the sense of the whirl is, as for the

mass unbalance, given by the sign of $Q_1 Q_2$:

$$\text{if } \Omega < \sqrt{\frac{k_1}{ms^2 + as}} \qquad \text{FW} \tag{2.206}$$

$$\text{if } \sqrt{\frac{k_1}{ms^2 + as}} < \Omega < \sqrt{\frac{k_2}{ms^2 + as}} \qquad \text{BW} \tag{2.207}$$

$$\text{if } \sqrt{\frac{k_2}{ms^2 + as}} < \Omega \qquad \text{FW} \tag{2.208}$$

For the rotor defined by (2.159) and (2.160), with $s = 0.5$:

$$Q_1 = \frac{(1.570 \times 10^6 - 5.009\Omega^2)F}{10.71\Omega^4 - 9.884 \times 10^6\Omega^2 + 1.877 \times 10^{12}} \tag{2.209}$$

$$Q_2 = \frac{(1.195 \times 10^6 - 5.009\Omega^2)F}{10.71\Omega^4 - 9.884 \times 10^6\Omega^2 + 1.877 \times 10^{12}} \tag{2.210}$$

The maximum amplitude (that is, $|Q_1|$ or $|Q_2|$) of the response, with $F = 1N$, is presented in Figure 2.14.

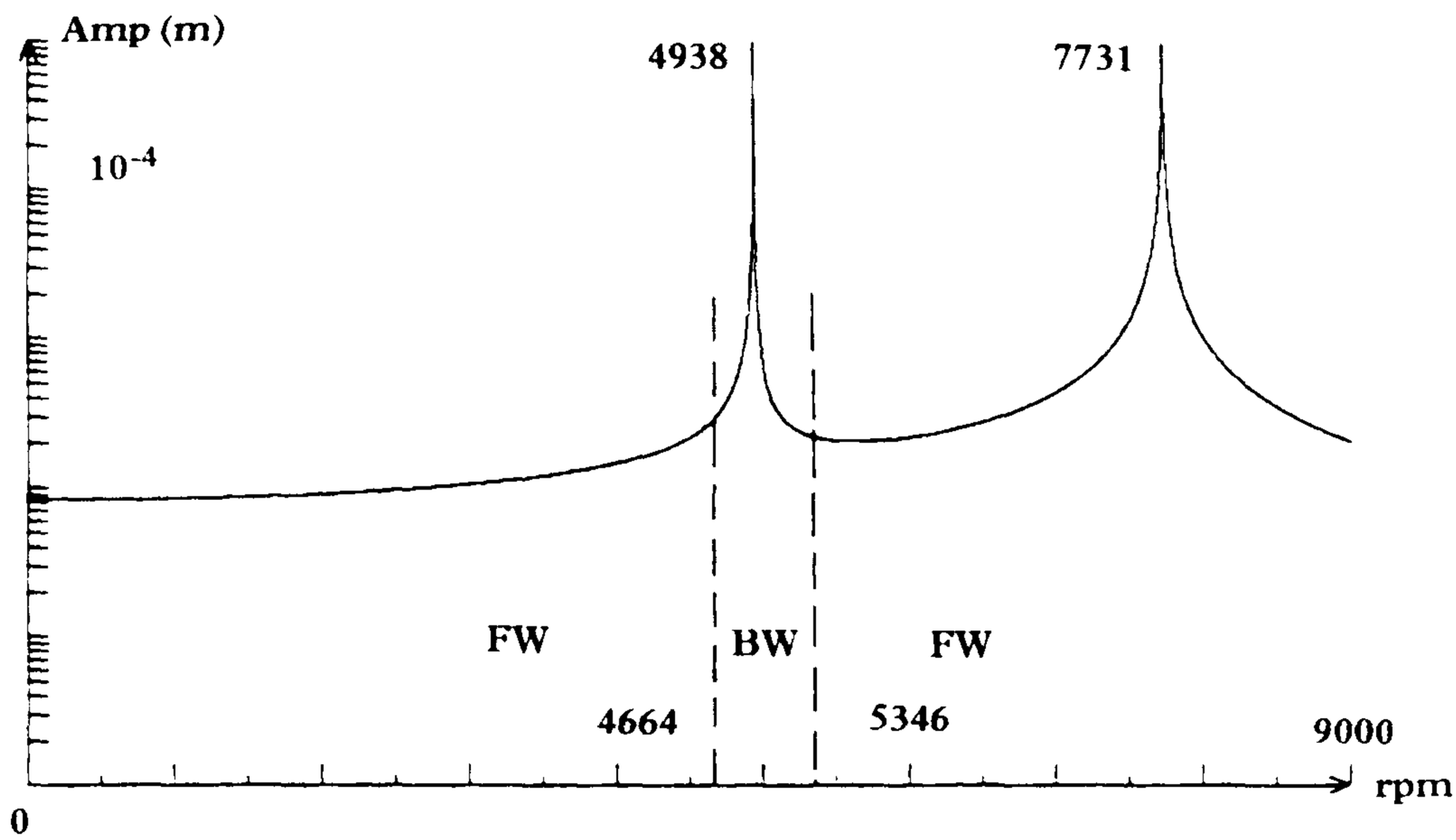

Figure 2.14. Asynchronous force response

Harmonic force fixed in space

The force is the same as just considered, and the equations to be solved are

$$m\ddot{q}_1 - a\Omega\dot{q}_2 + k_1 q_1 = F\sin\omega t \tag{2.211}$$

$$m\ddot{q}_2 + a\Omega\dot{q}_1 + k_2 q_2 = 0 \tag{2.212}$$

Solutions are sought as for (2.148) and (2.149), and

$$Q_1 = \frac{(k_2 - m\omega^2)F}{(k_1 - m\omega^2)(k_2 - m\omega^2) - a^2\Omega^2\omega^2} \tag{2.213}$$

$$Q_2 = \frac{-a\Omega\omega F}{(k_1 - m\omega^2)(k_2 - m\omega^2) - a^2\Omega^2\omega^2} \tag{2.214}$$

The critical frequencies are given by the equation

$$m^2\omega^4 - (k_1 m + k_2 m + a^2\Omega^2)\omega^2 + k_1 k_2 = 0 \tag{2.215}$$

which is the same as (2.164) with $r = \pm j\omega$. The two natural frequencies appear. The orbits, as $Q_1 \neq Q_2$, are ellipses, and the whirl given by the sign of the product $Q_1 Q_2$ is backward for $\omega < \omega_{20} = (k_2/m)^{1/2}$; otherwise the whirl is forward.

For the rotor defined by (2.159) and (2.160):

$$Q_1 = \frac{(1.570 \times 10^6 - 14.29\omega^2)F}{204.3\omega^4 - (3.954 \times 10^7 + 8.243 \times 10^{-2}\Omega^2)\omega^2 + 1.877 \times 10^{12}} \tag{2.216}$$

$$Q_2 = \frac{-2.871\Omega\omega F}{204.3\omega^4 - (3.954 \times 10^7 + 8.243 \times 10^{-2}\Omega^2)\omega^2 + 1.877 \times 10^{12}} \tag{2.217}$$

The maximum amplitude (that is, $|Q_1|$ or $|Q_2|$) of the response with $F = 1N$ has been calculated at $N = 4000$ rpm and is presented in Figure 2.15.

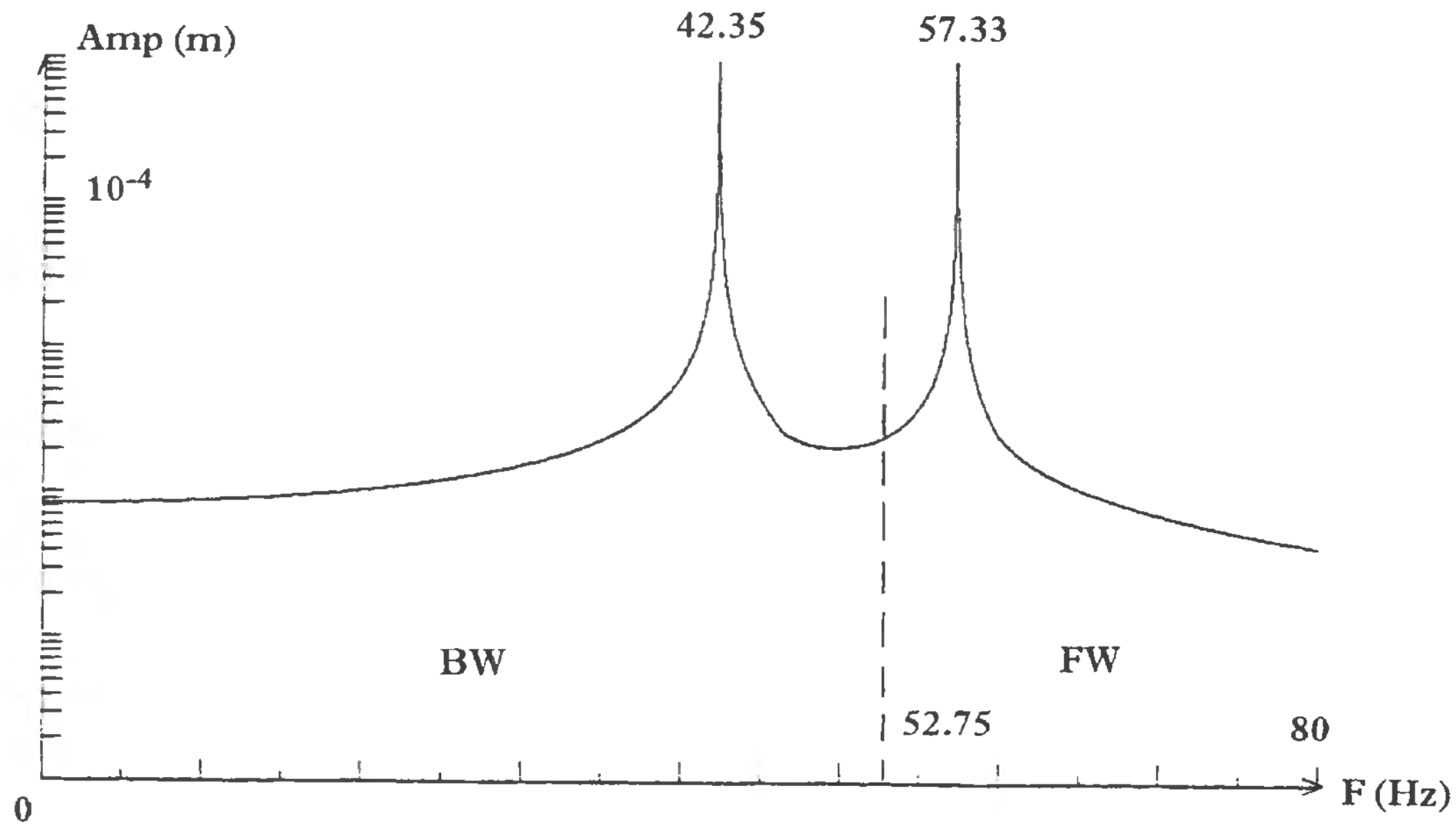

Figure 2.15. Harmonic force fixed in space response

2.4 INSTABILITY

When a system is not subjected to external forces and has only free motion due to its initial conditions, its motion, under specific conditions, grows indefinitely with time. The system is then said to be unstable.

2.4.1 Determination of instability

The determination of instability comes from a study of the system in free motion. When the natural frequencies are sought, a series of frequencies and modes are obtained as in the foregoing. Couples of solutions r_i as in (2.65) and (2.68), or (2.169) and (2.170), are obtained, and if viscous damping is present their general expressions are

$$r_i = -a_i \pm jb_i \tag{2.218}$$

which, as for a one-degree-of-freedom system, is better written

$$r_i = -\frac{\alpha_i \omega_i}{\sqrt{1-\alpha_i^2}} \pm j\omega_i \tag{2.219}$$

Hence

$$\omega_i = b_i \tag{2.220}$$

$$\alpha_i = \frac{a_i}{\sqrt{a_i^2 + b_i^2}} \tag{2.221}$$

where ω_i is the ith frequency and α_i the corresponding viscous damping factor. If the first term on the right-hand side of (2.219) (call it $-a_i$) is positive, the solution which appears in free motion grows indefinitely with time and the system is unstable.

The stability can also be determined from the Routh–Hurwitz criterion, which is very useful for a system modeled with a small number of degrees of freedom, as in this chapter, but does not give the frequency of the system which is unstable. The frequencies of the system, as in equation (2.62) for example, are the roots of a characteristic equation which can be written as

$$r^n + a_1 r^{n-1} + \cdots + a_{n-1} r + a_n = 0 \tag{2.222}$$

Then the following table for H is built:

$$H = \begin{bmatrix} a_1 & 1 & 0 & 0 & 0 & 0 & 0 & 0 & \cdot & \cdot \\ a_3 & a_2 & a_1 & 1 & 0 & 0 & 0 & 0 & \cdot & \cdot \\ a_5 & a_4 & a_3 & a_2 & a_1 & 1 & 0 & 0 & \cdot & \cdot \\ a_7 & a_6 & a_5 & a_4 & a_3 & a_2 & a_1 & 1 & \cdot & \cdot \\ \cdot & \cdot & \cdot & \cdot & \cdot & \cdot & \cdot & \cdot & \cdot & \cdot \\ \cdot & \cdot & \cdot & \cdot & \cdot & \cdot & \cdot & \cdot & \cdot & \cdot \\ \cdot & \cdot & \cdot & \cdot & \cdot & \cdot & \cdot & \cdot & \cdot & \cdot \end{bmatrix} \tag{2.223}$$

and n coefficients $H_1, \ldots, H_n$ can be obtained. Their expressions are

$$H_1 = \det[H_1] = a_1 \tag{2.224}$$

$$H_2 = \det[H_2] = \det \begin{vmatrix} a_1 & 1 \\ a_3 & a_2 \end{vmatrix} = a_1 a_2 - a_3 \tag{2.225}$$

$$H_n = \det[H_n] \tag{2.226}$$

The Routh–Hurwitz criterion demonstrates that if all the quantities $H_1 \cdots H_n$ are positive the system is stable.

2.4.2 An application

Let us reconsider the bearing in Section 2.1.3, and let us suppose that its stiffness characteristics are k_{xx}, k_{xz}, k_{zx} and k_{zz} and that its damping characteristics are $c_{xx} = c_{zz}$, $c_{xz} = c_{zx} = 0$. The equations of free motion become

$$m\ddot{q}_1 - a\Omega\dot{q}_2 + c\dot{q}_1 + k_1 q_1 + k_{12} q_2 = 0 \tag{2.227}$$

$$m\ddot{q}_2 + a\Omega\dot{q}_1 + c\dot{q}_2 + k_2 q_2 + k_{21} q_1 = 0 \tag{2.228}$$

and

$$k_1 = k + k_{xx} f^2(l_2) \tag{2.229}$$

$$k_2 = k + k_{zz} f^2(l_2) \tag{2.230}$$

$$k_{12} = k_{xz} f^2(l_2) \tag{2.231}$$

$$k_{21} = k_{zx} f^2(l_2) \tag{2.232}$$

$$c = c_{xx} f^2(l_2) = c_{zz} f^2(l_2) \tag{2.233}$$

Solutions of free motion are sought as in (2.58) and (2.59), and so

$$\begin{bmatrix} mr^2 + cr + k_1 & -a\Omega r + k_{12} \\ a\Omega r + k_{21} & mr^2 + cr + k_2 \end{bmatrix} \begin{bmatrix} Q_1 \\ Q_2 \end{bmatrix} = 0 \tag{2.234}$$

The characteristic equation obtained from (2.234) is

$$\begin{aligned} & r^4 + \frac{2c}{m} r^3 + \left(\frac{k_1}{m} + \frac{k_2}{m} + \frac{c^2}{m^2} + \frac{a^2\Omega^2}{m^2}\right) r^2 \\ & + \left[\frac{ck_1}{m^2} + \frac{ck_2}{m^2} + \frac{a}{m^2}(k_{21} - k_{12})\Omega\right] r + \frac{k_1 k_2 - k_{12} k_{21}}{m^2} = 0 \end{aligned} \tag{2.235}$$

where the quantities a_1, a_2, a_3 and a_4 defined in the Routh–Hurwitz criterion are

$$a_1 = \frac{2c}{m} \tag{2.236}$$

$$a_2 = \frac{k_1}{m} + \frac{k_2}{m} + \frac{c^2}{m^2} + \frac{a^2\Omega^2}{m^2} \tag{2.237}$$

$$a_3 = \frac{ck_1}{m^2} + \frac{ck_2}{m^2} + \frac{a}{m^2}(k_{21} - k_{12})\Omega \tag{2.238}$$

$$a_4 = \frac{k_1 k_2 - k_{21} k_{12}}{m^2} \tag{2.239}$$

First let us suppose that the damping coefficient is very small and equal to ε; then

$$H_1 = \frac{2\varepsilon}{m} \tag{2.240}$$

$$H_2 = -\frac{a\Omega}{m^2}(k_{21} - k_{12}) \tag{2.241}$$

$$H_3 = -\frac{a^2\Omega^2}{m^4}(k_{21} - k_{12})^2 \tag{2.242}$$

$$H_4 = -\frac{(k_1 k_2 - k_{12} k_{21}) a^2 \Omega^2 (k_{21} - k_{12})^2}{m^6} \tag{2.243}$$

The quantity H_3 is obviously negative, and the system is unstable. It must be considered that terms such as k_{12} and k_{21} come from bearings, such as hydrodynamic bearings, with which a significant damping has to be associated. Then from (2.236)–(2.239):

$$H_1 = \frac{2c}{m} \tag{2.244}$$

$$H_2 = \frac{ck_1}{m^2} + \frac{ck_2}{m^2} + \frac{2c^3}{m^3} - \frac{a}{m^2}(k_{21} - k_{12})\Omega + \frac{2c}{m^3} a^2 \Omega^2 \tag{2.245}$$

$$H_3 = \left[\frac{ck_1}{m^2} + \frac{ck_2}{m^2} + \frac{a\Omega}{m^2}(k_{21} - k_{12})\right] H_2 - \frac{4c^2}{m^4}(k_1 k_2 - k_{21} k_{12}) \tag{2.246}$$

$$H_4 = \frac{k_1 k_2 - k_{12} k_{21}}{m^2} H_3 \tag{2.247}$$

A simple observation of these expressions shows that under specific conditions one of them can be a negative quantity and the system can be unstable.

Returning to the rotor studied, and supposing that

$$k_{xx} = 2 \times 10^5 \text{ N/m}, \quad k_{zz} = 5 \times 10^5 \text{ N/m}$$

$$k_{xz} = -k_{zx} = 4 \times 10^4 \text{ N/m}$$

$$c_{xx} = c_{zz} = 10^2 \text{ N/m/s}, \quad c_{xz} = c_{zx} = 0$$

Equations (2.227) and (2.228) become

$$14.29\ddot{q}_1 - 2.871\Omega\dot{q}_2 + 75.00\dot{q}_1 + 1.345 \times 10^6 q_1 + 3.000 \times 10^4 q_2 = 0 \tag{2.248}$$

$$14.29\ddot{q}_2 + 2.871\Omega\dot{q}_1 + 75.00\dot{q}_2 + 1.570 \times 10^6 q_2 - 3.000 \times 10^4 q_1 = 0 \tag{2.249}$$

and the characteristic equation is

$$\begin{aligned} r^4 + 10.49r^3 + (2.040 \times 10^5 + 4.034 \times 10^{-2}\Omega^2)r^2 \\ + (1.070 - 8.430 \times 10^2\Omega)r + 1.034 \times 10^{10} = 0 \end{aligned} \tag{2.250}$$

The solutions of Equation (2.250) give the Campbell diagram shown in Figure 2.16. The lowest frequency $F_1(N)$ becomes unstable for 1395 rpm $< N$.

The Routh–Hurwitz criterion is now used, and Equation (2.250) gives

$$H_1 = 10.49 \tag{2.251}$$

$$H_2 = 1.070 \times 10^6 + 8.430 \times 10^2\Omega + 0.4233\Omega^2 \tag{2.252}$$

$$H_3 = 6.644 \times 10^9 - 2.435 \times 10^5\Omega - 2.577 \times 10^5\Omega^2 - 3.568 \times 10^2\Omega^3 \tag{2.253}$$

$$H_4 = 1.034 \times 10^{10} H_3 \tag{2.254}$$

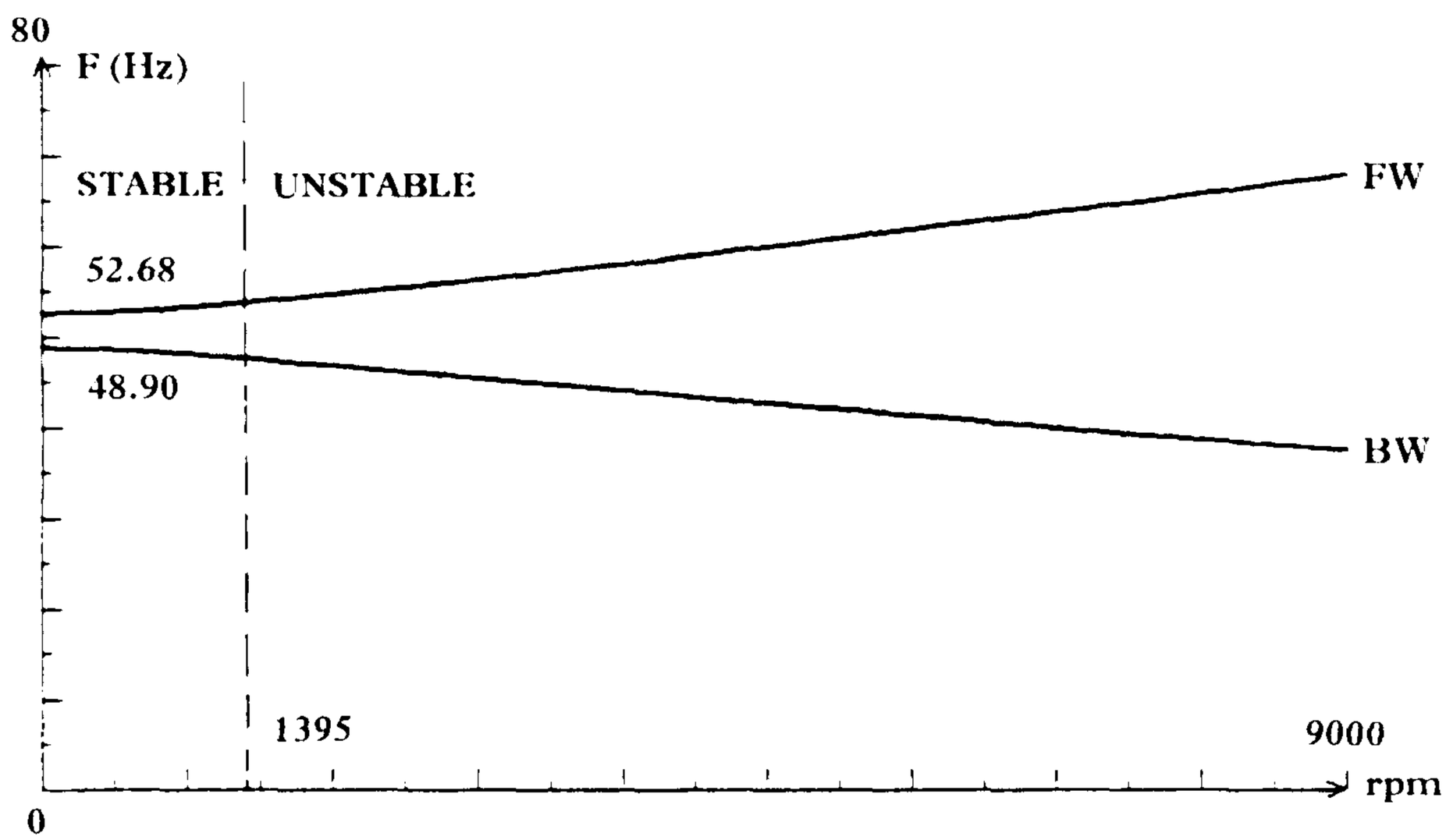

Figure 2.16. Campbell diagram

H_1 and H_2 are positive quantities. H_3 can be a negative quantity; the system is unstable for 146.1 rad/s $< \Omega$ or 1395 rpm $< N$.

2.5 DAMPED ROTORS

In what follows, the rotor studied previously in Section 2.3 is supposed to be viscously damped through a bearing. The corresponding general equations cannot be solved by hand calculations, and the equations and how to solve them are briefly presented here.

2.5.1 Natural frequencies as a function of the speed of rotation: the Campbell diagram

The equations are

$$m\ddot{q}_1 - a\Omega\dot{q}_2 + c_1\dot{q}_1 + k_1 q_1 = 0 \tag{2.255}$$

$$m\ddot{q}_2 + a\Omega\dot{q}_1 + c_2\dot{q}_2 + k_2 q_2 = 0 \tag{2.256}$$

Solutions are sought as for (2.58) and (2.59), and the characteristic equation is

$$\begin{aligned} m^2 r^4 + m(c_1 + c_2)r^3 + (k_1 m + k_2 m + c_1 c_2 + a^2\Omega^2)r^2 \\ + (k_2 c_1 + k_1 c_2)r + k_1 k_2 = 0 \end{aligned} \tag{2.257}$$

In general, the values of the damping coefficients c_1 and c_2 are low and the roots of (2.257) are pairs of complex conjugate quantities which can be written as in (2.219). In addition, if the damping coefficients c_1 and c_2 are high, at least one of the roots of the characteristic equation can be such that a frequency disappears, and then one solution can be such that

$$r_i = -a_i \tag{2.258}$$

Let us again consider the bearing in Section 2.1.3, and let us now suppose that its characteristics are $k_{xx} = 2 \times 10^5$ N/m, $k_{zz} = 5 \times 10^5$ N/m, $k_{xz} = k_{zx} = 0$, $c_{xx} = \beta \times 2 \times 10^5$ N/m/s, $c_{zz} = \beta \times 5 \times 10^5$ N/m/s,

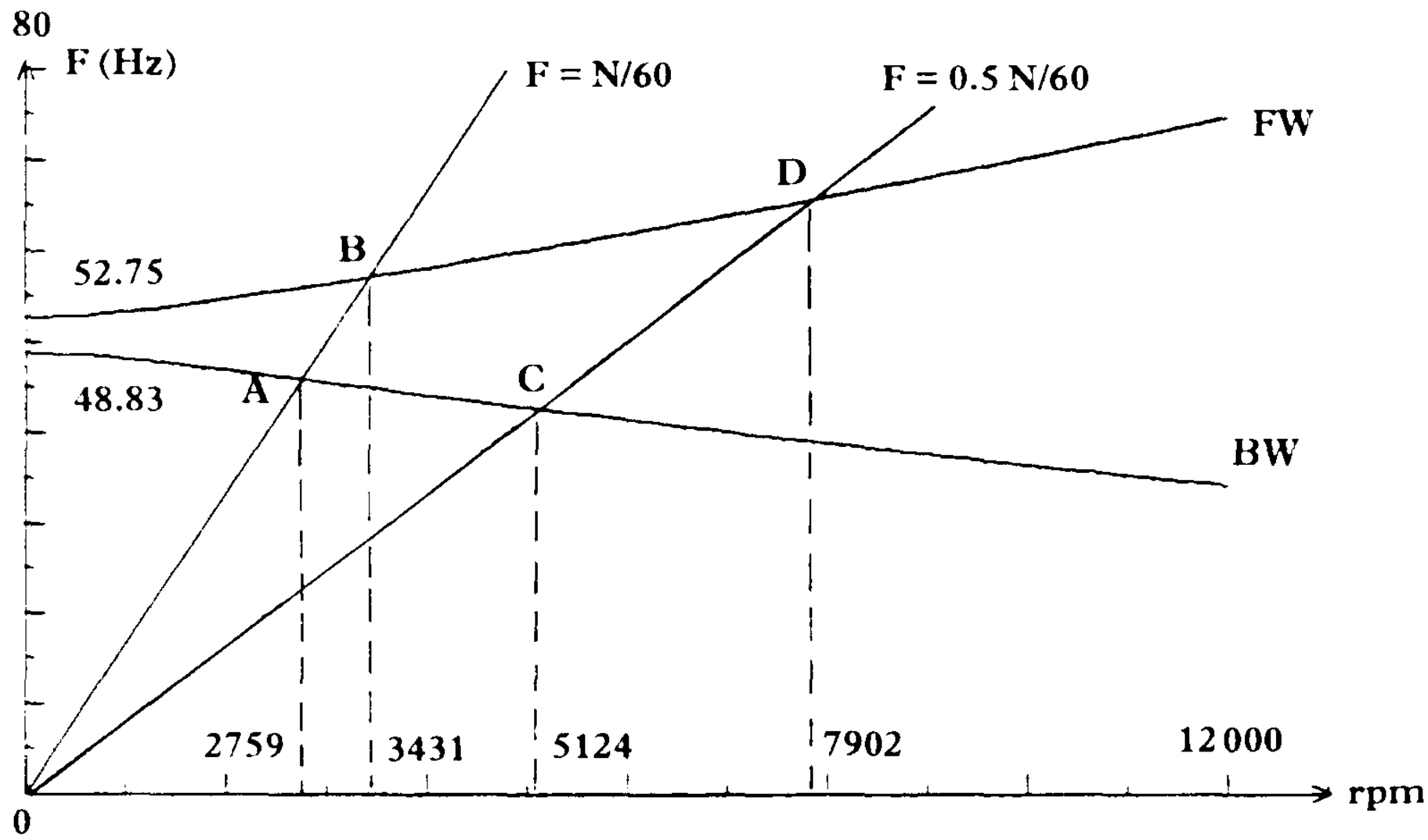

Figure 2.17. Campbell diagram: $\beta = 0.0002$

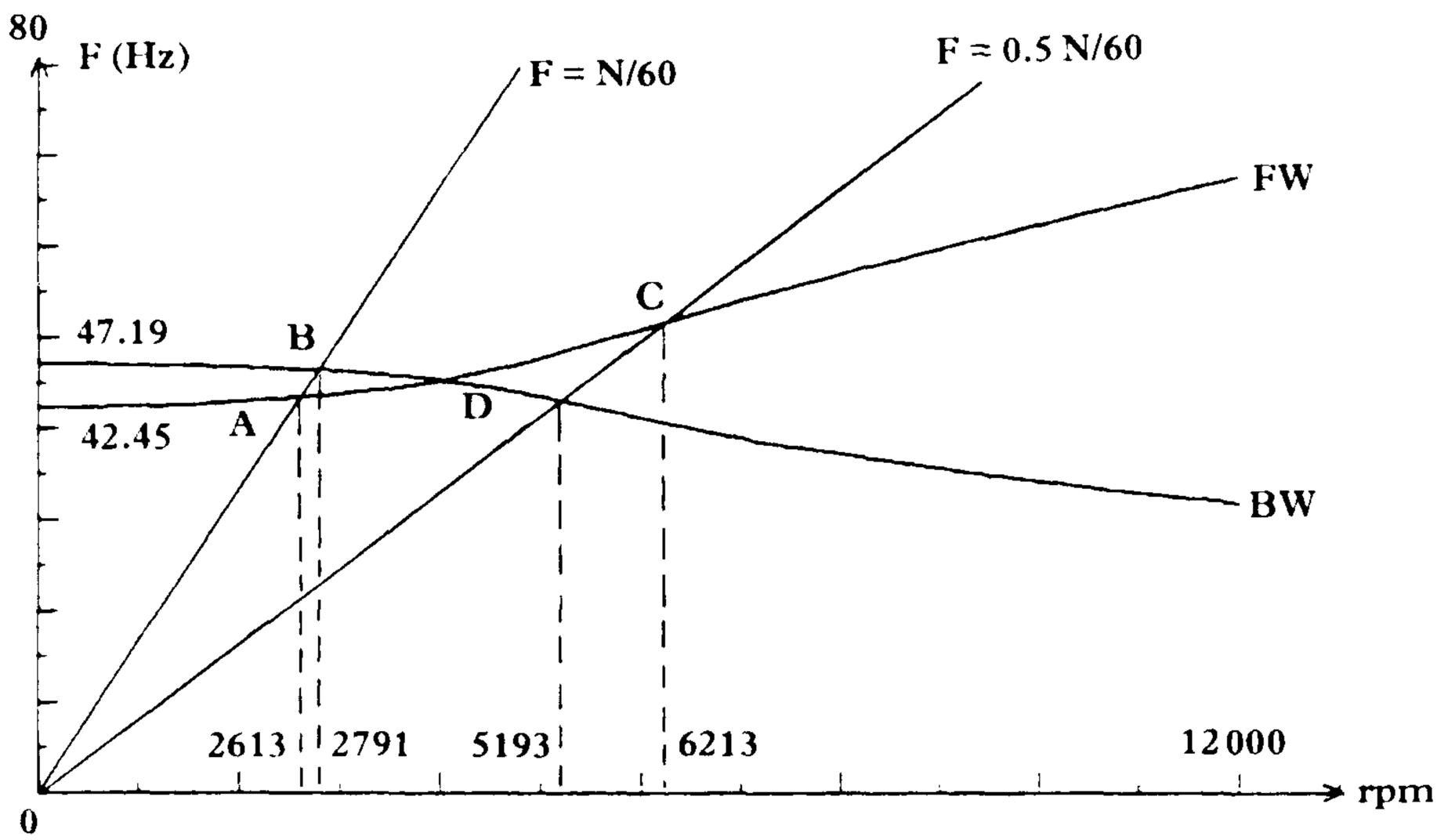

Figure 2.18. Campbell diagram: $\beta = 0.015$

$c_{xz} = c_{zx} = 0$. Equations (2.255) and (2.256) become

$$14.29\ddot{q}_1 - 2.871\Omega\dot{q}_2 + \beta \times 1.5 \times 10^5\dot{q}_1 + 1.345 \times 10^6 q_1 = 0 \qquad (2.259)$$

$$14.29\ddot{q}_2 + 2.871\Omega\dot{q}_1 + \beta \times 3.75 \times 10^5\dot{q}_2 + 1.570 \times 10^6 q_2 = 0 \qquad (2.260)$$

The damping influence is observed by varying the value of β. Here, the Campbell diagram is presented for three values of β:

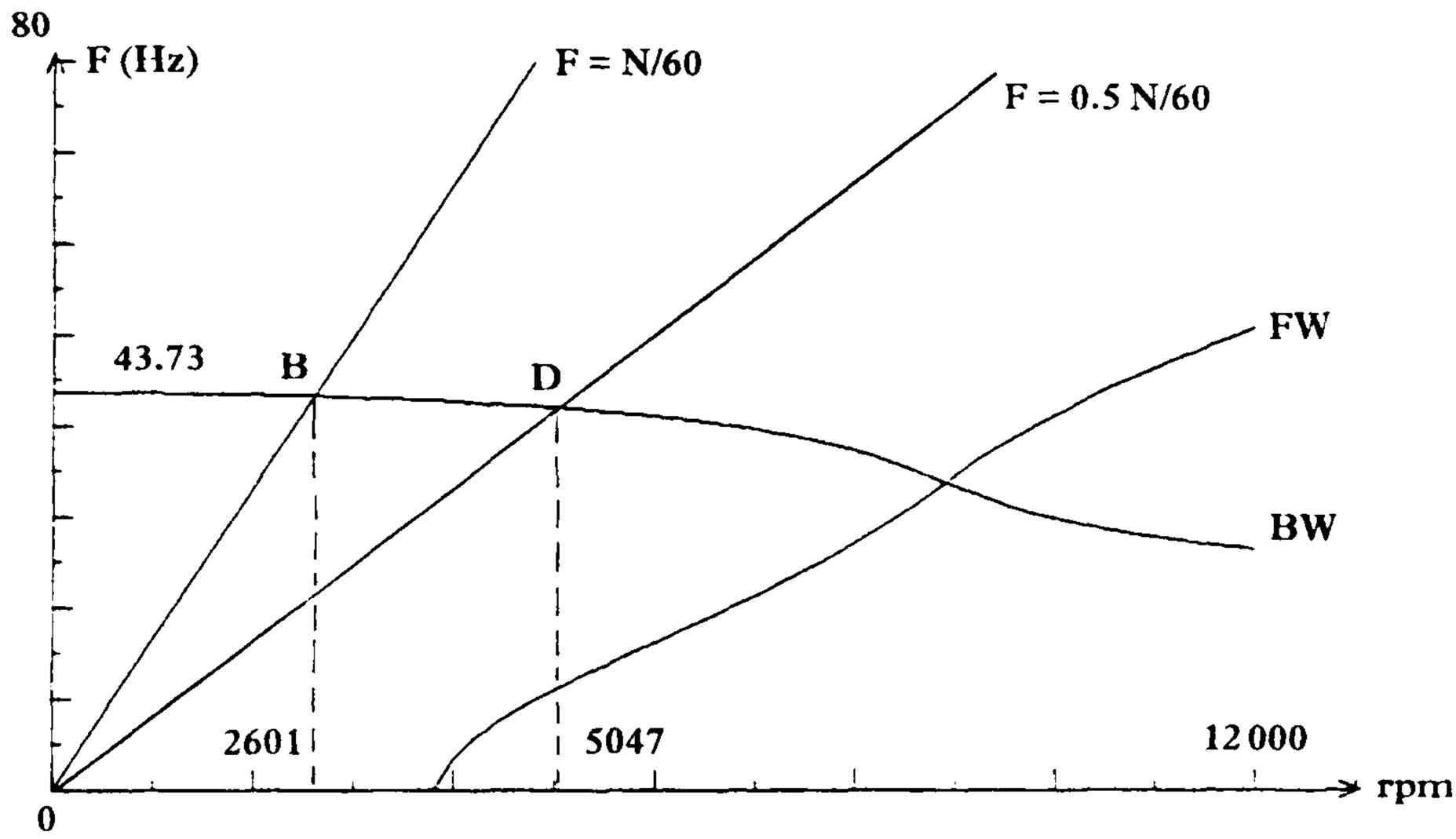

Figure 2.19. Campbell diagram: $\beta = 0.026$

- low damping ($\beta = 0.0002$): the diagram of Figure 2.17 is almost the same as that for $\beta = 0$;
- high damping ($\beta = 0.015$): the diagram of Figure 2.18 is now rather different;
- very high damping ($\beta = 0.026$): until the speed of rotation has a significant value, only one frequency appears (Figure 2.19).

2.5.2 Response to forces of excitation

As the rotor is asymmetric, orbits are elliptical, and the responses to forces of excitation shown in the figures correspond to half the major axis of the ellipses.

Mass unbalance

The mass unbalance is the same as in (2.157) and (2.158), and the equations to be solved are

$$m\ddot{q}_1 - a\Omega\dot{q}_2 + c_1\dot{q}_1 + k_1 q_1 = m^* d\Omega^2 \sin\Omega t \qquad (2.261)$$

$$m\ddot{q}_2 + a\Omega\dot{q}_1 + c_2\dot{q}_2 + k_2 q_2 = m^* d\Omega^2 \cos\Omega t \qquad (2.262)$$

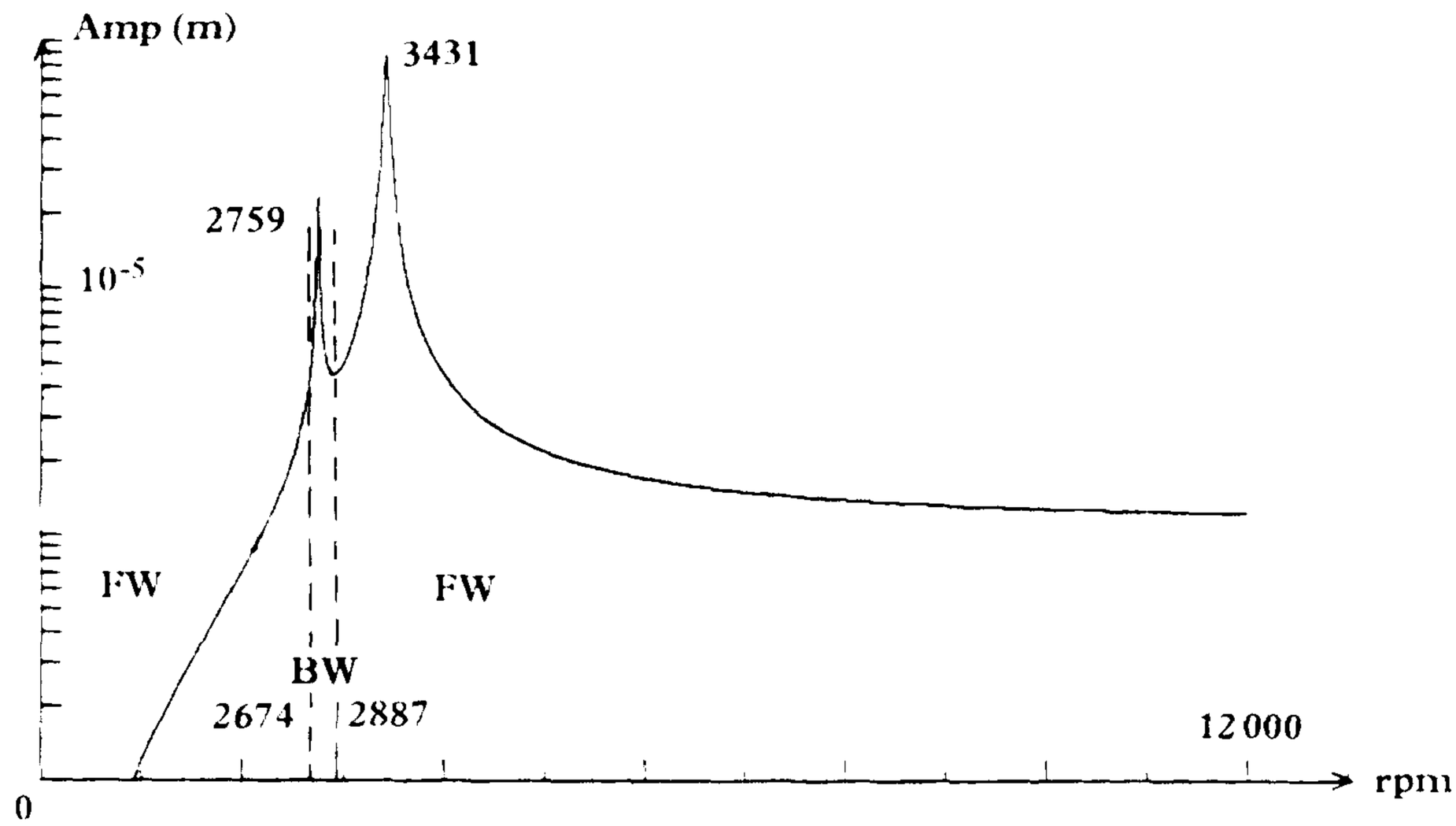

Figure 2.20. Mass unbalance response: $\beta = 0.0002$

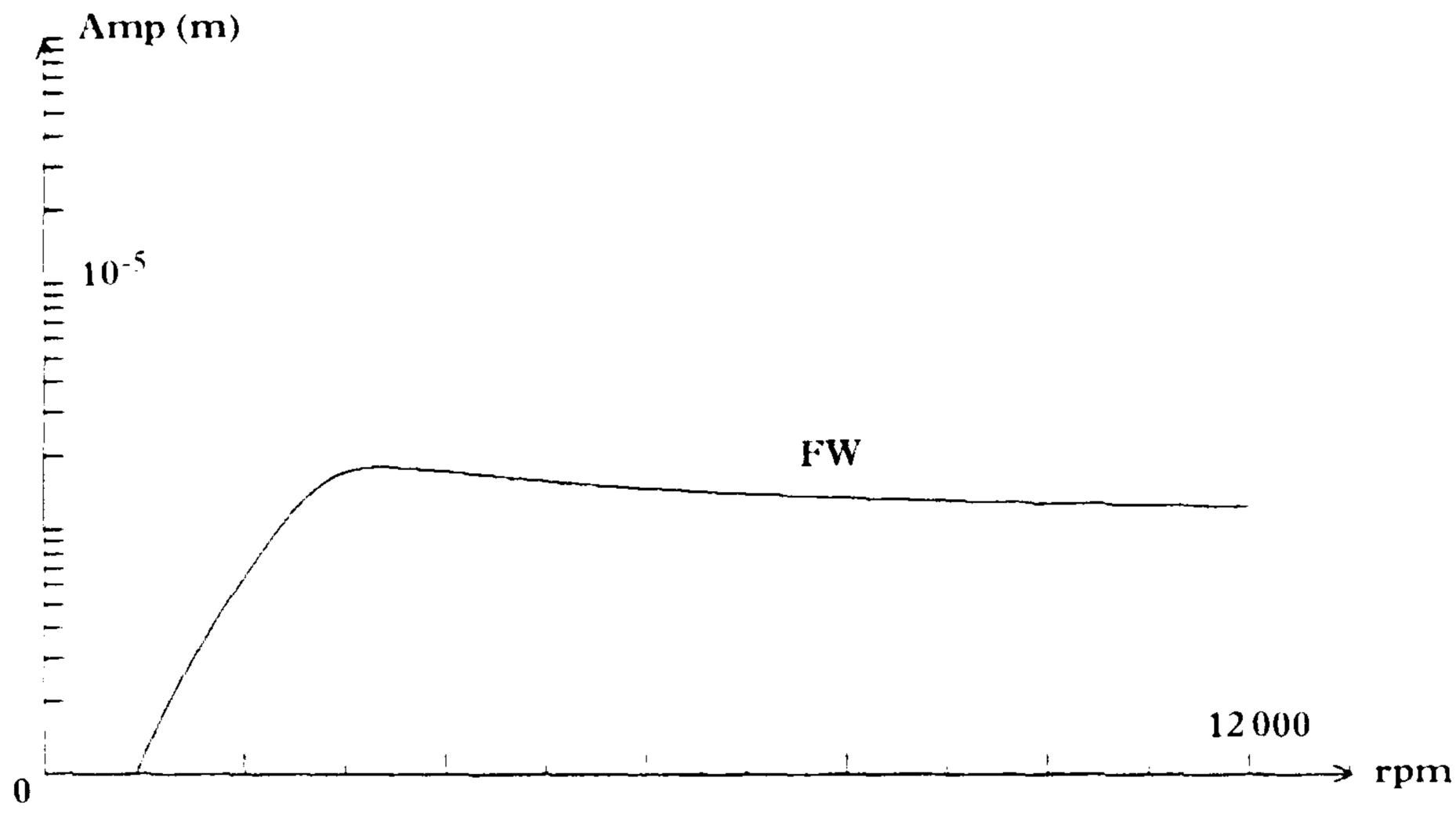

Figure 2.21. Mass unbalance response: $\beta = 0.015$

As the system is damped, solutions of equations are now to be sought in the form

$$q_1 = A_1 \sin \Omega t + B_1 \cos \Omega t \tag{2.263}$$

$$q_2 = A_2 \sin \Omega t + B_2 \cos \Omega t \tag{2.264}$$

These are substituted in (2.261) and (2.262); and since equations must hold for all time, each equation yields two equations corresponding to the

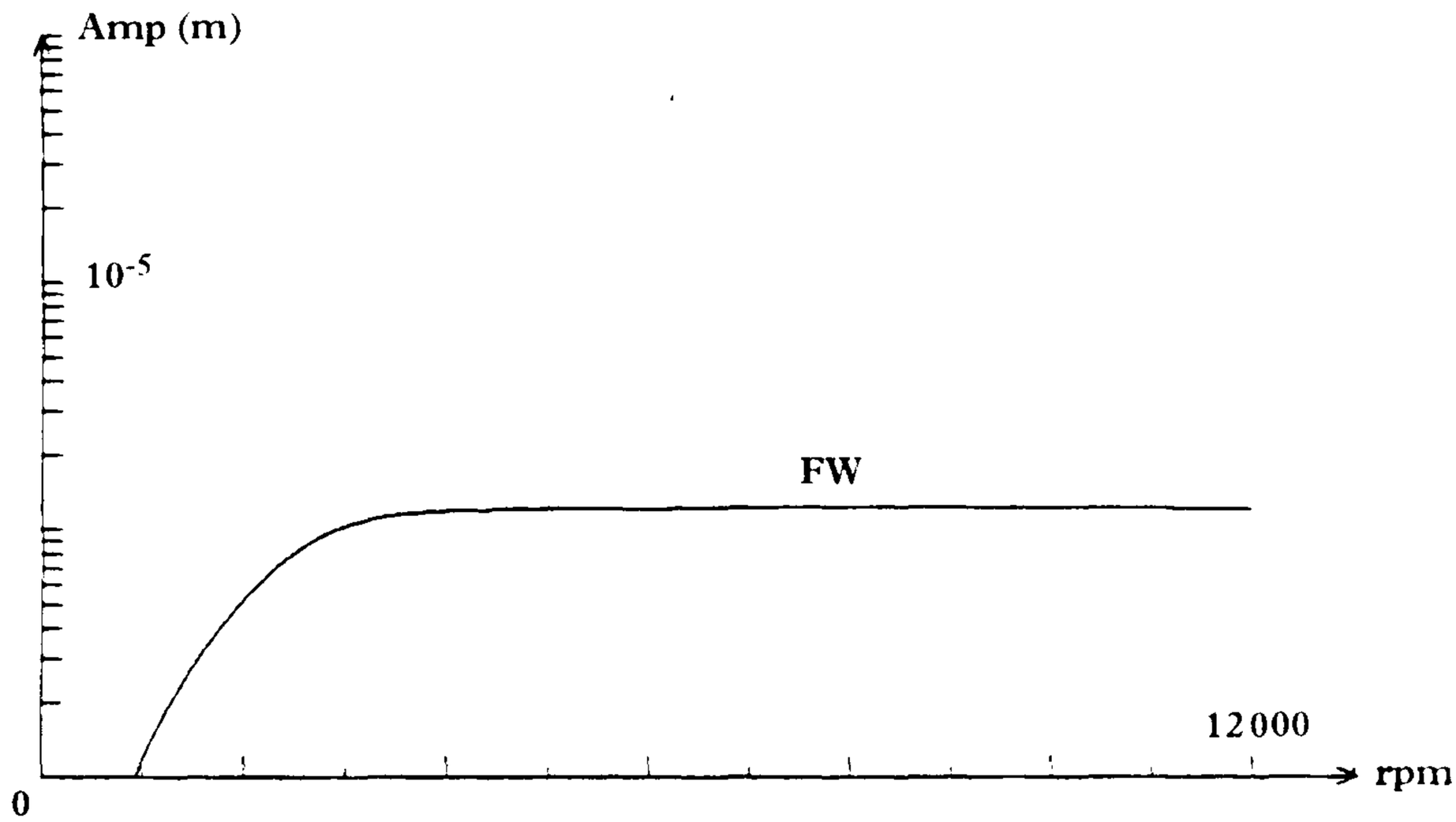

Figure 2.22. Mass unbalance response: $\beta = 0.026$

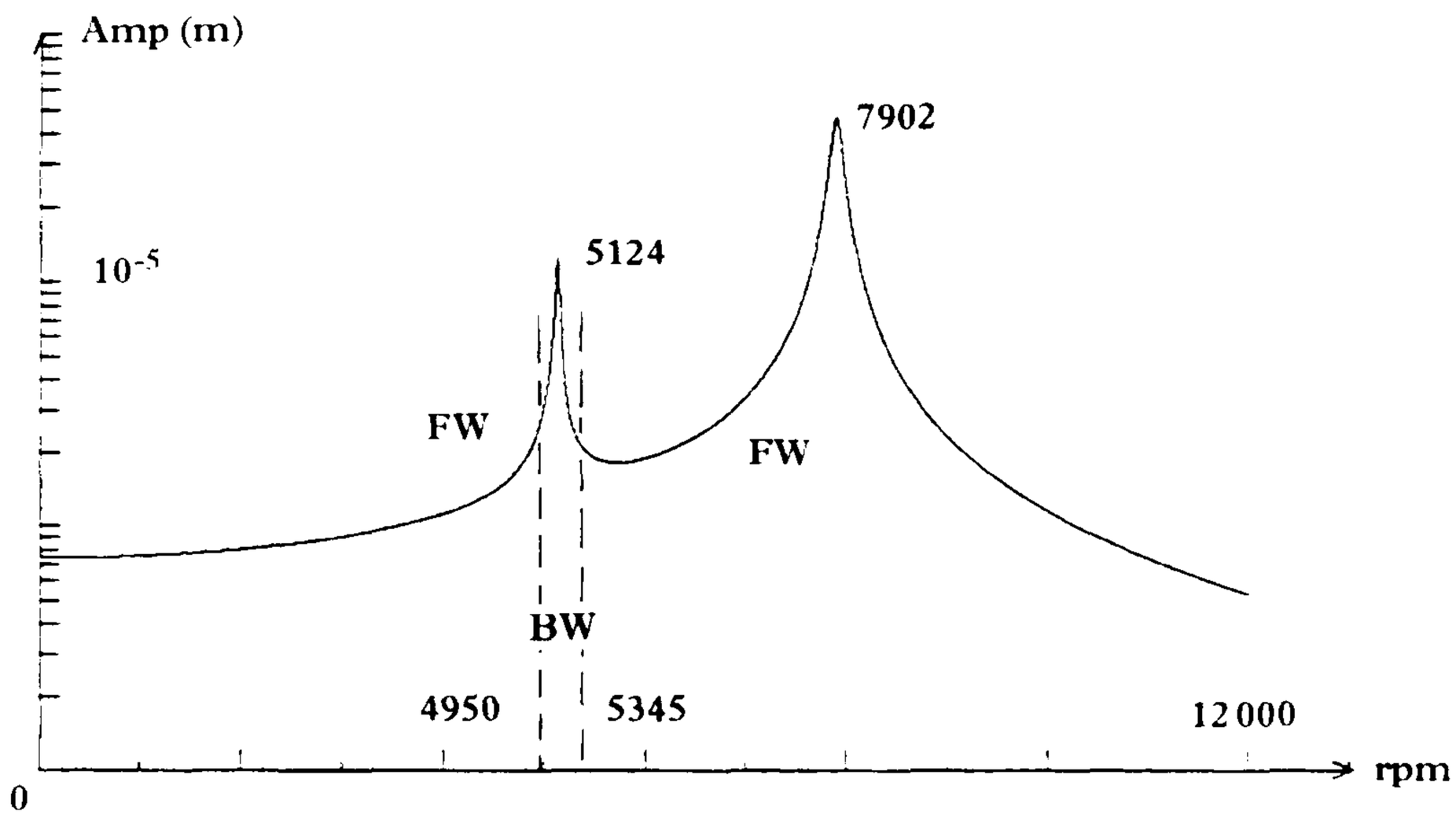

Figure 2.23. Asynchronous force response: $\beta = 0.0002$

vanishing of the coefficients of $\sin \Omega t$ and $\cos \Omega t$. This gives a set of linear equations which, in matrix form, can be written as

$$\begin{bmatrix} k_1 - m\Omega^2 & -c_1\Omega & 0 & a\Omega^2 \\ c_1\Omega & k_1 - m\Omega^2 & -a\Omega^2 & 0 \\ 0 & -a\Omega^2 & k_2 - m\Omega^2 & -c_2\Omega \\ a\Omega^2 & 0 & c_2\Omega & k_2 - m\Omega^2 \end{bmatrix} \begin{bmatrix} A_1 \\ B_1 \\ A_2 \\ B_2 \end{bmatrix} = \begin{bmatrix} m^* d\Omega^2 \\ 0 \\ 0 \\ m^* d\Omega^2 \end{bmatrix} \tag{2.265}$$

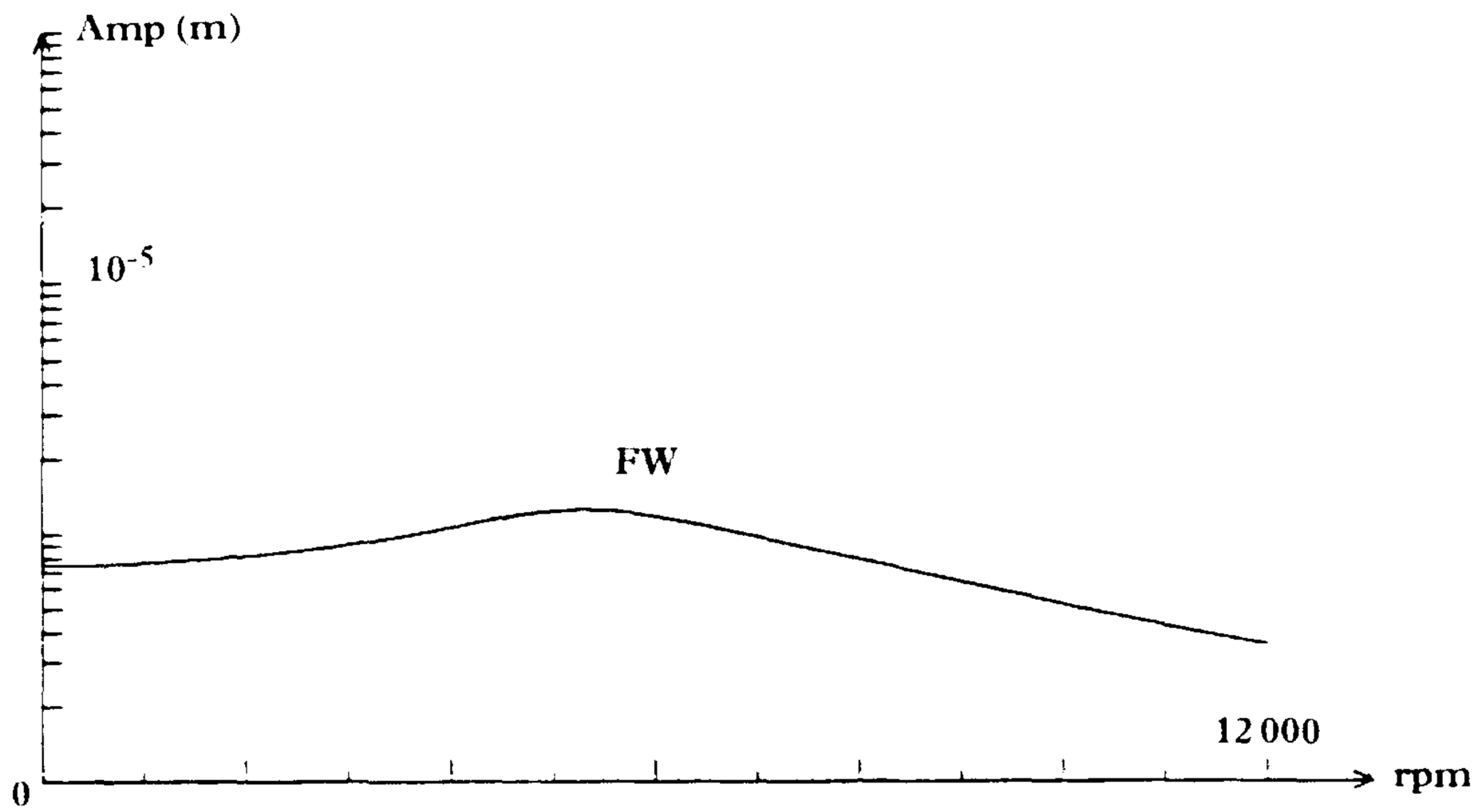

Figure 2.24. Asynchronous force response: $\beta = 0.015$

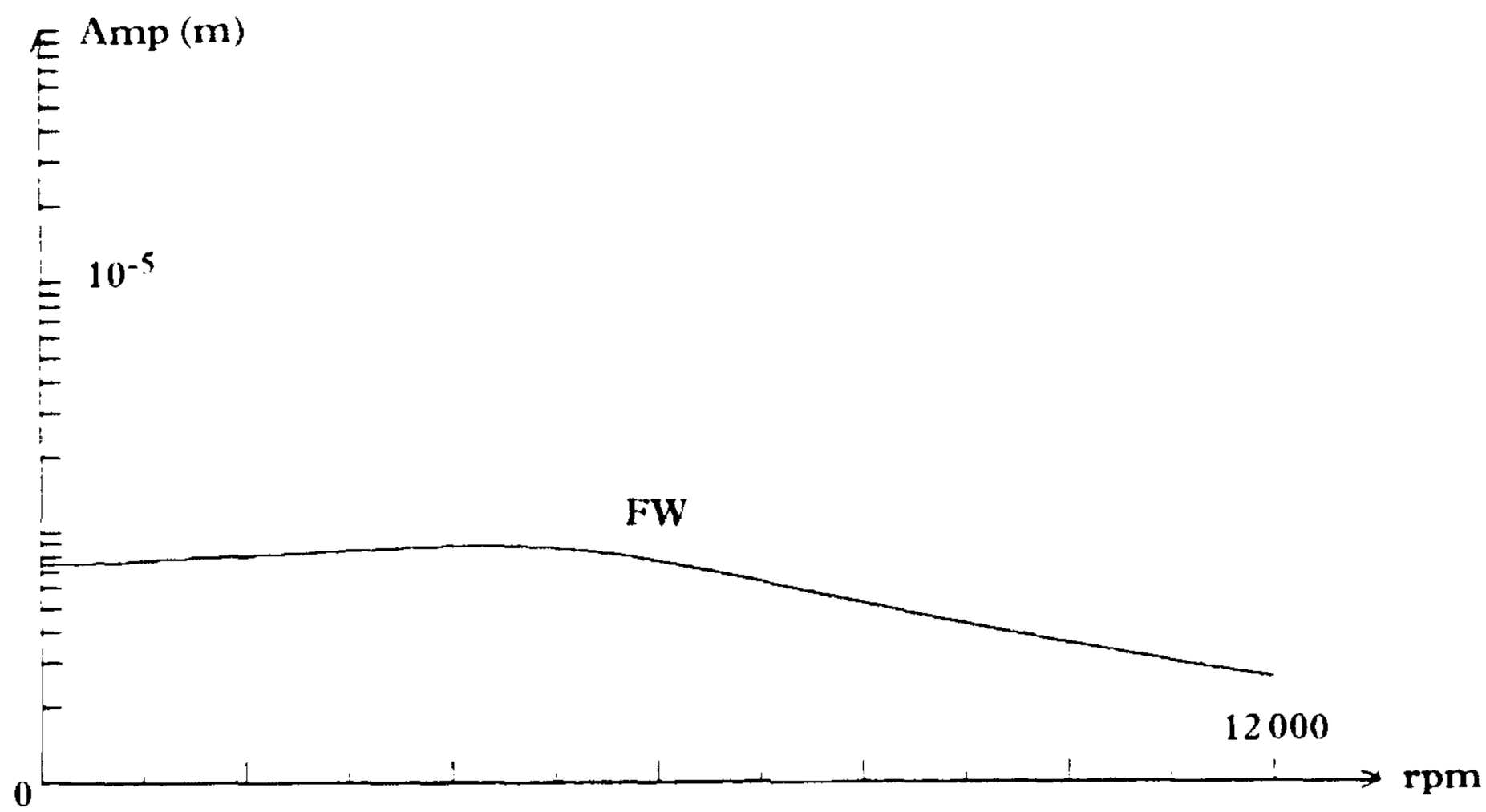

Figure 2.25. Asynchronous force response: $\beta = 0.026$

For given values of Ω, the solutions of (2.265) give $A_1(\Omega)$, $B_1(\Omega)$, $A_2(\Omega)$ and $B_2(\Omega)$; then q_1 and q_2 come from (2.263) and (2.264). The data used to get the response to mass unbalance are those of (2.159) and (2.160) with (2.259) and (2.260). In Figures 2.20–2.22, the responses are presented: two critical speeds appear for low damping, and for high and very high damping values the critical speeds disappear.

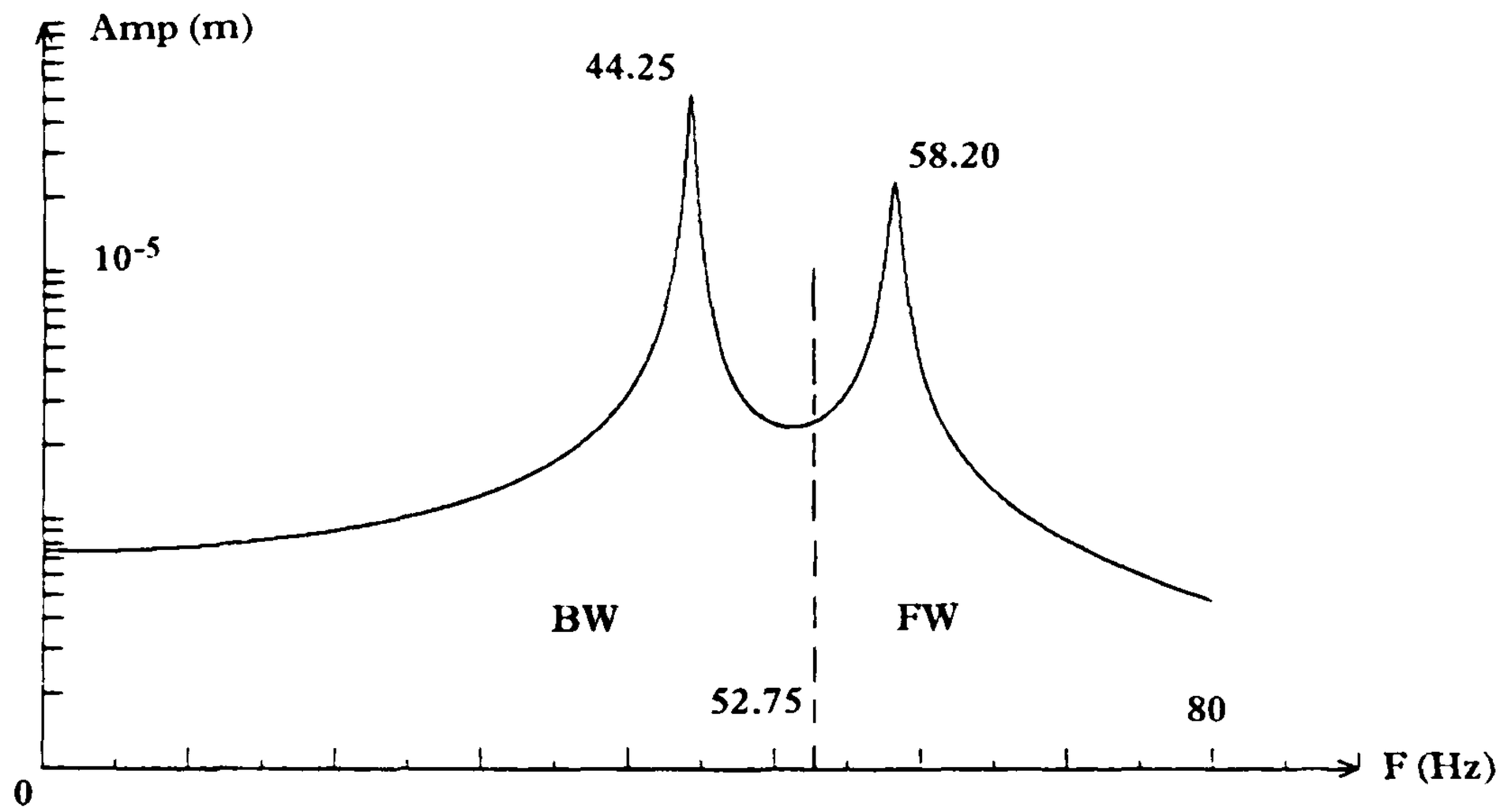

Figure 2.26. Harmonic force fixed in space response: $\beta = 0.0002$

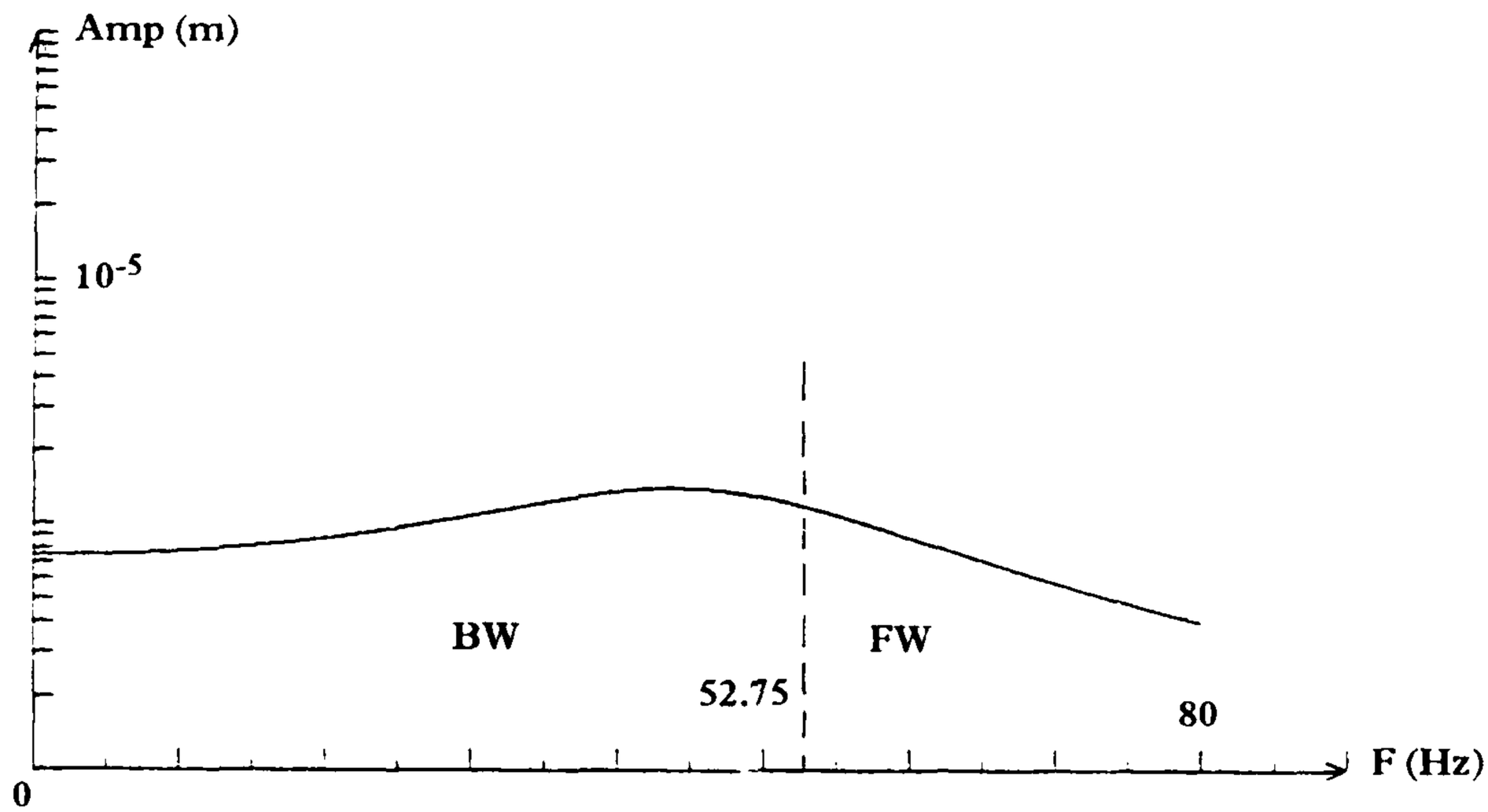

Figure 2.27. Harmonic force fixed in space response: $\beta = 0.015$

Asynchronous force

The components of the force are the same as before (i.e. see Equations (2.135) and (2.136)), and the solutions are to be sought as

$$q_1 = A_1 \sin s\Omega t + B_1 \cos s\Omega t \tag{2.266}$$

$$q_2 = A_2 \sin s\Omega t + B_2 \cos s\Omega t \tag{2.267}$$

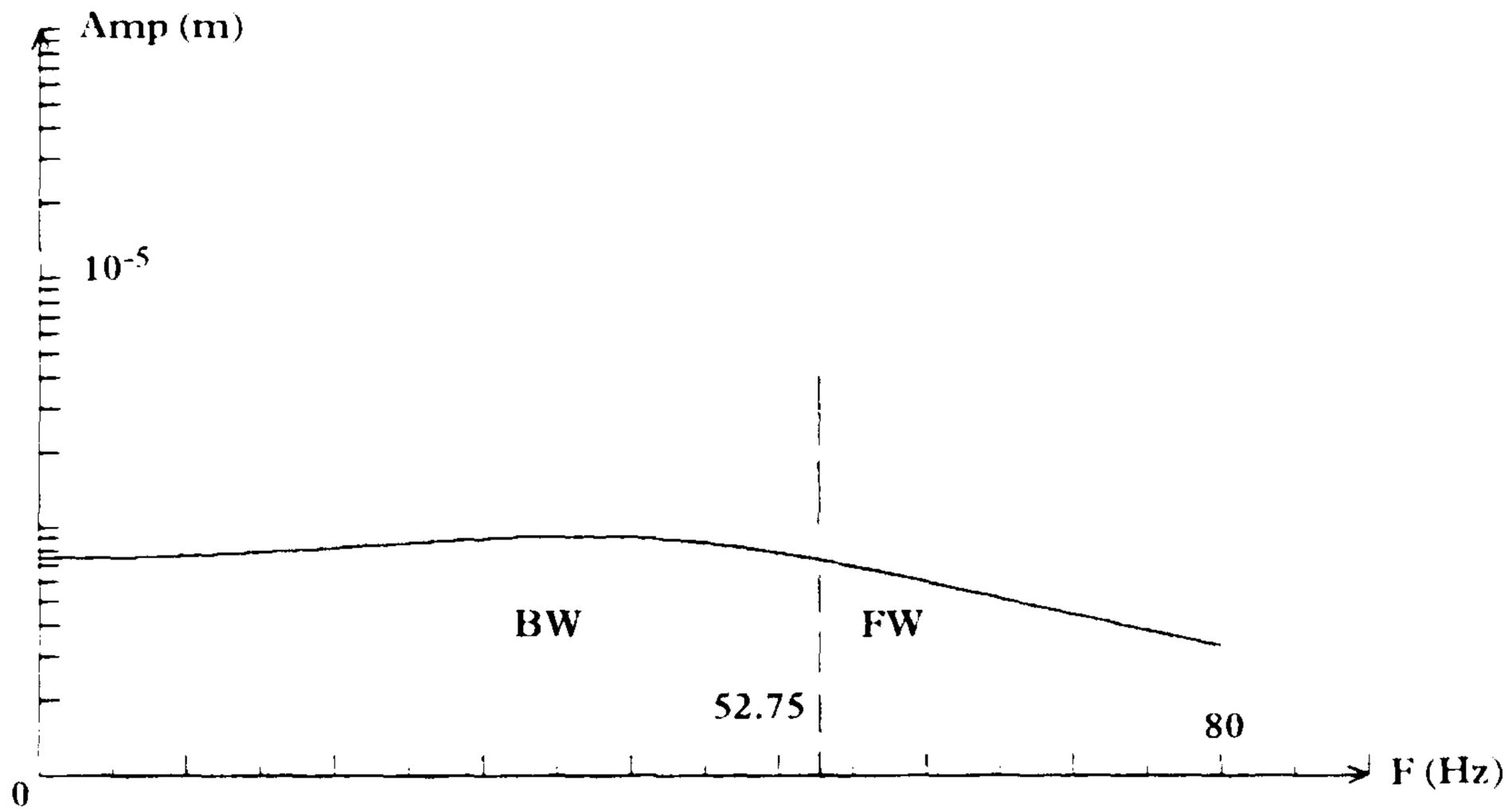

Figure 2.28. Harmonic force fixed in space response: $\beta = 0.026$

One proceeds as in the foregoing section, and the results are presented in Figures 2.23–2.25.

Harmonic force fixed in space

The components of the force are the same as before (i.e. see Equations (2.144) and (2.145)), and the solutions are to be sought as

$$q_1 = A_1 \sin \omega t + B_1 \cos \omega t \tag{2.268}$$

$$q_2 = A_2 \sin \omega t + B_2 \cos \omega t \tag{2.269}$$

One proceeds as in the foregoing section, and the results are presented in Figures 2.26–2.28 for a speed of rotation of 4000 rpm.

3

Multirotors: Simple Models, Basic Phenomena

This chapter deals with the dynamic behavior of coaxial multirotors. As with the monorotors in Chapter 2, the aim of this chapter is to show the main basic phenomena occurring in rotordynamics by using a simple but realistic example modeled by equations that are easy to solve by hand calculations. The Rayleigh-Ritz numerical method is again used here and two systems are studied: initially the first is symmetric, while the second is asymmetric since the behavior of symmetric and asymmetric systems is different. Lastly, the influence of damping is presented briefly. The main basic phenomena are:

- natural frequencies as a function of the speed of rotation, the Campbell diagram and instability.
- the effect of forces of excitation due to mass unbalance.

3.1 DETERMINATION OF THE MODEL

The simple model is an extension of the model used in Chapter 2 and is shown in Figure 3.1. The rotors are symmetric as the shaft cross-sections are constant and the non-symmetric effects derive from the stiffness k_{zz}. No damping is included in the model. The expressions for kinetic energy, strain energy and virtual work given in Chapter 1 are used for each element of the two rotors, and the constant term appearing in the expression for the kinetic energy is systematically canceled, since its contribution to the equations is nil. The stiffness of the roller bearings, points A, B, C and D, is presumed to be so high that at points A, B and D

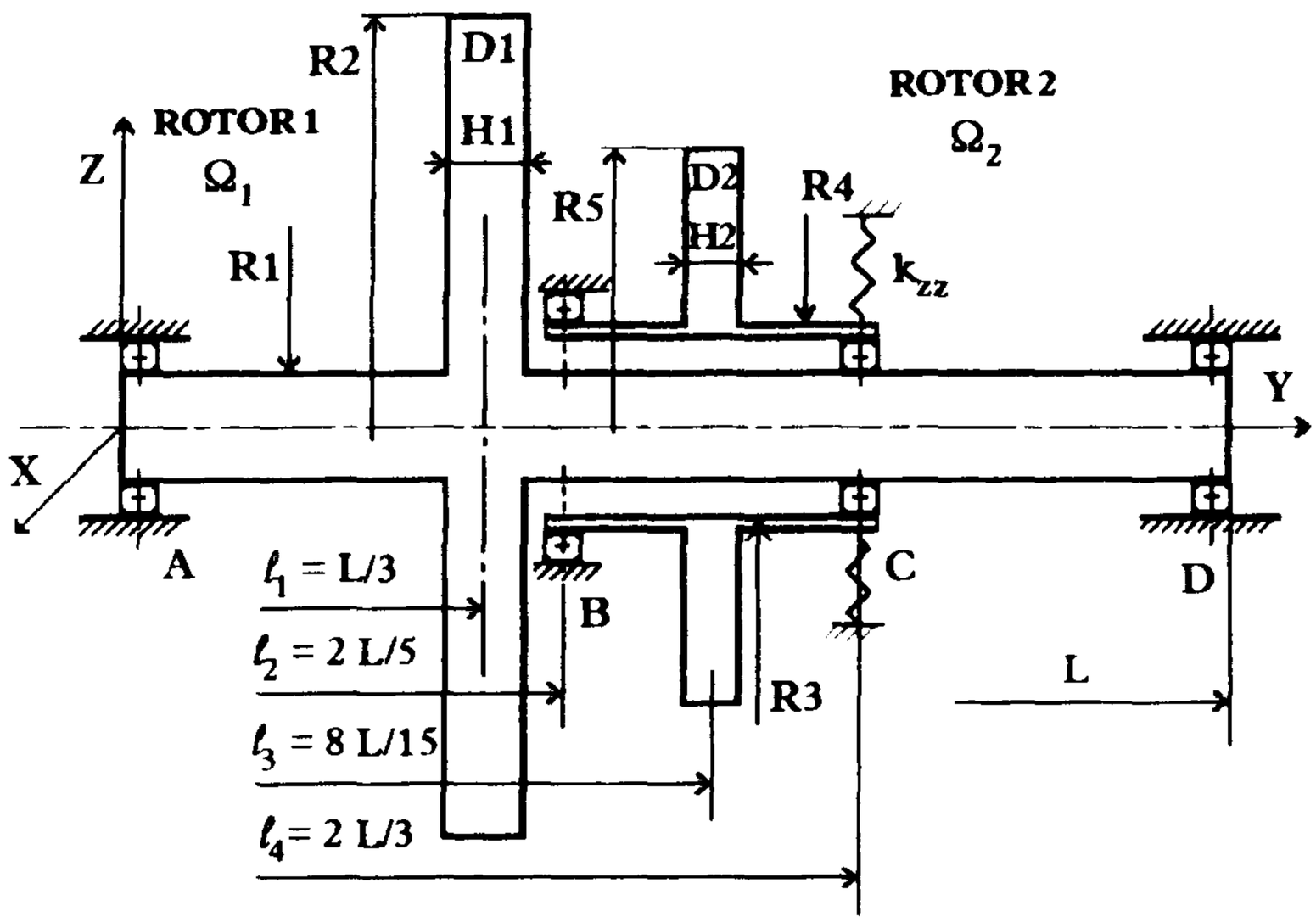

Figure 3.1. Model of the coaxial rotors

the rotors are considered as simply supported and at point C the displacements of rotors 1 and 2 are the same. The results obtained, which are shown in what follows, are very close to those obtained with a finite element model (Appendix 1). The expressions for the displacements for rotor 1 in the x and z directions are those of a simply supported beam in bending:

$$u_1(y,t) = \sin\frac{\pi y}{L} q_1(t) = f_1(y) q_1 \tag{3.1}$$

$$w_1(y,t) = \sin\frac{\pi y}{L} q_2(t) = f_1(y) q_2 \tag{3.2}$$

where q_1 and q_2 are generalized independent coordinates. As the angular displacements are small (see Figure 2.2, Chapter 2), they are approximated by

$$\theta_1 = \frac{\partial w_1}{\partial y} = \frac{\mathrm{d} f_1(y)}{\mathrm{d} y} q_2(t) = g_1(y) q_2 \tag{3.3}$$

and

$$\psi_1 = -\frac{\partial u_1}{\partial y} = -\frac{\mathrm{d} f_1(y)}{\mathrm{d} y} q_1(t) = -g_1(y) q_1 \tag{3.4}$$

The second-order derivatives of u_1 and w_1 are necessary to express the strain energy; their expressions are

$$\frac{\partial^2 u_1}{\partial y^2} = \frac{\mathrm{d}^2 f_1(y)}{\mathrm{d}y^2} q_1(t) = h_1(y) q_1 \tag{3.5}$$

$$\frac{\partial^2 w_1}{\partial y^2} = \frac{\mathrm{d}^2 f_1(y)}{\mathrm{d}y^2} q_2(t) = h_1(y) q_2 \tag{3.6}$$

Rotor 2 is assumed to be rigid, so that

$$u_2(y,t) = \frac{(y - l_2)}{l_4 - l_2} \sin \frac{\pi l_4}{L} q_1(t) = f_2(y) q_1 \tag{3.7}$$

$$w_2(y,t) = \frac{(y - l_2)}{l_4 - l_2} \sin \frac{\pi l_4}{L} q_2(t) = f_2(y) q_2 \tag{3.8}$$

and

$$\theta_2 = \frac{\partial w_2}{\partial y} = \frac{\mathrm{d} f_2(y)}{\mathrm{d}y} q_2(t) = g_2 q_2 \tag{3.9}$$

$$\psi_2 = -\frac{\partial u_2}{\partial y^2} = -\frac{\mathrm{d} f_2(y)}{\mathrm{d}y} q_1(t) = -g_2 q_1 \tag{3.10}$$

Since g_2 is a constant,

$$\frac{\partial^2 u_2}{\partial y^2} = \frac{\partial^2 w_2}{\partial y^2} = 0 \tag{3.11}$$

3.1.1 Kinetic energy

The kinetic energy of the two disks and of the two shafts is obtained from Equations (1.6) and (1.7) in Chapter 1 and respectively from Equations (3.1)–(3.4) and (3.7)–(3.10) above. It is expressed as

$$T = \tfrac{1}{2} m (\dot{q}_1^2 + \dot{q}_2^2) - \Omega_1 a_1 \dot{q}_1 q_2 - \Omega_2 a_2 \dot{q}_1 q_2 \tag{3.12}$$

with

$$m = M_{D1} f_1^2(l_1) + M_{D2} f_2^2(l_3) + I_{Dx1} g_1^2(l_1) + I_{Dx2} g_2^2$$
$$+ \rho S_1 \int_0^L f_1^2(y)\mathrm{d}y + \rho S_2 \int_{l_2}^{l_4} f_2^2(y)\mathrm{d}y$$
$$+ \rho I_1 \int_0^L g_1^2(y)\mathrm{d}y + \rho I_2 \int_{l_2}^{l_4} g_2^2(y)\mathrm{d}y \tag{3.13}$$

$$a_1 = I_{Dy1} g_1^2(l_1) + 2\rho I_1 \int_0^L g_1^2(y)\mathrm{d}y \tag{3.14}$$

$$a_2 = I_{Dy2} g_2^2 + 2\rho I_2 \int_{l_2}^{l_4} g_2^2(y)\mathrm{d}y \tag{3.15}$$

where subscripts 1 and 2 concern respectively rotors 1 and 2.

The two speeds of rotation are such that

$$\Omega_2 = n\Omega_1 = n\Omega \tag{3.16}$$

3.1.2 Strain energy

The strain energy comes from rotor 1. Using Equation (1.25) in Chapter 1 and Equations (3.5) and (3.6) gives, as the axial force is nil,

$$U_s = \tfrac{1}{2} k (q_1^2 + q_2^2) \tag{3.17}$$

with

$$k = \frac{\pi^4 E I_1}{2L^3} \tag{3.18}$$

3.1.3 Virtual work

The virtual work done by the force created by k_{zz} acting on the shaft can be written as

$$\delta W = -k_{zz} w(l_4)\, \delta w(l_4) \tag{3.19}$$

or

$$\delta W = -k_{zz} f_1^2(l_4) q_2 \delta q_2 \tag{3.20}$$

Hence the components of the generalized force are

$$F_{q1} = 0 \tag{3.21}$$

$$F_{q2} = -k_{zz} f_1^2(l_4) q_2 \tag{3.22}$$

3.1.4 Kinetic energy due to mass unbalances

The force due to mass unbalances, m_u, situated at a distance d from the rotation axis comes from the expression for the mass unbalance kinetic energy, Equation (1.34) in Chapter 1, and from Equations (3.1), (3.2), (3.7) and (3.8).

When the mass unbalance is situated on disk D_1, $y = l_1$, the corresponding kinetic energy is

$$T_1 = m_u \Omega_1 d f(l_1)(\dot{q}_1 \cos \Omega_1 t - \dot{q}_2 \sin \Omega_1 t) \tag{3.23}$$

and when the mass unbalance is situated on disk D_2, $y = l_3$, the corresponding kinetic energy is

$$T_2 = m_u \Omega_2 d f(l_3)(\dot{q}_1 \cos \Omega_2 t - \dot{q}_2 \sin \Omega_2 t) \tag{3.24}$$

3.1.5 Numerical data

The angular velocity Ω_1 is the reference and the values chosen for n are -5, -1 and 5. For the rotor as shown in Figure 3.1, the numerical data are $L = 0.4$ m, $R_1 = 0.02$ m, $R_2 = 0.15$ m, $R_3 = 0.03$ m, $R_4 = 0.035$ m, $R_5 = 0.1$ m, $H_1 = 0.03$ m, $H_2 = 0.02$ m, $E = 2 \times 10^{11}$ N/m^2, $\rho = 7800$ kg/m^3 and $k_{zz} = 8 \times 10^6$ N/m. The mass unbalance is characterized by $m_u d = 10$ g.mm.

3.2 SYMMETRIC SYSTEM

Here k_{zz} is taken as being equal to zero. The use of Lagrange's equations (Equations (2.49) and (2.50) of Chapter 2) gives the two general

equations

$$m\ddot{q}_1 - \Omega(a_1 + na_2)\dot{q}_2 + kq_1 = F_1(t) \tag{3.25}$$

$$m\ddot{q}_2 + \Omega(a_1 + na_2)\dot{q}_1 + kq_2 = F_2(t) \tag{3.26}$$

When the mass unbalance is situated on disk D_1, $y = l_1$, the force components are

$$F_1(t) = m_u f(l_1) d\Omega_1^2 \sin \Omega_1 t = m_1 d\Omega_1^2 \sin \Omega_1 t = m_1 d\Omega^2 \sin \Omega t \tag{3.27}$$

$$F_2(t) = m_u f(l_1) d\Omega_1^2 \cos \Omega_1 t = m_1 d\Omega_1^2 \cos \Omega_1 t = m_1 d\Omega^2 \cos \Omega t \tag{3.28}$$

When the mass unbalance is situated on disk D_2, $y = l_3$, the force components are

$$F_1(t) = m_u f(l_3) d\Omega_2^2 \sin \Omega_2 t = m_2 d\Omega_2^2 \sin \Omega_2 t = m_2 dn^2\Omega^2 \sin n\Omega t \tag{3.29}$$

$$F_2(t) = m_u f(l_1) d\Omega_2^2 \cos \Omega_2 t = m_2 d\Omega_2^2 \cos \Omega_2 t = m_2 dn^2\Omega^2 \cos n\Omega t \tag{3.30}$$

In addition, the terms of Equations (3.25) and (3.26) are $m = 17.46$ kg, $a_1 = 2.893$ kg, $a_2 = 1.651$ kg and $k = 1.913 \times 10^7$ N/m.

3.2.1 Natural frequencies as a function of the speed of rotation: the Campbell diagram

The systems are studied in free motion. Then Equations (3.25) and (3.26) become

$$m\ddot{q}_1 - \Omega(a_1 + na_2)\dot{q}_2 + kq_1 = 0 \tag{3.31}$$

$$m\ddot{q}_2 + \Omega(a_1 + na_2)\dot{q}_1 + kq_2 = 0 \tag{3.32}$$

Solutions must be sought in the form of Equations (2.58) and (2.59), Chapter 2, which, when substituted in Equations (3.31) and (3.32), give a homogeneous set of equations in Q_1 and Q_2. The characteristic equation

obtained is

$$m^2r^4 + (2km + (a_1 + na_2)^2\Omega^2)r^2 + k^2 = 0 \tag{3.33}$$

At rest ($\Omega = 0$) the solutions of (3.33) are $\pm j\omega_{10}$ and $\pm j\omega_{20}$, with

$$\omega_{10} = \omega_{20} = \sqrt{\frac{k}{m}} \tag{3.34}$$

Under rotating conditions the solutions are

$$r_1 = \pm j\omega_1 \tag{3.35}$$

$$r_2 = \pm j\omega_2 \tag{3.36}$$

with

$$\omega_1 = \left[\omega_{10}^2 + \frac{(a_1 + na_2)^2\Omega^2}{2m^2}\left(1 - \left(1 + \frac{4m^2\omega_{10}^2}{(a_1 + na_2)^2\Omega^2}\right)^{1/2}\right)\right]^{1/2} \tag{3.37}$$

$$\omega_2 = \left[\omega_{10}^2 + \frac{(a_1 + na_2)^2\Omega^2}{2m^2}\left(1 + \left(1 + \frac{4m^2\omega_{10}^2}{(a_1 + na_2)^2\Omega^2}\right)^{1/2}\right)\right]^{1/2} \tag{3.38}$$

From Equations (3.37) and (3.38) it can be observed that

$$\omega_1(\Omega) < \omega_{10} = \omega_{20} < \omega_2(\Omega) \tag{3.39}$$

The mode shapes are such that

$$Q_1 = \frac{\Omega(a_1 + na_2)rQ_2}{k + mr^2} \tag{3.40}$$

The sense of the whirl in the Campbell diagrams depends on the value of n. If $n < -a_1/a_2$, frequency $\omega_2(\Omega)$ corresponds to a backward whirl and $\omega_1(\Omega)$ to a forward whirl. If $-a_1/a_2 < n$, the direction of the whirl is

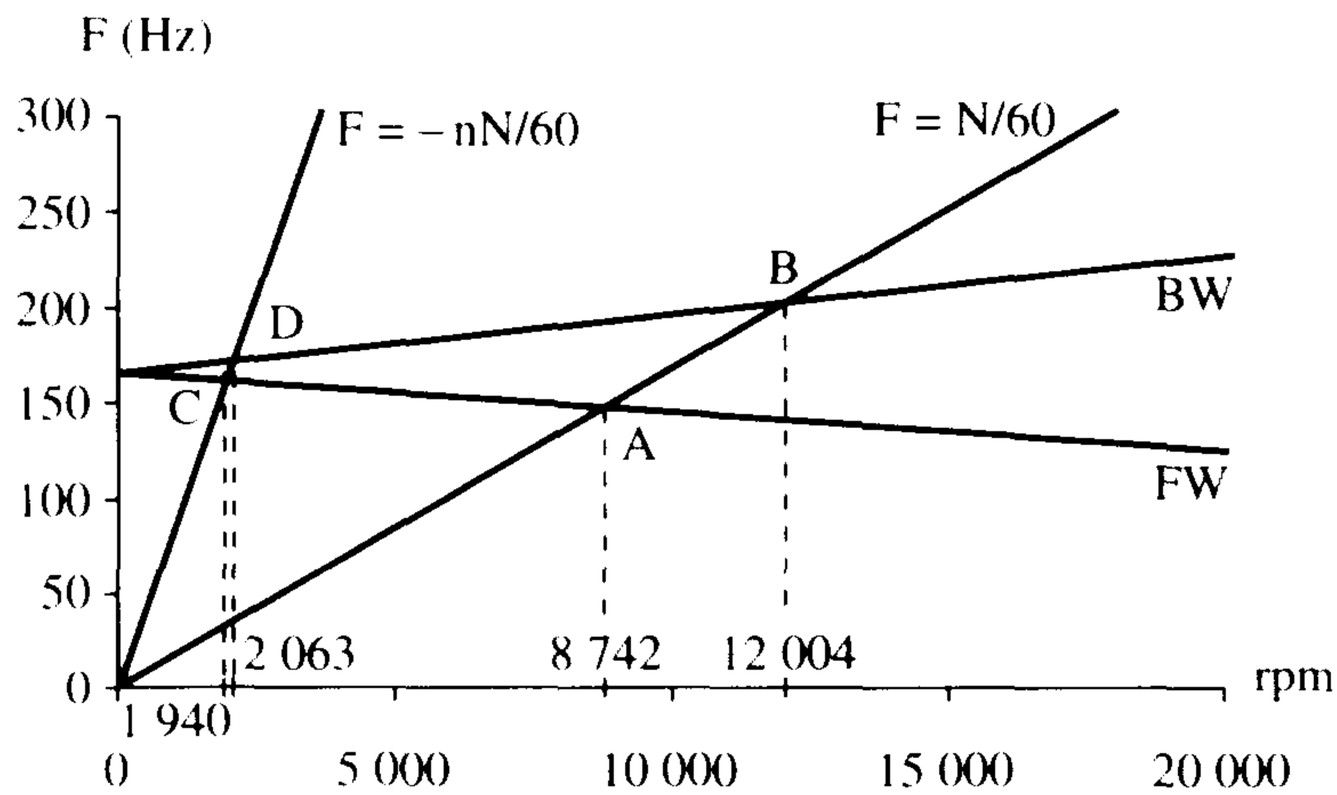

Figure 3.2. Campbell diagram: $n = -5$

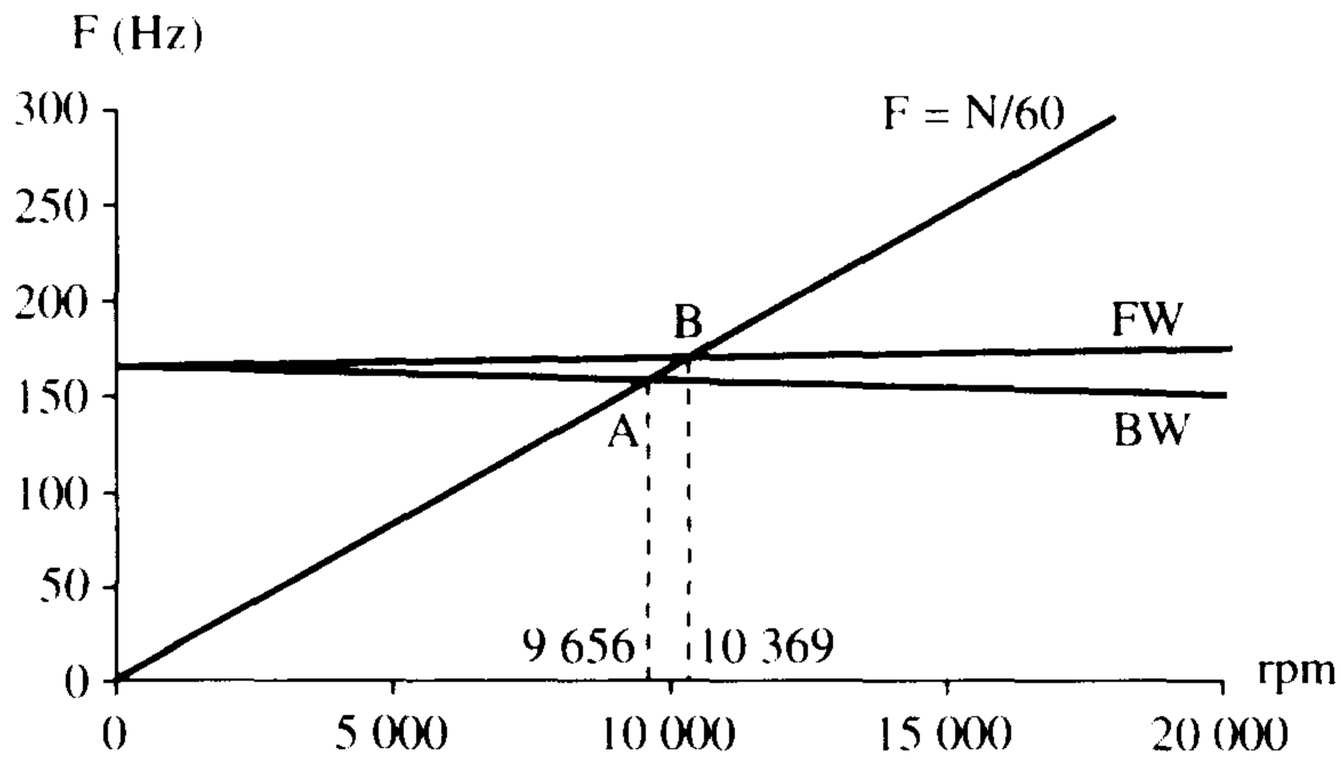

Figure 3.3. Campbell diagram: $n = -1$

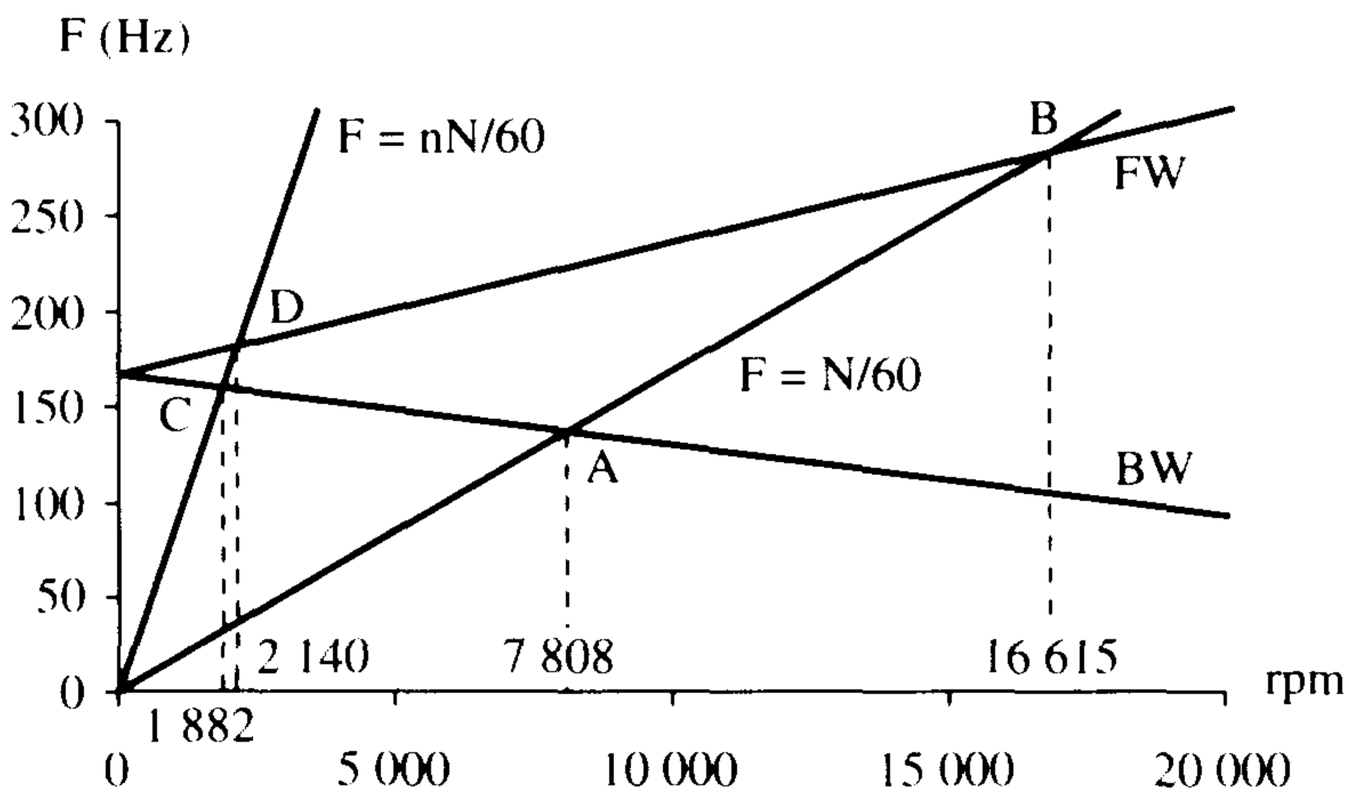

Figure 3.4. Campbell diagram: $n = 5$

changed. The Campbell diagrams, with $F_1 = \omega_1/2\pi = F_1(N)$ and $F_2 = \omega_2/2\pi = F_2(N)$, where $N = 30\Omega/\pi$ is the speed of rotation of rotor 1 expressed in rpm, are presented respectively for $n = -5, -1$ and 5 in Figures 3.2, 3.3 and 3.4. The straight lines correspond to $F = N/60$ and $F = |n|N/60$. At the intersections of curves $F_1(N)$ and $F_2(N)$ with the straight lines, a frequency of the system equals a frequency of rotation of each rotor. It is of interest, as in the symmetric rotor equations (2.117)–(2.120) of Chapter 2, to obtain the general expressions for the frequencies corresponding to points A, B, C and D. At points A and B,

$$\omega = \Omega \tag{3.41}$$

and use of the characteristic equation (3.33) with $r = \pm j\omega$ gives

$$\Omega_1 = \sqrt{\frac{k}{m + (a_1 + na_2)}} \tag{3.42}$$

$$\Omega_2 = \sqrt{\frac{k}{m - (a_1 + na_2)}} \tag{3.43}$$

which correspond to points A and B. At points C and D,

$$\omega = |n|.\Omega \tag{3.44}$$

and this gives

$$\Omega_1 = \sqrt{\frac{k}{n(mn + (a_1 + na_2))}} \tag{3.45}$$

$$\Omega_2 = \sqrt{\frac{k}{n(mn - (a_1 + na_2))}} \tag{3.46}$$

which correspond to points C and D.

3.2.2 Response to forces due to mass unbalances

Here, only the steady-state response is calculated. The general solution of Equations (3.31) and (3.32) is not considered. The mass unbalance

response is predicted with the mass unbalance located on disk D_1 (rotor 1) or disk D_2 (rotor 2).

Mass unbalance on rotor 1

The system is governed by Equations (3.25) and (3.26) with the forces given in Equations (3.27) and (3.28). As there is no damping, the solutions are sought in the form

$$q_1 = Q_1 \sin \Omega t \tag{3.47}$$

$$q_2 = Q_2 \cos \Omega t \tag{3.48}$$

Substituting (3.47) and (3.48) in the system equations gives

$$Q_1 = Q_2 = \frac{m_1 d \Omega^2}{k + (a_1 + n a_2 - m)\Omega^2} \tag{3.49}$$

As $Q_1 = Q_2$ the orbits described by the rotors are circles. The critical speed is

$$\Omega_c = \sqrt{\frac{k}{m - (a_1 + n a_2)}} \tag{3.50}$$

which corresponds to Equation (3.43) and to points A (for $n = -5$, Figure 3.2) and B (for $n = -1$, Figure 3.3, and $n = 5$, Figure 3.4). In each case there is only one critical speed which corresponds to the intersection between $F = N/60$ and the forward frequency, as shown in Figures 3.5, 3.6 and 3.7 for $n = -5$, -1 and 5 respectively.

Mass unbalance on rotor 2

In this case the forces are given by Equations (3.29) and (3.30) and the solutions are sought in the form

$$q_1 = Q_1 \sin n\Omega t \tag{3.51}$$

$$q_2 = Q_2 \cos n\Omega t \tag{3.52}$$

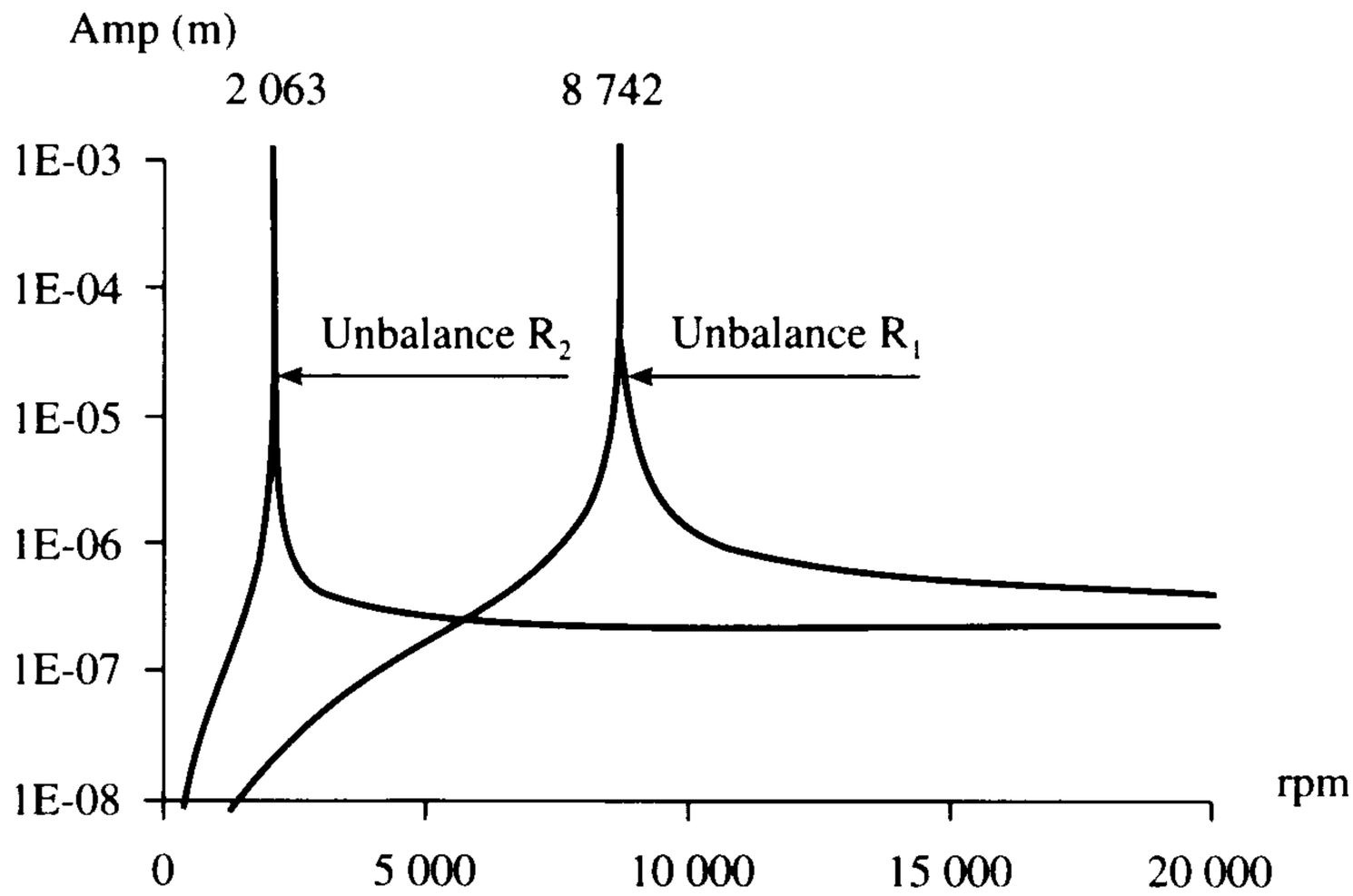

Figure 3.5. Mass unbalance response: $n = -5$

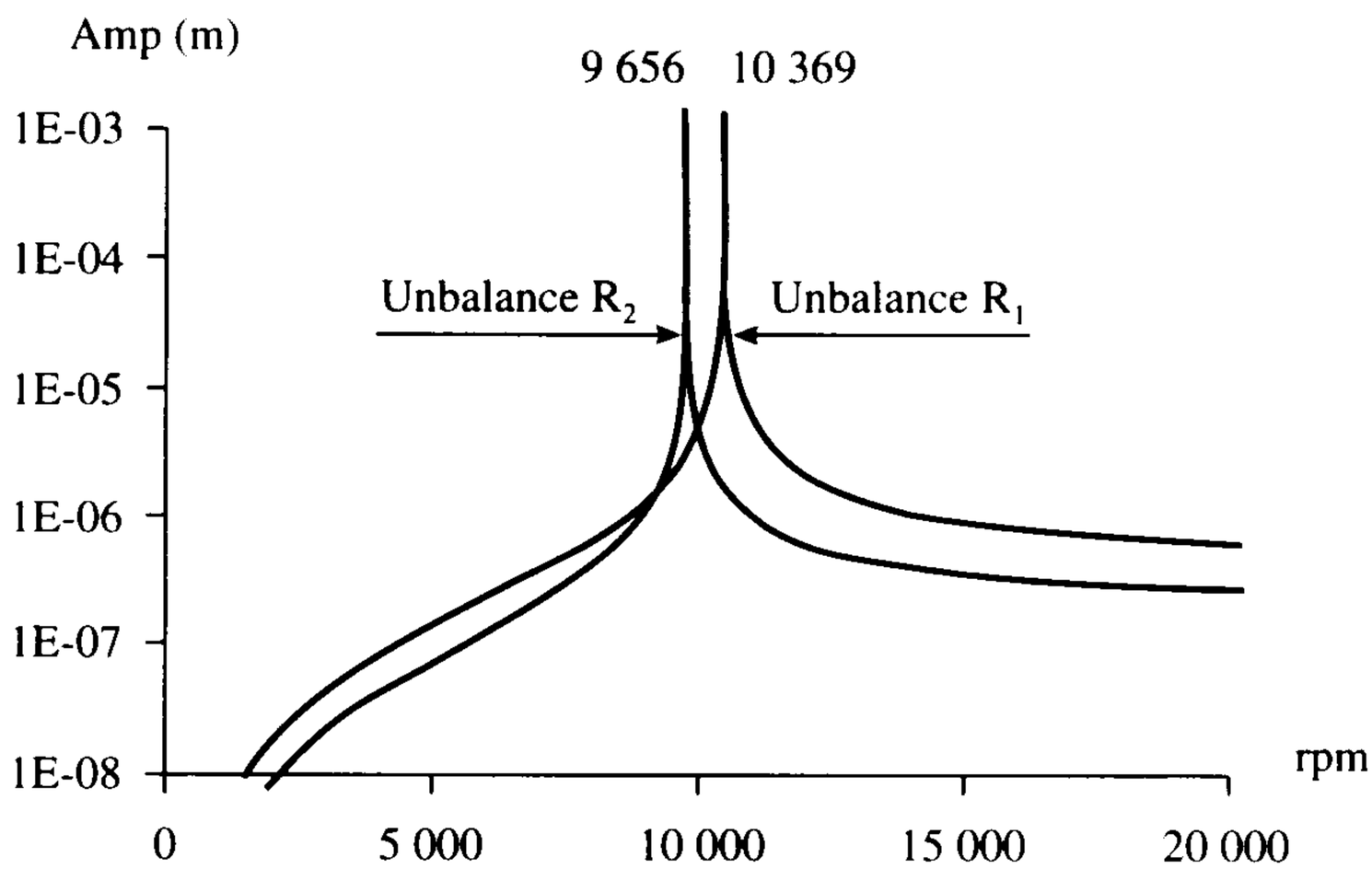

Figure 3.6. Mass unbalance response: $n = -1$

and thus

$$Q_1 = Q_2 = \frac{m_2 d n^2 \Omega^2}{k + (a_1 + n a_2 - mn) n \Omega^2} \tag{3.53}$$

As $Q_1 = Q_2$ the orbits described by the rotors are circles. The critical speed is

$$\Omega_c = \sqrt{\frac{k}{n(mn - (a_1 + n a_2))}} \tag{3.54}$$

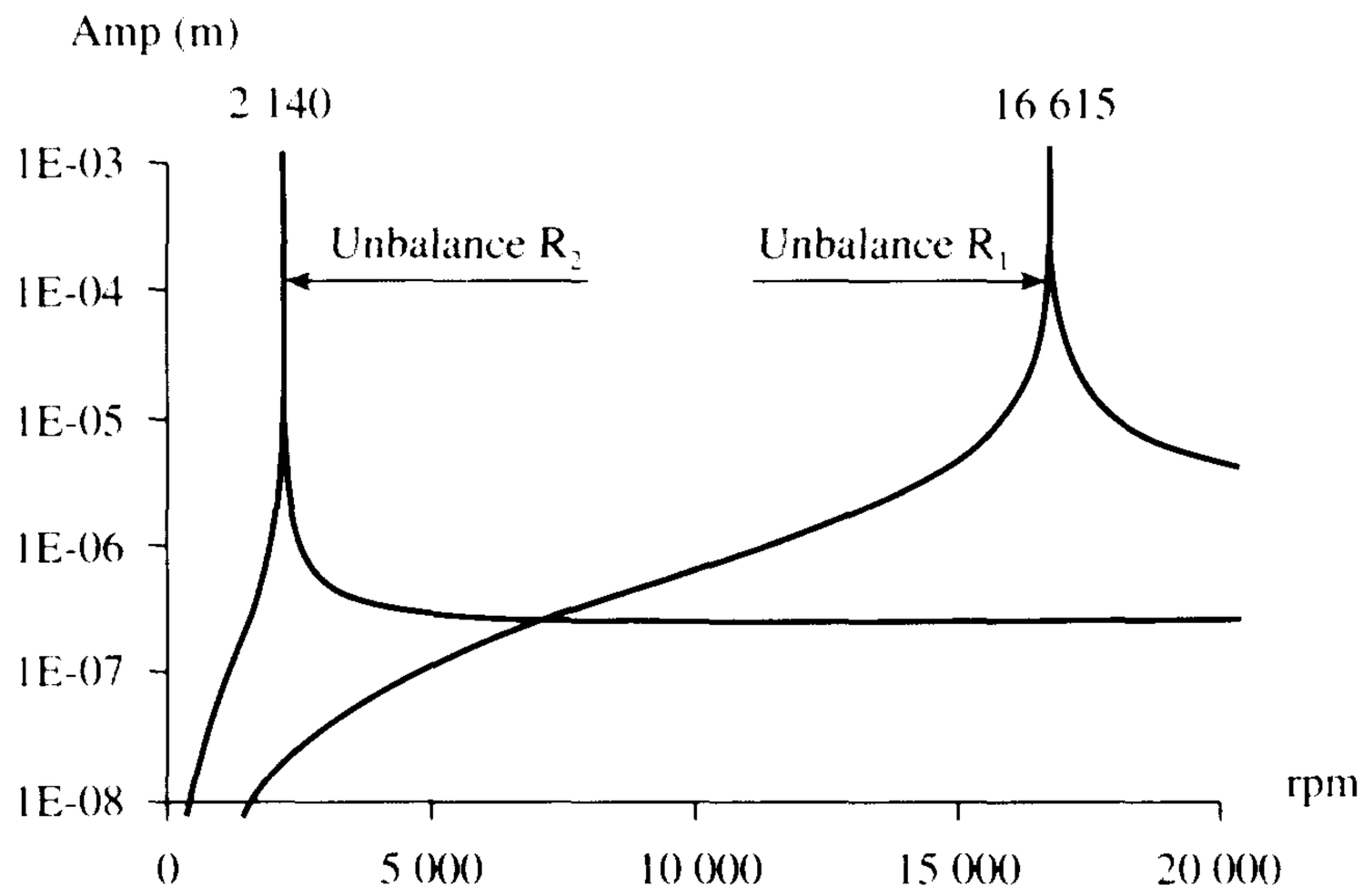

Figure 3.7. Mass unbalance response: $n = 5$

which corresponds to Equation (3.46) and to points D (for $n = -5$, Figure 3.2) A (for $n = -1$, Figure 3.3) and D (for $n = 5$, Figure 3.4). In this case there is only one critical speed which corresponds to the intersection between $F = |n|N/60$ and the forward frequency when $n > 0$ or the backward frequency when $n < 0$, as shown in Figure 3.5–3.7.

Sense of the whirl

Expressions (3.1) and (3.2) show that the displacements along x and z of a point on rotor 1 are proportional respectively to q_1 and q_2. Expressions (3.7) and (3.8) show that the displacements along x and z of a point on rotor 2 are also proportional respectively to q_1 and q_2. The sense of the whirl is obtained easily from the displacement of the point of one of the rotors expressed by q_1 and q_2. Let us define

$$0\vec{A} = \begin{bmatrix} q_1 \\ 0 \\ q_2 \end{bmatrix} \tag{3.55}$$

then

$$d0\vec{A} = \begin{bmatrix} \dfrac{dq_1}{dt}\,dt \\ 0 \\ \dfrac{dq_2}{dt}\,dt \end{bmatrix} \tag{3.56}$$

and the cross-product is

$$0\vec{A} \wedge d0\vec{A} = \begin{bmatrix} 0 \\ q_2 \dfrac{dq_1}{dt} dt - q_1 \dfrac{dq_2}{dt} dt \\ 0 \end{bmatrix} \tag{3.57}$$

When the mass unbalance is on rotor 1, using Equations (3.47)–(3.49) gives

$$0\vec{A} \wedge d0\vec{A} = \begin{bmatrix} 0 \\ Q_1^2 \Omega\, dt \\ 0 \end{bmatrix} = \begin{bmatrix} 0 \\ Q_2^2 \Omega\, dt \\ 0 \end{bmatrix} \tag{3.58}$$

As $Q_2^2 \Omega\, dt$ is a positive quantity the whirl is forward.

When the mass unbalance is on rotor 2, using Equations (3.51)–(3.53) gives

$$0\vec{A} \wedge d0\vec{A} = \begin{bmatrix} 0 \\ nQ_1^2 \Omega\, dt \\ 0 \end{bmatrix} = \begin{bmatrix} 0 \\ nQ_2^2 \Omega\, dt \\ 0 \end{bmatrix} \tag{3.59}$$

thus the whirl is the same whatever the rotation speed; the whirl is forward if $n > 0$ and backward if $n < 0$.

3.3 ASYMMETRIC SYSTEM

The asymmetry is introduced by k_{zz} as shown in Equations (3.21) and (3.22). Equations (3.25) and (3.26) become

$$m\ddot{q}_1 - \Omega(a_1 + na_2)\dot{q}_2 + k_1 q_1 = F_1(t) \tag{3.60}$$

$$m\ddot{q}_2 + \Omega(a_1 + na_2)\dot{q}_1 + k_2 q_2 = F_2(t) \tag{3.61}$$

where

$$k_1 = k \tag{3.62}$$

$$k_2 = k + k_{zz} f_1^2(l_4) \tag{3.63}$$

The value of k_2 is 2.513×10^7N/m and the force components are still expressed by the sets (3.27) and (3.28) or (3.29) and (3.30).

3.3.1 Natural frequencies as a function of the speed of rotation: the Campbell diagram

Once again the system is studied in free motion. Equations (3.60) and (3.61) become

$$m\ddot{q}_1 - \Omega(a_1 + na_2)\dot{q}_2 + k_1 q_1 = 0 \tag{3.64}$$

$$m\ddot{q}_2 + \Omega(a_1 + na_2)\dot{q}_1 + k_2 q_2 = 0 \tag{3.65}$$

Solutions must be sought in the form of Equations (2.58) and (2.59), Chapter 2, which when substituted in Equations (3.64) and (3.65) lead to the characteristic equation

$$m^2 r^4 + (k_1 m + k_2 m + (a_1 + na_2)^2 \Omega^2) r^2 + k_1 k_2 = 0 \tag{3.66}$$

At rest ($\Omega = 0$) the solutions are $\pm j\omega_{10}$ and $\pm j\omega_{20}$ with

$$\omega_{10} = \sqrt{\frac{k_1}{m}} \tag{3.67}$$

$$\omega_{20} = \sqrt{\frac{k_2}{m}} \tag{3.68}$$

Under rotating conditions the solutions are $\pm j\omega_1$ and $\pm j\omega_2$ with

$$\omega_1 = \left[\frac{\omega_{10}^2 + \omega_{20}^2}{2} + \frac{(a_1 + na_2)^2\Omega^2}{2m^2} - \left[\left(\frac{\omega_{10}^2 + \omega_{20}^2}{2} + \frac{(a_1 + na_2)^2\Omega^2}{2m^2}\right)^2 - \omega_{10}^2\omega_{20}^2\right]^{1/2}\right]^{1/2} \tag{3.69}$$

$$\omega_2 = \left[\frac{\omega_{10}^2 + \omega_{20}^2}{2} + \frac{(a_1 + na_2)^2\Omega^2}{2m^2} + \left[\left(\frac{\omega_{10}^2 + \omega_{20}^2}{2} + \frac{(a_1 + na_2)^2\Omega^2}{2m^2}\right)^2 - \omega_{10}^2\omega_{20}^2\right]^{1/2}\right]^{1/2} \tag{3.70}$$

From Equations (3.69) and (3.70) it can be observed that

$$\omega_1(\Omega) < \omega_{10} < \omega_{20} < \omega_2(\Omega) \tag{3.71}$$

The Campbell diagrams $F_1 = \omega_1/2\pi = F_1(N)$ and $F_2 = \omega_2/2\pi = F_2(N)$ are presented respectively for $n = -5, -1, 5$ in Figures 3.8, 3.9 and 3.10. At the intersections of curves $F_1(N)$ and $F_2(N)$ with the straight lines $F = N/60$ and $F = |n|N/60$, a frequency of the system equals a frequency of rotation of one of the rotors. At points A and B, or C and D, a natural frequency of the rotors equals respectively the frequency of rotation of rotor 1 or the frequency of rotation of rotor 2. The general

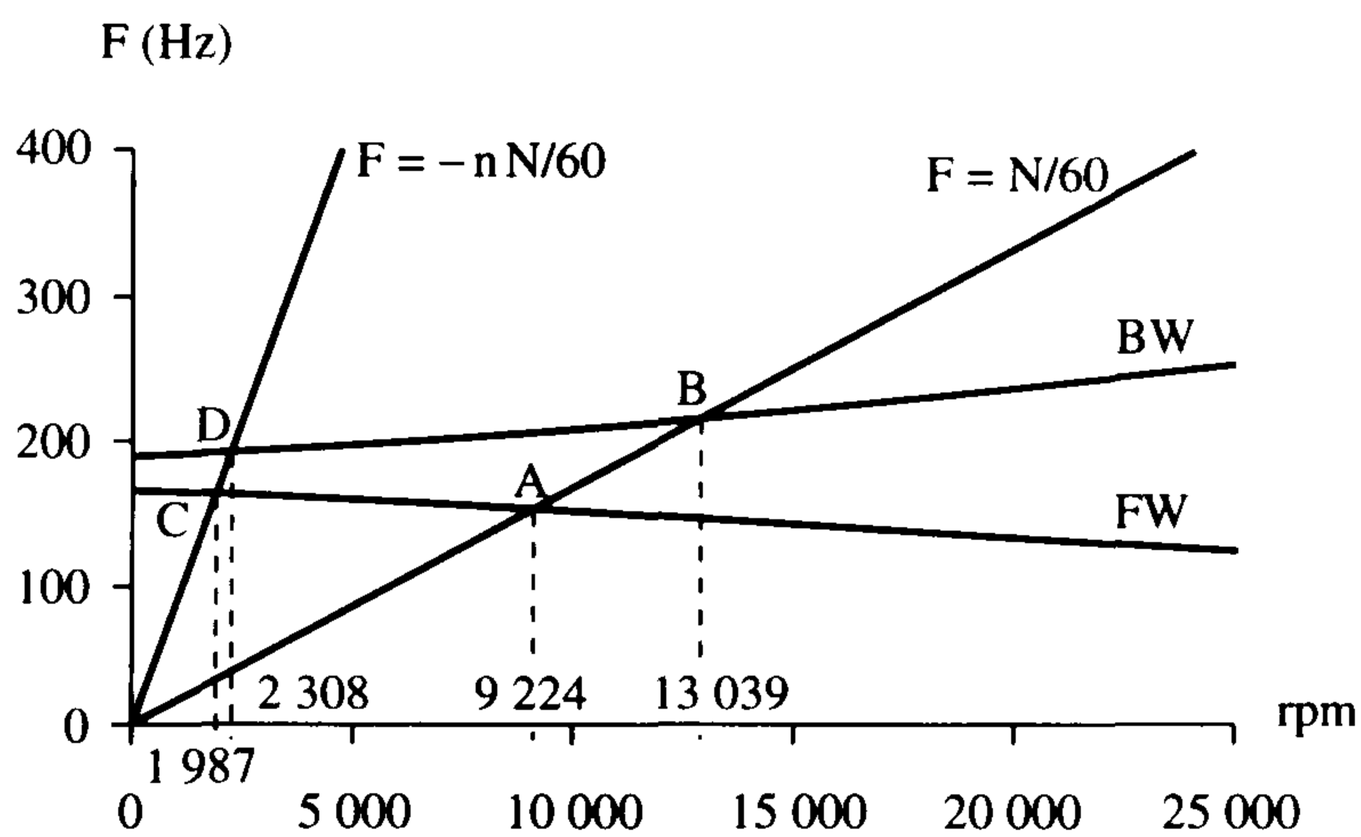

Figure 3.8. Campbell diagram: $n = -5$

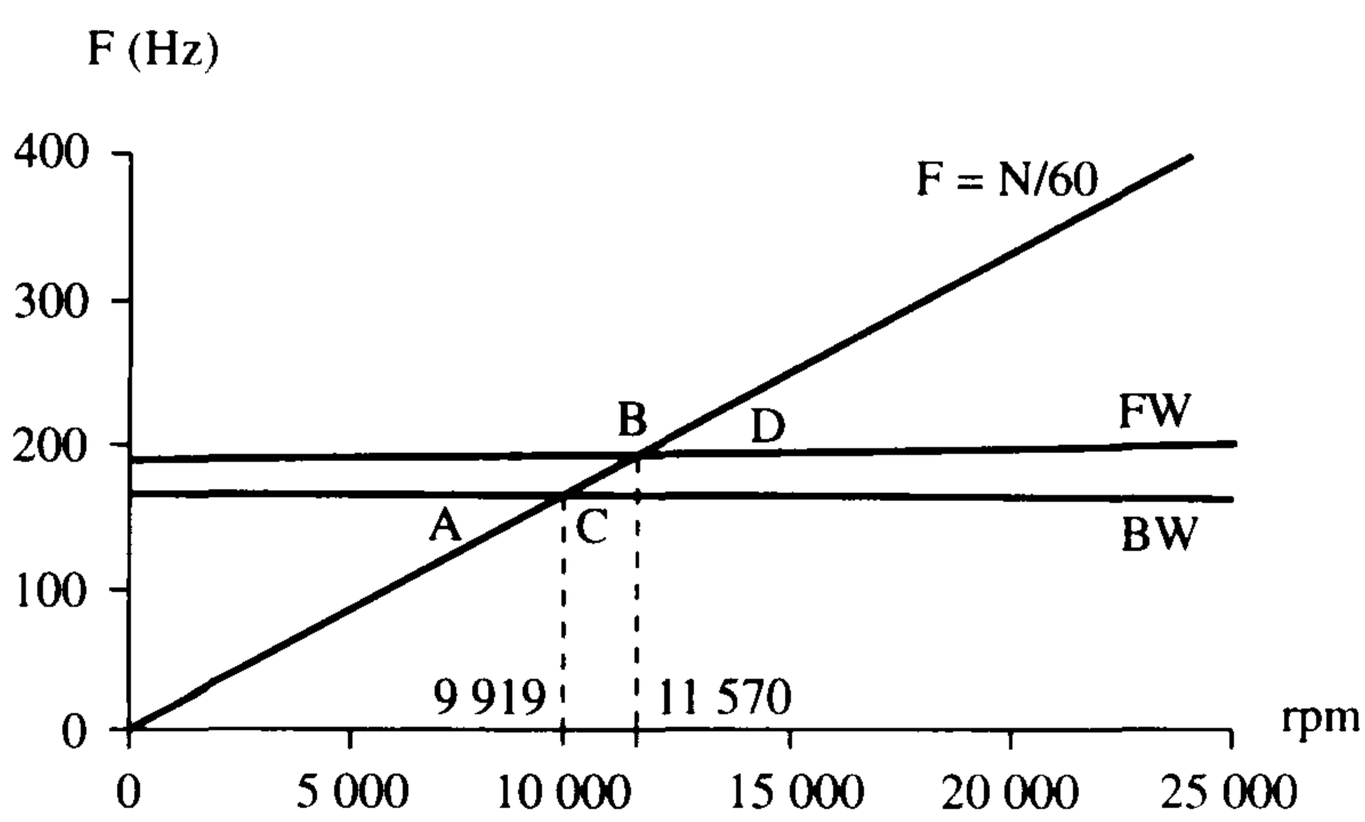

Figure 3.9. Campbell diagram: $n = -1$

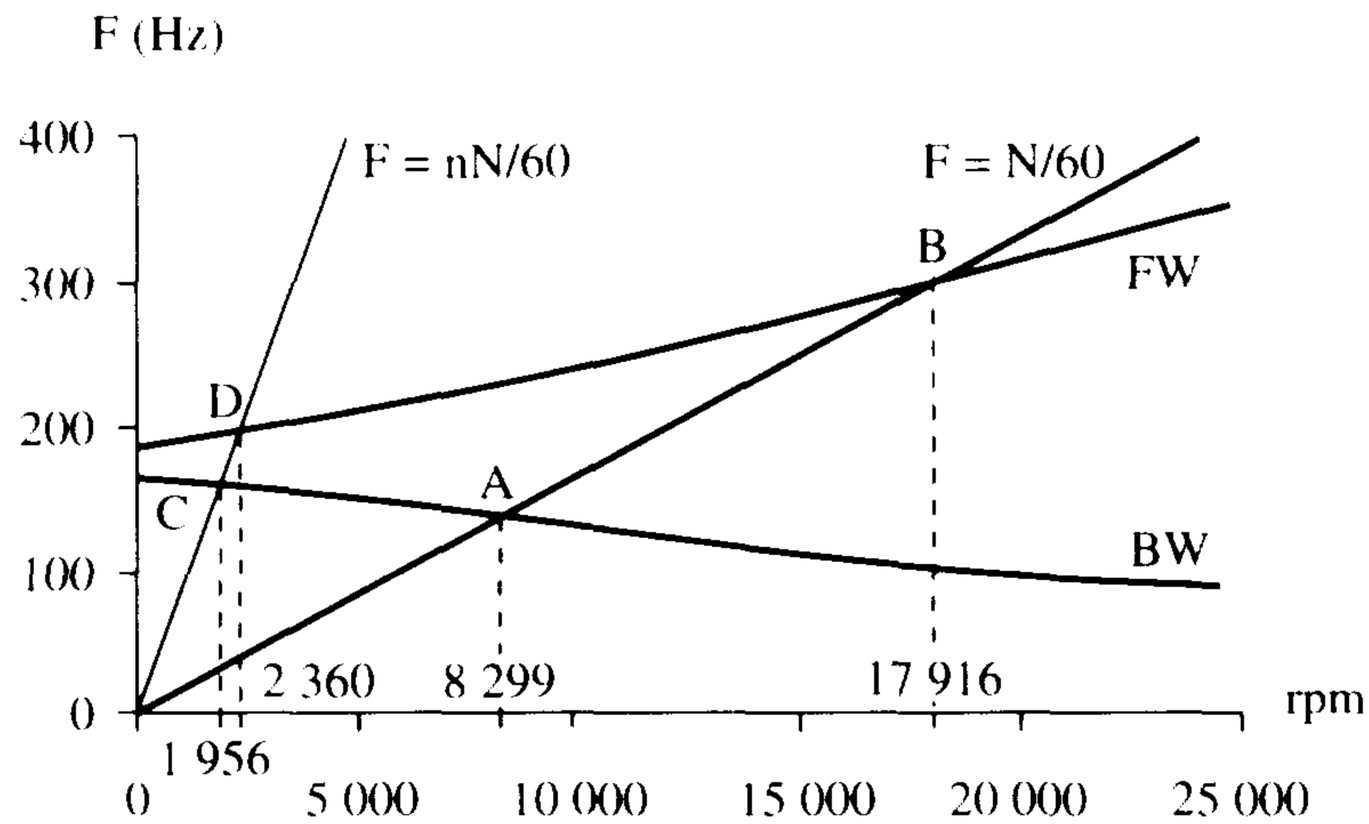

Figure 3.10. Campbell diagram: $n = 5$

equations which give the values of the frequencies at points A and B, or C and D, can be obtained from Equation (3.66). This gives, for points A and B,

$$\Omega^4(m^2 - (a_1 + na_2)^2) - (k_1 + k_2)m\Omega^2 + k_1 k_2 = 0 \tag{3.72}$$

and for points C and D,

$$\Omega^4(m^2 n^4 - n^2(a_1 + na_2)^2) - (k_1 + k_2)m^2 n^2 \Omega^2 + k_1 k_2 = 0 \tag{3.73}$$

3.3.2 Response to forces due to mass unbalances

Here, only the steady-state response is calculated. The general solution of Equations (3.60) and (3.61) is not considered. The mass unbalance response is predicted with the mass unbalance located on disk D_1 (rotor 1) or disk D_2 (rotor 2).

Mass unbalance on rotor 1

The system is governed by Equations (3.60) and (3.61) with the forces given in Equations (3.27) and (3.28). The solutions are sought in the form

of (3.47) and (3.48), which gives

$$Q_1 = \frac{m_1 d\Omega^2(k_2 - (m + a_1 + na_2)\Omega^2)}{(k_1 - m\Omega^2)(k_2 - m\Omega^2) - (a_1 + na_2)^2\Omega^4} \tag{3.74}$$

$$Q_2 = \frac{m_1 d\Omega^2(k_1 - (m + a_1 + na_2)\Omega^2)}{(k_1 - m\Omega^2)(k_2 - m\Omega^2) - (a_1 + na_2)^2\Omega^4} \tag{3.75}$$

As $Q_1 \neq Q_2$ the orbits described by the rotors are ellipses. The critical speeds correspond to

$$(k_1 - m\Omega^2)(k_2 - m\Omega^2) - (a_1 + na_2)^2\Omega^4 = 0 \tag{3.76}$$

which is the same equation as (3.72). Hence the two frequencies, which are the solutions of Equation (3.72), give critical speeds. The mass unbalance responses for $n = -5$, -1 and 5, respectively, are shown in Figures 3.11, 3.12 and 3.13.

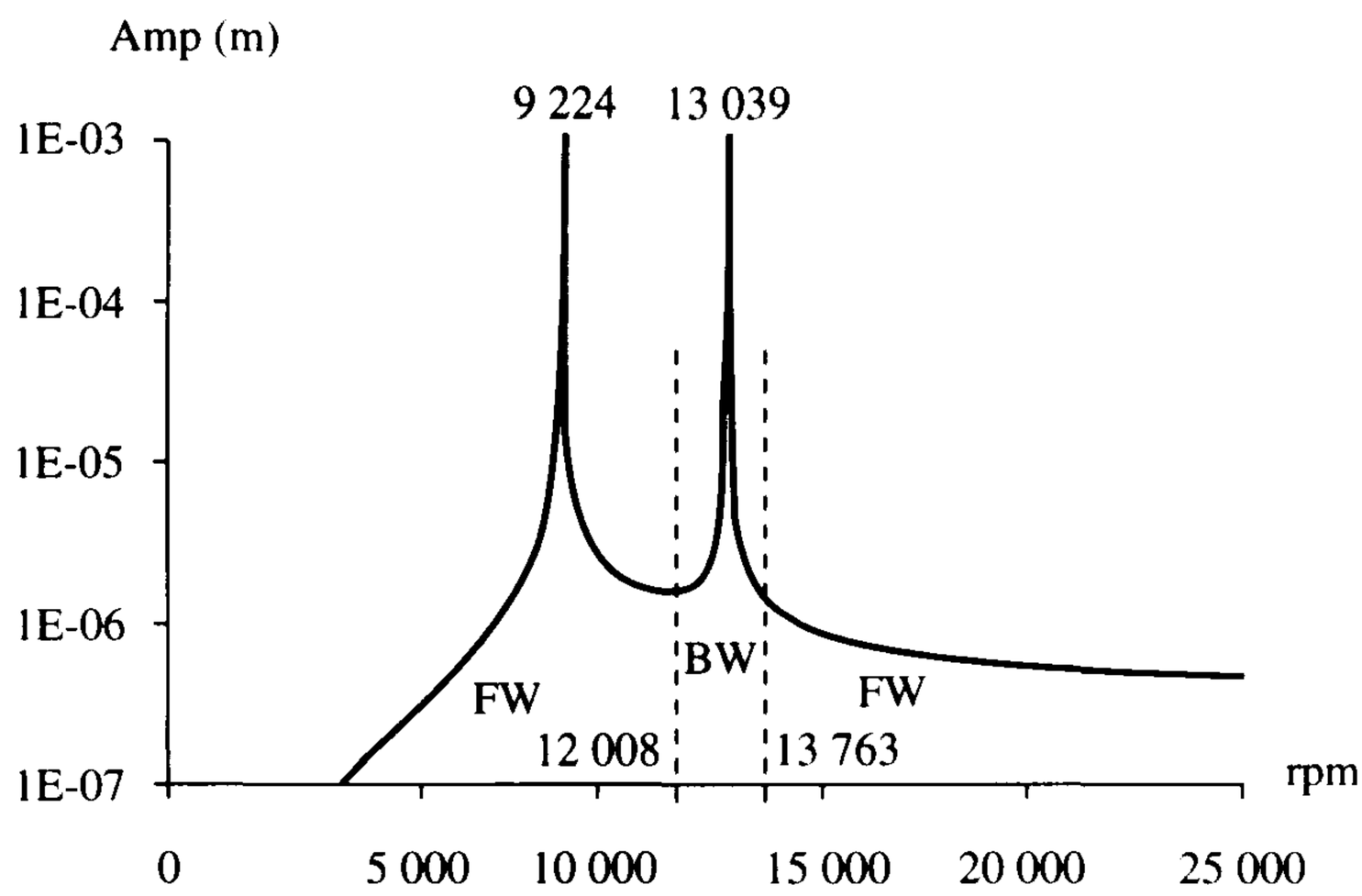

Figure 3.11. Mass unbalance response (mass on rotor 1): $n = -5$

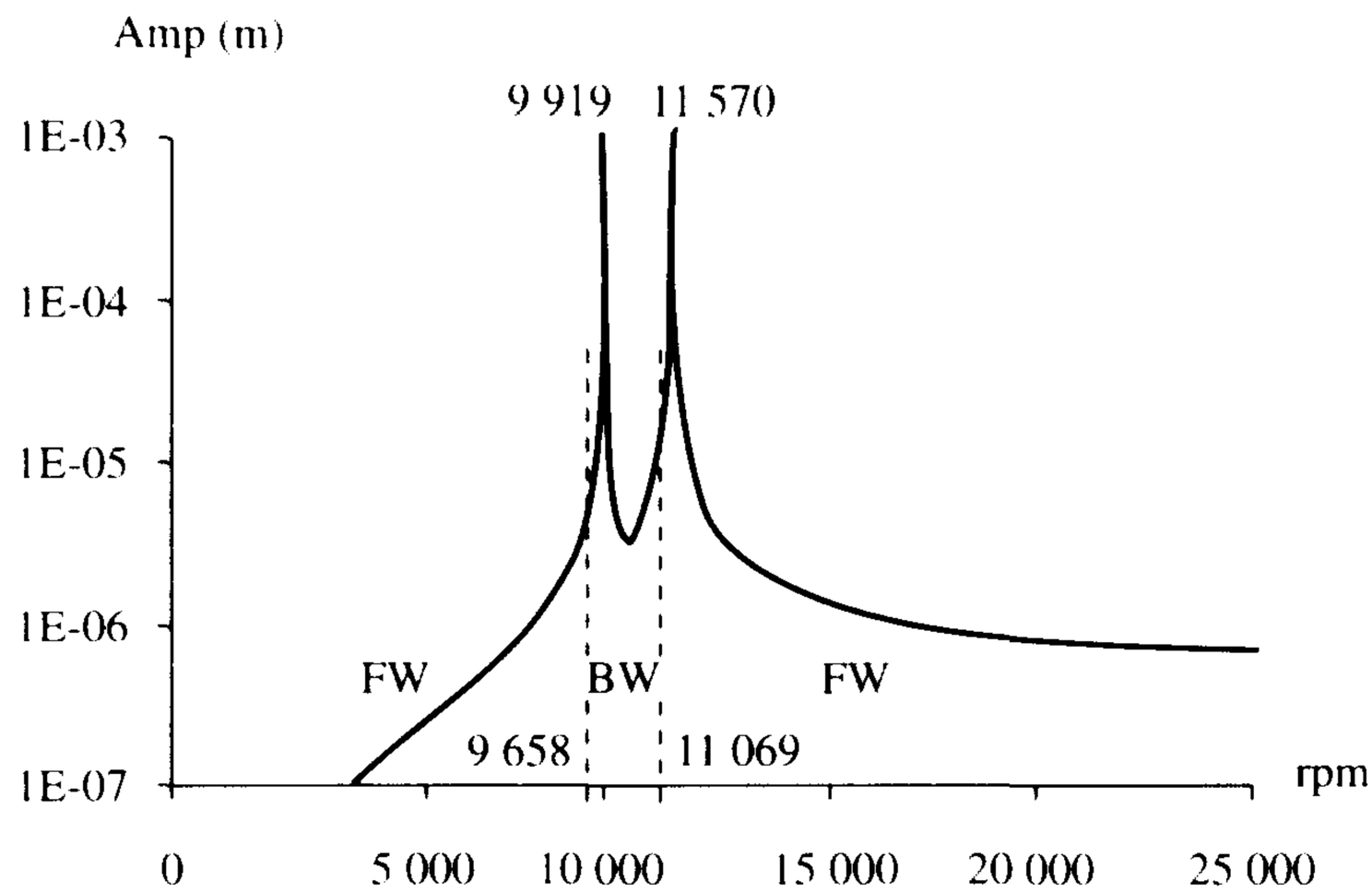

Figure 3.12. Mass unbalance response (mass on rotor 1): $n = -1$

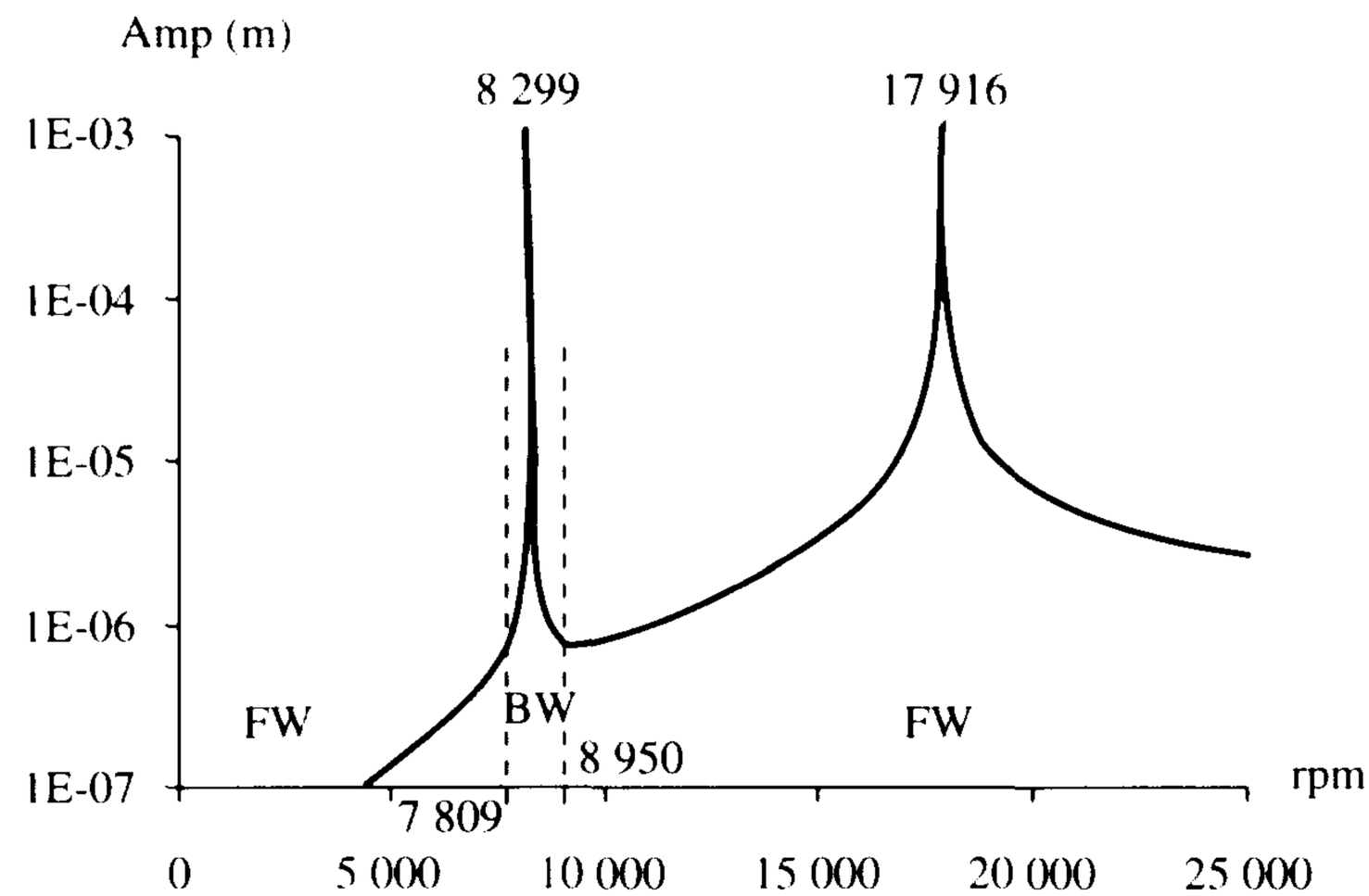

Figure 3.13. Mass unbalance response (mass on rotor 1): $n = 5$

Mass unbalance on rotor 2

Here the forces are given by Equations (3.29) and (3.30), and the solutions are sought in the form of (3.51) and (3.52), which gives

$$Q_1 = \frac{m_2 d n^2 \Omega^2 (k_2 - (mn + a_1 + na_2) n\Omega^2)}{(k_1 - mn^2\Omega^2)(k_2 - mn^2\Omega^2) - (a_1 + na_2)^2 n^2 \Omega^4} \tag{3.77}$$

$$Q_2 = \frac{m_2 d n^2 \Omega^2 (k_1 - (mn + a_1 + na_2) n\Omega^2)}{(k_1 - mn^2\Omega^2)(k_2 - mn^2\Omega^2) - (a_1 + na_2)^2 n^2 \Omega^4} \tag{3.78}$$

As $Q_1 \neq Q_2$ the orbits described by the rotors are ellipses. The critical speeds correspond to

$$(k_1 - mn^2\Omega^2)(k_2 - mn^2\Omega^2) - n^2\Omega^4(a_1 + na_2)^2 = 0 \tag{3.79}$$

which is the same equation as (3.73). Hence the two frequencies, which are the solutions of Equation (3.73), give critical speeds. The mass unbalance responses for $n = -5$, -1 and 5, respectively, are shown in Figures 3.14, 3.15 and 3.16. Practically as residual mass unbalances are

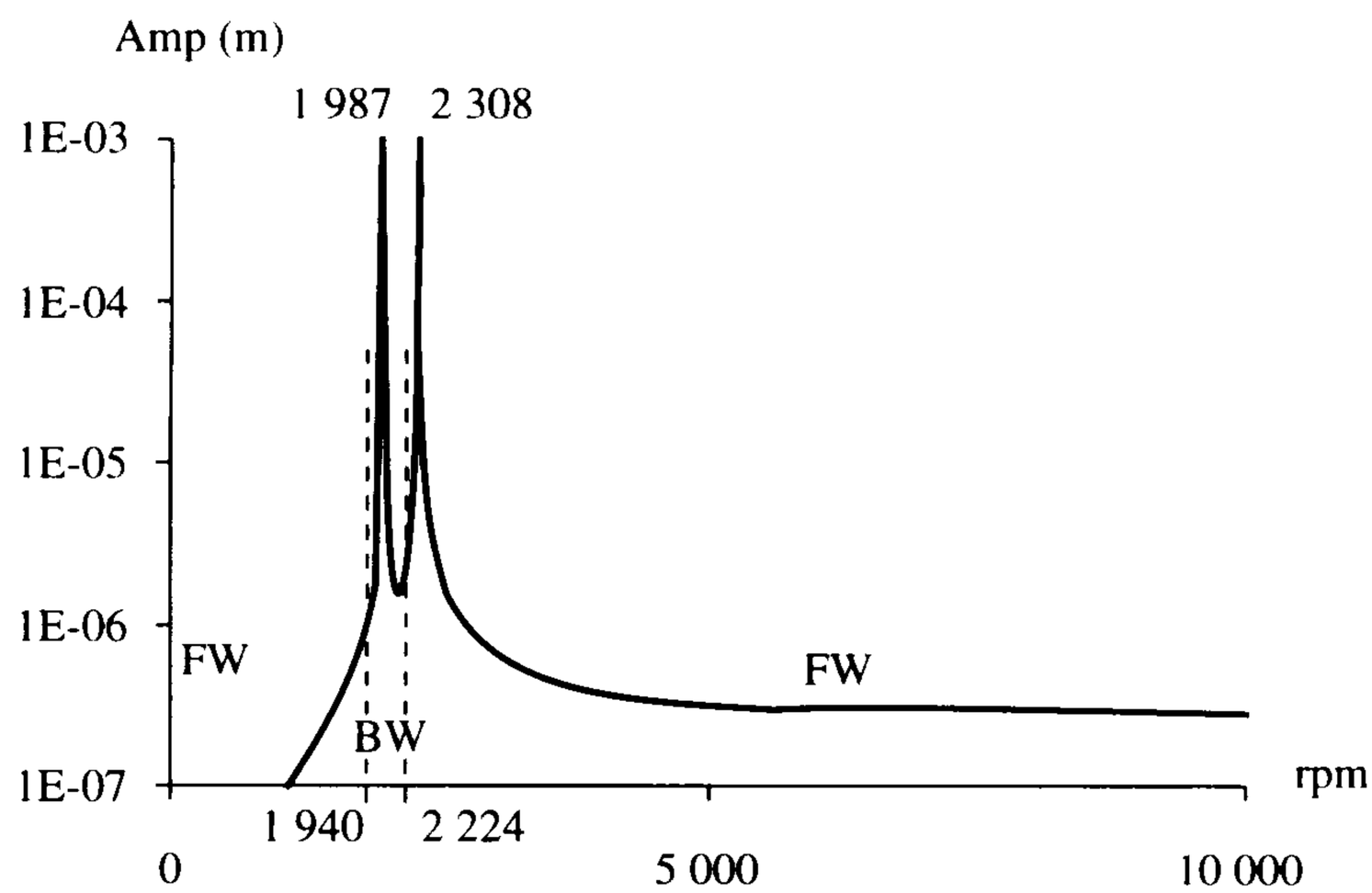

Figure 3.14. Mass unbalance response (mass on rotor 2): $n = -5$

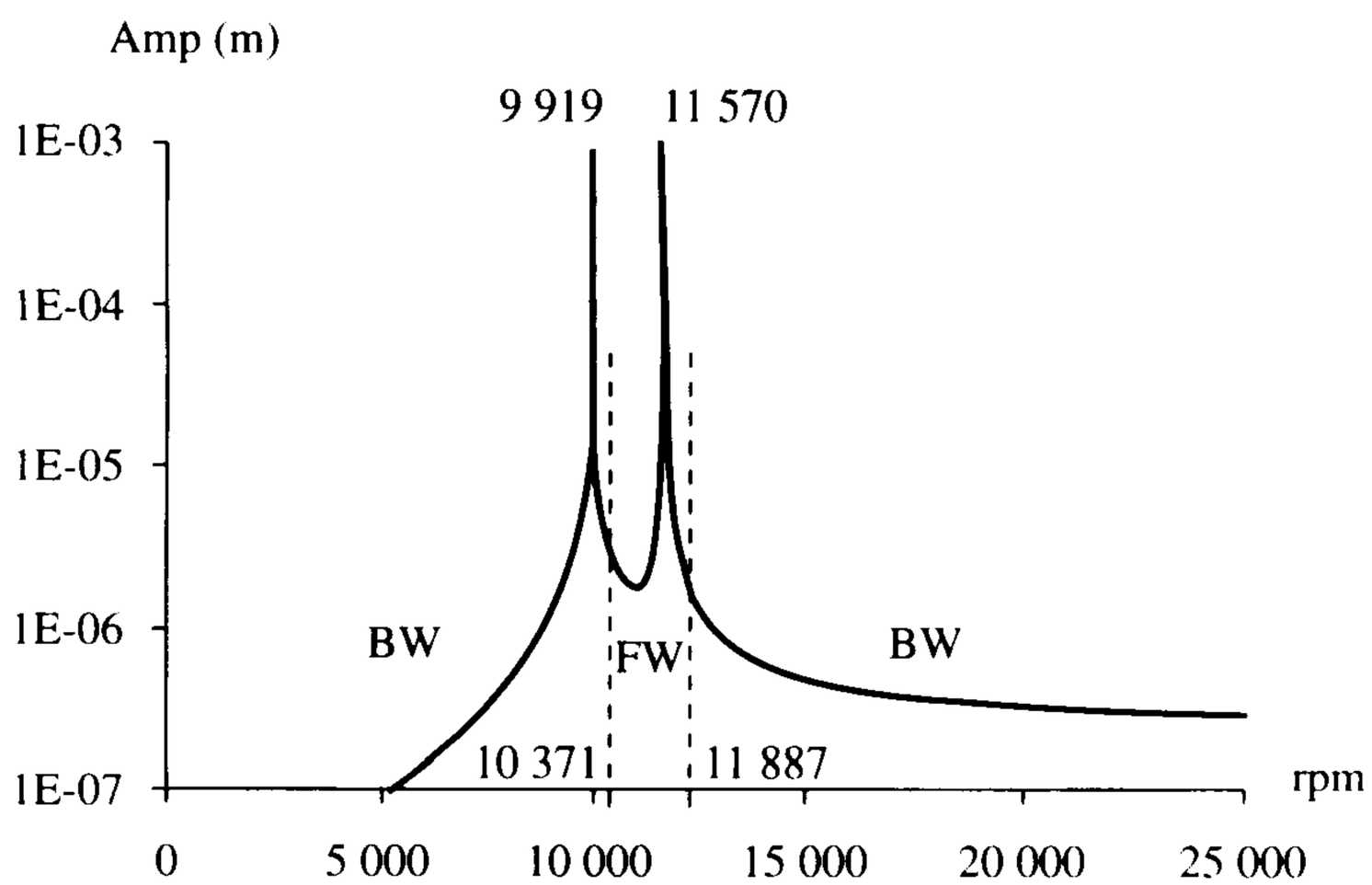

Figure 3.15. Mass unbalance response (mass on rotor 2): $n = -1$

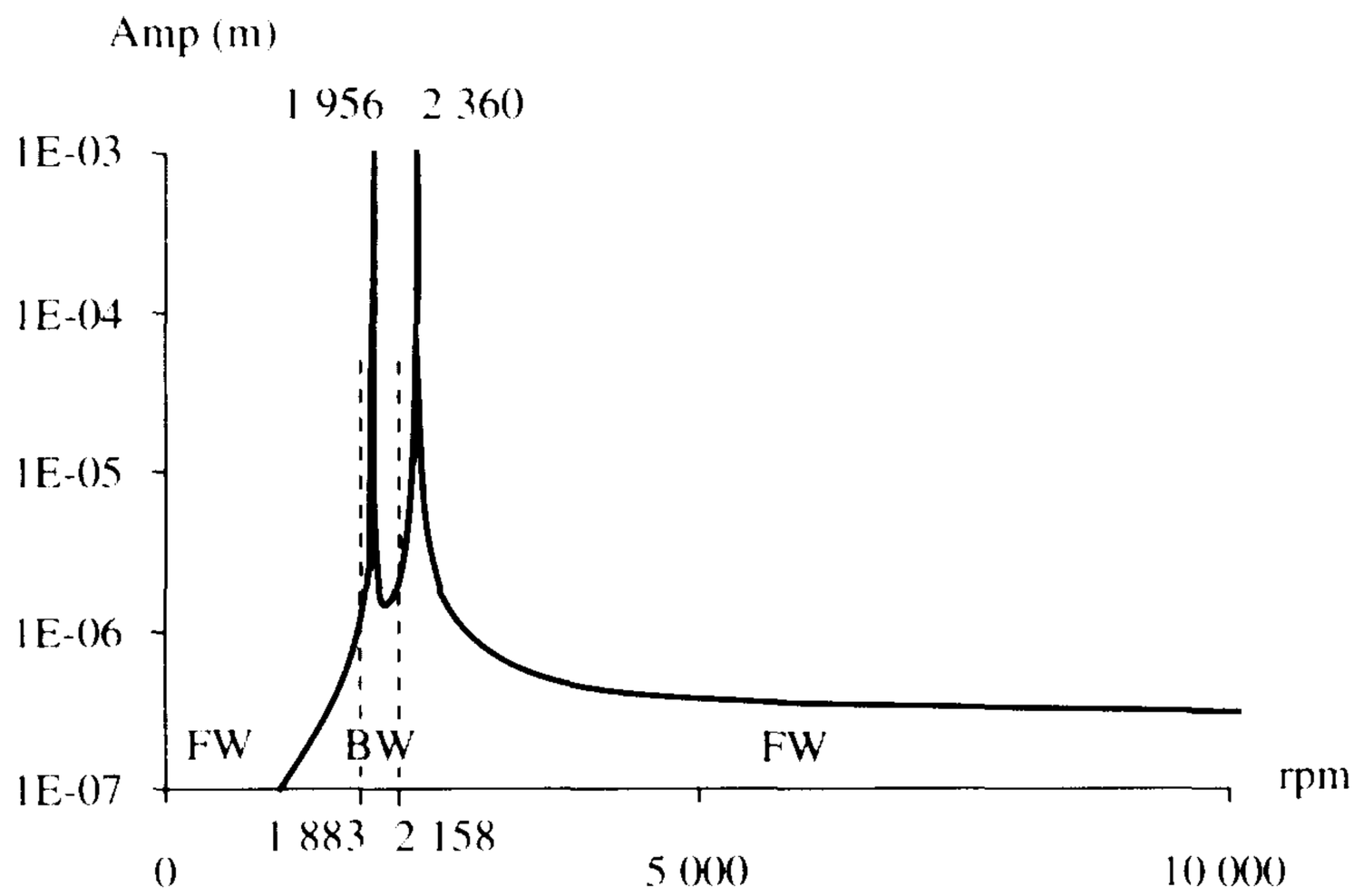

Figure 3.16. Mass unbalance response (mass on rotor 2): $n = 5$

simultaneously on the two rotors the four critical speeds would be observed.

Sense of the whirl

As for the symmetric systems, the sense of the whirl is given by expression (3.57). When the mass unbalance is on rotor 1, Equations (3.47), (3.48), (3.74) and (3.75) give

$$0\vec{A} \wedge \frac{\mathrm{d}0\vec{A}}{\mathrm{d}t} = \begin{bmatrix} 0 \\ Q_1 Q_2 \Omega \mathrm{d}t \\ 0 \end{bmatrix} \tag{3.80}$$

and the sign of $Q_1 Q_2 \Omega dt$ is the sign of $Q_1 Q_2$, which is that of

$$P_1 = (k_2 - (m + a_1 + na_2)\Omega^2)(k_1 - (m + a_1 + na_2)\Omega^2) \tag{3.81}$$

If $P_1 > 0$ the whirl is forward (FW), and if $P_1 < 0$ the whirl is backward (BW). In terms of the frequencies Ω_1 and Ω_2 such that is

$$\Omega_1 = \sqrt{\frac{k_1}{m + a_1 + na_2}} \tag{3.82}$$

$$\Omega_2 = \sqrt{\frac{k_2}{m + a_1 + na_2}} \tag{3.83}$$

we have a forward whirl for $\Omega < \Omega_1$ or $\Omega_2 < \Omega$ and a backward whirl for $\Omega_1 < \Omega < \Omega_2$. In addition, it is interesting to know what happens at the critical speeds ω_1 and ω_2. As the critical speeds are solutions of Equation (3.72), the expression

$$F(\omega^2) = \omega^4(m^2 - (a_1 + na_2)^2) - (k_1 + k_2)m\omega^2 + k_1 k_2 \tag{3.84}$$

is a positive quantity when $\omega < \omega_1$ or $\omega > \omega_2$. If $0 < a_1 + na_2$ the value of $F(\omega^2)$ for $\omega = \Omega$, which is

$$F(\Omega_1^2) = F\left(\frac{k_1}{m + a_1 + na_2}\right) = \frac{k_1(a_1 + na_2)(k_2 - k_1)}{m + a_1 + na_2} \tag{3.85}$$

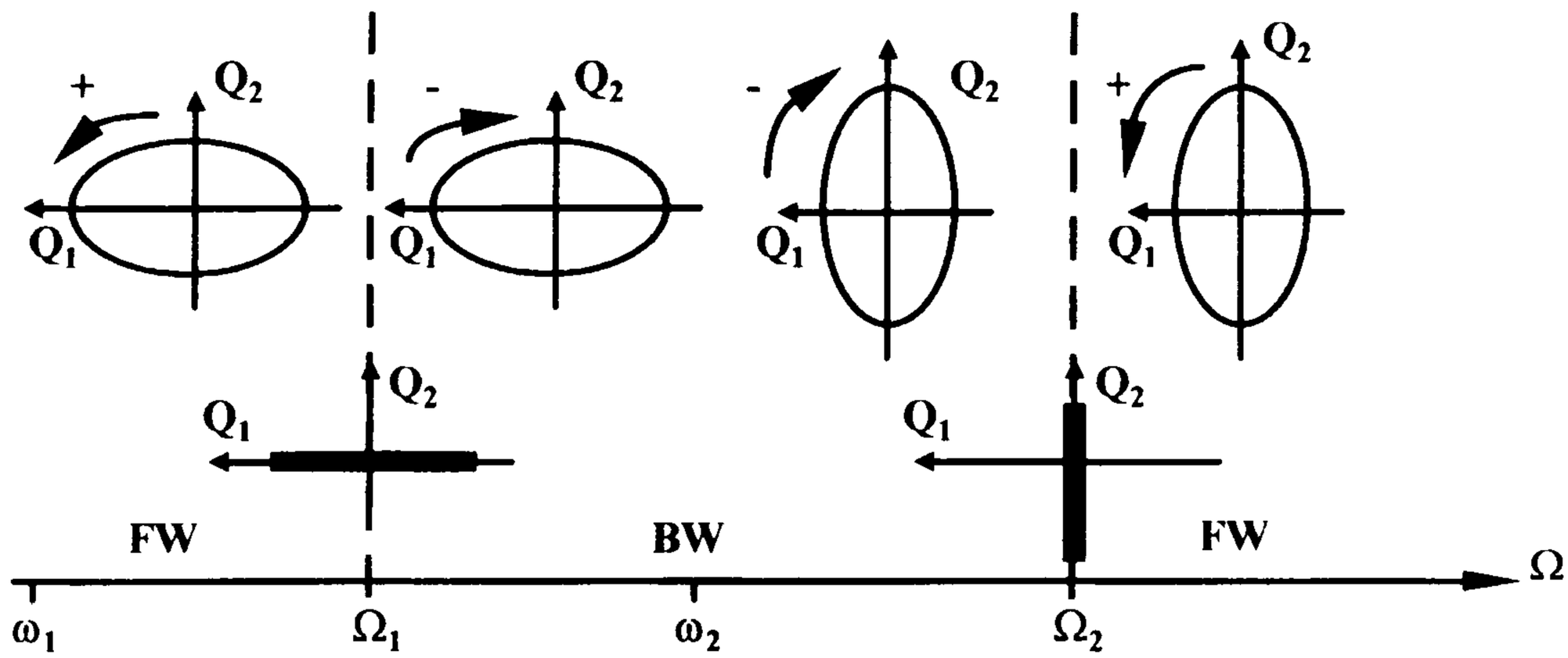

(a) : n < - (a_1 / a_2)

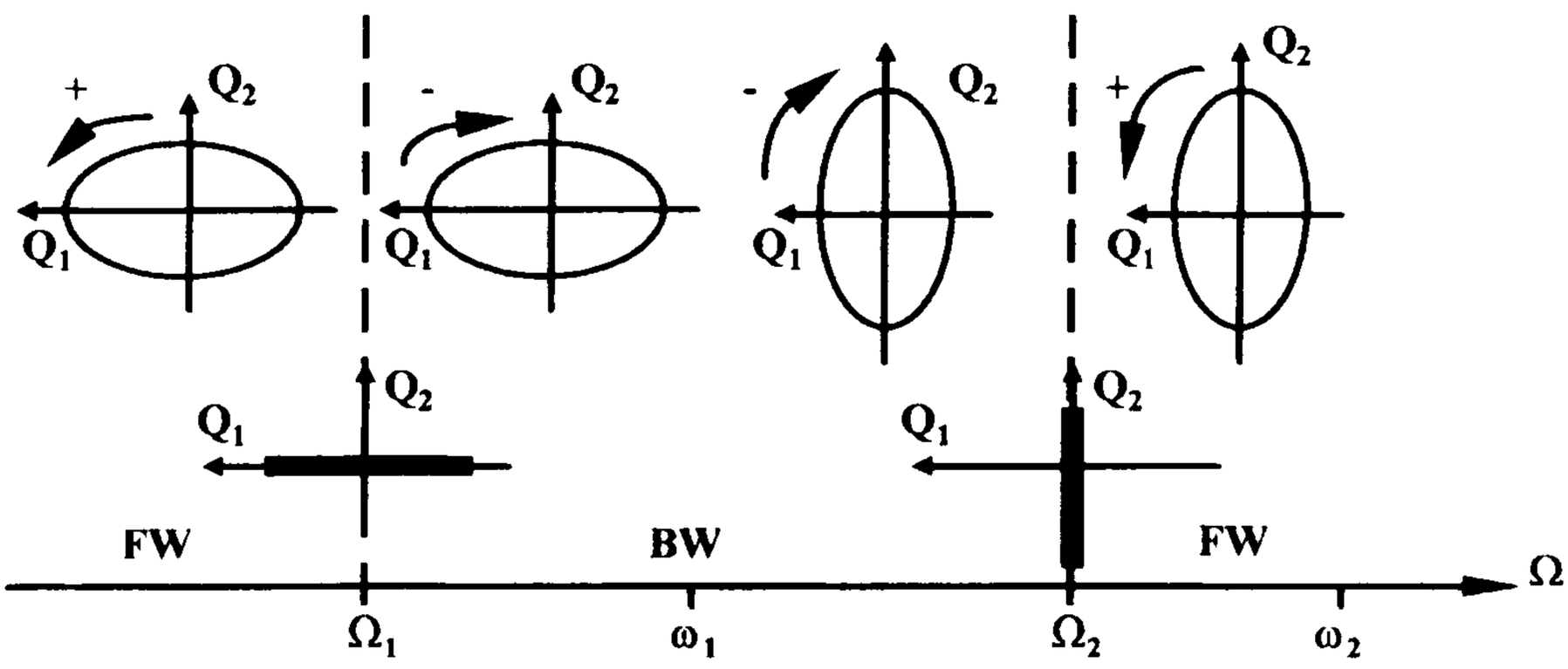

(b) : n > - (a_1 / a_2)

Figure 3.17. Sense of the whirl: mass unbalance on rotor 1

is also a positive quantity. In addition, since

$$F(\Omega_2^2) = F\left(\frac{k_2}{m + a_1 + na_2}\right) = \frac{k_2(a_1 + na_2)(k_1 - k_2)}{m + a_1 + na_2} \tag{3.86}$$

$F(\Omega_2^2)$ is a negative quantity. Hence, for $n > -(a_1/a_2)$,

$$\Omega_1 < \omega_1 < \Omega_2 < \omega_2 \text{ (Figure 3.17(b))} \tag{3.87}$$

The sense of the whirl is shown in Figure 3.17.

When the mass unbalance is on rotor 2, Equations (3.51), (3.52), (3.77) and (3.78) give

$$0\vec{A} \wedge \frac{\mathrm{d}0\vec{A}}{\mathrm{d}t} = \begin{bmatrix} 0 \\ n\Omega Q_1 Q_2 \mathrm{d}t \\ 0 \end{bmatrix} \tag{3.88}$$

and the sign of $n\Omega Q_1 Q_2 dt$ is the sign of $nQ_1 Q_2$, which is that of

$$P_2 = n(k_2 - (mn + a_1 + na_2)n\Omega^2)(k_1 - (mn + a_1 + na_2)n\Omega^2) \tag{3.89}$$

It is now appropriate to define the frequencies Ω_1 and Ω_2 as

$$\Omega_1 = \sqrt{\frac{k_1}{n(mn + a_1 + na_2)}} \tag{3.90}$$

$$\Omega_2 = \sqrt{\frac{k_2}{n(mn + a_1 + na_2)}} \tag{3.91}$$

and it is also of particular interest to know what happens to critical speeds ω_1 and ω_2. These frequencies are the solutions of Equation (3.73) and the sign of the expression

$$F(\omega^2) = \omega^4(m^2n^4 - n^2(a_1 + na_2)^2) - (k_1 + k_2)mn^2\omega^2 + k_1 k_2 \tag{3.92}$$

has to be considered. It can be shown that

$$F(\Omega_1^2) = F\left(\frac{k_1}{n(mn + a_1 + na_2)}\right) = \frac{k_1(a_1 + na_2)(k_2 - k_1)}{mn + a_1 + na_2} \tag{3.93}$$

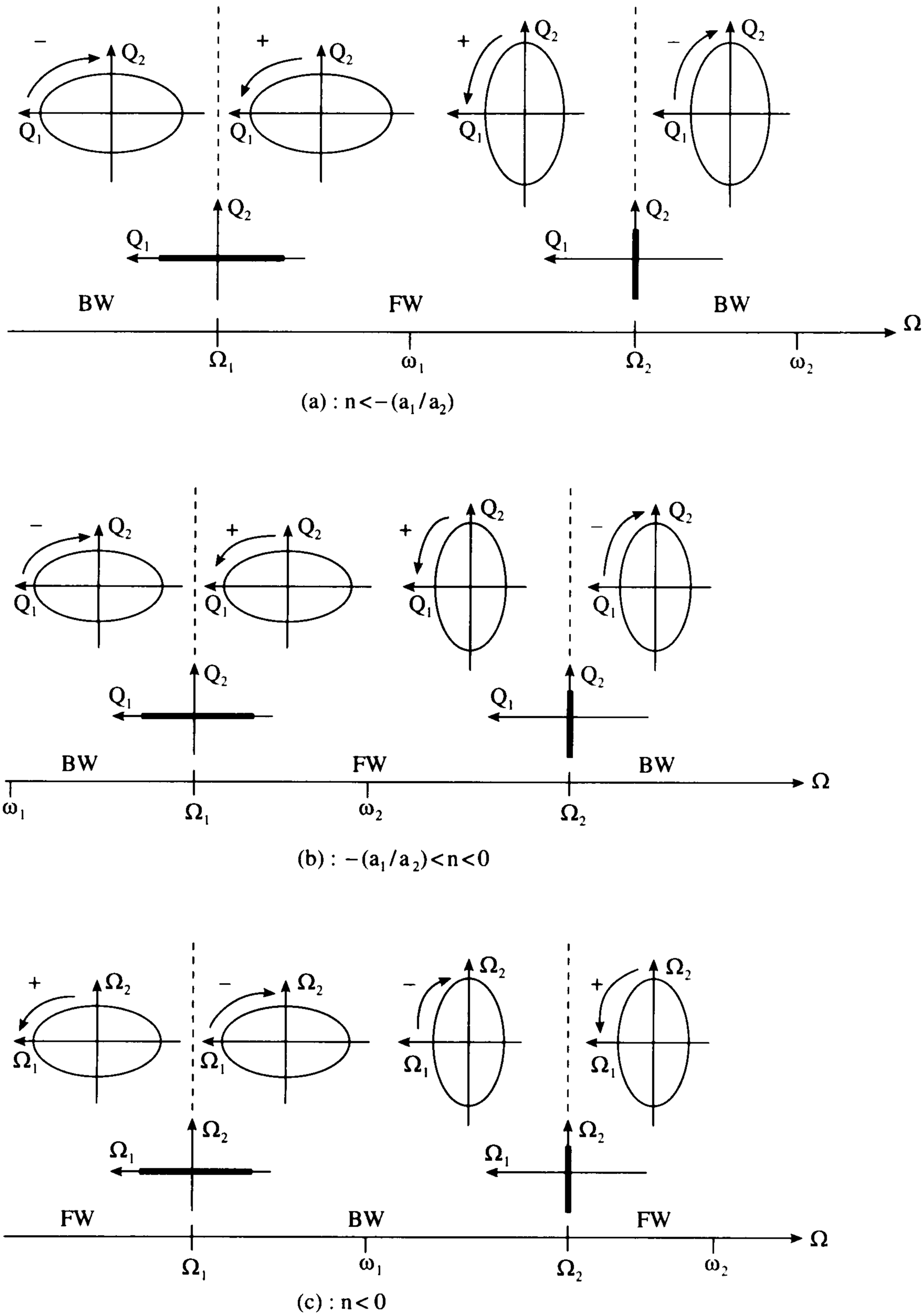

Figure 3.18. Sense of the whirl: mass unbalance on rotor 2

and

$$F(\Omega_2^2) = F\left(\frac{k_2}{n(mn + a_1 + na_2)}\right) = \frac{k_2(a_1 + na_2)(k_1 - k_2)}{mn + a_1 + na_2} \tag{3.94}$$

It can be shown moreover that if $n < -a_1/a_2$,

$$\Omega_1 < \omega_1 < \Omega_2 < \omega_2 \text{ (see Figure 3.18(a))} \tag{3.95}$$

if $-a_1/a_2 < n < 0$,

$$\omega_1 < \Omega_1 < \omega_2 < \Omega_2 \text{ (see Figure 3.18(b))} \tag{3.96}$$

and if $n > 0$,

$$\Omega_1 < \omega_1 < \Omega_2 < \omega_2 \text{ (see Figure 3.18(c))} \tag{3.95}$$

Expressions (3.95) and (3.97) are the same but the sense of the whirl is different: see Figure 3.18.

3.4 DAMPED SYSTEM

In what follows, the coaxial rotors studied previously in this chapter are assumed to be viscously damped by a bearing. Let us then suppose that the bearing characteristics, located at $y = l_4$, are

$$k_{xx} = 2 \times 10^6 \text{ N/m}, \quad k_{zz} = 8 \times 10^6 \text{ N/m}, \quad k_{xz} = k_{zx} = 0$$
$$c_{xx} = \beta k_{xx} \text{ N/m/s}, \quad c_{zz} = \beta k_{zz} \text{ N/m/s}, \quad c_{xz} = c_{zx} = 0$$

The motion equations are

$$m\ddot{q}_1 - \Omega(a_1 + na_2)\dot{q}_2 + c_1\dot{q}_1 + k_1 q_1 = F_1(t) \tag{3.98}$$
$$m\ddot{q}_2 + \Omega(a_1 + na_2)\dot{q}_1 + c_2\dot{q}_2 + k_2 q_2 = F_2(t) \tag{3.99}$$

where

$$k_1 = 2.063 \times 10^7 \text{ N/m}, \quad k_2 = 2.513 \times 10^7 \text{ N/m} \tag{3.100}$$
$$c_1 = \beta \times 1.5 \times 10^6 \text{ N/m/s}, \quad c_2 = \beta \times 6 \times 10^6 \text{ N/m/s} \tag{3.101}$$

Equations (3.98) and (3.99) cannot be solved by hand calculations.

3.4.1 Natural frequencies as a function of the speed of rotation: the Campbell diagram

The system is studied in free motion. The solutions must be sought in the form of Equations (2.58) and (2.59), Chapter 2, which, when substituted in Equations (3.98) and (3.99) without the right member, lead to the characteristic equation

$$m^2r^4 + m(c_1 + c_2)r^3 + (k_1m + k_2m + c_1c_2 + (a_1 + na_2)^2\Omega^2)r^2 + (k_2c_1 + k_1c_2)r + k_1k_2 = 0 \tag{3.102}$$

As in Section 2.5.1, if the values of the damping coefficients c_1 and c_2 are low, the roots of (3.102) are pairs of complex conjugate quantities

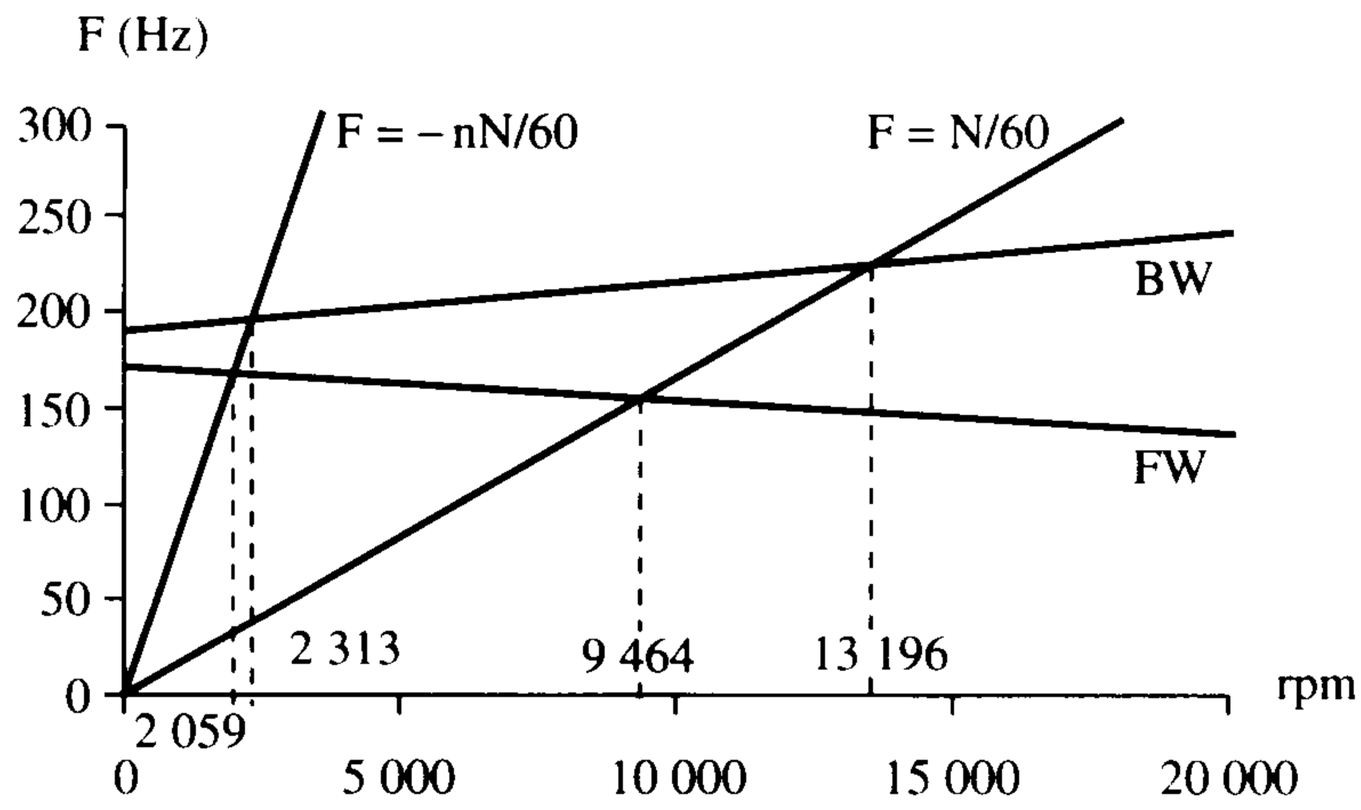

Figure 3.19. Campbell diagram: $(\beta = 0.0001, n = -5)$

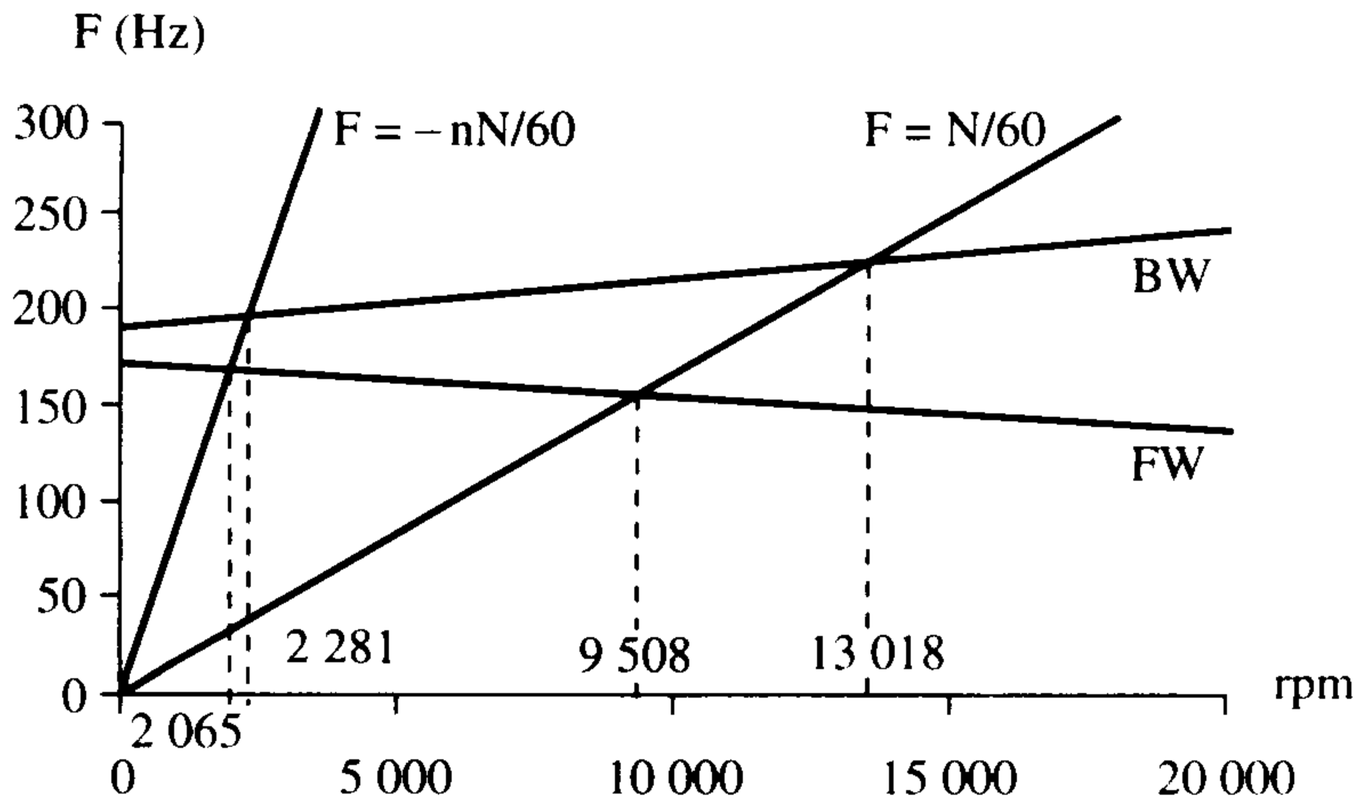

Figure 3.20. Campbell diagram: $(\beta = 0.001, n = -5)$

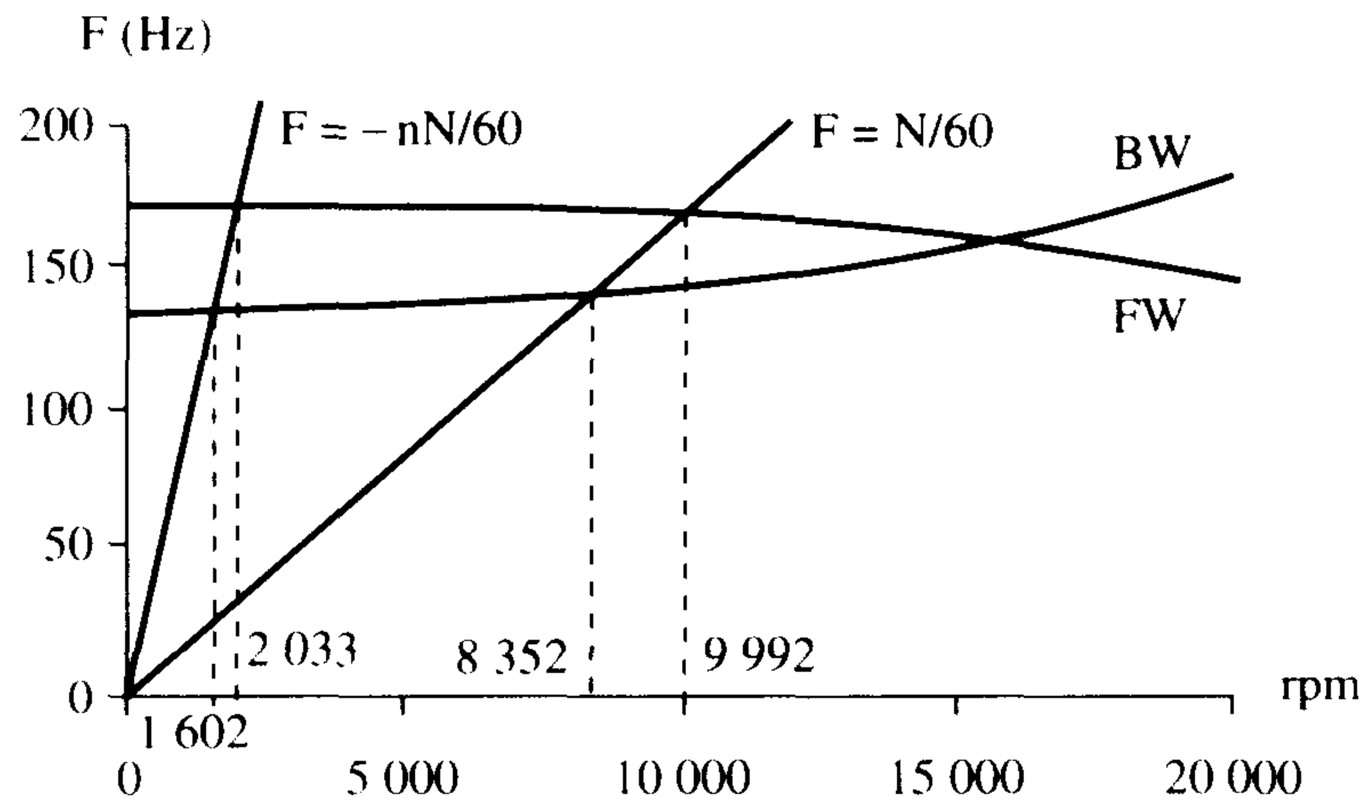

Figure 3.21. Campbell diagram: $(\beta = 0.005, n = -5)$

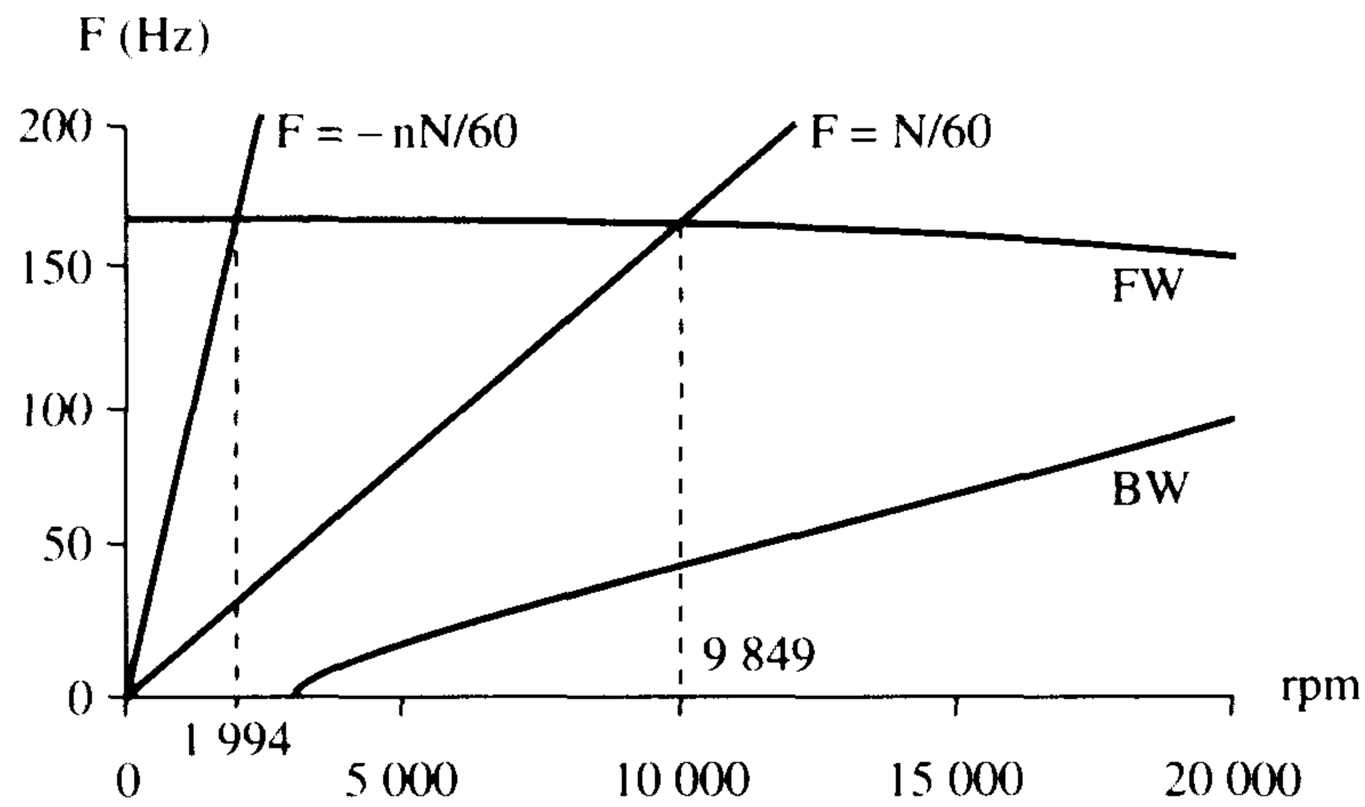

Figure 3.22. Campbell diagram: $(\beta = 0.007, n = -5)$

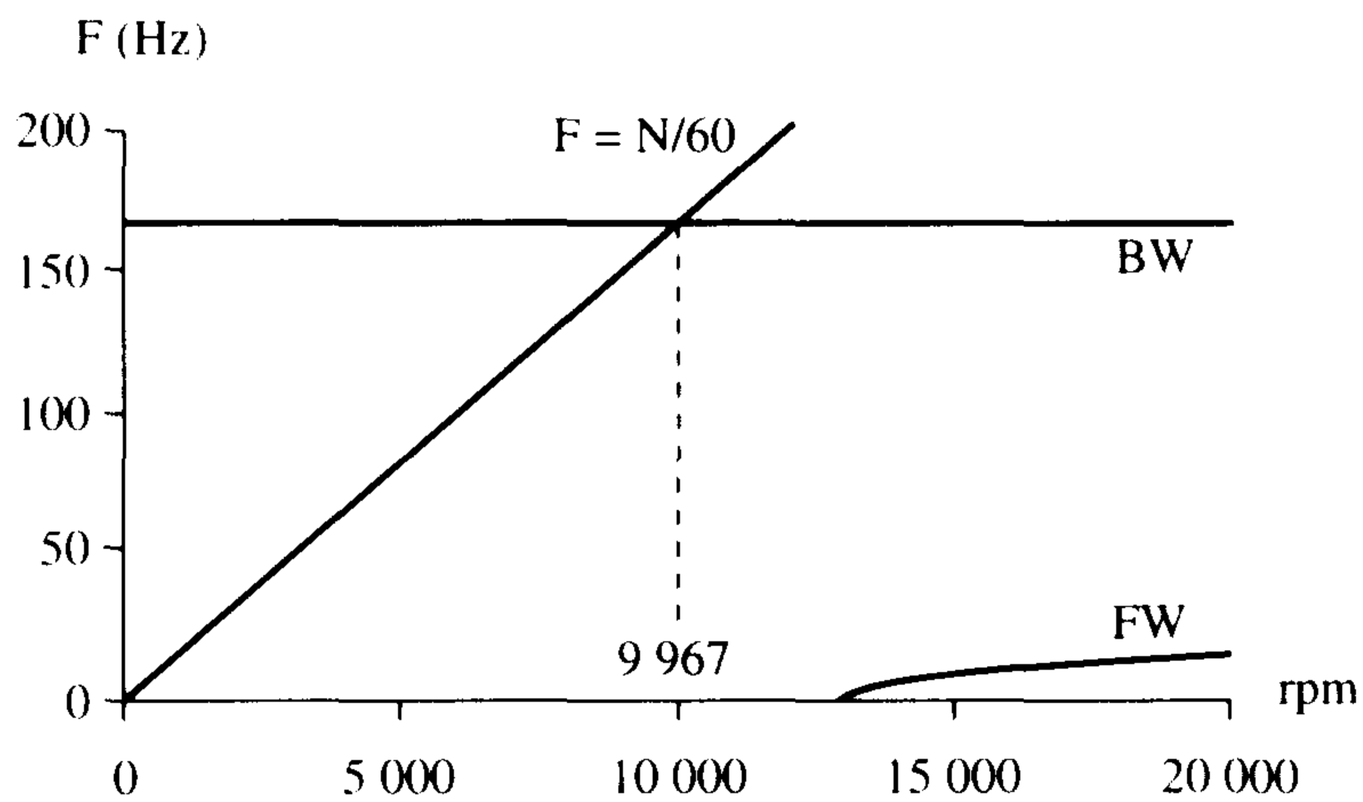

Figure 3.23. Campbell diagram: $(\beta = 0.007, n = -1)$

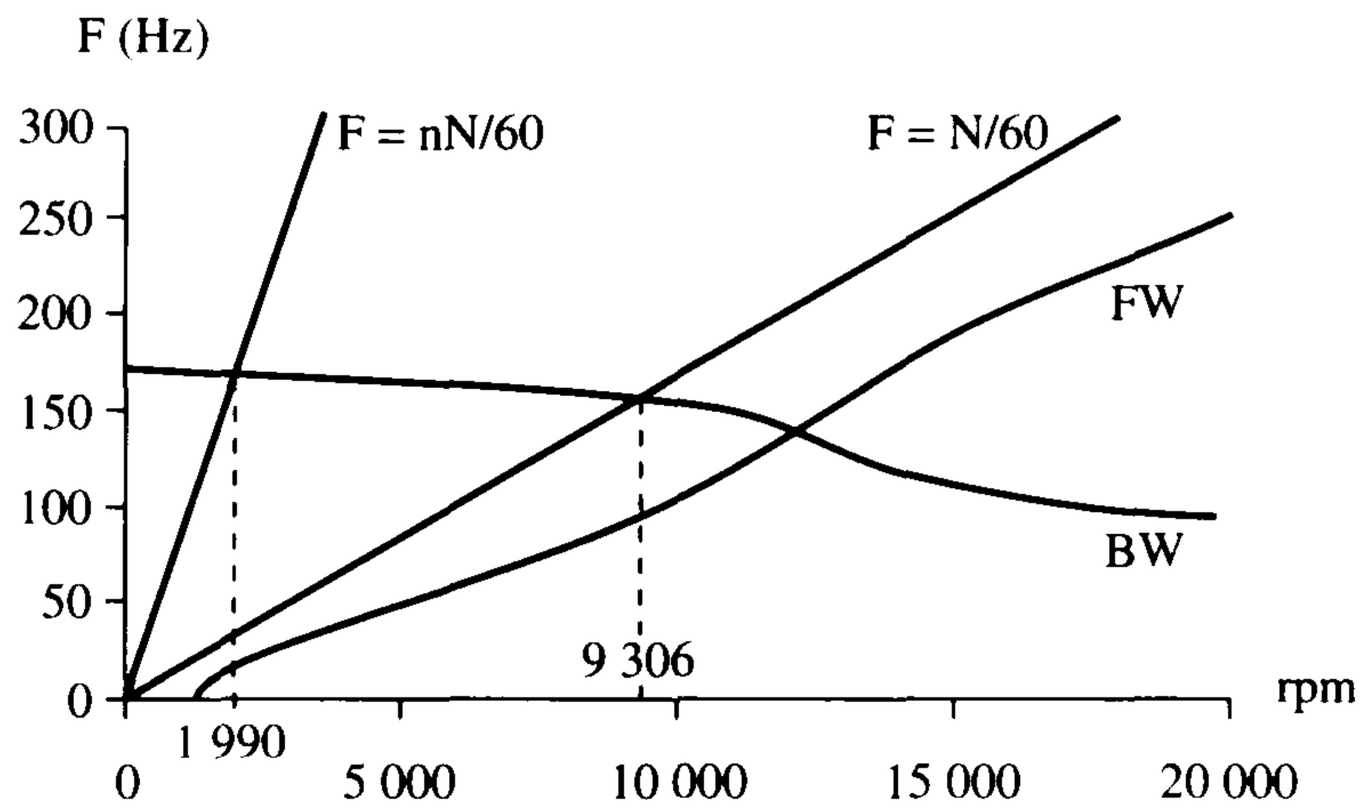

Figure 3.24. Campbell diagram: ($\beta = 0.007, n = 5$)

and, if the damping coefficients increase, it is possible to obtain real roots.

Figures 3.19, 3.20, 3.21 and 3.22 show the Campbell diagrams, with the speed ratio $n = -5$, when the damping varies. The results shown in Figure 3.19 ($\beta = 0.0001$) and Figure 3.20 ($\beta = 0.001$) are almost the same as those of Figure 3.8 for $\beta = 0$.

With high damping, $\beta = 0.005$, the diagram, Figure 3.21, is now rather different. When the damping increases to $\beta = 0.007$, Figure 3.22, only one frequency appears until the rotation speed has a significant value. For the damping corresponding to $\beta = 0.007$, the Campbell diagrams for $n = -1$ and $n = 5$ are shown in Figures 3.23 and 3.24.

3.4.2 Response to forces due to mass unbalances

As in Section 3.3.2, only the steady-state response is calculated. The results presented have been limited to $n = -5$.

Mass unbalance on rotor 1

The system is governed by Equations (3.98) and (3.99) with the forces given by Equations (3.27) and (3.28). Since the system is damped, the solutions of the equations must now be sought in the form

$$q_1 = A_1 \sin \Omega t + B_1 \cos \Omega t \tag{3.103}$$

$$q_2 = A_2 \sin \Omega t + B_2 \cos \Omega t \tag{3.104}$$

These are substituted in (3.98) and (3.99). This gives a set of linear

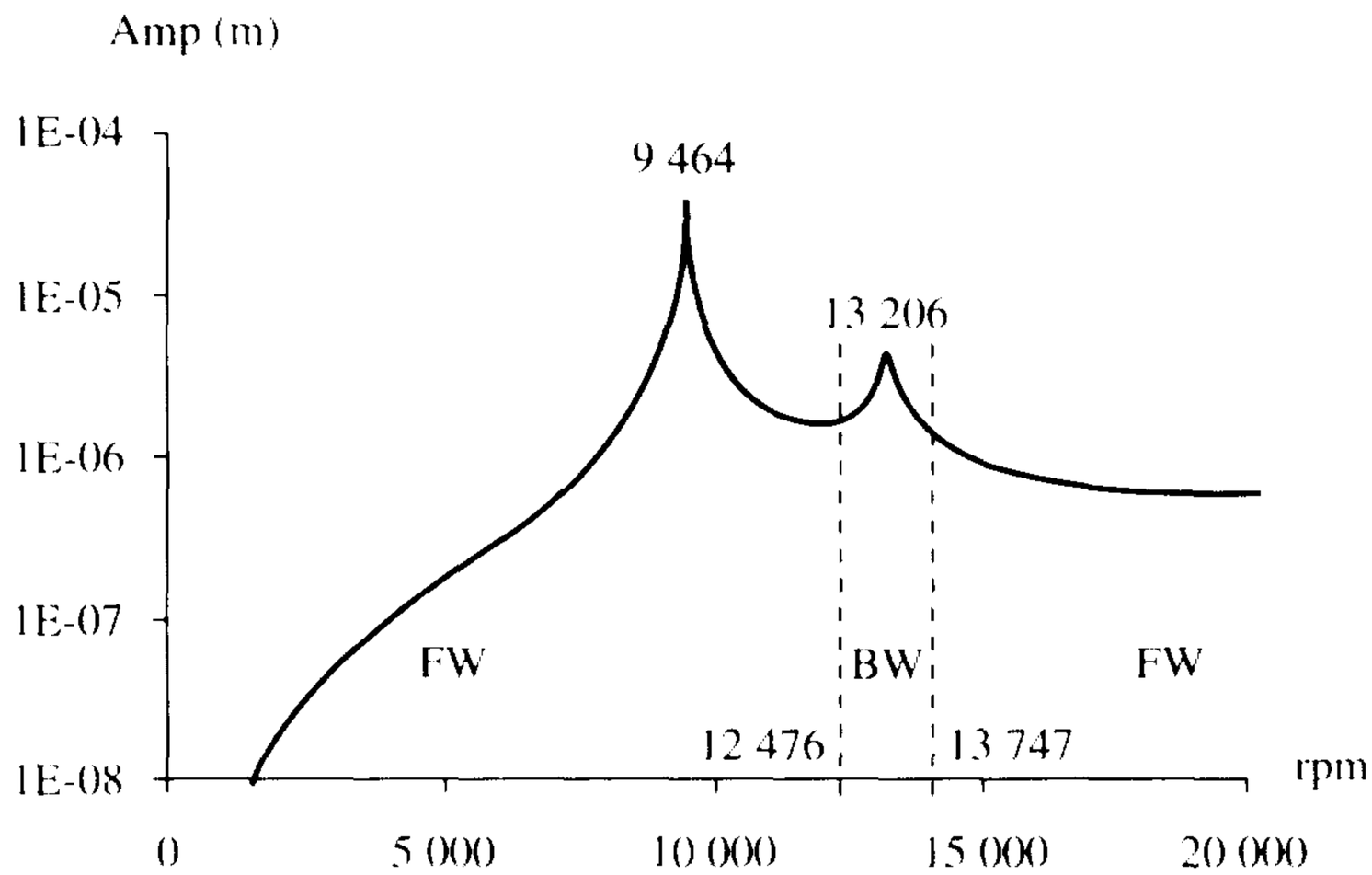

Figure 3.25. Mass unbalance response (mass on rotor 1): $n = -5, \beta = 0.0001$

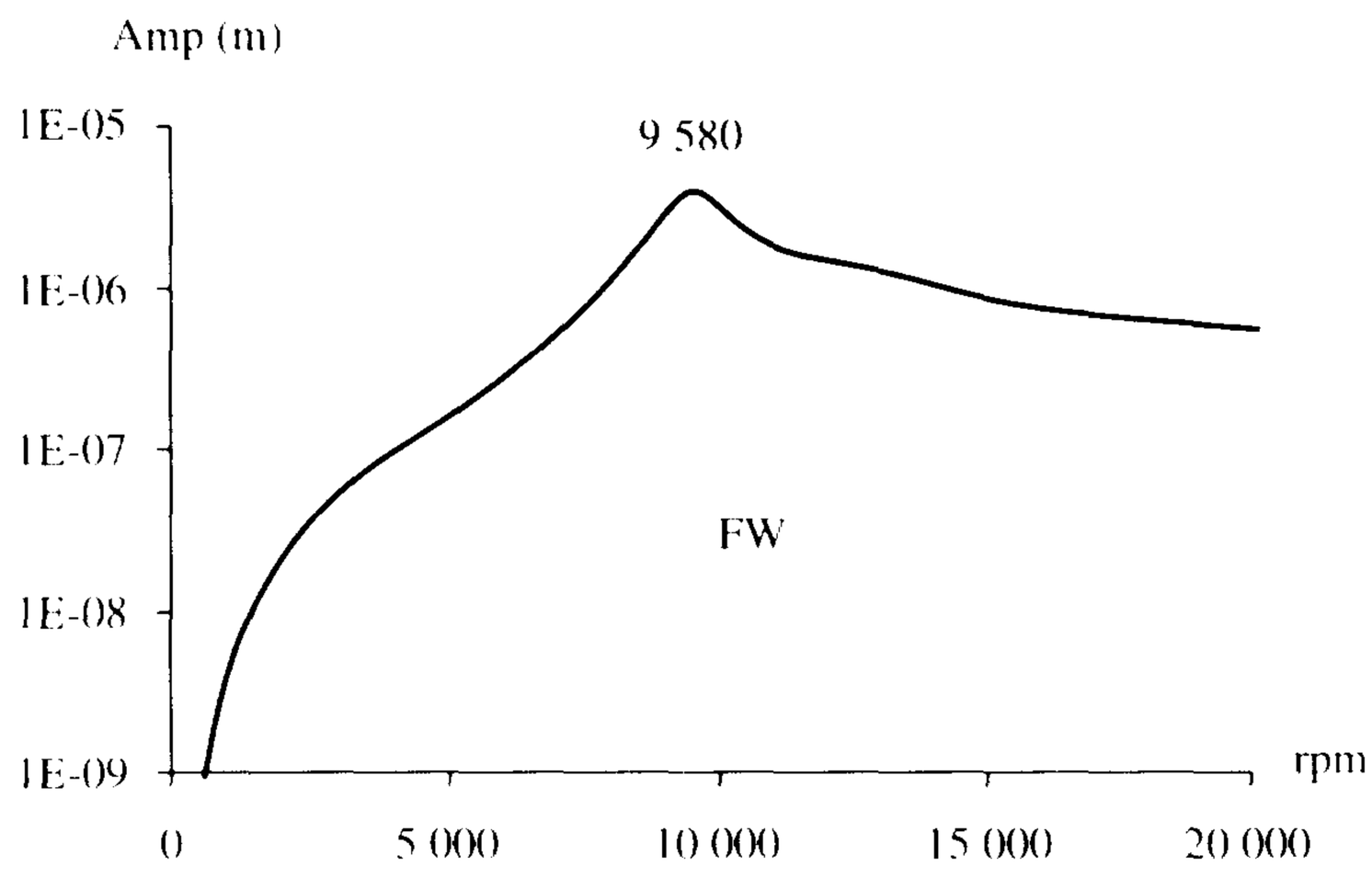

Figure 3.26. Mass unbalance response (mass on rotor 1): $n = -5, \beta = 0.001$

equations:

$$\begin{bmatrix} k_1 - m\Omega^2 & -c_1\Omega & 0 & (a_1+na_2)\Omega^2 \\ c_1\Omega & k_1 - m\Omega^2 & -(a_1+na_2)\Omega^2 & 0 \\ 0 & -(a_1+na_2)\Omega^2 & k_2 - m\Omega^2 & -c_2\Omega \\ (a_1+na_2)\Omega^2 & 0 & c_2\Omega & k_2 - m\Omega^2 \end{bmatrix} \begin{bmatrix} A_1 \\ B_1 \\ A_2 \\ B_2 \end{bmatrix} = \begin{bmatrix} m_1 d\Omega^2 \\ 0 \\ 0 \\ m_1 d\Omega^2 \end{bmatrix} \tag{3.105}$$

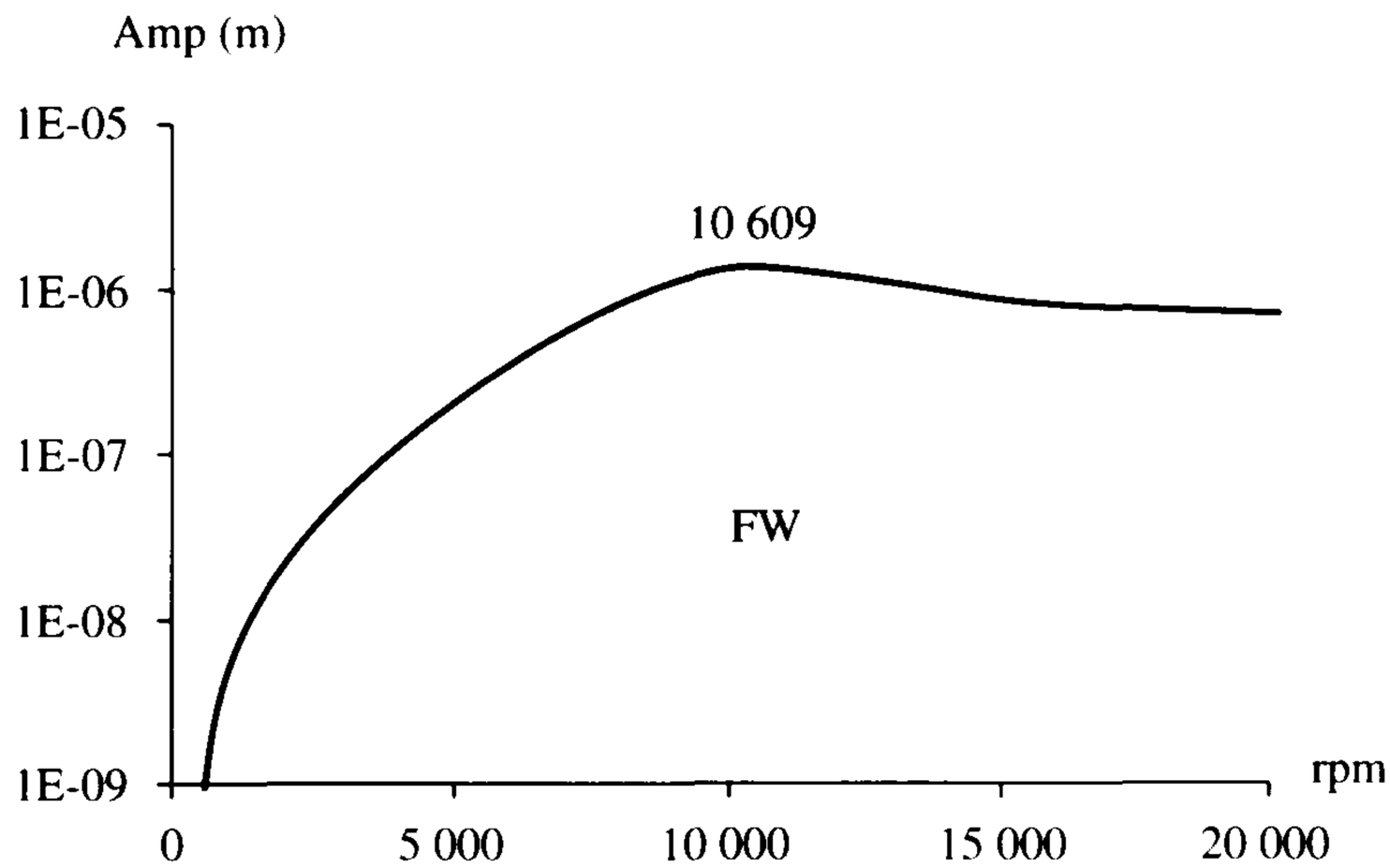

Figure 3.27. Mass unbalance response (mass on rotor 1): $n = -5, \beta = 0.005$

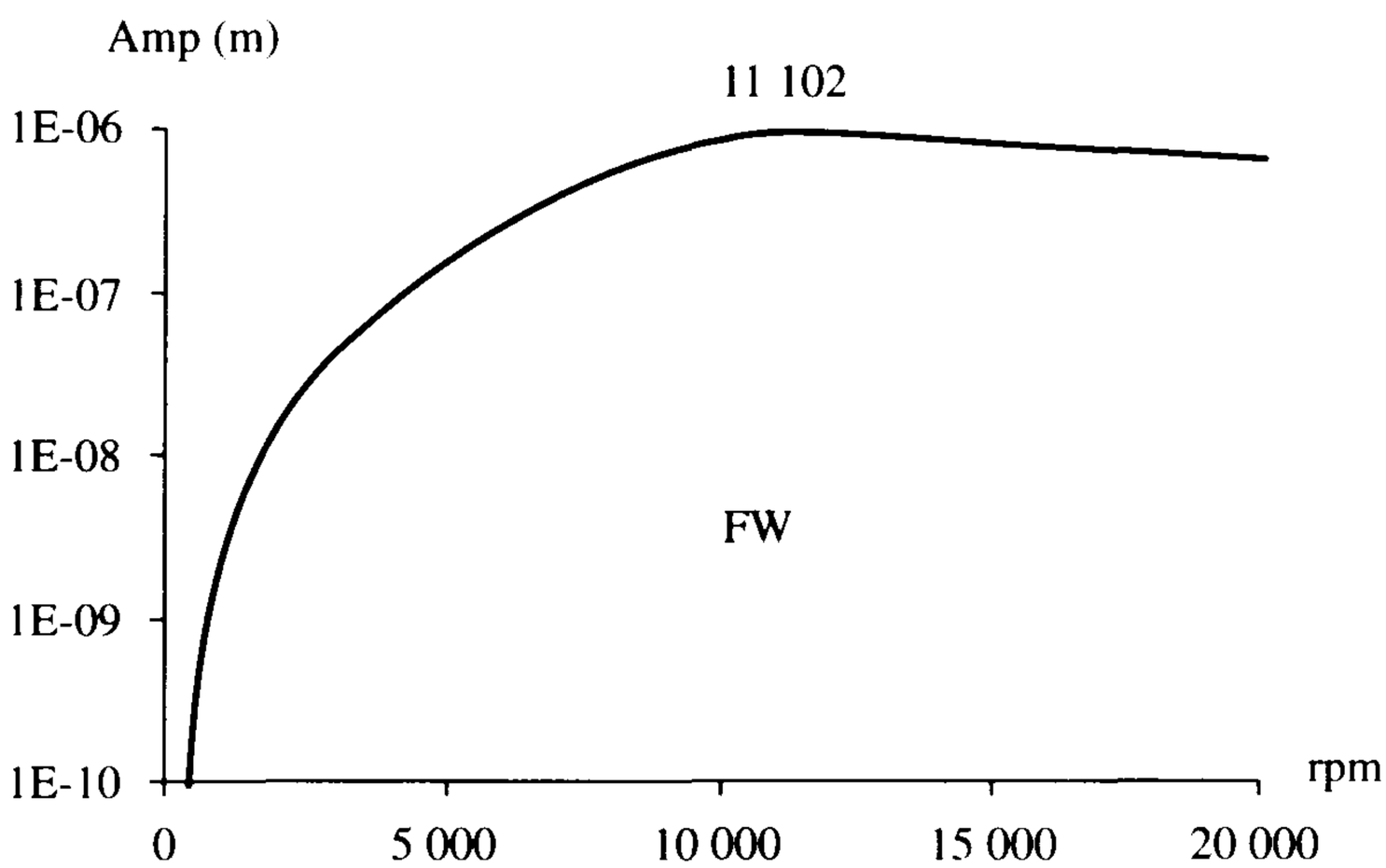

Figure 3.28. Mass unbalance response (mass on rotor 1): $n = -5, \beta = 0.007$

For each value of Ω, the solution of (3.105) gives $A_1(\Omega)$, $B_1(\Omega)$, $A_2(\Omega)$ and $B_2(\Omega)$, and using Equations (3.103) and (3.104) leads to q_1 and q_2.

In Figures 3.25 and 3.26 the responses are presented for $\beta = 0.0001$ and $\beta = 0.001$. In the first case two critical speeds appear; in the second only one critical speed exists. Figures 3.27 and 3.28 show the responses for $\beta = 0.005$ and $\beta = 0.007$: the damping is then so high that no critical speed appears.

Mass unbalance on rotor 2

The system is governed by Equations (3.98) and (3.99) with the forces given in Equations (3.29) and (3.30). The solutions are to be sought in the form

$$q_1 = A_1 \sin n\Omega t + B_1 \cos n\Omega t \tag{3.106}$$

$$q_2 = A_2 \sin n\Omega t + B_2 \cos n\Omega t \tag{3.107}$$

These are substituted in (3.98) and (3.99). This gives a set of linear

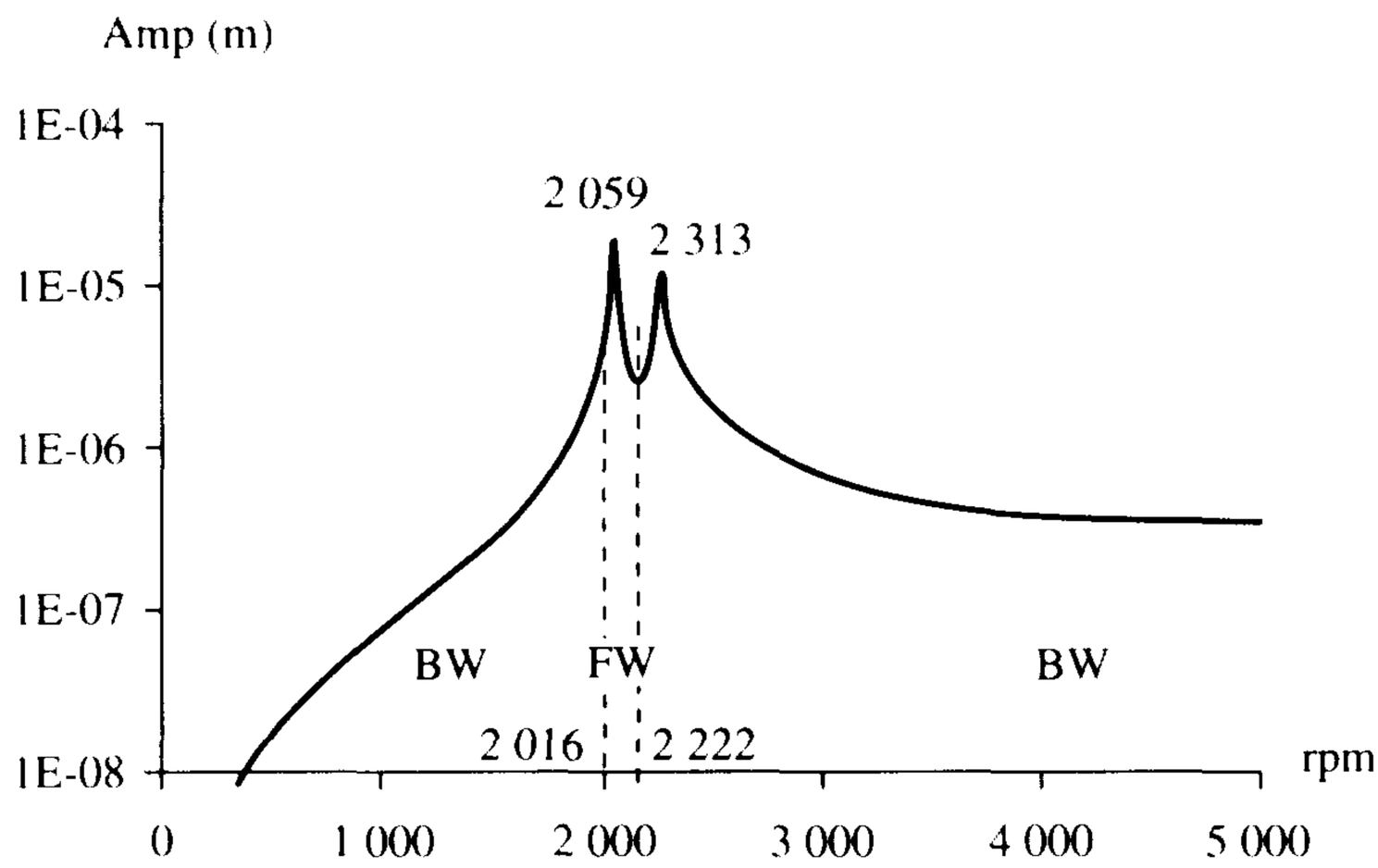

Figure 3.29. Mass unbalance response (mass on rotor 2): $n = -5, \beta = 0.0001$

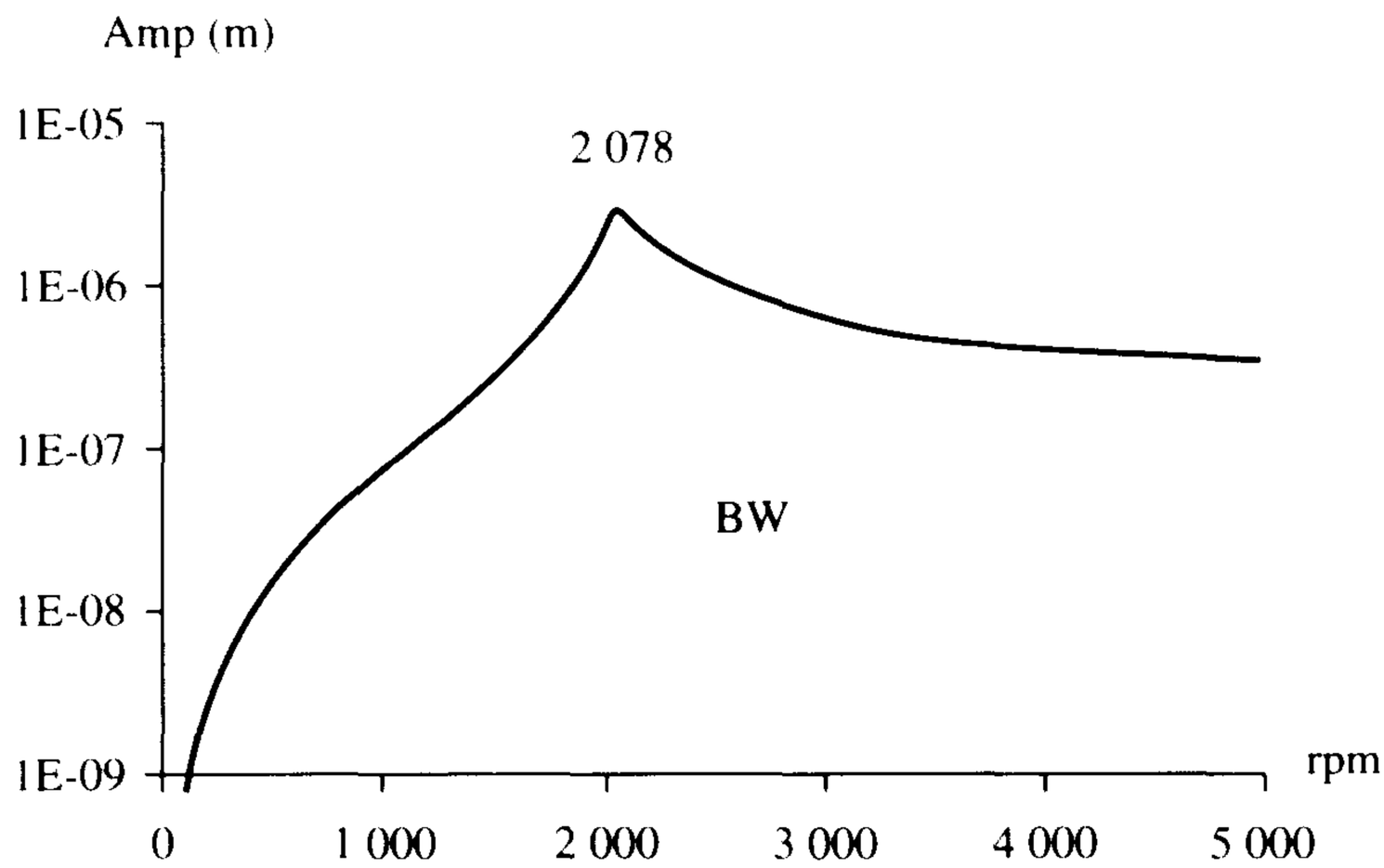

Figure 3.30. Mass unbalance response (mass on rotor 2): $n = -5, \beta = 0.001$

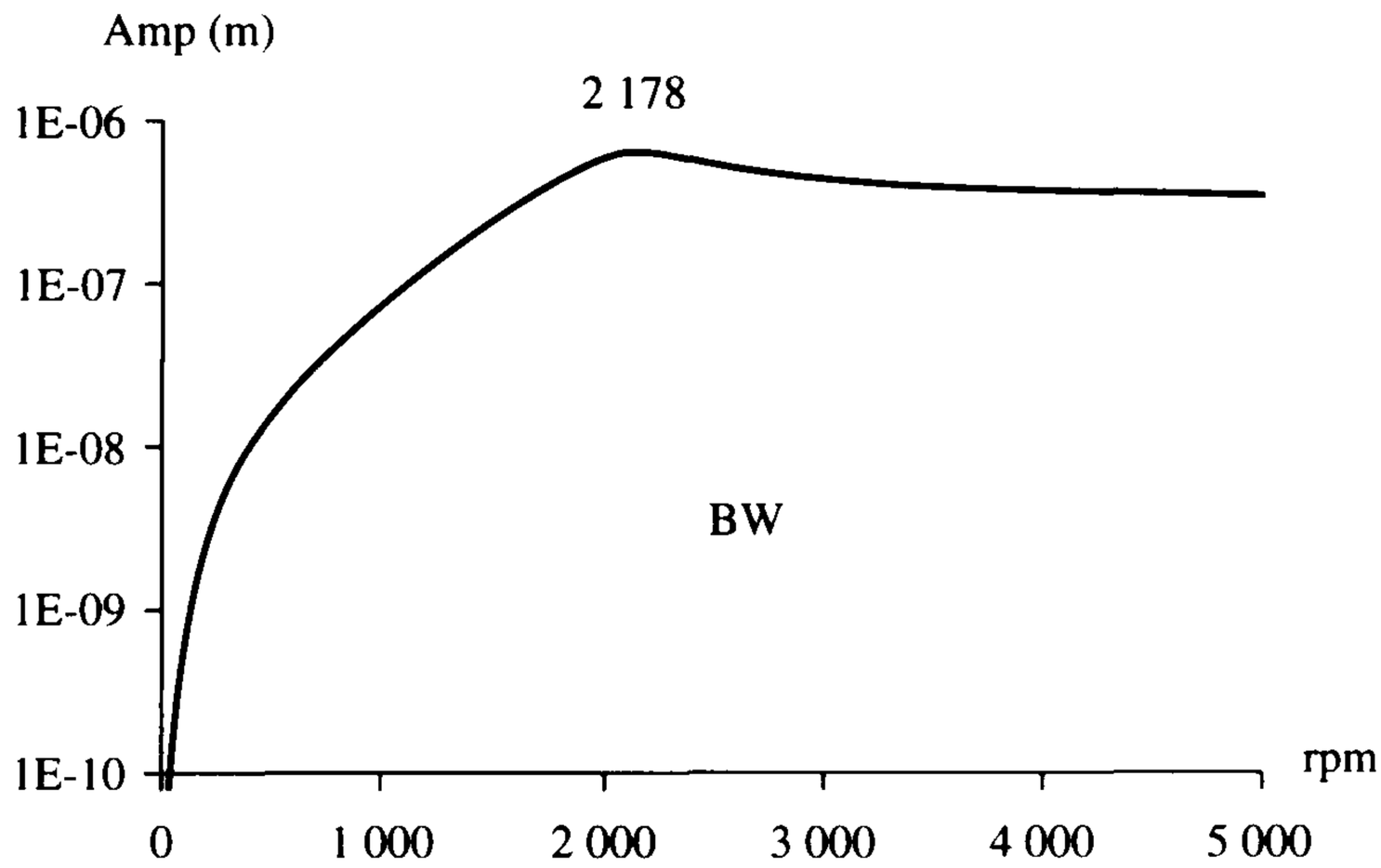

Figure 3.31. Mass unbalance response (mass on rotor 2): $n = -5, \beta = 0.005$

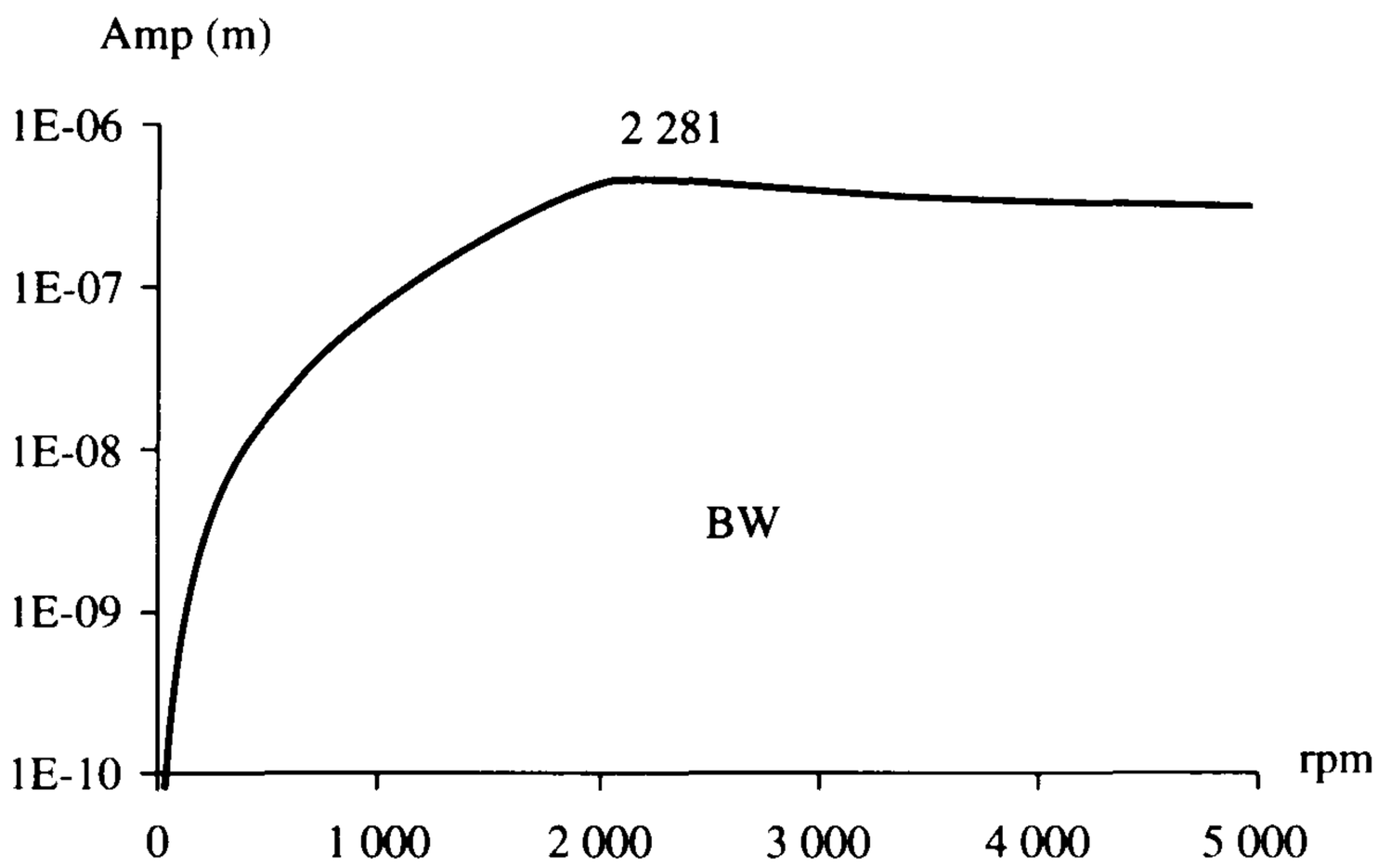

Figure 3.32. Mass unbalance response (mass on rotor 2): $n = -5, \beta = 0.007$

equations:

$$\begin{bmatrix} k_1 - mn^2\Omega^2 & -c_1 n\Omega & 0 & (a_1 + na_2)n\Omega^2 \\ c_1 n\Omega & k_1 - mn^2\Omega^2 & -(a_1 + na_2)n\Omega^2 & 0 \\ 0 & -(a_1 + na_2)n\Omega^2 & k_2 - mn^2\Omega^2 & -c_2 n\Omega \\ (a_1 + na_2)n\Omega^2 & 0 & c_2 n\Omega & k_2 - mn^2\Omega^2 \end{bmatrix}$$

$$\times \begin{bmatrix} A_1 \\ B_1 \\ A_2 \\ B_2 \end{bmatrix} = \begin{bmatrix} m_2 d n^2 \Omega^2 \\ 0 \\ 0 \\ m_2 d n^2 \Omega^2 \end{bmatrix} \tag{3.108}$$

For each value of Ω, the solution of (3.108) gives $A_1(\Omega)$, $A_2(\Omega)$, $B_1(\Omega)$ and $B_2(\Omega)$, and using Equations (3.106) and (3.107) leads to q_1 and q_2. The mass unbalance responses are shown in Figures 3.29 to 3.32. For $\beta = 0.0001$, Figure 3.29, two critical speeds appear. In Figure 3.30, $\beta = 0.001$, only one critical speed appears. In Figures 3.31 and 3.32, when the damping increases, no critical speed appears.

4

Rotor Equations: Solutions of Equations

This chapter is concerned with rotors in turbomachinery. It is devoted to monorotors and multirotors coupled by aerodynamics. General equations are presented, and the numerical methods used to solve these equations are given briefly.

4.1 FINITE ELEMENTS OF THE ROTOR PARTS

As in Chapters 1 and 2, the following have to be considered: disk, shaft, bearings and mass unbalance [46, 53].

4.1.1 The disk

At a given node the rotor has four degrees of freedom: two displacements u and w, and two slopes about the X and Z axes which are respectively θ and ψ. Then, if the nodal displacement vector δ of the disk center is

$$\delta = [u, w, \theta, \psi]^{\mathrm{T}} \tag{4.1}$$

the application of Lagrange's equations to Equation (1.6) in Chapter 1 gives

$$\frac{d}{dt}\left(\frac{\partial T}{\partial \dot{\delta}}\right) - \frac{\partial T}{\partial \delta} = \begin{bmatrix} M_{\mathrm{D}} & 0 & 0 & 0 \\ 0 & M_{\mathrm{D}} & 0 & 0 \\ 0 & 0 & I_{\mathrm{D}x} & 0 \\ 0 & 0 & 0 & I_{\mathrm{D}x} \end{bmatrix} \begin{bmatrix} \ddot{u} \\ \ddot{w} \\ \ddot{\theta} \\ \ddot{\psi} \end{bmatrix} + \Omega \begin{bmatrix} 0 & 0 & 0 & 0 \\ 0 & 0 & 0 & 0 \\ 0 & 0 & 0 & -I_{\mathrm{D}y} \\ 0 & 0 & I_{\mathrm{D}y} & 0 \end{bmatrix} \begin{bmatrix} \dot{u} \\ \dot{w} \\ \dot{\theta} \\ \dot{\psi} \end{bmatrix} \tag{4.2}$$

where the first matrix is the classical mass matrix and the second one is the gyroscopic (Coriolis) matrix.

4.1.2 The shaft

The shaft is modeled as a beam with a constant circular cross-section. The finite element used has two nodes, so the matrices are eighth-order, including four displacements and four slopes (Figure 4.1). The relations between displacements and slopes are

$$\theta = \frac{\partial w}{\partial y} \tag{4.3}$$

$$\psi = -\frac{\partial u}{\partial y} \tag{4.4}$$

and the nodal displacement vector is

$$\delta = [u_1, w_1, \theta_1, \psi_1, u_2, w_2, \theta_2, \psi_2]^{\mathrm{T}} \tag{4.5}$$

which includes the displacements δu and δw corresponding respectively to the motions in the X and Z directions; that is

$$\delta_u = [u_1, \psi_1, u_2, \psi_2]^{\mathrm{T}} \tag{4.6}$$

$$\delta_w = [w_1, \theta_1, w_2, \theta_2]^{\mathrm{T}} \tag{4.7}$$

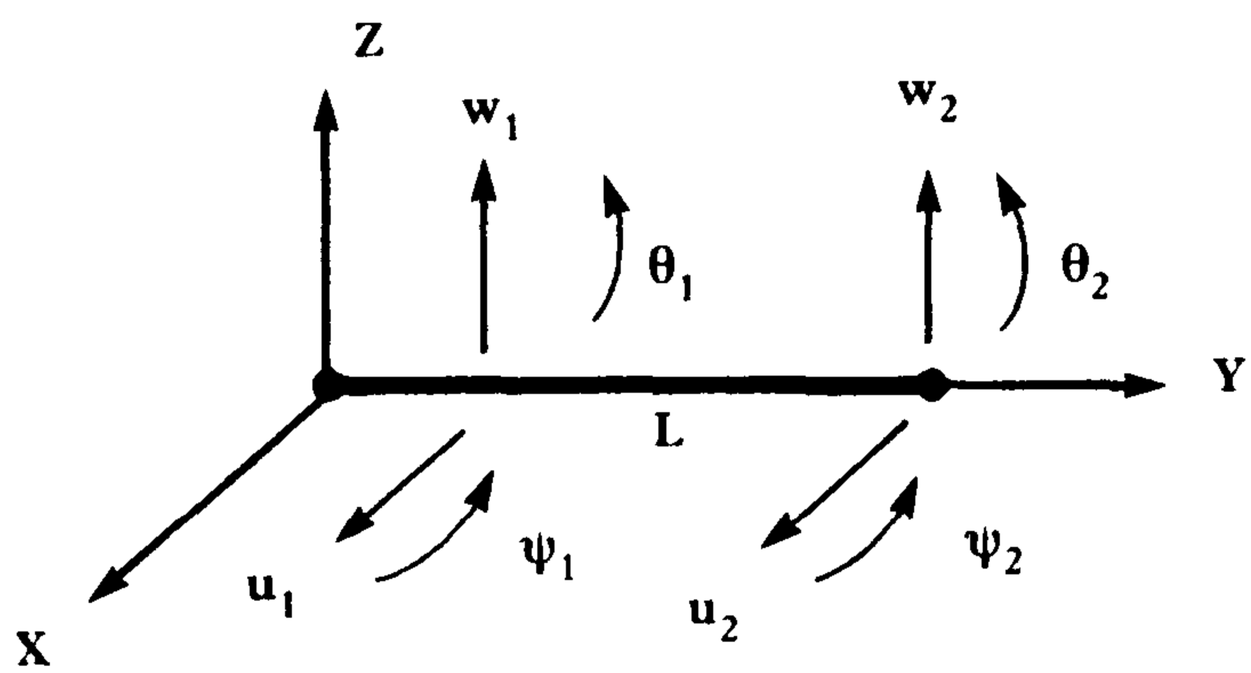

Figure 4.1. Shaft finite element

The finite element is built from

$$u = N_1(y)\delta u \tag{4.8}$$

$$w = N_2(y)\delta w \tag{4.9}$$

where $N_1(y)$ and $N_2(y)$ are the typical displacement functions of a beam in bending:

$$N_1(y) = \left[1 - \frac{3y^2}{L^2} + \frac{2y^3}{L^3};\ -y + \frac{2y^2}{L} - \frac{y^3}{L^2};\ \frac{3y^2}{L^2} - \frac{2y^3}{L^3};\ \frac{y^2}{L} - \frac{y^3}{L^2}\right] \tag{4.10}$$

$$N_2(y) = \left[1 - \frac{3y^2}{L^2} + \frac{2y^3}{L^3};\ y - \frac{2y^2}{L} + \frac{y^3}{L^2};\ \frac{3y^2}{L^2} - \frac{2y^3}{L^3};\ -\frac{y^2}{L} + \frac{y^3}{L^2}\right] \tag{4.11}$$

The kinetic energy of the shaft is obtained from Equation (1.7) in Chapter 1, which gives, in a compact form,

$$\begin{aligned} T = &\frac{\rho S}{2}\int_0^L [\delta\dot{u}^{\mathrm{T}} N_1^{\mathrm{T}} N_1 \delta\dot{u} + \delta\dot{w}^{\mathrm{T}} N_2^{\mathrm{T}} N_2 \delta\dot{w}]\mathrm{d}y \\ &+ \frac{\rho I}{2}\int_0^L \left[\delta\dot{u}^{\mathrm{T}} \frac{\mathrm{d}N_1^{\mathrm{T}}}{\mathrm{d}y}\frac{\mathrm{d}N_1}{\mathrm{d}y}\delta\dot{u} + \delta\dot{w}^{\mathrm{T}} \frac{\mathrm{d}N_2^{\mathrm{T}}}{\mathrm{d}y}\frac{\mathrm{d}N_2}{\mathrm{d}y}\delta\dot{w}\right]\mathrm{d}y \\ &- 2\rho I\Omega \int_0^L \delta\dot{u}^{\mathrm{T}} \frac{\mathrm{d}N_1^{\mathrm{T}}}{\mathrm{d}y}\frac{\mathrm{d}N_2}{\mathrm{d}y}\delta w \mathrm{d}y + \rho I L \Omega^2 \end{aligned} \tag{4.12}$$

Substituting (4.10) and (4.11) and their derivatives in Equation (4.12) gives, after integration:

$$\begin{aligned} T = &\tfrac{1}{2}\delta\dot{u}^{\mathrm{T}} M_1 \delta\dot{u} + \tfrac{1}{2}\delta\dot{w}^{\mathrm{T}} M_2 \delta\dot{w} + \tfrac{1}{2}\delta\dot{u}^{\mathrm{T}} M_3 \delta\dot{u} \\ &+ \tfrac{1}{2}\delta\dot{w}^{\mathrm{T}} M_4 \delta\dot{w} + \Omega\delta\dot{u}^{\mathrm{T}} M_5 \delta w + \rho I L \Omega^2 \end{aligned} \tag{4.13}$$

where the matrices M_1 and M_2 are the classical mass matrices, M_3 and M_4 give the influence of the secondary effect of rotatory inertia, and M_5 gives the gyroscopic effect. As has been observed previously, the last term which is a constant, is not considered any more. The application of Lagrange's equations to (4.13) gives

$$\frac{\mathrm{d}}{\mathrm{d}t}\left(\frac{\partial T}{\partial \dot{\delta}}\right) - \frac{\partial T}{\partial \delta} = (M + M_s)\ddot{\delta} + C\dot{\delta} \tag{4.14}$$

where M and M_s are obtained respectively from M_1, M_2 and M_3, M_4, and the matrix C comes from M_5. These matrices are

$$M = \frac{\rho SL}{420}\begin{bmatrix} 156 & 0 & 0 & -22L & 54 & 0 & 0 & 13L \\ 0 & 156 & 22L & 0 & 0 & 54 & -13L & 0 \\ 0 & 22L & 4L^2 & 0 & 0 & 13L & -3L^2 & 0 \\ -22L & 0 & 0 & 4L^2 & -13L & 0 & 0 & -3L^2 \\ 54 & 0 & 0 & -13L & 156 & 0 & 0 & 22L \\ 0 & 54 & 13L & 0 & 0 & 156 & -22L & 0 \\ 0 & -13L & -3L^2 & 0 & 0 & -22L & 4L^2 & 0 \\ 13L & 0 & 0 & -3L^2 & 22L & 0 & 0 & 4L^2 \end{bmatrix} \tag{4.15}$$

$$M_s = \frac{\rho I}{30L}\begin{bmatrix} 36 & 0 & 0 & -3L & -36 & 0 & 0 & -3L \\ 0 & 36 & 3L & 0 & 0 & -36 & 3L & 0 \\ 0 & 3L & 4L^2 & 0 & 0 & -3L & -L^2 & 0 \\ -3L & 0 & 0 & 4L^2 & 3L & 0 & 0 & -L^2 \\ -36 & 0 & 0 & 3L & 36 & 0 & 0 & 3L \\ 0 & -36 & -3L & 0 & 0 & 36 & -3L & 0 \\ 0 & 3L & -L^2 & 0 & 0 & -3L & 4L^2 & 0 \\ -3L & 0 & 0 & -L^2 & 3L & 0 & 0 & 4L^2 \end{bmatrix} \tag{4.16}$$

$$C = \frac{\rho I\Omega}{15L}\begin{bmatrix} 0 & -36 & -3L & 0 & 0 & 36 & -3L & 0 \\ 36 & 0 & 0 & -3L & -36 & 0 & 0 & -3L \\ 3L & 0 & 0 & -4L^2 & -3L & 0 & 0 & L^2 \\ 0 & 3L & 4L^2 & 0 & 0 & -3L & -L^2 & 0 \\ 0 & 36 & 3L & 0 & 0 & -36 & 3L & 0 \\ -36 & 0 & 0 & 3L & 36 & 0 & 0 & 3L \\ 3L & 0 & 0 & L^2 & -3L & 0 & 0 & -4L^2 \\ 0 & 3L & -L^2 & 0 & 0 & -3L & 4L^2 & 0 \end{bmatrix} \tag{4.17}$$

The strain energy of the shaft is obtained from (4.8), (4.9) and Equation (1.25) in Chapter 1, which give

$$\begin{aligned} U = {} & \frac{EI}{2}\int_0^L \left[\delta u^{\mathrm{T}} \frac{\mathrm{d}^2 N_1^{\mathrm{T}}}{\mathrm{d}y^2}\frac{\mathrm{d}^2 N_1}{\mathrm{d}y^2}\delta u + \delta w^{\mathrm{T}} \frac{\mathrm{d}^2 N_2^{\mathrm{T}}}{\mathrm{d}y^2}\frac{\mathrm{d}^2 N_2}{\mathrm{d}y^2}\delta w\right]\mathrm{d}y \\ & + \frac{F_0}{2}\int_0^L \left[\delta u^{\mathrm{T}} \frac{\mathrm{d}N_1^{\mathrm{T}}}{\mathrm{d}y}\frac{\mathrm{d}N_1}{\mathrm{d}y}\delta u + \delta w^{\mathrm{T}} \frac{\mathrm{d}N_2^{\mathrm{T}}}{\mathrm{d}y}\frac{\mathrm{d}N_2}{\mathrm{d}y}\delta w\right]\mathrm{d}y \end{aligned} \tag{4.18}$$

After integration U becomes

$$U = \tfrac{1}{2}\delta u^{\mathrm{T}} K_1 \delta u + \tfrac{1}{2}\delta w^{\mathrm{T}} K_2 \delta w + \tfrac{1}{2}\delta u^{\mathrm{T}} K_3 \delta u + \tfrac{1}{2}\delta w^{\mathrm{T}} K_4 \delta w \tag{4.19}$$

where K_1 and K_2 are the classical stiffness matrices, and K_3 and K_4 the matrices due to the axial forces. It is also frequently necessary to take into account the shear effect, which is characterized by the quantity

$$a = \frac{12EI}{GS_{\mathrm{r}}L^2} \tag{4.20}$$

with the shear modulus

$$G = \frac{E}{2(1+v)} \tag{4.21}$$

where v is Poisson's ratio, and $S_{\mathrm{r}}(\simeq S)$ is the reduced area of the cross-section.

The influence of the shear effect which gives a matrix K_{S} is not demonstrated here, but its influence is included in the classical stiffness matrix [31]. The classical stiffness matrix K_{C} comes from K_1, K_2 and K_{S}, and the matrix K_{F} due to the axial force comes from K_3 and K_4. Then if Lagrange's equations are applied to (4.19) we have

$$\frac{\partial U}{\partial \delta} = K\delta \tag{4.22}$$

with

$$K = K_{\mathrm{C}} + K_{\mathrm{F}} \tag{4.23}$$

The expressions of the matrices are as follows:

$$K_{\mathrm{C}} = \frac{EI}{(1+a)L^3}\begin{bmatrix} 12 & 0 & 0 & -6L & -12 & 0 & 0 & -6L \\ 0 & 12 & 6L & 0 & 0 & -12 & 6L & 0 \\ 0 & 6L & (4+a)L^2 & 0 & 0 & -6L & (2-a)L^2 & 0 \\ -6L & 0 & 0 & (4+a)L^2 & 6L & 0 & 0 & (2-a)L^2 \\ -12 & 0 & 0 & 6L & 12 & 0 & 0 & 6L \\ 0 & -12 & -6L & 0 & 0 & 12 & -6L & 0 \\ 0 & 6L & (2-a)L^2 & 0 & 0 & -6L & (4+a)L^2 & 0 \\ -6L & 0 & 0 & (2-a)L^2 & 6L & 0 & 0 & (4+a)L^2 \end{bmatrix} \tag{4.24}$$

(If $a = 0$, (4.24) is the classical stiffness matrix of a beam in bending.)

$$K_F = \frac{F}{30L}\begin{bmatrix} 36 & 0 & 0 & -3L & -36 & 0 & 0 & -3L \\ 0 & 36 & 3L & 0 & 0 & -36 & 3L & 0 \\ 0 & 3L & 4L^2 & 0 & 0 & -3L & -L^2 & 0 \\ -3L & 0 & 0 & 4L^2 & 3L & 0 & 0 & -L^2 \\ -36 & 0 & 0 & 3L & 36 & 0 & 0 & 3L \\ 0 & -36 & -3L & 0 & 0 & 36 & -3L & 0 \\ 0 & 3L & -L^2 & 0 & 0 & -3L & 4L^2 & 0 \\ -3L & 0 & 0 & -L^2 & 3L & 0 & 0 & 4L^2 \end{bmatrix} \tag{4.25}$$

4.1.3 Bearings and seals

The main characteristics link forces and displacements, and the influence of slopes and bending moments is neglected here. The matrices are directly obtained from (1.26) and (1.27) in Chapter 1, which give

$$F_u = -k_{xx}u - k_{xz}w - c_{xx}\dot{u} - c_{xz}\dot{w} \tag{4.26}$$

$$F_w = -k_{zz}w - k_{zx}u - c_{zz}\dot{w} - c_{zx}\dot{u} \tag{4.27}$$

As $F_\theta = F_\psi = 0$, we have

$$\begin{bmatrix} F_u \\ F_\theta \\ F_w \\ F_\psi \end{bmatrix} = -\begin{bmatrix} k_{xx} & 0 & k_{xz} & 0 \\ 0 & 0 & 0 & 0 \\ k_{zx} & 0 & k_{zz} & 0 \\ 0 & 0 & 0 & 0 \end{bmatrix}\begin{bmatrix} u \\ \theta \\ w \\ \psi \end{bmatrix} - \begin{bmatrix} c_{xx} & 0 & c_{xz} & 0 \\ 0 & 0 & 0 & 0 \\ c_{zx} & 0 & c_{zz} & 0 \\ 0 & 0 & 0 & 0 \end{bmatrix}\begin{bmatrix} \dot{u} \\ \dot{\theta} \\ \dot{w} \\ \dot{\psi} \end{bmatrix} \tag{4.28}$$

The first matrix is a stiffness matrix and the second a viscous damping matrix. These matrices are generally asymmetric (i.e. $k_{xz} \neq k_{zx}$ and $c_{xz} \neq c_{zx}$) and the terms of the matrices can vary significantly as a function of the speed of rotation.

4.1.4 Mass unbalance

The general expression for the kinetic energy of the mass unbalance was given in Equation (1.34) in Chapter 1, and the application of Lagrange's

equations gives

$$\frac{\mathrm{d}}{\mathrm{d}t}\frac{\partial T}{\partial \dot{\delta}} - \frac{\partial T}{\partial \delta} = -m_{\mathrm{u}} d \Omega^2 \begin{bmatrix} \sin \Omega t \\ \cos \Omega t \end{bmatrix} \tag{4.29}$$

with

$$\delta = [u, w]^{\mathrm{T}} \tag{4.30}$$

The expression (4.29) corresponds to a mass unbalance situated on the z axis at $t = 0$. When industrial rotors are studied, the influence of several mass unbalances acting simultaneously has to be considered. For a mass unbalance situated at $t = 0$ at an angular position α with respect to the z axis, the forces become

$$\begin{bmatrix} F_u \\ F_w \end{bmatrix} = m_{\mathrm{u}} d \Omega^2 \begin{bmatrix} \sin(\Omega t + \alpha) \\ \cos(\Omega t + \alpha) \end{bmatrix} \tag{4.31}$$

which can be written as

$$\begin{bmatrix} F_u \\ F_w \end{bmatrix} = F_2 \sin \Omega t + F_3 \cos \Omega t \tag{4.32}$$

with

$$F_2 = m_{\mathrm{u}} d \Omega^2 \begin{bmatrix} \cos \alpha \\ -\sin \alpha \end{bmatrix} \tag{4.33}$$

and

$$F_3 = m_{\mathrm{u}} d \Omega^2 \begin{bmatrix} \sin \alpha \\ \cos \alpha \end{bmatrix} \tag{4.34}$$

4.2 EQUATIONS FOR MONOROTORS

When Lagrange's equations are applied to a monorotor the general system equation becomes

$$M\ddot{\delta} + C(\Omega)\dot{\delta} + K\delta = F(t) \tag{4.35}$$

with

$$F(t) = F_1 + F_2 \sin \Omega t + F_3 \cos \Omega t + F_4 \sin s\Omega t + F_5 \cos s\Omega t + F_6 \sin \omega t + F_7 \cos \omega t \tag{4.36}$$

where δ is the vector containing now all the nodal displacements; M is the symmetric mass matrix; C is the asymmetric matrix, including an antisymmetric gyroscopic matrix function of Ω, and a frequently asymmetric matrix owing to the characteristics of the bearings; K is the stiffness matrix, frequently asymmetric owing to the characteristics of the bearings; and $F(t)$, the force vector, includes a constant vector F_1 corresponding, for example, to the gravity influence, F_2, F_3 and F_4, F_5 corresponding respectively to the mass unbalances and the asynchronous forces, and F_6 and F_7 corresponding to harmonic forces fixed in space.

4.3 EQUATIONS FOR COAXIAL MULTIROTORS

Figure 4.2 shows two coaxial rotors linked by an intershaft bearing [3]. The two rotors R_1 and R_2 rotate at different speeds Ω_1 and Ω_2 and are aerodynamically coupled.

The displacements u_1 and w_1 for rotor 1 and u_2 and w_2 for rotor 2 correspond to the same point on the axis of rotation. As the intershaft bearing can be considered as short, the slope influence is neglected. Let R_1 and R_2 be the reactions of rotor 1 and rotor 2 on the bearing, the mass of which is neglected (or concentrated on rotors 1 and 2). If

$$R_1 = \begin{bmatrix} R_{1x} \\ R_{1z} \end{bmatrix} \tag{4.37}$$

and

$$R_{1x} = F_{u1} \tag{4.38}$$

$$R_{1z} = F_{w1} \tag{4.39}$$

then

$$R_1 = \begin{bmatrix} k_{xx} & k_{xz} \\ k_{zx} & k_{zz} \end{bmatrix} \begin{bmatrix} u_1 - u_2 \\ w_1 - w_2 \end{bmatrix} + \begin{bmatrix} c_{xx} & c_{xz} \\ c_{zx} & c_{zz} \end{bmatrix} \begin{bmatrix} \dot{u}_1 - \dot{u}_2 \\ \dot{w}_1 - \dot{w}_2 \end{bmatrix} \tag{4.40}$$

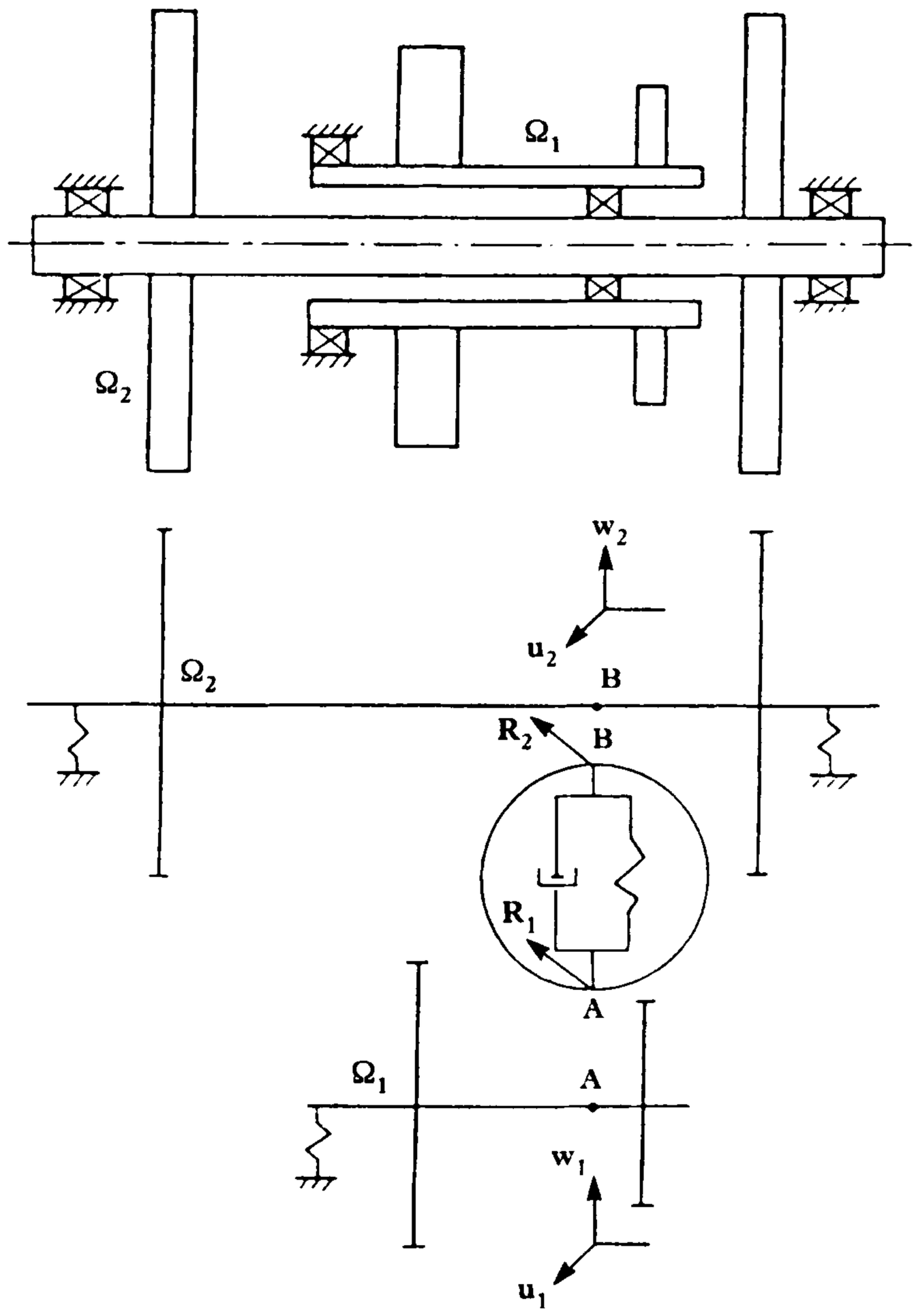

Figure 4.2. Dual rotor model

which can be compacted to

$$R_1 = K\begin{bmatrix} u_1 - u_2 \\ w_1 - w_2 \end{bmatrix} + C\begin{bmatrix} \dot{u}_1 - \dot{u}_2 \\ \dot{w}_1 - \dot{w}_2 \end{bmatrix} \tag{4.41}$$

with

$$K = \begin{bmatrix} k_{xx} & k_{xz} \\ k_{zx} & k_{zz} \end{bmatrix} \tag{4.42}$$

$$C = \begin{bmatrix} c_{xx} & c_{xz} \\ c_{zx} & c_{zz} \end{bmatrix} \tag{4.43}$$

As the mass of the bearing is neglected,

$$R_1 + R_2 = 0 \tag{4.44}$$

and so finally

$$\begin{bmatrix} R_1 \\ R_2 \end{bmatrix} = \begin{bmatrix} K & -K \\ -K & K \end{bmatrix} \begin{bmatrix} u_1 \\ w_1 \\ u_2 \\ w_2 \end{bmatrix} + \begin{bmatrix} C & -C \\ -C & C \end{bmatrix} \begin{bmatrix} \dot{u}_1 \\ \dot{w}_1 \\ \dot{u}_2 \\ \dot{w}_2 \end{bmatrix} \tag{4.45}$$

T and U, the kinetic and strain energies are now calculated for each rotor. Lagrange's equations are written, and so

$$\text{Rotor 1: } M_1\ddot{\delta}_1 + C_1(\Omega_1)\dot{\delta}_1 + K_1\delta_1 = F_1(t) - R_1 \tag{4.46}$$

$$\text{Rotor 2: } M_2\ddot{\delta}_2 + C_2(\Omega_2)\dot{\delta}_2 + K_2\delta_2 = F_2(t) - R_2 \tag{4.47}$$

where M_1, M_2, C_1, C_2, K_1, K_2, $F_1(t)$ and $F_2(t)$ are matrices such as those of Section 4.2, and where δ_1 and δ_2 are the nodal displacements. From (4.45), (4.46) and (4.47), R_1 and R_2 can be canceled, and so

$$M\ddot{\delta} + C(\Omega_1, \Omega_2)\dot{\delta} + K\delta = F(t) \tag{4.48}$$

where M is the symmetric mass matrix, C is the asymmetric matrix, K is the asymmetric stiffness matrix, and δ is the nodal displacement vector.

The three matrices M, C and K come respectively from the assembly of M_1 and M_2 ; $C_1(\Omega_2)$ and C bearings; and K_1, K_2 and K bearings. In addition, owing to the aerodynamic properties of the system:

$$\Omega_1 = a\Omega_2 + b \tag{4.49}$$

where a and b are known constants.

Coupling between shafts can also be a mechanical coupling with $a \neq 0$, $b = 0$ as in [9] and application 7.7, or with $a = -1$, $b = 0$ as in [19], [41] and application 7.6.

4.4 SOLUTION OF EQUATIONS

Owing to the relation (4.49), which must be taken in association with (4.48), the equations of monorotors and coaxial multirotors can be

considered to be of the same type; that is

$$M\ddot{\delta} + C(\Omega)\dot{\delta} + K\delta = F(t) \tag{4.50}$$

which is the same equation as (4.35). As in Chapter 2, it is necessary to obtain:

- the natural frequencies as a function of the speed of rotation, the Campbell diagram, and zones of instability;
- the effects of the forces of excitation: mass unbalance, asynchronous force, harmonic force fixed in space.

In general the order of the system has to be reduced. Either Equation (4.50) has to be solved by the direct method, or the order N of the system of equations is greatly reduced and the new equations obtained from a pseudo-modal method are solved.

4.4.1 The pseudo-modal method

The pseudo-modal method [2, 4] allows a big reduction in computer time and core memory. The results obtained are very close to those obtained by the direct method. In addition it is possible here to introduce in the equations modal dampings, which is of interest when the damping is low, the mechanism of damping not well known and the modes reasonably uncoupled. From Equation (4.50) a modal basis is defined by the solutions of

$$M\ddot{\delta} + K^*\delta = 0 \tag{4.51}$$

M is the mass matrix; K^* is the stiffness matrix, obtained from K, where terms such as k_{xz} and k_{zx} introduced by the bearings are canceled. The n lowest mode shapes of (4.51) are easily obtained using a simultaneous iterative technique. The n first modes $\phi_1, \ldots, \phi_n$ form a matrix:

$$\phi = [\phi_1, \ldots, \phi_n] \tag{4.52}$$

which is used to obtain a new set of equations from

$$\delta = \phi p \tag{4.53}$$

This gives, from (4.50) after a premultiplication by ϕ^{T}:

$$\phi^{\mathrm{T}}M\phi\ddot{p} + \phi^{\mathrm{T}}C(\Omega)\phi\dot{p} + \phi^{\mathrm{T}}K\phi p = \phi^{\mathrm{T}}F(t) \tag{4.54}$$

Then modal damping can be introduced in the equations: by analogy with a one-degree-of-freedom system (mass, spring, viscous damper), terms c_i such as

$$c_i = 2\alpha_i\sqrt{\phi_i^{\mathrm{T}}K\phi_i \cdot \phi_i^{\mathrm{T}}M\phi_i} \tag{4.55}$$

are added on the diagonal of the matrix $\phi^{\mathrm{T}}C\phi$. The values of α_i, the modal damping factor, are essentially taken from machine designer experience.

Natural frequencies, the Campbell diagram, zones of instability

The solutions of (4.54) with no external forces:

$$\phi^{\mathrm{T}}M\phi\ddot{p} + \phi^{\mathrm{T}}C(\Omega)\phi\dot{p} + \phi^{\mathrm{T}}K\phi p = 0 \tag{4.56}$$

are sought for different values of Ω. The form chosen is

$$p = Pe^{rt} \tag{4.57}$$

which gives

$$[r^2m + rc + k]P = 0 \tag{4.58}$$

with

$$m = \phi^{\mathrm{T}}M\phi = \mathrm{diag}\ \{\phi_i^{\mathrm{T}}M\phi_i\} \tag{4.59}$$

$$k = \phi^{\mathrm{T}}K\phi = \mathrm{diag}\ \{\phi_i^{\mathrm{T}}K^*\phi_i\} + \phi_i^{\mathrm{T}}K^{**}\phi_i \tag{4.60}$$

and

$$K^{**} = K - K^*$$

In addition:

$$c = \phi^{\mathrm{T}}C\phi + \mathrm{diag}\ \{C_i\} \tag{4.62}$$

Equation (4.58) can be written as

$$\begin{bmatrix} 0 & I \\ -k^{-1}m & -k^{-1}c \end{bmatrix} \begin{bmatrix} rP \\ P \end{bmatrix} = \frac{1}{r} \begin{bmatrix} rP \\ P \end{bmatrix} \tag{4.63}$$

The eigenvalues/eigenvectors (natural frequencies and mode shapes) of (4.63) are complex quantities and are obtained using the Q.R. [56] algorithm. Eigenvalues are of the type $-\alpha_i\omega_i/(1-\alpha_i^2)^{1/2} \pm j\omega_i$, where ω_i is the frequency and α_i is the viscous damping factor; if $-\alpha_i\omega_i/(1-\alpha_i^2)^{1/2} > 0$ the system is unstable. From the results obtained, the Campbell diagram can be drawn and the critical speeds found.

Response to forces of excitation

Here the steady-state response is calculated; hence the general solution of (4.50) with $F(t) = 0$ does not have to be used.

Constant force

$$K\delta = F_1 \tag{4.64}$$

It is easy to solve the equations directly by the well-known Gaussian method.

Mass unbalance

The equations to be solved are

$$m\ddot{p} + c\dot{p} + kp = f_2 \sin \Omega t + f_3 \cos \Omega t \tag{4.65}$$

with

$$f_2 = \phi^{\mathrm{T}} F_2 \tag{4.66}$$

$$f_3 = \phi^{\mathrm{T}} F_3 \tag{4.67}$$

Solutions are sought as

$$p = p_2 \sin \Omega t + p_3 \cos \Omega t \tag{4.68}$$

and identification of the terms in $\sin \Omega t$ and $\cos \Omega t$ gives the equation

$$\begin{bmatrix} k - m\Omega^2 & -\Omega c \\ \Omega c & k - m\Omega^2 \end{bmatrix} \begin{bmatrix} p_2 \\ p_3 \end{bmatrix} = \begin{bmatrix} f_2 \\ f_3 \end{bmatrix} \tag{4.69}$$

This system (4.69) is solved for given values of Ω, and the values of $p_2(\Omega)$ and $p_3(\Omega)$ associated with (4.53) give the displacement vector

$$\delta = \phi[p_2(\Omega) \sin \Omega t + p_3(\Omega) \cos \Omega t] \tag{4.70}$$

Asynchronous force

The equations to be solved are

$$m\ddot{p} + c\dot{p} + kp = f_4 \sin s\Omega t + f_5 \cos s\Omega t \tag{4.71}$$

with

$$f_4 = \phi^{\mathrm{T}} F_4 \tag{4.72}$$

$$f_5 = \phi^{\mathrm{T}} F_5 \tag{4.73}$$

Solutions are sought as

$$p = p_4 \sin s\Omega t + p_5 \cos s\Omega t \tag{4.74}$$

and identification of the terms in $\sin s\Omega t$ and $\cos s\Omega t$ gives the equation

$$\begin{bmatrix} k - m(s\Omega)^2 & -s\Omega c \\ s\Omega c & k - m(s\Omega)^2 \end{bmatrix} \begin{bmatrix} p_4 \\ p_5 \end{bmatrix} = \begin{bmatrix} f_4 \\ f_5 \end{bmatrix} \tag{4.75}$$

This system is solved for any value of Ω, and

$$\delta = \phi[p_4(s\Omega) \sin s\Omega t + p_5(s\Omega) \cos s\Omega t] \tag{4.76}$$

Harmonic force fixed in space

The equations to be solved are

$$m\ddot{p} + c\dot{p} + kp = f_6 \sin \omega t + f_7 \cos \omega t \tag{4.77}$$

with

$$f_6 = \phi^{\mathrm{T}} F_6 \tag{4.78}$$

$$f_7 = \phi^{\mathrm{T}} F_7 \tag{4.79}$$

Solutions are sought as

$$p = p_6 \sin \omega t + p_7 \cos \omega t \tag{4.80}$$

and identification of the terms in $\sin \omega t$ and $\cos \omega t$ gives the equation

$$\begin{bmatrix} k - m\omega^2 & -\omega c \\ \omega c & k - m\omega^2 \end{bmatrix} \begin{bmatrix} p_6 \\ p_7 \end{bmatrix} = \begin{bmatrix} f_6 \\ f_7 \end{bmatrix} \tag{4.81}$$

The system is solved for any value of ω, and

$$\delta = \phi[p_6(\omega) \sin \omega t + p_7(\omega) \cos \omega t] \tag{4.82}$$

Here the system rotates at a constant speed of rotation Ω and the frequency of excitation ω changes.

4.4.2 The direct method

In this case the number of equations of the system (4.50) is not reduced: the N degrees of freedom are kept.

Natural frequencies, the Campbell diagram, zones of instability

The solutions of (4.50) with no external forces are sought. The form chosen is

$$\delta = \Delta e^{rt} \tag{4.83}$$

which has to be substituted in

$$M\ddot{\delta} + C\dot{\delta} + K\delta = 0 \tag{4.84}$$

where $C = C(\Omega)$. Then

$$(r^2 M + rC + K)\Delta = 0 \tag{4.85}$$

Using the identity

$$M\Delta = M\Delta \tag{4.86}$$

gives, when combined with Equation (4.85):

$$\begin{bmatrix} 0 & M \\ M & C \end{bmatrix} \begin{bmatrix} r\Delta \\ \Delta \end{bmatrix} = \frac{1}{r} \begin{bmatrix} M & 0 \\ 0 & -K \end{bmatrix} \begin{vmatrix} r\Delta \\ \Delta \end{vmatrix} \tag{4.87}$$

Equation (4.87) is better written as

$$AX = \lambda BX \tag{4.88}$$

where

$$A = \begin{bmatrix} 0 & M \\ M & C \end{bmatrix} \tag{4.89}$$

$$B = \begin{bmatrix} M & 0 \\ 0 & -K \end{bmatrix} \tag{4.90}$$

$$\lambda = l/r \tag{4.91}$$

$$X = \begin{bmatrix} r\Delta \\ \Delta \end{bmatrix} \tag{4.92}$$

The solutions of the eigenvalue/eigenvector problem defined in (4.87) are obtained here by a simultaneous iterative technique [7], which is very efficient at getting the lowest eigenvalues. Eigenvalues/eigenvectors are complex quantities, and as matrices A and B are real matrices the eigenvalues must be pairs of complex conjugates. Let us, for example, consider the two lowest eigenvalues:

$$r_1 = -\frac{\alpha_1\omega_1}{\sqrt{1-\alpha_1^2}} \pm j\omega_1 \tag{4.93}$$

and the corresponding eigenvectors

$$\Delta_1 = R_1 \pm jI_1 \tag{4.94}$$

The understanding of a complex mode shape is not obvious, as for an undamped system, and it is necessary to go back to the solution for free

motion. The corresponding solution is

$$\begin{aligned}\delta =&(R_1 + jI_1)\exp\left(-\frac{\alpha_1\omega_1}{\sqrt{1-\alpha_1^2}} + j\omega_1\right)t \\ &+ (R_1 - jI_1)\exp\left(-\frac{\alpha_1\omega_1}{\sqrt{1-\alpha_1^2}} - j\omega_1\right)t\end{aligned} \tag{4.95}$$

which can be written as

$$\begin{aligned}\delta = &\exp\left(-\frac{\alpha_1\omega_1}{\sqrt{1-\alpha_1^2}}\right)t[(R_1 + jI_1)(\cos\omega_1 t + j\sin\omega_1 t) \\ &+ (R_1 - jI_1)(\cos\omega_1 t - j\sin\omega_1 t)]\end{aligned} \tag{4.96}$$

Then

$$\delta = 2\exp\left(-\frac{\alpha_1\omega_1}{\sqrt{1-\alpha_1^2}}\right)t[R_1\cos\omega_1 t - I_1\sin\omega_1 t] \tag{4.97}$$

Expression (4.97) does not contain any complex quantity. The exponential expression decreases to zero for a stable system as time passes. The quantity

$$\frac{\delta}{2\exp(\cdots)t} = R_1\cos\omega_1 t - I_1\sin\omega_1 t \tag{4.98}$$

is the mode. Then for a node of the structure in general, the components of the displacements are

$$u = u_r\cos\omega_i t + u_i\sin\omega_i t \tag{4.99}$$

$$w = w_r\cos\omega_i t + w_i\sin\omega_i t \tag{4.100}$$

and the orbits are ellipses. At the critical speeds, owing to unbalance the shape of the rotors looks like the mode shape which appears in free motion.

Response to forces of excitation

As in the foregoing analysis, the steady-state response is first calculated and one proceeds as for the pseudo-modal method, but all the degrees of freedom are kept in the calculations.

5

A Computer Program*

This chapter describes a computer program developed to analyze the dynamic behavior of rotors in bending. An initial computer program devoted to the dynamic behavior of monorotors was developed at LMSt in 1981, and later a computer program for industrial use was developed in close association with Thermodyn. More recently the computer program has been equipped with an efficient preprocessor and postprocessor. Called SYSROTOR, it is now distributed by SYSTUS International Another computer program for calculating the dynamic behavior of coaxial multirotors in bending has been developed by LMSt and is used in aeronautical companies. The laboratory (see Appendix 2) carries out significant research in rotordynamics and develops specific prototype computer programs in the fields of earthquake influence, asymmetry of rotating elements, equations with periodic coefficients in stiffness and mass matrices bending–torsion coupling.

5.1 PRESENTATION OF SYSROTOR

The SYSROTOR computer program contains three parts:

- A preprocessor which displays the model.
- A solver which computes the natural frequencies, the associated mode shapes and the responses to mass unbalances, asynchronous forces and harmonic forces fixed in space.
- A postprocessor which displays and draws the Campbell diagram, the responses to excitation forces, the modes and rotor deflections.

* A free reduced version for PC use is available on the Internet: see Appendix 2.

The program contains about 10000 lines and needs a core memory of 500 kbytes. The matrices of the system have been arranged using the skyline technique, which saves significant core memory space and is especially useful when dealing with multirotors. Disk capacity depends on the number of degrees of freedom of the system studied: for most industrial applications a capacity of 20 Mbytes is sufficient. The program has been implemented on a PC and workstations such as HP, SUN, etc.

The operating diagram is shown in Figure 5.1.

Simultaneous use of the preprocessor and the text editor permits organization of the data. An output file (*trageo. txt*) contains the elements of the geometry and the error messages; the option solution uses the file *.dat* (data) as input and the file *.arc* (archives) as input–output, depending on whether it is an initial computation or a computation using previous results. The file *.lis* (listing) contains all the data and results obtained from the computation: they can be displayed using a text editor and

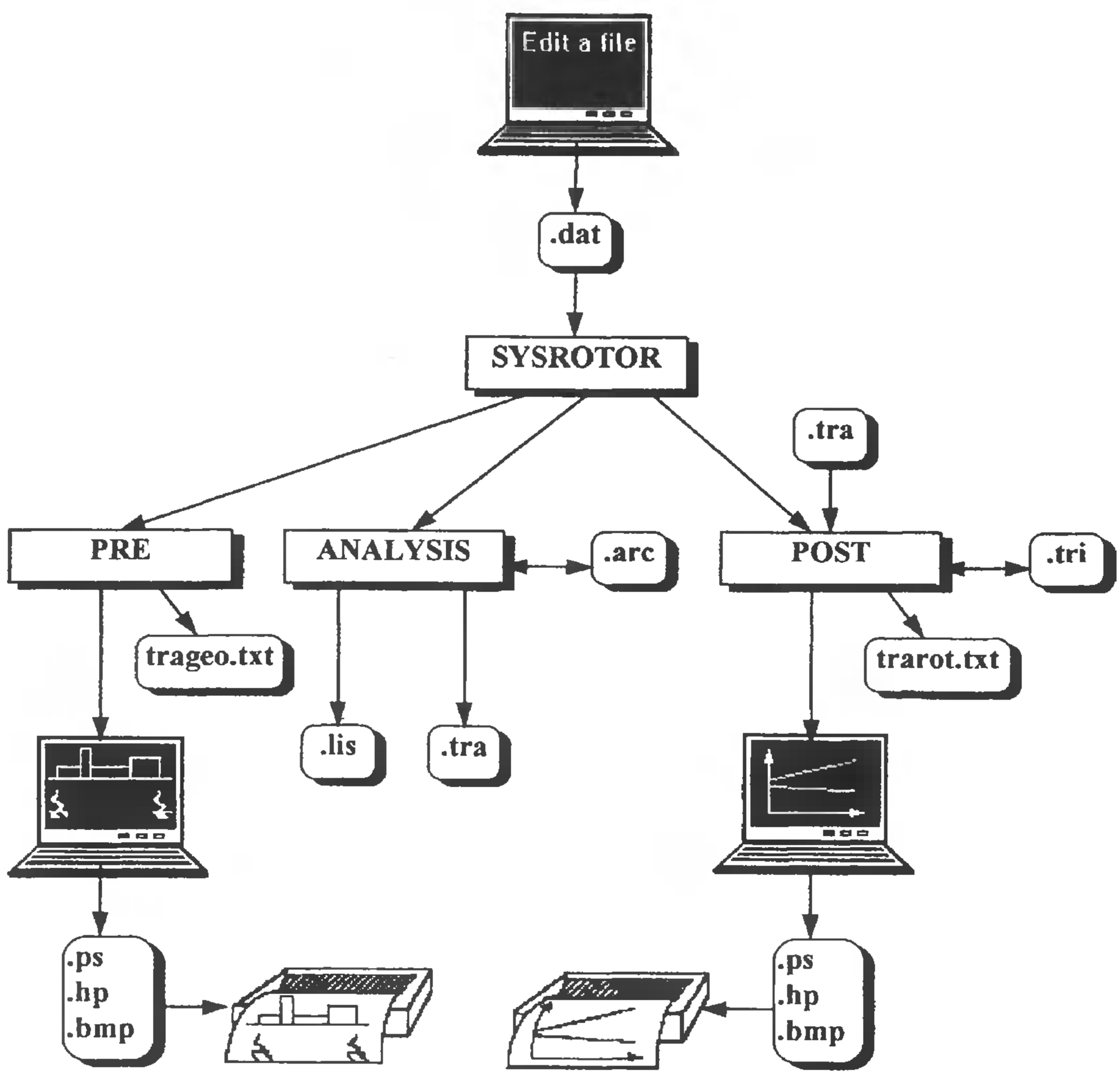

Figure 5.1. Operating diagram

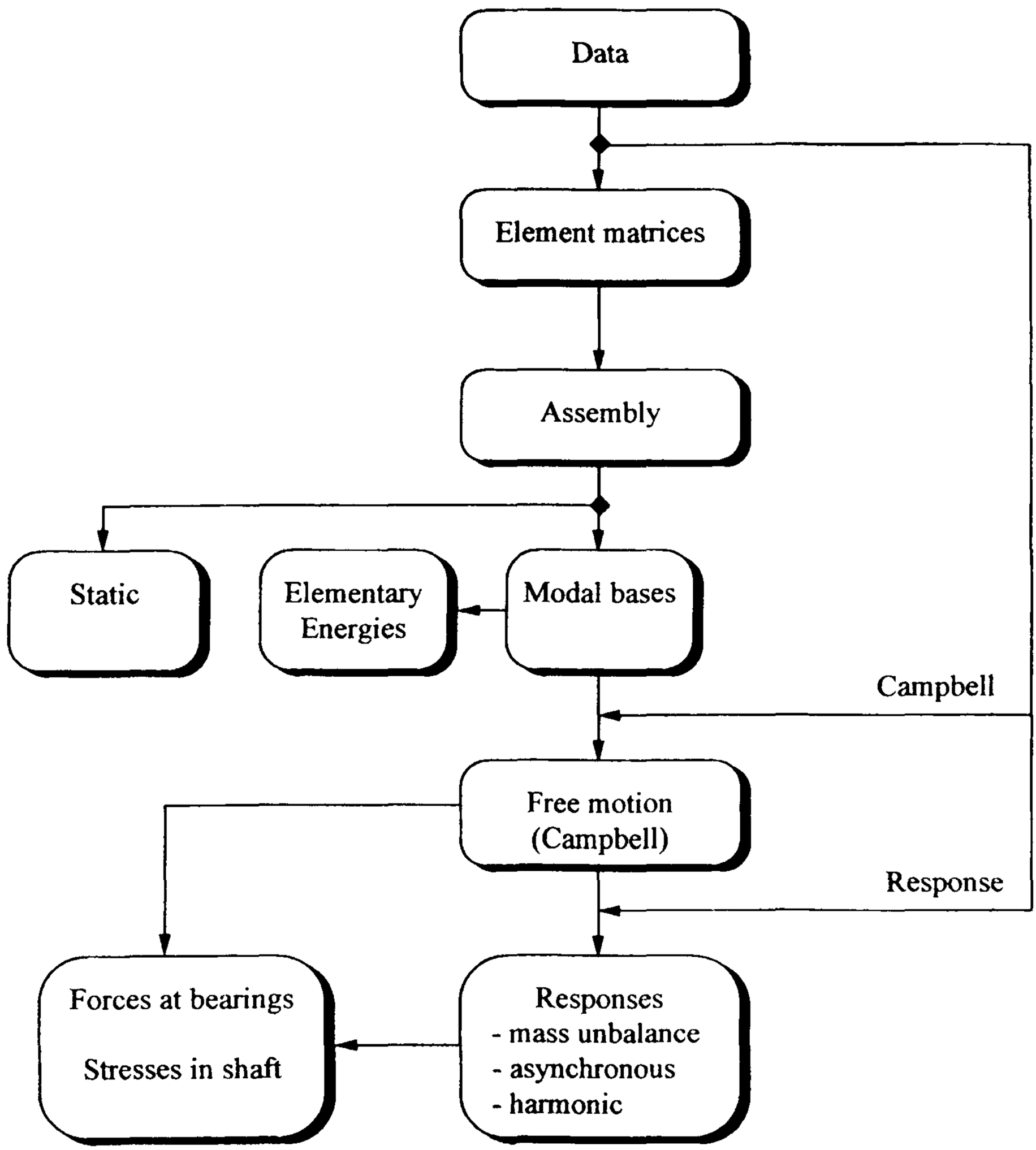

Figure 5.2. Solver

printed. The file *.tra* (tracing) contains the information necessary for the postprocessor.

Finally, the file *trarot.txt* contains informations on the execution and message errors. Plots can be requested in color or in black and white. Output files are denoted *.ps* (postscript format), *.hp* (hpgl format) or *.bmp* (bitmap format). The file *.tri* contains the frequency sort results used when drawing the Campbell diagram.

The solver is schematically presented in Figure 5.2.

Elementary matrices

The elementary matrices, corresponding to the mass, stiffness, gyroscopic and damping effects, are calculated and stored in a file. In addition, supplementary matrices can be added; they are useful, for example, for taking into account the rotor mounting. The mounting effect can be calculated separately using a finite element computer program and the corresponding matrices obtained through a substructuring technique.

Static

This type of simple calculation is mostly used when it is necessary to subject the static behavior of rotors only to the effect of gravity. First the equivalent nodal forces are obtained; in addition, concentrated forces and torques can be taken into account. This calculation is performed without modal reduction.

Modal basis

For industrial applications, the pseudo-modal method is used as it is very efficient; the direct method is 20 to 100 times more time-consuming. The direct method is used essentially to check the results obtained by the pseudo-modal method. When calculating the modal basis, elementary energies at rest are obtained. They are obviously not the same as the energies when the system is rotating, but their values are of great interest when it is necessary to modify the rotor in order to modify critical speeds. In addition, the pseudo-modal method is very useful when one wants to introduce modal damping factors which are frequently known from the general behavior of the system.

Free motion

Bearing characteristics which are a function of the speed of rotation are used. This gives the natural frequencies as functions of the speed of rotation, i.e. the Campbell diagram, the corresponding modes and the critical speeds. If the rotor is unstable the instability zones are also

obtained. Force and moment components and stresses in the elements of the shaft are predicted with the maximum displacement chosen. When industrial applications with many bearings are concerned, it is not easy to define the whirl as forward or backward. Indeed, some parts of the rotor can be in forward whirl and others in backward whirl. The following method is used here. The maximum axes of the ellipses described by the nodes are calculated, and all the values are added with a positive sign if the whirl is positive, otherwise they are added with a negative sign. The sign of the sum of all those quantities gives the forward (positive addition) or backward (negative addition) whirl. For monorotors it is usually sufficient to perform the calculation for about ten speeds of rotation, so disk memory capacity is not a problem.

Forced response

Several mass unbalances or several asynchronous forces can be simultaneously applied. Also, several harmonic forces with different phases can be applied. Here, too, the characteristics of the bearing are functions of the speed of rotation, and again force and moment components in the bearings and stresses in the elements are calculated. The responses can be calculated at all the nodes or at certain selected nodes. As the rotors are in general asymmetric, orbits are elliptical, and the responses to the excitation forces presented correspond to half the major axes of these ellipses. The deflected position of the shaft is drawn for speeds of rotation chosen from among those calculated; this is of interest as it shows how the shaft deflects when the speed of rotation changes. These calculations need far more memory than for free motion. Sweeping of the speed of rotation must usually be done by small increments. If the system has low damping, the calculations have to be performed for hundreds of speeds of rotation.

5.2 DATA FILE

The following gives a brief description of the data file, in this case a data file concerning a simple model of an industrial rotor, comments on data and results.

5.2.1 Brief description of data file

Rec. 1: TITLE (2 lines of 80 characters)

Rec. 2: GENERAL DATA (2I5, F5.0, 7I5, 2F10.0) (1 line)
analy_typ, nb_nodes, cod_geom, nb_freq, cod_resu_writ, cod_data_writ, cod_force_analy, <cod_shear>, <nb_modes>, <maxnb_iter>, <eigenval_prec>,
<eigenvec_prec>

---

anly_typ = 0 (static forces except gravity)
= 1 (static forces and gravity)
= 2 (modal basis)
= 3 (response)
= 4 (modes in rotation)
= 5 (2 + 4)
= 6 (2 + 3)
= 7 (2 + 3 + 4)

---

cod_geom = 1. (inertial form)
= 2. (dimensional form)

---

cod_resu_writ = 0 (frequencies)
= 1 (frequencies and modes)
= 2 (global modal matrices + elementary modal matrices %)
= 3 (2 + elementary modal matrices)
= 4 (elementary modal matrices)

---

cod_data_writ = 0 (none)
= 1 (data read)
= 2 (data generated automatically)
= 3 (1 + 2)

---

cod_force_analy = 0 (none)
= 1 (forces at bearings)
= 2 (1 + stresses in shaft elements)

---

cod_shear = <0> (no shear)
= 1 (shear)

Rec. 3: NODE COORDINATES (I5, F10.0, I5)
node_nb, y_coord, <node_step>;
/ For automatic node generation: /
/ 1, 0., or 1, 0., /
/ 2, 0.1, 5, 0.4, 1, /
/ 3, 0.2, /
/ 4, 0.3, /
/ 5, 0.4, /
Index 99999

Rec. 4: BOUNDARY CONDITIONS (5I5)
node_nb, <x_block>, <z_block>, <rx_block>, <rz_block>
Index 99999

Rec. 5: TYPE AND NUMBER OF ELEMENTS IN REC. 6 (2I5)
elem_typ, nb_elem

---

elem_typ = 1 (shaft element)
= 2 (disk element)
= 3 (bearing element)
= 4 (sup. stiffness element)
= 5 (sup. mass element)
= 6 (sup. gyroscopic element)
= 7 (sup. damping element)

Rec. 6: DESCRIPTION OF ELEMENTS DECLARED IN REC. 5 (9I5)
elem_nb, nodel_nb, node2_nb, mat_nb, <nodel_prop_nb>
or <stiff_prop_nb>, <node2_prop_nb> or <damp_prop_nb>,
<elem_nb_step>, <node_nb_step>, <prop_nb_step>
/ For automatic element generation:
/ 1,1,2,1,12,12, or 1,1,2,1,12,12 /
/ 2,2,3,1,12,12, 5,5,6,1,12,12,1,1,0, /
/ 3,3,4,1,12,12, /
/ 4,4,5,1,12,12, /
/ 5,5,6,1,12,12, /
Index 99999

Rec. 7: CHARACTERISTICS OF MATERIALS (I5, 3F10.0)
mat_nb, Young_mod, density, Poisson_ratio

Rec. 8: PROPERTIES (I5, 5F15.0)

/Shaft with cod_geom=1./
prop_nb, section, section_inertia, <axial_F>, <1.>,
<shear_factor>

/Shaft with cod_geom =2./
prop_nb, outer_rad, inner_rad, <axial_F>, <2.>,
<shear_factor>

/Disk with cod_geom=1./
prop_nb, mass, mass_inertia_X, <mass_inertia_Y>, <1.>

/Disk with cod_geom=2./
prop_nb, outer_rad, inner_rad, thickness, <2.>

/Bearing: stiffness/
prop_nb, kxx, kzz, kxz, <kzx>

/Bearing: damping/
prop_nb, cxx, czz, cxz, <czx>

Rec. 8b: VARIABLE BEARING CHARACTERISTICS (I5, 5F15.0)

/Stiffness/
prop_nb, rotation_speed, kxx_at_speed, kzz_at_speed,
kxz_at_speed, kzx_at_speed

/ Damping /
prop_nb, rotation_speed, cxx_at_speed, czz_at_speed,
cxz_at_speed, czx_at_speed

Index 99999

Rec. 9: GENERAL DATA FOR SUPPLEMENTARY ELEMENTS (4I5)
elem_nb, cod_sym, cod_read, nb_records

---

cod_sym = −1 (anti-symmetrical)
= 0 (symmetrical)
= 1 (any)

---

cod_read = 0 (line by line)
= 1 (line number, column number, value)

Rec. 10: SUPPLEMENTARY ELEMENT MATRIX (line by line) (8F15.0)
/ If cod_sym = −1 or 0, only the upper half of the matrix is/
/ described and the first term is the diagonal term./

Rec. 11: SUPPLEMENTARY ELEMENT MATRIX (line number, column number, value) 4(2I5, F15.0)
line_nb, column_nb, term
/If cod_sym= −1 or 0, only the upper half of the matrix is described/

Index 99999

Rec. 12: NUMBER OF MODAL DAMPING FACTORS FOR REC. 13 (I5) (1 line)
nb_damp_factors

Rec. 13: MODAL DAMPING FACTORS DECLARED IN REC.12 (8F10.0)

Index 99999

Rec. 14: GRAVITY (I5, 2F10.0) (1 line)
0, 0x_g_angle, g_accel

Rec. 15: EXTERNAL STATIC FORCES (I5, 4F10.0)
node_nb, force_x, force_z, moment_x, moment_z

If record 14 or 15 is present: Index 99999

Rec. 16: ROTATIONAL AND EXCITATION SPEEDS (I5, 3F10.0)
(1 to 3 lines)
speed_typ, ini_speed, final_speed, speed_step

---

speed_typ = 0 (rotor rotational speeds for frequency and mode analysis)
= 1 (rotor rotational speeds for response analysis)
= 2 (asynchronous force rotational speeds)
= 3 (fixed direction harmonic force excitation speeds)

Index 99999

Rec. 17: MASS UNBALANCE (I5, 3F10.0)
node_nb, mass, distance_axis, angle_ini_position

Rec. 18: ASYNCHRONOUS FORCES (I5, 2F10.0)
node_nb, amplitude, angle_ini_position

Rec. 18b: FIXED DIRECTION HARMONIC FORCES (I5, 3F10.0)
node_nb, amplitude, angle_position, phase
Index 99999

Rec. 19: LIST OF NODES FOR WHICH RESPONSE IS TO BE COMPUTED (16I5)
/ For automatic generation:/
/1,2,3,4,5 or 1, −5,/
Index 99999

Note:<> identifies a default value.

5.2.2 Data file of a simple model of an industrial rotor

The data for a simple model of an industrial rotor schematized in Figure 5.3 are:

Disks D1 : $M = 1.2\,\text{kg}$, $I_d = 1.2 \times 10^{-3}\,\text{kg}\,\text{m}^2$, $I_p = 2.4 \times 10^{-3}\,\text{kg}\,\text{m}^2$
D2 : $M = 1.0\,\text{kg}$, $I_d = 1.0 \times 10^{-3}\,\text{kg}\,\text{m}^2$, $I_p = 2.0 \times 10^{-3}\,\text{kg}\,\text{m}^2$

Bearings P1 : $k_{xx} = 8 \times 10^7\,\text{N/m}$, $k_{zz} = 1 \times 10^8\,\text{N/m}$
$k_{xz} = -1 \times 10^7\,\text{N/m}$, $k_{zx} = -6 \times 10^7\,\text{N/m}$
$c_{xx} = 8 \times 10^3\,\text{N s/m}$, $c_{zz} = 1.2 \times 10^4\,\text{N s/m}$
$c_{xz} = -3 \times 10^3\,\text{N s/m}$, $c_{zx} = -3 \times 10^3\,\text{N s/m}$
P2 : $k_{xx} = 5 \times 10^7\,\text{N/m}$, $k_{zz} = 7 \times 10^7\,\text{N/m}$
$k_{xz} = -2 \times 10^7\,\text{N/m}$, $k_{zx} = -4 \times 10^7\,\text{N/m}$
$c_{xx} = 6 \times 10^3\,\text{N s/m}$, $c_{zz} = 8 \times 10^3\,\text{N s/m}$
$c_{xz} = -1.5 \times 10^3\,\text{N s/m}$, $c_{zx} = -1.5 \times 10^3\,\text{N s/m}$

The shaft is made of steel and the two disks are in aluminum. The model contains twelve nodes, two disks and two bearings, and the finite element modeling is shown in Figure 5.4. The maximum operating speed is 50000 rpm. The data are:

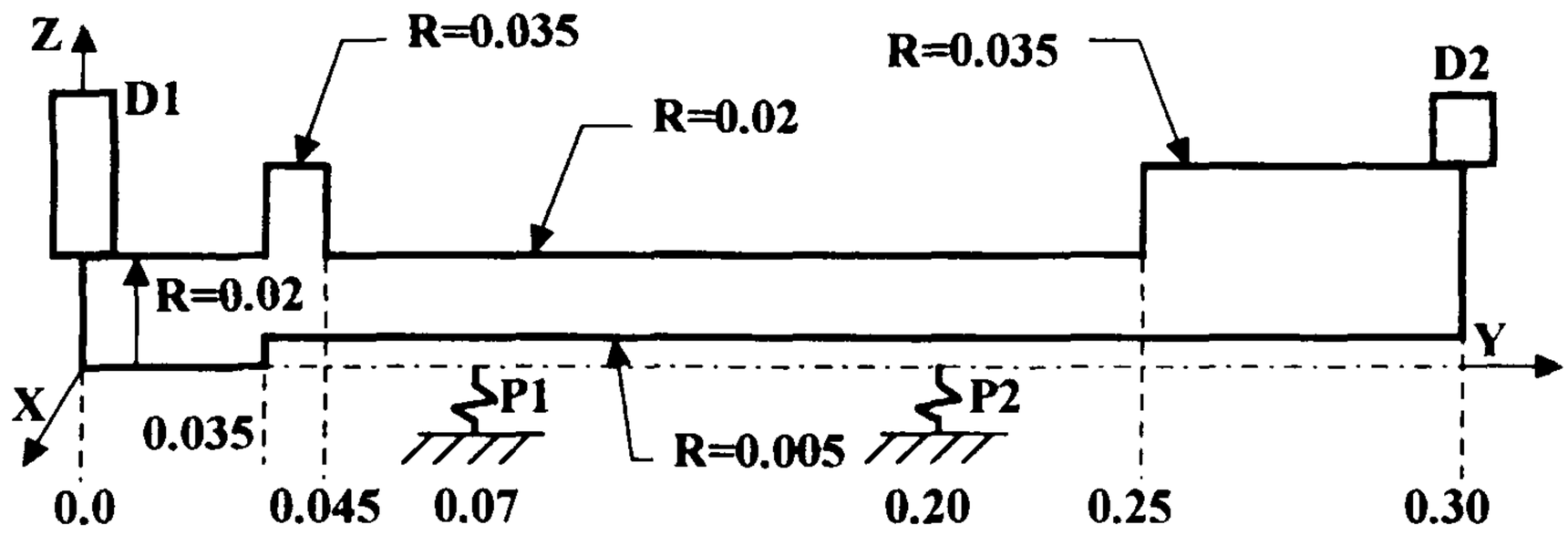

Figure 5.3. Rotor dimensions

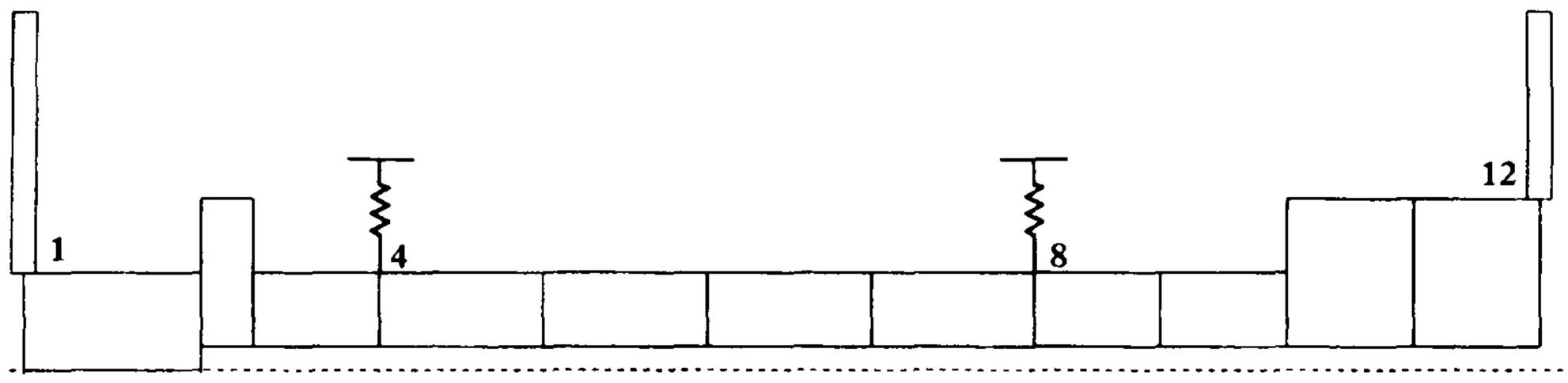

Figure 5.4. Finite element model

```
Simple model of an industrial rotor
Campbell diagram and mass unbalance response
7,12,2.,8,0,3,0,1,
1,.0,
2,.035,
3,.045,
4,.07,
8,.20,1,
10,.25,1,
12,.30,1,
99999
99999
1,11,
1,1,2,1,1,1,
2,2,3,1,2,2,
3,3,4,1,3,3,
9,9,10,1,3,3,1,1,0,
10,10,11,1,2,2,
11,11,12,1,2,2,
2,2,
```

```
12,1,0,0,4,
13,12,0,0,5,
3,2,
14,4,0,0,6,7,
15,8,0,0,8,9,
99999
1,2.E11,7800.,.3,
1,.02,
2,.035,.005,
3,.02,.005,
4,1.2,1.2E-3,2.4E-3,1.,
5,1.,1.E-3,2.E-3,1.,
6,8.E7,1.E8,-1.E7,-6.E7,
7,8.E3,1.2E4,-3.E3,-3.E3,
8,5.E7,7.E7,-2.E,-4.E7,
9,6.E3,8.E3,-1.5E3,-1.5E3,
99999
99999
99999
0,0.,50000.,5000.,
1,0.,50000.,50.,
99999
1,0.0005,0.001,
12,0.0005,0.001,180.,
99999
1,-12,
99999
```

5.2.3 Comments on the data

Line no.	Content	Comments
1	Simple model of an industrial rotor	
2	Campbell diagram and mass unbalance response	Title
3	7,12,2.,8,0,3,0,1, general data	Analysis of modal basis, frequencies and modes in rotation, mass unbalance response. Shafts and disks are defined by their dimensions, eight frequencies are computed, and shear is taken into account Twelve modes (8 + 4) are used for analysis by default

4	1,.0,	node	Node 1 is situated at $y = 0$ m
5	2,.035,	node	Node 2 is situated at $y = 0.035$ m
6	3,.045,	node	Node 3 is situated at $y = 0.045$ m
7	4,.07,	node	Node 4 is situated at $y = 0.07$ m
8	8,0.2,1	node	Node 8 is situated at $y = 0.2$ m, and nodes 5, 6 and 7 are generated with an increment of 1 on the node numbers
9	10,.25,1,	node	Node 10 is situated at $y = 0.25$ m, and node 9 is generated with an increment of 1 on the node number
10	12,.30,1,	node	Node 12 is situated at $y = 0.3$ m, and node 11 is generated with an increment of 1 on the node number
11	99999		Index
12	99999		Index
13	1,11,	shafts	Eleven shaft elements (type 1) are defined
14	1,1,2,1,1,1,	shafts	Element 1 from node 1 to node 2 is made of material 1. Property 1 is assigned to node 1 and node 2
15	2,2,3,1,2,2,	shafts	Element 2 from node 2 to node 3 is made of material 1. Property 2 is assigned to node 2 and node 3
16	3,3,4,1,3,3,	shafts	Element 3 from node 3 to node 4 is made of material 1. Property 3 is assigned to node 3 and node 4
17	9,9,10,1,3,3,1,1,0,	shafts	Element 9 from node 9 to node 10 is made of material 1. Property 3 is assigned to node 9 and node 10. Elements 4, 5, 6, 7 and 8 are generated with an increment of 1 on the element numbers and node numbers, and an increment of 0 on the properties (all elements have property 3)
18	10,10,11,1,2,2,	shafts	Element 10 from node 10 to node 11 is made of material 1. Property 2 is assigned to node 10 and node 11
19	11,11,12,1,2,2	shafts	Element 11 from node 11 to node 12 is made of material 1. Property 2 is assigned to node 11 and node 12
20	2,2	disks	Two disk elements (type 2) are defined
21	12,1,0,0,4,	disks	Element 12 is situated on node 1 and is defined by property 4 assigned to node 1
22	13,12,0,0,5,	disks	Element 13 is situated on node 12 and is defined by property 5 assigned to node 12
23	3,2,	bearings	Two bearing elements (type 3) are defined

24	14,4,0,0,6,7,	bearings	Element 14 is situated on node 4 and is defined by stiffness property 6 and damping property 7
25	15,8,0,0,8,9,	bearings	Element 15 is situated on node 8 and is defined by stiffness property 8 and damping property 9
26	99999		Index
27	1,2.E11,7800.,.3,	material	Material 1 is defined by a Young's modulus of $2.E+11$ N/m^2, a density of 7800 kg/m^3 and Poisson's ratio of 0.3
28	1,.02,	properties	Property 1 defines an outer radius of 0.02 m (inner radius = 0)
29	2,.035,.005,	properties	Property 2 defines an outer radius of 0.035 m, and an inner radius of 0.005 m
30	3,.02,.005,	properties	Property 3 defines an outer radius of 0.02 m, and an inner radius of 0.005 m
31	4,1.2,1.2E−3,2.4E−3,1.,	properties	Property 4 defines a mass of 1.2, diametral inertia of 0.0012 and polar inertia of 0.0024. The last digit (1.) indicates that these are inertia values and not dimensions, as indicated by the first data line code
32	5,1.,1.E−3,2.E−3,1.,	properties	Property 5 defines a mass of 1, diametral inertia of 0.001 and polar inertia of 0.002. The last digit (1.) indicates that these are inertia values and not dimensions, as indicated by the first data line code
33	6,8.E7,1.E8,−1.E7,−6.E7,		Property 6 defines $k_{xx} = 8.\mathrm{E}+7, k_{zz} = 1.\mathrm{E}+8, k_{xz} = -1.\mathrm{E}+7$ and $k_{zx} = -6.\mathrm{E}+7$
34	7,8.E3,1.2E4,−3.E3,−3.E3,		Property 7 defines $c_{xx} = 8.\mathrm{E}+3, c_{zz} = 1.2\mathrm{E}+4, c_{xz} = -3.\mathrm{E}+3$ and $c_{zx} = -3.\mathrm{E}+3$
35	8,5.E7,7.E7,−2.E7,−4.E7,		Property 8 defines $k_{xx} = 5.\mathrm{E}+7, k_{zz} = 7.\mathrm{E}+7, k_{xz} = -2.\mathrm{E}+7$ and $k_{zx} = -4.\mathrm{E}+7$
36	9,6.E3,8.E3,−1.5E3,−1.5E3,		Property 9 defines $c_{xx} = 6.\mathrm{E}+3, c_{zz} = 8\mathrm{E}+3, c_{xz} = -1.5\mathrm{E}+3$ and $c_{zx} = -1.5\mathrm{E}+3$
37	99999		Index
38	99999		Index
39	99999		Index
40	0,0.,50000.,5000.,	speed for Campbell	Modes and frequencies in rotation from 0 to 50 000 rpm with an increment of 5000 rpm
41	1,0.,50000.,50.,	speed for mass unbalance response	Mass unbalance response from 0 to 50 000 rpm with an increment of 50 rpm

42	99999		Index
43	1,0.0005,0.001,	unbalance	The unbalance is 0.5 g mm on disk 1
44	12,0.0005,0.001,180.,	unbalance	The unbalance is 0.5 g mm on disk 2 in phase opposition
45	99999		Index
46	1,–12,	nodes	The response is computed for all nodes
47	99999		Index

5.2.4 Results

The following results are given:

- The Campbell diagram, Figure 5.5.
- The first four mode shapes at 50 000 rpm, Figure 5.6(a)–(d).
- The mass unbalance response at four nodes, Figure 5.7.
- The deflections due to the mass unbalance for five speeds of rotation, Figure 5.8(a)–(e).

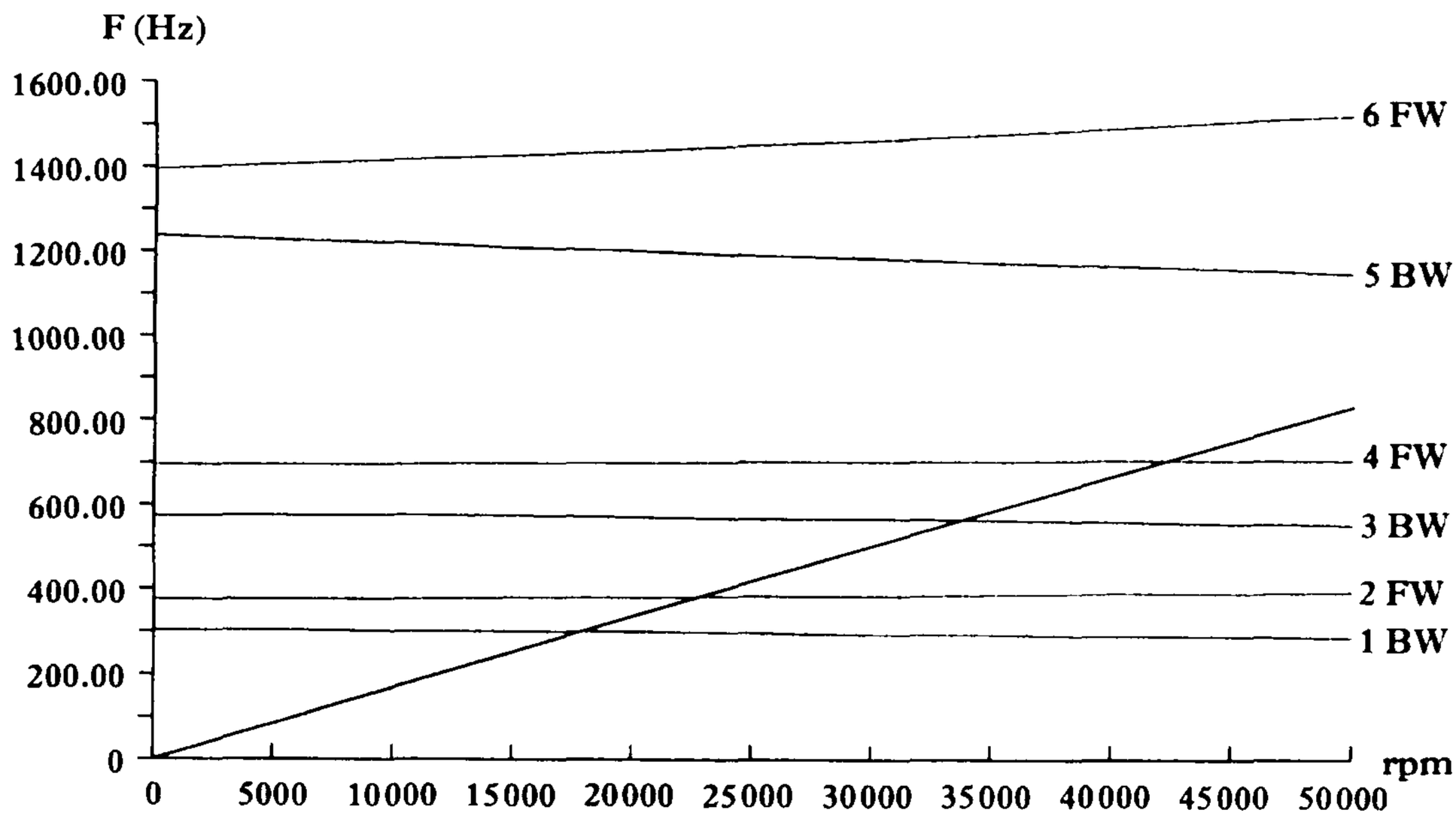

Figure 5.5. Campbell diagram

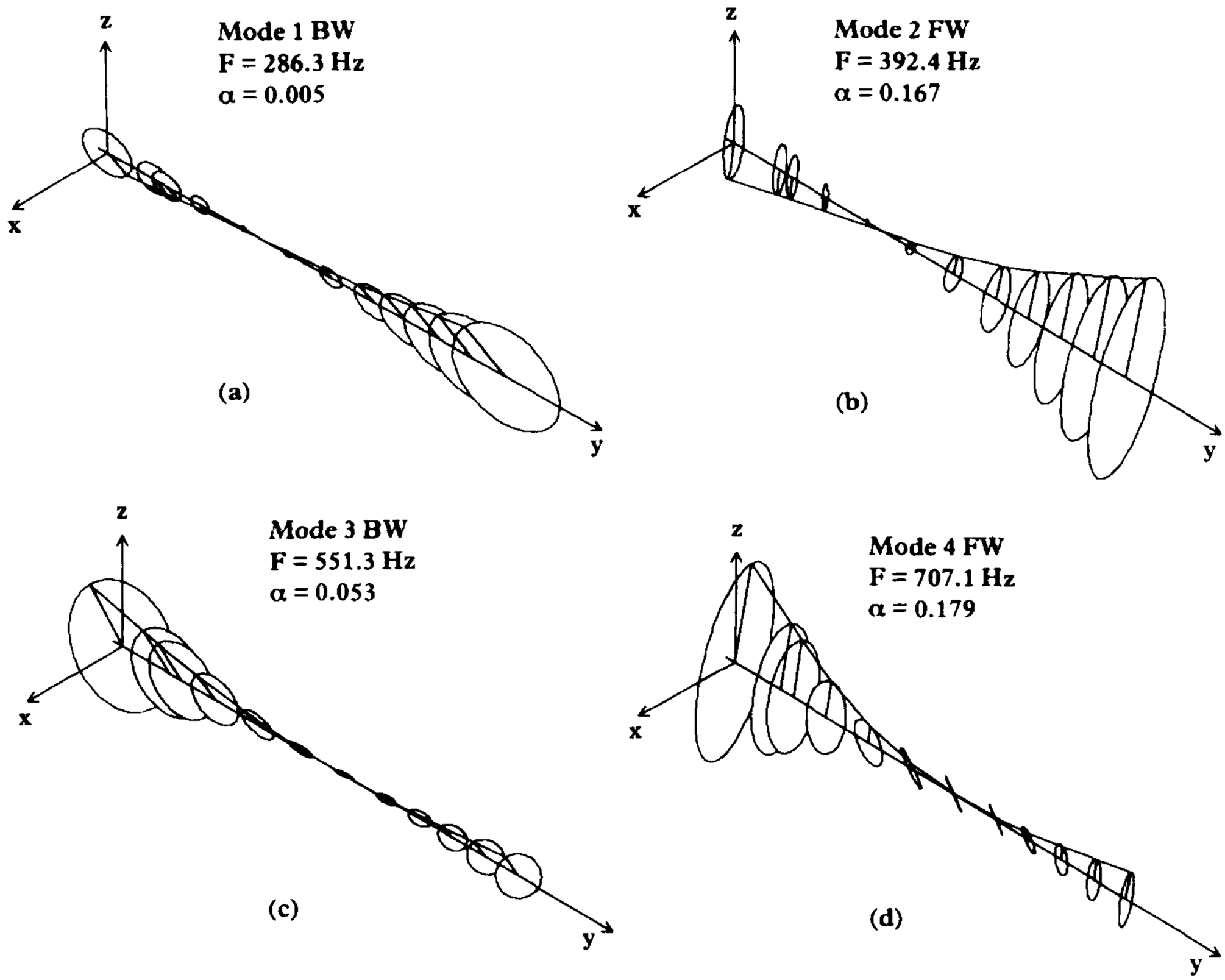

Figure 5.6. Mode shapes at 50 000 rpm

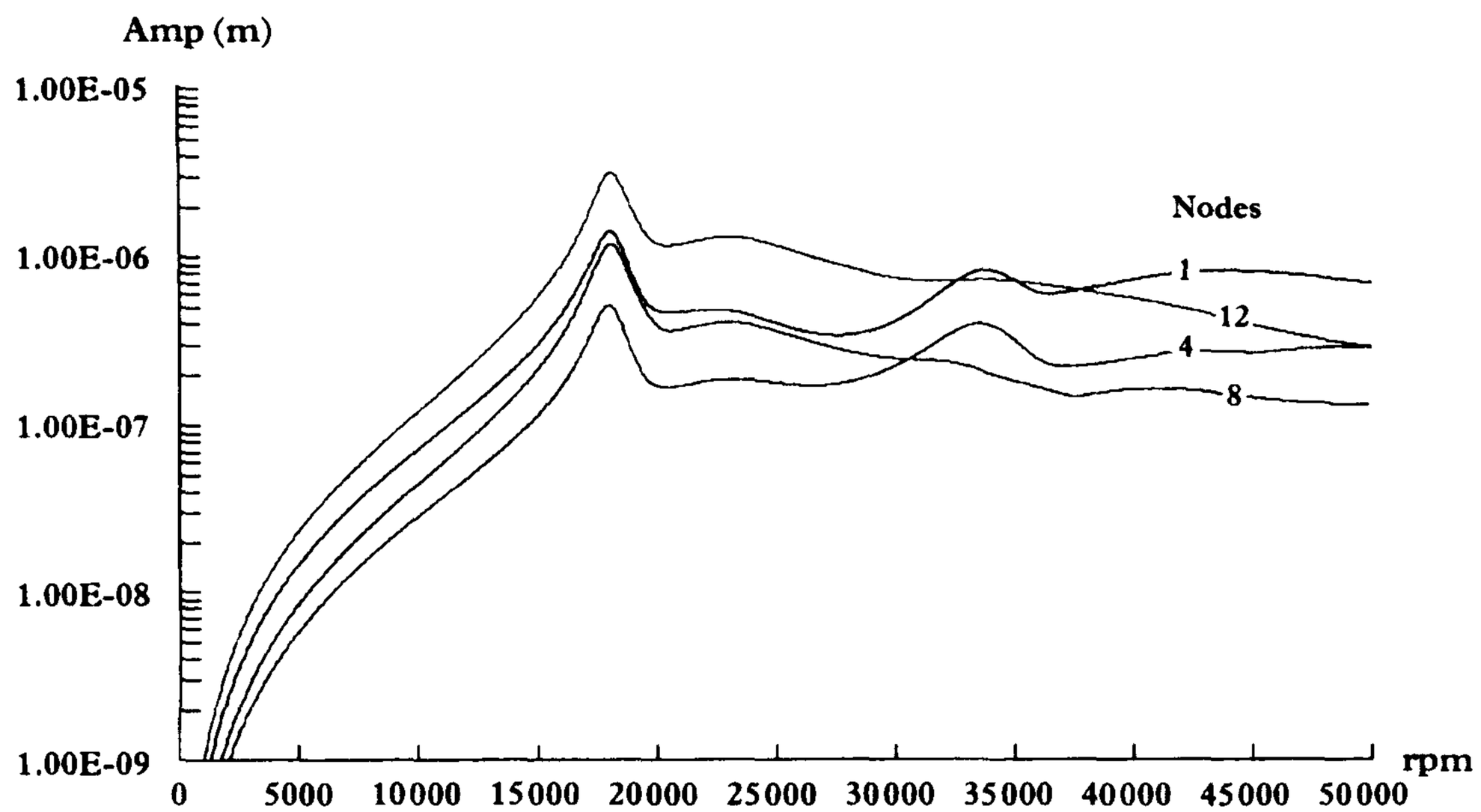

Figure 5.7. Mass unbalance response

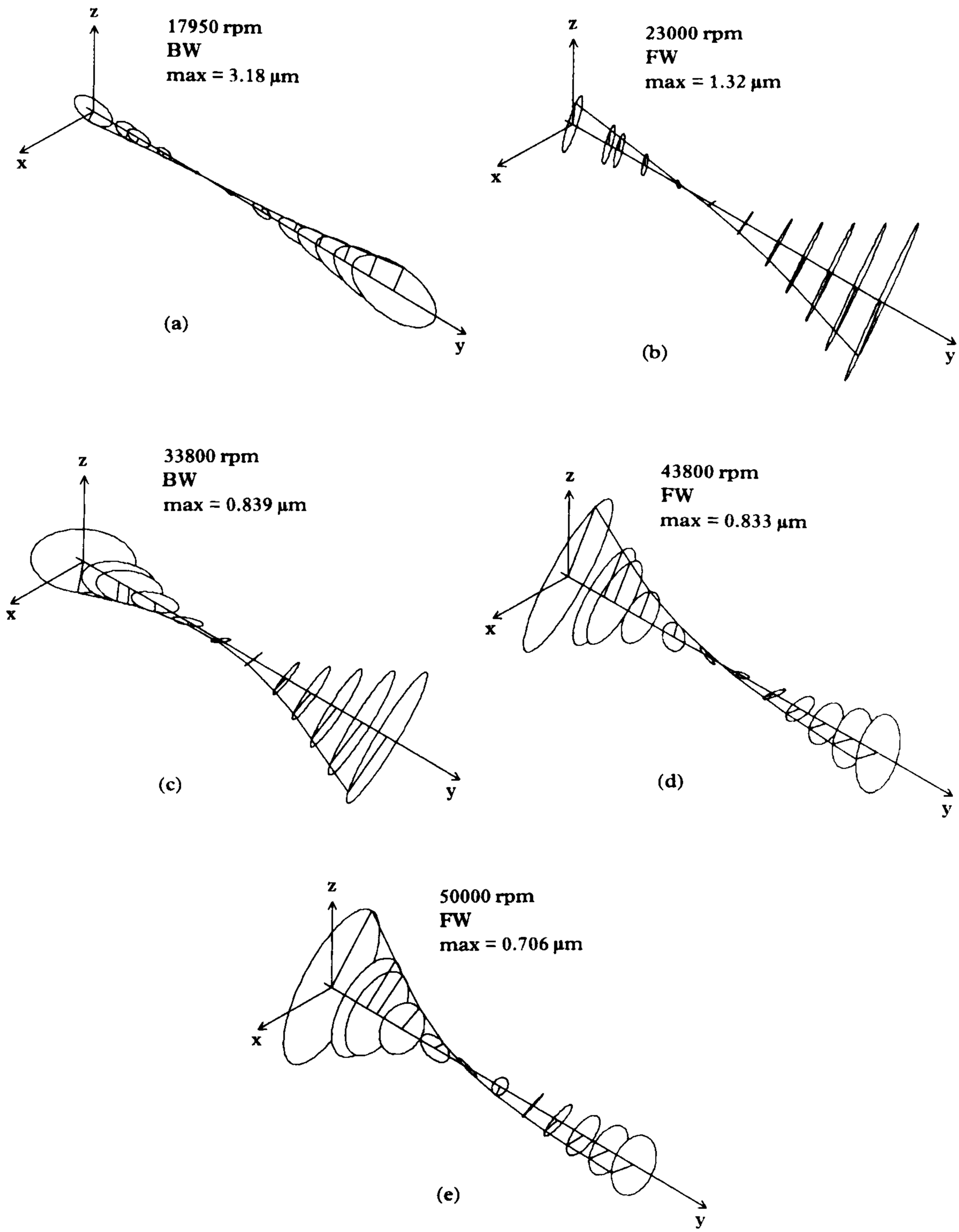

Figure 5.8. Rotor deflections

6

Towards Industrial Applications

In this chapter, in order to show some specific aspects, relatively simple examples modeled using finite elements are presented. The first example is designed to show the degree of confidence which can be given to the pseudo-modal method. A second example shows the influence of the model. Next, representation of the natural frequencies as a function of the bearing stiffness is presented. The fourth section is concerned with force transmissibility due to bearings. Lastly, some comments on bearings are given.

6.1 THE PSEUDO-MODAL METHOD

The direct method, which does not reduce the number of equations, is the reference. These reference results are compared with those obtained using the pseudo-modal method, which uses a different number of modes n. The rotor used here is shown in Figure 6.1.

The rotor uses 13 shaft finite elements which have the same length. The data are (lengths in meters)

$$L_1 = 0.2 \quad L_2 = 0.3 \quad L_3 = 0.5 \quad L_4 = 0.3$$

and the shaft cross-sectional radius is 0.05 m. The disk data are given in Table 6.1.

The disk and shaft are made of steel and characterized by

$$E = 2 \times 10^{11}\,\mathrm{N/m^2}$$
$$\rho = 7800\,\mathrm{kg/m^3}$$
$$\nu = 0.3$$

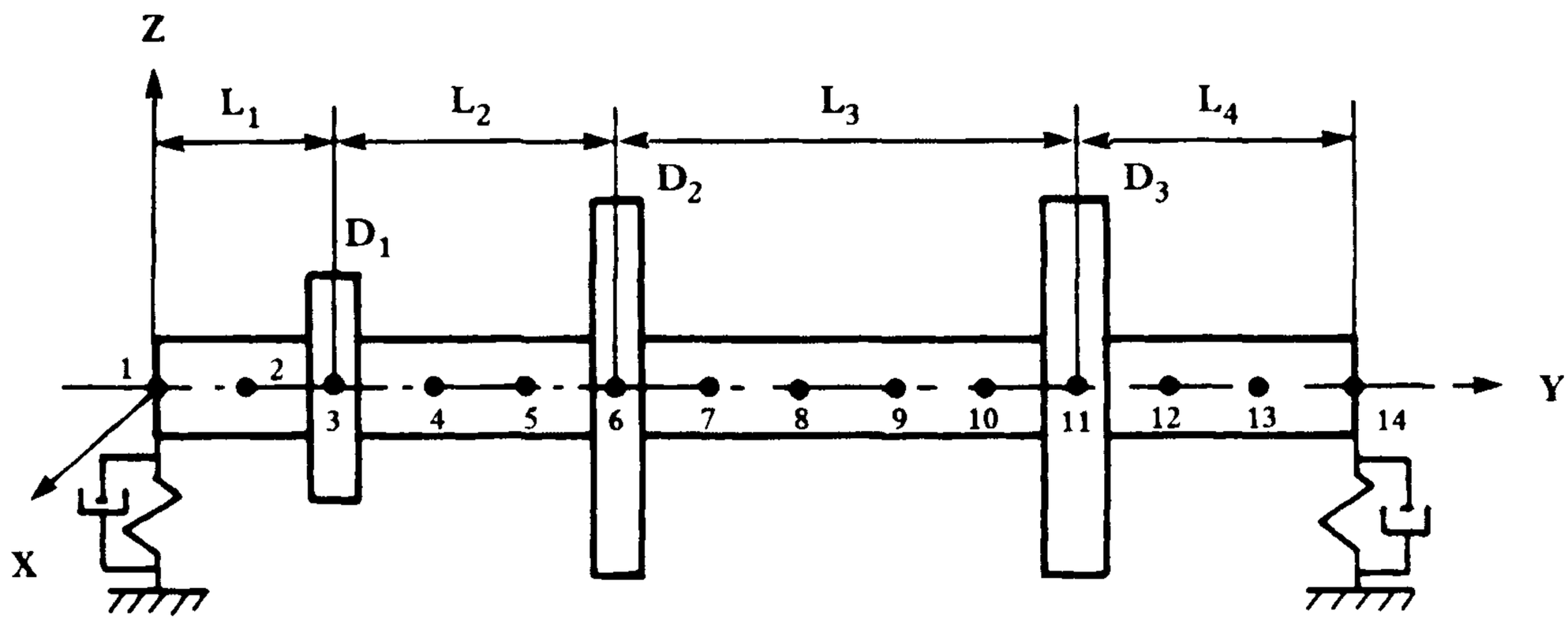

Figure 6.1. Rotor model

Table 6.1. Disk data

Disk	D_1	D_2	D_3
Thickness (m)	0.05	0.05	0.06
Inner radius (m)	0.05	0.05	0.05
Outer radius (m)	0.12	0.2	0.2

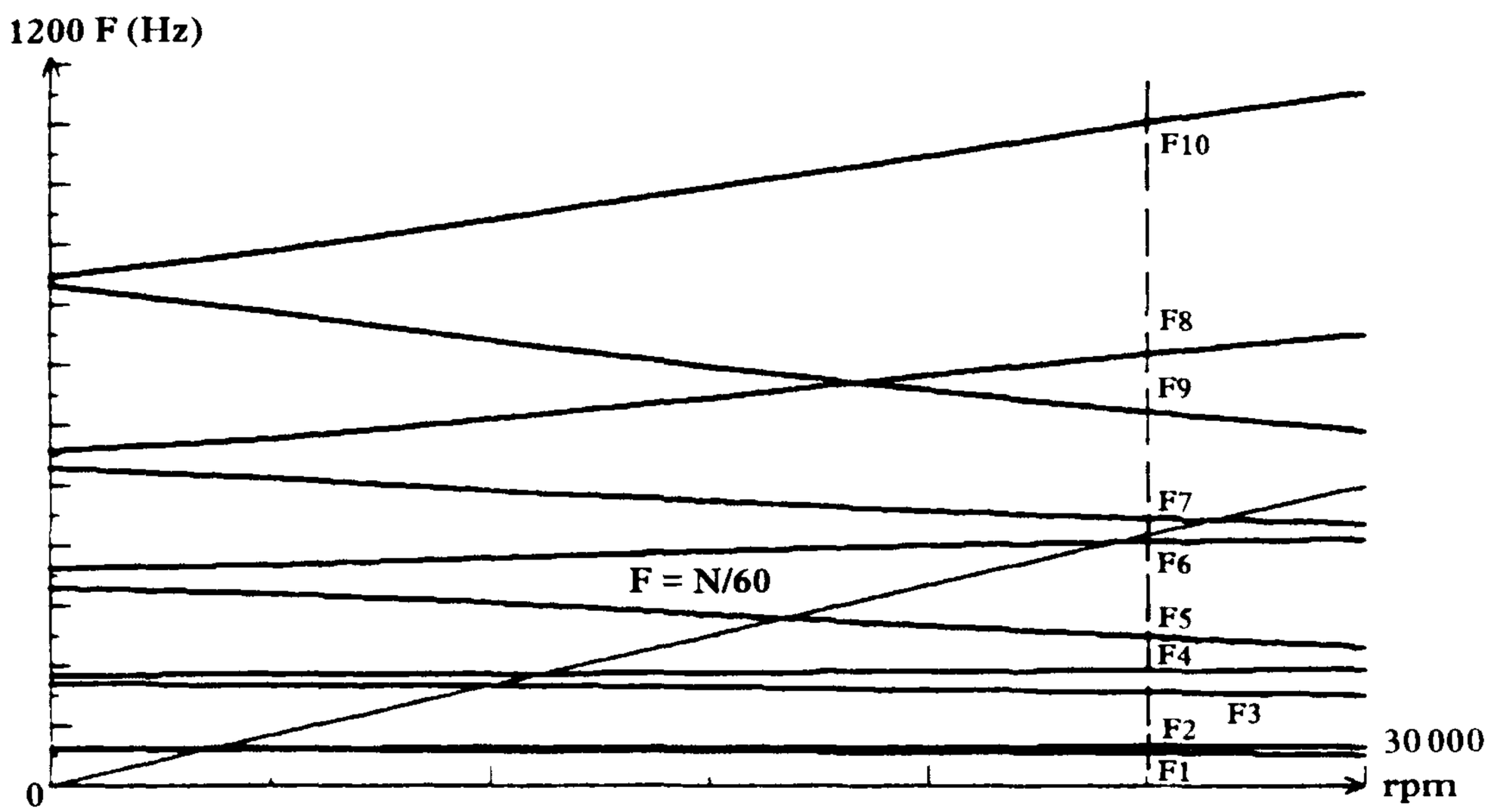

Figure 6.2. Campbell diagram

Table 6.2. Frequencies in hertz at 25 000 rpm

Frequency	Reference Value	2 Modes	4 Modes	6 Modes	8 Modes	10 Modes	12 Modes	14 Modes
F1	55,41	56,14 1,3%	56,13 1,3%	55,7 0,5%	55,48 0,1%	55,47 0,1%	55,43 0%	55,43 0%
F2	67,20	68,05 1,3%	68,04 1,3%	67,46 0,4%	67,26 0,1%	67,25 0,1%	67,22 0%	67,21 0%
F3	157,9		160,3 1,5%	160,2 1,5%	160 1,3%	158,4 0,3%	158,1 0,1%	157,9 0%
F4	193,6		196,3 1,4%	196,2 1,3%	195,9 1,2%	194,1 0,3%	193,8 0,1%	193,7 0,1%
F5	249,9			270,7 8,3%	254,5 1,8%	253,4 1,4%	251,2 0,5%	250,9 0,4%
F6	407,5			448,3 10,0%	413 1,3%	410,7 0,8%	409,4 0,5%	408,5 0,2%
F7	446,7				453,2 1,5%	452,5 1,3%	448,2 0,3%	447,3 0,1%
F8	714,9				759,9 6,3%	758,6 6,1%	720,1 0,7%	720,1 0,7%
F9	622,7					635,7 2,1%	628,1 0,9%	624,5 0,3%
F10	1076					1144 6,3%	1082 0,6%	1080 0,4%

The two bearings are assumed to be identical and characterized by

$$k_{xx} = 5 \times 10^7 \,\mathrm{N/m} \quad k_{zz} = 7 \times 10^7 \,\mathrm{N/m} \quad k_{xz} = k_{zx} = 0$$
$$c_{xx} = 5 \times 10^2 \,\mathrm{N/m/s} \quad c_{zz} = 7 \times 10^2 \,\mathrm{N/m/s} \quad c_{xz} = c_{zx} = 0$$

The speed of rotation of the rotor ranges from zero to 30 000 rpm.

6.1.1 The Campbell diagram

The ten lowest frequencies obtained by the direct method, as a function of the speed of rotation, are presented in Figure 6.2.

The frequencies at 25 000 rpm are shown in Table 6.2, where the pseudo-modal results with $n = 2, 4, \ldots, 14$ are compared with the reference. The percentage accuracy of the frequency is also given.

6.1.2 Mass unbalance response

A mass unbalance of 200 g mm is assumed to be situated on disk D_2. The results for the reference (displacement node 6) are shown in Figure 6.3. The pseudo-modal results are shown in Figures 6.4–6.7 for a number of modes ($n = 2, 4, 6, 8$). The results (critical speed of rotation, amplitude of the response at node 6, and percentage accuracy of the amplitude) are summarized in Table 6.3.

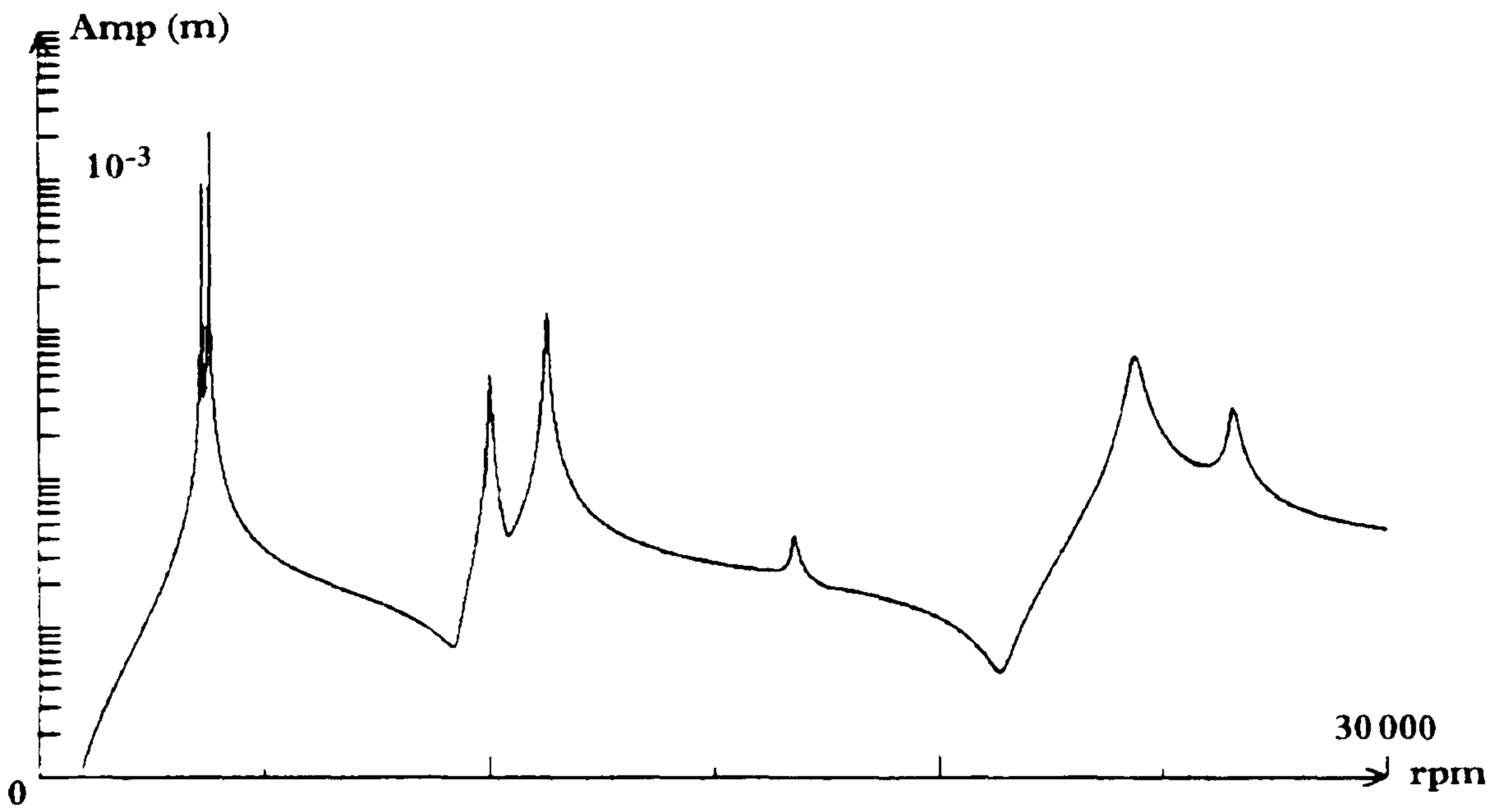

Figure 6.3. Mass unbalance response: reference

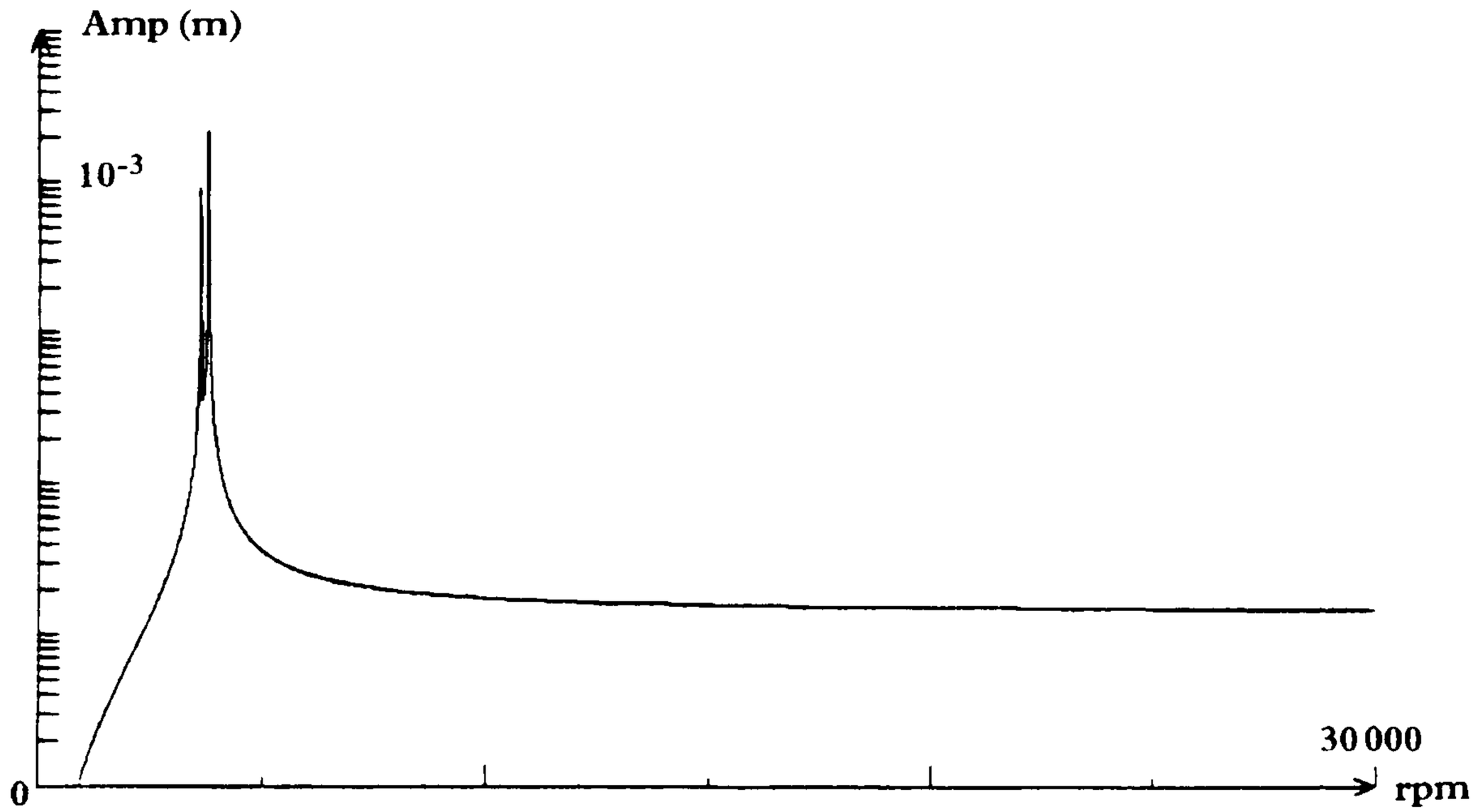

Figure 6.4. Mass unbalance response: $n = 2$

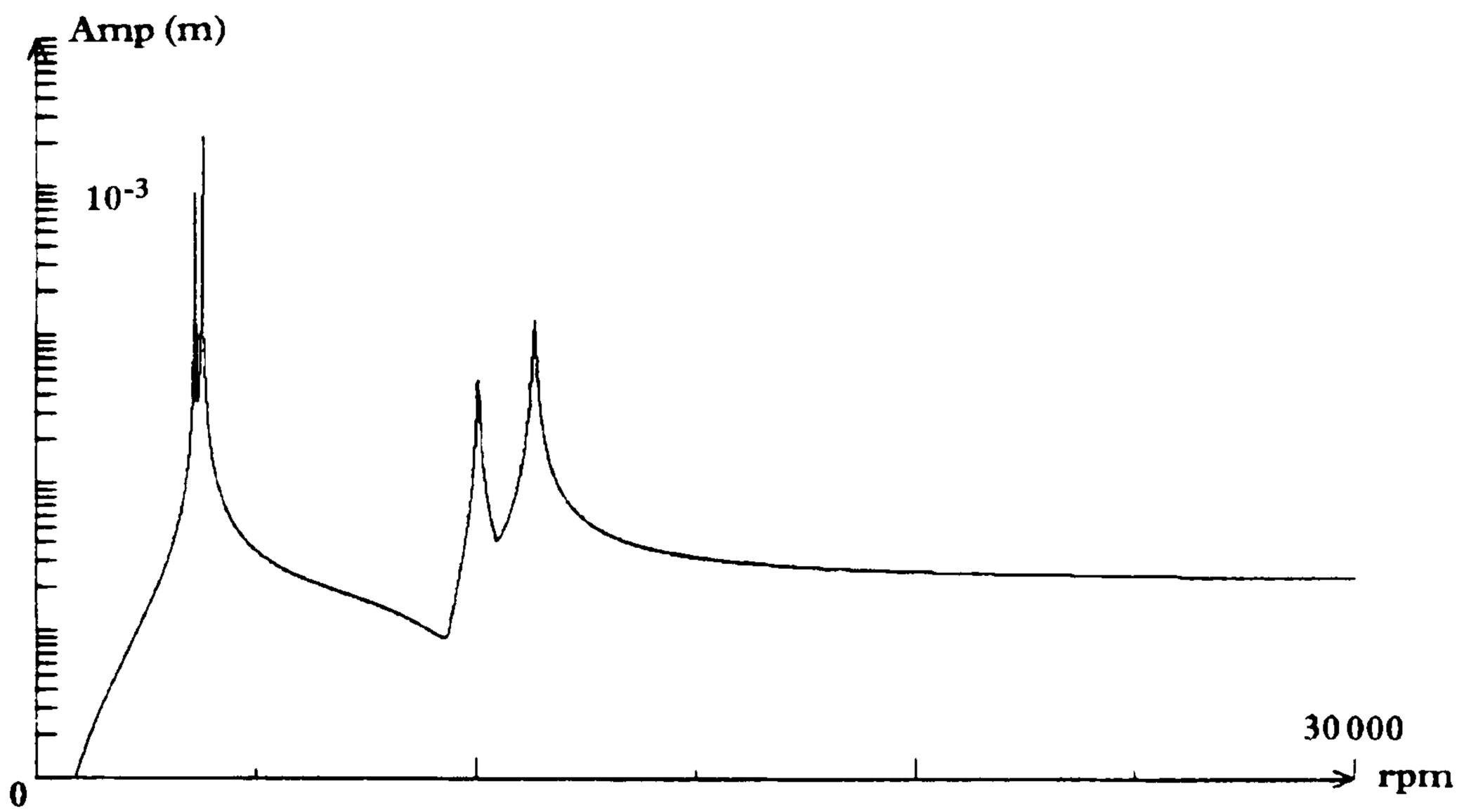

Figure 6.5. Mass unbalance response: $n = 4$

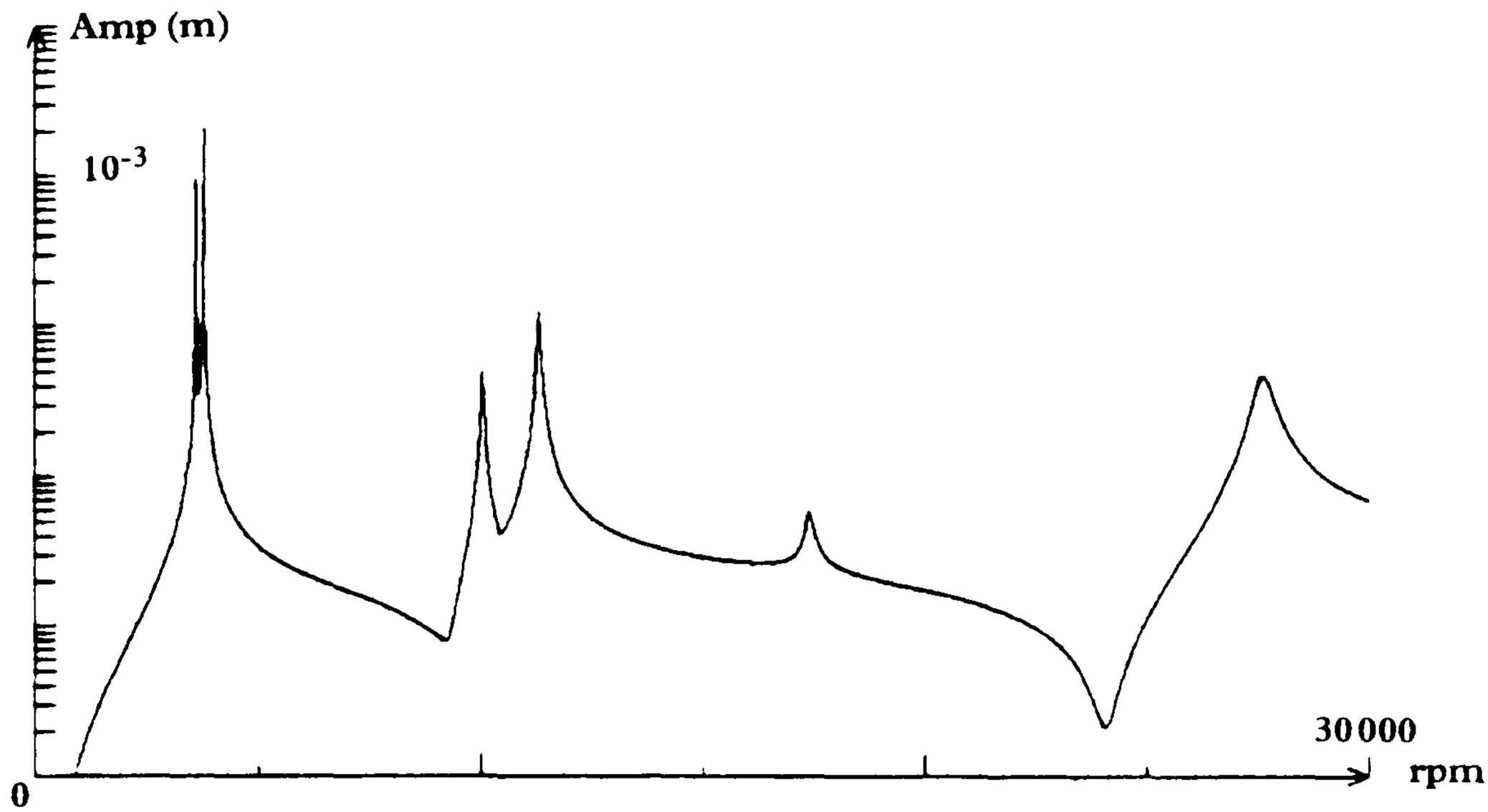

Figure 6.6. Mass unbalance response: $n = 6$

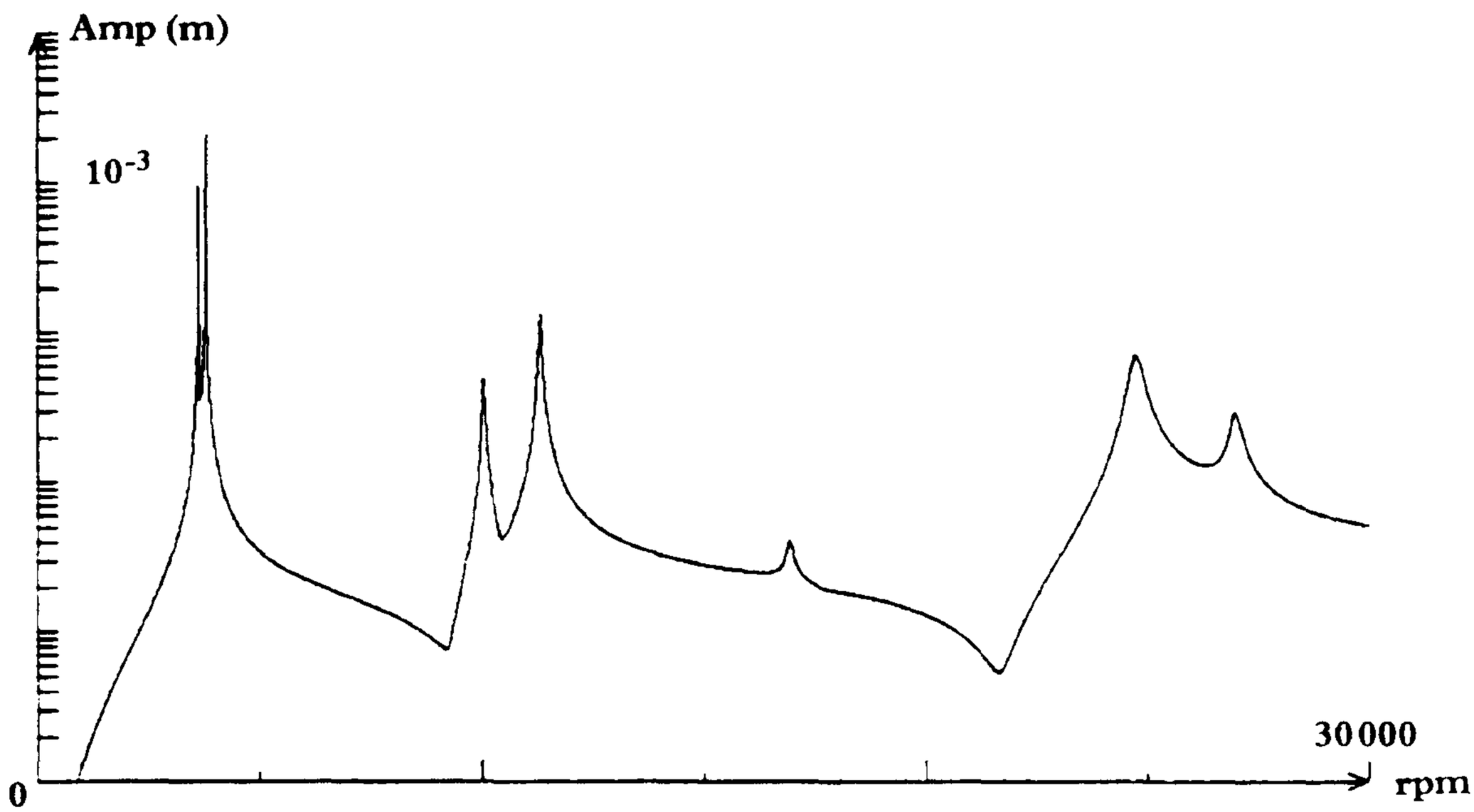

Figure 6.7. Mass unbalance response: $n = 8$

Table 6.3. Critical speeds and unbalance response as a function of n

Critical Speed	Reference Value	$n = 2$	$n = 4$	$n = 6$	$n = 8$	$n = 10$	$n = 12$	$n = 14$
C1	3620,4	3621,2	3621,2	3620,7	3620,4	3620,4	3620,4	3620,4
	9,38E-04	9,10E-04	9,12E-04	9,38E-04	9,41E-04	9,40E-04	9,38E-04	9,38E-04
		−3,0%	−2,8%	0%	0,3%	0,2%	0%	0%
C2	3798,1	3799,4	3799,3	3798,5	3798,2	3798,1	3798,1	3798,1
	2,10E-03	2,18E-03	2,18E-03	2,09E-03	2,09E-03	2,09E-03	2,10E-03	2,10E-03
		3,8%	3,8%	−0,5%	−0,5%	−0,5%	0%	0%
C3	10018		10041	10041	10037	10022	10019	10018
	5,00E-05		5,05E-05	5,04E-05	4,96E-05	4,97E-05	5,02E-05	5,00E-05
			1,0%	0,8%	−0,8%	−0,6%	0,4%	0%
C4	11279		11312	11313	11308	11285	11281	11279
	1,30E-04		1,26E-04	1,28E-04	1,33E-04	1,32E-04	1,30E-04	1,30E-04
			−3%	−1,5%	2,3%	1,5%	0%	0%
C5	16785			17399	16918	16883	16824	16816
	4,21E-06			5,89E-06	4,10E-06	4,28E-06	4,27E-06	4,20E-06
				39.9%	−2,6%	1,7%	1,4%	−0,2%
C6	24408			27629	24763	24615	24533	24472
	6,84E-05			4,84E-05	7,20E-05	6,59E-05	6,57E-05	7,04E-05
				−29,2%	5,3%	−3,7%	−3,9%	2,9%
C7	26615				27010	26951	26708	26651
	3,09E-05				2,94E-05	2,75E-05	3,31E-05	3,21E-05
					−4,9%	−11,0%	7,1%	3,9%

The results obtained by the pseudo-modal method are very satisfactory if a sufficient number of modes is used to reduce the number of equations. This was shown for industrial applications presented in [4].

6.2 INFLUENCE OF MODELING

6.2.1 Number of shaft elements

The rotor in Figure 6.1 is used again and the results are limited to the value of frequencies at 25 000 rpm. The calculations have been performed using 26 and 13 shaft finite elements of equal length, as well as on a very rough model with only four finite elements. In the latter case the five nodes are obviously located at the bearings and disk locations.

The results, presented in Table 6.4, show that the differences between a model using 13 and 26 finite elements are always lower than 0.1 percent. The results obtained using only four finite elements are also quite accurate and demonstrate that it is not always necessary to use a large number of shaft finite elements to obtain satisfactory results.

6.2.2 Models of the disk

The disks and shaft can be assembled in different ways (Figure 6.8). In model 1, the disk is wedged or mounted on a grooved shaft. It is reasonable to assume that the disk does not change the stiffness of the shaft, and the inertia characteristics of the disk are concentrated at the corresponding shaft element node.

In model 2, the disk is shrunk on the shaft, or the disk–shaft assembly is solid. Here one assumes that the disk increases the stiffness of the shaft, the radius of which is supposed to be increased by $h/2$, where h is the disk thickness near the shaft. The disk characteristics are lumped at node 2. In this situation the inertia characteristics, if h is important, can be lumped at three nodes, as in model 3.

Table 6.4. Frequencies in hertz at 25 000 rpm ($n = 14$)

4FE	55,42	67,21	157,9	193,7	250,1	408,7	447,4	725,7	624,0	1129
13FE	55,43	67,21	157,9	193,7	250,9	408,5	447,3	720,1	624,5	1080
26FE	55,43	67,21	157,9	193,7	250,9	408,4	447,3	719,8	624,5	1079

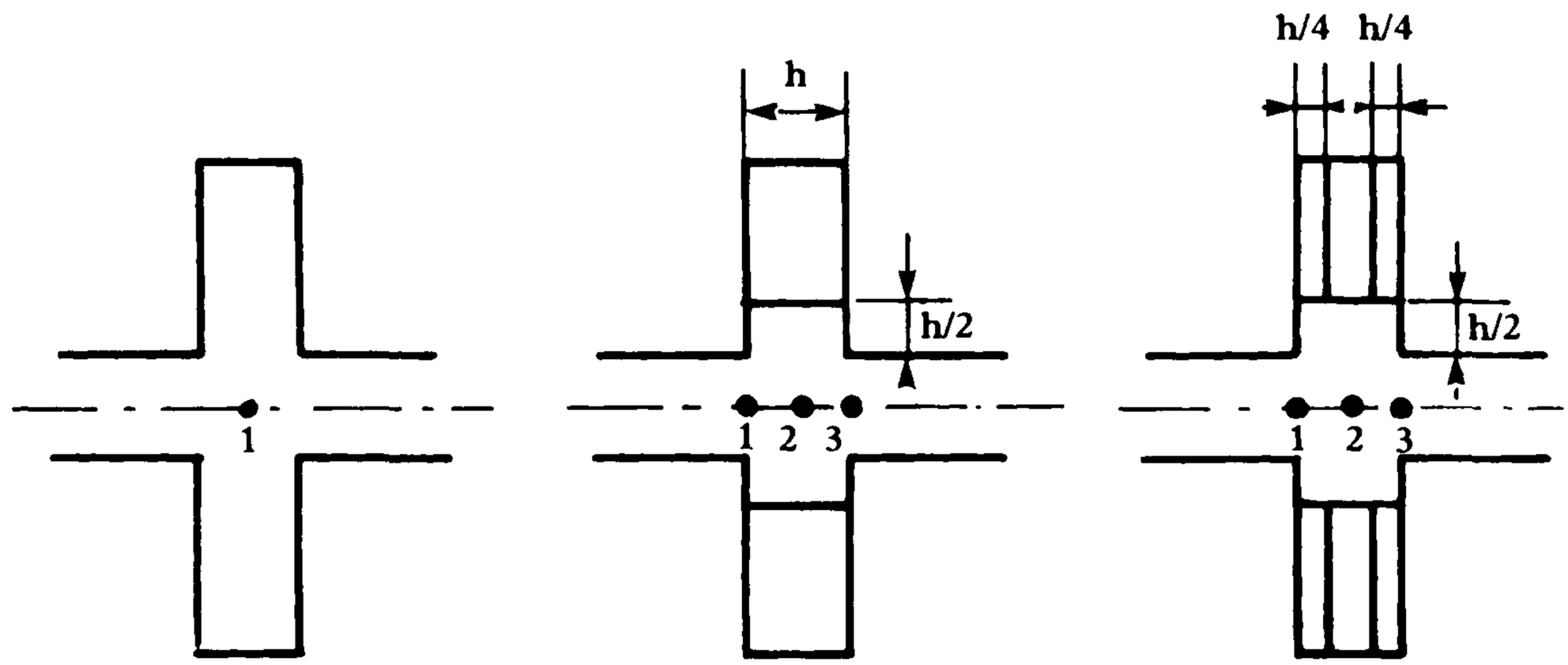

Figure 6.8. Shaft–disk models

Table 6.5. Frequencies in hertz at 25 000 rpm for different models

Frequencies	Model 1	Model 2	Model 3
F1	55,43	58,34 5,2%	58,35 5,3%
F2	67,21	70,02 4,0%	70,03 4,0%
F3	157,9	164,5 4,0%	164,7 4,1%
F4	193,7	203,2 4,7%	203,3 4,7%
F5	250,9	260,9 3,8%	261,7 4,1%
F6	408,5	425,2 3,9%	425,2 3,9%
F7	447,3	488,1 8,4%	489,6 8,6%
F8	720,1	751,9 4,2%	749,7 3,9%
F9	624,5	695,4 10%	705,1 11%
F10	1080	1163 7,1%	1160 6,9%

The frequencies at 25 000 rpm using 13 shaft finite elements and $13 + (2 \times 3) = 19$ shaft finite elements (models 2 and 3) are presented in Table 6.5. The number of modes used is $n = 14$.

The results obtained with models 2 and 3 are very similar, but these results are fairly different from those obtained using model 1. It is thus necessary in real situations to know how the disks and shafts are assembled in rotors.

6.3 NATURAL FREQUENCIES: THE BEARING STIFFNESS DIAGRAM

Rotation effects are not considered for the shaft and the disks. The bearing stiffness diagram (Figure 6.9) is the representation of the evolution of the rotor frequencies versus bearing stiffness, which are supposed to be:

- identical for all the bearings;

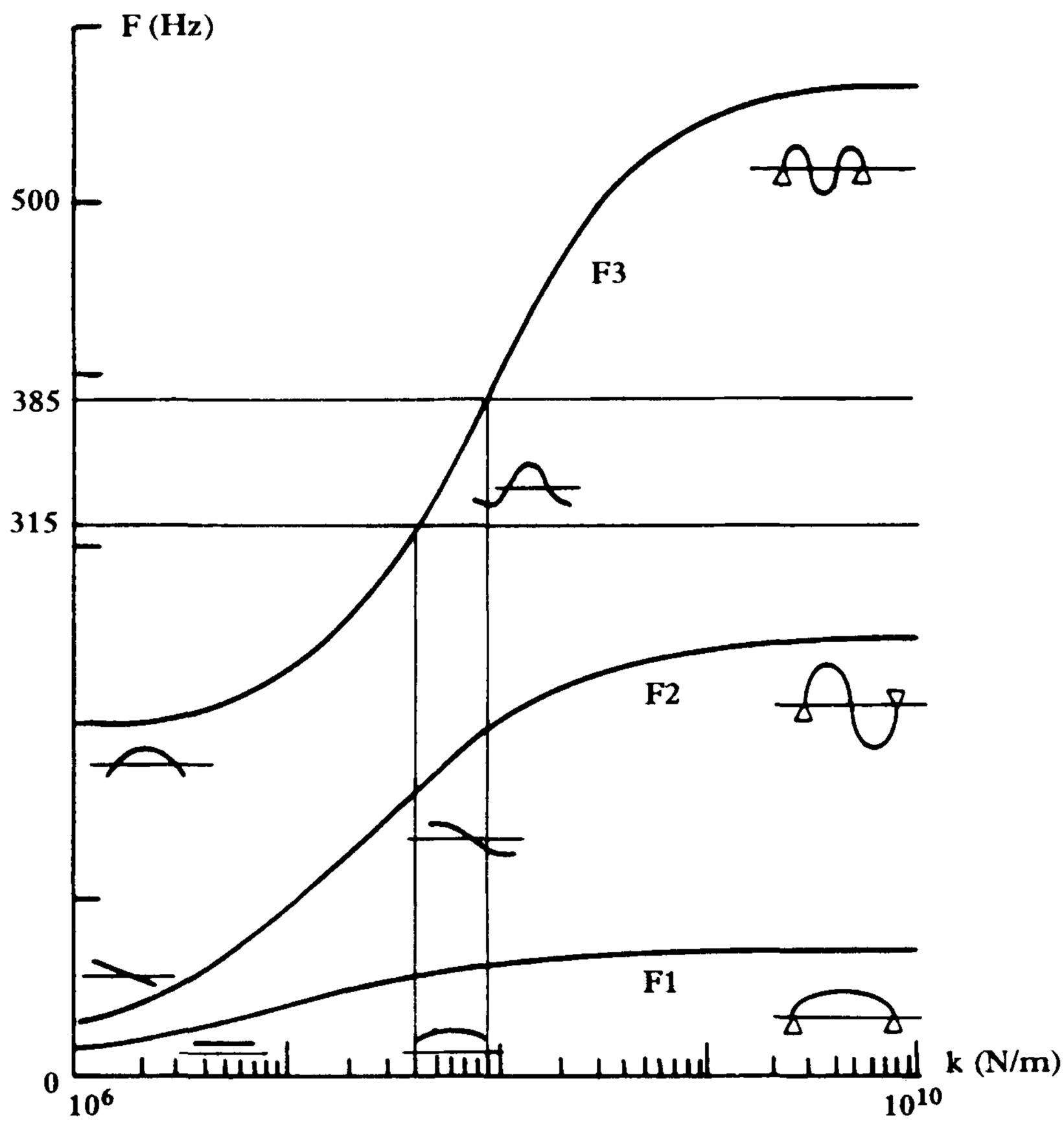

Figure 6.9. Frequencies versus equivalent bearing stiffness

- equal to the equivalent stiffness.

$$k_x = \sqrt{k_{xx}^2 + \Omega^2 c_{xx}^2} \tag{6.1}$$

with

$$k_x = k_z = k \tag{6.2}$$

$$k_{xz} = k_{zx} = c_{xz} = c_{zx} = 0 \tag{6.3}$$

where Ω is the angular speed of rotation.

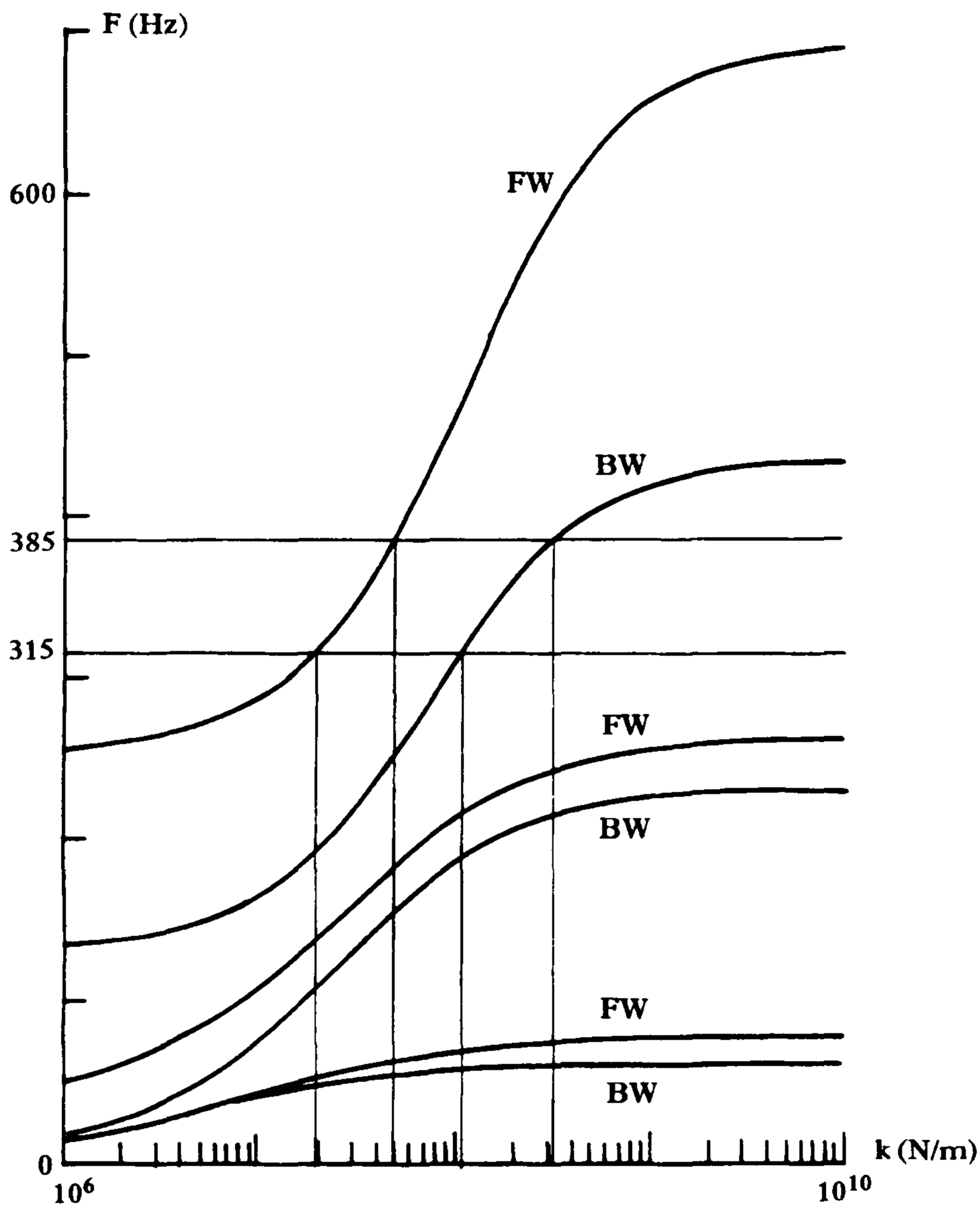

Figure 6.10. Frequencies including gyroscopic effects versus equivalent bearing stiffness

This diagram is very useful in the preliminary phase of the design of a rotor, by giving information about the comparative stiffnesses of the shaft and the bearings. This is recommended (and sometimes required) by turbomachinery standards, such as those of the American Petroleum Institute (API).

When the gyroscopic effect is low the frequencies are not a function of the speed of rotation. It can be shown from the diagram that if the operating speed of the rotor is 21 000 rpm (350 Hz), frequencies in the range 315–385 Hz must be avoided ($\pm$ 10 percent of the operating speed). It can be concluded roughly that the equivalent bearing stiffness should be out of the range 4×10^7 to 9×10^7 N/m.

When the gyroscopic effect is significant it is necessary to include in the prediction its influence at the nominal speed of rotation (21 000 rpm). Six frequencies appear now (3 in FW, 3 in BW)–Figure 6.10. It can be concluded roughly that the equivalent bearing stiffness must be from the range 2×10^7 to 5×10^7 N/m (FW critical speeds) or 1×10^8 to 3.1×10^8 N/m (BW critical speeds). The API diagrams thus give guidance on the stiffnesses to be used for bearings.

6.4 TRANSMISSIBILITY

6.4.1. Elementary model

The system shown in Figure 6.11 represents an elementary model of a rotating machine of mass $M - m$ submitted to the unbalance md. The machine is fixed to the foundation through a spring k and a viscous damper c. The mass m rotates at a constant speed of rotation Ω, and the

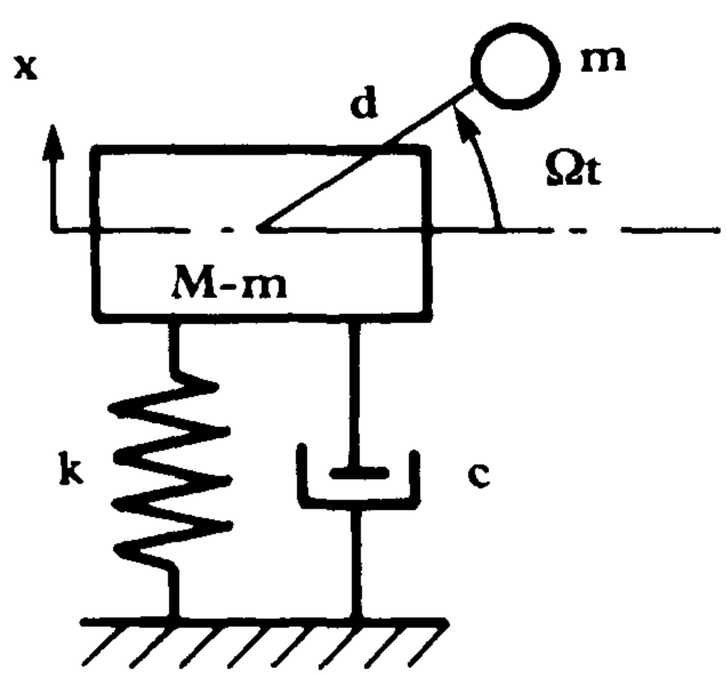

Figure 6.11. Elementary model

system equation is

$$M\ddot{x} + c\dot{x} + kx = md\Omega^2 \sin \Omega t \tag{6.4}$$

In steady-state motion the displacement is

$$x = X \sin(\Omega t - \phi) \tag{6.5}$$

and it is easy to relate X, the displacement amplitude, and F_t, the force transmitted to the foundations:

$$F_t = X\sqrt{k^2 + c^2\Omega^2} \tag{6.6}$$

These expressions can be shown to be

$$X = \frac{md\Omega^2}{\sqrt{(k - M\Omega^2)^2 + c^2\Omega^2}} \tag{6.7}$$

$$F_t = md\Omega^2\sqrt{\frac{k^2 + c^2\Omega^2}{(k - M\Omega^2)^2 + c^2\Omega^2}} \tag{6.8}$$

These can be written in a more convenient form for use as:

$$X = \frac{md}{M}\frac{(\Omega/\omega)^2}{\sqrt{[1 - (\Omega/\omega)^2]^2 + (2\alpha\Omega/\omega)^2}} \tag{6.9}$$

$$F_t = \frac{mdk(\Omega/\omega)^2}{M}\sqrt{\frac{1 + (2\alpha\Omega/\omega)^2}{[1 - (\Omega/\omega)^2]^2 + (2\alpha\Omega/\omega)^2}} \tag{6.10}$$

with ω, the natural frequency, and α, the viscous damping factor, such that

$$\omega = \sqrt{k/M} \tag{6.11}$$

$$c = 2\alpha\sqrt{kM} \tag{6.12}$$

The quantities MX/md and MF_t/kmd are presented in Figures 6.12 and 6.13 as a function of (Ω/ω) in the conditions of no damping $(\alpha = 0)$ and with some damping $(\alpha = 0.1)$.

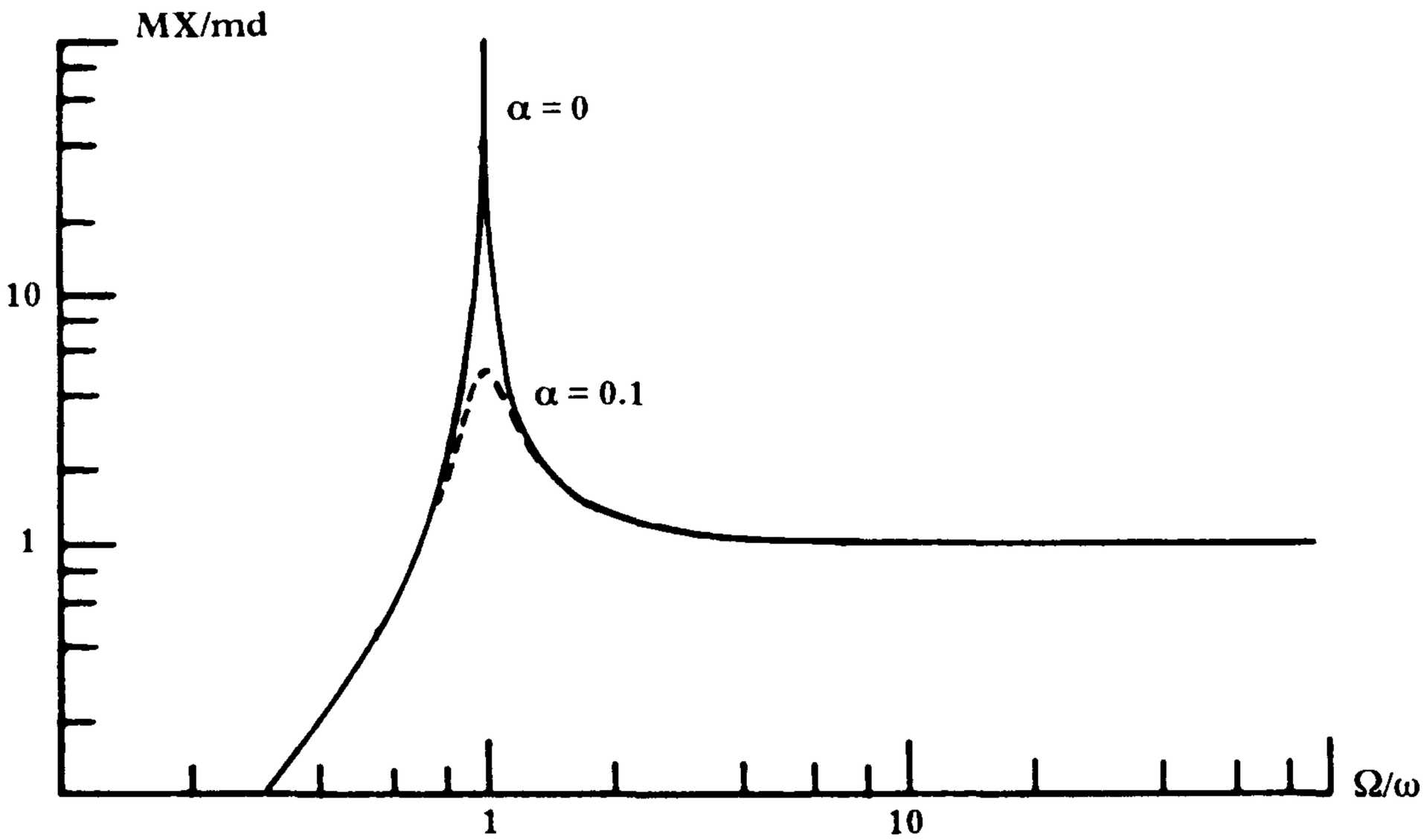

Figure 6.12. Response amplitude

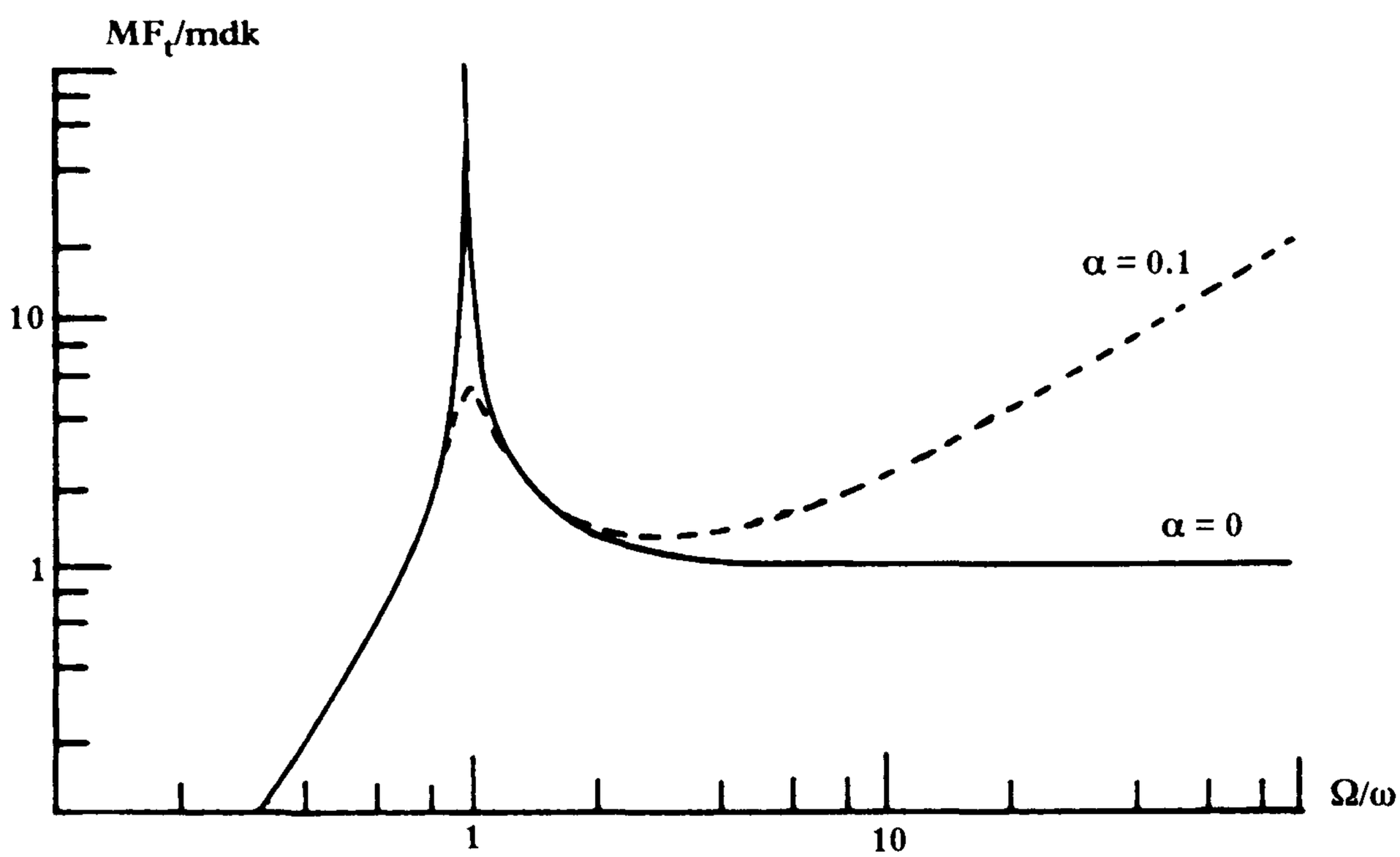

Figure 6.13. Transmissibility

It must be noted that when there is no damping $MX/md = MF_t/kmd$, and in what could be considered as supercritical operating conditions ($\Omega/\omega > 1$), these quantities tend towards unity. When damping is present in resonant conditions, both X and F_t stay limited, but in operating conditions MX/md tends towards unity and MF_t/kmd increase; hence the addition of damping increases the transmissibility.

6.4.2 Simple rotor

The rotor used for illustration is the symmetric rotor defined in Chapter 2. Its model uses nine finite elements (Figure 6.14), and the bearing values are

$$k_{xx} = k_{zz} = 10^7 \,\mathrm{N/m} \tag{6.13}$$

$$k_{xz} = k_{zx} = 0 \tag{6.14}$$

$$c_{xx} = c_{zz} = c \tag{6.15}$$

$$c_{xz} = c_{zx} = 0 \tag{6.16}$$

The mass unbalance 15 g mm is located on the disk. The results (Figures 6.15 and 6.16) show that the amplitude of the response (node 1), when the speed of rotation is far enough from the critical speed, is constant and not affected by the value of the damping.

Now let u and w be respectively the displacements at node 1 in the x and z directions. Here the whirl is always forward, and

$$u = A \cos \Omega t \tag{6.17}$$

$$w = -A \sin \Omega t \tag{6.18}$$

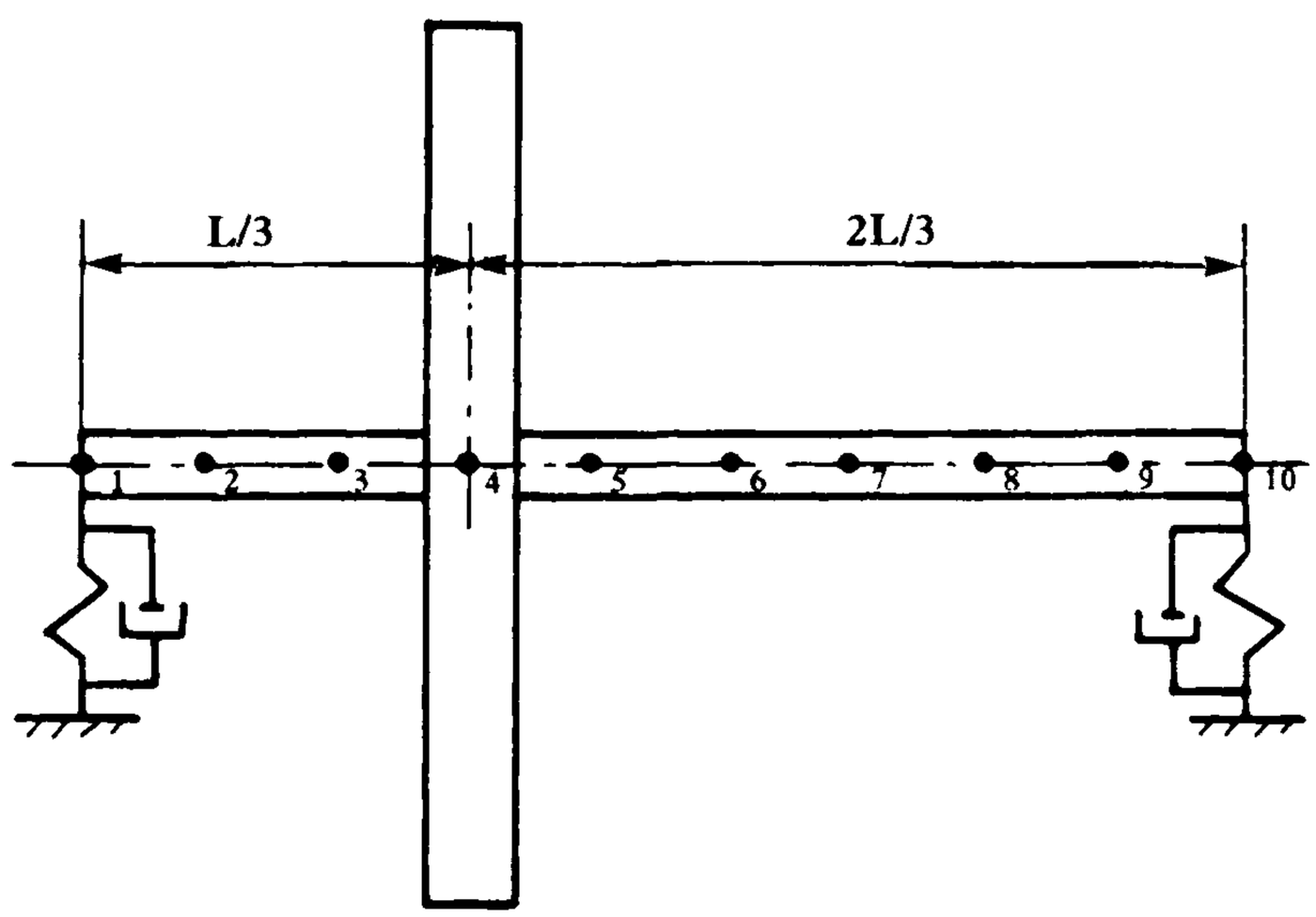

Figure 6.14. Rotor model

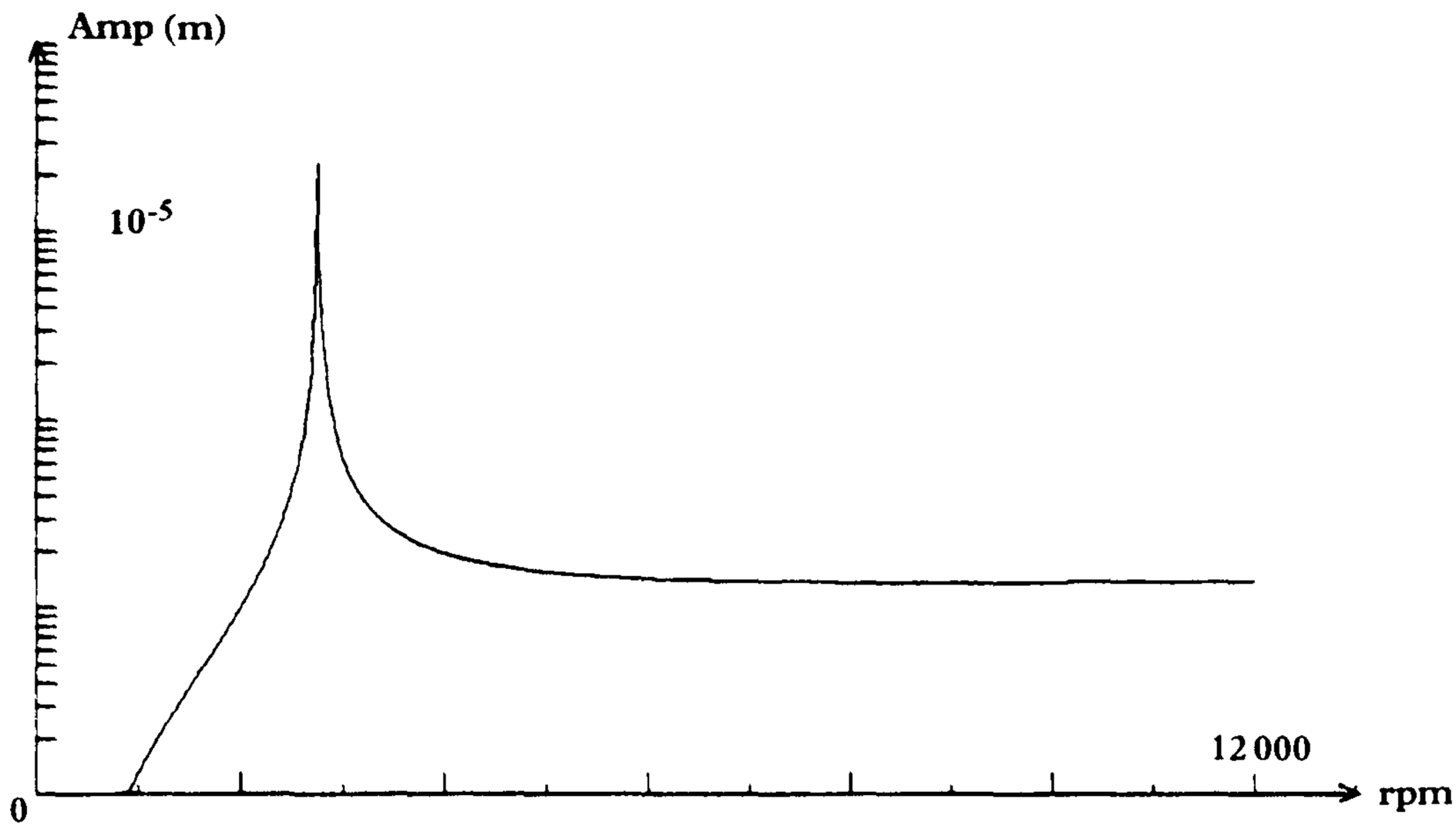

Figure 6.15. Mass unbalance response, displacement: $c = 10^3$ N/m/s

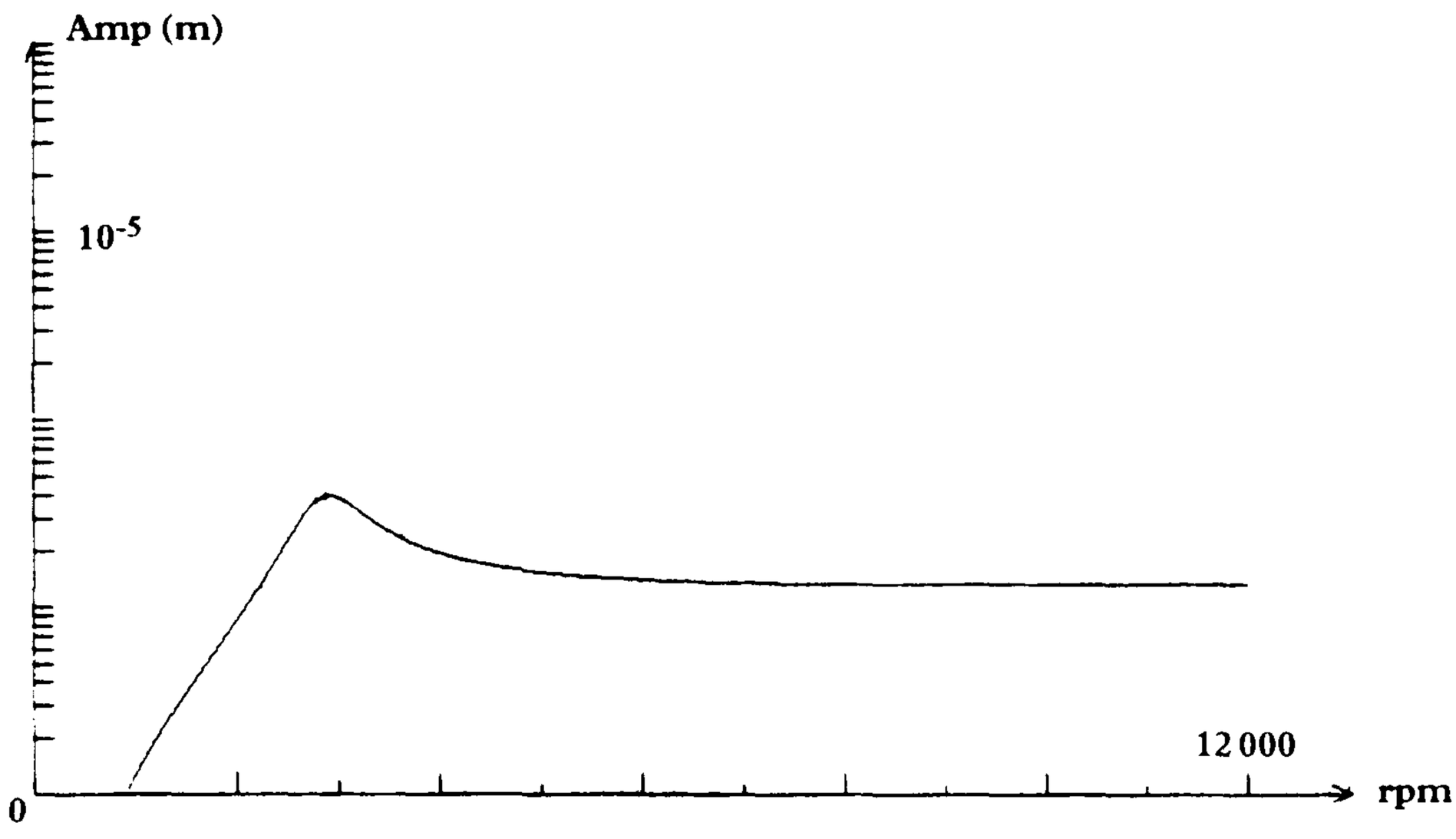

Figure 6.16. Mass unbalance response, displacement: $c = 10^5$ N/m/s

The two components of the force transmitted are

$$F_x = k_{xx}u + c_{xx}\dot{u} \tag{6.19}$$

$$= Ak\cos\Omega t - Ac\Omega\sin\Omega t \tag{6.20}$$

$$F_z = k_{zz}w + c_{zz}\dot{w} \tag{6.21}$$

$$= -Ak\sin\Omega t - Ac\Omega\cos\Omega t \tag{6.22}$$

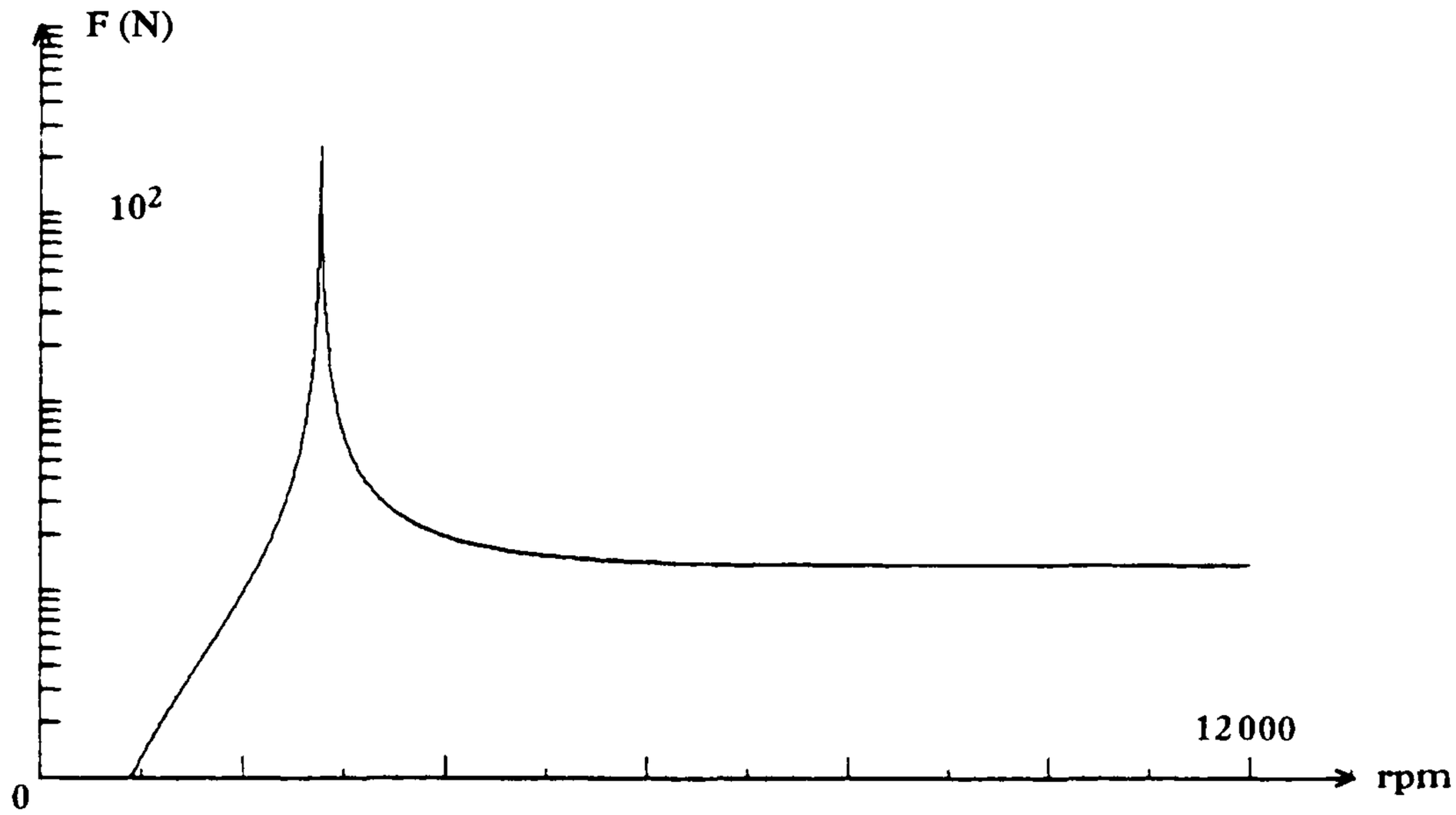

Figure 6.17. Mass unbalance response, force transmitted: $c = 10^3$ N/m/s

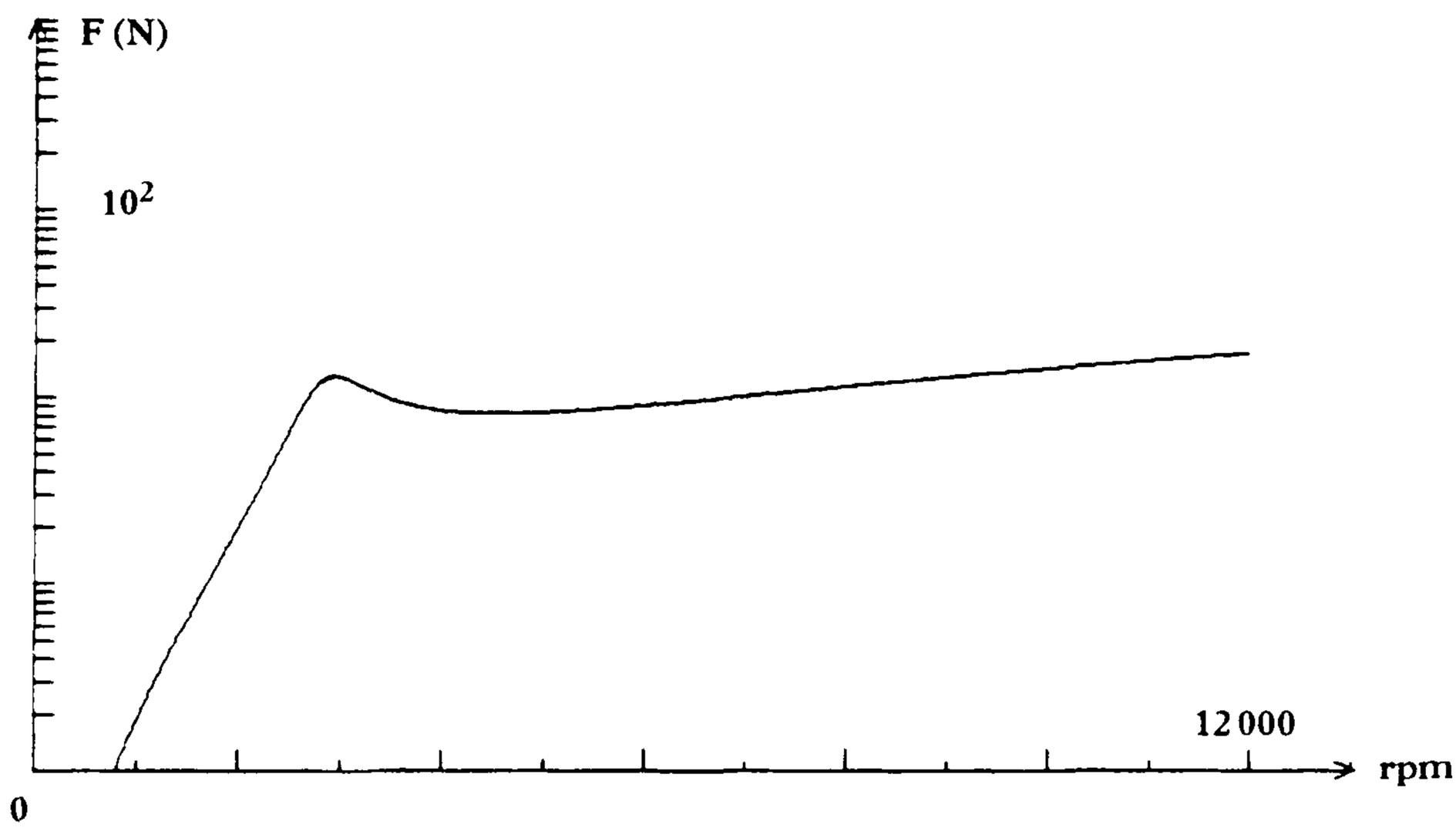

Figure 6.18. Mass unbalance response, force transmitted: $c = 10^5$ N/m/s

Hence the amplitude of the transmitted force is

$$F_t = \sqrt{F_x^2 + F_z^2} \tag{6.23}$$

$$= A\sqrt{k^2 + c^2\Omega^2} \tag{6.24}$$

When the speed of rotation is far enough from the critical speed, the amplitude of the displacement A is constant, and when c grows F_t increases. This appears clearly in Figures 6.17 and 6.18. In the range of

rotation considered, when c grows from 10^3 to 10^5 N/m/s, F_t is roughly multiplied by 10 at 10 000 rpm.

The two examples show why we should be interested in damping when dealing with critical speeds: it decreases both response and transmissibility amplitudes. However, it must be remembered that increasing the bearing damping can increase transmissibility beyond the critical speed.

6.5 BEARINGS

Bearing characteristics must be used when the behavior of a rotor in bending is predicted. The characteristics of the assembly bearing support, which can be quite different from those of the bearing alone, must be used. Two main kinds of bearings are commonly used: roller bearings and fluid film bearings.

6.5.1 Roller bearings

Roller bearings are quite difficult to model at the design stage; however, use of the Hertz contact theory gives stiffness properties, and damping, which is small, can be evaluated [34].

The Q factor of a given mode i can be known from the manufacturer's experience when dealing with a family of machines [3, 9], or it can sometimes be estimated by a rule of thumb [19]. The Q factor ($Q_i = 1/(2\alpha_i)$) can be easily introduced in equations when the pseudo-modal method is used.

The roller bearing characteristics can be obtained from experiments, with prototypes (see application 7.1). It should be noted that in this application the roller bearings are mounted with elastomer rings and the stiffness and damping properties come mostly from the elastomer element.

6.5.2 Fluid film bearings

Most of the fluid film bearings are hydrostatic bearings (the load is supported by hydrostatic pressure) or hydrodynamic bearings (the load is supported by the hydrodynamic pressure generated by rotor motion). Their stiffness and viscous damping characteristics are obtained from the solution of Reynolds equations [8, 20, 51].

7

Industrial Applications

This chapter covers the bending analysis of a selection of industrial rotors. The basic calculations are as follows.

Natural frequencies and modes, viscous damping factor and stability

It is necessary to obtain the natural frequencies as a function of the speed of rotation. These calculations give, simultaneously, the modes, the viscous damping factor and the stability or instability of the system. When one damping factor is negative the system is unstable; it is then generally said that the rotor is subjected to self-excited vibrations. The Campbell (interference) diagram clearly shows the possible resonances due to:

- unbalance: the intersections with $F = N/60$
- coupling misalignment: the intersections with $F = 2N/60$
- blade, vane, nozzle and diffusers: the intersections with $F = sN/60$
- internal aerodynamic excitations, as in centrifugal compressors: the intersections with $F = 0.5N/60$ ($0.5N/60$ is the highest value of the excitation frequency range).

N is the speed of rotation in rpm.

Response to forces of excitation

The response can be synchronous (unbalance effect) or asynchronous.

The 1979 edition of the American Petroleum Institute standards for steam turbines, gas turbines and centrifugal compressors defines mass

unbalance U_B by

$$md\Omega^2 = \frac{Mg}{2} \tag{7.1}$$

then

$$U_{\mathrm{B}} = md \approx \frac{5M}{\Omega^2} \tag{7.2}$$

where U_{B} is the unbalance in kg m, M is the mass of the rotor in kg, and Ω is 105/100 of the maximum value of the speed of rotation in rad/s. This unbalance is equivalent to the balancing class equal to $1000M/\Omega$, according to an International Standards Organization definition (ISO 1940). In the 1988 edition of the API, this criterion was changed to meet the ISO definition.

The same API standards recommend that the vibration levels at the bearing locations should not exceed

$$a = 1391/\sqrt{N} \approx 450/\sqrt{\Omega} \tag{7.3}$$

if the runout is supposed to be zero, where N is the maximum continuous speed of rotation in rpm, and a, the single peak amplitude, is in microns or micrometers (μm), a very convenient unit. (Note that 1 mill $= 10^{-3}$ in $= 25.4\,\mu\mathrm{m}$)

The procedure frequently adopted is a calculated simulation of the tests recommended by API standards to discover the sensitivity of the rotor to unbalance when a critical speed is within the specified operating speed range. The following two cases are considered:

Case 1: The mass unbalance is situated at the center of inertia of the rotor. This case is related to the so-called cylindrical (translational) mode and the first bending mode.

Case 2: The mass unbalance is divided into two equal quantities $U_{\mathrm{B}}/2$, which are situated at the two ends of the rotor in phase opposition. This case is related to the so-called conical mode and the second bending mode.

This type of calculation is very useful in the design and dynamic behavior prediction of industrial rotors, taking into account characteristics of the

shaft and bearings as accurately as possible. It is a necessary complement to the study of natural frequencies and modes, the viscous damping factor and stability.

The 1995 edition of the API standard concerning centrifugal compressors uses the value of the Q factor for each critical speed. These values are useful for appreciating the response amplitudes of the system for each critical speed. The mass unbalances and the maximum amplitudes are defined for each critical speed. The mass unbalance is

$$U_B = \frac{2 \times 6350M}{N} \tag{7.4}$$

where N, in rpm, is the operating speed which is closest to the critical speed, and U_B is in g mm. In practice the critical speed is used. The mass unbalance must be situated in such a way that the maximum displacements are obtained at the critical speed. Hence the mass unbalance must be located at points corresponding to the maximum displacements for this critical speed. For centrifugal compressors the modes concerned are commonly conical and cylindrical modes. The maximum amplitude is

$$a = \frac{25.4}{2}\sqrt{\frac{1200}{N}} \tag{7.5}$$

The operating speed ranges which must be avoided, Figure 7.1, are obtained from the value of the Q factor:

$$Q = \frac{N_c}{N_{c2} - N_{c1}} \tag{7.6}$$

If $Q < 2.5$, there is no forbidden speed range and the corresponding speed is no longer considered as a critical speed.

If $2.5 < Q < 3.55$, there is a forbidden speed range defined by

$$SM_1 = \frac{5}{100}N_c \tag{7.7}$$

$$SM_2 = \frac{15}{100}N_c \tag{7.8}$$

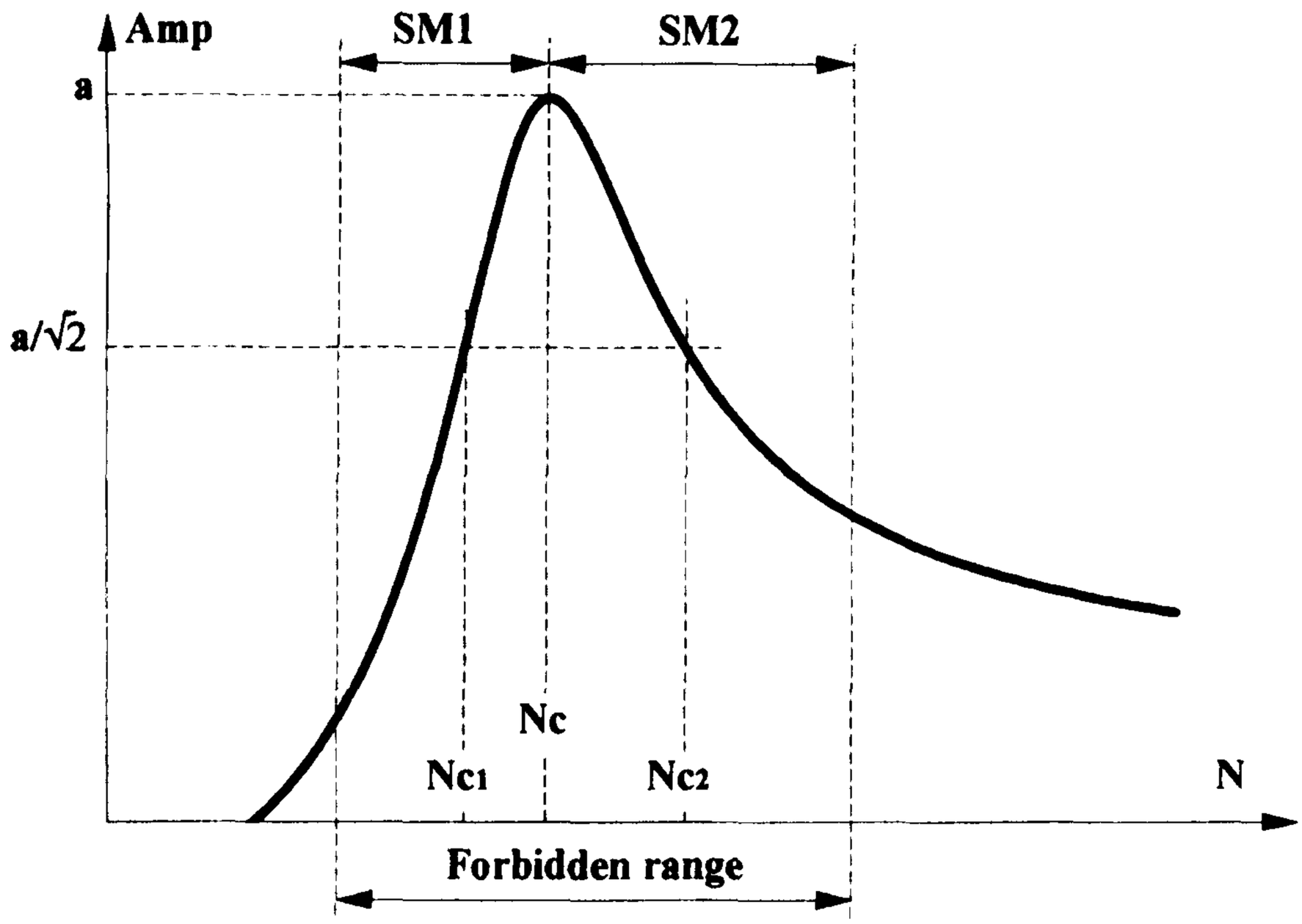

Figure 7.1. Response around a critical speed

If $3.55 < Q$, there is a forbidden speed range defined by

$$SM_1 = \left(100 - \left(84 + \frac{6}{Q-3}\right)\right)N_c \tag{7.9}$$

$$SM_2 = \left(\left(126 - \frac{6}{Q-3}\right) - 100\right)N_c \tag{7.10}$$

In addition it is recommended that for all speeds of rotation the maximum amplitude should not exceed 75 percent of the minimum clearances.

The first six applications of [40] were designed by the manufacturers according to the 1979 edition of the API standards. Applications 7.3 and 7.4 were designed by he manufacturer according to the 1995 edition of the API standards. Application 7.5 was presented previously in [40].

The computer program used for the first five applications was presented in Chapter 5 and all the results were obtained using the pseudo-modal method.

7.1 HYBRID TURBOMOLECULAR PUMP

The main characteristics of the hybrid turbomolecular pump used for gas analysis, leak detection and process monitoring, Figure 7.2, are:

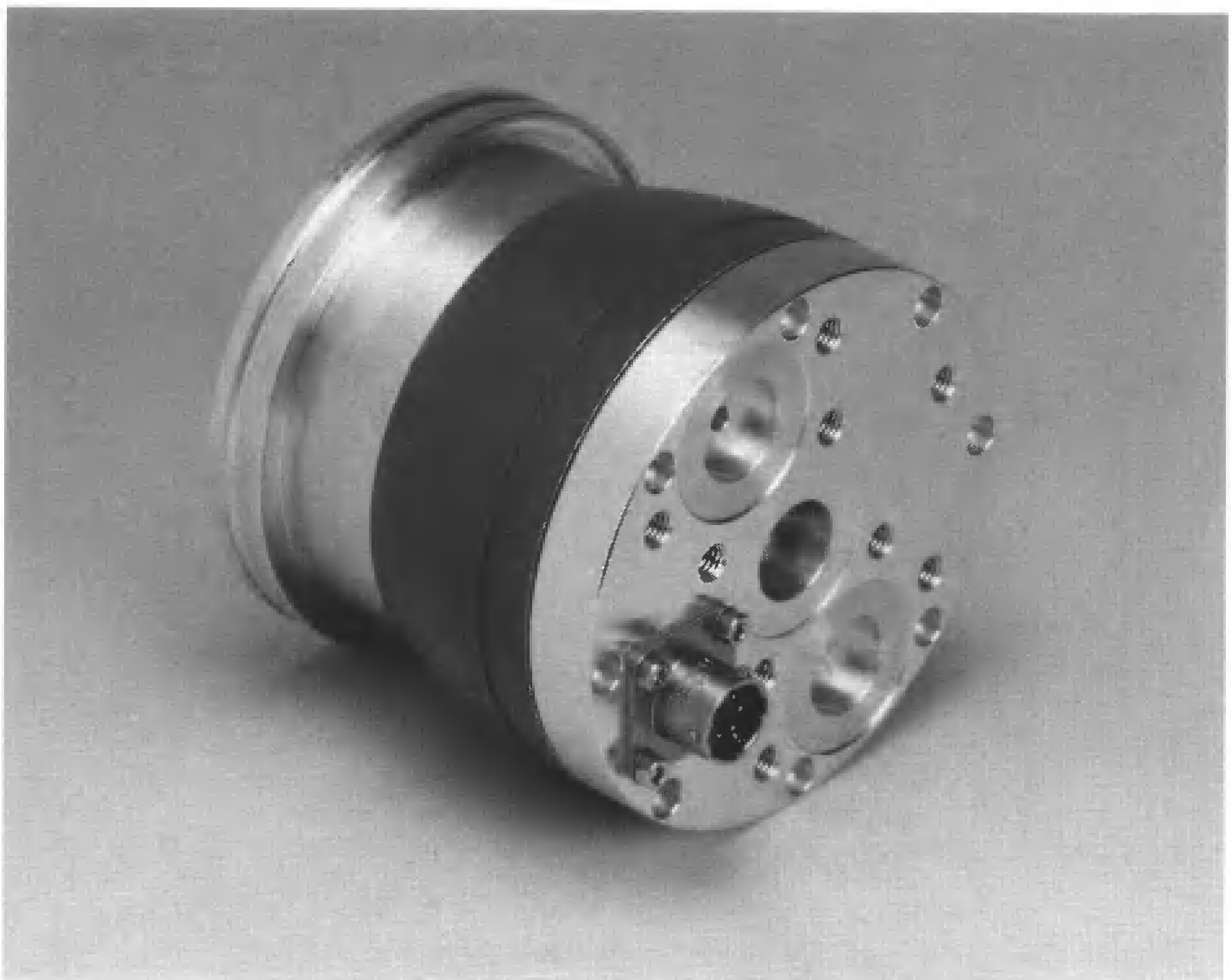

Figure 7.2. Hybrid turbomolecular pump (Picture courtesy ALCATEL-CIT)

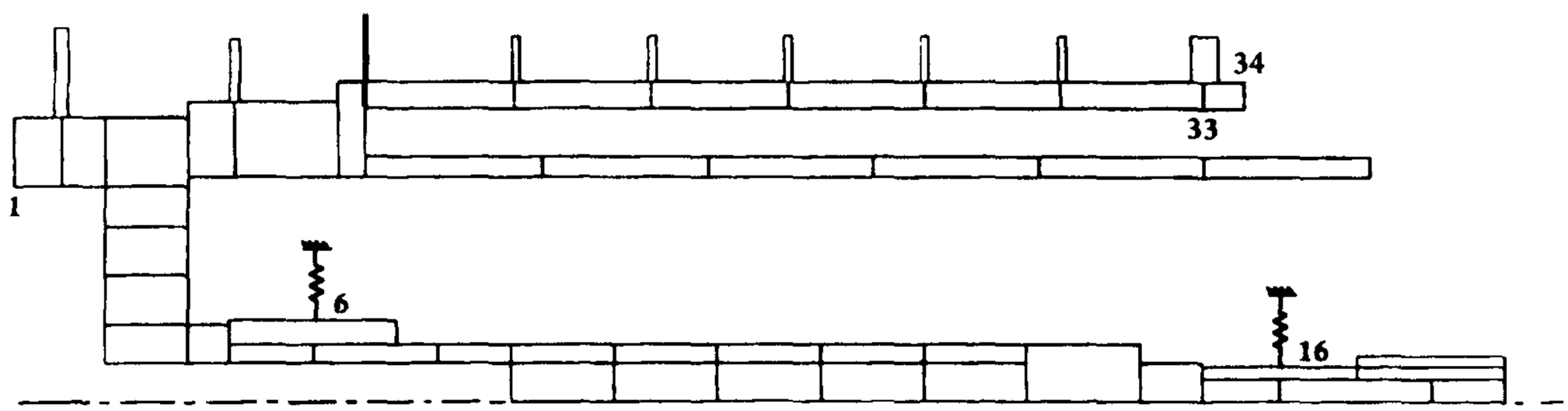

Figure 7.3. Finite element model

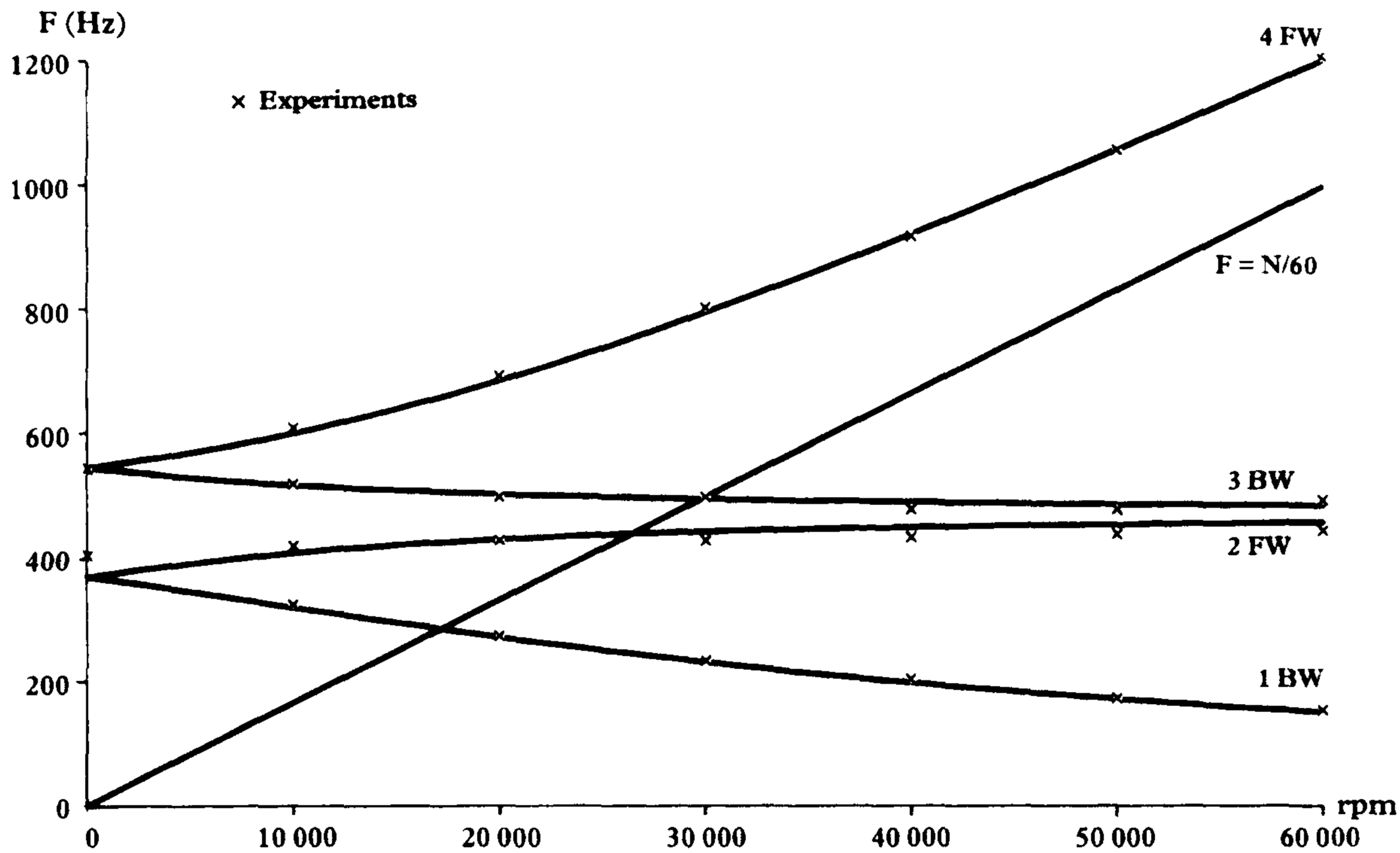

Figure 7.4. Campbell diagram

- an inlet pressure of 10^{-3} mbar (0.1 Pa) with a compression ratio of 2×10^7
- a mass of 1.2 kg and a rotor mass of 0.2 kg
- a rotor driven by an electric motor built into the shaft, and two ceramic ball bearings mounted with elastomeric rings
- an operating speed range from 36 000 to 60 000 rpm.

The finite element model, Figure 7.3, uses 42 shaft elements and 13 disks. The two bearing characteristics, which include stiffness and viscous damping coefficients, are assumed to be constant and symmetric.

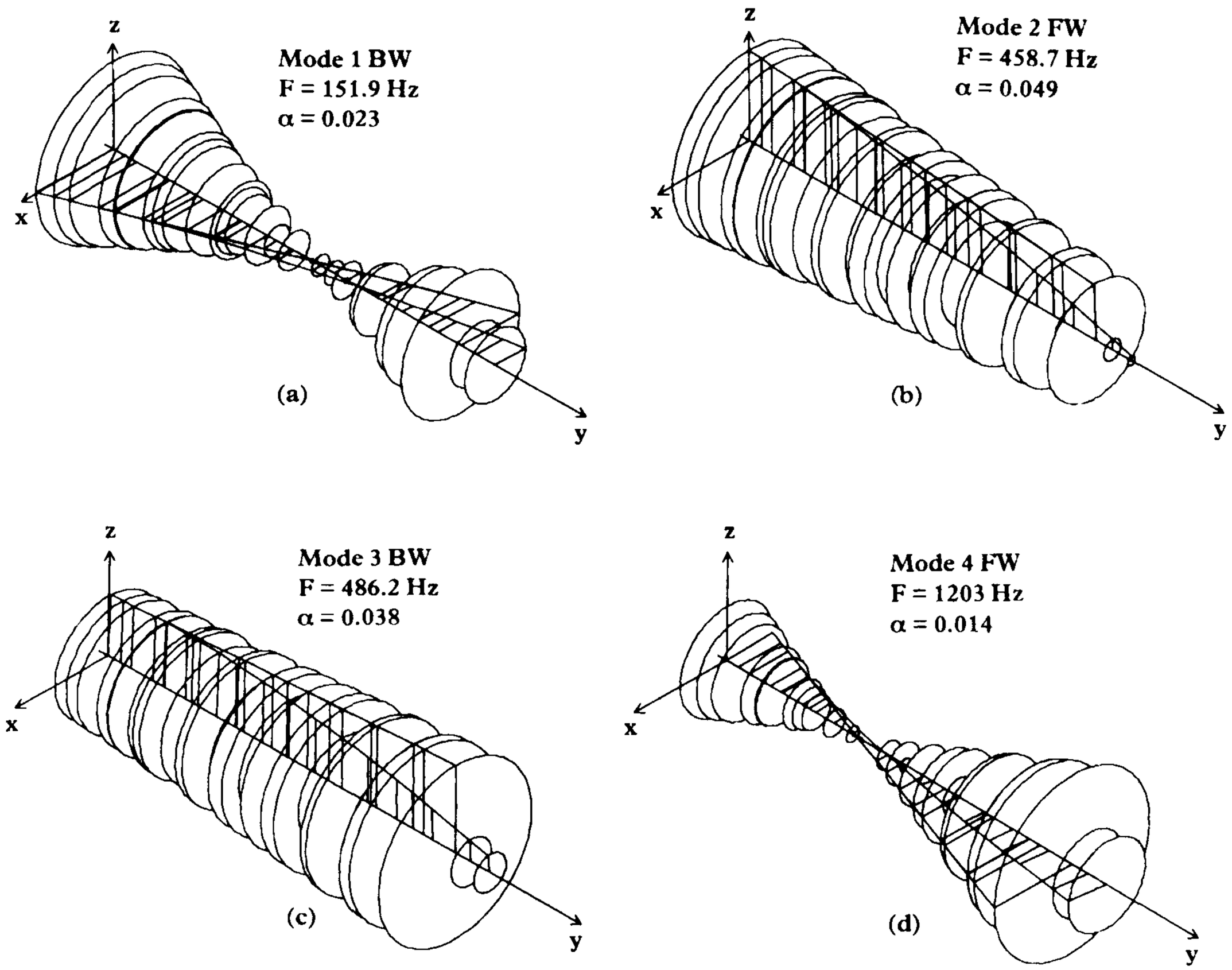

Figure 7.5. Mode shapes at 60 000 rpm

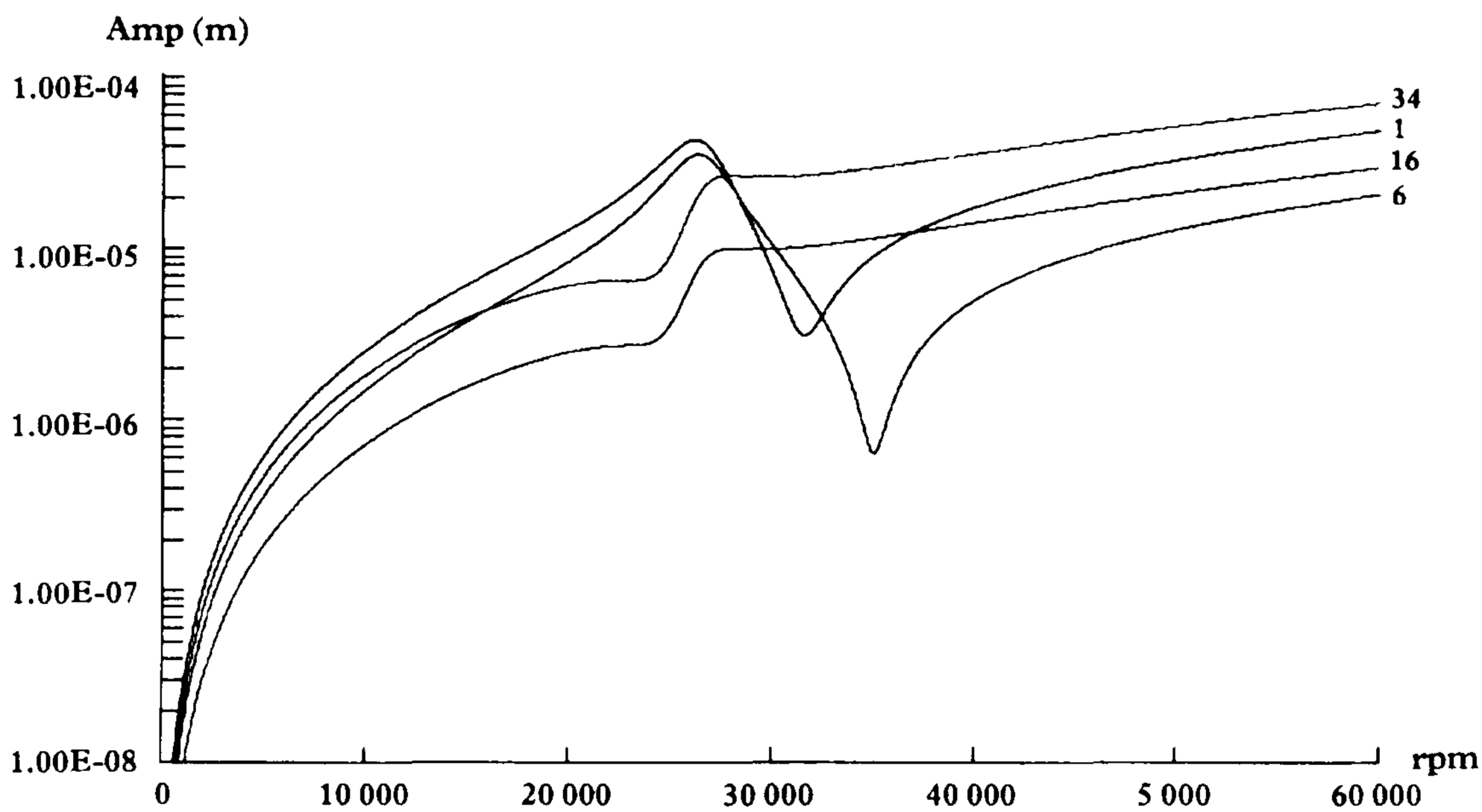

Figure 7.6. Mass unbalance response

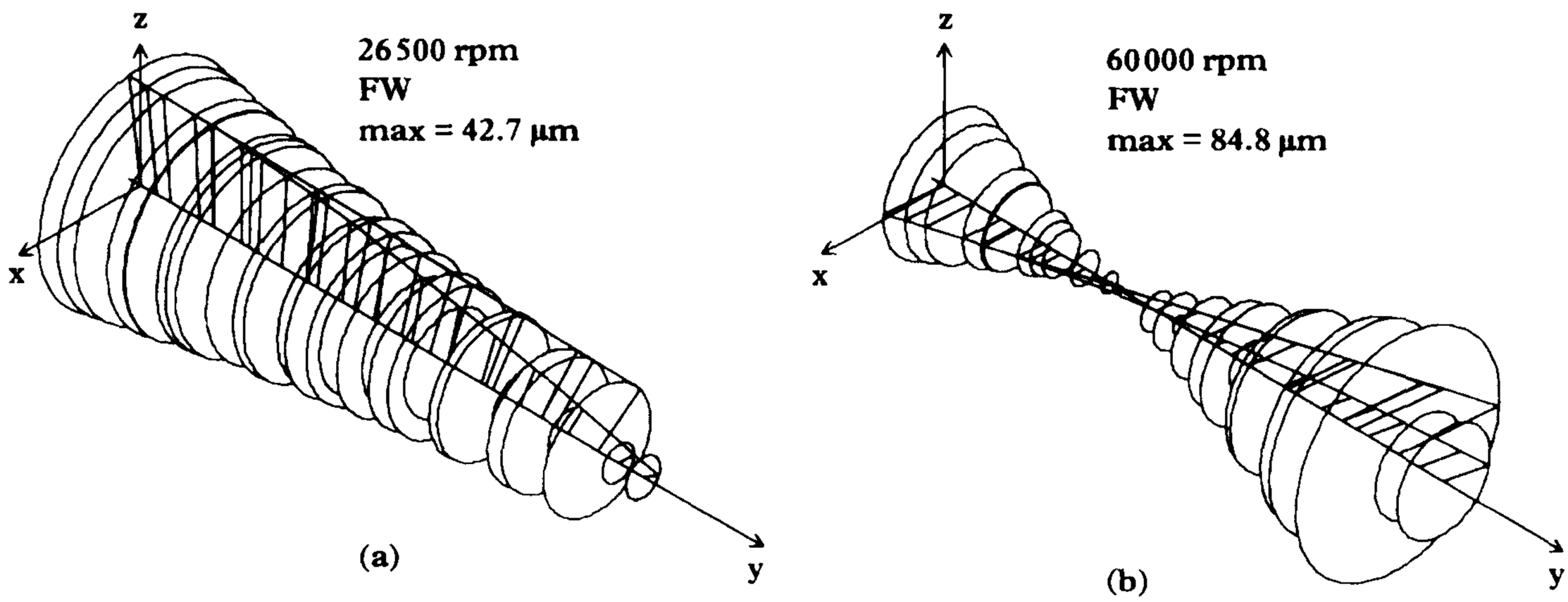

Figure 7.7. Rotor deflections

7.1.1 The Campbell diagram

The diagram is shown in Figure 7.4 and no instability occurs. The mode shapes at the highest operating speed are shown in Figure 7.5. A critical speed appears at 26 500 rpm.

7.1.2 Mass unbalance response

The mass unbalance response is calculated with two equal masses in phase opposition situated at nodes 1 and 33. The unbalance response, Figure 7.6, shows a maximum amplitude at 26 500 rpm. Between 40 000 and 60 000 rpm the amplitudes increase slowly and continuously. Rotor deflections at 26 500 rpm and 60 000 rpm are shown in Figure 7.7.

7.1.3 Remarks

The pump, supported by soft mounts and rotating at up to 60 000 rpm, has been subjected to a harmonic force fixed in space (Section 2.2.2). This frequency response, at a constant speed of rotation Ω, gives the points of the Campbell diagram. The values obtained at 20 000 rpm have been used for estimating bearing stiffnesses and modal damping (Section 6.5). These values have been used for calculating the frequencies as a function of the speed of rotation. Experimental and finite element results are presented in Table 7.1 and agreement is shown to be very good.

Table 7.1. Finite elements and experimental results

Speed of rotation (rpm)	f_1 (Hz)			f_2 (Hz)			f_3 (Hz)			f_4 (Hz)		
	FE	EXP	%	FE	EXP	%	FE	EXP	%	FE	EXP	%
0	369.4	405	−8.8%	369.4	405	−8.8%	564.6	545	0.3%	546.6	545	0.3%
10 000	320.4	325	−1.4%	408.2	420	−2.8%	518.3	520	−0.3%	601.4	610	−1.4%
20 000	272.8	275	−0.8%	431.3	430	0.3%	504.2	500	0.8%	687.3	695	−1.1%
30 000	232.2	235	−1.2%	443.9	430	3.2%	496.5	500	−0.7%	797.1	805	−1%
40 000	199.2	205	−2.8%	451.1	435	3.7%	491.7	480	2.4%	922.8	920	0.3%
50 000	172.9	175	−1.2%	455.6	440	3.5%	488.5	480	1.8%	1059.3	1060	0.0%
60 000	151.9	155	−2%	458.7	445	3.1%	486.2	495	−1.8%	1203.3	1210	−0.6%

7.2 TURBOCHARGER

The main characteristics of the turbocharger used for cars [24], Figure 7.8, are:

- a rotor mass of 140 g
- two hydrodynamic bearings
- an operating speed range from 80 000 to 200 000 rpm.

The finite element model, Figure 7.9, uses 44 shaft elements and four disks. The turbine, shown on the left of the figure, is mounted sliding on the shaft and fixed by a nut. The amplitudes of the displacements between the turbine disk and the shaft are lower than the clearances, hence a specific model is used: nodes 6 to 12 (shaft) and 28 to 34 (turbine) are independent.

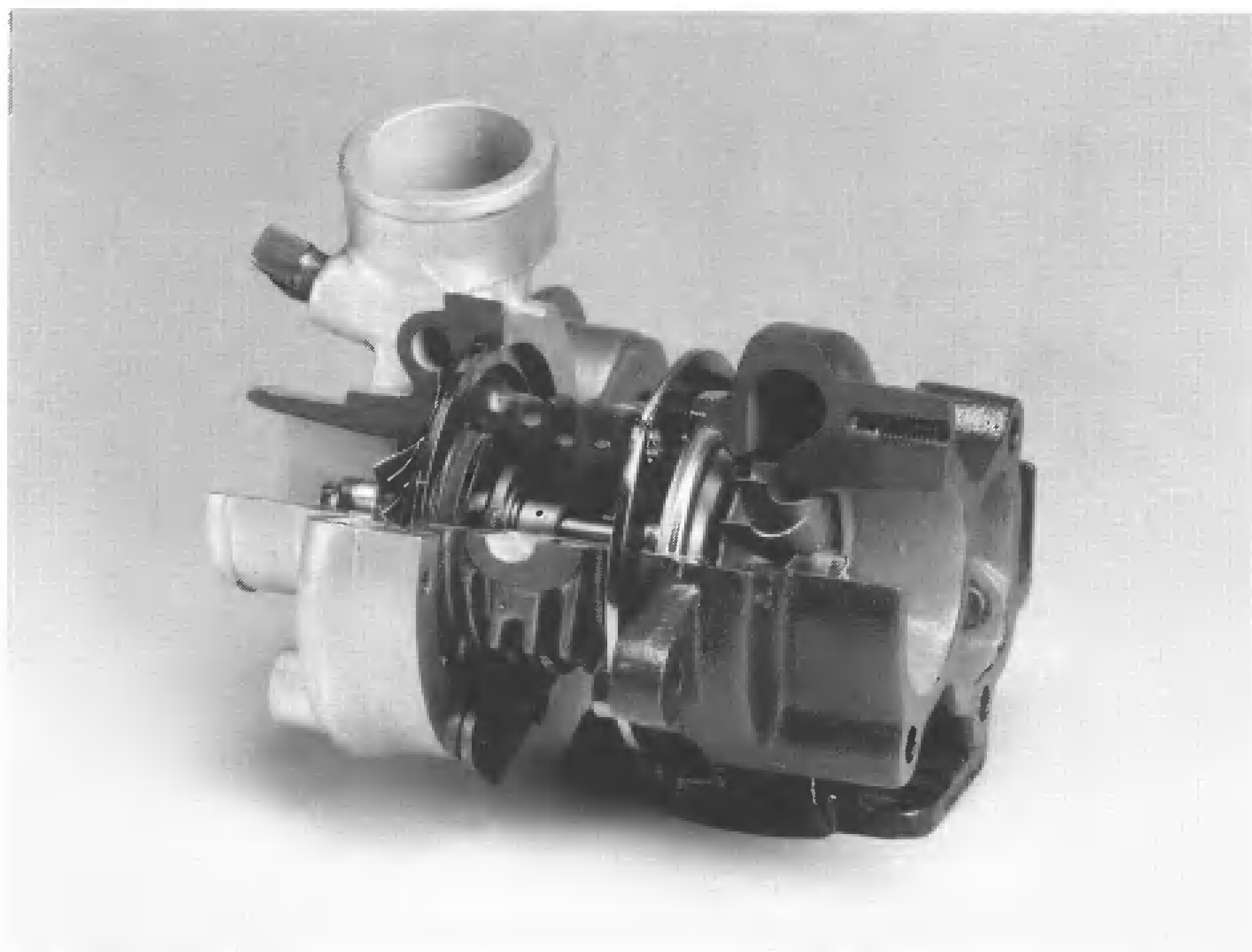

Figure 7.8. Turbocharger (Picture courtesy Allied Signal Turbo SA)

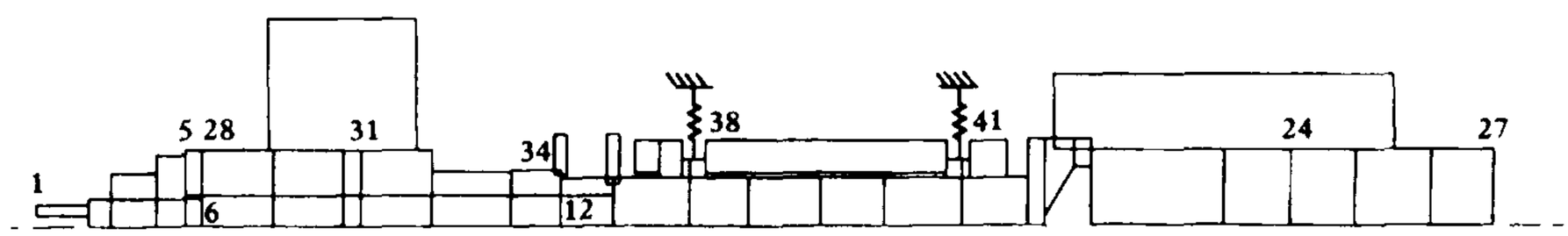

Figure 7.9. Finite element model

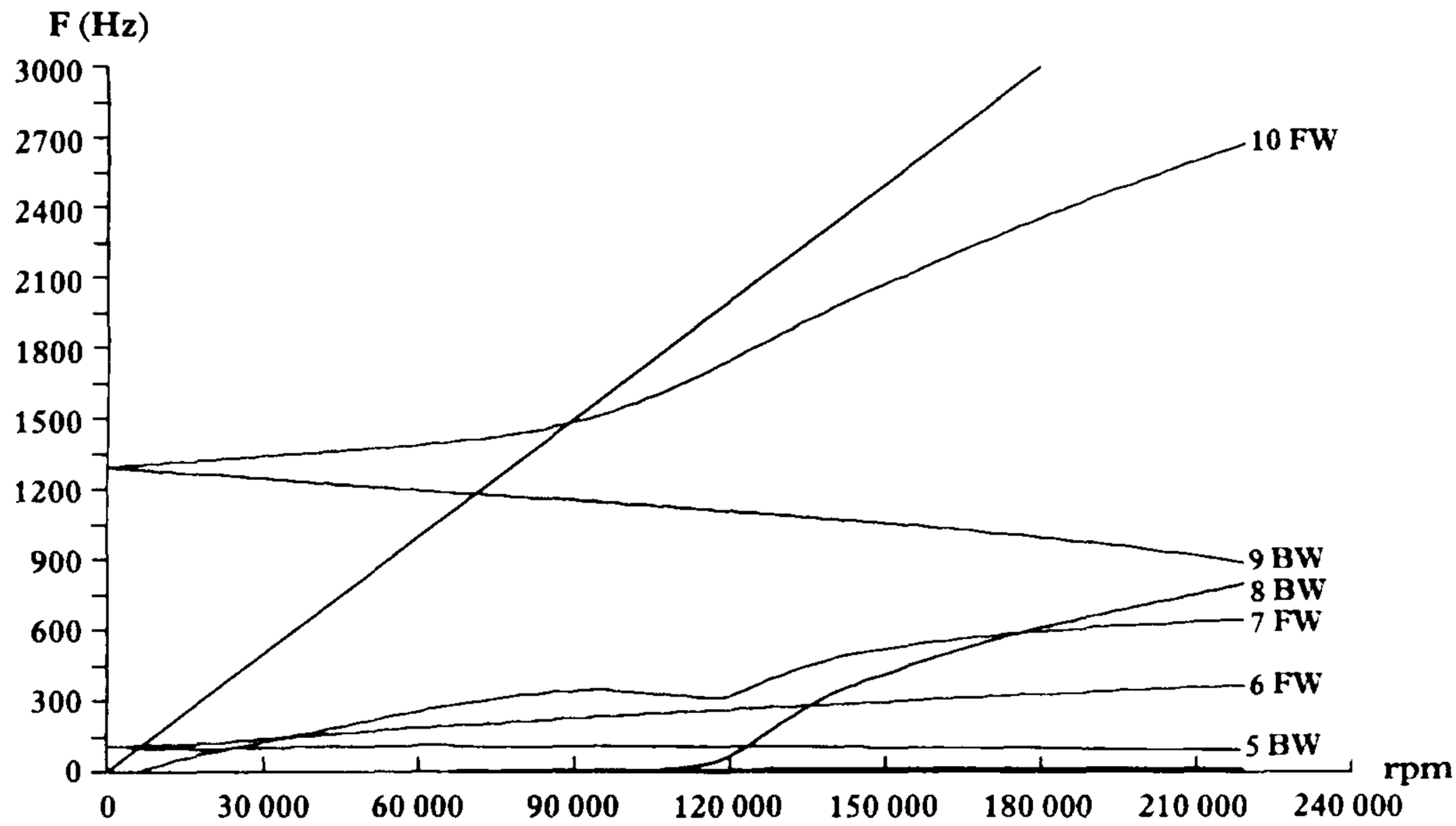

Figure 7.10. Campbell diagram

7.2.1 The Campbell diagram

The Campbell diagram is shown in Figure 7.10 and no instability occurs. As the damping is very high, the first modes to be considered are modes 9 and 10. Mode 10 gives a critical speed at 90 000 rpm and mode shapes are presented at 200 000 rpm which is the maximum operating speed, Figure 7.11.

7.2.2 Mass unbalance response

Several mass unbalance possibilities have been tested and two are presented. The first mass unbalance response, Figure 7.12, corresponds to two equal masses in phase and situated on the turbine and on the compressor. The deflections at three speeds of rotation are presented in

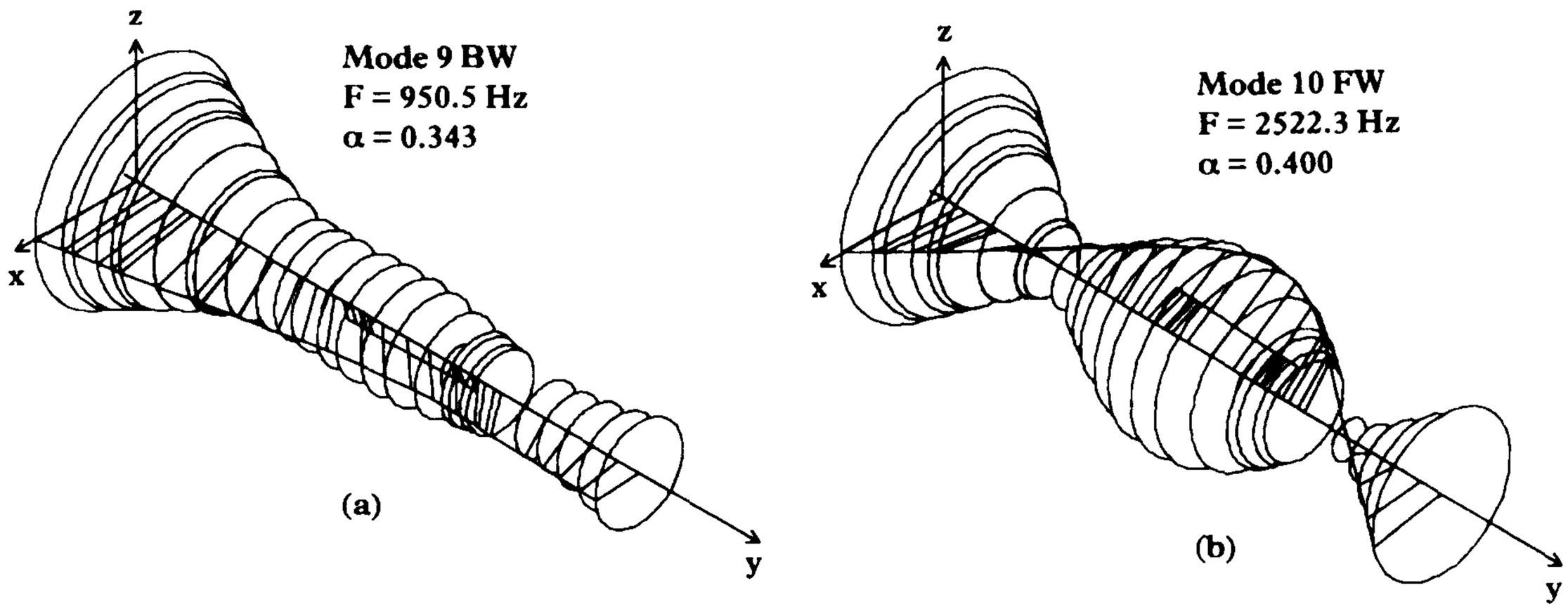

Figure 7.11. Mode shapes at 200 000 rpm

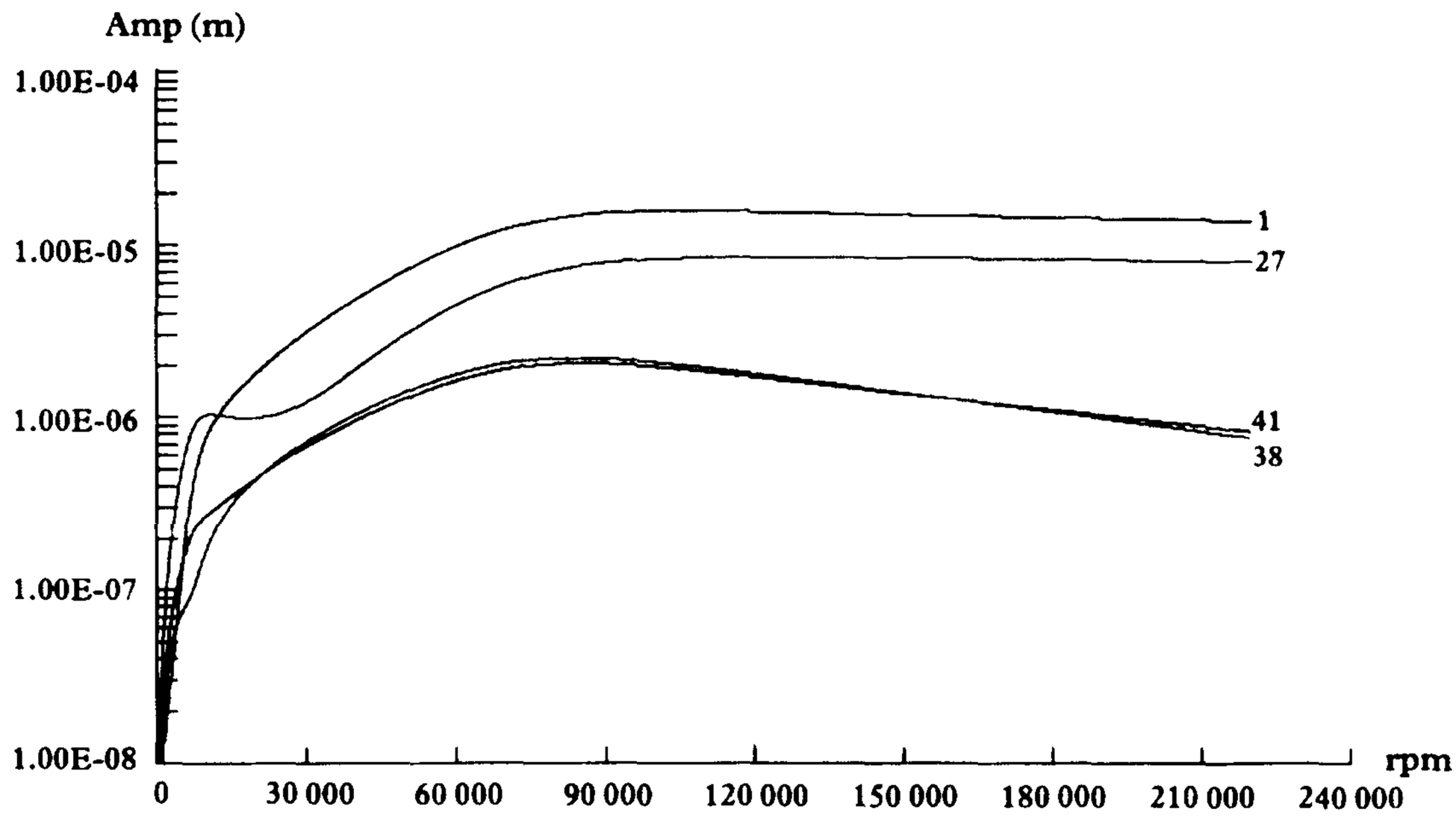

Figure 7.12. Mass unbalance response (two masses in phase)

Figure 7.13. A second mass unbalance response, Figure 7.14, corresponds to three mass unbalances: two (in phase) are on the compressor and on the turbine nut, the third (in phase opposition) is situated on the turbine. The deflections at three speeds of rotation are presented in Figure 7.15.

7.2.3 Remarks

No critical speed occurs and the prediction is in good agreement with both experimental and field results.

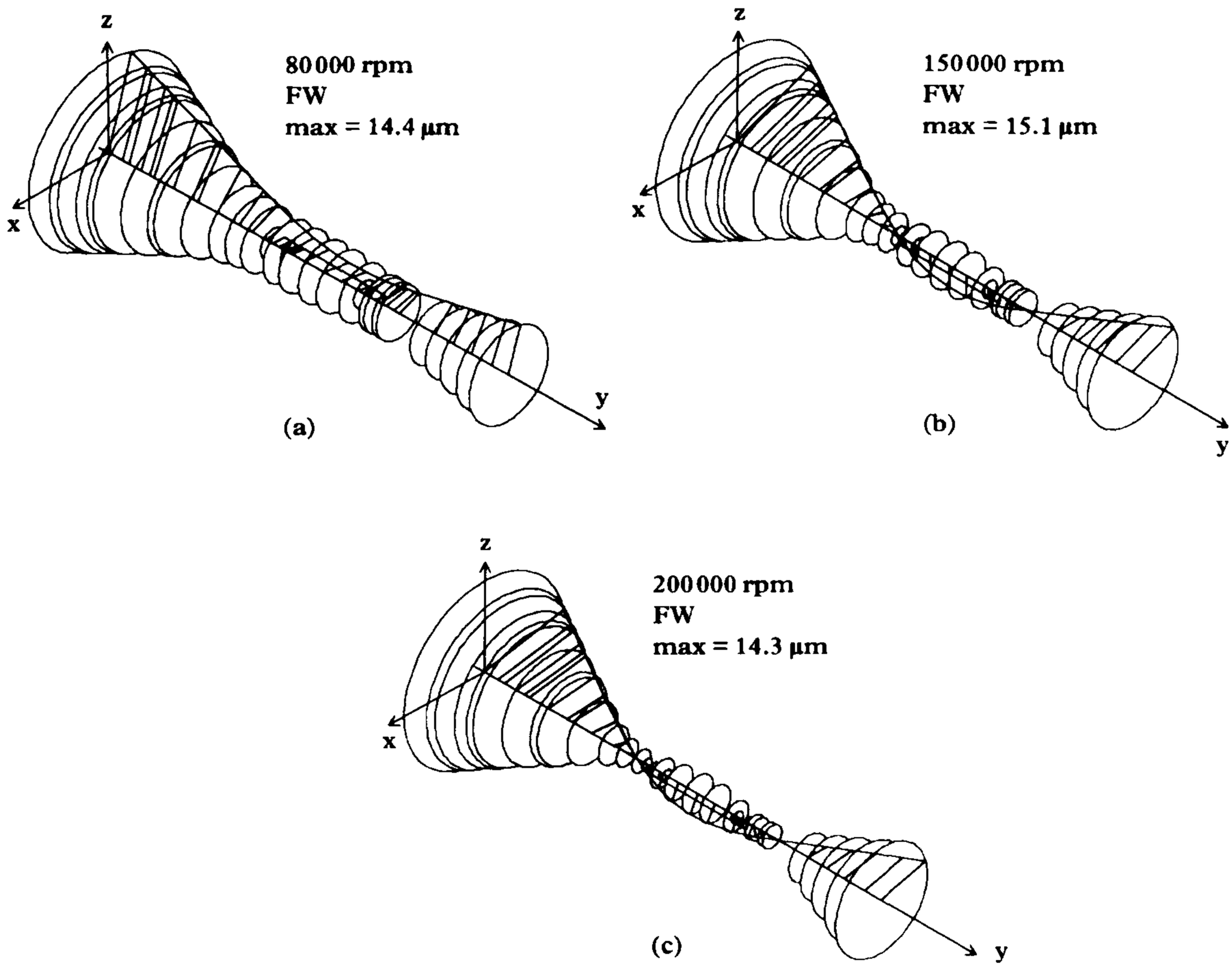

Figure 7.13. Rotor deflections (two masses in phase)

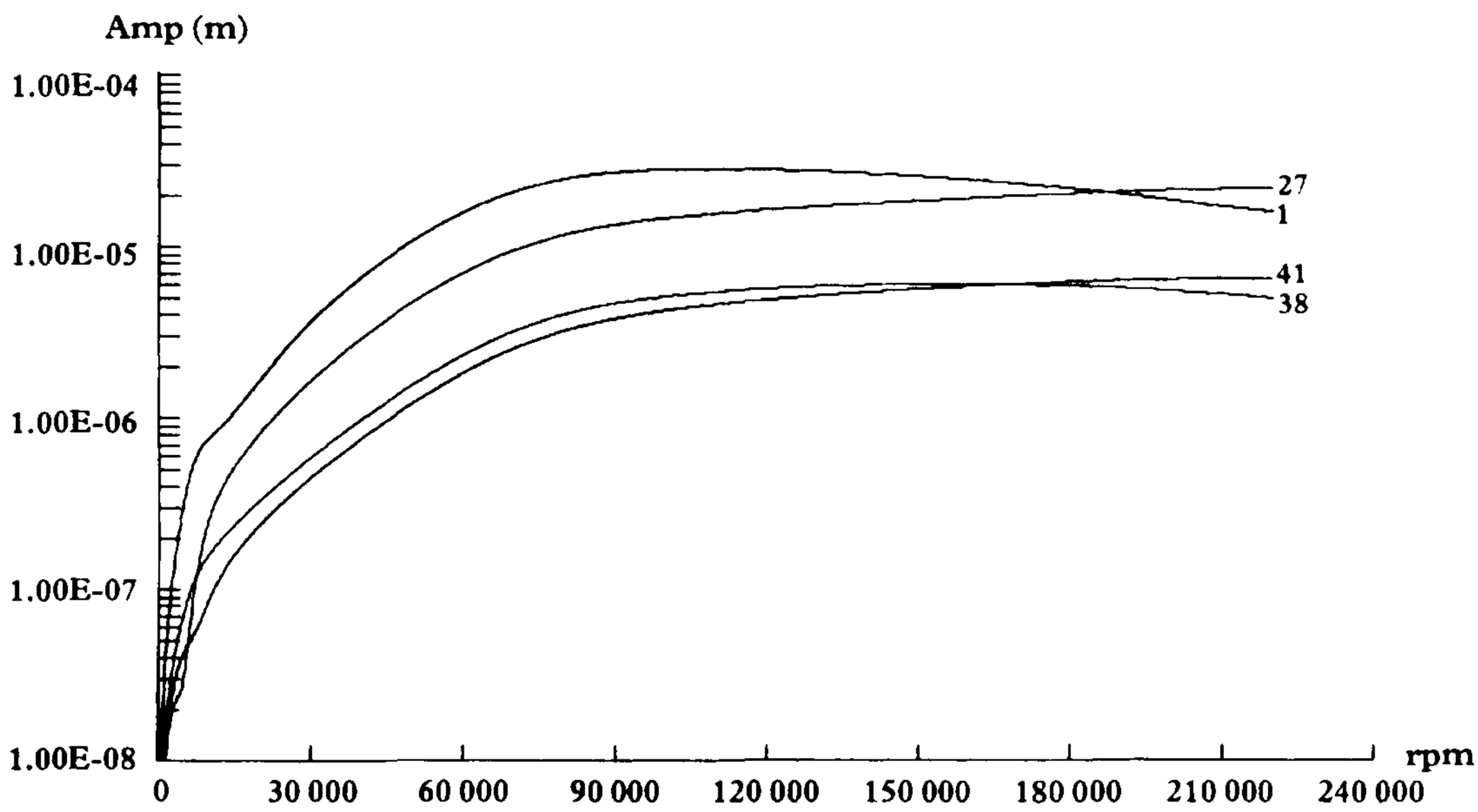

Figure 7.14. Mass unbalance response (three masses)

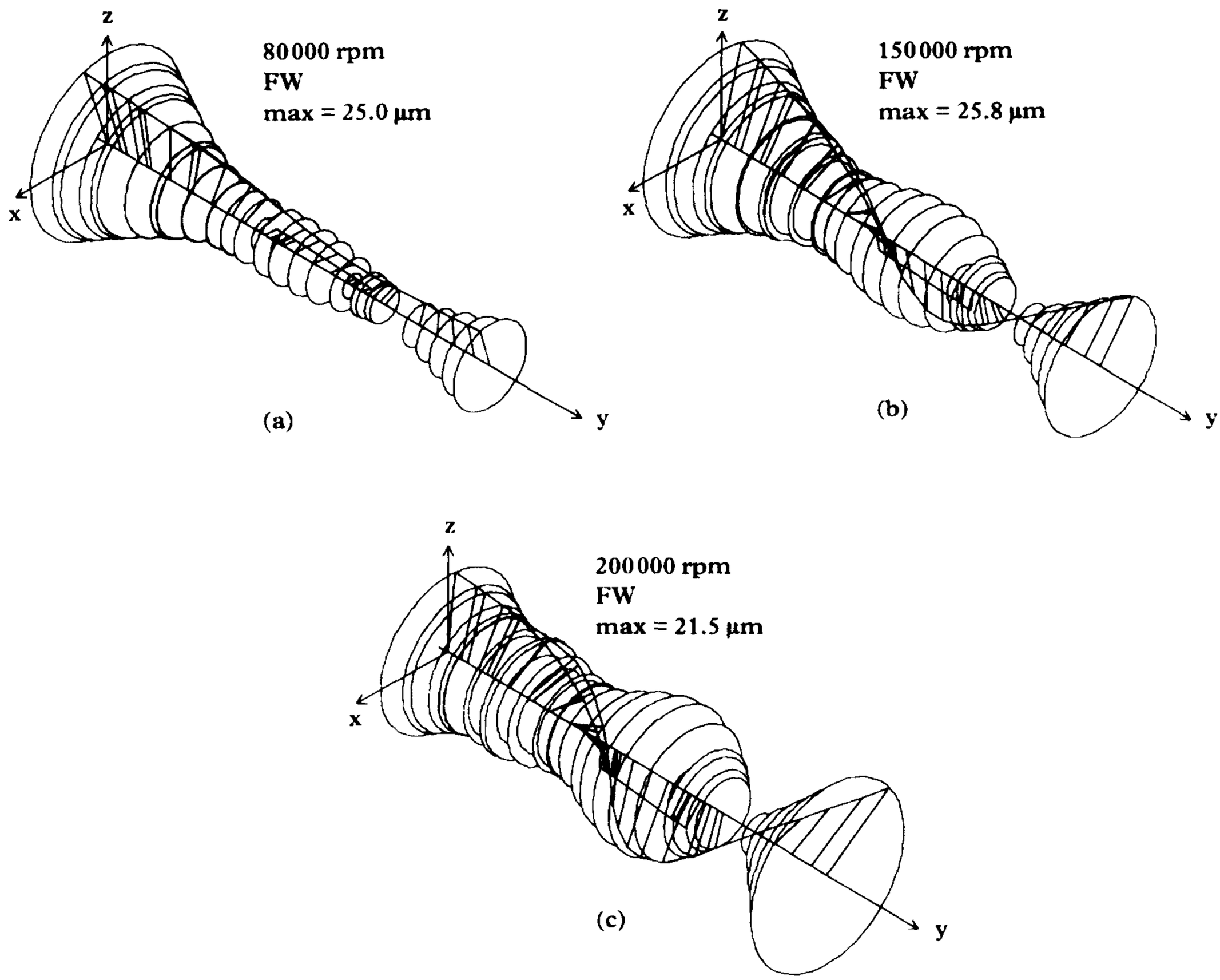

Figure 7.15. Rotor deflections (three masses)

7.3 CENTRIFUGAL COMPRESSOR

The main characteristics of the compressor, Figure 7.16, used to collect petroleum with gas-lift are:

- a power of 5.3 MW at a nominal speed of rotation of 13 800 rpm
- two hydrodynamic bearings with five tilting pads
- a rotor of length 1.8 m and mass 295 kg.

The finite element model, Figure 7.17, uses 71 shaft elements and 17 disks. The seals are modeled in the same way as the bearings and also include stiffness and viscous damping coefficients which are a function of the speed of rotation.

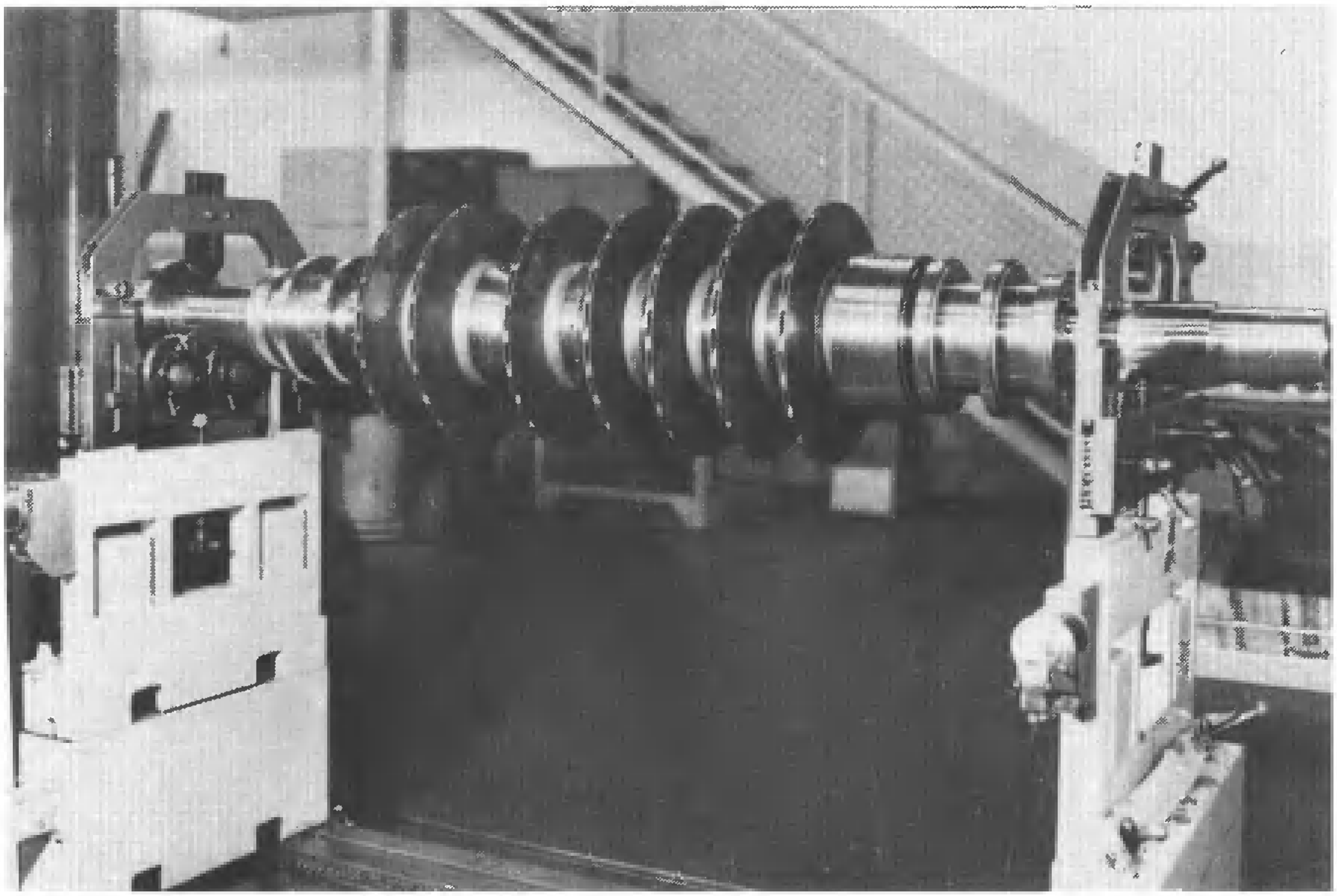

Figure 7.16. Centrifugal compressor (Picture courtesy Thermodyn)

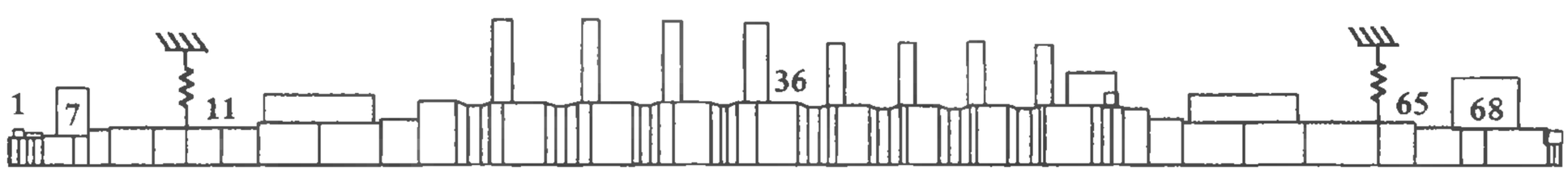

Figure 7.17. Finite element model

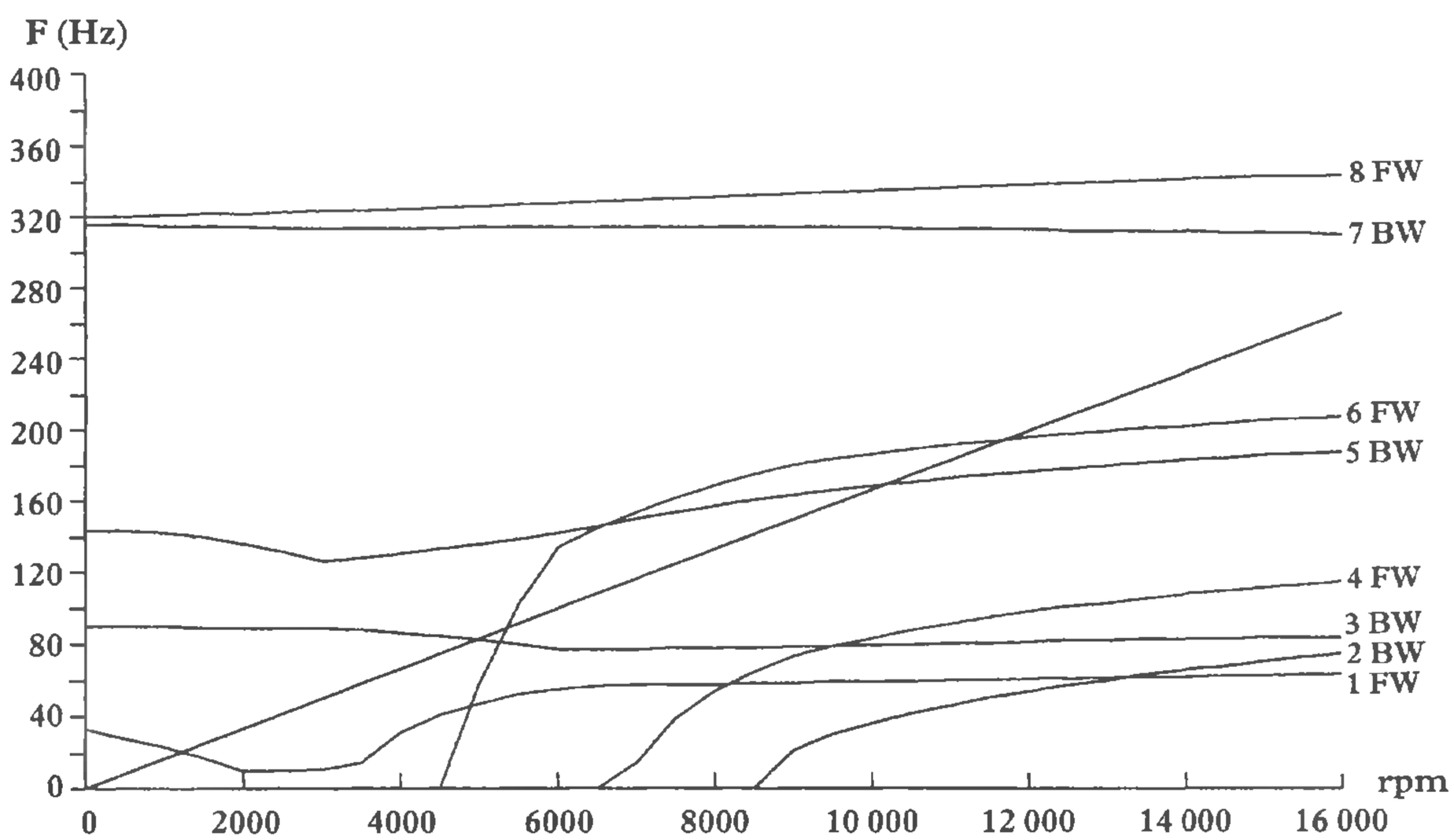

Figure 7.18. Campbell diagram

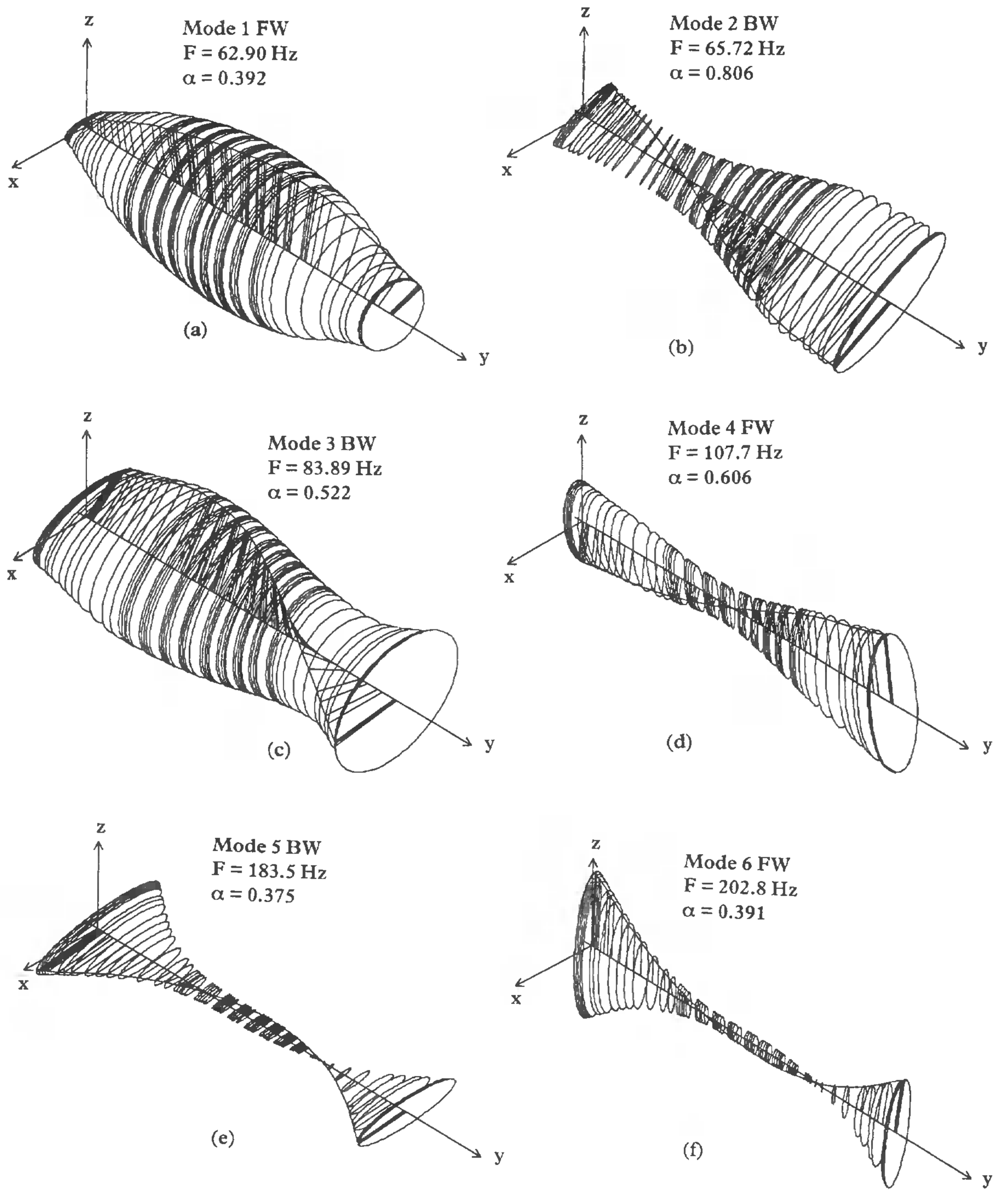

Figure 7.19. Mode shapes at 13 800 rpm

7.3.1 The Campbell diagram

The diagram is shown in Figure 7.18, and no instability occurs. The first six modes are highly damped and the mode shapes at 13 800 rpm are shown in Figure 7.19.

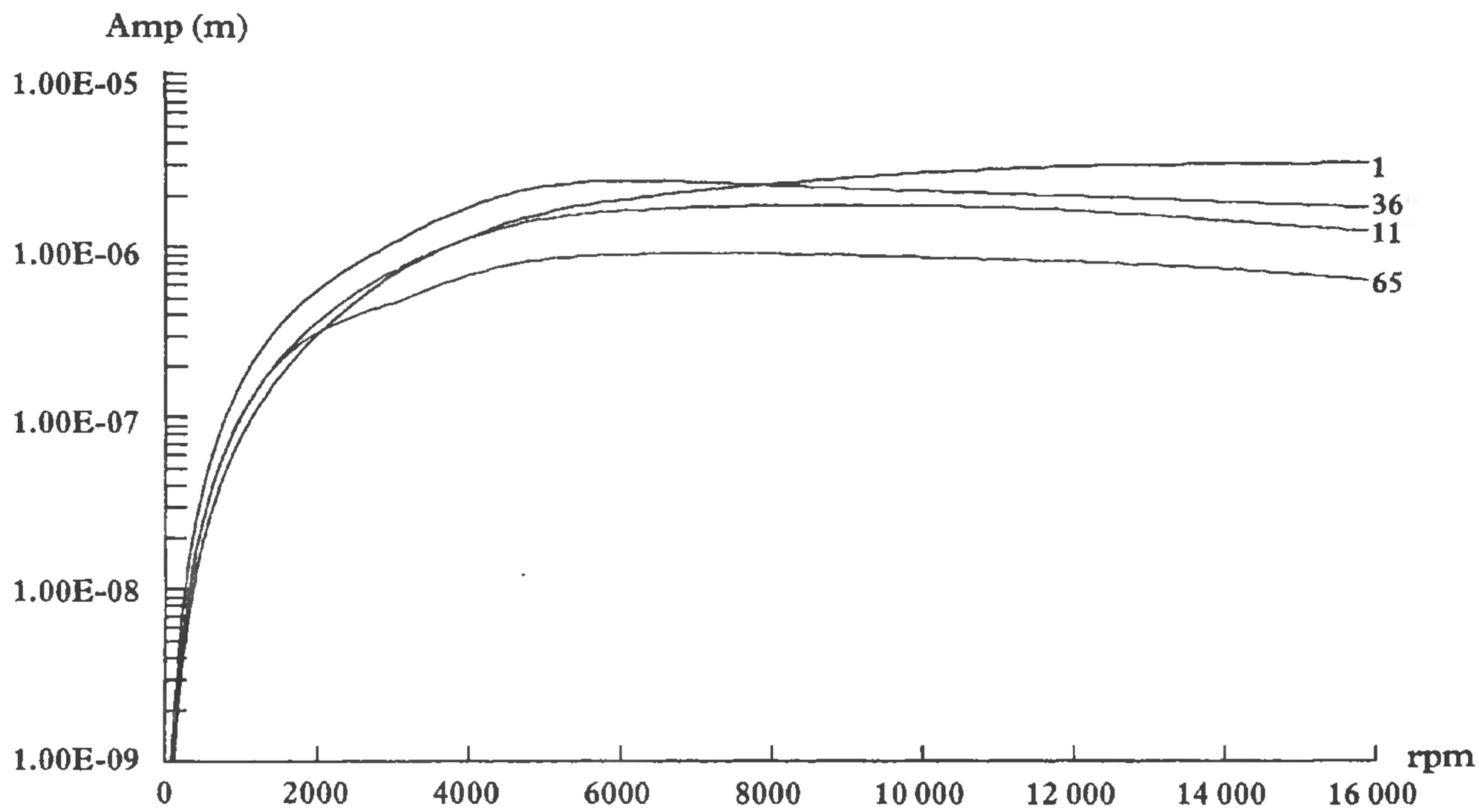

Figure 7.20. Case 1: mass unbalance response

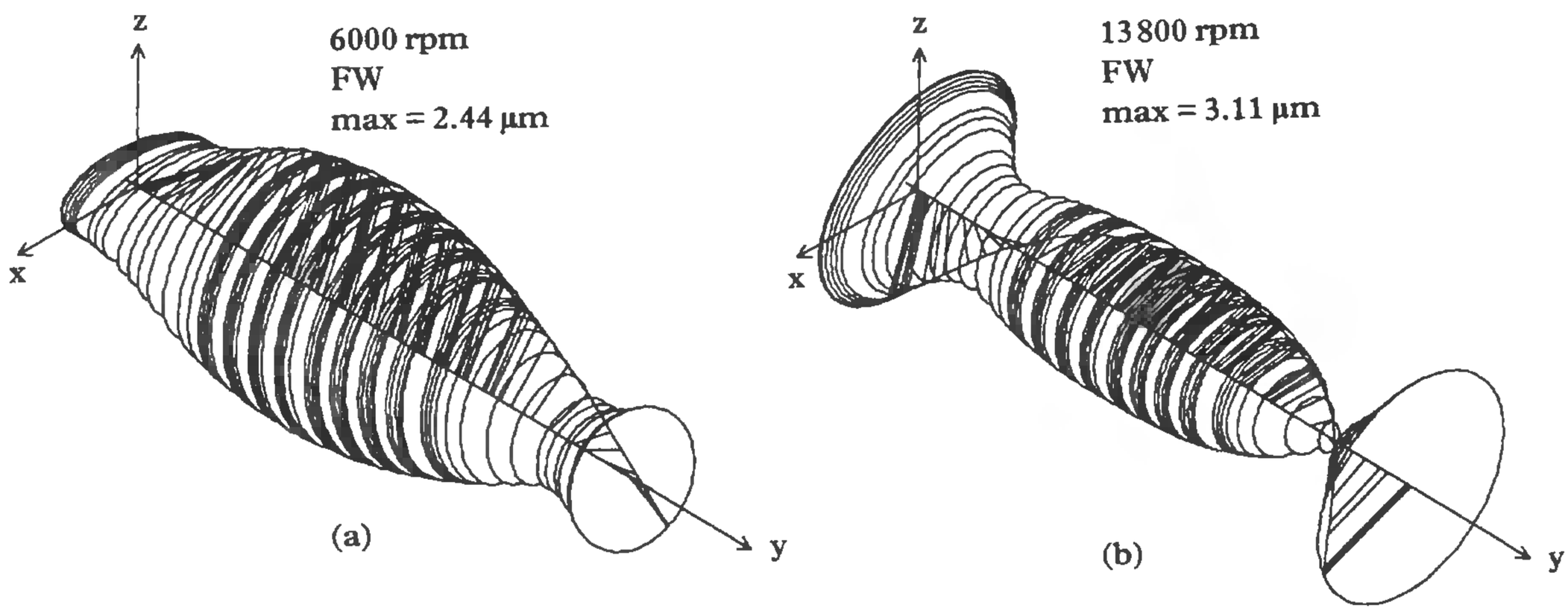

Figure 7.21. Case 1: rotor deflections

7.3.2 Mass unbalance response

The mass unbalance defined by the 1995 API standards is 272 g mm and the maximum displacement at the bearing locations is 12 μm.

Case 1: The mass unbalance is located near the middle of the rotor, node 36. The response is shown in Figure 7.20 and the rotor deflections are presented in Figure 7.21 for two speeds of rotation.

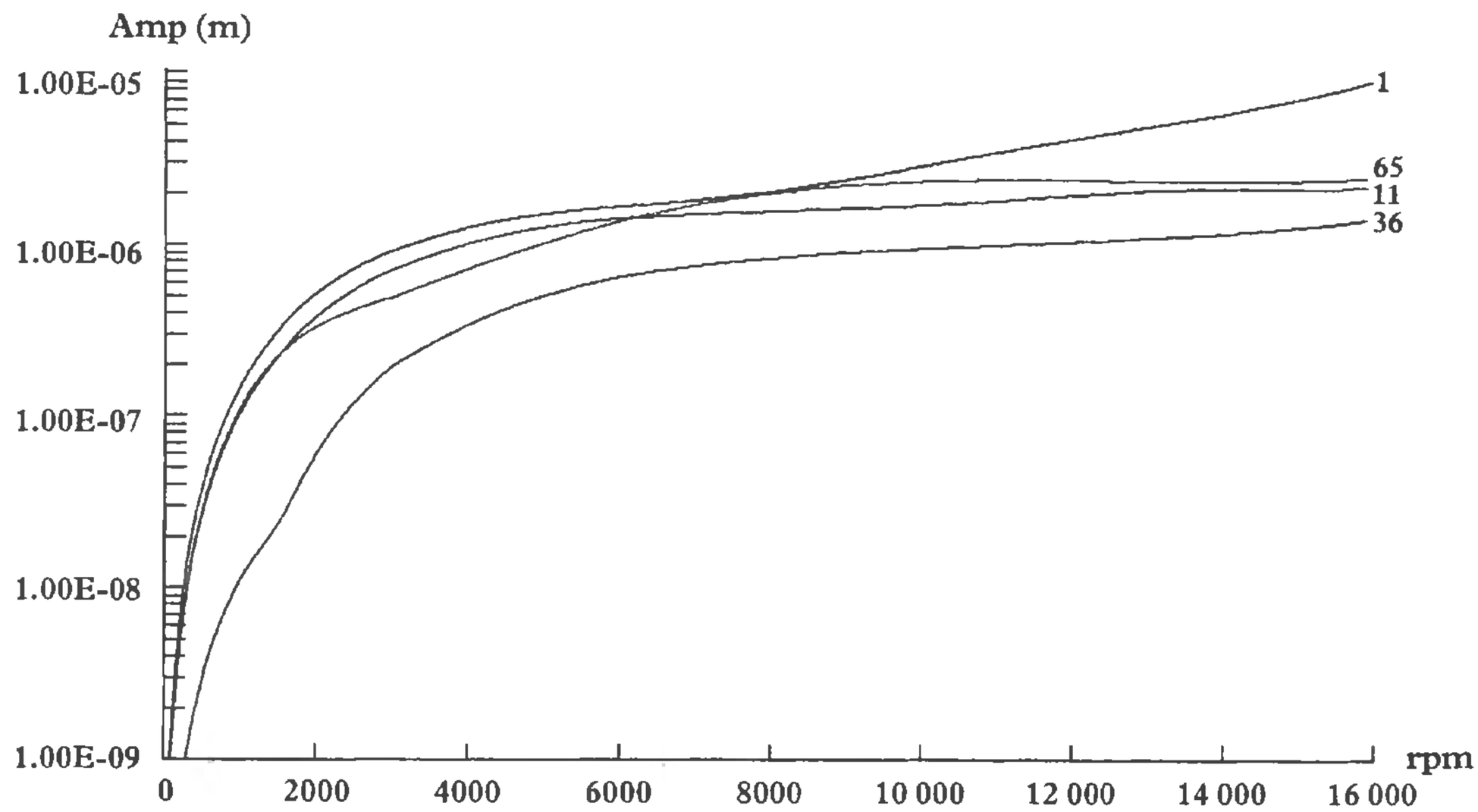

Figure 7.22. Case 2: mass unbalance response

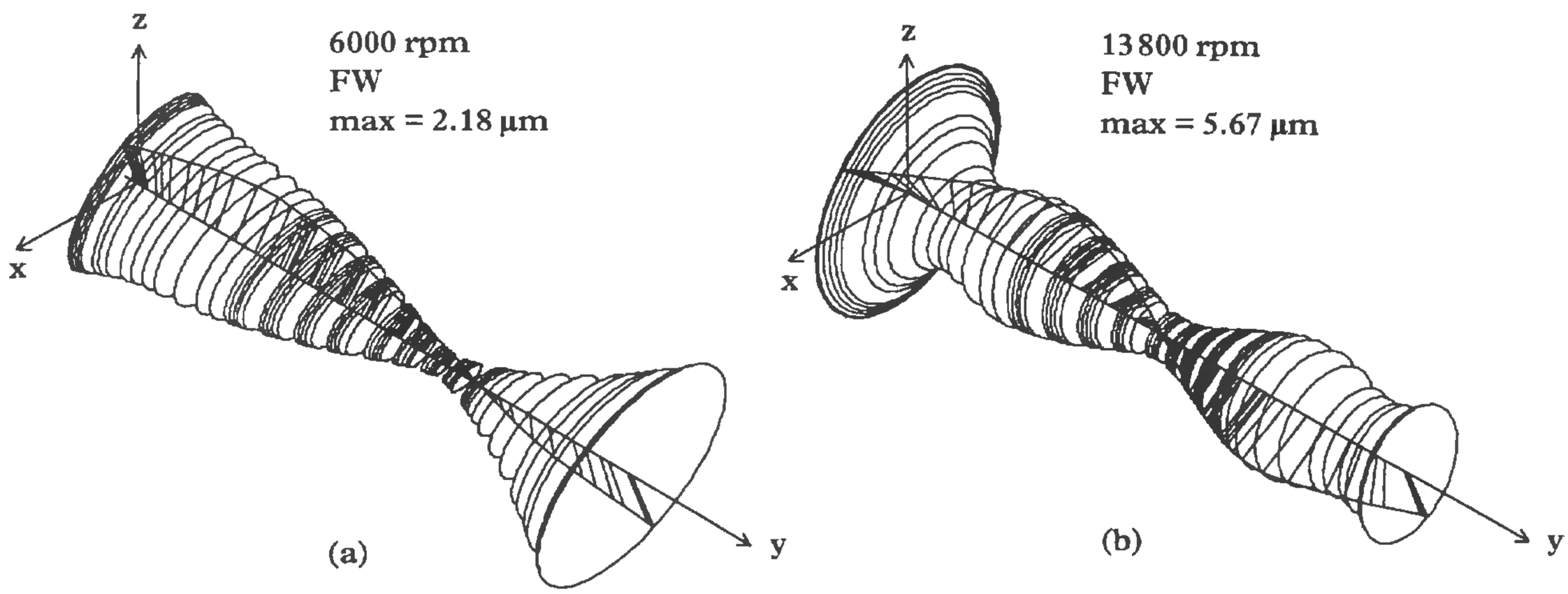

Figure 7.23. Case 2: rotor deflections

Case 2: The masses, in phase opposition, are situated near the two ends of the rotor, at nodes 7 and 68. The response is shown in Figure 7.22 and the rotor deflections are presented in Figure 7.23.

7.3.3 Remarks

In the two cases concerned the Q factor is less than 2.5 and no critical speed exists. The maximum amplitude calculated is 5.7 µm, which is half of the maximum admissible displacement. These results were confirmed in the field.

7.4 STEAM TURBINE

The steam turbine, presently being developed, is similar to that shown in Figure 7.24. It will be used for driving a centrifugal compressor through a step-up gear. The main characteristics are:

- a nominal power of 23 MW at 4800 rpm
- two hydrodynamic bearings with five tilting pads
- a rotor mass of 4200 kg.

The finite element model, Figure 7.25, uses 68 shaft elements and 10 disks. Numerical simulations have been achieved for three clearance values (maximum, average, minimum) and the minimum clearance results are presented in what follows.

7.4.1 The Campbell diagram

The diagram is shown in Figure 7.26 and no instability occurs. It shows five possible critical speeds. The first two modes have little damping and

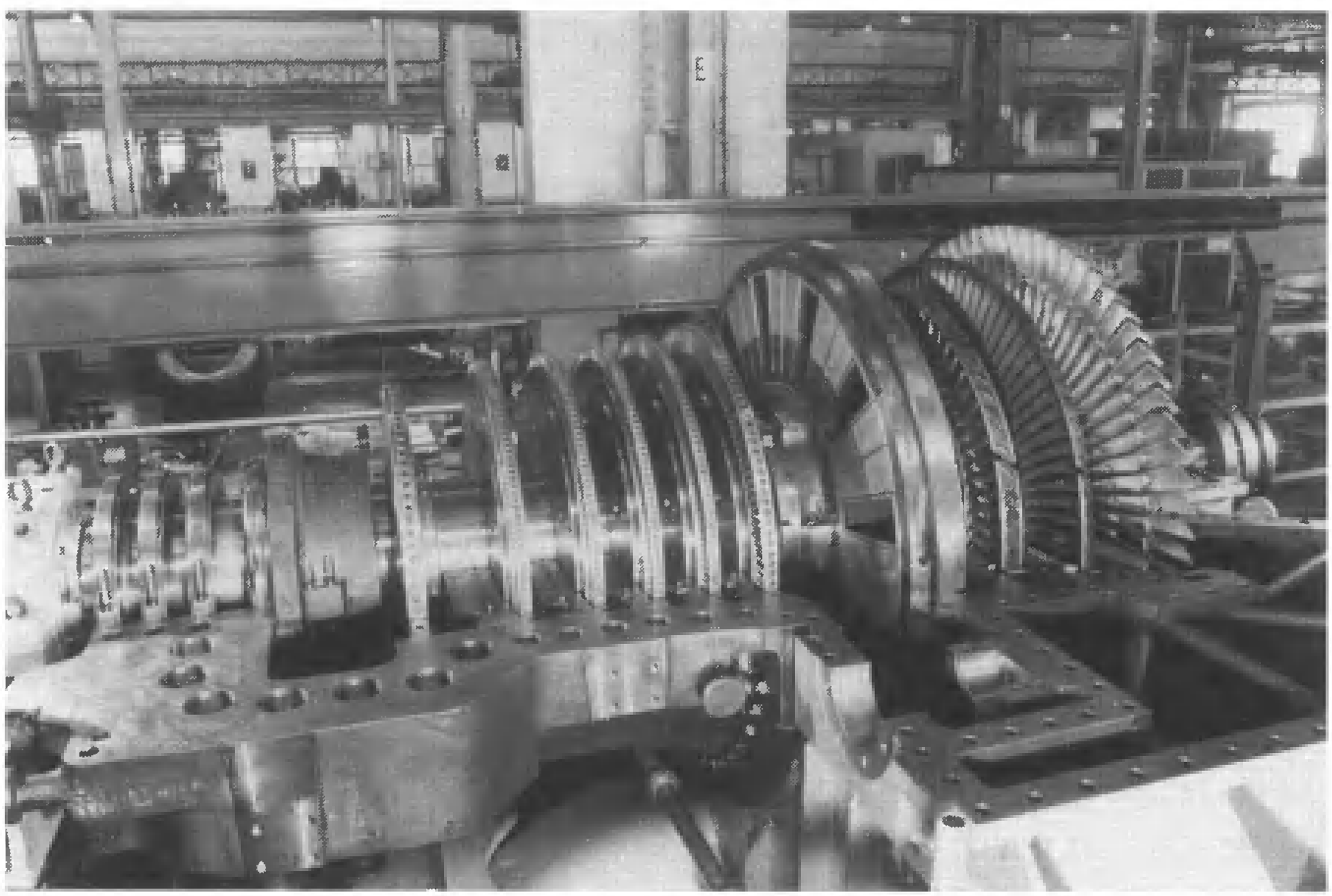

Figure 7.24. Steam turbine (Picture courtesy Thermodyn)

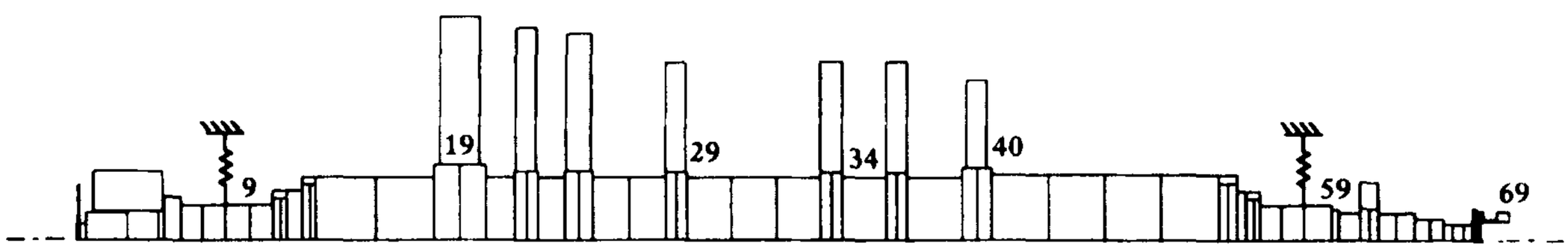

Figure 7.25. Finite element model

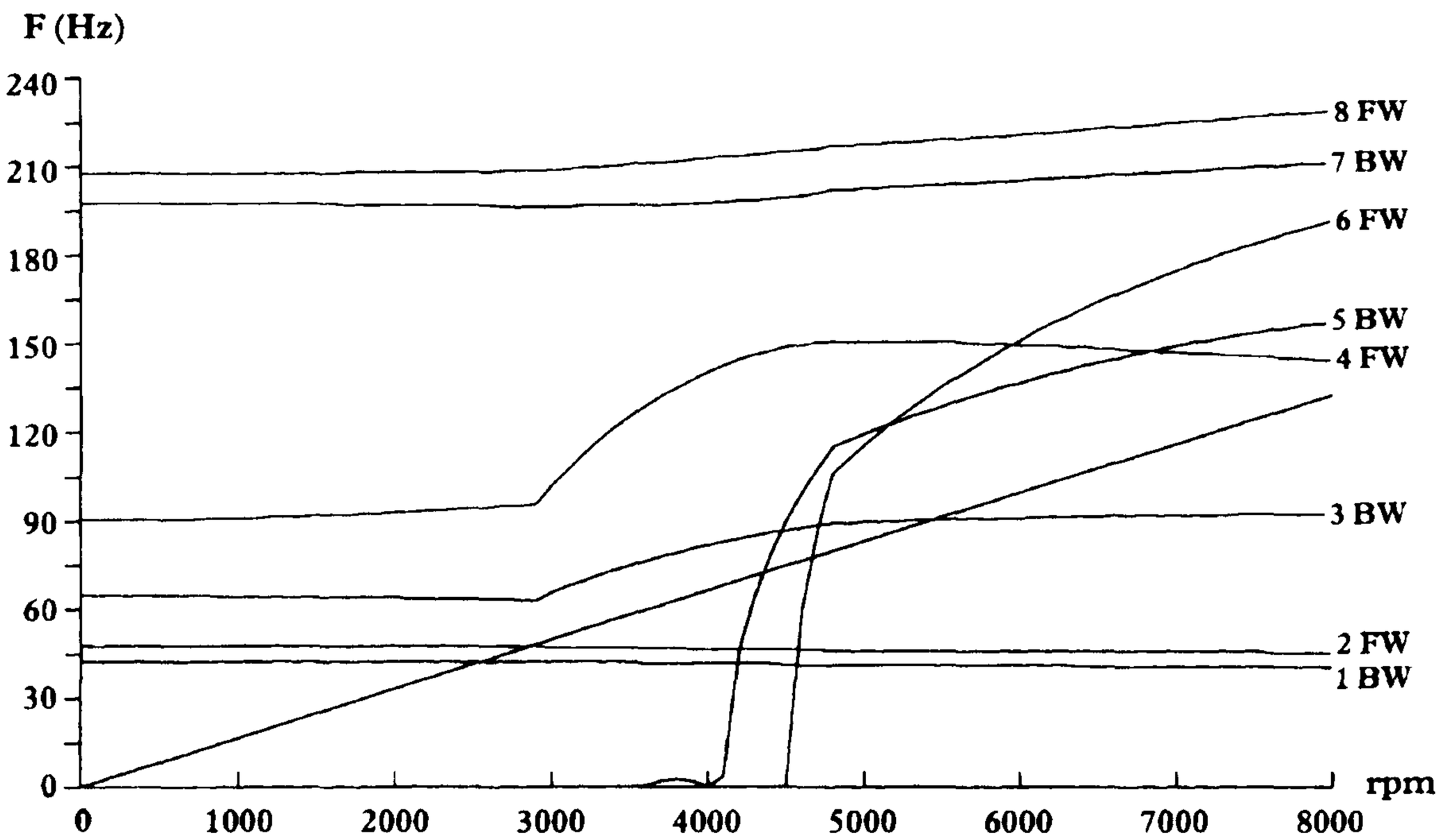

Figure 7.26. Campbell diagram

modes 3 to 6 are highly damped; they are presented at 4800 rpm in Figure 7.27.

7.4.2 Mass unbalance response

The mass unbalance defined by the 1995 API standards, at 4800 rpm, is 11 112 g mm and the critical speed appears at 2865 rpm. It is therefore necessary to use a mass unbalance of 18 618 g mm.

Case 1: The two mass unbalances are located, in phase, near the middle of the rotor, at nodes 21 and 34. The response is shown in Figure 7.28 and the rotor deflections at the critical speed and at the nominal speed are shown in Figure 7.29.

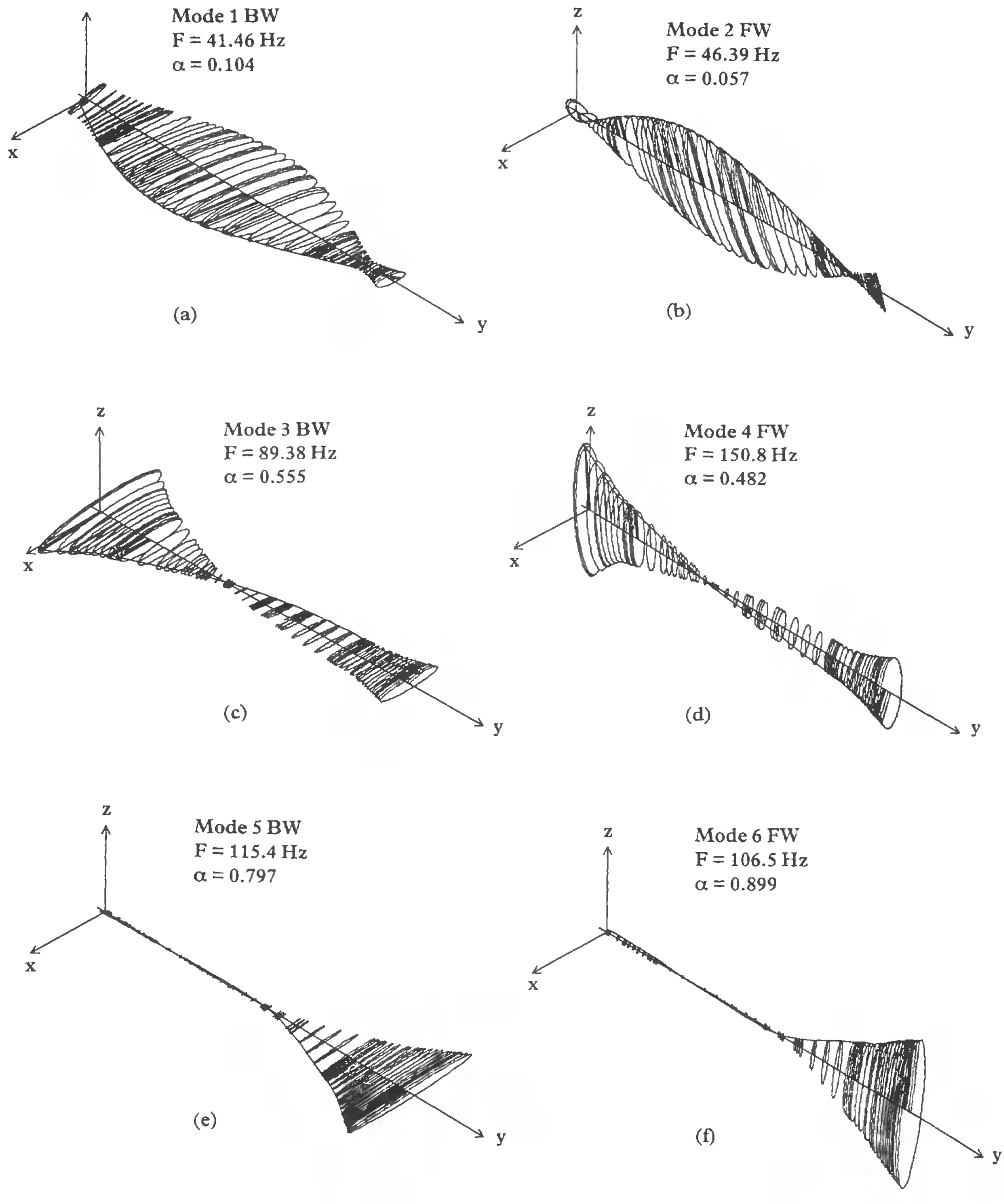

Figure 7.27. Mode shapes at 4800 rpm

Case 2: The two mass unbalances are located, in phase opposition, at nodes 19 and 40. The response is shown in Figure 7.30 and the rotor deflections at the same speed of rotation as in case 1 are shown in Figure 7.31.

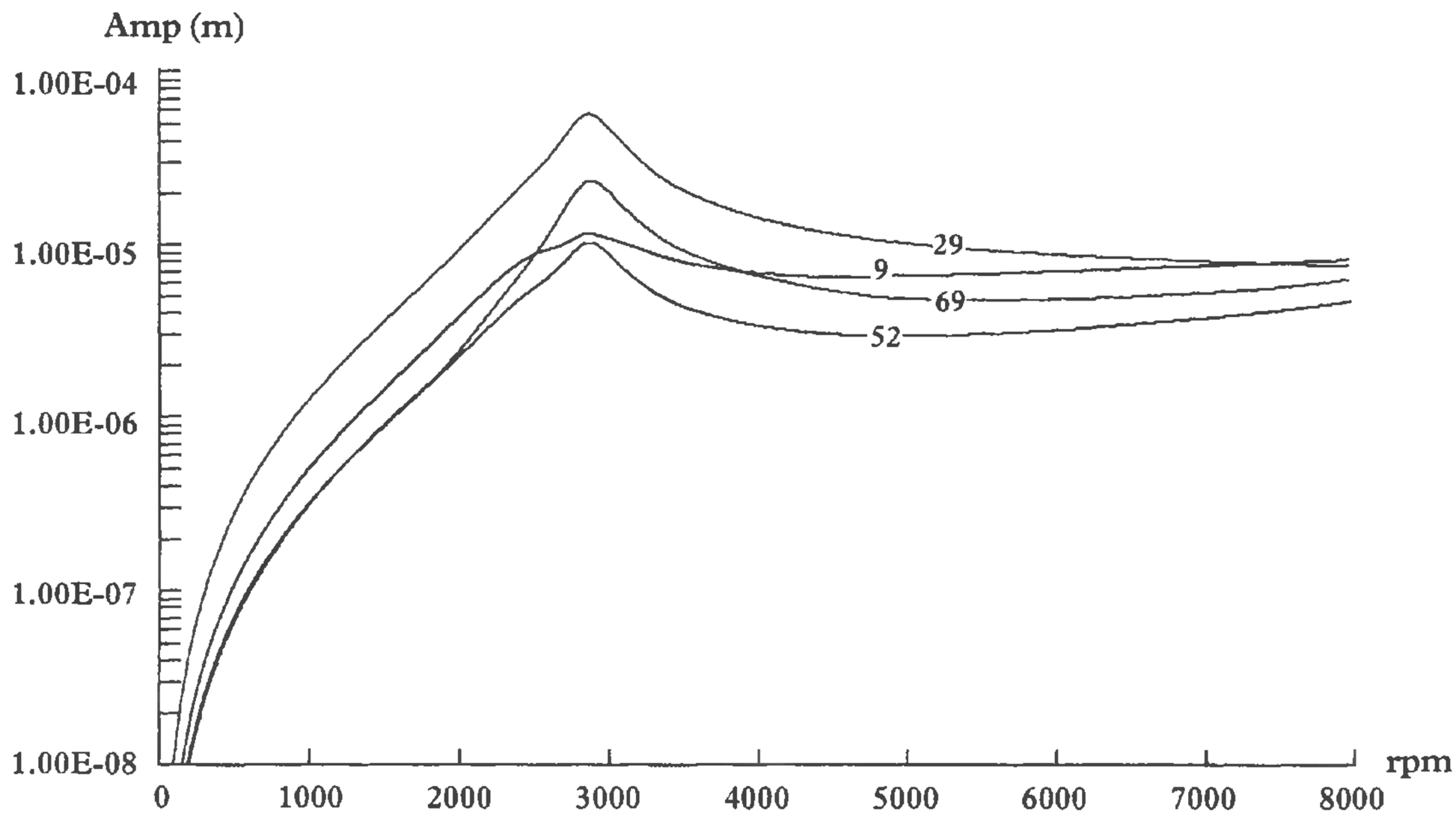

Figure 7.28. Case 1: mass unbalance response

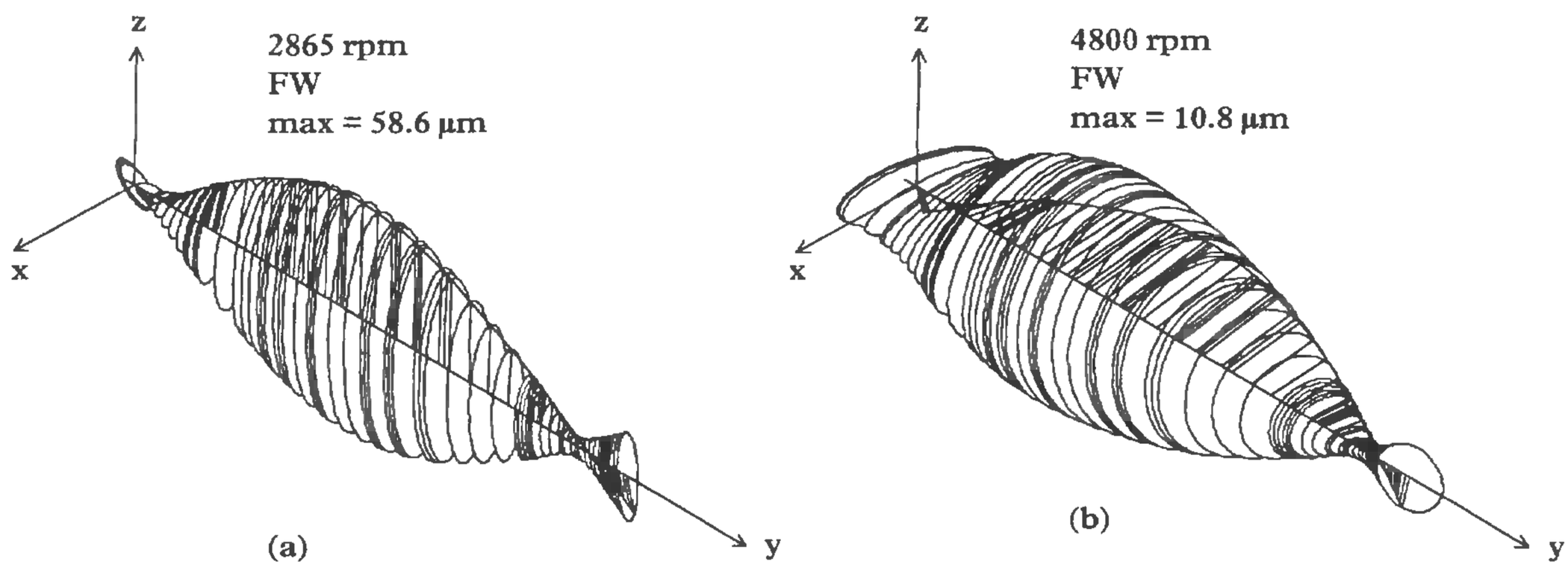

Figure 7.29. Case 1: rotor deflections

7.4.3 Remarks

The damping values for nodes 1 to 6 clearly show that the possible critical speeds were limited at the intersection of $F = N/60$ for the first two modes.

One critical speed appears clearly in case 1. The deflection at node 29 is 57.5 μm and the speeds of rotation corresponding to a -3 dB bandwidth are 2684 rpm and 3070 rpm, hence $Q = 7.4$. Application of Equations (7.9) and (7.10) gives the prohibited operating speed range (2366 to 3573 rpm). The deflections calculated at these two rotation

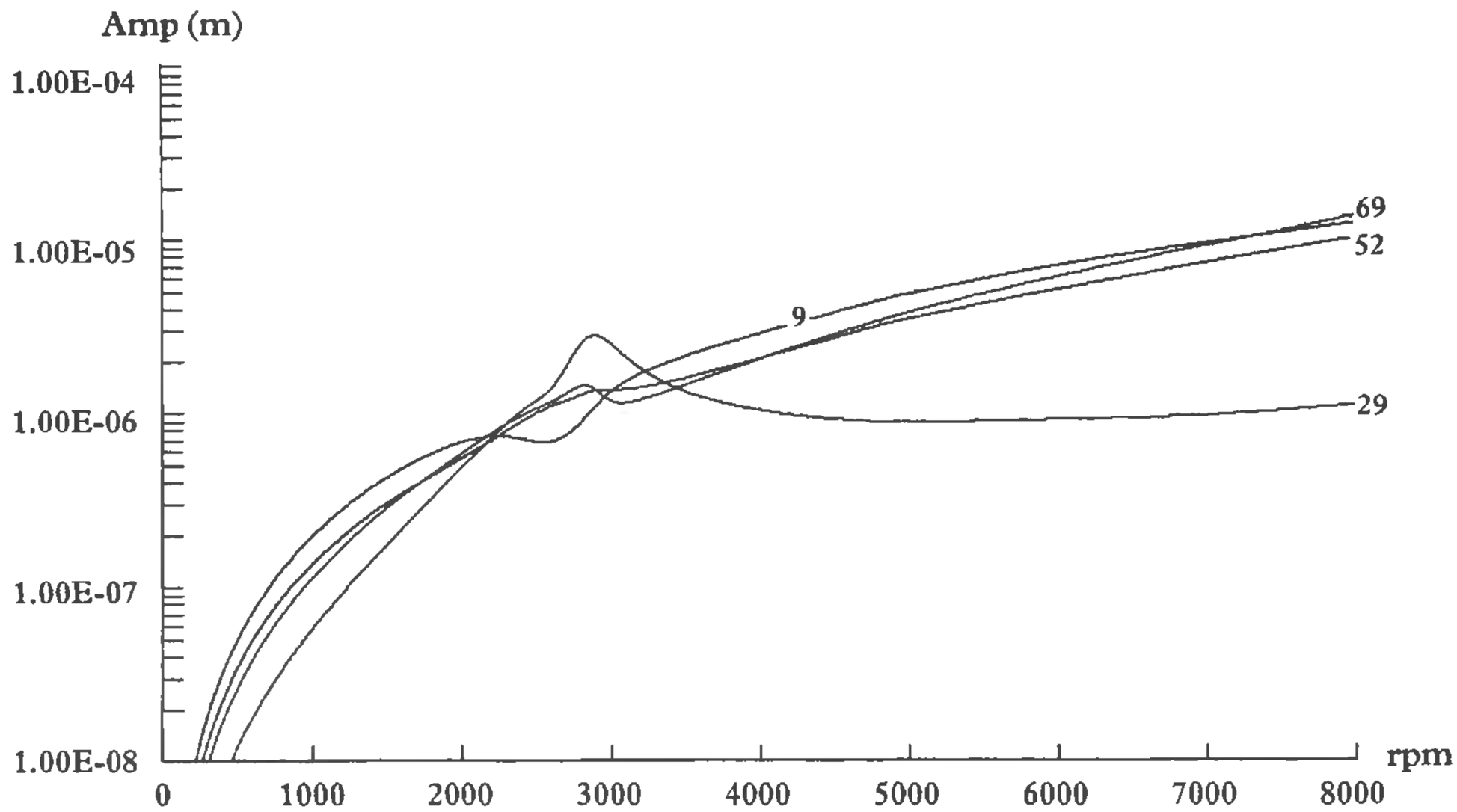

Figure 7.30. Case 2: mass unbalance response

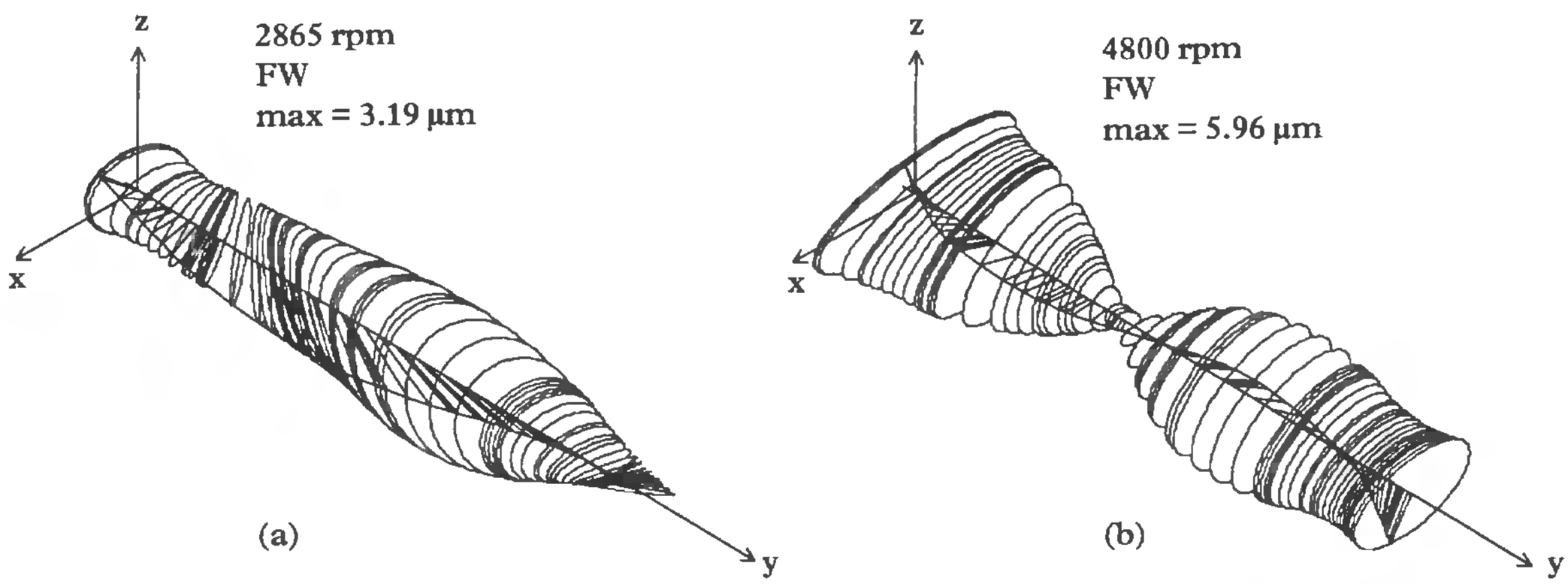

Figure 7.31. Case 2: rotor deflections

speeds are respectively 20 and 19.4 µm. Equation (7.5) gives a maximum displacement of 26 µm at the critical speeds and 20 µm at the nominal speeds.

7.5 CENTRIFUGAL COMPRESSOR FITTED WITH ACTIVE MAGNETIC BEARINGS

This industrial prototype of an oil-free centrifugal compressor (Figure 7.32) is used for natural-gas compression in a gas-treatment unit in south-west France (ELF Aquitaine). This is the first European application of a

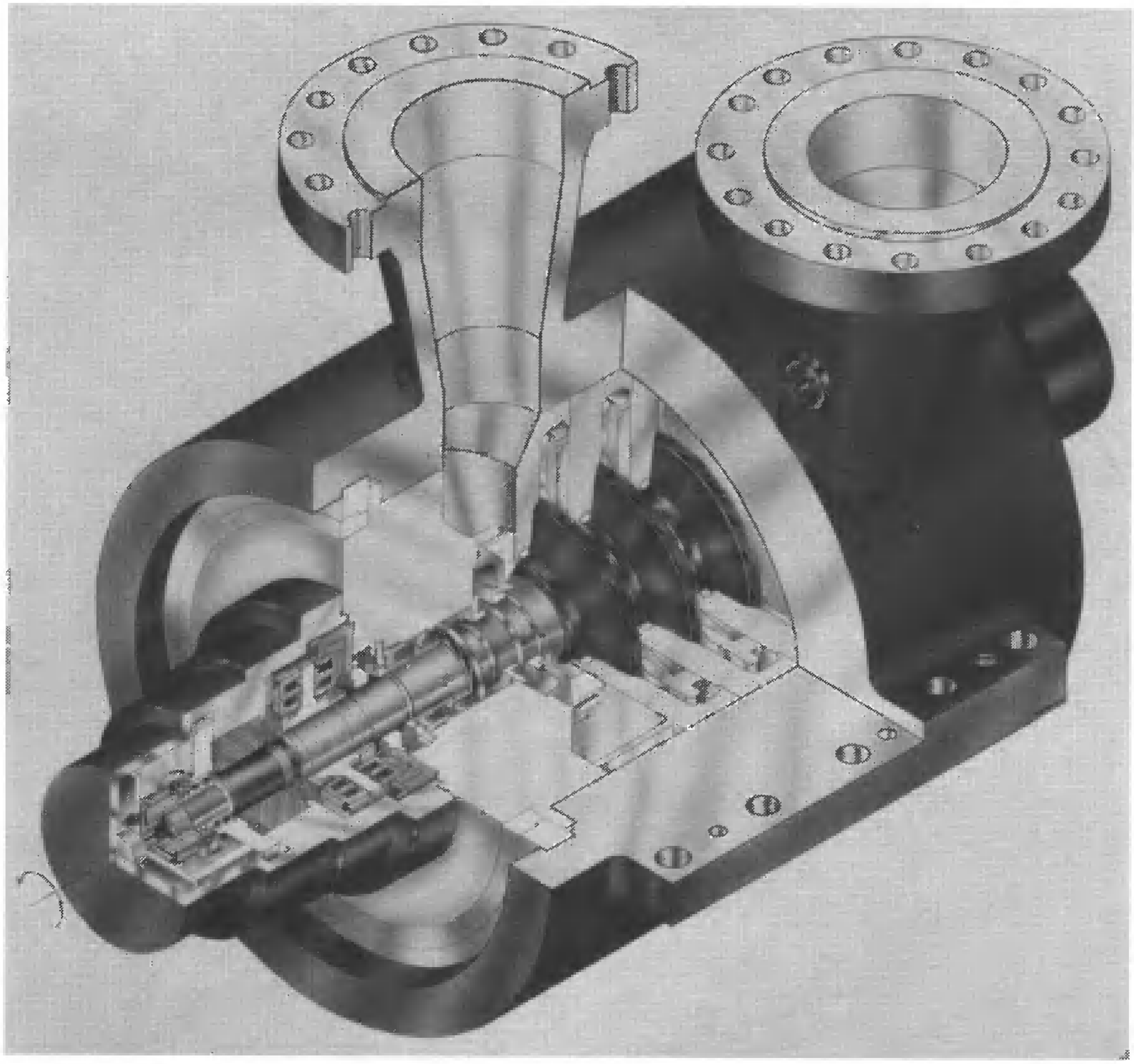

Figure 7.32. Oil-free centrifugal compressor (Picture courtesy Thermodyn, ELF Aquitaine and S2M)

centrifugal compressor fitted with active magnetic bearings (from S2M, Société de Mécanique Magnétique) and dry gas seals (type 28 AT from Crane Packing).

The main characteristics of this multistage compressor are:

- a power of 3700 kW at a nominal speed of rotation of 13 600 rpm
- a flow rate of 5200 m^3/h – the suction pressure is 36 bar and the discharge pressure 66 bar
- three impellers
- two radial active magnetic bearings which support the rotor

- one active magnetic thrust bearing
- an electronic control cabinet for the radial and thrust bearing servosystem
- a rotor of length 1.698 m and mass 199.3 kg
- a flexible diaphragm coupling.

In addition, a small device made up of a mass and a viscoelastic material is mounted at one end of the rotor in order to damp the highest modes, for which the electronic control system is not efficient because of their high frequencies.

Two auxiliary ball bearings are introduced in case of failure of the magnetic bearings (and to support the rotor at standstill).

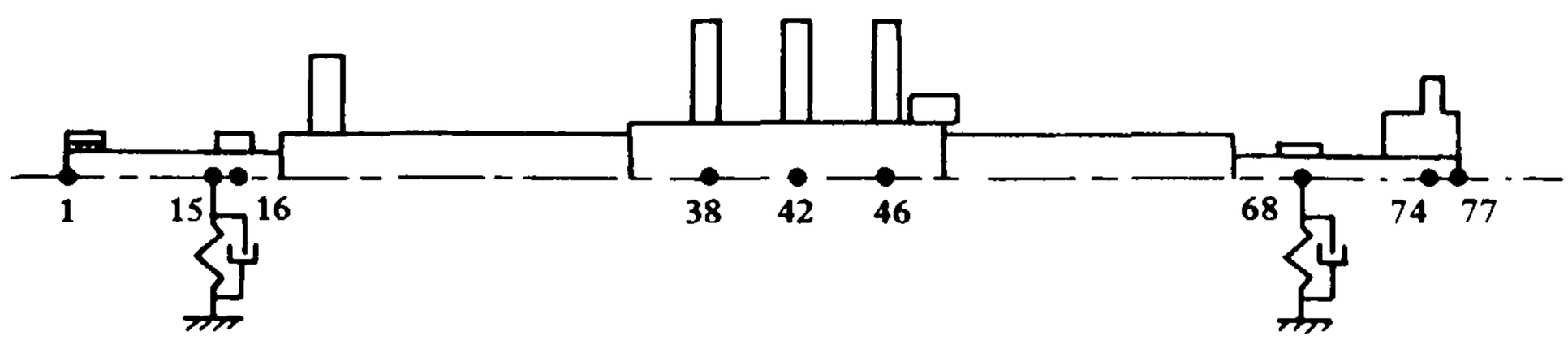

Figure 7.33. Finite element model

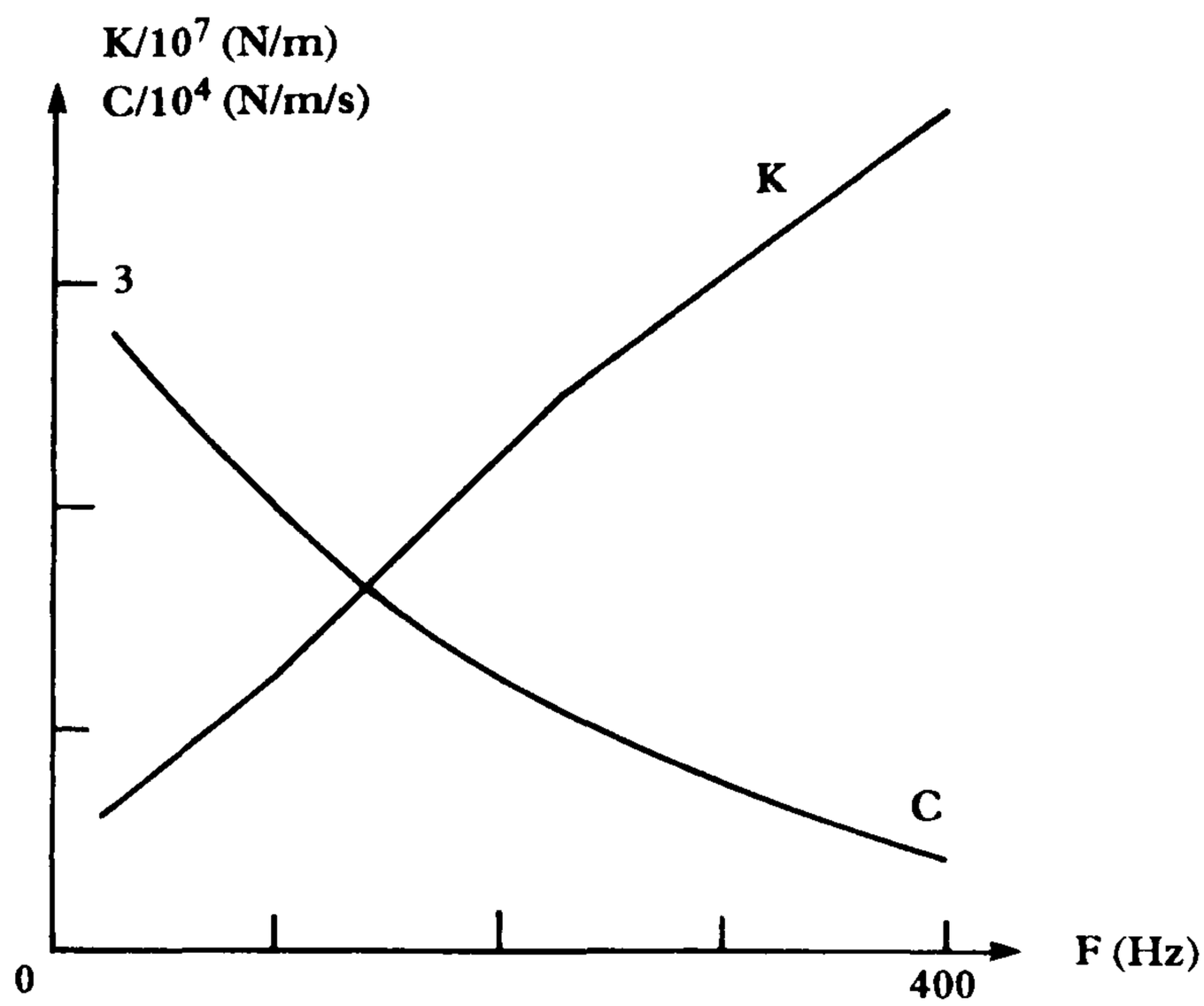

Figure 7.34. Stiffness and viscous damping characteristics

The finite element model (Figure 7.33) includes 76 shaft elements, 32 disks and two bearings. The magnetic bearing characteristics, stiffness and viscous damping, include isotropic diagonal terms and no cross-coupling terms. These characteristics, shown in Figure 7.34, are a function of the frequency of excitation and are given by the control system design, but do not depend on the speed of rotation.

7.5.1 The Campbell diagram

The diagram is shown in Figure 7.35. As the bearing characteristics are a function of the frequency, an iterative procedure has to be implemented for each speed of rotation. Frequencies F7 and F8 vary significantly with the speed of rotation and are mostly due to the motion of the small damper added at the rotor end. They are to be considered as local and not excitable modes.

The mode shapes at 13 600 rpm are shown in Figure 7.36. The viscous damping factors are very high as a consequence of the rotor arrangement and of the design of the derivative action of the controller. The stiffness

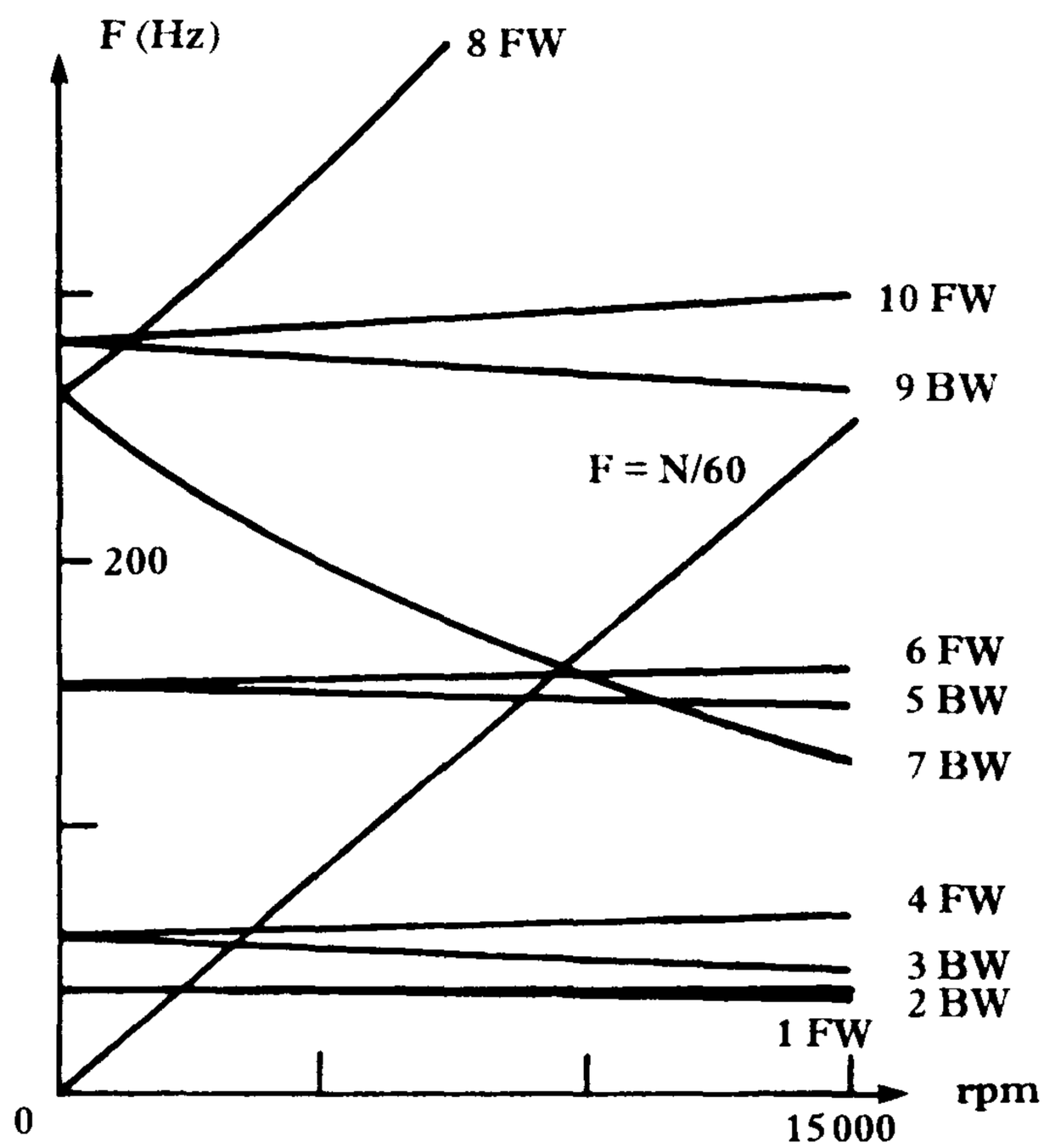

Figure 7.35. Campbell diagram

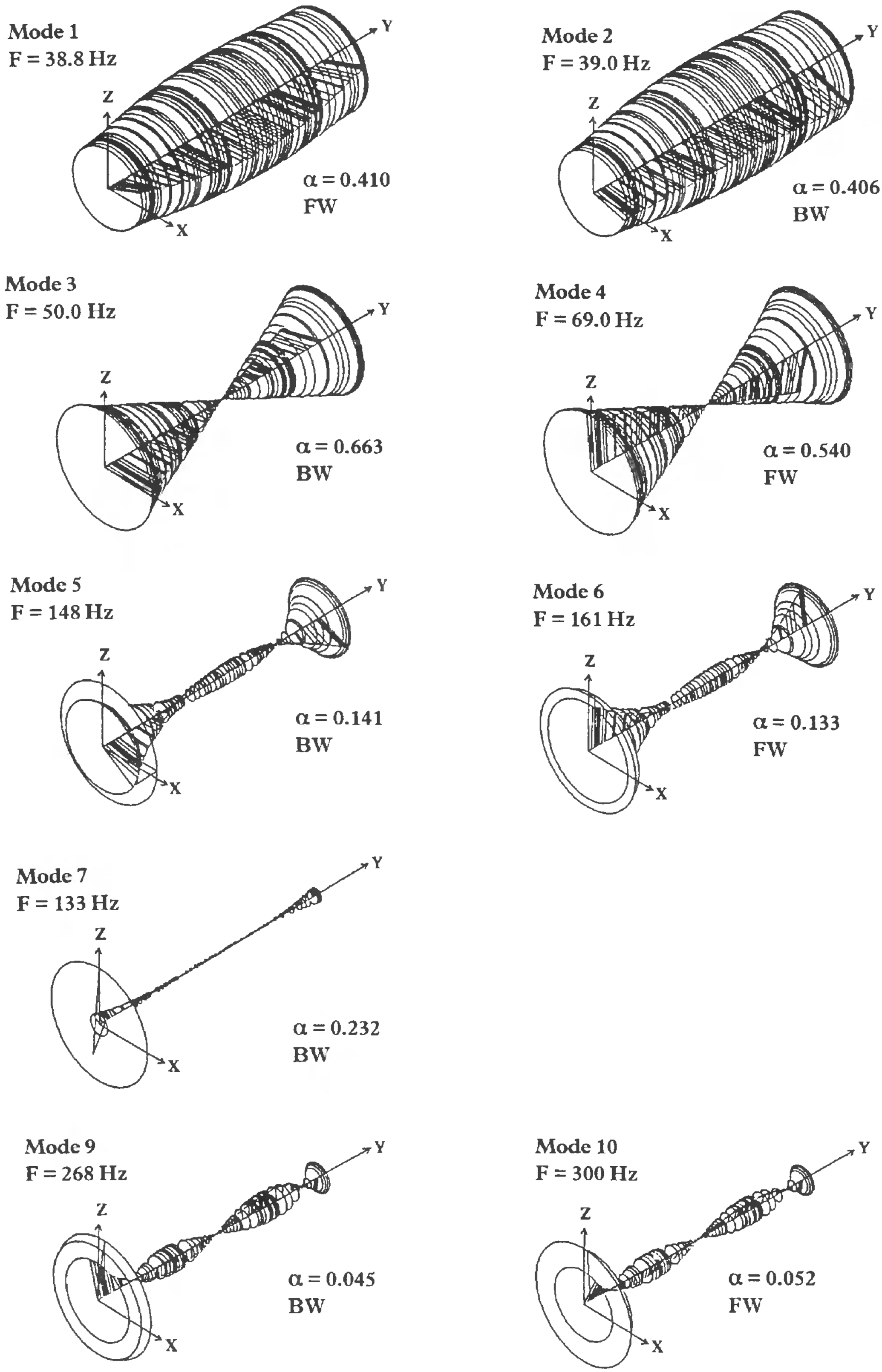

Figure 7.36. Mode shapes at 13 600 rpm

of an active magnetic bearing is about 10 to 15 times lower than the stiffness of a hydrodynamic bearing. So, it can be seen on the Campbell diagram that the operating speed of the compressor is located between the third and fourth critical speeds; this is now commonly accepted for such a multistage rotor. During the design, special attention must be paid to the damping, more than to the critical speed versus the nominal speed. This is why the arrangement with the thrust bearing inside the radial bearing was chosen, because it leads to a higher damping.

7.5.2 Mass unbalance response

From Equations (7.2) and (7.3), the mass unbalance is 446 g mm and the maximum allowable displacement 11.9 μm.

Case 1

The mass unbalance is at node 42. The response at this node and at nodes 15 and 68, which define the bearing positions, is presented in Figure 7.37. The maximum displacement noted at 9740 rpm is that of the mass of the device and is 16.1 μm. The displacement of the mass of the device is 9.24 μm at the nominal speed, and the maximum displacement at the bearings

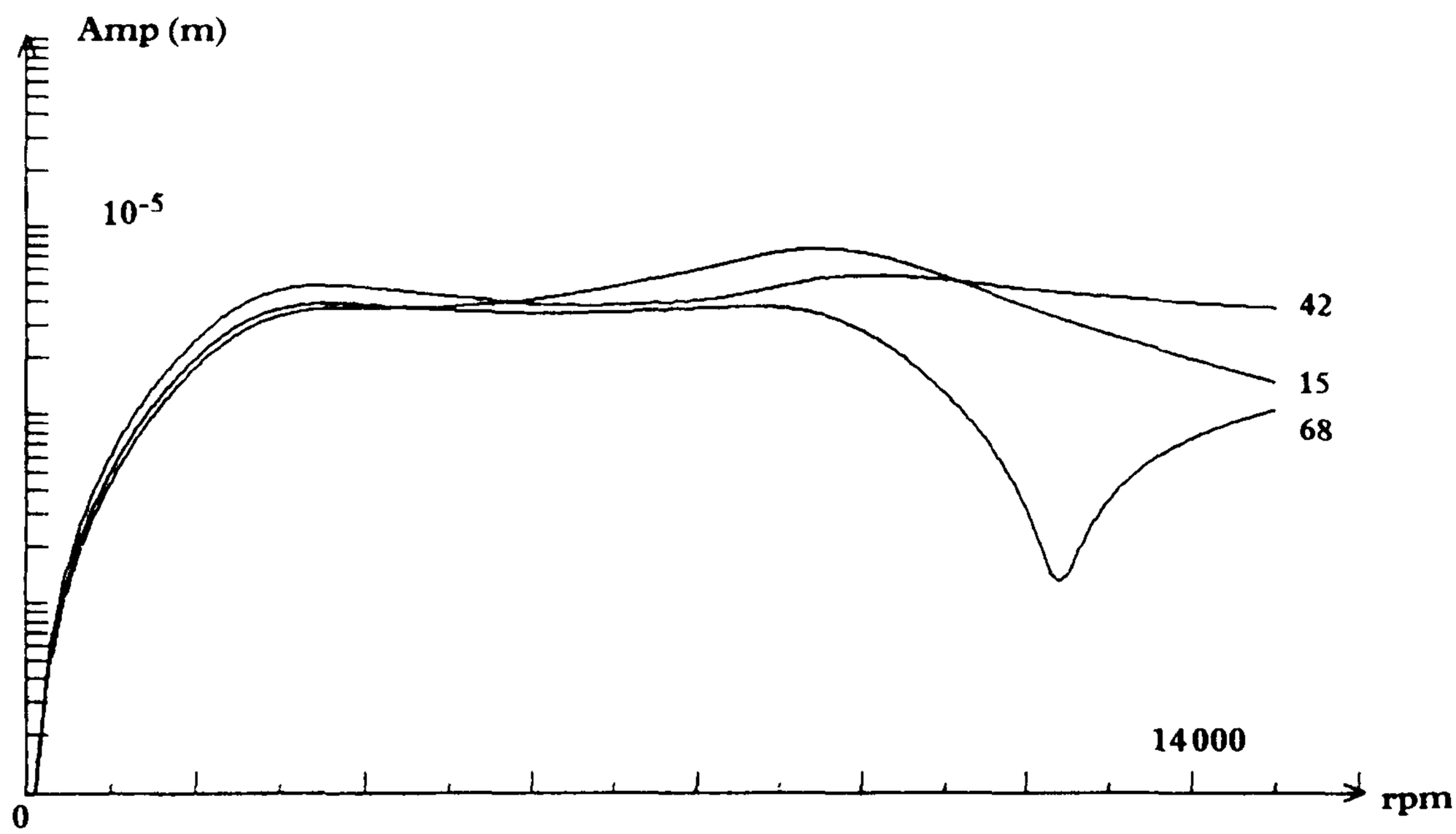

Figure 7.37. Case 1: mass unbalance response

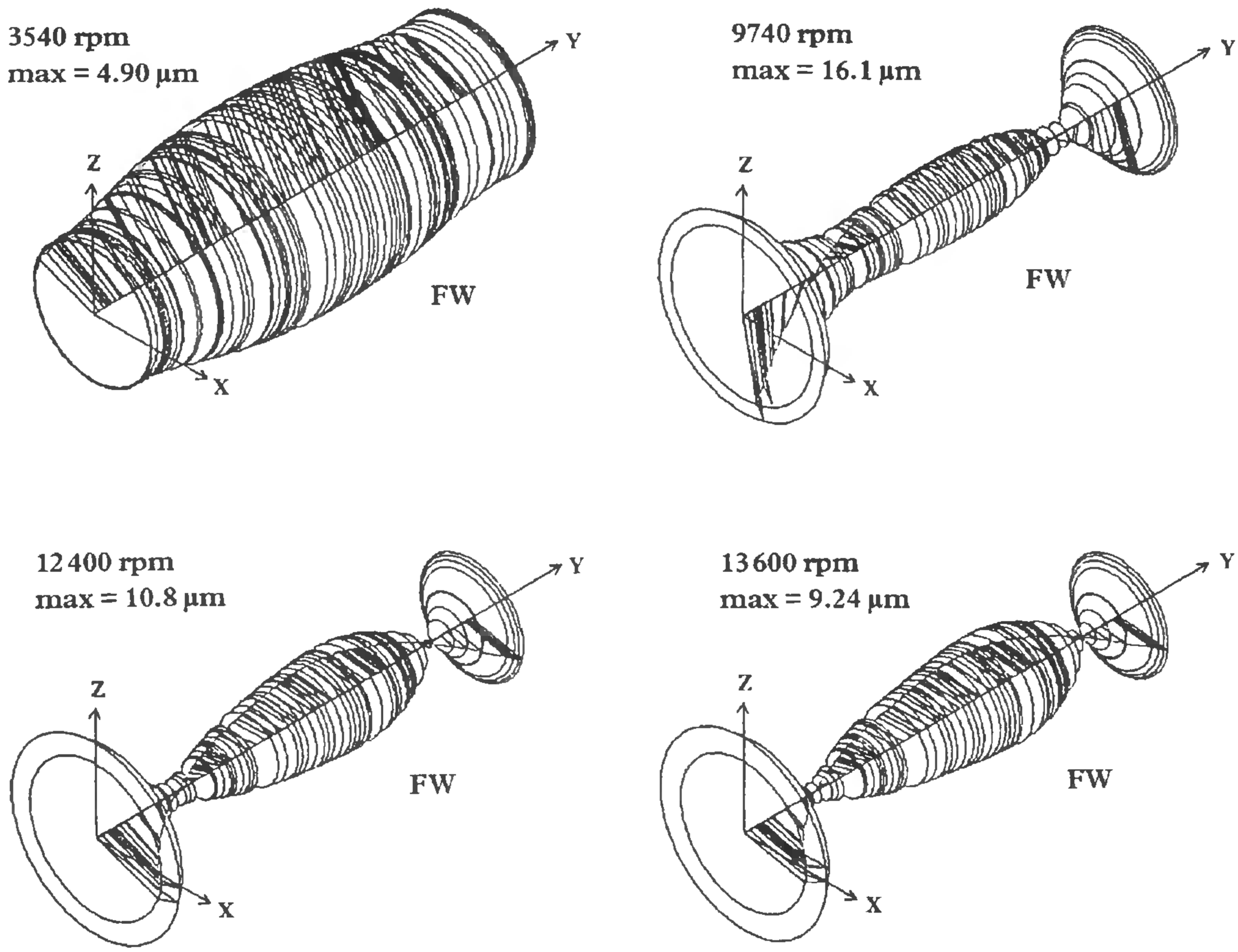

Figure 7.38. Case 1: rotor deflections

is 2.34 µm. In Figure 7.38 the rotor deflections at four speeds of rotation, including the nominal speed, are shown.

Case 2

The mass unbalance is at nodes 16 and 74. The unbalance response shows no maximum and is presented in Figure 7.39. The displacement maximum at the operating speed, 11.8 µm, is at node 77. In Figure 7.40 the rotor deflections at four speeds of rotation, including the nominal speed, are shown.

7.5.3 Remarks

The rotor is stable and damping is very high. The largest displacement is that of the small damping device and this does not cause a problem. All

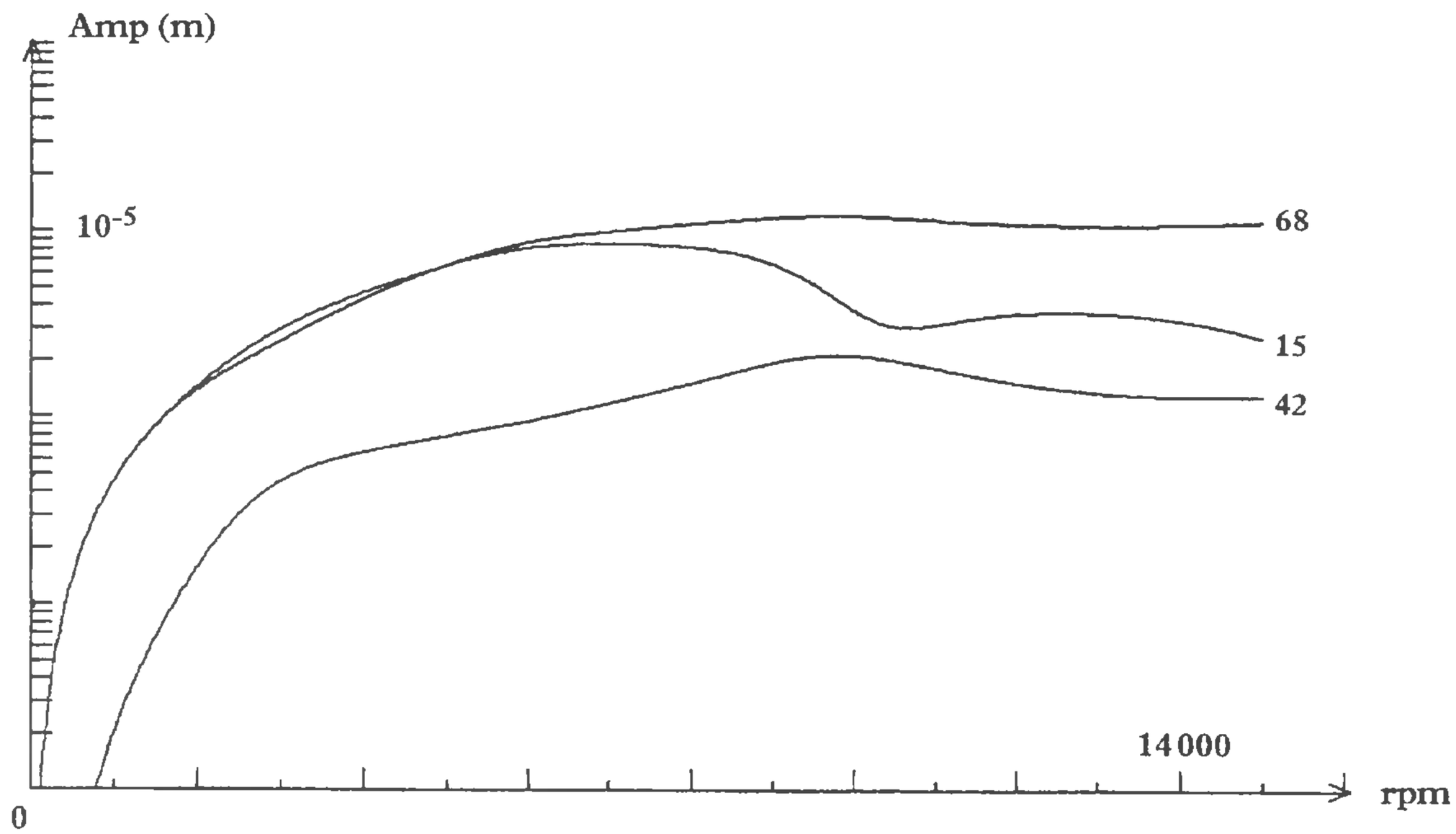

Figure 7.39. Case 2: mass unbalance response

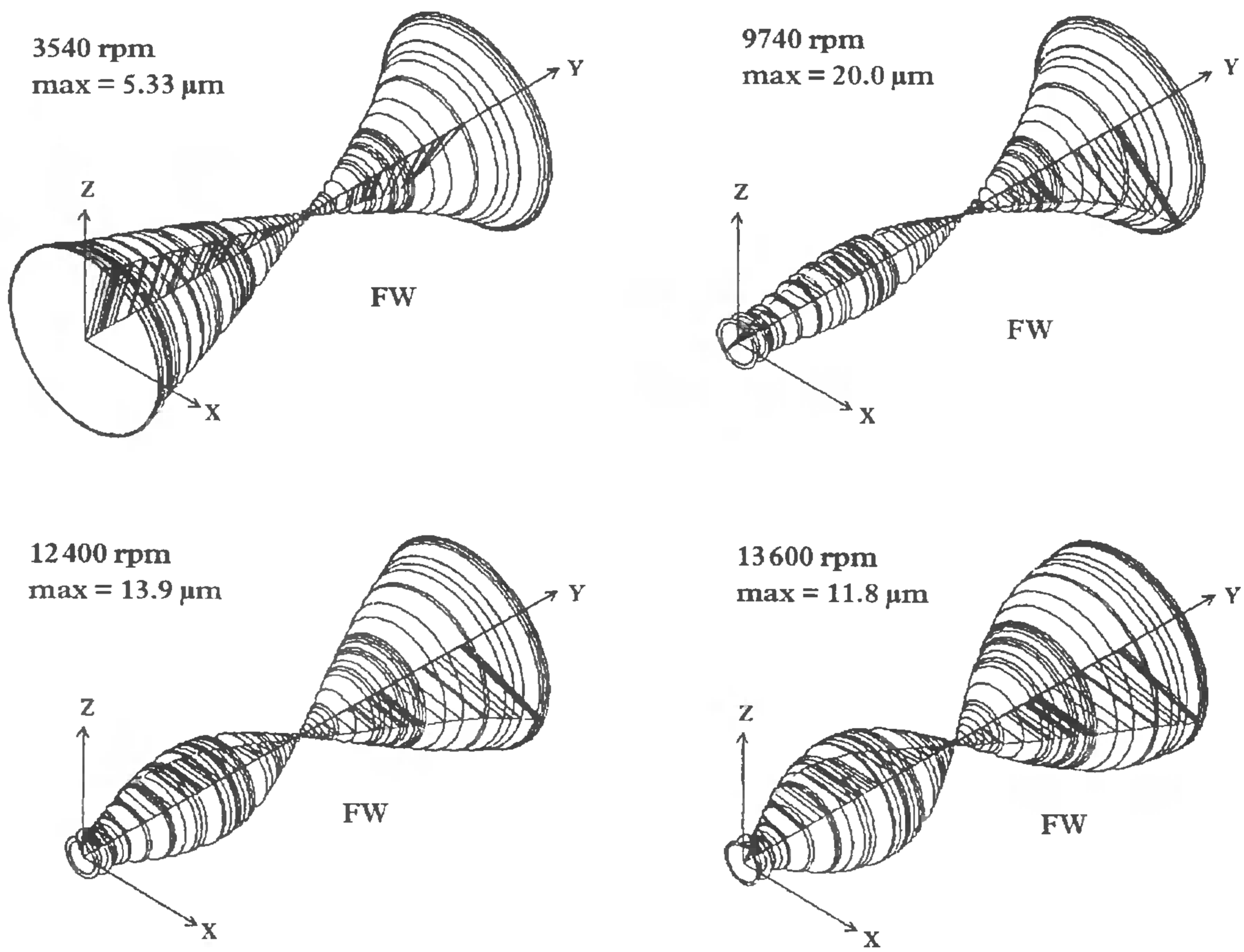

Figure 7.40. Case 2: rotor deflections

the maximum displacements of the rotor obtained in cases 1 and 2 are lower than the API recommendation. This is very important, because the stiffness of an active magnetic bearing is much lower than the stiffness of a hydraulic bearing (for which the API recommendations are established) and it is nevertheless found that the same criteria may be used.

These calculations were performed for synchronous excitation. It is important with such applications, where the aerodynamic excitations are high in relation to the stiffness of the bearings, to consider the response to subsynchronous excitation at a frequency roughly half the speed of rotation. In this case, the high damping leads to very low displacements.

This oil-free centrifugal compressor has been in continuous industrial operation since October 1987.

7.6 PROPFAN

The propfan studied [19, 41] in the European project DUPRIN (Ducted Propfan Investigation) is shown in Figure 7.41. The propfan is driven by a four-stage compressed air turbine giving a power of 160 kW and a speed of rotation of up to 16 000 rpm (see Figure 7.42); the coupling between the propfan shafts and the turbine concerns only torsion. The bending

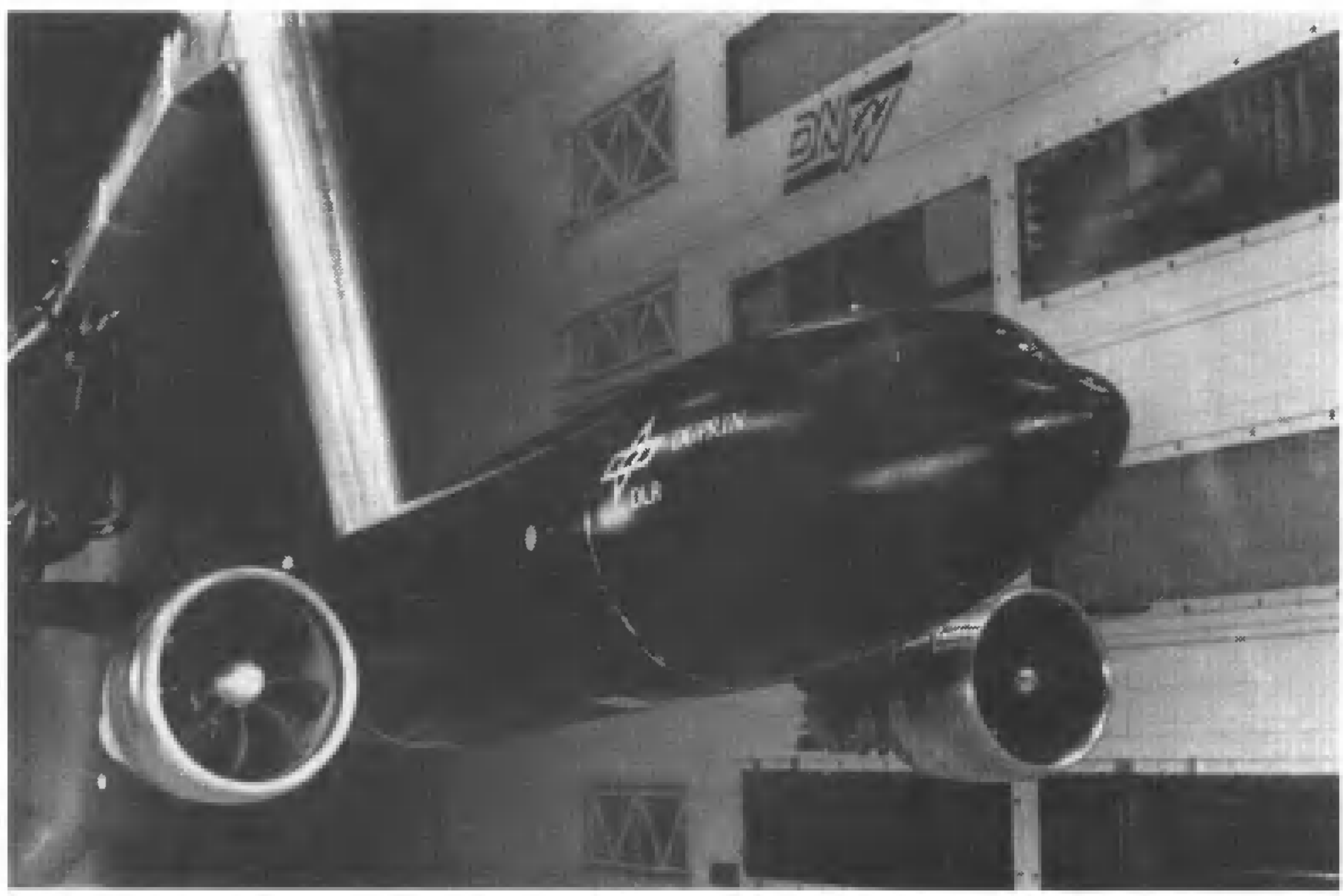

Figure 7.41. The DUPRIN propfan (Picture courtesy Dutch Airbus, DLR, Aérospatiale, Technofan and all the European partners)

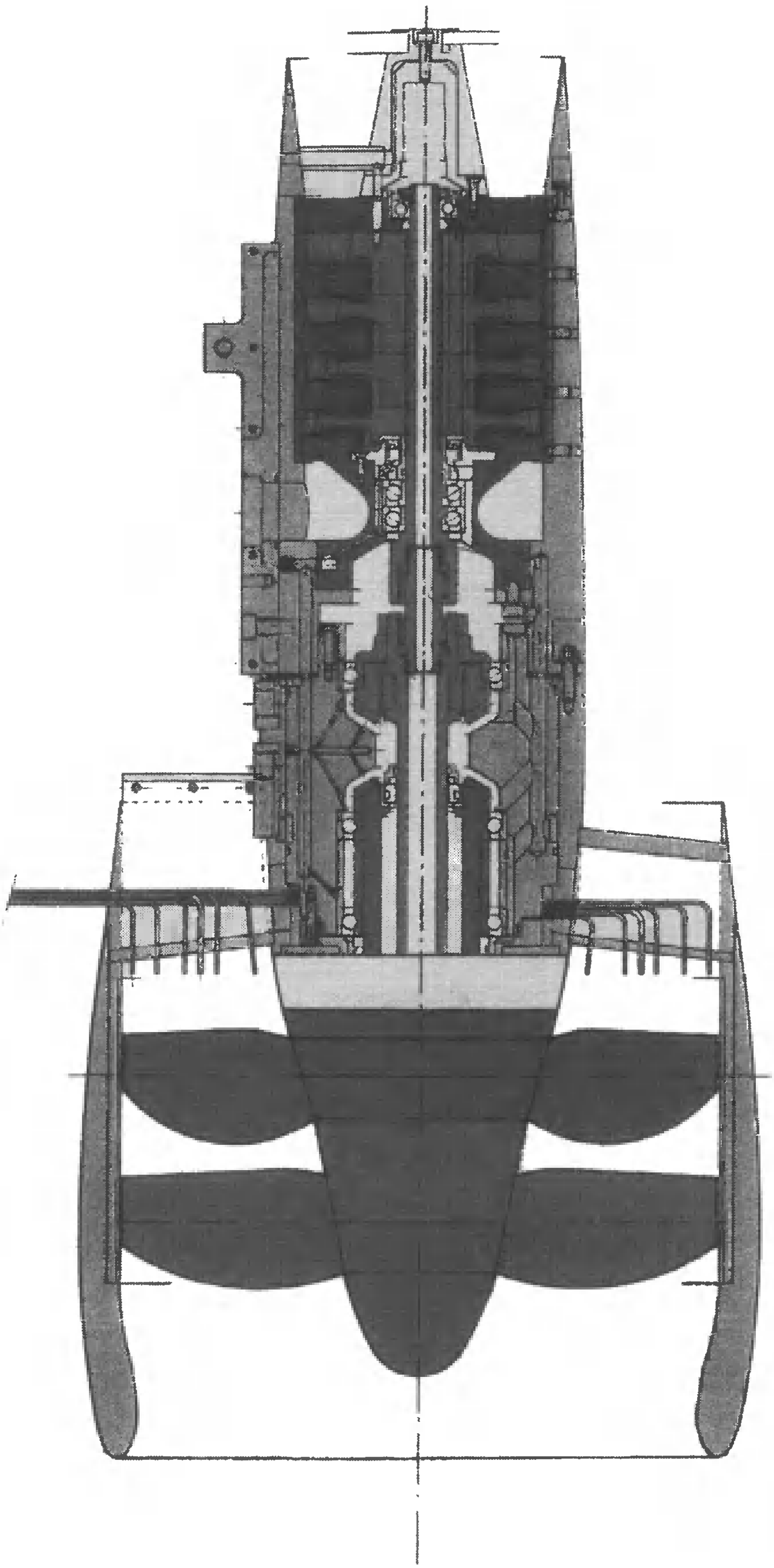

Figure 7.42. The DUPRIN propfan cross-section

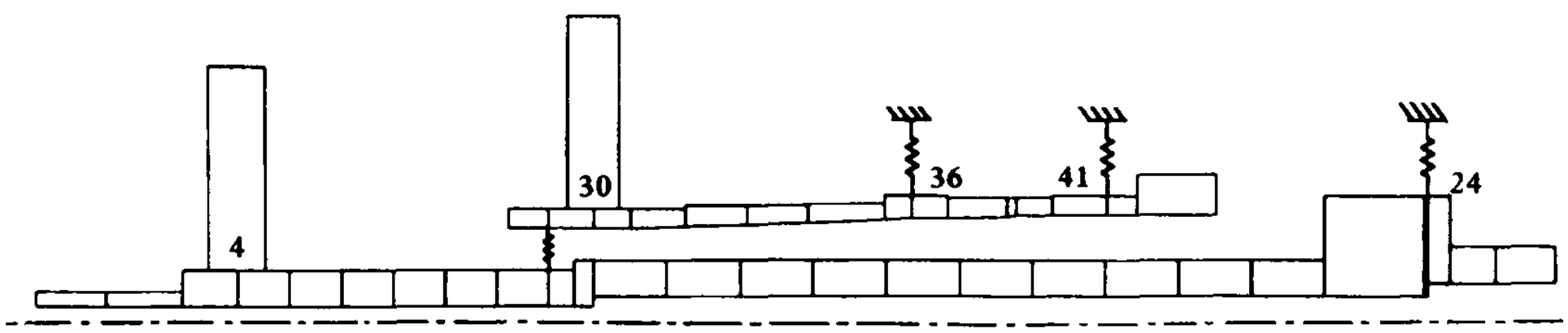

Figure 7.43. Finite element model

dynamic behavior of the propfan can therefore be studied independently from the turbine and it is sufficient to model the dashed parts of Figure 7.42. The finite element model of the propfan (see Figure 7.43) is based on beam elements for the shafts, rigid disk elements for disks, and stiffness for the roller bearings which are isotropic and linear. In the z-axis the stiffness of the bearing must include the stiffness of the casing. In this case the system is asymmetric. The Q factor is estimated as being 50 for each mode.

7.6.1 The Campbell diagram

The diagram is shown in Figure 7.44. The two mode shapes at the highest operating speed are shown in Figure 7.45. Two critical speeds appear when the mass unbalance is situated either on rotor 1 or on rotor 2.

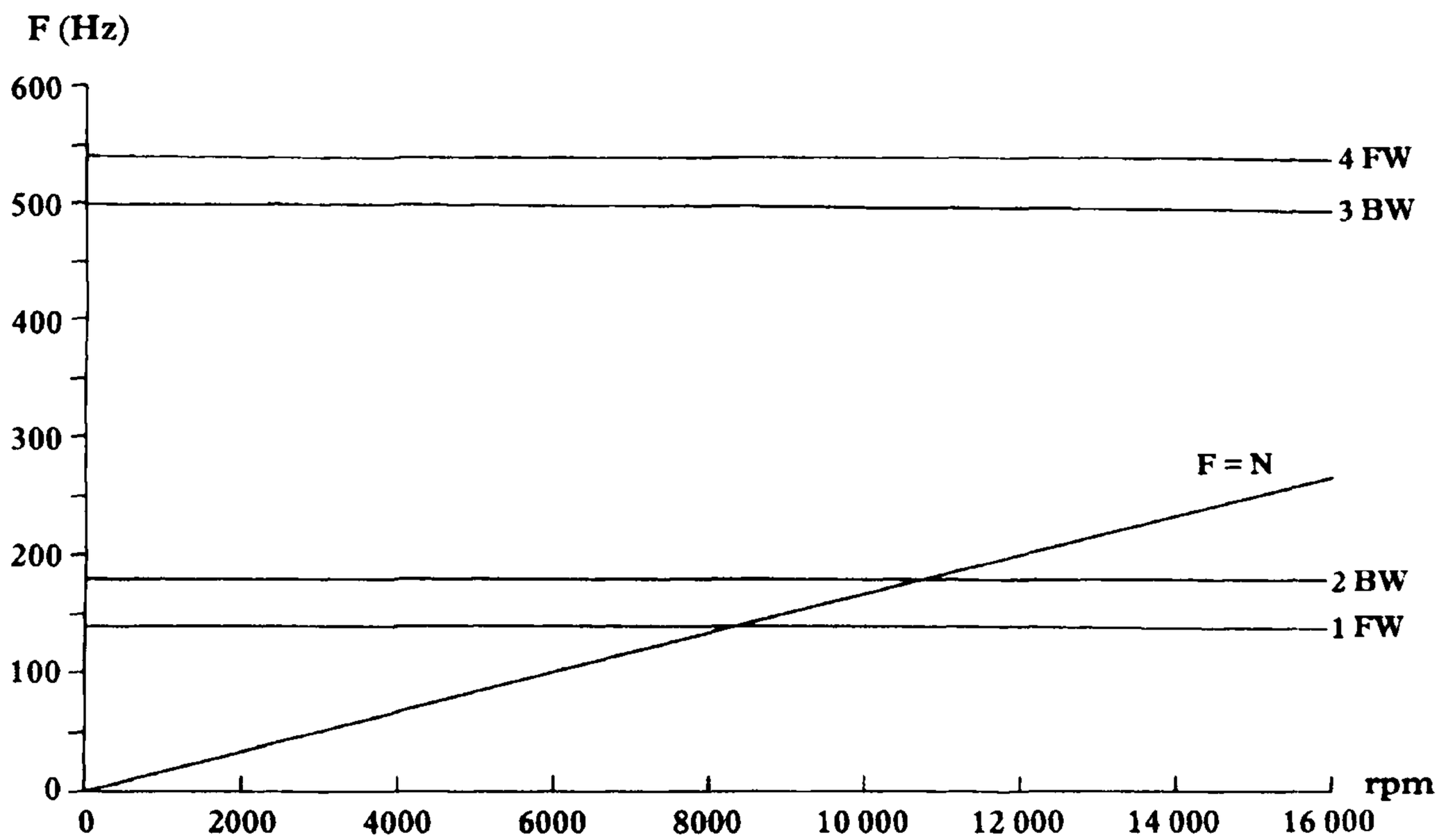

Figure 7.44. Campbell diagram

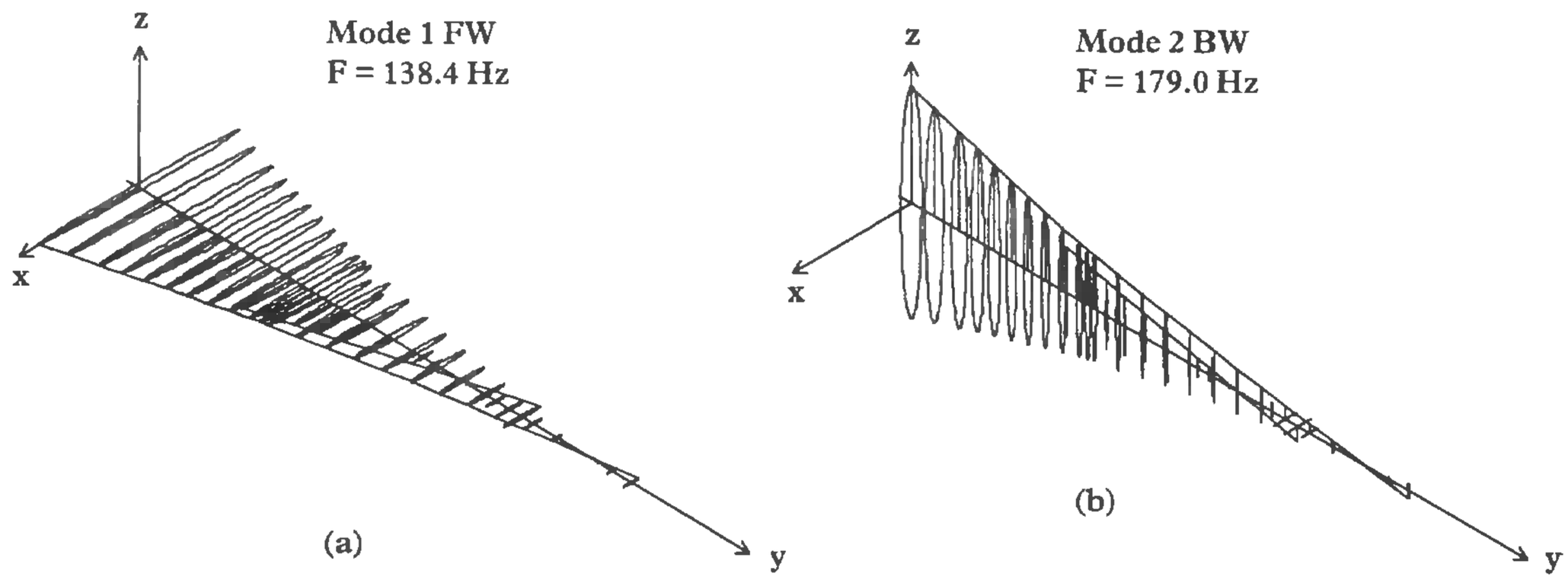

Figure 7.45. Mode shapes at 16 000 rpm

7.6.2 Mass unbalance response

For the mass unbalance on rotor 1, the mass is located at node 4 and the response is shown in Figure 7.46. The rotor deflections at the critical speeds and at the nominal speed are shown in Figure 7.47.

For the mass unbalance on rotor 2, the mass is located at node 30 and the response is shown in Figure 7.48. The same two critical speeds appear. Rotor deflections at the critical speeds and at the nominal speed are shown in Figure 7.49.

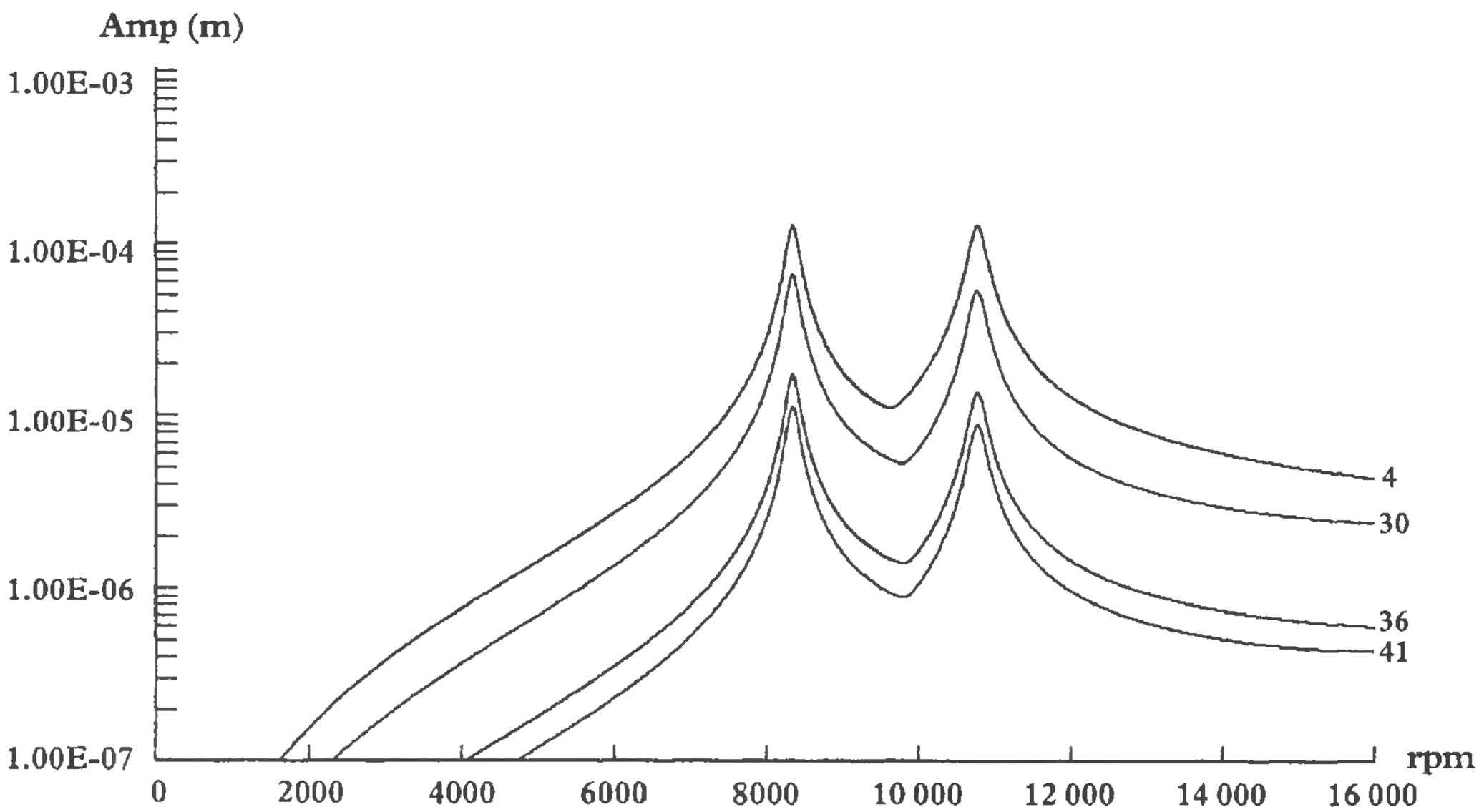

Figure 7.46. Mass unbalance response (mass on rotor 1)

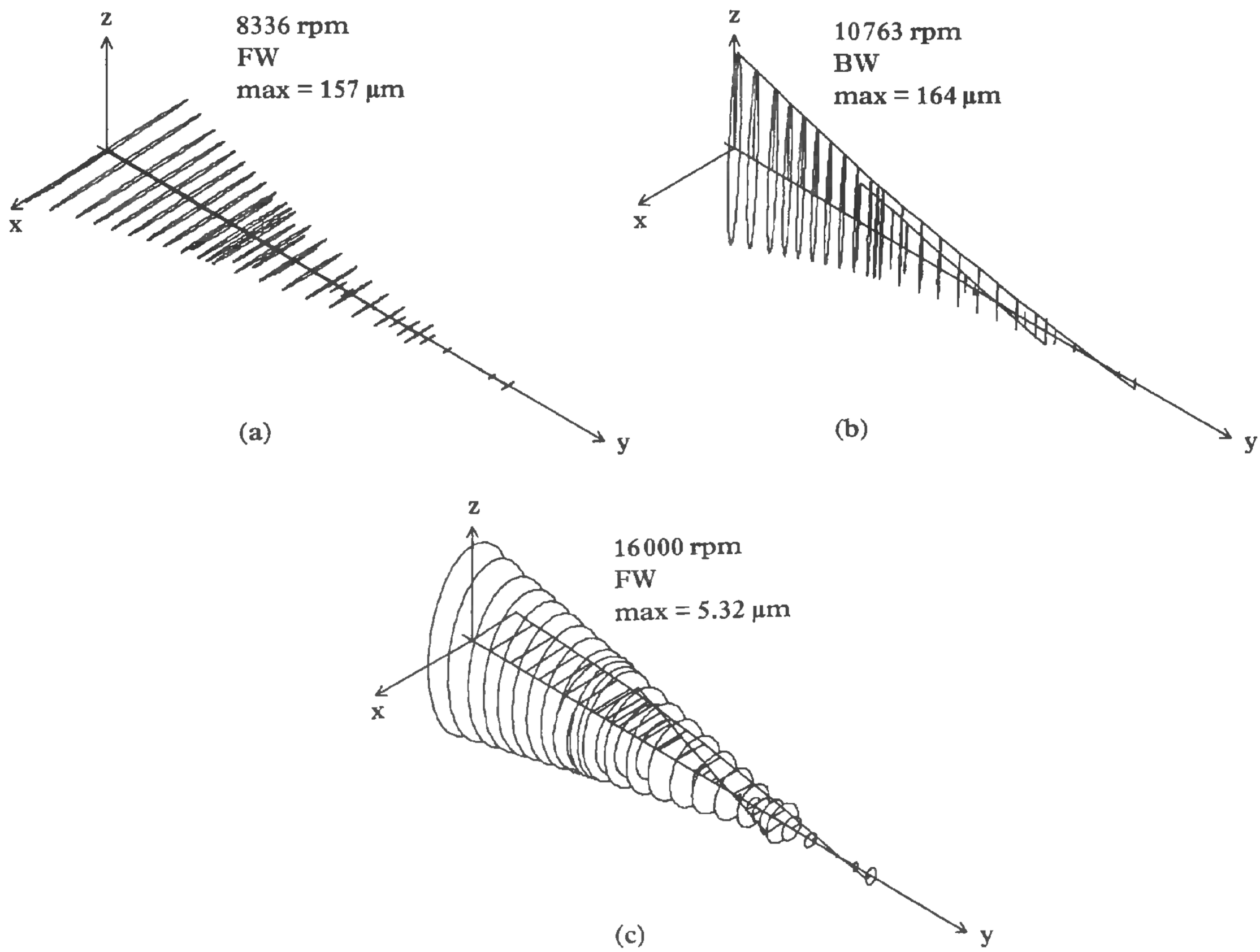

Figure 7.47. Rotor deflections (mass on rotor 1)

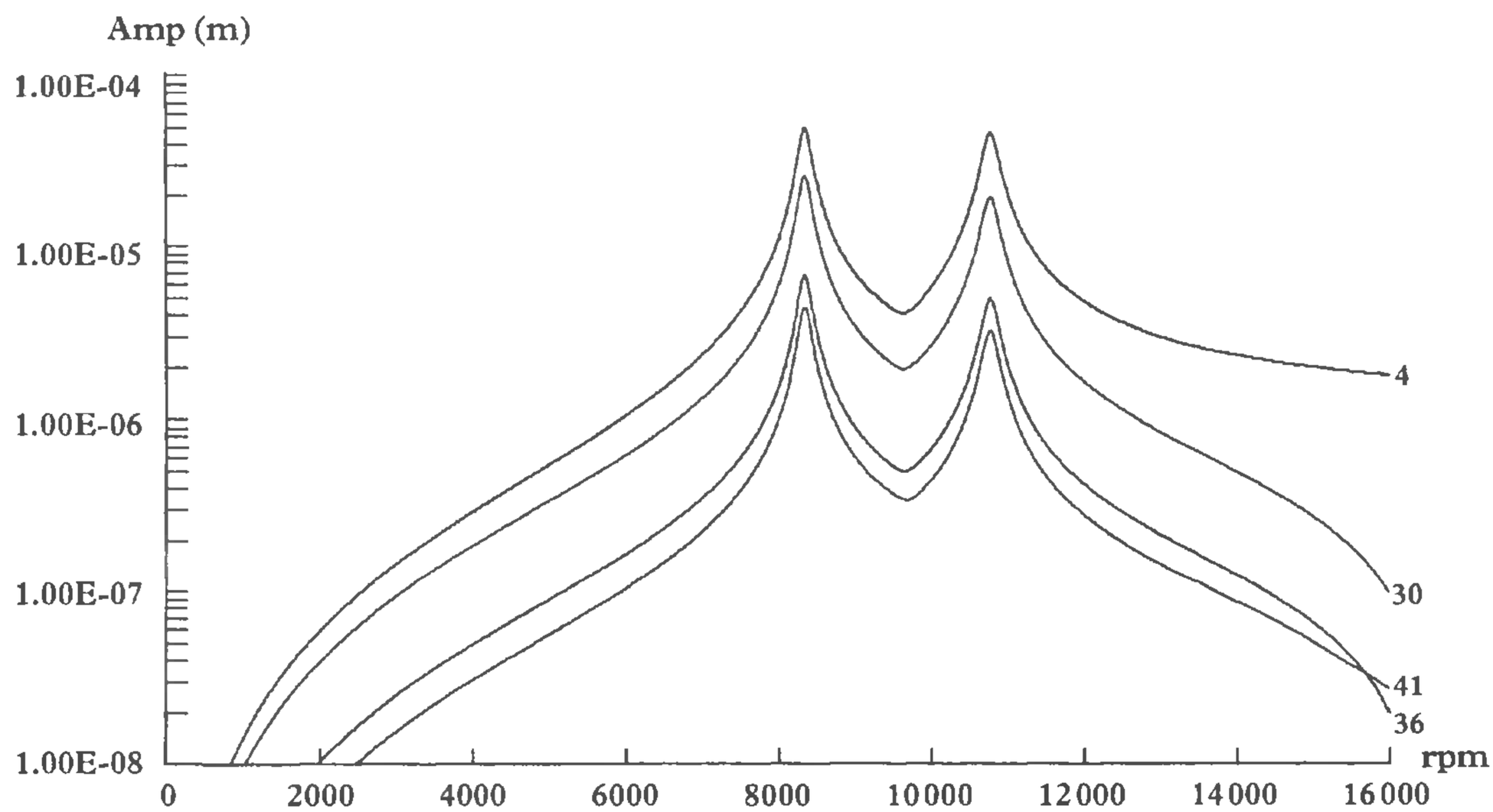

Figure 7.48. Mass unbalance response (mass on rotor 2)

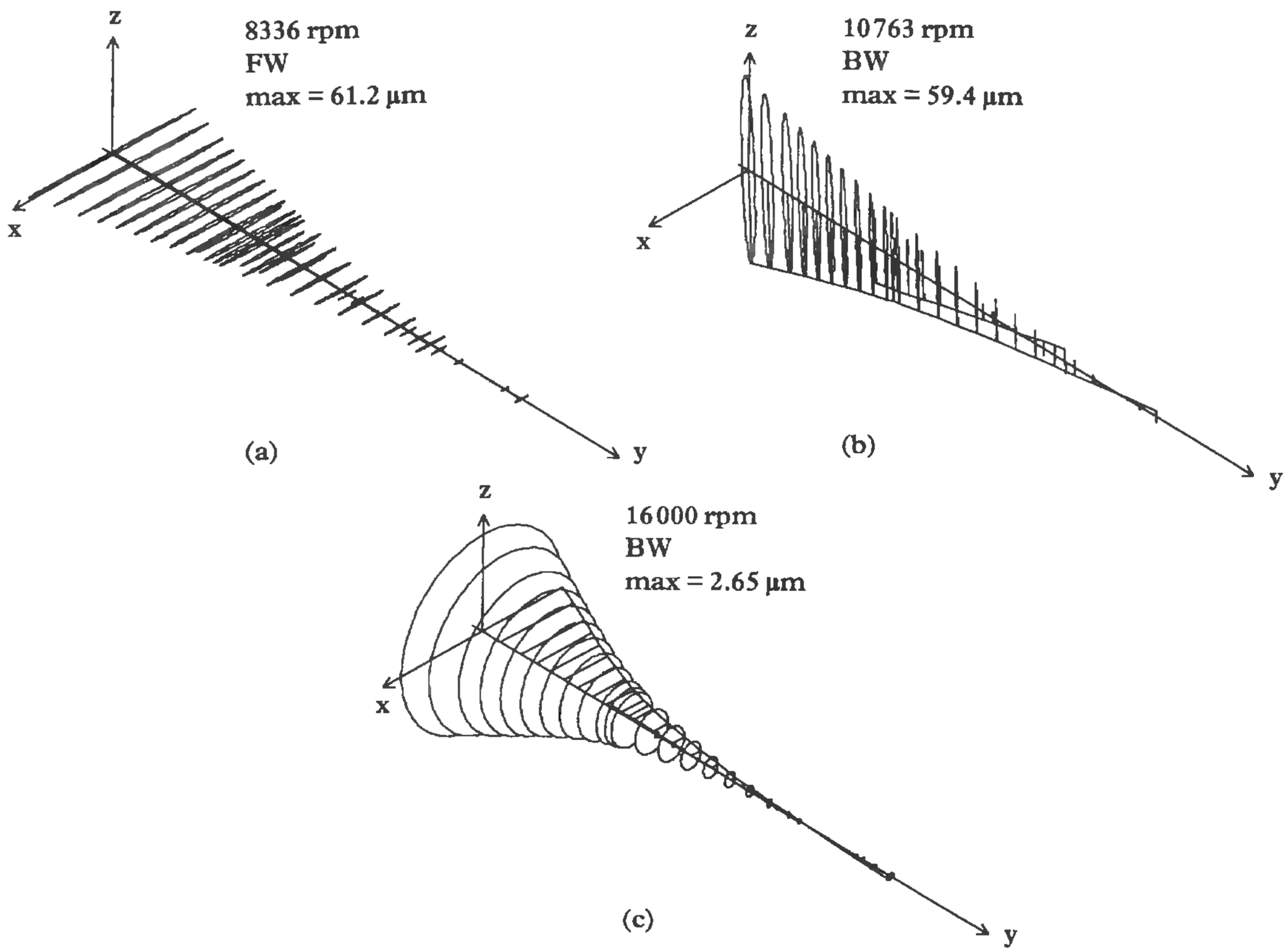

Figure 7.49. Rotor deflections (mass on rotor 2)

7.6.3 Remarks

It should be noted that the gyroscopic effect is low as the two disks are identical and counter-rotate at the same speed of rotation.

It is difficult to compare the amplitudes of the experimental and theoretical mass unbalance responses, because of the residual mass unbalances and the damping values, though here the predicted results compare well with the experiments.

7.7 AIR TURBINE STARTER

The air turbine starter studied, similar to the air turbine starter described in [9], is used for starting fighter aircraft engines and is presented schematically in Figure 7.50. Its main characteristics are:

- two counter-rotating rotors connected by a reduction gear (ratio = 5.3)
- a power of 130 kW

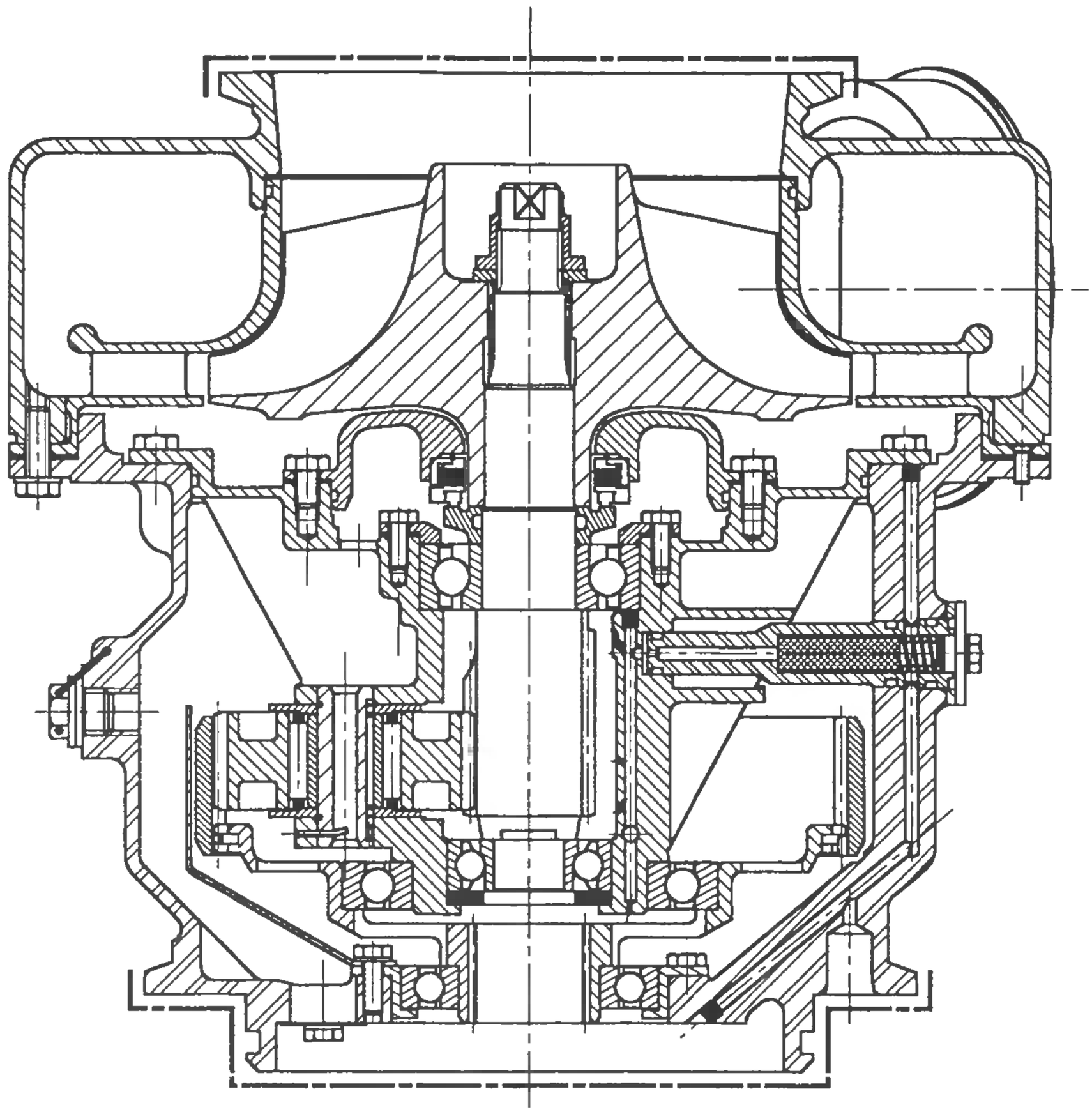

Figure 7.50. Air turbine starter (Picture courtesy Microturbo)

- a total mass of about 7 kg
- a maximum of the turbine speed of rotation at 69 000 rpm.

The finite element model, Figure 7.51, uses 58 nodes. The stiffness of the roller bearings can be considered as isotropic and constant with the speed of rotation, and the stator is modeled by reduced stiffness and mass matrices. The Q factor is estimated to be 25.

7.7.1 The Campbell diagram

The Campbell diagram, Figure 7.52, shows the critical speed (at point A) when the mass unbalance is located on the ring gear (node 36) or the critical speeds (at points C and D) when the mass unbalance is located on

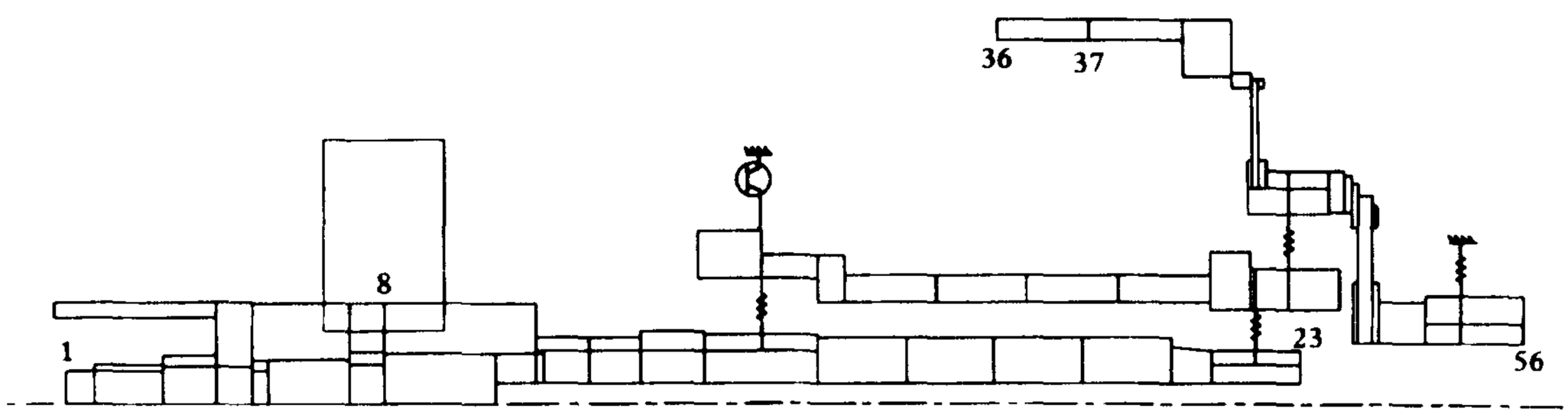

Figure 7.51. Finite element model

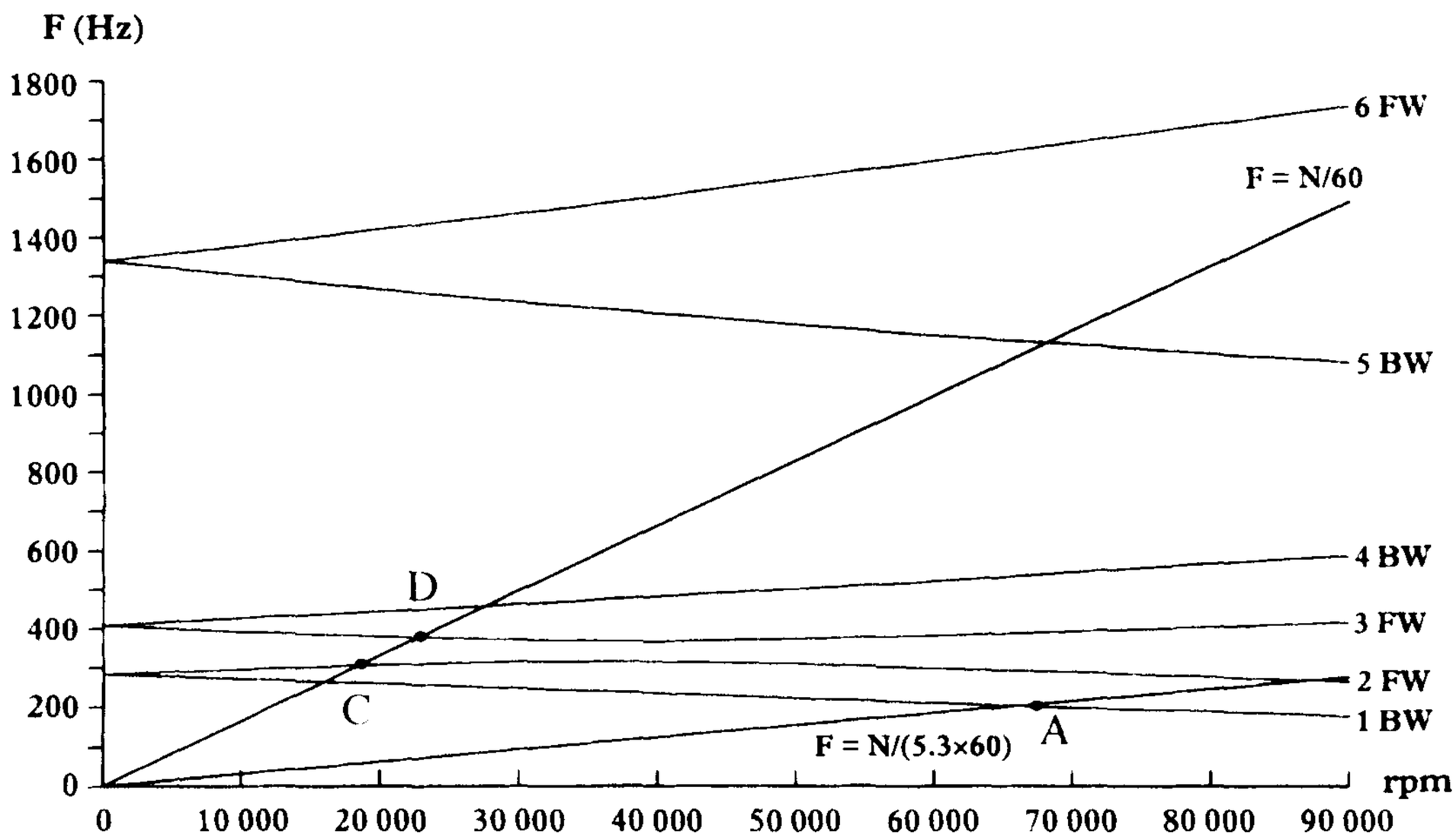

Figure 7.52. Campbell diagram

the turbine disk (node 8). The first four mode shapes at 60 000 rpm are shown in Figure 7.53.

7.7.2 Mass unbalance response

The mass unbalance response with a mass unbalance located on the turbine disk is presented in Figure 7.54. The rotor deflections at the critical speeds are shown in Figure 7.55.

The mass unbalance response with a mass unbalance located on the ring gear is presented in Figure 7.56. The rotor deflections at the critical speeds are shown in Figure 7.57.

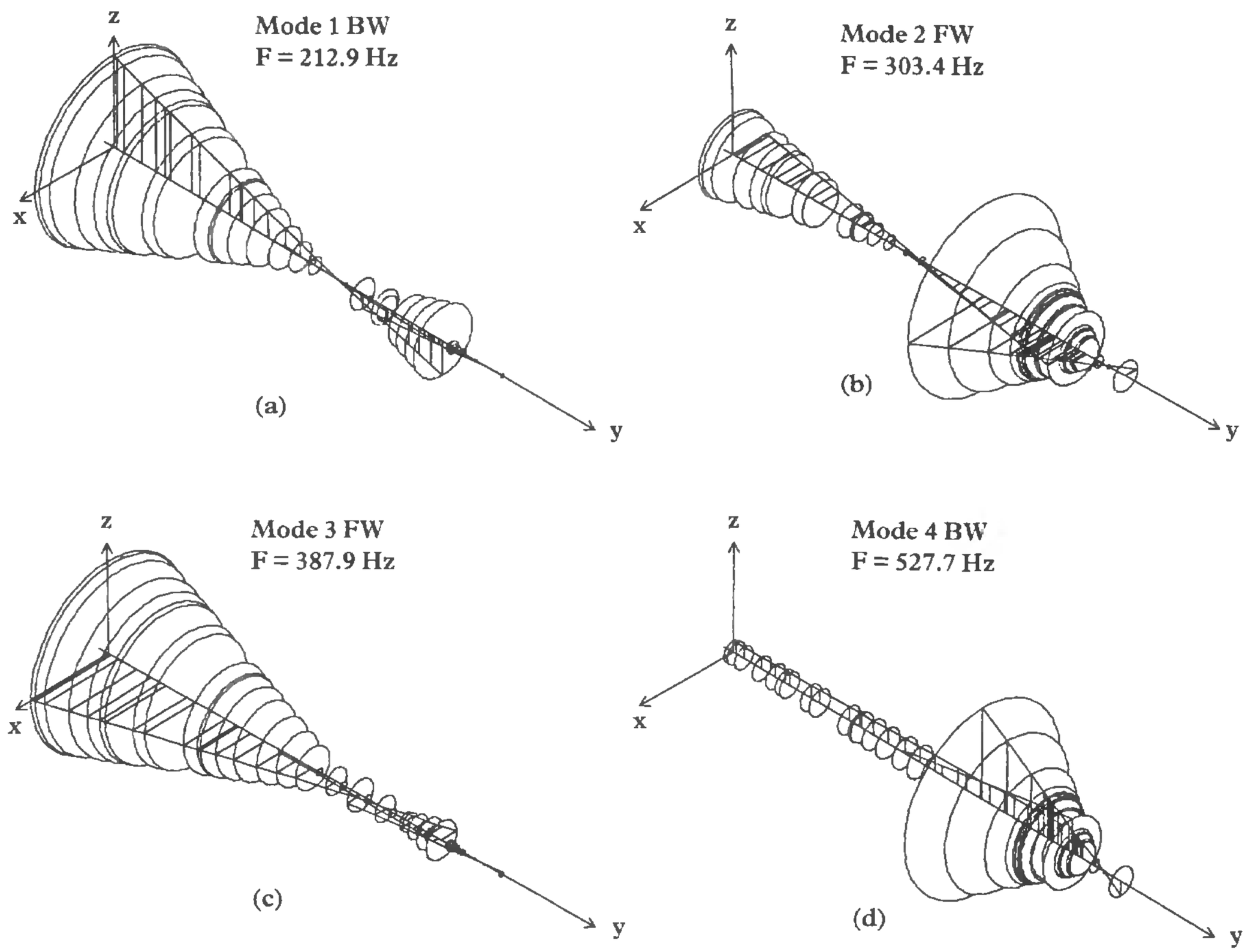

Figure 7.53. Mode shapes at 60 000 rpm

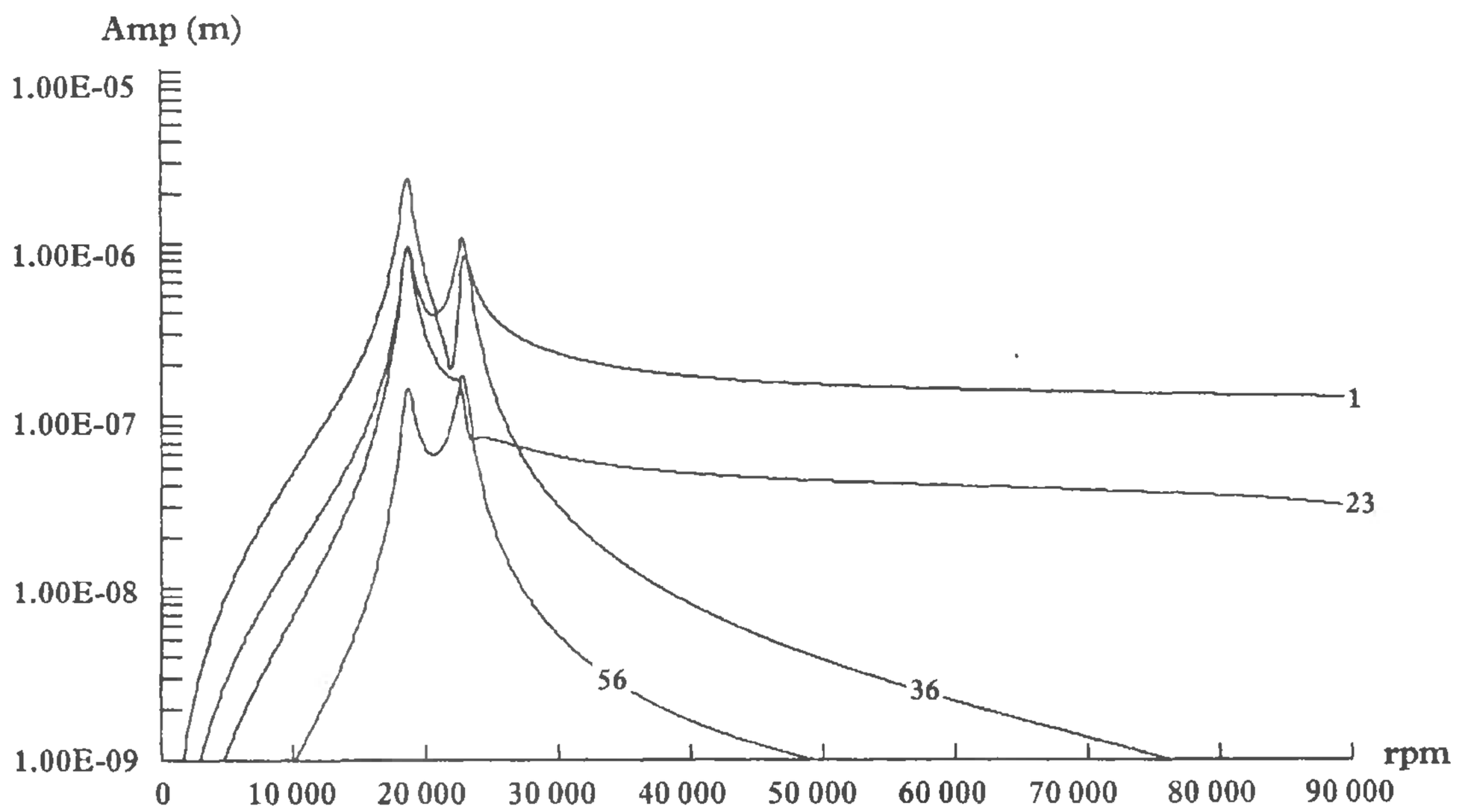

Figure 7.54. Mass unbalance response (mass on rotor 1)

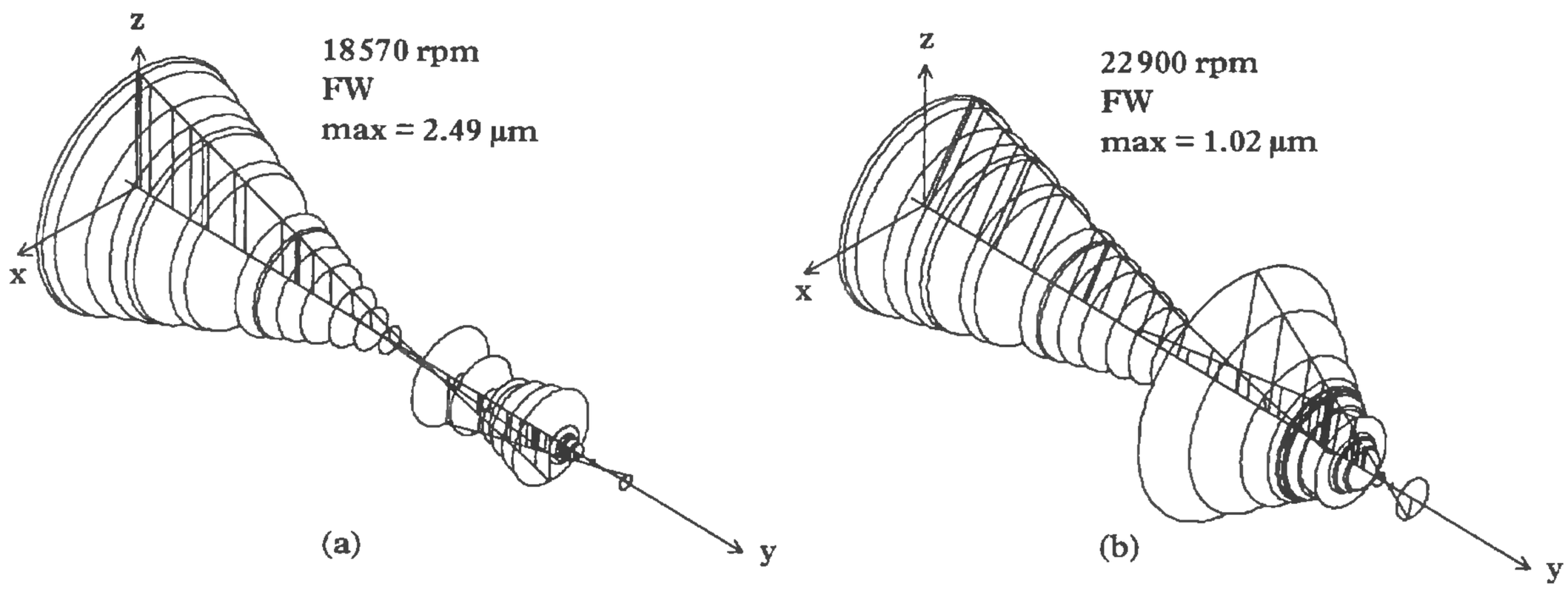

Figure 7.55. Rotor deflections (mass on rotor 1)

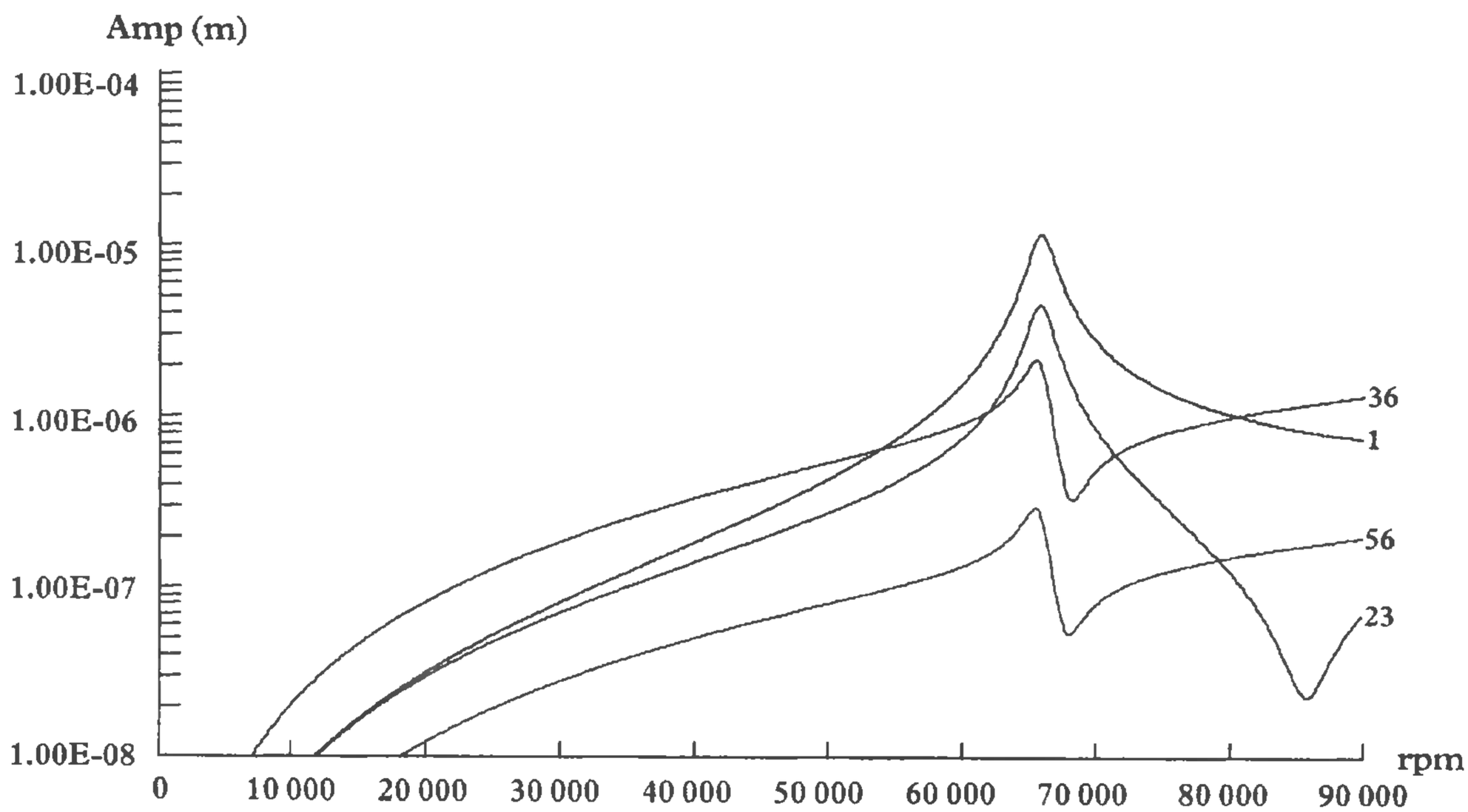

Figure 7.56. Mass unbalance response (mass on rotor 2)

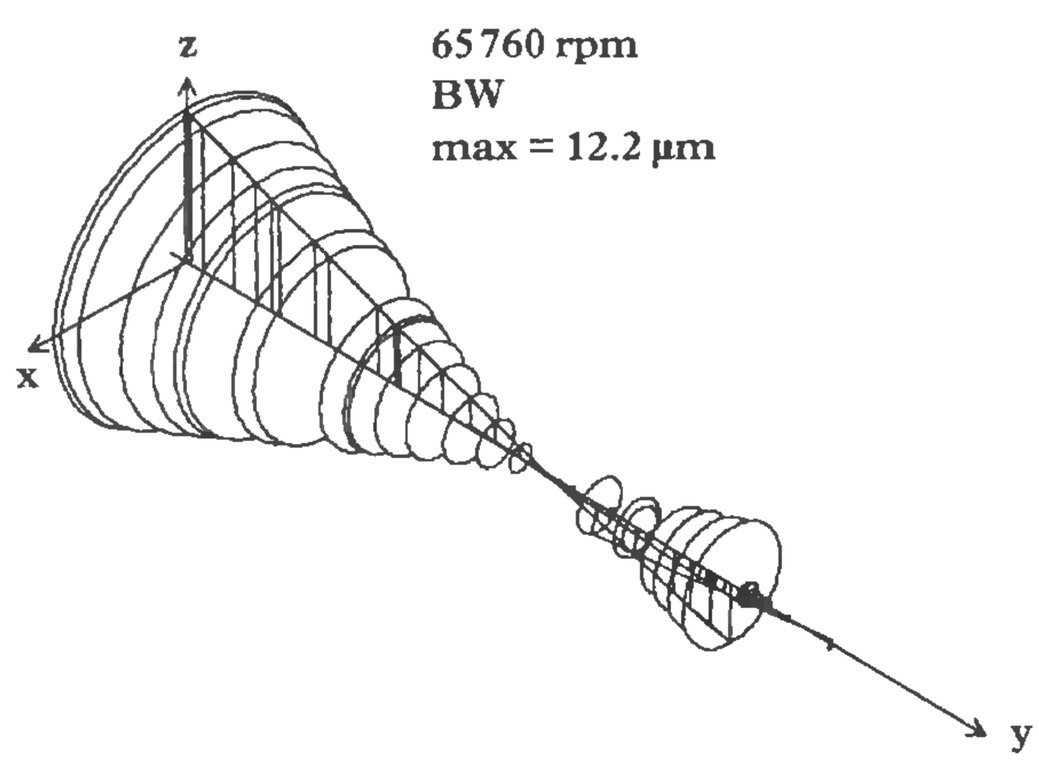

Figure 7.57. Rotor deflection (mass on rotor 2)

Table 7.2. Finite elements and experimental results

CRITICAL SPEEDS (RPM)	1	2	3
Prediction	18 556	22 796	65 758
Experiment	18 140	23 000	66 280

7.7.3 Remarks

Experimental and finite element results are presented in Table 7.2 and agreement is shown to be good.

It is difficult to compare the amplitudes calculated with experimental values, because the mass unbalances exist simultaneously on the two rotors. In addition the damping value is an estimate.

8

Transient Motions

It is now more and more important to know what happens when a rotor starts up, stops or goes through a critical speed, effects known as transient motions. In this chapter the characteristics of the bearings will be assumed to be constant. The equations given in Chapter 1 have to be adapted [33, 38].

8.1 EQUATIONS AND SOLUTIONS

The angular velocity $\dot{\phi}$ is no longer constant and is a function of time; that is

$$\dot{\phi} = \dot{\phi}(t) \tag{8.1}$$

Equation (1.6) in Chapter 1, which gives the kinetic energy T_D of a disk, becomes

$$T_D = \tfrac{1}{2}M_{\mathrm{D}}(\dot{u}^2 + \dot{w}^2) + \tfrac{1}{2}I_{\mathrm{D}x}(\dot{\theta}^2 + \dot{\psi}^2) + \tfrac{1}{2}I_{\mathrm{D}y}(\dot{\phi}^2 + 2\dot{\phi}\dot{\psi}\theta) \tag{8.2}$$

As in Chapter 1, the kinetic energy T_{S} of the shaft of length L is obtained by an extension of the expression which gives the kinetic energy of the disk, and

$$\begin{aligned} T_{\mathrm{S}} = &\frac{\rho S}{2}\int_0^L (\dot{u}^2 + \dot{w}^2)\mathrm{d}y + \frac{\rho I}{2}\int_0^L (\dot{\psi}^2 + \dot{\theta}^2)\mathrm{d}y + \rho I\int_0^L \dot{\phi}^2\mathrm{d}y \\ &+ 2\rho I\int_0^L \dot{\phi}\dot{\psi}\theta\mathrm{d}y \end{aligned} \tag{8.3}$$

Expression (8.3) is better written as

$$T_S = \frac{\rho S}{2}\int_0^L (\dot{u}^2 + \dot{w}^2)\mathrm{d}y + \frac{\rho I}{2}\int_0^L (\dot{\psi}^2 + \dot{\theta}^2)\mathrm{d}y + \rho I L \dot{\phi}^2 + 2\rho I \dot{\phi}\int_0^L \dot{\psi}\theta \mathrm{d}y \tag{8.4}$$

The quantities u, w, ψ, θ and ϕ can be considered as generalized independent coordinates, and if Lagrange's equations are applied to Equation (8.2) it comes

$$\frac{\mathrm{d}}{\mathrm{d}t}\left(\frac{\partial T_D}{\partial \dot{u}}\right) - \frac{\partial T_D}{\partial u} = M_D \ddot{u} \tag{8.5}$$

$$\frac{\mathrm{d}}{\mathrm{d}t}\left(\frac{\partial T_D}{\partial \dot{w}}\right) - \frac{\partial T_D}{\partial w} = M_D \ddot{w} \tag{8.6}$$

$$\frac{\mathrm{d}}{\mathrm{d}t}\left(\frac{\partial T_D}{\partial \dot{\theta}}\right) - \frac{\partial T_D}{\partial \theta} = I_{Dx}\ddot{\theta} - I_{Dy}\dot{\phi}\dot{\psi} \tag{8.7}$$

$$\frac{\mathrm{d}}{\mathrm{d}t}\left(\frac{\partial T_D}{\partial \dot{\psi}}\right) - \frac{\partial T_D}{\partial \psi} = I_{Dx}\ddot{\psi} + I_{Dy}\dot{\phi}\dot{\theta} + I_{Dy}\ddot{\phi}\theta \tag{8.8}$$

$$\frac{\mathrm{d}}{\mathrm{d}t}\left(\frac{\partial T_D}{\partial \dot{\phi}}\right) - \frac{\partial T_D}{\partial \phi} = I_{Dy}\ddot{\phi} + I_{Dy}\ddot{\psi}\theta + I_{Dy}\dot{\psi}\dot{\theta} \tag{8.9}$$

Equation (8.9) can be used to obtain the torque which is necessry to impose the angular velocity $\dot{\phi}$. This equation will not be used in what follows, and the angular velocity is supposed to be known. Using the same nodal displacements as in Chapter 4, that is:

$$\delta = [u, w, \theta, \psi]^{\mathrm{T}} \tag{8.10}$$

Equations (8.5)–(8.8) are written in a compact form and

$$\frac{\mathrm{d}}{\mathrm{d}t}\left(\frac{\partial T_D}{\partial \dot{\delta}}\right) - \frac{\partial T_D}{\partial \delta} = M_D\ddot{\delta} + \dot{\phi}C_D\dot{\delta} + \ddot{\phi}K_{DT}\delta \tag{8.11}$$

where M_D is the mass matrix of Equation (4.2) in Chapter 4. Matrix C_D is the Coriolis matrix of the same equation, divided by Ω. K_{DT} is a stiffness matrix in which only term $\{4, 3\}$, the value of which is I_{Dy}, is non-zero.

Next, using from Chapter 4 the same nodal displacement vector (Equations (4.5)–(4.7)) and the same shape functions (Equations (4.8) and (4.9)), the expression for the kinetic energy of the shaft can be written as:

$$\begin{aligned} T_S = & \tfrac{1}{2}\delta\dot{u}^T M_1 \delta\dot{u} + \tfrac{1}{2}\delta\dot{w}^T M_2 \delta\dot{w} + \tfrac{1}{2}\delta\dot{u}^T M_3 \delta\dot{u} \\ & + \tfrac{1}{2}\delta\dot{w}^T M_4 \delta\dot{w} + \dot{\phi}\delta\dot{u}^T M_5 \delta w + \rho I L \dot{\phi}^2 \end{aligned} \tag{8.12}$$

where M_1, M_2, and M_3 and M_4 are the matrices given in Chapter 4, and M_5 is the matrix M_5 of Chapter 4 divided by Ω. Application of Lagrange's equation to (8.12) gives

$$\frac{\mathrm{d}}{\mathrm{d}t}\left(\frac{\partial T_S}{\partial \dot{\delta}}\right) - \frac{\partial T_S}{\partial \delta} = (M + M_S)\ddot{\delta} + \dot{\phi} C_S \dot{\delta} + \ddot{\phi} K_{ST} \delta \tag{8.13}$$

where M and M_S are the matrices (4.15) and (4.16) in Chapter 4, and C_S is the matrix (4.17) divided by Ω. The matrix K_{ST} is a stiffness matrix given below:

$$K_{ST} = \frac{\rho I}{15L}\begin{bmatrix} 0 & -36 & -3L & 0 & 0 & 36 & -3L & 0 \\ 0 & 0 & 0 & 0 & 0 & 0 & 0 & 0 \\ 0 & 0 & 0 & 0 & 0 & 0 & 0 & 0 \\ 0 & 3L & 4L^2 & 0 & 0 & -3L & -L^2 & 0 \\ 0 & 36 & 3L & 0 & 0 & -36 & 3L & 0 \\ 0 & 0 & 0 & 0 & 0 & 0 & 0 & 0 \\ 0 & 0 & 0 & 0 & 0 & 0 & 0 & 0 \\ 0 & 3L & -L^2 & 0 & 0 & -3L & 4L^2 & 0 \end{bmatrix} \tag{8.14}$$

As the mass unbalance m_u is much smaller than the mass of the rotor, its kinetic energy T_u becomes

$$T_u = m_u d\dot{\phi}(\dot{u}\cos\phi - \dot{w}\sin\phi) \tag{8.15}$$

and the application of Lagrange's equations gives

$$\frac{\mathrm{d}}{\mathrm{d}t}\left(\frac{\partial T_{\mathrm{U}}}{\partial \dot{u}}\right) - \frac{\partial T_{\mathrm{U}}}{\partial u} = md\ddot{\phi}\cos\phi - md\dot{\phi}^2\sin\phi \tag{8.16}$$

$$\frac{\mathrm{d}}{\mathrm{d}t}\left(\frac{\partial T_{\mathrm{U}}}{\partial \dot{w}}\right) - \frac{\partial T_{\mathrm{U}}}{\partial w} = -md\ddot{\phi}\sin\phi - md\dot{\phi}^2\cos\phi \tag{8.17}$$

The strain energy of the shaft is not affected by the transient motion and is given by (1.25) in Chapter 1 and (4.22) in Chapter 4.

The bearing characteristics used are those given by (1.28) in Chapter 1 and (4.28) in Chapter 4, where the characteristics of stiffness and viscous damping are supposed in this case to be constant.

Now δ includes all the degrees of freedom of the rotor, and the general differential equation of the system can be written as

$$M\ddot{\delta} + (C_1 + \dot{\phi}C_2]\dot{\delta} + [K_1 + \ddot{\phi}K_2]\delta = \dot{\phi}^2F_1(\phi) + \ddot{\phi}F_2(\phi) \tag{8.18}$$

Equation (8.18) now has to be solved and the nodal displacement vector δ has to be known at given instants t. It is common to use a step-by-step numerical integration procedure to solve this type of equation, but this requires much computer time. Here the Newmark method is used, assuming the mean acceleration to be constant; that is

$$\dot{\delta}(t + \Delta t) = \dot{\delta}(t) + \frac{\Delta t}{2}[\ddot{\delta}(t) + \ddot{\delta}(t + \Delta t)] \tag{8.19}$$

and

$$\delta(t + \Delta t) = \delta(t) + \frac{\Delta t^2}{4}[\ddot{\delta}(t) + \ddot{\delta}(t + \Delta t)] \tag{8.20}$$

The behavior of the system–that is, $\delta(t)\dot{\delta}(t)$ and $\ddot{\delta}(t)$–being known at the instant t, the equilibrium is written at the instant $t + \Delta t$. Using (8.18),

(8.19) and (8.20):

$$\left\{\frac{4M}{(\Delta t)^2}+\frac{2}{\Delta t}[C_1+\dot{\phi}(t+\Delta t)C_2]+[K_1+\ddot{\phi}(t+\Delta t)K_2]\right\}\delta(t+\Delta t)$$
$$=\dot{\phi}^2(t+\Delta t)F_1(\phi(t+\Delta t))+\ddot{\phi}(t+\Delta t)F_2(\phi(t+\Delta t))$$
$$-\left\{\frac{4M}{(\Delta t)^2}+\frac{2}{\Delta t}[C_1+\dot{\phi}(t)C_2]\right\}\delta(t)$$
$$-\left\{\frac{4M}{\Delta t}+[C_1+\dot{\phi}(t)C_2]\right\}\dot{\delta}(t)-M\ddot{\delta}(t) \tag{8.21}$$

The solution of the system (8.21) gives $\delta(t+\Delta t)$, and then Equations (8.20) and (8.19) give respectively $\ddot{\delta}(t+\Delta t)$ and $\dot{\delta}(t+\Delta t)$. The procedure begins at $t_0=0$ with the initial conditions $\delta(0)$ and $\dot{\delta}(0)$ known. The acceleration vector $\ddot{\delta}(0)$ is easily obtained by writing that at instant t_0 the quantities $\delta(0)$, $\dot{\delta}(0)$ and $\ddot{\delta}(0)$ satisfy Equation (8.18). Then at the first step Δt, Equation (8.21) gives

$$\left\{\frac{4M}{(\Delta t)^2}+\frac{2}{\Delta t}[C_1+\dot{\phi}(\Delta t)C_2]+K_1+\ddot{\phi}(\Delta t)K_2\right\}\delta(\Delta t)$$
$$=\dot{\phi}^2(\Delta t)F_1(\phi(\Delta t))+\ddot{\phi}(\Delta t)F_2(\phi(\Delta t))-M\ddot{\delta}(0) \tag{8.22}$$

Thus $\delta(\Delta t)$ is obtained, then $\ddot{\delta}(\Delta t)$ and $\dot{\delta}(\Delta t)$. The system (8.21) has to be solved for each increment of time, and the order of the system has to be significantly decreased to lead to acceptable computer time and core memory. The reduction of the order of the system is made through either a modal or a substructure method. Here, too, the pseudo-modal method presented in Chapter 4 (Section 4.4.1) is used; that is, the lowest modes of

$$M\ddot{\delta}+K_1^*\delta=0 \tag{8.23}$$

are used. The matrix K_1^* is the symmetric stiffness matrix obtained from K_1. This matrix is such that terms like k_{xz} and k_{zx} coming from bearings are canceled.

8.2 SPEED OF ROTATION LAW

For industrial applications the law can be considered to be close to an exponential function. This means that when the rotor starts the speed of rotation increases rapidly, and the acceleration is small when the rotor is close to the operating speed. However, a linear law, which gives a constant acceleration, is also of interest.

8.2.1 Exponential law

The expression for the speed of rotation, $\dot{\phi}(t)$, is

$$\dot{\phi}(t) = A + Be^{-\lambda t} \tag{8.24}$$

Expressions for the two constants can be obtained easily from the values of $\dot{\phi}(t)$ at the initial instant (t_0, Ω_0) and at the final instant (t_f, Ω_f):

$$B = \frac{\Omega_f - \Omega_0}{e^{-\lambda t_f} - e^{-\lambda t_0}} \tag{8.25}$$

$$A = \frac{\Omega_f e^{\lambda t_f} - \Omega_0 e^{\lambda t_0}}{e^{-\lambda t_f} - e^{-\lambda t_0}} \tag{8.26}$$

In addition, $\ddot{\phi}(t)$ and $\phi(t)$ are also obtained:

$$\ddot{\phi}(t) = \frac{\mathrm{d}\dot{\phi}(t)}{\mathrm{d}t} \tag{8.27}$$

$$= -\lambda B e^{-\lambda t} \tag{8.28}$$

and, if at t_0 the value of $\phi(t)$ is ϕ_0:

$$\phi(t) = \int \dot{\phi}(t)\mathrm{d}t \tag{8.29}$$

$$= At - \frac{B}{\lambda} e^{-\lambda t} + C \tag{8.30}$$

with

$$C = \phi_0 - At_0 - \frac{B}{\lambda} e^{-\lambda t_0} \tag{8.31}$$

8.2.2 Linear law

$$\dot{\phi}(t) = A + Bt \tag{8.32}$$

Using the same initial conditions as in Section 8.2.1, we have

$$B = \frac{\Omega_0 - \Omega_f}{t_0 - t_f} \tag{8.33}$$

$$A = \frac{\Omega_0 t_f - \Omega_f t_0}{t_f - t_0} \tag{8.34}$$

Hence

$$\ddot{\phi}(t) = \frac{\Omega_f - \Omega_0}{t_f - t_0} \tag{8.35}$$

$$\phi(t) = At + \frac{Bt^2}{2} + C \tag{8.36}$$

with

$$C = \phi_0 - At_0 \frac{Bt_0^2}{2} \tag{8.37}$$

8.3 BEHAVIOR OF A SIMPLE ROTOR

The rotor studied (Figure 8.1) is the asymmetric rotor of Chapter 2, which has the properties given in Section 2.1.6. Equations (8.2), (8.4) and (8.15) above give

$$T_D = 6.902(\dot{q}_1^2 + \dot{q}_2^2) - 2.870\dot{\phi}\dot{q}_1 q_2 \tag{8.38}$$

$$T_S = 0.2454(\dot{q}_1^2 + \dot{q}_2^2) - 1.512 \times 10^{-3}\dot{\phi}\dot{q}_1 q_2 \tag{8.39}$$

$$T_U = 1.299 \times 10^{-5}\dot{\phi}(\dot{q}_1 \cos\phi - \dot{q}_2 \sin\phi) \tag{8.40}$$

The strain energy and the components of the force vector are given respectively by Equations (2.45), (2.47) and (2.48) in Chapter 2. In

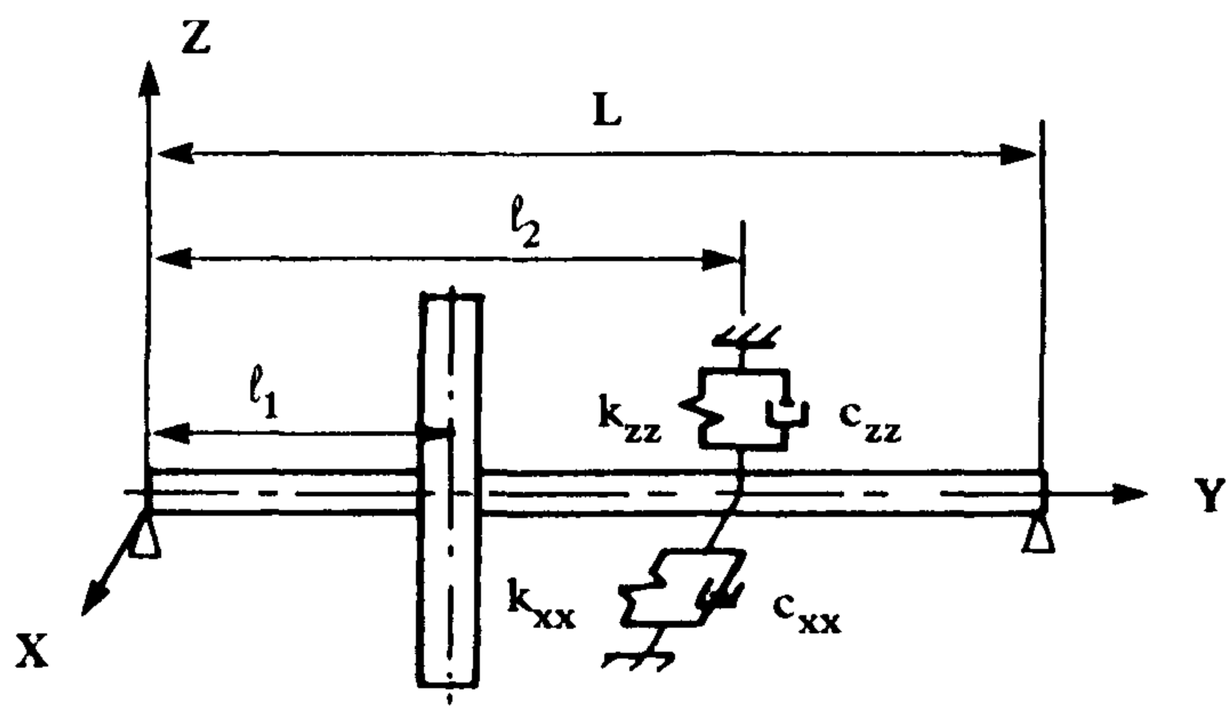

Figure 8.1. Model of the rotor

addition the two dampers c_1 and c_2 are supposed to be such that their values are proportional to the stiffnesses of the bearing in the x and z directions respectively (Equations (2.259) and (2.260) in Chapter 2). The rotor equations are

$$14.29\ddot{q}_1 - 2.871\dot{\phi}\dot{q}_2 - 2.871\ddot{\phi}q_2 + \beta 1.5 \times 10^5\dot{q}_1 + 1.345 \times 10^6 q_1$$
$$= 1.299 \times 10^{-5}\dot{\phi}^2 \sin\phi - 1.299 \times 10^{-5}\ddot{\phi}\cos\phi \tag{8.41}$$

$$14.29\ddot{q}_2 + 2.871\dot{\phi}\dot{q}_1 + \beta 3.75 \times 10^5\dot{q}_1 + 1.57 \times 10^6 q_1$$
$$= 1.299 \times 10^{-5}\dot{\phi}^2 \cos\phi + 1.299 \times 10^{-5}\ddot{\phi}\sin\phi \tag{8.42}$$

The following calculations have been performed:

- linear law followed by a constant speed of rotation
- exponential law followed by a constant speed of rotation.

8.3.1 Linear law followed by a constant speed of rotation

The constant speed of rotation is 5000 rpm. At first, $\beta = 0.0002$ and the responses are presented for the three following linear laws:

$$\dot{\phi} = 416.7t \text{ (Figure 8.2)} \tag{8.43}$$

$$\dot{\phi} = 1250t \text{ (Figure 8.3)} \tag{8.44}$$

$$\dot{\phi} = 5000t \text{ (Figure 8.4)} \tag{8.45}$$

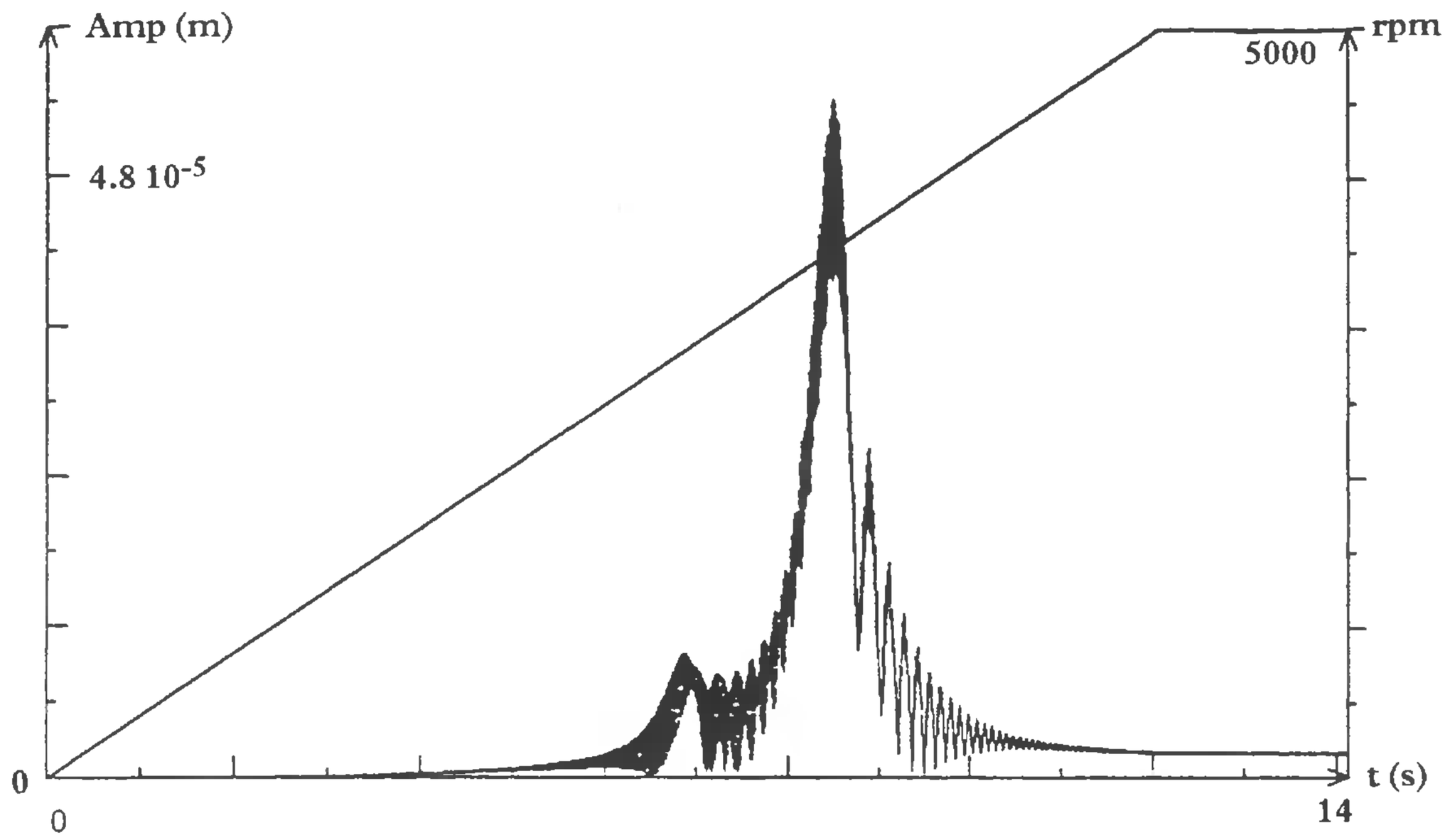

Figure 8.2. Transient response law: Equation (8.43)

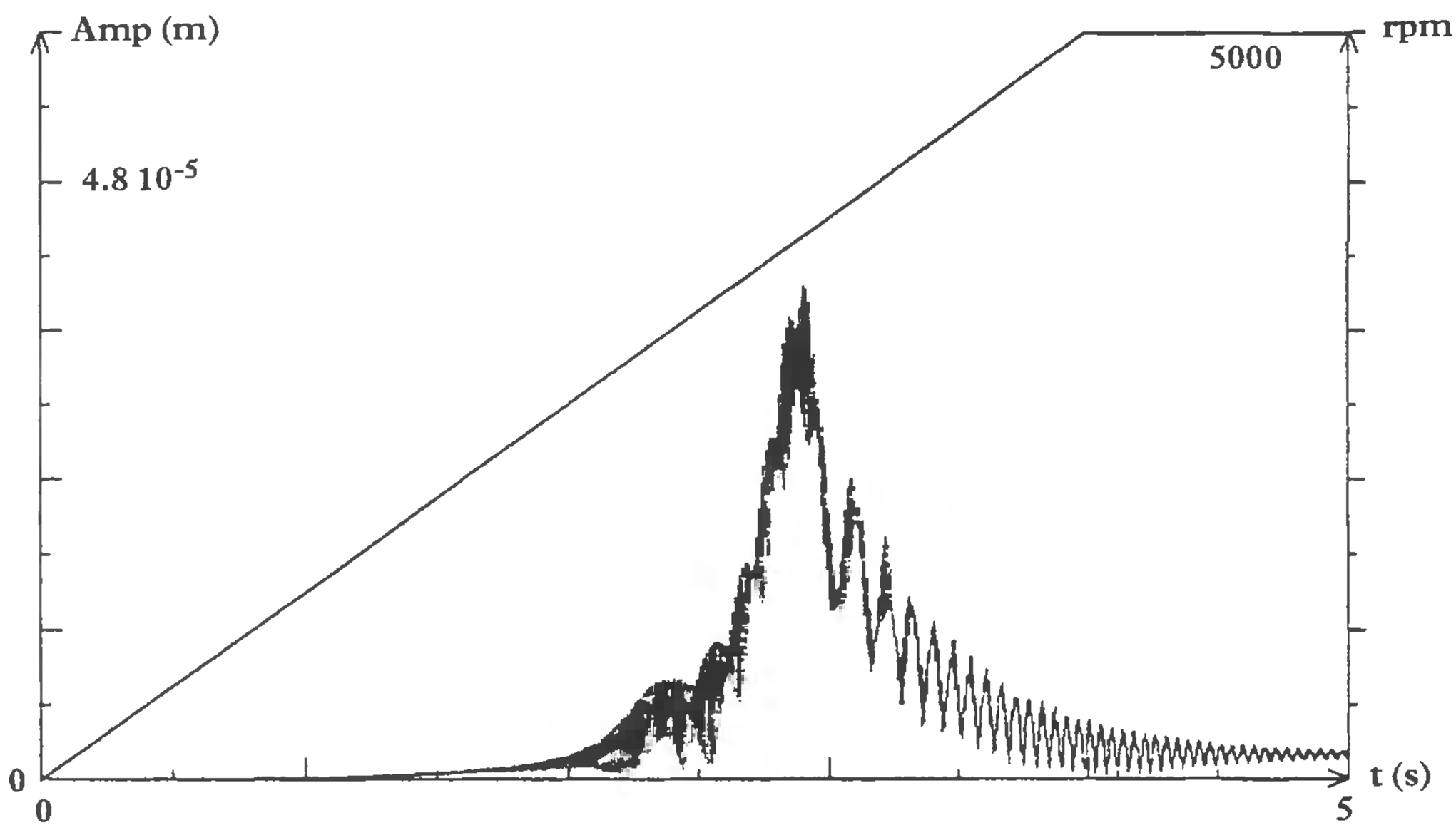

Figure 8.3. Transient response law: Equation (8.44)

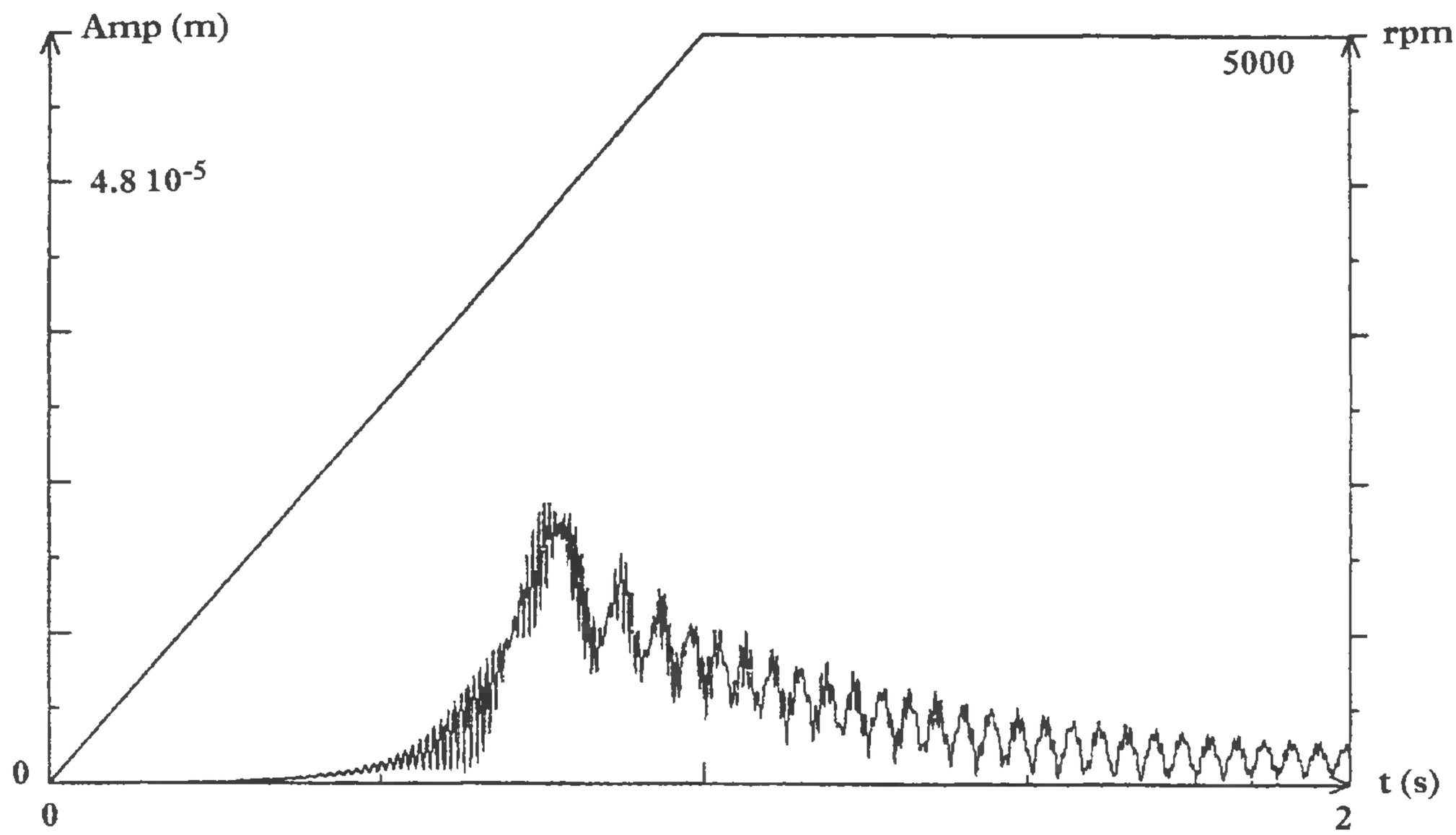

Figure 8.4. Transient response law: Equation (8.45)

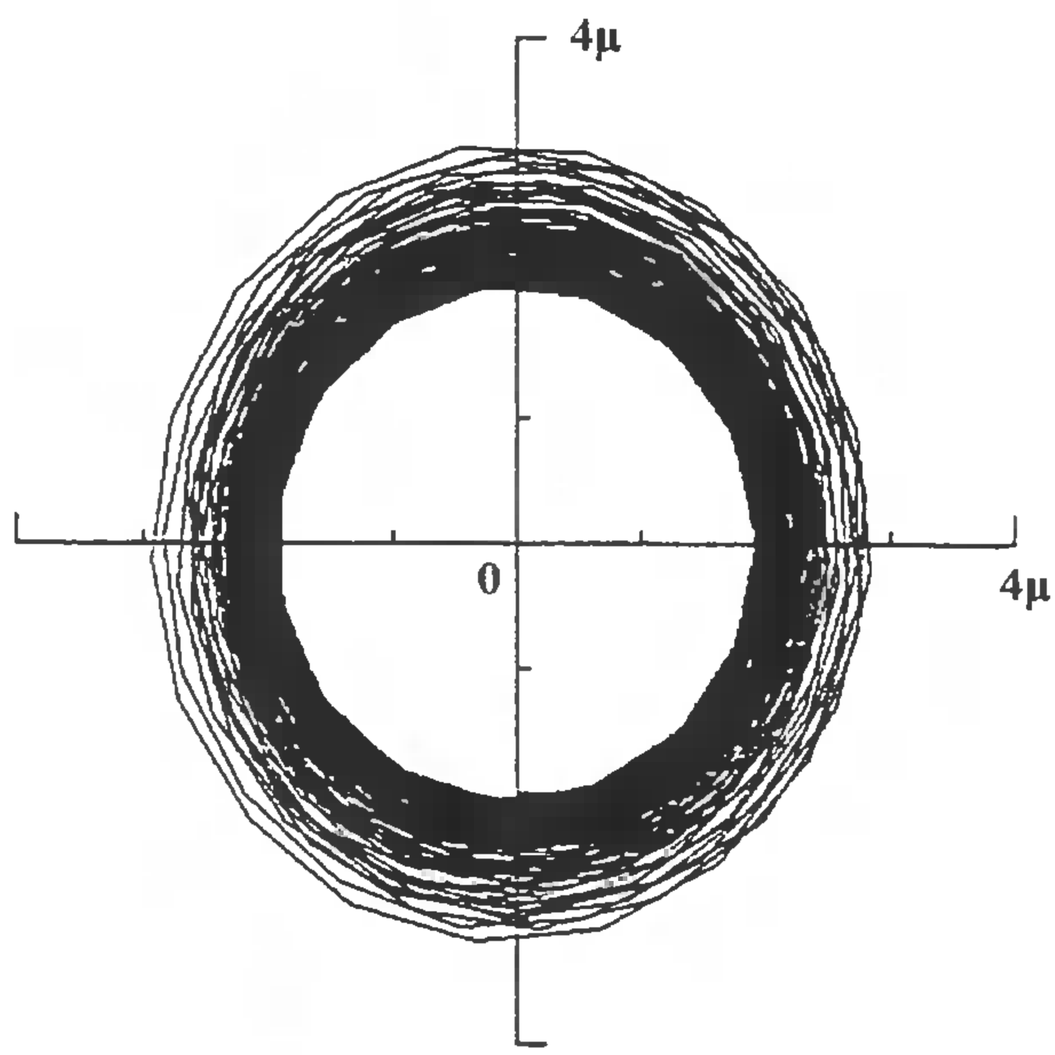

Figure 8.5. Stabilization of the response at 5000 rpm

The steady-state motion at 5000 rpm, with law (8.43), is shown in Figure 8.5, and the amplitude maximum in the z direction corresponds to the value of the response at 5000 rpm, presented for steady motion in Figure 2.20 in Chapter 2.

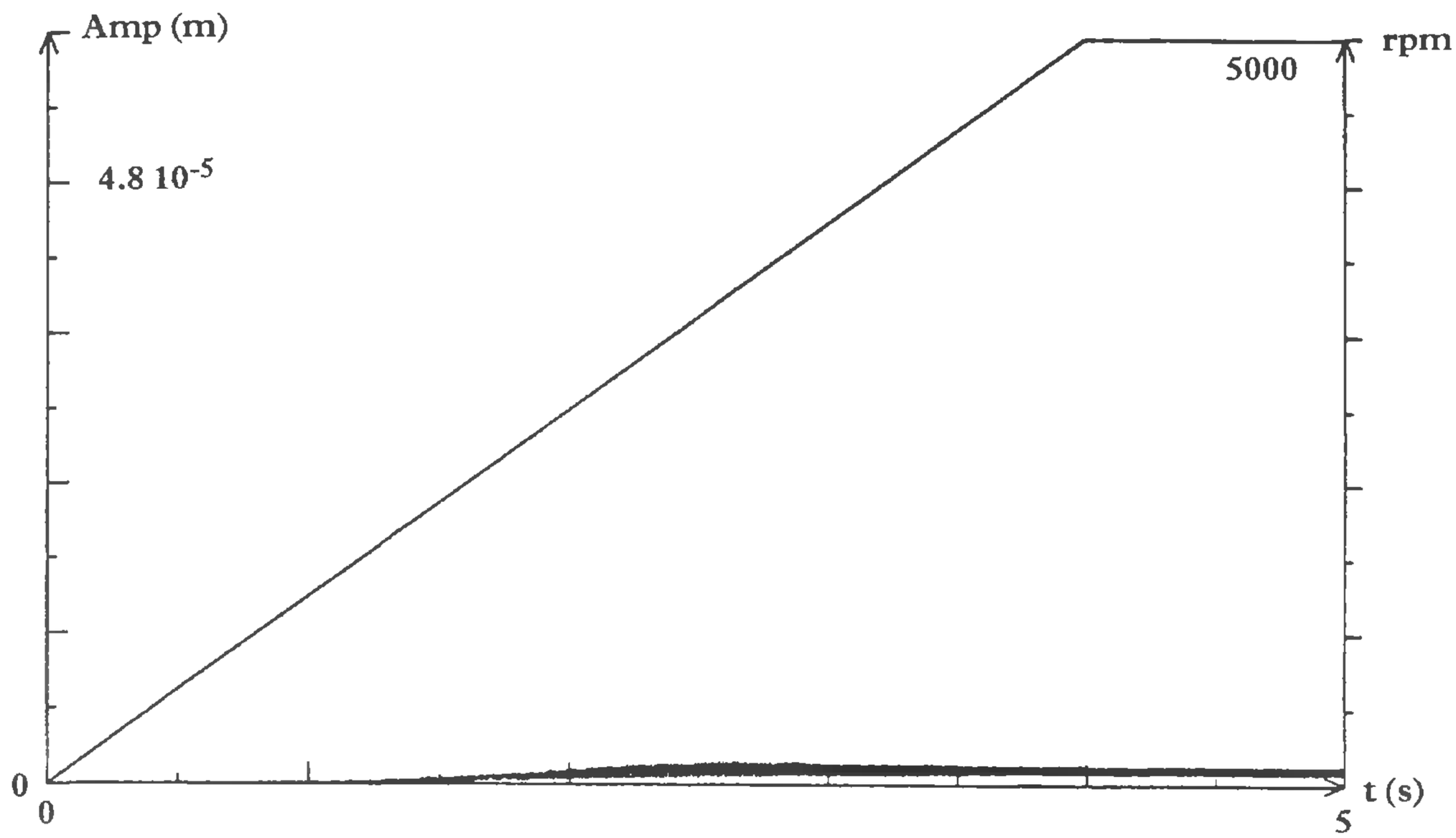

Figure 8.6. Transient response law: Equation (8.44), $\beta = 0.015$

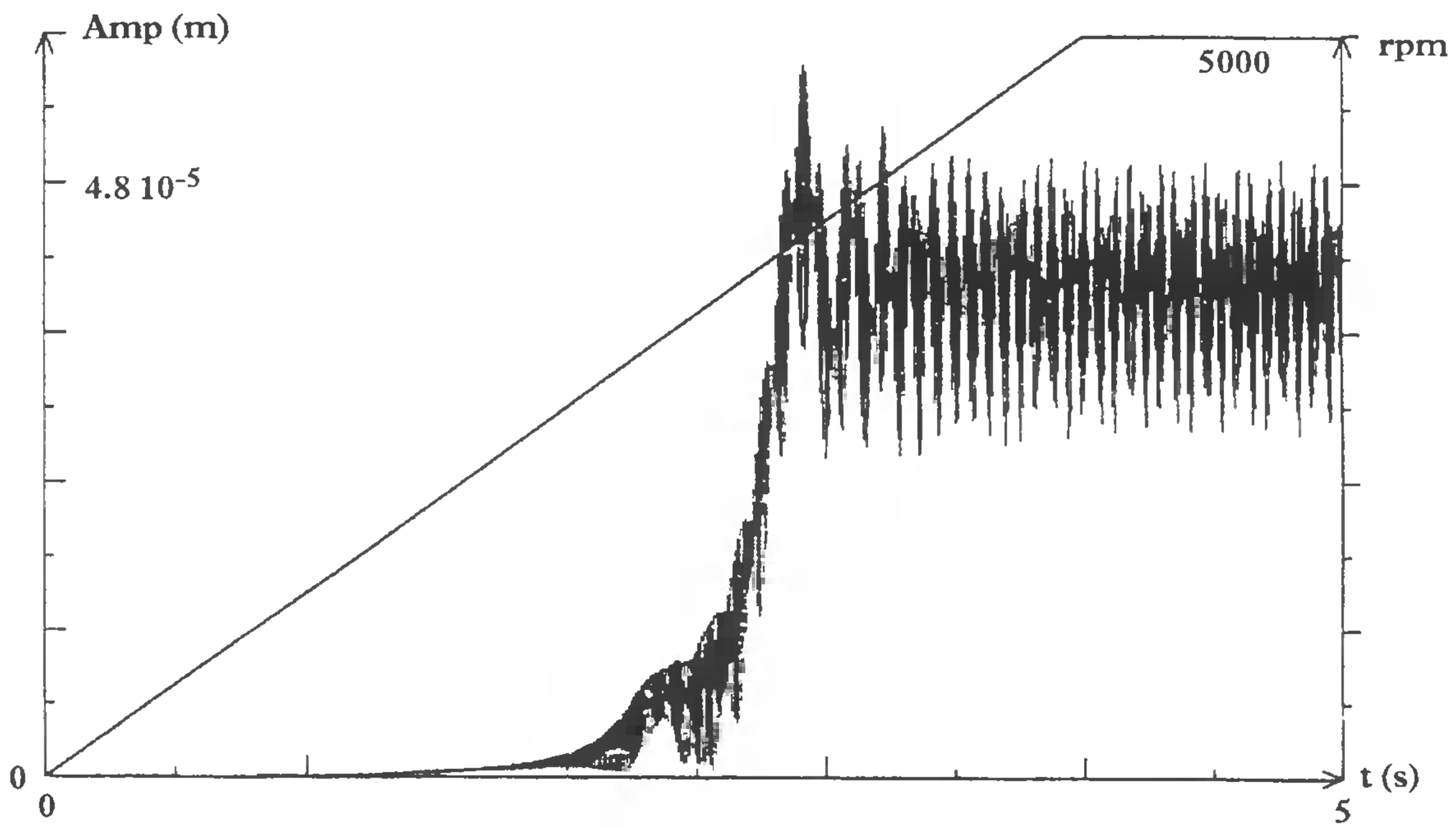

Figure 8.7. Transient response law: Equation (8.44), $\beta = 0$

The response with $\beta = 0.015$ is presented in Figure 8.6 with the law (8.44). The amplitude corresponds to the value of the response at 5000 rpm in Figure 2.21 in Chapter 2.

The response with $\beta = 0$ is presented in Figure 8.7 with law (8.44). The mean value of the response at 5000 rpm is different from the value of

the response at 5000 rpm which can be observed in Figure 2.13 in Chapter 2. This comes from the transient motion, equation with no external forces, which cannot vanish because of lack of damping.

8.3.2 Exponential law followed by a constant speed of rotation

The constant speed of rotation is again 5000 rpm and $\beta = 0.0002$. The responses are presented for

$$\dot{\phi} = 5100(1 - e^{-0.3273t}) \quad \text{(Figure 8.8)} \tag{8.46}$$

$$\dot{\phi} = 5100(1 - e^{-0.9830t}) \quad \text{(Figure 8.9)} \tag{8.47}$$

$$\dot{\phi} = 5100(1 - e^{-3.832t}) \quad \text{(Figure 8.10)} \tag{8.48}$$

8.3.3 Comments

It can be observed that:

- The higher the speed of rotation, the lower is the maximum amplitude.

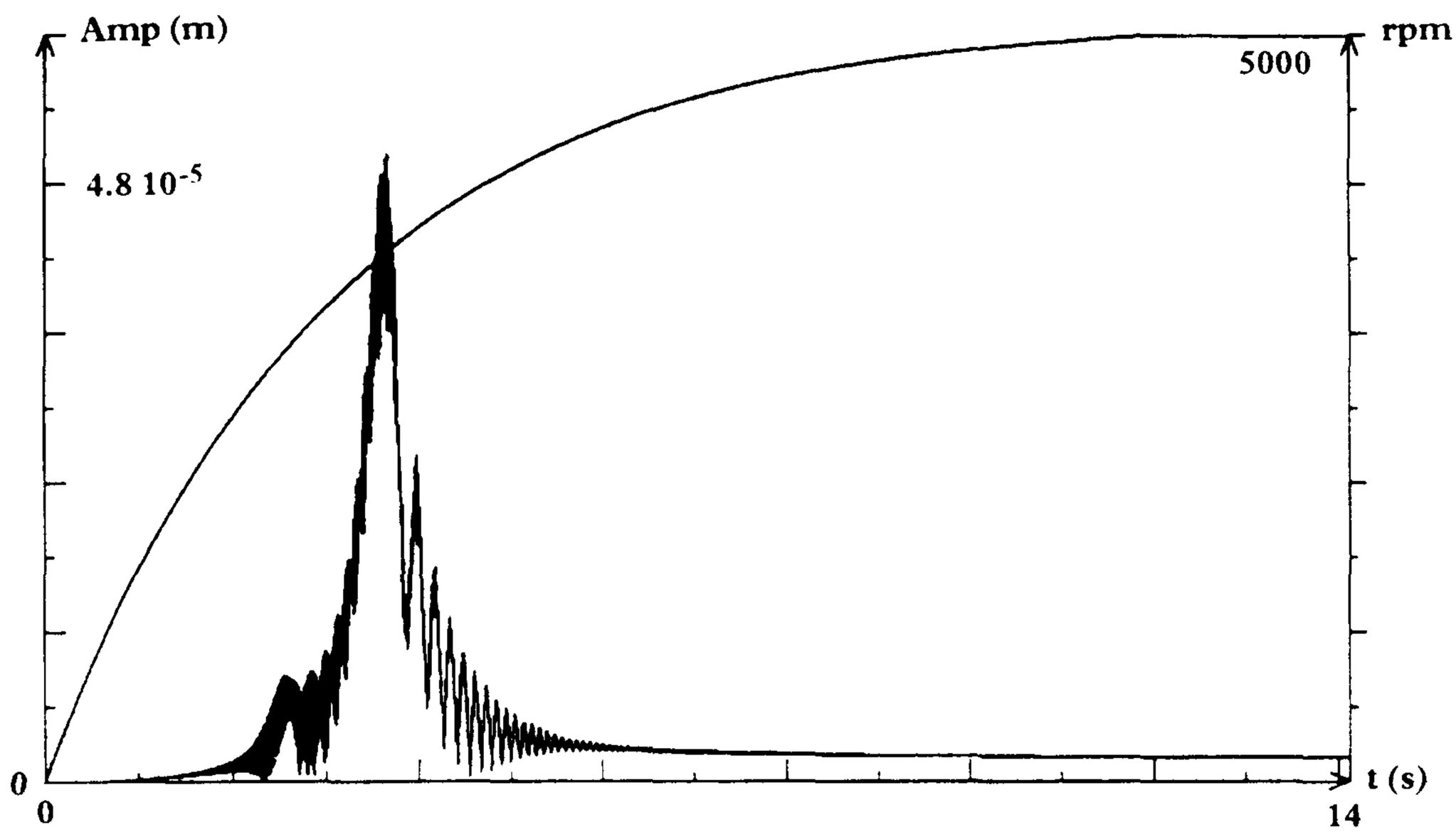

Figure 8.8. Transient response law: Equation (8.46)

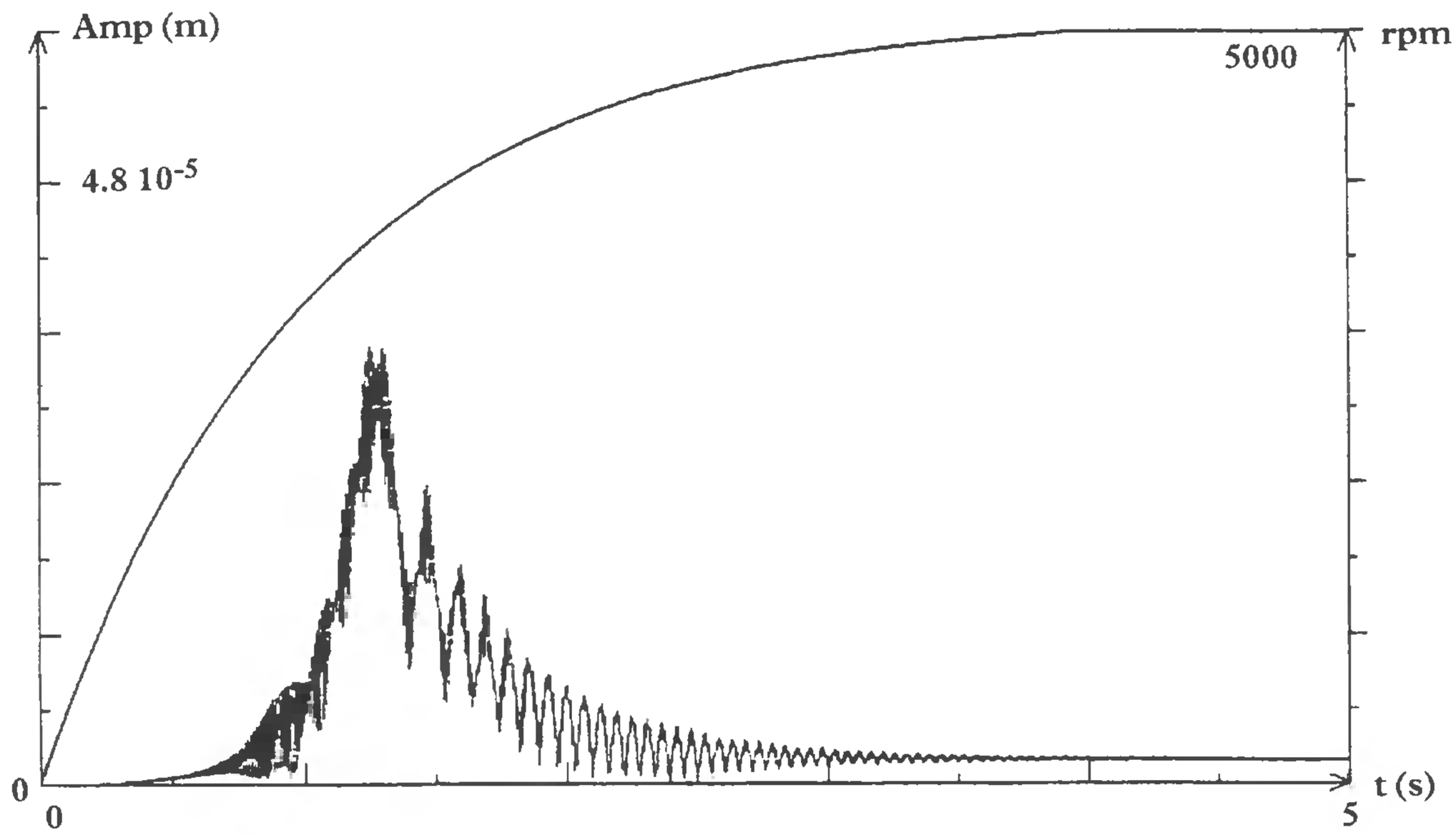

Figure 8.9. Transient response law: Equation (8.47)

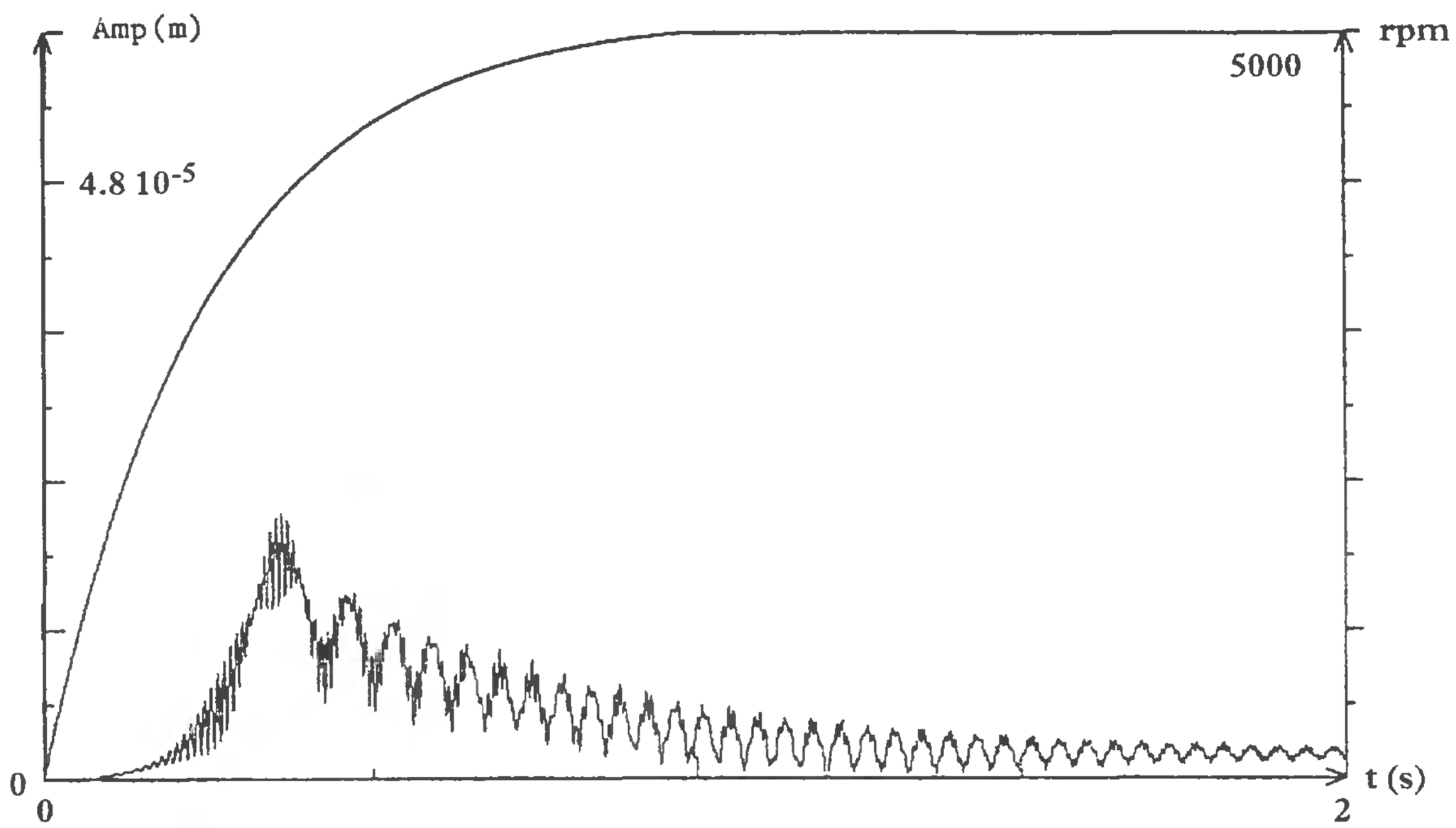

Figure 8.10. Transient response law: Equation (8.48)

- The peaks due to FW and BW resonant frequencies appear clearly with low damping (Figures 8.2 and 8.8).
- The higher the damping, the lower is the amplitude response.
- The responses due to the linear and exponential laws are similar.

8.4 EXPERIMENTAL AND THEORETICAL RESULTS FOR A THREE-DISK ROTOR

The experimental device shown in Figure 8.11 has been developed and tested at the Laboratoire de Mécanique des Structures. The characteristics of this steel-made rotor and of the experimental setup are given in detail in [35]. The shaker shown in the figure was used in another experiment.

The basic characteristics are a 4 kW electric motor, a rotor length of 0.95 m and diameter 0.035 m, three disks (diameter 0.250 m, thickness 0.03 m), base mounting weight about 600 kg. The law for the speed of

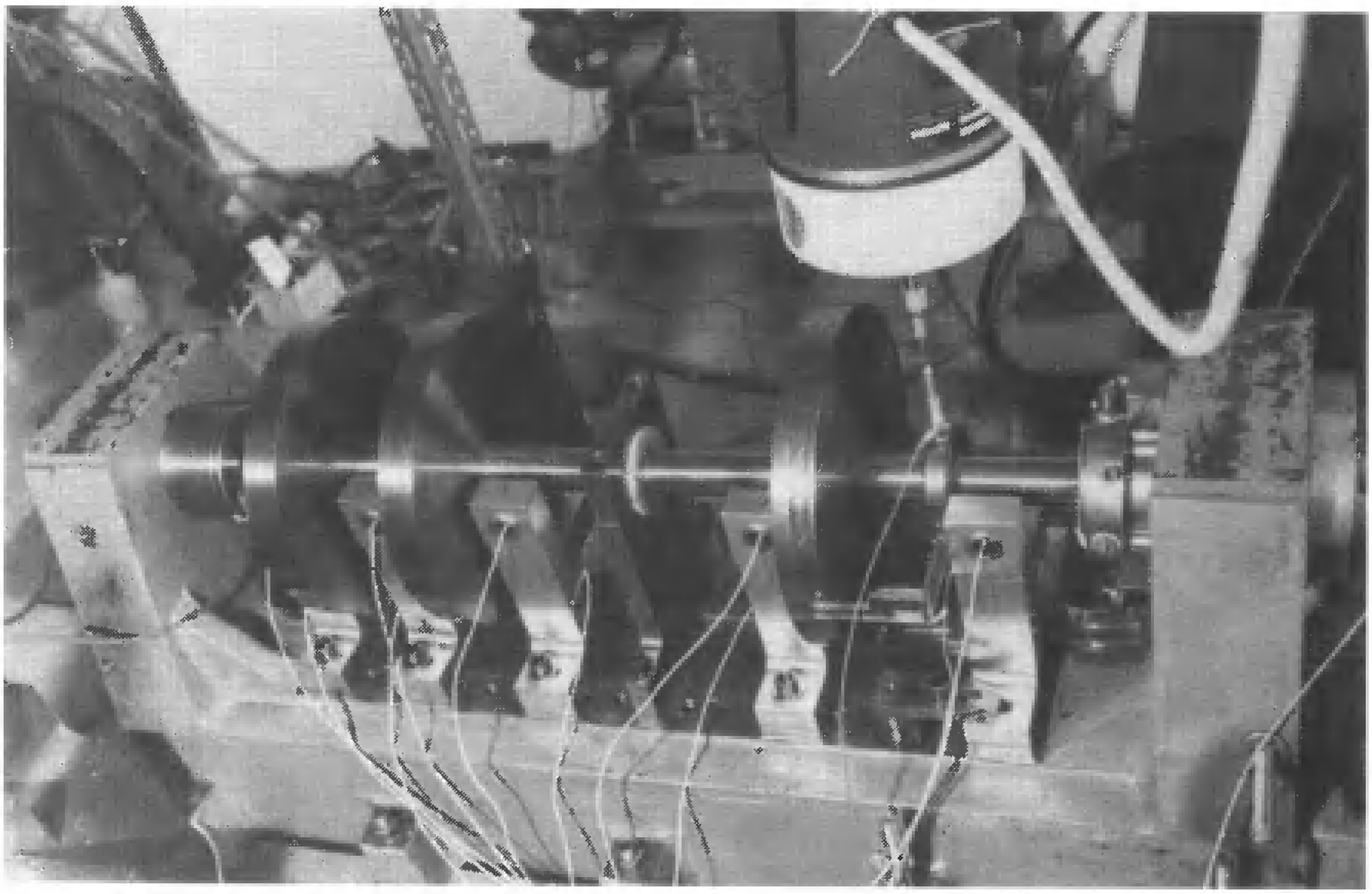

Figure 8.11. Experimental setup

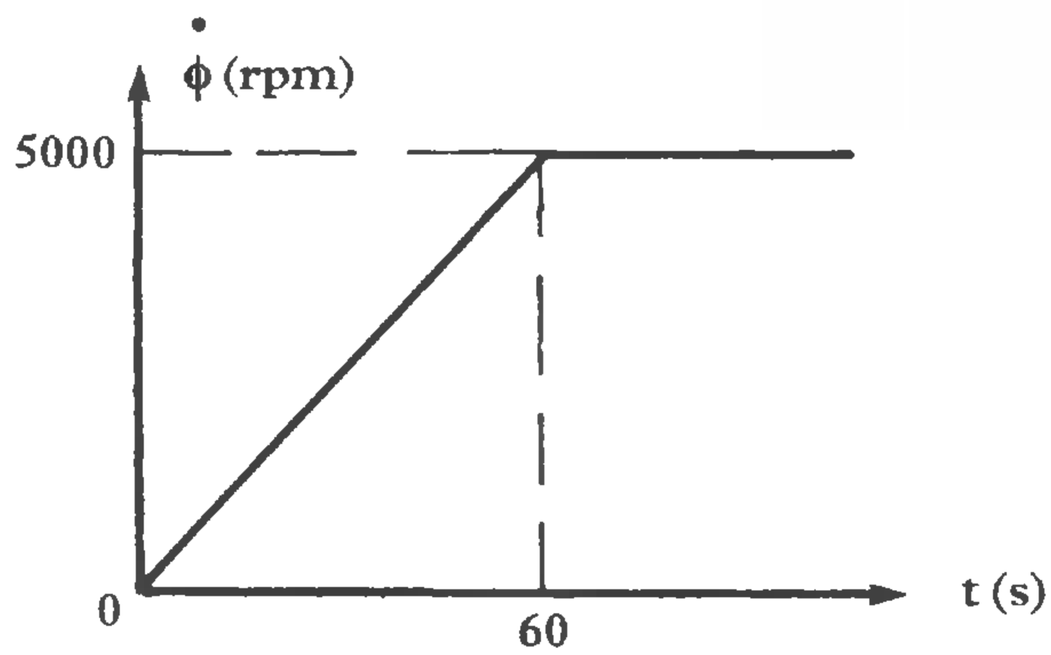

Figure 8.12. Speed of rotation law

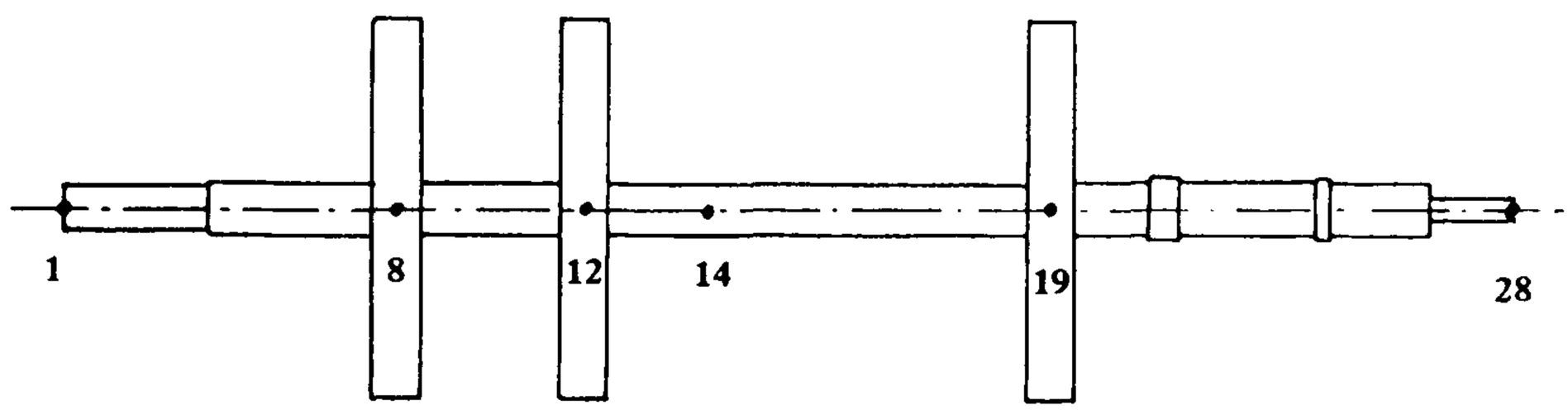

Figure 8.13. Rotor model

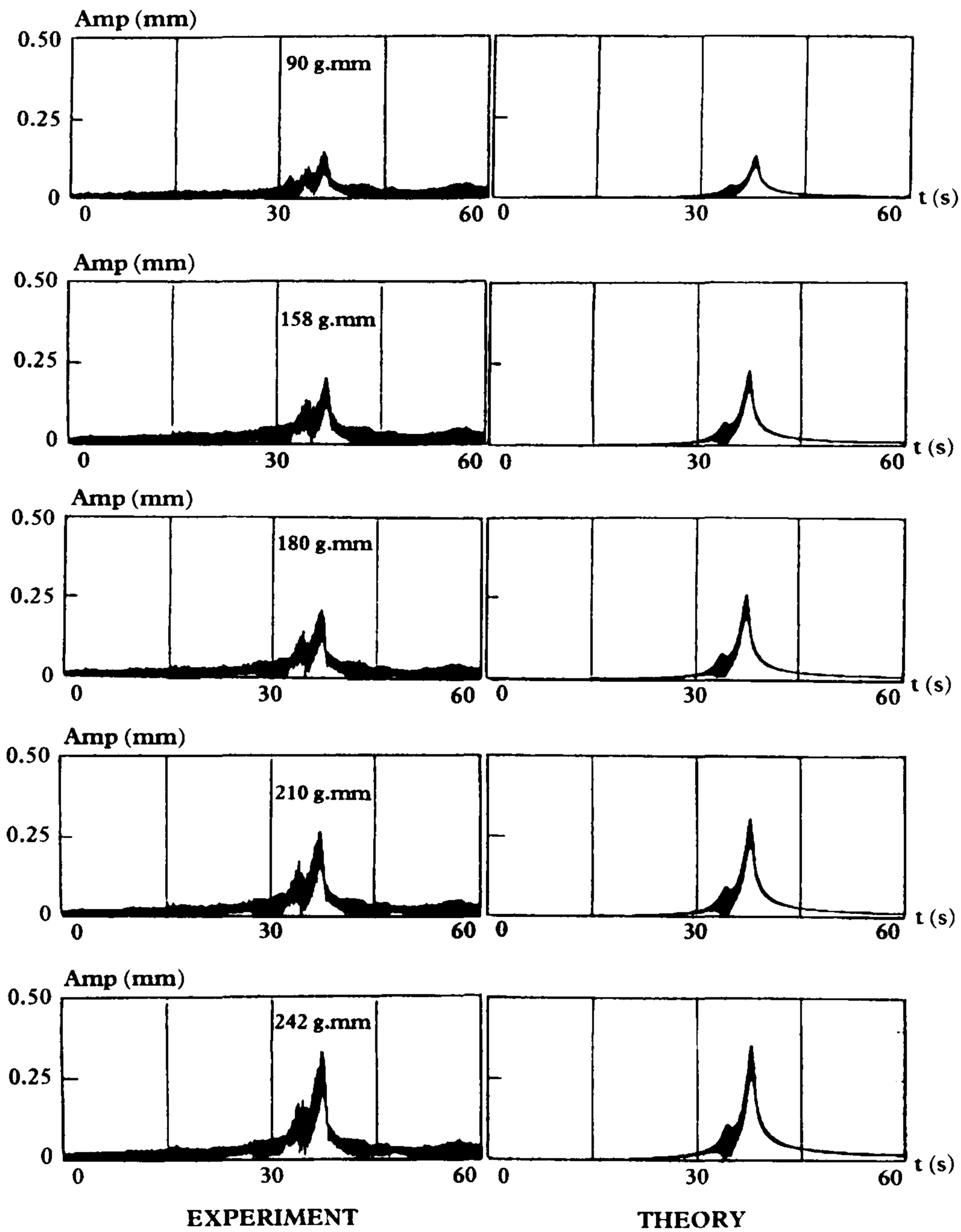

Figure 8.14. Response amplitudes for several mass unbalances

rotation is linear (Figure 8.12). The measurements are performed using eddy-current-non-contact probes.

The finite element model is shown in Figure 8.13.

Experimental and theoretical response results at node 14 are shown in Figure 8.14 for several mass unbalances situated on one disk (node 12). The agreement between experience and theory is satisfactory, and the two FW and BW resonant frequencies due to unbalance appear clearly.

8.5 BEHAVIOR OF AN INDUSTRIAL ROTOR

The rotor of the example shown in [40], Section 5.1, has been used and the characteristics of the bearings are supposed constant. The operating speed of rotation is 50 000 rpm and the exponential law used is

$$\dot{\phi} = 51000(1 - e^{-1.966t}) \tag{8.49}$$

The unbalance responses, node 1, have been calculated for an aluminum disk; these are shown in Figures 8.15 and 8.16 for the two cases. The unbalance with a steel disk is shown in Figure 8.17 for case 1 only: the displacement grows indefinitely as the system is unstable.

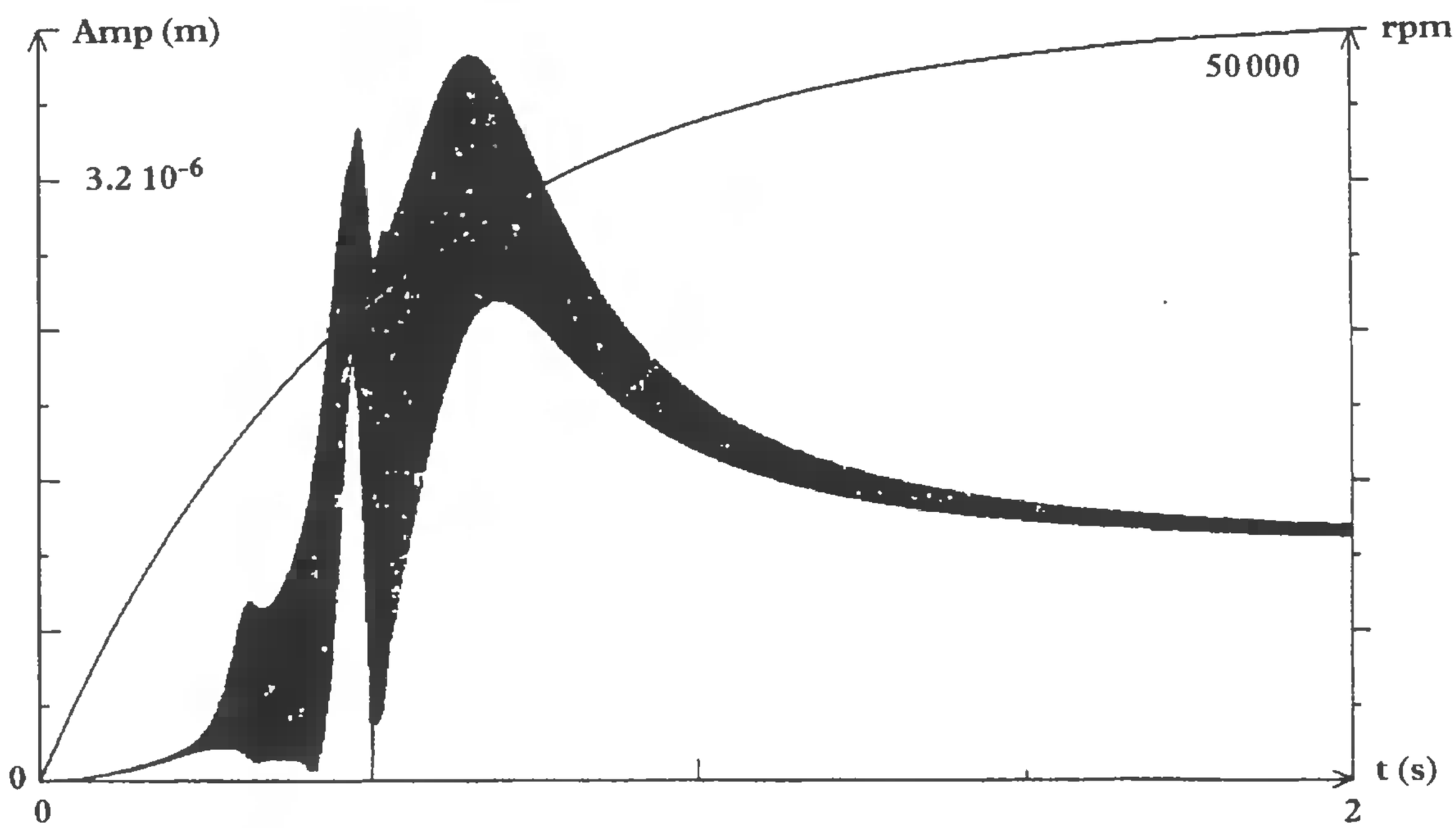

Figure 8.15. Transient response, case 1: aluminum disks

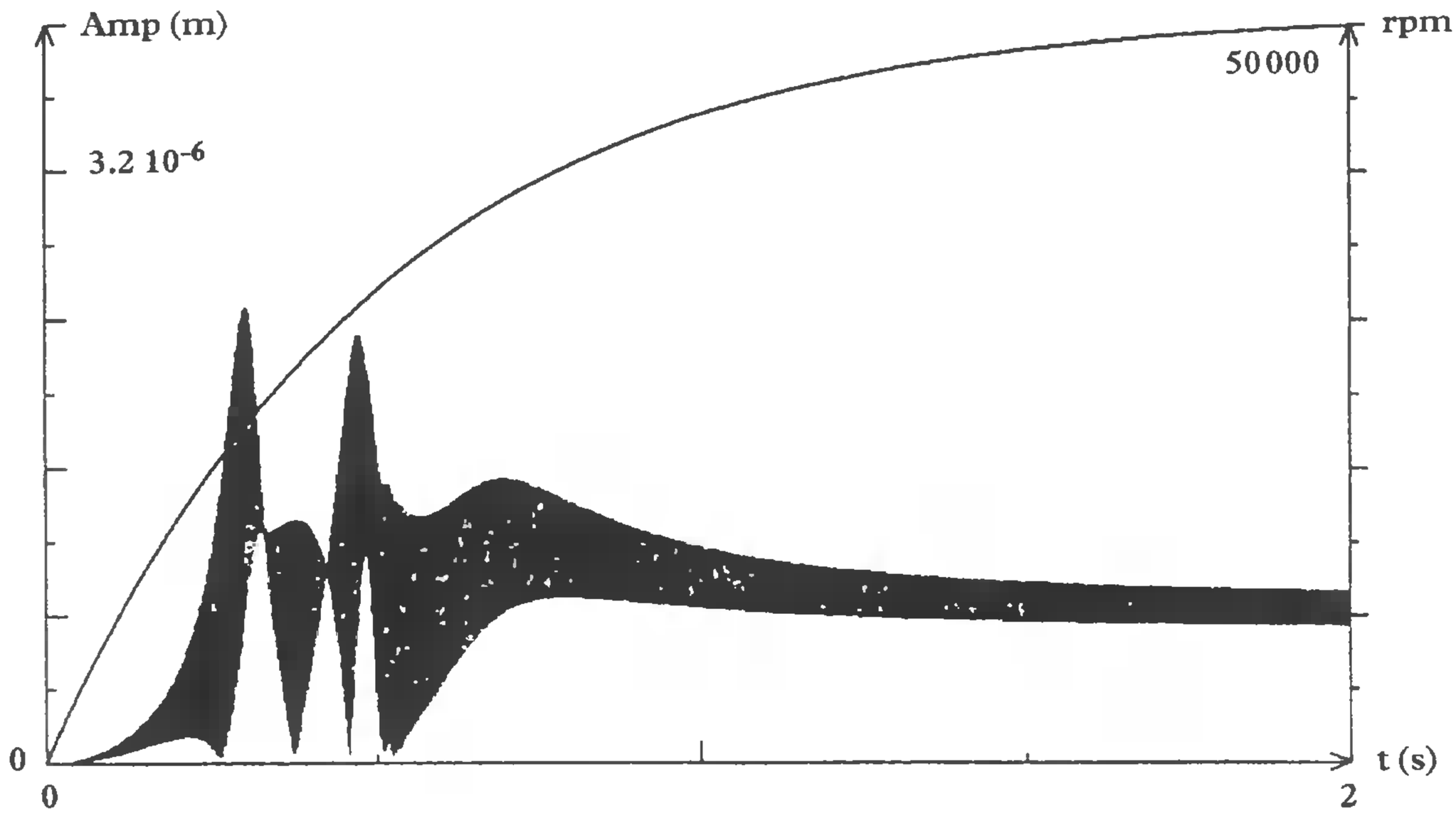

Figure 8.16. Transient response, case 2: aluminum disks

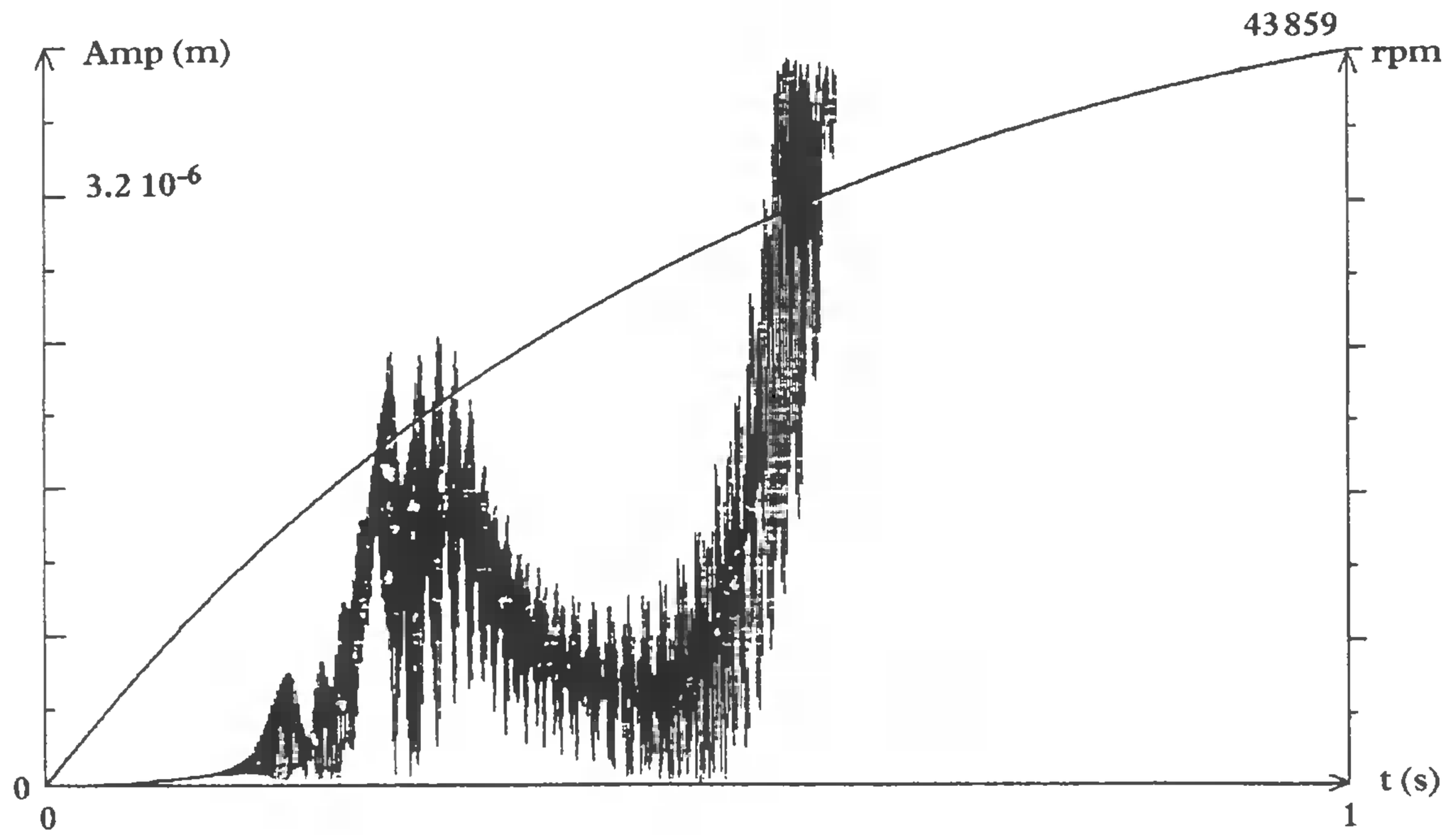

Figure 8.17. Transient response, case 1: steel disks

9

Torsion

Natural frequencies and modes of branched systems in torsion have to be predicted, to ensure that the frequency of the entire unit which is closest to the operating speed is a sufficient margin above or below that speed. In addition, when electric motors or generators are present in the unit their transient behavior during start-up or short-circuit conditions must be predicted. Torques, and consequently stresses in shaft elements, can then be significantly higher than the steady-state values for the system.

Damping has not been introduced in the models presented here because it is generally low. Its influence on natural frequencies is not significant, and the maximum response during transients cannot be affected.

9.1 DETERMINATION OF THE MINIMUM SHAFT RADIUS

The minimum shaft radius R given by the strength of material is

$$R = \left(\frac{2T_n}{\pi\tau_{\max}}\right)^{1/3} \tag{9.1}$$

where T_n is the nominal torque, and $\tau_{\max}$ is the maximum admissible shearing stress, depending on the shaft material. As the power is

$$P = T_n\Omega \tag{9.12}$$

Equation (9.1) can be written as

$$R = \left(\frac{2P}{\pi\Omega\tau_{\max}}\right)^{1/3} \tag{9.3}$$

The transient torque T_t, if it has to be considered, is in most cases higher than the nominal torque. The minimum shaft radius R^* is then

$$R^* = R\left(\frac{T_t}{T_n}\right)^{1/3} \tag{9.4}$$

9.2 EQUATIONS OF A BRANCHED SYSTEM IN TORSION

9.2.1 Basic elements

The disk

The disk (Figure 9.1) rotates at a given velocity Ω, its mass moment of inertia is I, and the angular displacement θ_1 is measured with respect to an instantaneous shaft position. The kinetic energy is

$$T = I\dot{\theta}_1^2/2 \tag{9.5}$$

The shaft

The shaft element (Figure 9.2) of length L has a circular cross-section of radius R, and its mass moment of inertia per unit length is

$$I_\theta = \rho\pi R^4/2 \tag{9.6}$$

The element inertia, $I_\theta L$, can be discretized easily, and half of the inertia is lumped at each of two nodes 1 and 2. Then:

$$T = \frac{\rho\pi R^4 L}{8}(\dot{\theta}_1^2 + \dot{\theta}_2^2) \tag{9.7}$$

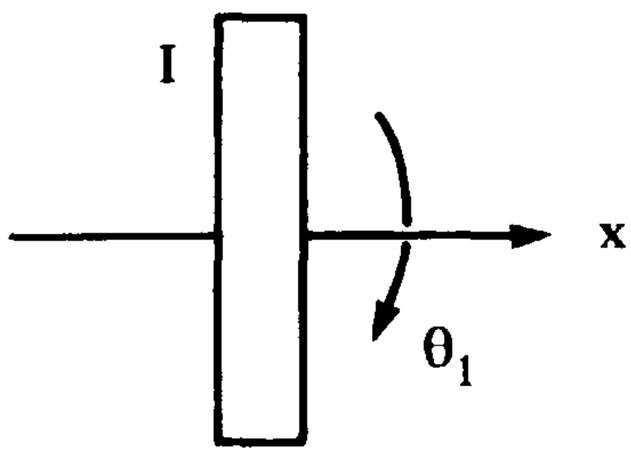

Figure 9.1. Disk

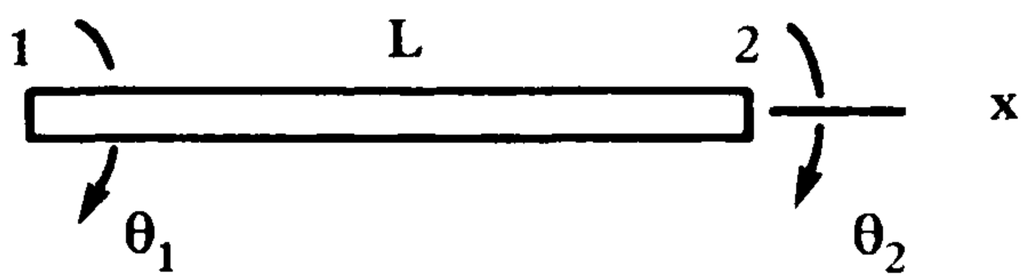

Figure 9.2. Shaft

and the corresponding mass matrix is

$$M = \frac{\rho \pi R^4 L}{4} \begin{bmatrix} 1 & 0 \\ 0 & 1 \end{bmatrix} \tag{9.8}$$

When this diagonal mass matrix is used, the model is said to be a discrete model.

The expression for the kinetic energy T can be calculated as in [37]. A linear hypothesis for the element is chosen; that is:

$$\theta = \left[1 - \frac{x}{L}, \frac{x}{L}\right] \begin{bmatrix} \theta_1 \\ \theta_2 \end{bmatrix} \tag{9.9}$$

Since

$$T = \frac{1}{2} \int_0^L I_\theta \dot{\theta}^2 \mathrm{d}x \tag{9.10}$$

we have, from (9.9):

$$T = \frac{I_\theta L}{12} \begin{bmatrix} \dot{\theta}_1 \\ \dot{\theta}_2 \end{bmatrix}^T \begin{bmatrix} 2 & 1 \\ 1 & 2 \end{bmatrix} \begin{bmatrix} \dot{\theta}_1 \\ \dot{\theta}_2 \end{bmatrix} \tag{9.11}$$

with the mass matrix

$$M = \frac{I_\theta L}{6} \begin{bmatrix} 2 & 1 \\ 1 & 2 \end{bmatrix} \tag{9.12}$$

This non-diagonal mass matrix is consistent with the bending matrices of Chapter 4. When this matrix is used here the model is said to be a finite element model.

The strain energy of the element is given by

$$U = \frac{1}{2} \int_0^L GJ \left(\frac{\partial \theta}{\partial x}\right)^2 \mathrm{d}x \tag{9.13}$$

where J is the polar moment of inertia ($I_\theta = \rho J$ for a circular cross-section) and G is the shear modulus. Using Equations (9.9) and (9.13) gives

$$U = \frac{GJ}{2L}(\theta_1 - \theta_2)^2 \tag{9.14}$$

$$= \tfrac{1}{2}k(\theta_1 - \theta_2)^2 \tag{9.15}$$

Then the stiffness of the element is

$$k = GJ/L \tag{9.16}$$

In matrix form, (9.14) can be expressed as

$$U = \frac{GJ}{L}\begin{bmatrix}\theta_1\\ \theta_2\end{bmatrix}^T \begin{bmatrix}1 & -1\\ -1 & 1\end{bmatrix}\begin{bmatrix}\theta_1\\ \theta_2\end{bmatrix} \tag{9.17}$$

with the stiffness matrix

$$K = \frac{GJ}{L}\begin{bmatrix}1 & -1\\ -1 & 1\end{bmatrix} \tag{9.18}$$

Connection elements

When two different shafts are coupled with gears (Figure 9.3), the corresponding strain energy is

$$U = k\delta^2/2 \tag{9.19}$$

with

$$\delta = R_1\theta_1 + R_2\theta_2 \tag{9.20}$$

and k is the global stiffness of the teeth gear. When the stiffness is very high the teeth do not deform; the strain energy is then zero, and

$$R_1\theta_1 + R_2\theta_2 = 0 \tag{9.21}$$

or

$$\theta_2 = -n\theta_1 \tag{9.22}$$

where n is the coupling ratio.

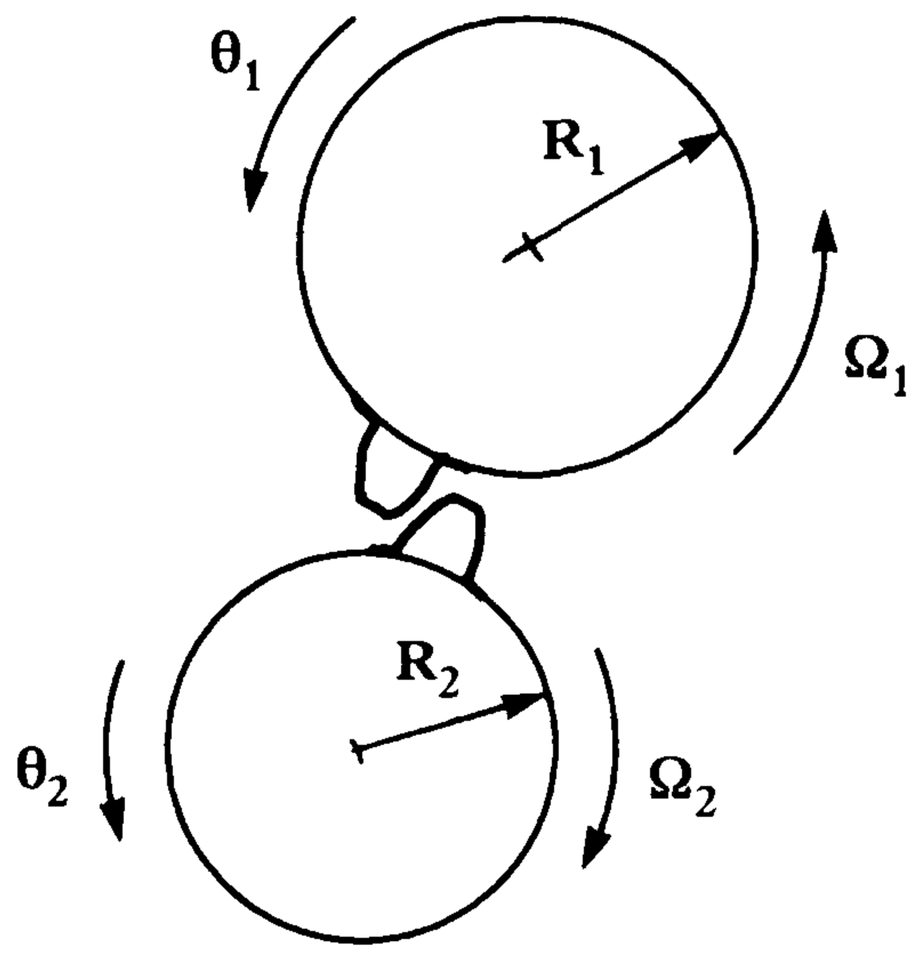

Figure 9.3. Connection element

9.2.2 Discrete model

Let us consider the branched system shown in Figure 9.4. The system can be supposed to be the simple model of a unit consisting of an electric motor (I_1, I_2), a multiplier (I_3, I_4) and a compressor (I_5). The stiffnesses of the shaft elements are k_1, k_2 and k_3. Assuming that relation (9.22) holds, the kinetic energy and the strain energy are, from (9.5) and (9.15):

$$T = \tfrac{1}{2}[I_1\dot{\theta}_1^2 + I_2\dot{\theta}_2^2 + I_3\dot{\theta}_3^2 + I_4\dot{\theta}_4^2 + I_5\dot{\theta}_5^2] \tag{9.23}$$

$$U = \tfrac{1}{2}[k_1(\theta_2 - \theta_1)^2 + k_2(\theta_3 - \theta_2)^2 + k_3(\theta_5 - \theta_4)^2] \tag{9.24}$$

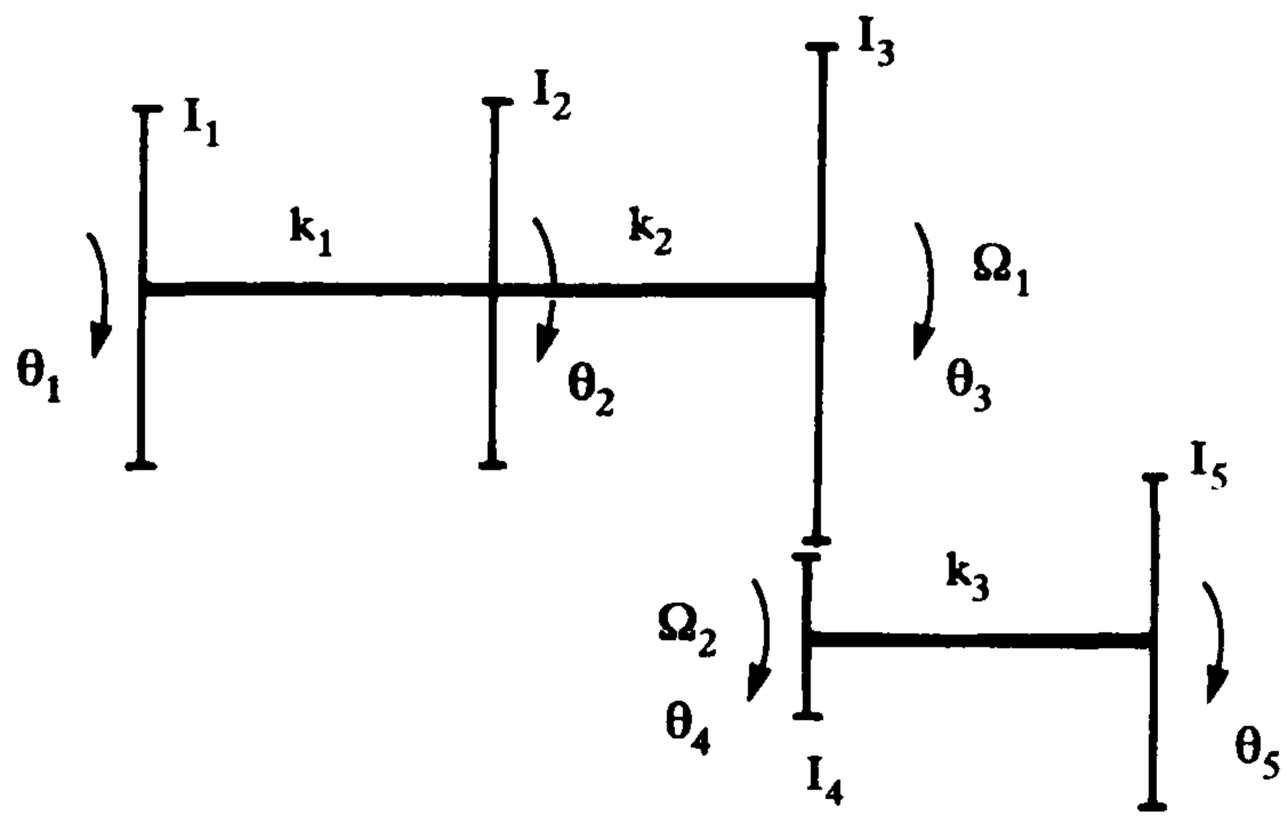

Figure 9.4. Branched system

It is easier to cancel one degree of freedom ($\theta_4 = -n\theta_3$) than to use one Lagrange multiplier; then:

$$T = \tfrac{1}{2}[I_1\dot{\theta}_1^2 + I_2\dot{\theta}_2^2 + (I_3 + n^2 I_4)\dot{\theta}_3^2 + I_5\dot{\theta}_5^2] \tag{9.25}$$

$$U = \tfrac{1}{2}[k_1(\theta_2 - \theta_1)^2 + k_2(\theta_3 - \theta_2)^2 + k_3(\theta_5 + n\theta_3)^2] \tag{9.26}$$

If, in addition, torques $T_1, \ldots, T_5$ act on each disk, their virtual work is

$$\delta W = T_1\delta\theta_1 + T_2\delta\theta_2 + T_3\delta\theta_3 + T_4\delta\theta_4 + T_5\delta\theta_5 \tag{9.27}$$

$$= T_1\delta\theta_1 + T_2\delta\theta_2 + (T_3 - T_4 n)\delta\theta_3 + T_5\delta\theta_5 \tag{9.28}$$

Application of Lagrange's equations to (9.25), (9.26) and (9.28) gives

$$\begin{bmatrix} I_1 & 0 & 0 & 0 \\ 0 & I_2 & 0 & 0 \\ 0 & 0 & I_3 + n^2 I_4 & 0 \\ 0 & 0 & 0 & I_5 \end{bmatrix} \begin{bmatrix} \ddot{\theta}_1 \\ \ddot{\theta}_2 \\ \ddot{\theta}_3 \\ \ddot{\theta}_5 \end{bmatrix} + \begin{bmatrix} k_1 & -k_1 & 0 & 0 \\ -k_1 & k_1 + k_2 & -k_2 & 0 \\ 0 & -k_2 & k_2 + n^2 k_3 & nk_3 \\ 0 & 0 & nk_3 & k_3 \end{bmatrix} \begin{bmatrix} \theta_1 \\ \theta_2 \\ \theta_3 \\ \theta_5 \end{bmatrix} = \begin{bmatrix} T_1 \\ T_2 \\ T_3 - nT_4 \\ T_5 \end{bmatrix} \tag{9.29}$$

Assuming now that the gear teeth are deformed its strain energy (see Equations (9.19) and (9.20)) has to be added to (9.24). Applying Lagrange equations gives

$$\begin{bmatrix} I_1 & 0 & 0 & 0 & 0 \\ 0 & I_2 & 0 & 0 & 0 \\ 0 & 0 & I_3 & 0 & 0 \\ 0 & 0 & 0 & I_4 & 0 \\ 0 & 0 & 0 & 0 & I_5 \end{bmatrix} \begin{bmatrix} \ddot{\theta}_1 \\ \ddot{\theta}_2 \\ \ddot{\theta}_3 \\ \ddot{\theta}_4 \\ \ddot{\theta}_5 \end{bmatrix} + \begin{bmatrix} k_1 & -k_1 & 0 & 0 & 0 \\ -k_1 & k_1 + k_2 & -k_2 & 0 & 0 \\ 0 & -k_2 & k_2 + R_3^2 k & R_3 R_4 k & 0 \\ 0 & 0 & R_3 R_4 k & k_3 + R_4^2 k & -k_3 \\ 0 & 0 & 0 & -k_3 & k_3 \end{bmatrix} \begin{bmatrix} \theta_1 \\ \theta_2 \\ \theta_3 \\ \theta_4 \\ \theta_5 \end{bmatrix} = \begin{bmatrix} T_1 \\ T_2 \\ T_3 \\ T_4 \\ T_5 \end{bmatrix} \tag{9.30}$$

9.2.3 Solutions of Equations (9.29) and (9.30)

Since the same method is used to solve both equations, only the solution of (9.29) is presented here.

Natural frequencies and modes

It is very easy to solve Equation (9.29) with no external forces and to draw the Campbell diagram and modes.

Transient motion: at start-up

The general expression for the start-up torque T_{st} at zero speed is given from the appropriate laws of electromagnetism:

$$T_{st} = a + be^{-\lambda t} \sin \omega t \tag{9.31}$$

where a, b and $\lambda(> 0)$ are known constants and ω is the frequency of the electric current. The torque acts on disk I_2 and there is no torque on disks I_1, I_3, I_4 or I_5. At start-up ($t_0 = 0$) the initial conditions are displacements $\theta_1(0)$, $\theta_2(0)$, $\theta_3(0)$ and $\theta_5(0)$ and velocities $\dot{\theta}_1(0)$, $\dot{\theta}_2(0)$, $\dot{\theta}_3(0)$, and $\dot{\theta}_5(0)$ all equal to zero.

The initial conditions for the acceleration come from (9.29) and are

$$\ddot{\theta}_1(0) = 0 \tag{9.32}$$

$$\ddot{\theta}_2(0) = \frac{T_{st}(0)}{I_2} = \frac{a}{I_2} \tag{9.33}$$

$$\ddot{\theta}_3(0) = 0 \tag{9.34}$$

$$\ddot{\theta}_5(0) = 0 \tag{9.35}$$

The solution of the transient motion is, as in Chapter 8, obtained by the Newmark method. The angular displacements θ_1, θ_2, θ_3 and θ_5 are then known as functions of time. Hence the torque in each shaft element is obtained from

$$T_{1,2} = k_1(\theta_2 - \theta_1) \tag{9.36}$$

$$T_{2,3} = k_2(\theta_3 - \theta_2) \tag{9.37}$$

$$T_{4,5} = k_3(\theta_5 + n\theta_3) \tag{9.38}$$

Transient motion: short-circuit

The general expression of the short-circuit torque T_{sc} is

$$T_{sc} = be^{-\lambda t} \sin \omega t \tag{9.39}$$

The shafts rotate at constant speeds and the branched system is in steady-state motion at the initial instant $t_0 = 0$. Before the short-circuit, the motor gives a power $P = T_n \Omega_1$. The compressor is supposed to receive the same power and then creates a resistant torque T_R such that

$$T_R = T_n \frac{\Omega_1}{\Omega_2} = \frac{T_n}{n} \tag{9.40}$$

where Ω_1 and Ω_2 are the speeds of rotation of shafts 1 and 2 respectively, and T_n is the nominal torque on shaft 1. The initial conditions have to be known. The angular positions come from

$$\begin{bmatrix} k_1 & -k_1 & 0 & 0 \\ -k_1 & k_1 + k_2 & -k_2 & 0 \\ 0 & -k_2 & k_2 + n^2 k_3 & nk_3 \\ 0 & 0 & nk_3 & k_3 \end{bmatrix} \begin{bmatrix} \theta_1 \\ \theta_2 \\ \theta_3 \\ \theta_5 \end{bmatrix} = \begin{bmatrix} 0 \\ T_n \\ 0 \\ T_R \end{bmatrix} \tag{9.41}$$

As the system is free (one rigid body mode) the angles are obtained within an additive constant. Thus we can write $\theta_2 = 0$, and then (9.41) gives the following initial conditions:

$$\theta_1 = \theta_2 = 0 \tag{9.42}$$

$$\theta_3 = -T_n / k_2 \tag{9.43}$$

$$\theta_5 = \frac{T_n [k_2 + n^2 k_3]}{n k_2 k_3} \tag{9.44}$$

and the angular velocities are

$$\dot{\theta}_1 = \dot{\theta}_2 = \dot{\theta}_3 = \dot{\theta}_5 = 0 \tag{9.45}$$

The values of the angular accelerations at the initial instant are obtained

from the equations of motion; that is:

$$\begin{bmatrix} I_1 & 0 & 0 & 0 \\ 0 & I_2 & 0 & 0 \\ 0 & 0 & I_3 + n^2 I_4 & 0 \\ 0 & 0 & 0 & I_5 \end{bmatrix} \begin{bmatrix} \ddot{\theta}_1 \\ \ddot{\theta}_2 \\ \ddot{\theta}_3 \\ \ddot{\theta}_5 \end{bmatrix} + \begin{bmatrix} k_1 & -k_1 & 0 & 0 \\ -k_1 & k_1 + k_2 & -k_2 & 0 \\ 0 & -k_2 & k_2 + n^2 k_3 & nk_3 \\ 0 & 0 & nk_3 & k_3 \end{bmatrix} \begin{bmatrix} \theta_1 \\ \theta_2 \\ \theta_3 \\ \theta_5 \end{bmatrix}$$

$$= \begin{bmatrix} 0 \\ T_{sc}(0) \\ 0 \\ T_R \end{bmatrix} = \begin{bmatrix} 0 \\ T_{sc}(0) \\ 0 \\ T_n/n \end{bmatrix} \tag{9.46}$$

where the torque T_R still exists and where $T_{sc}(0)$ is the value of the short-circuit torque at $t_0 = 0$. Using (9.42), (9.43), (9.44) and (9.46) we obtain

$$\ddot{\theta}_2 = \frac{T_{sc}(0) - T_n}{I_2} \tag{9.47}$$

$$\ddot{\theta}_1 = \ddot{\theta}_3 = \ddot{\theta}_5 = 0 \tag{9.48}$$

All the initial conditions being known, the procedure can be applied.

9.3 ANALYSIS OF A BRANCHED SYSTEM IN TORSION

The geometry of the system is as in Figure 9.4. The coupling ratio is

$$\theta_4 = -3\theta_3 \tag{9.49}$$

and the values of the disk inertias and shaft stiffnesses are

$$\begin{aligned} I_1 &= 0.248\,11\ \text{kg m}^2 \\ I_2 &= 0.119\,65\ \text{kg m}^2 \\ I_3 &= 0.942\,03\ \text{kg m}^2 \\ I_4 &= 0.019\,38\ \text{kg m}^2 \\ I_5 &= 0.089\,74\ \text{kg m}^2 \\ k_1 &= k_2 = 1.5733 \times 10^5\ \text{N/m} \\ k_3 &= 1.1800 \times 10^5\ \text{N/m} \end{aligned} \tag{9.50}$$

The frequencies and modes are shown in Figure 9.5.

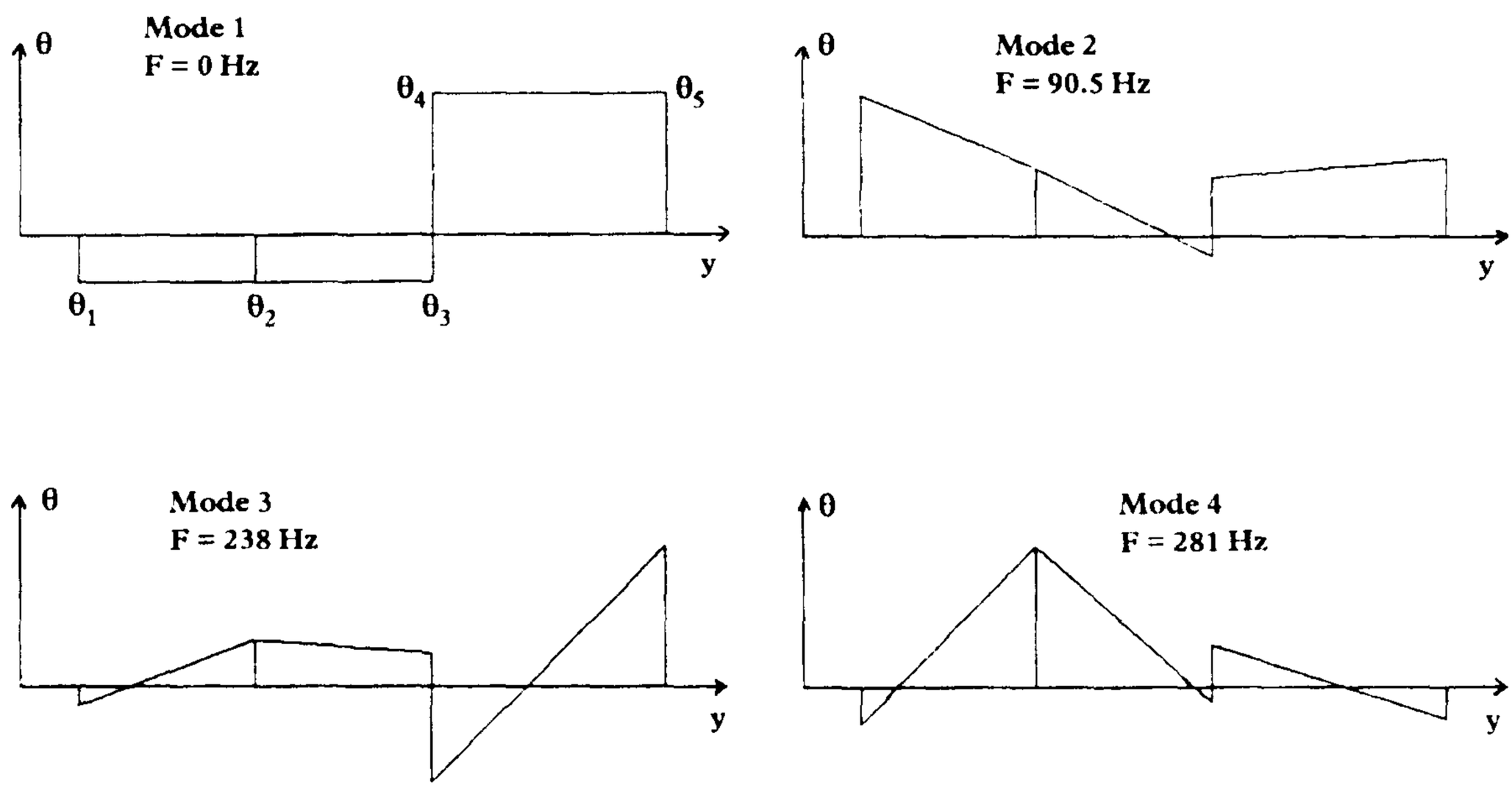

Figure 9.5. Mode shapes

At start-up

At start-up the torque is

$$T_{st} = T_n[0.8 - 6e^{-0.25t} \sin(\omega t + 0.1)] \tag{9.51}$$

This is shown in Figure 9.6. (The frequency of the electric current is 100π rad/s).

The ratios of the torques in each element over the nominal torque are shown in Figures 9.7, 9.8 and 9.9. The maxima are

$$\begin{aligned} T_{1,2}/T_n &= 2.571 \text{ at } t = 0.2849\text{s} \\ T_{2,3}/T_n &= 9.122 \text{ at } t = 0.2348\text{s} \\ T_{4,5}/T_n &= 1.712 \text{ at } t = 0.014\,16\text{s} \end{aligned} \tag{9.52}$$

During a Short-circuit

The general expression for the torque is

$$T_{sc} = 6T_n e^{-t/0.03} \sin \omega t \tag{9.53}$$

This is shown in Figure 9.10.

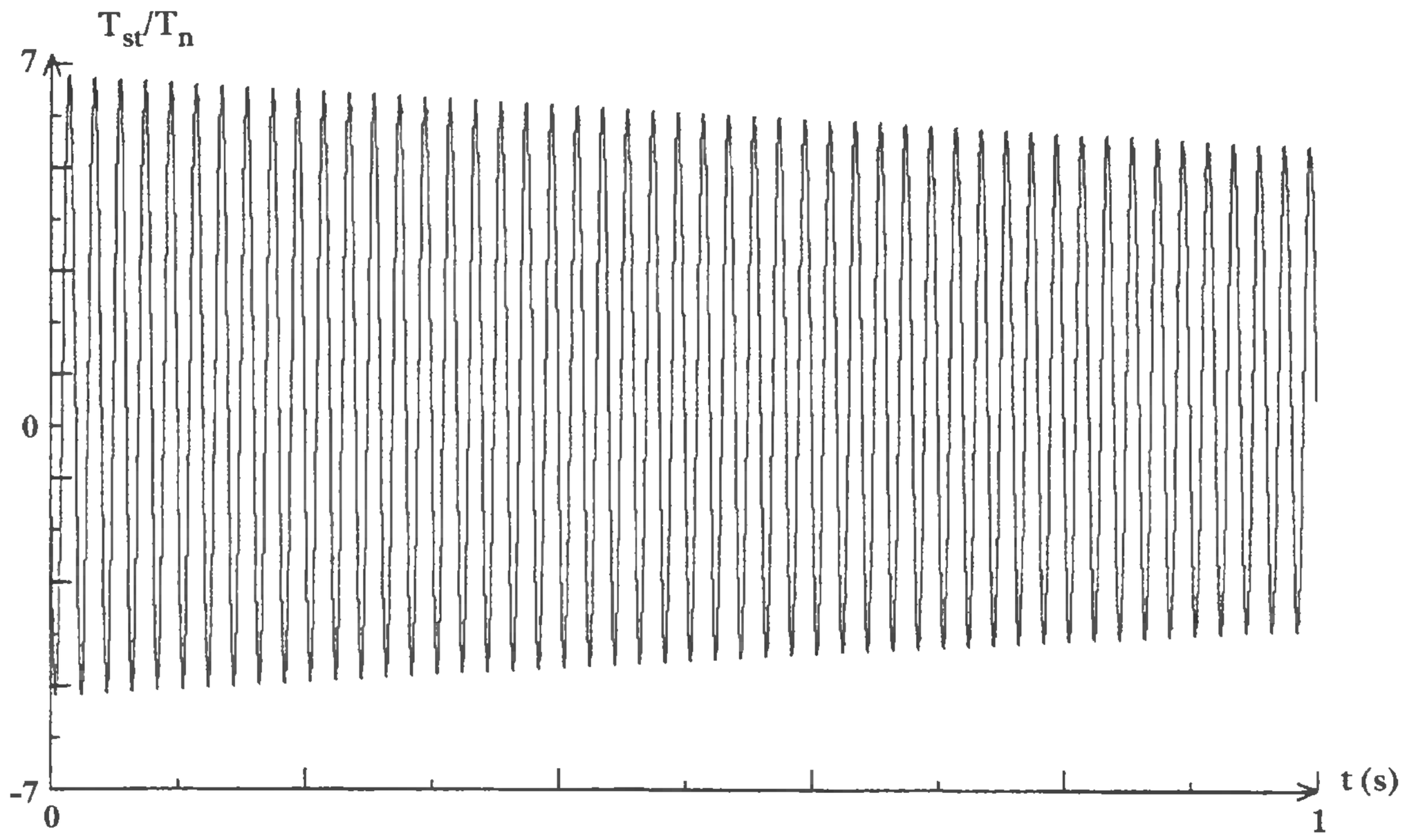

Figure 9.6. Start-up torque over nominal torque, T_{st}/T_n, versus time

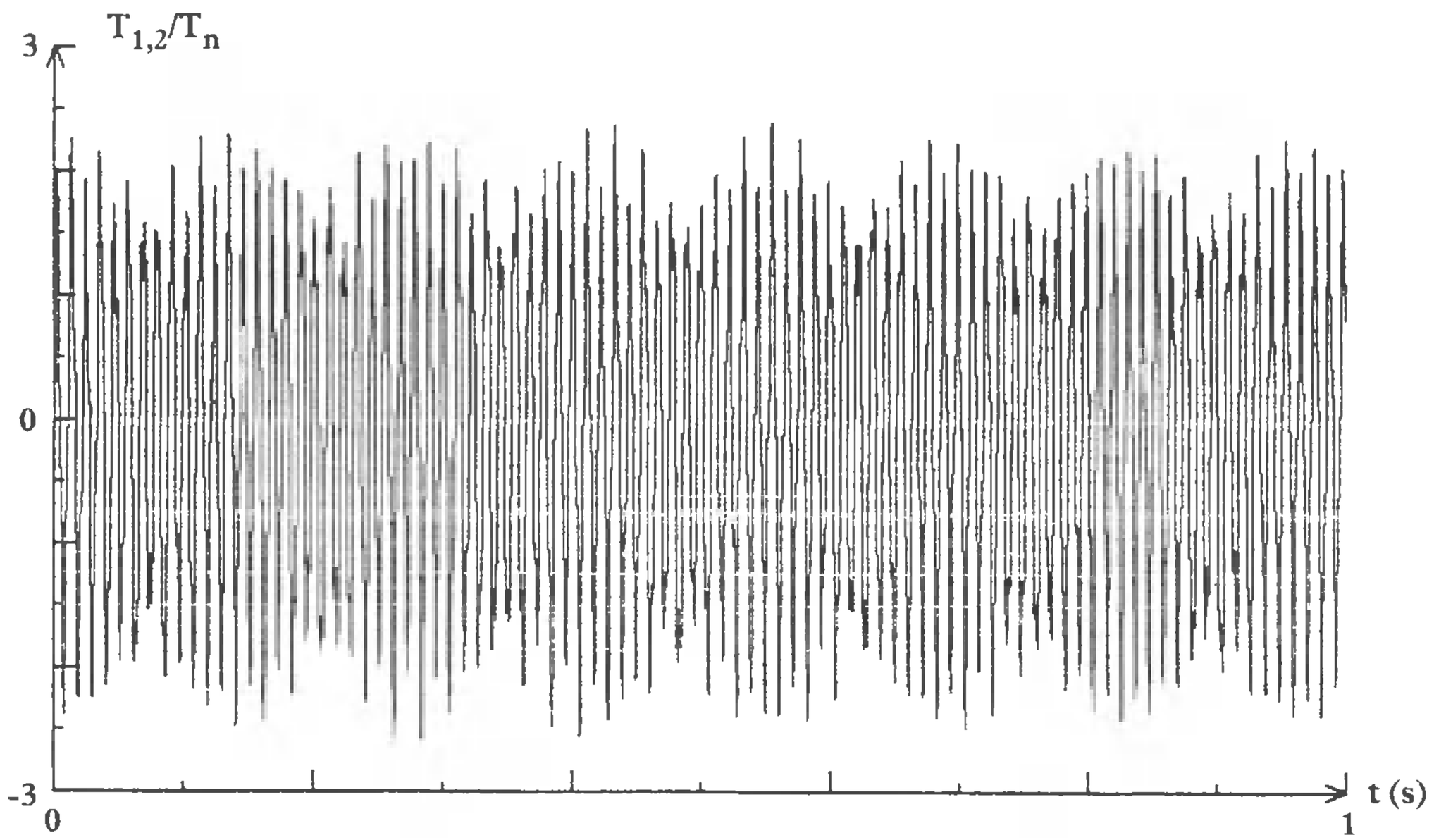

Figure 9.7. Start-up: $T_{1,2}/T_n$ versus time

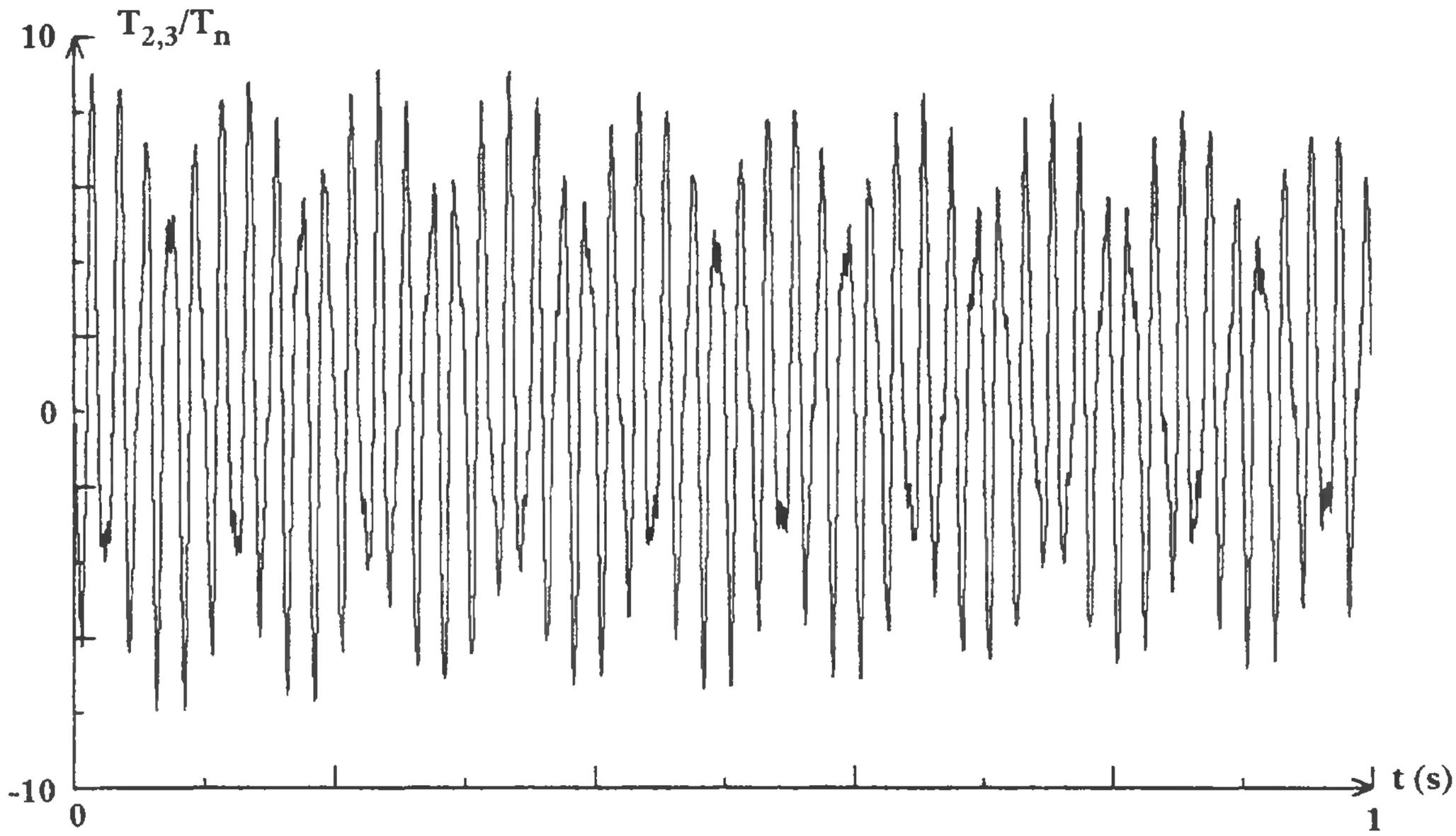

Figure 9.8. Start-up: $T_{2,3}/T_n$ versus time

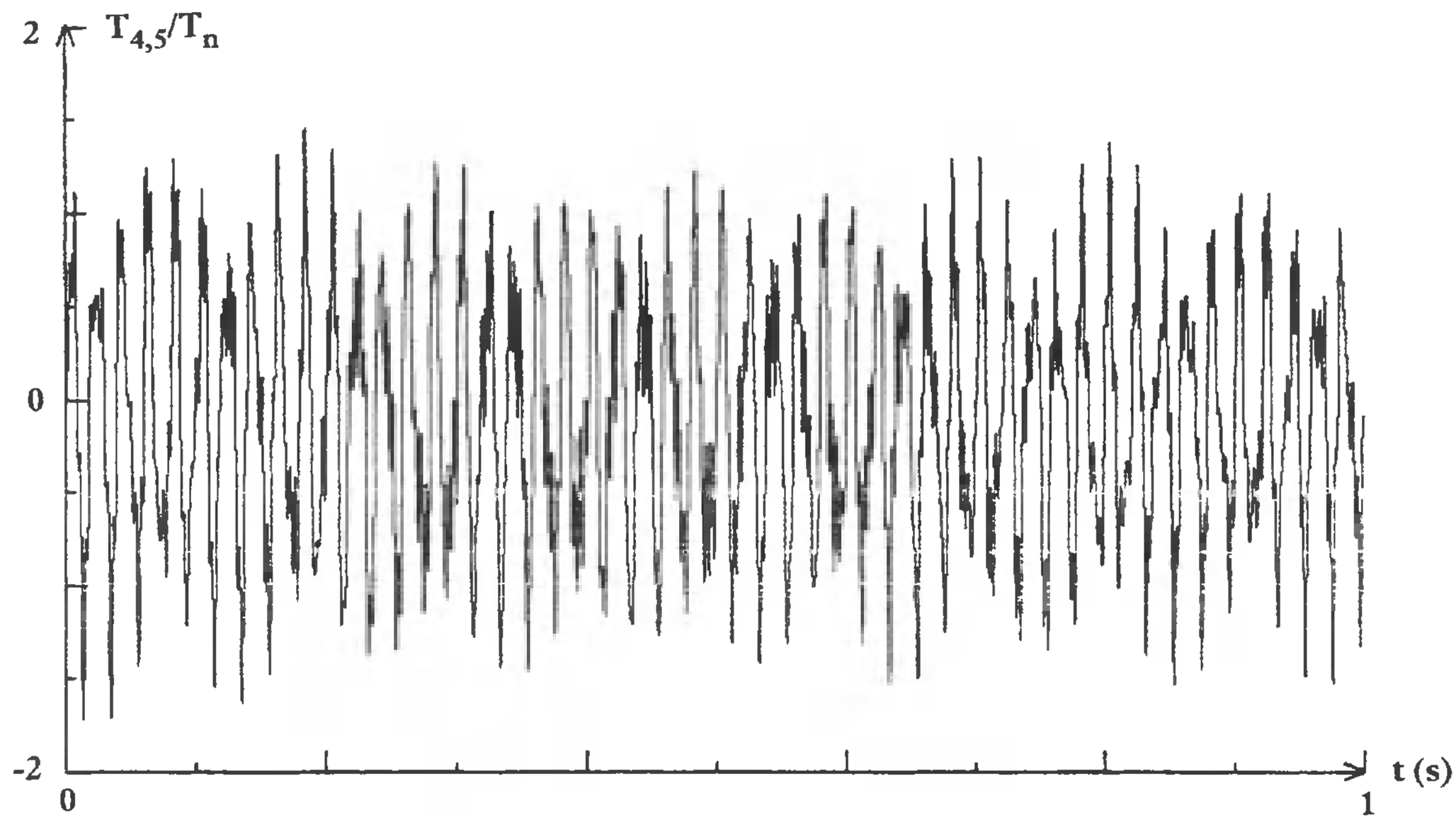

Figure 9.9. Start-up: $T_{4,5}/T_n$ versus time

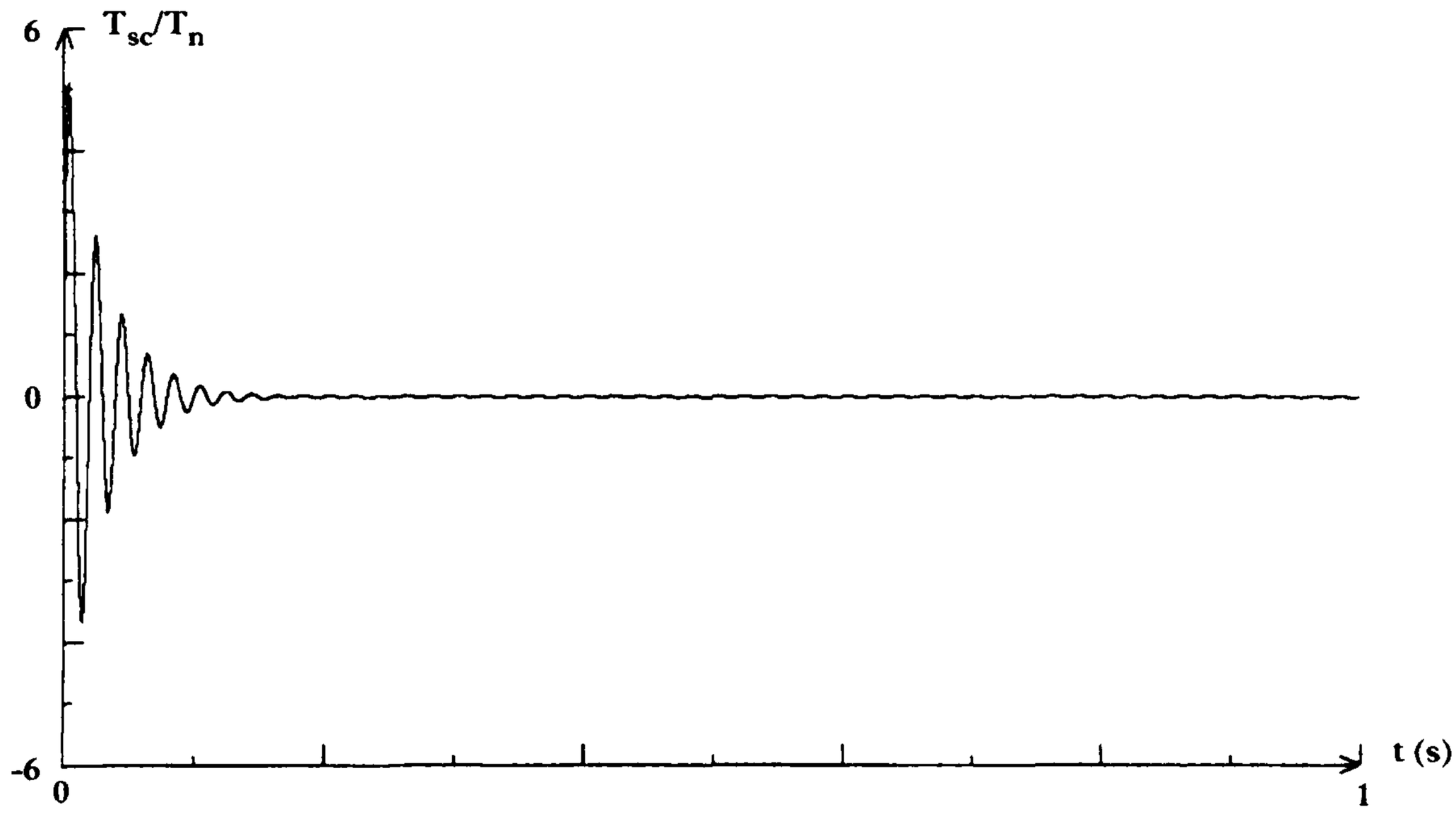

Figure 9.10. Short-circuit torque over nominal torque, T_{sc}/T_n, versus time

The initial conditions are

$$\begin{aligned} \theta_1 &= 0 \\ \theta_2 &= 0 \\ \theta_3 &= -1.9056 \times 10^{-5} T_n \,\text{rad} \\ \theta_5 &= 6.5642 \times 10^{-5} T_n \,\text{rad} \end{aligned} \tag{9.54}$$

The ratios of the torques in each element over the nominal torque are shown in Figure 9.11, 9.12 and 9.13. The maxima are

$$\begin{aligned} T_{1,2}/T_n &= 3.472 \,\text{at}\; t = 0.551\,\text{s} \\ T_{2,3}/T_n &= 6.129 \,\text{at}\; t = 0.00750\,\text{s} \\ T_{4,5}/T_n &= 2.063 \,\text{at}\; t = 0.009\,\text{s} \end{aligned} \tag{9.55}$$

Conclusion

The short-circuit and start-up torques are both higher than T_n, and formula (9.4) has to be used, where T_t is the highest value of the transient torques in (9.52) and (9.55).

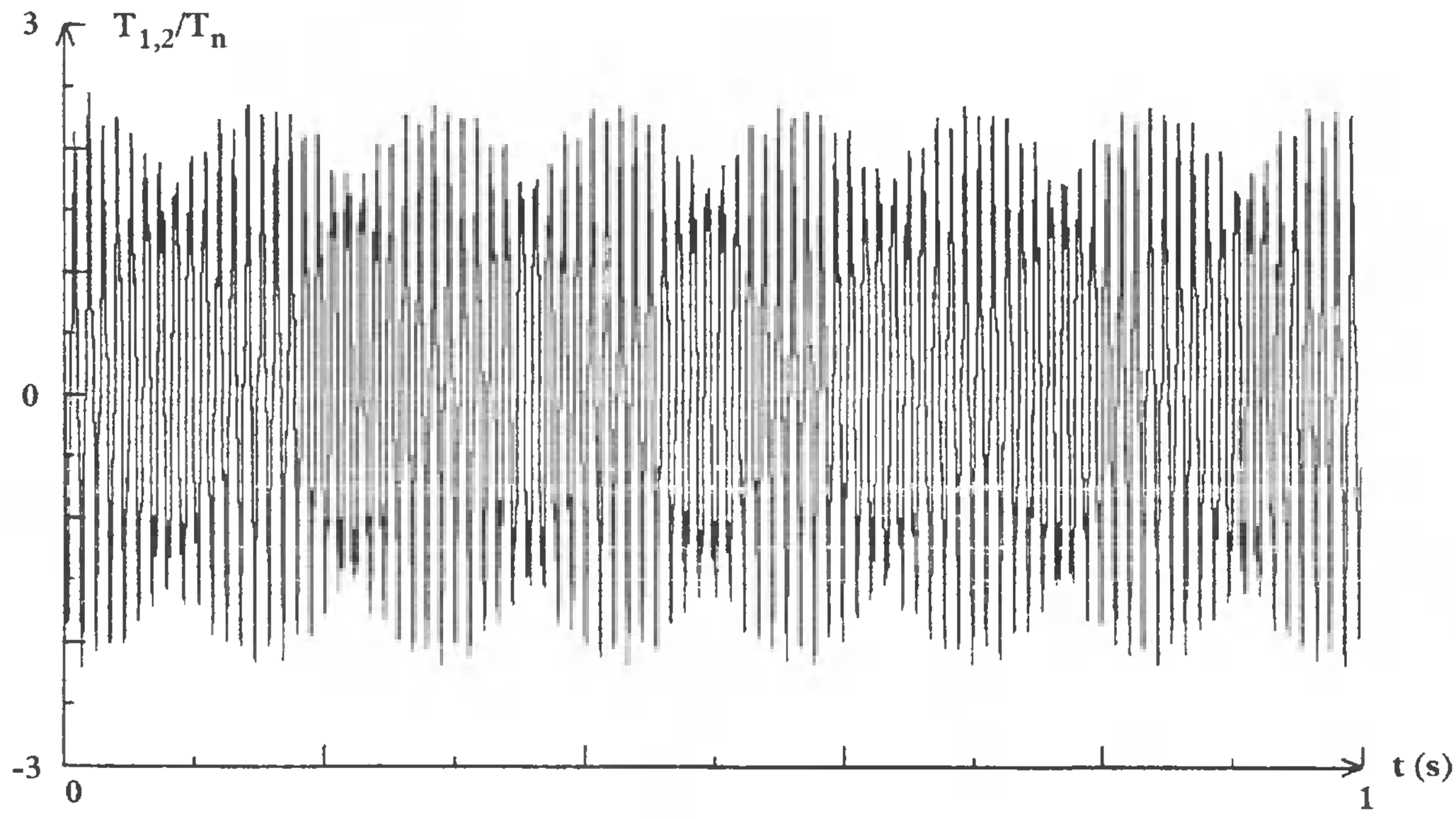

Figure 9.11. Short-circuit: $T_{1,2}/T_n$ versus time

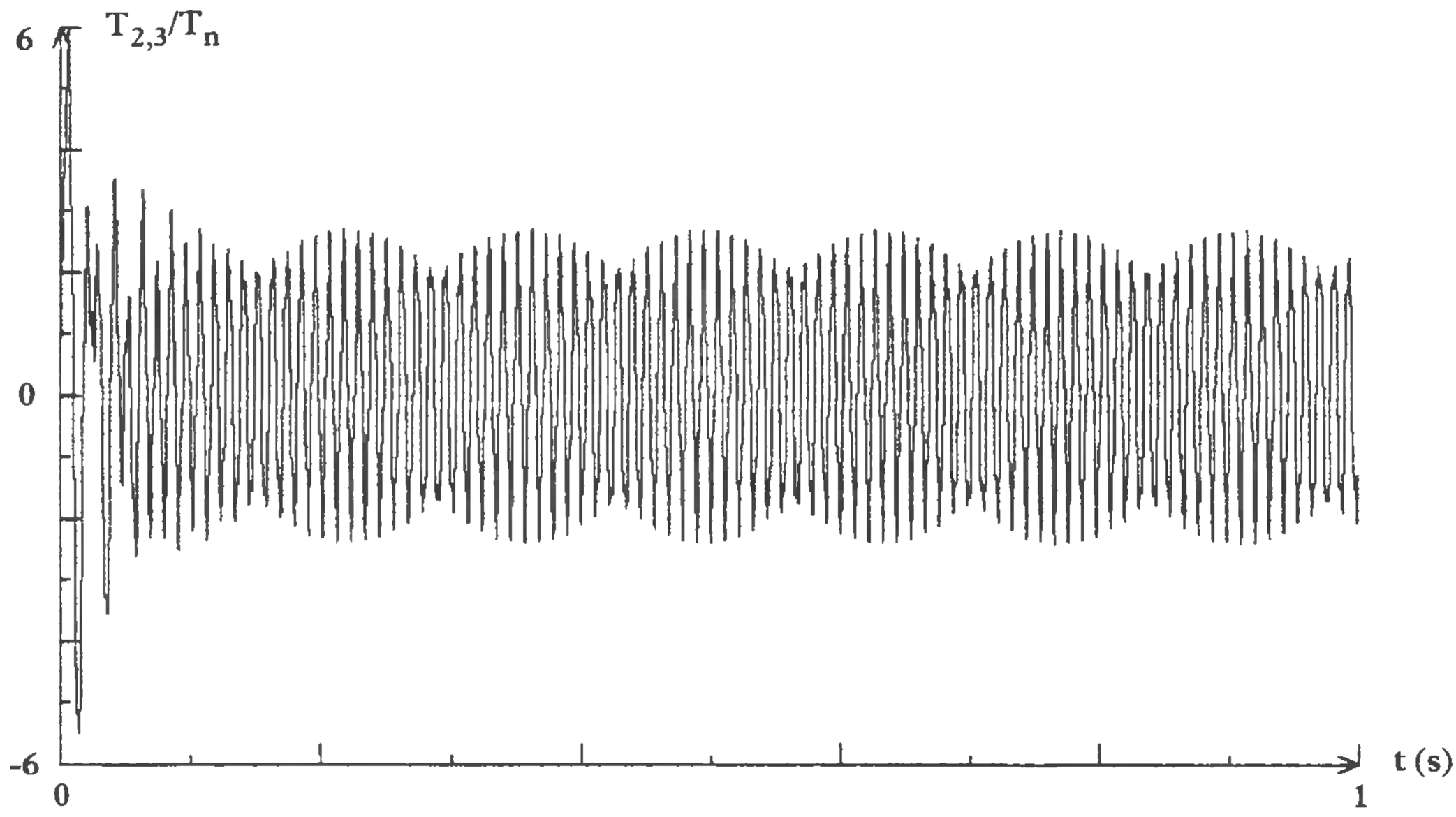

Figure 9.12. Short-circuit: $T_{2,3}/T_n$ versus time

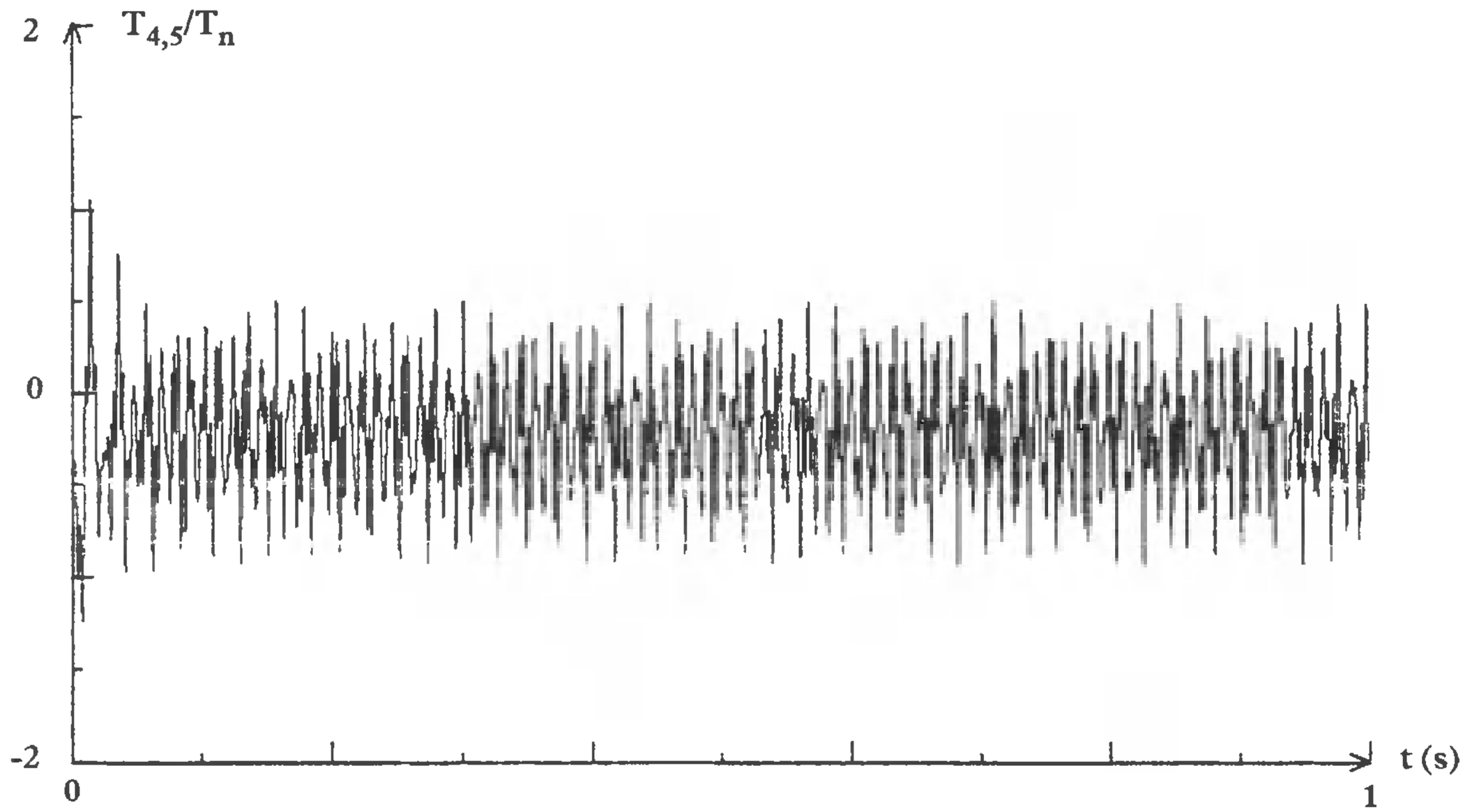

Figure 9.13. Short-circuit: $T_{4,5}/T_n$ versus time

9.4 INDUSTRIAL ELECTRIC-MOTOR/ CENTRIFUGAL-COMPRESSOR UNIT

The whole unit is shown in Figure 9.14. The centrifugal compressor is the one fitted with active magnetic bearings presented in Chapter 7. A direct start-up synchronous electric motor drives the compressor through a multiplier.

This branched system has been studied in torsion using the discrete model with 16 degrees of freedom shown in Figure 9.15.

The Campbell diagram

The frequencies and modes, which are not functions of the speed of rotation, are calculated first: the Campbell diagram is shown in Figure 9.16. Since the compressor operating speed is 13 600 rpm, a possible critical speed must not exist in the range 12240 to 14960 rpm. It appears clearly that this requirement is fulfilled. The mode shapes corresponding to the six lowest frequencies are presented in Figure 9.17.

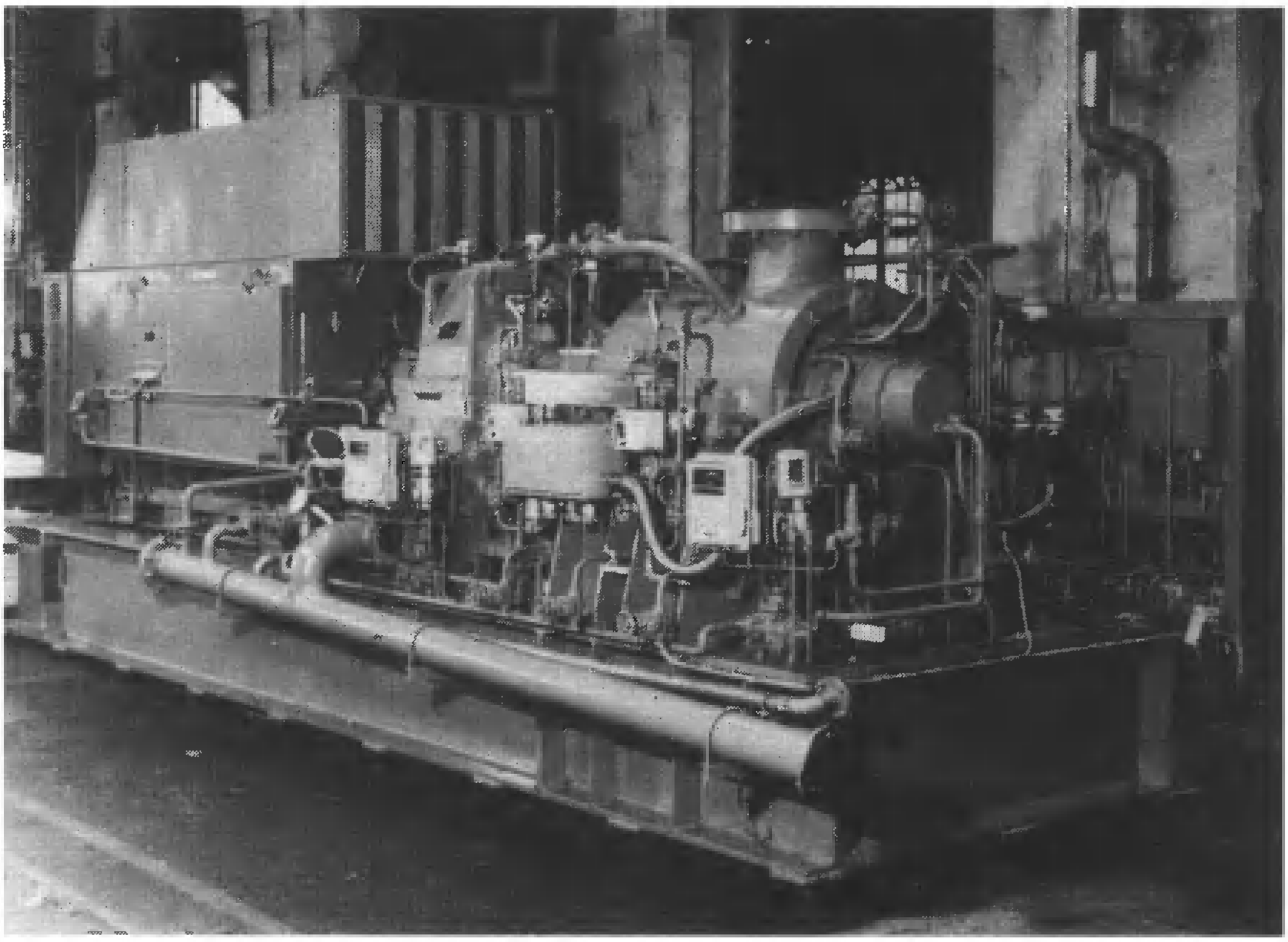

Figure 9.14. Electric-motor/centrifugal-compressor unit (Picture courtesy of Thermodyn)

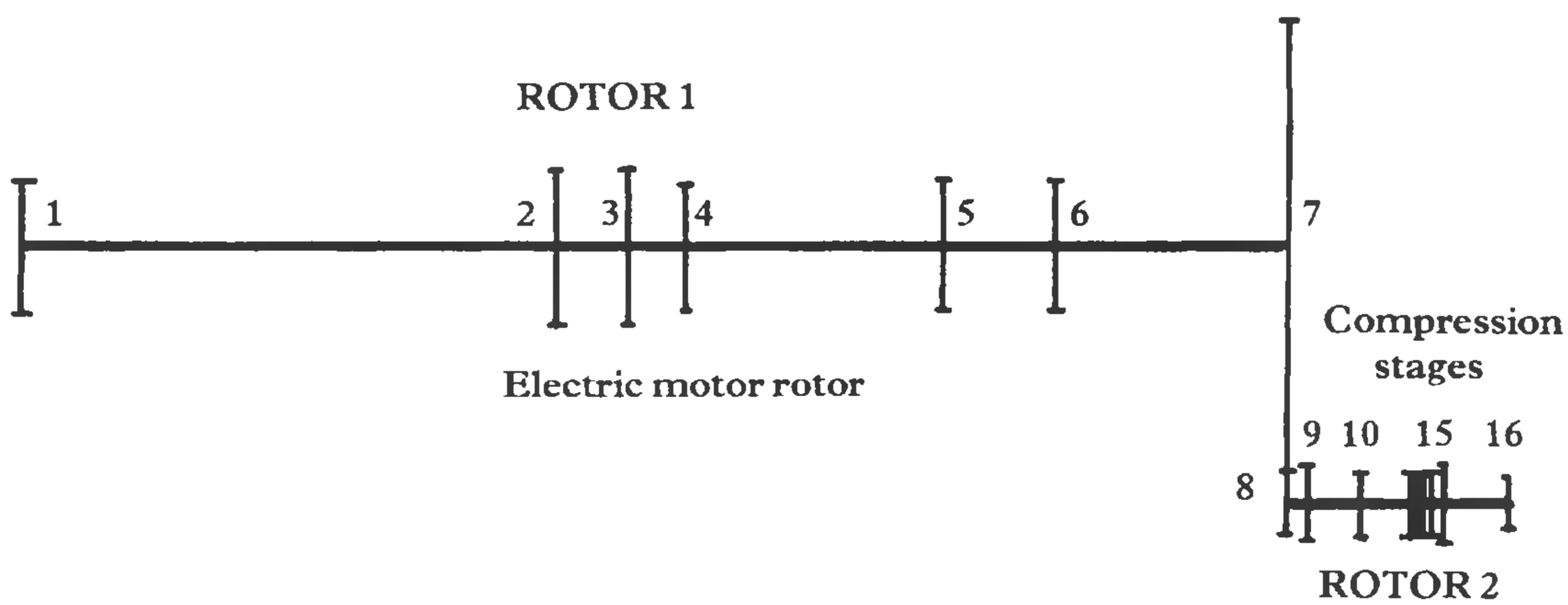

Figure 9.15. Discrete model of electric motor-compressor unit

At start-up

The electric motor is a direct start-up synchronous motor which experiences two phenomena: flux variation up to the steady state when the electric power is switched on, and excitation to a varying frequency when the speed of rotation rises to the operating speed. In what follows

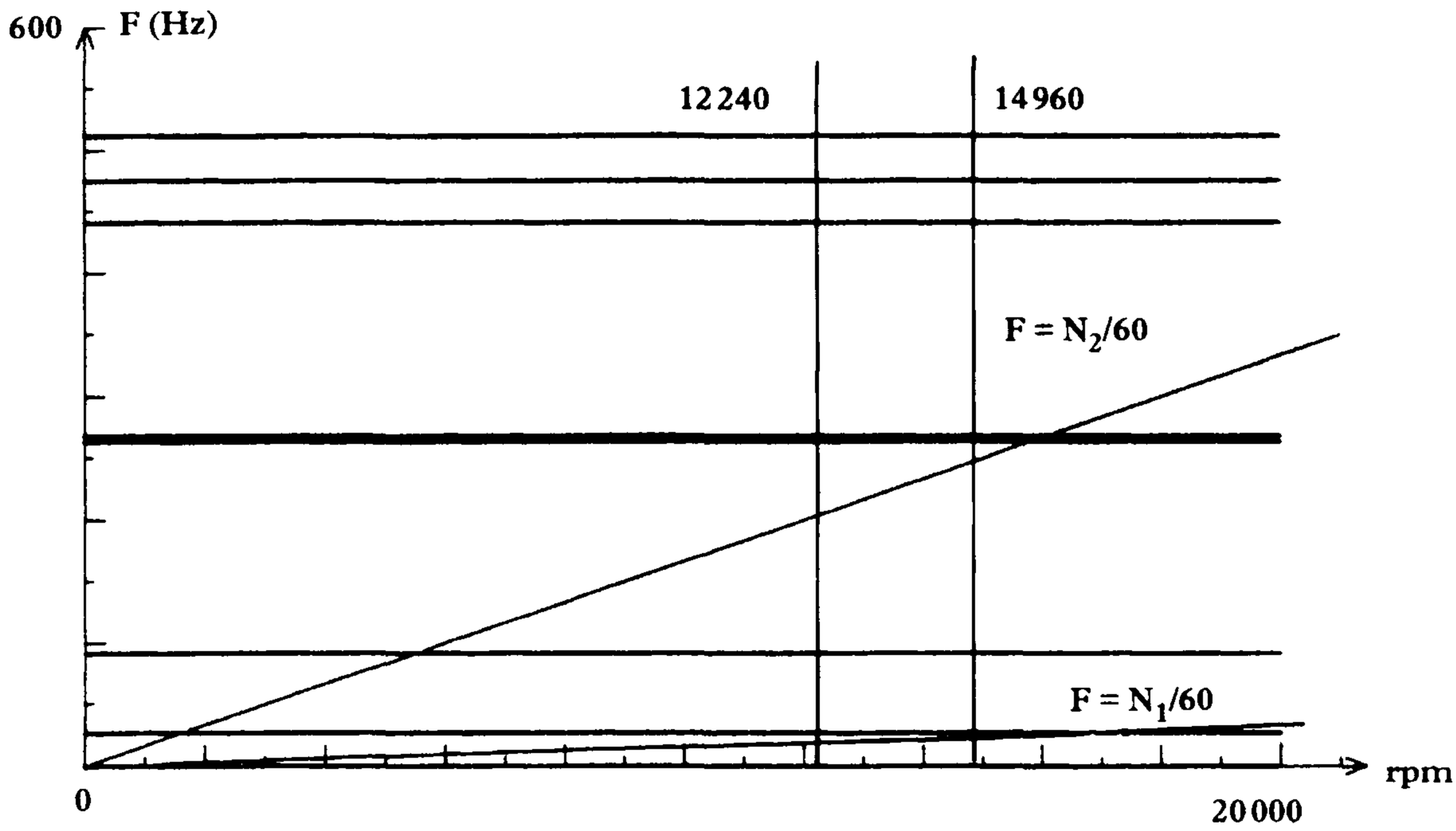

Figure 9.16. Campbell diagram

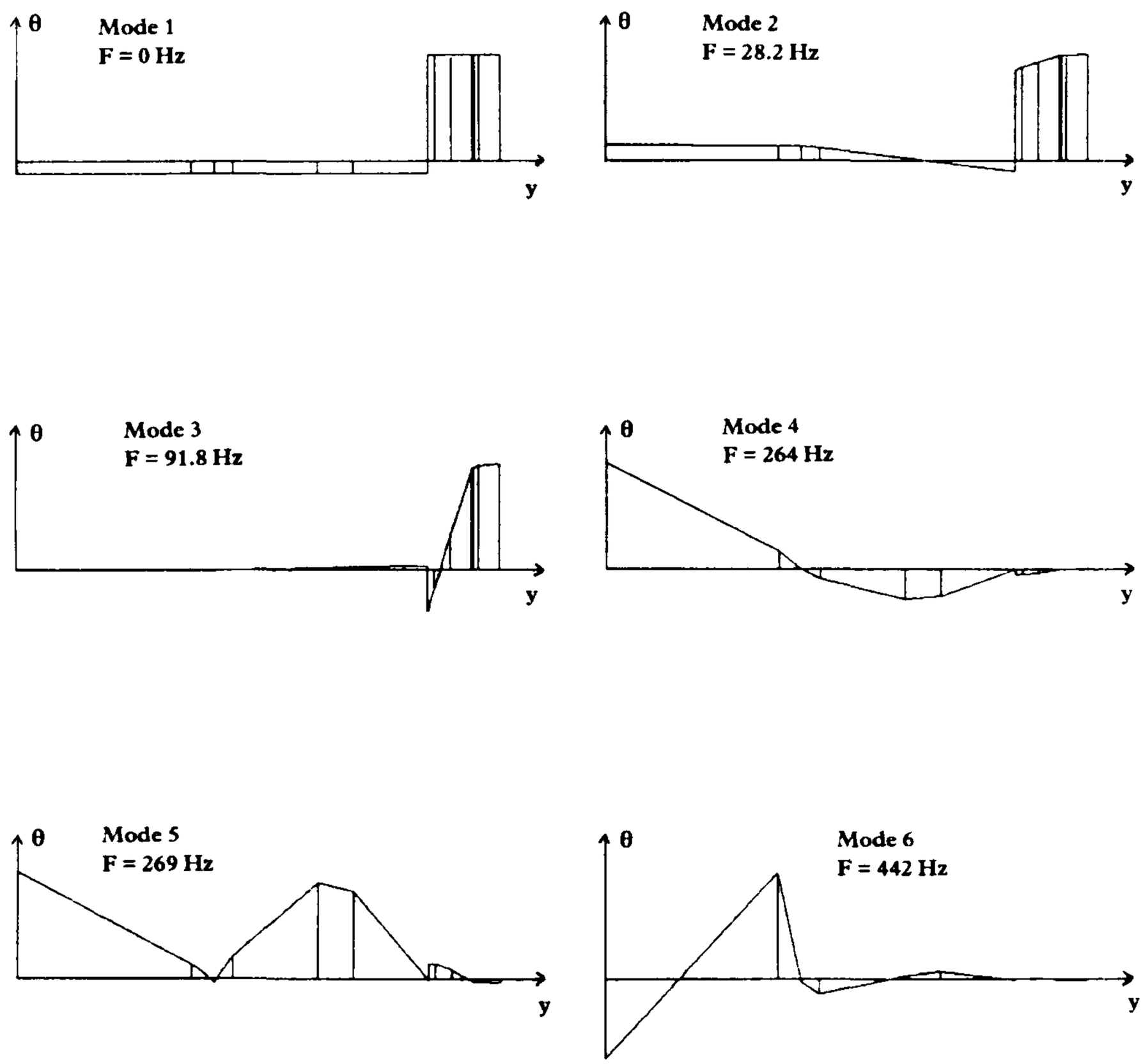

Figure 9.17. Mode shapes

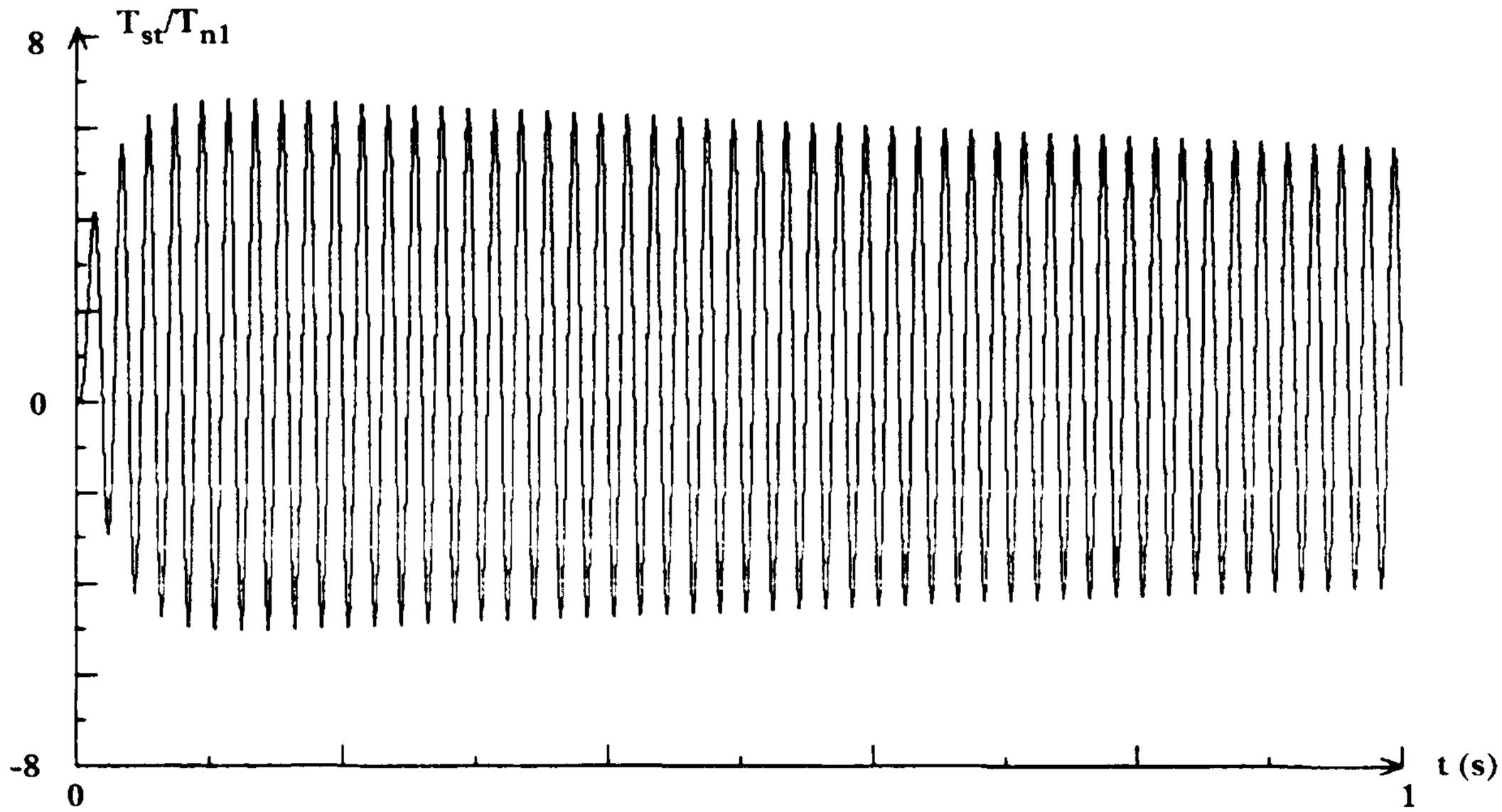

Figure 9.18. Start-up: T_{st}/T_{n1} versus time

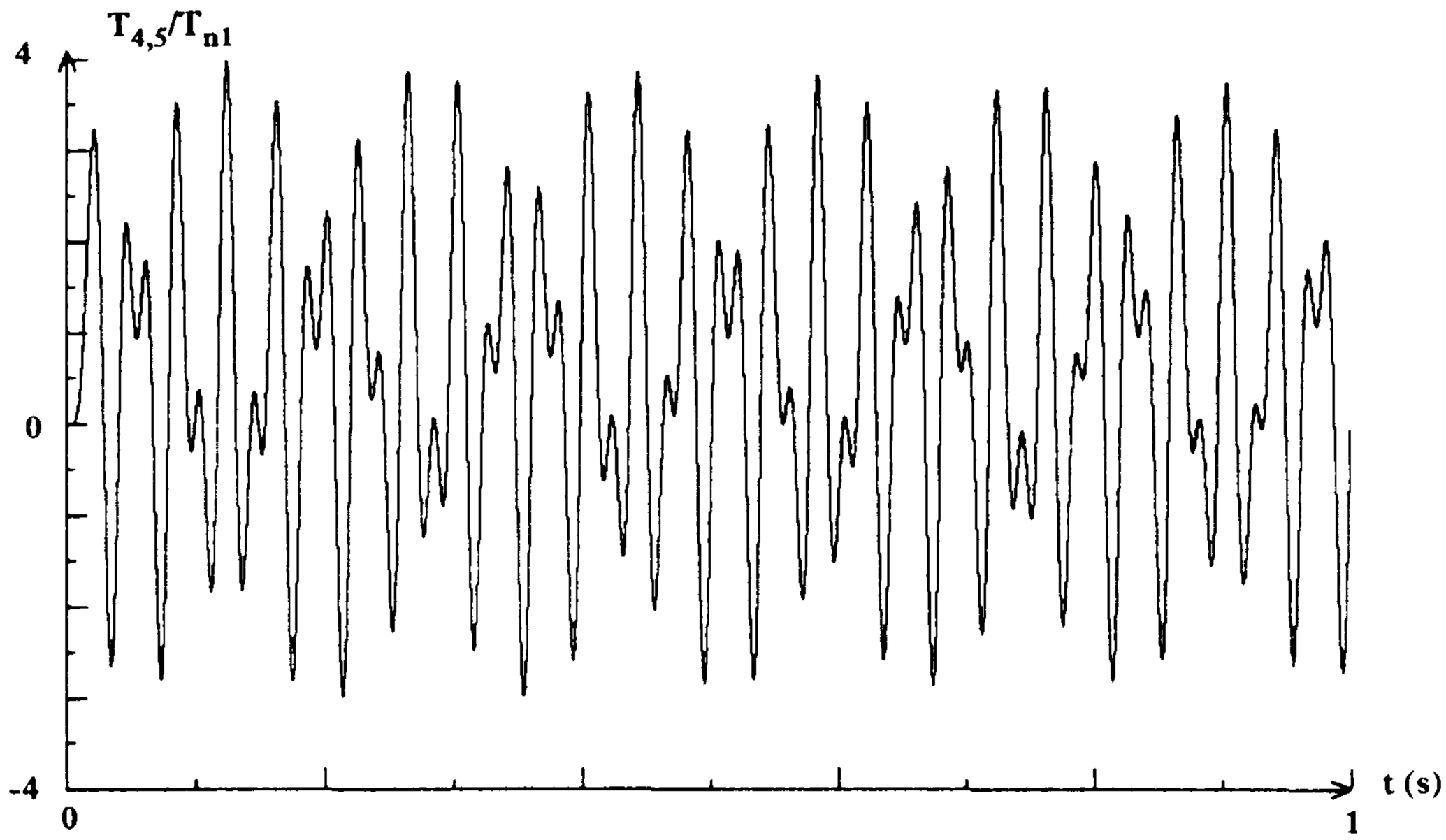

Figure 9.19. Start-up: $T_{4,5}/T_{n1}$ versus time

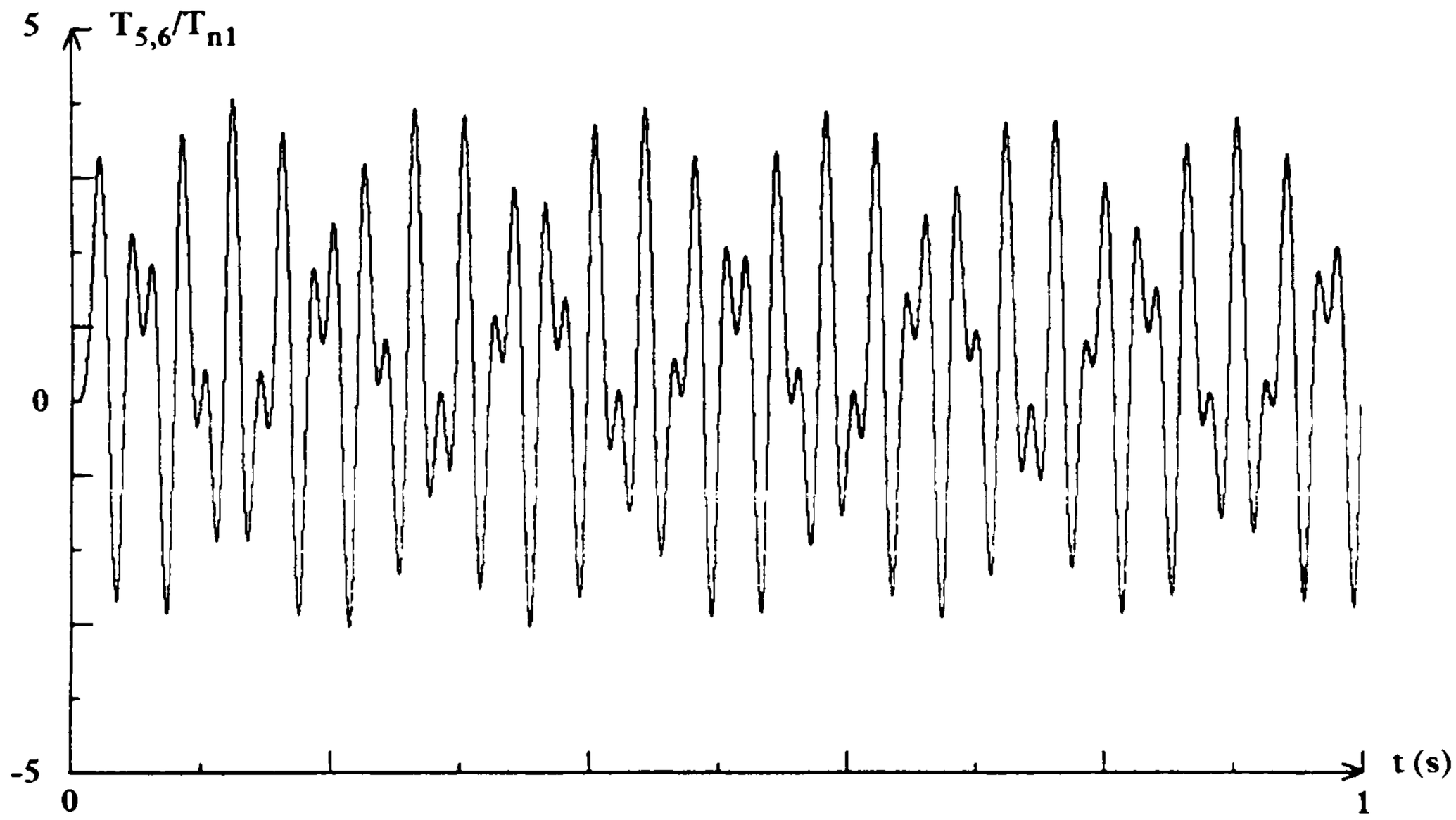

Figure 9.20. Start-up: $T_{5,6}/T_{n1}$ versus time

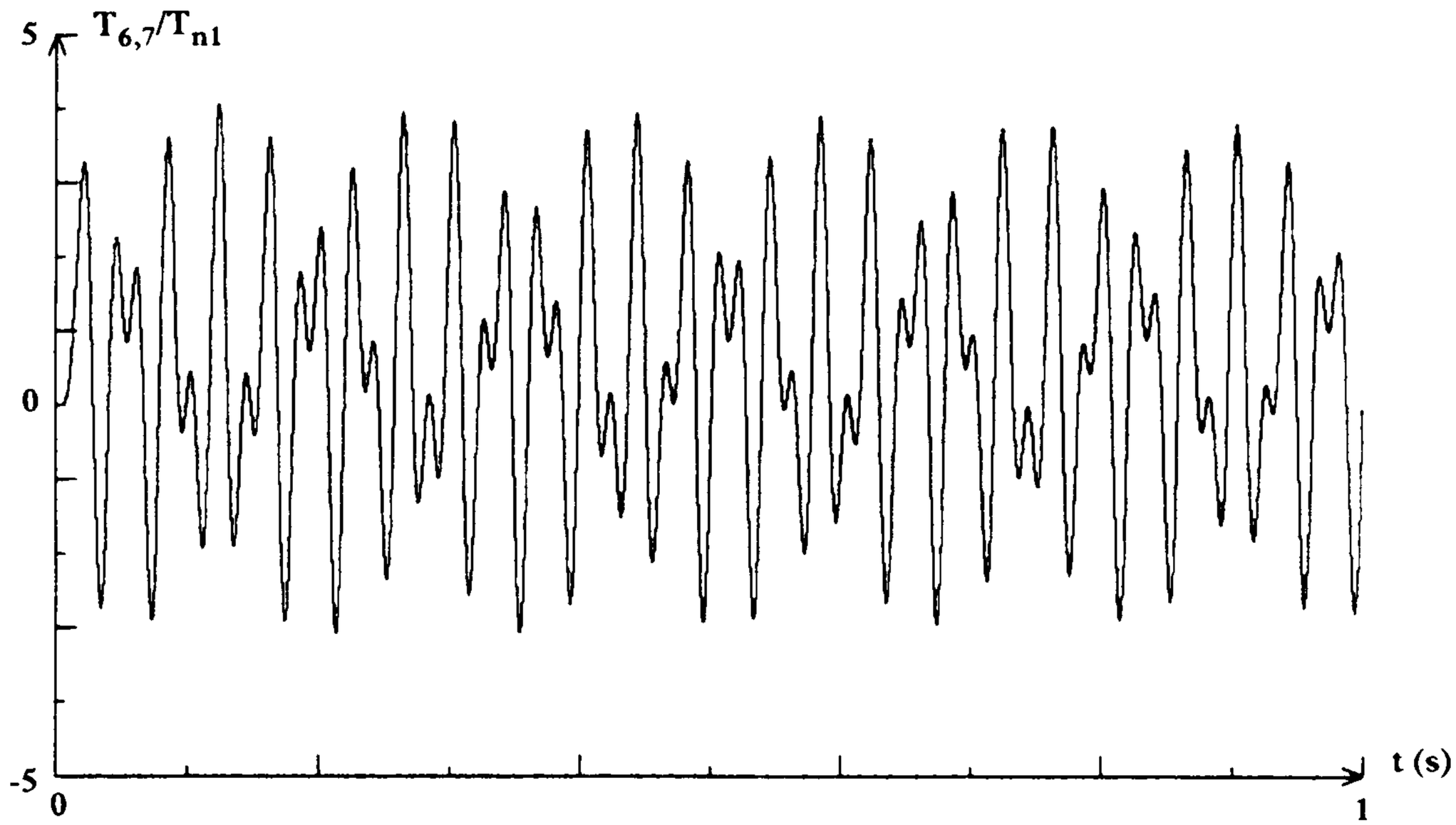

Figure 9.21. Start-up: $T_{6,7}/T_{n1}$ versus time

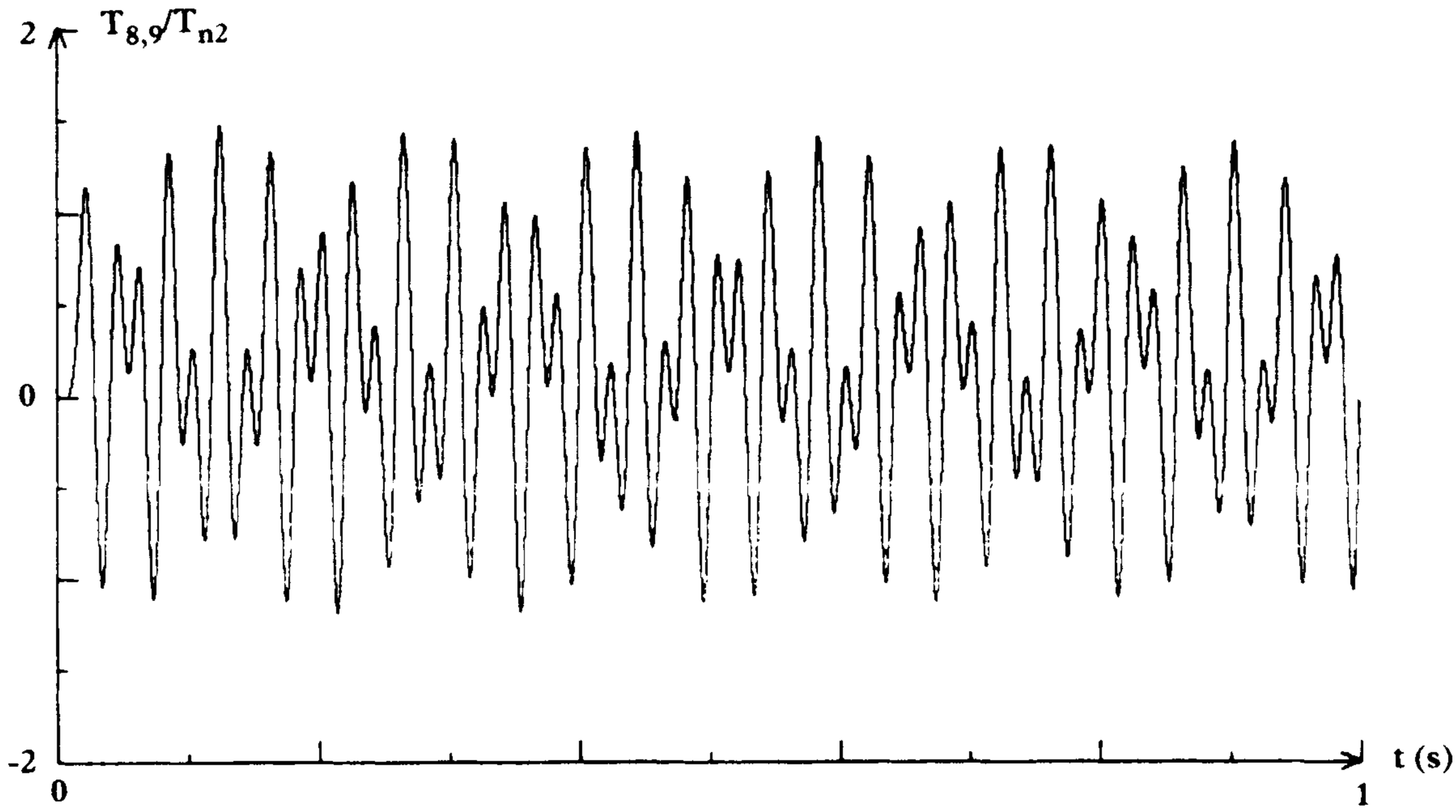

Figure 9.22. Start-up: $T_{8,9}/T_{n2}$ versus time

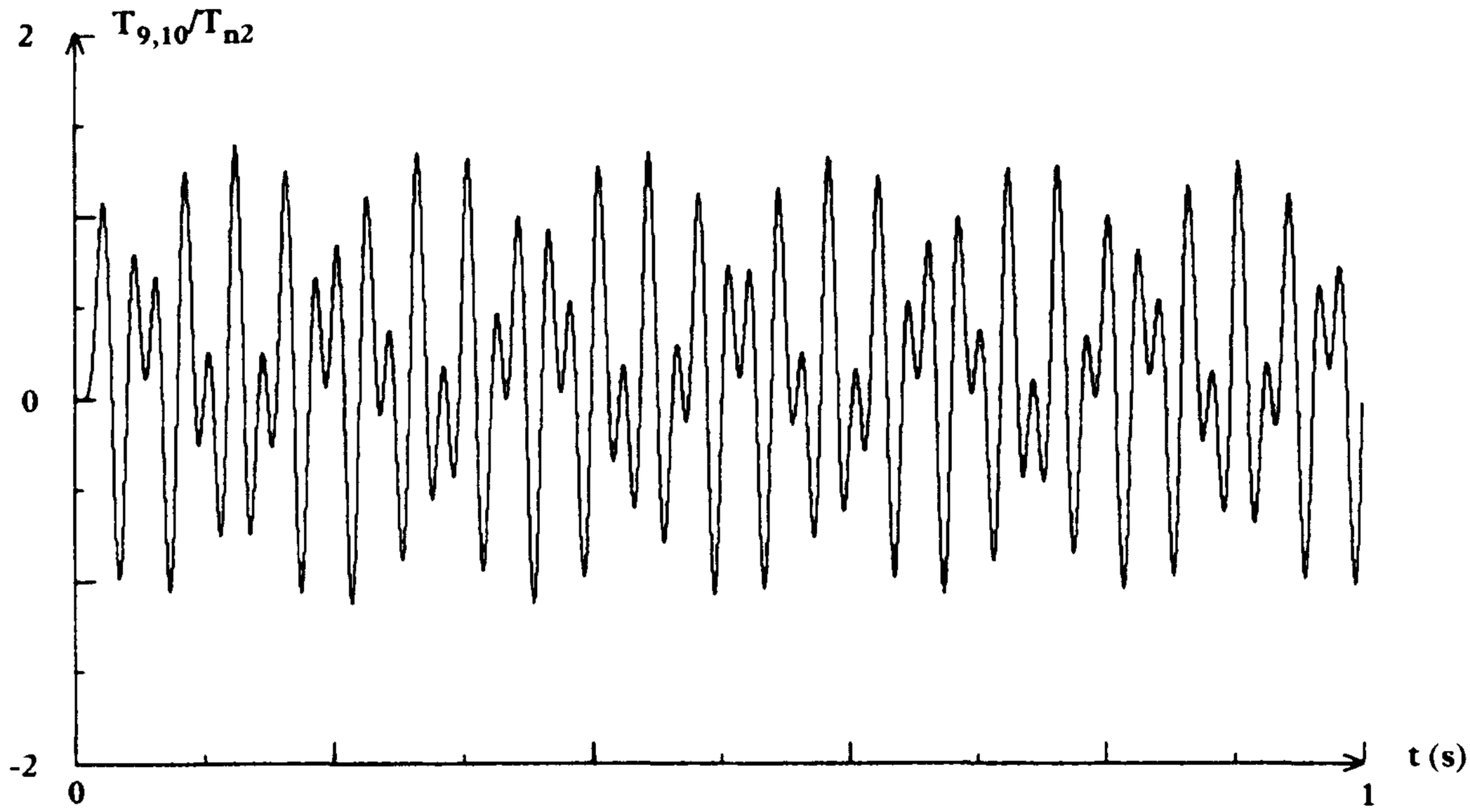

Figure 9.23. Start-up: $T_{9,10}/T_{n2}$ versus time

the first phenomenon is analyzed. The torque is

$$T_{st} = T_{n1}[0.8 + 0.8e^{-t/0.023} + 6e^{-t/0.023} \sin(\omega t - 0.132) - 6e^{-t/4.65} \sin(\omega t + 0.132)] \tag{9.56}$$

where T_{n1} is the nominal torque in shaft 1. Similarly, T_{n2} is the nominal torque in shaft 2, and

$$P = T_{n1}\Omega_1 = T_{n2}\Omega_2 \tag{9.57}$$

Expression (9.56) gives the torque (shown in Figure 9.18) at the air-gap of the electric motor; the frequency is 50 Hz ($\omega = 100\pi$ rad/s).

The most sensitive elements are the couplings and, in general, the low-speed rotor – see Equation (9.57). The torque ratios over T_{n1} in elements 4–5, 5–6 and 6–7, and over T_{n2} in elements 8–9 and 9–10, are shown in Figures 9.19–9.23. The maxima are

$$\begin{aligned} T_{6,7}/T_{n1} &= 4.078 \text{ at } t = 0.1248 \text{ s (low-speed rotor)} \\ T_{8,9}/T_{n2} &= 1.480 \text{ at } t = 0.1248 \text{ s (high-speed rotor)} \end{aligned} \tag{9.58}$$

During a short-circuit

The three-phase short-circuit torque is

$$\frac{T_{sc}}{T_{n1}} = 6.65e^{-t/0.063} \sin \omega t - 3.32e^{-t/0.136} \sin 2\omega t + 0.47e^{-t/0.07} \tag{9.59}$$

This is presented in Figure 9.24. The value of the two-phase short-circuit torque is roughly 1.3 times the value of the three-phase short-circuit torque. The initial conditions are obtained using the technique shown in Section 9.2.3.

The torque ratios for the short-circuit condition are presented in Figures 9.25–9.29. The maxima are

$$\begin{aligned} T_{6,7}/T_{n1} &= 3.882 \text{ at } t = 0.01316 \text{ s (low-speed rotor)} \\ T_{8,9}/T_{n2} &= 2.509 \text{ at } t = 0.07917 \text{ s (high-speed rotor)} \end{aligned} \tag{9.60}$$

Then the ratio maximum is 4.078 for the low-speed rotor and 2.509 for the high-speed rotor.

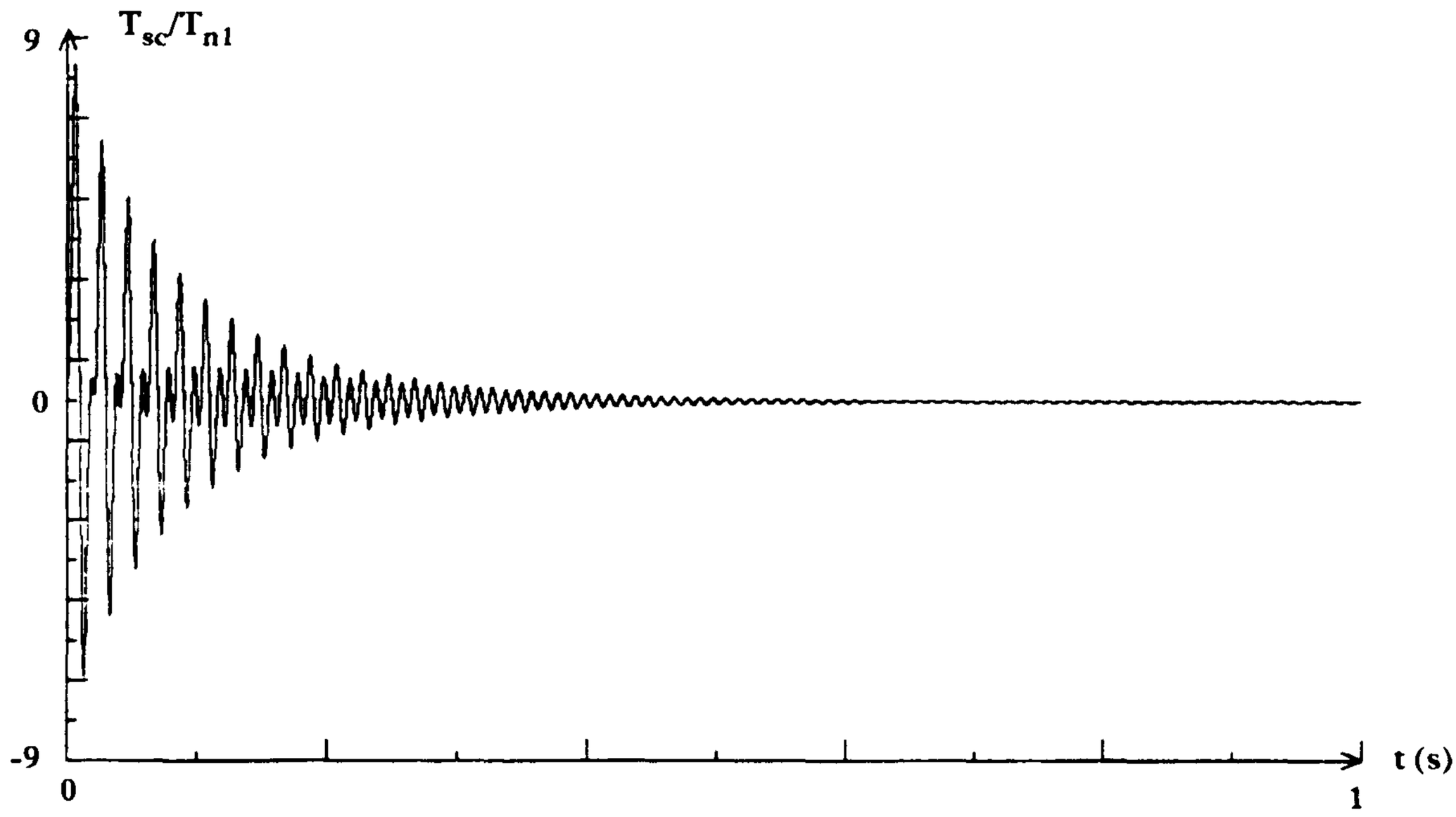

Figure 9.24. Short-circuit: T_{sc}/T_{n1} versus time

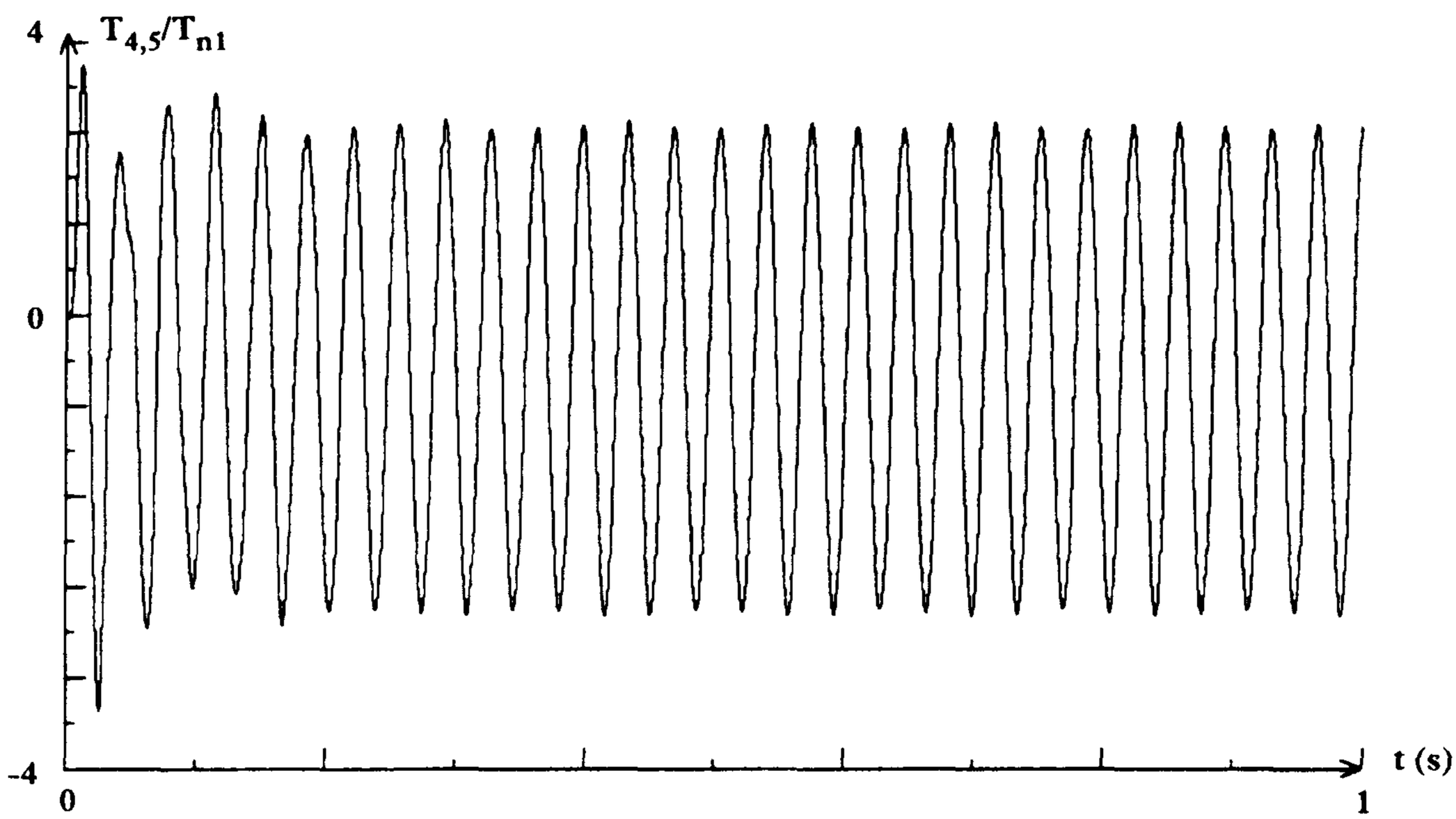

Figure 9.25. Short-circuit: $T_{4,5}/T_{n1}$ versus time

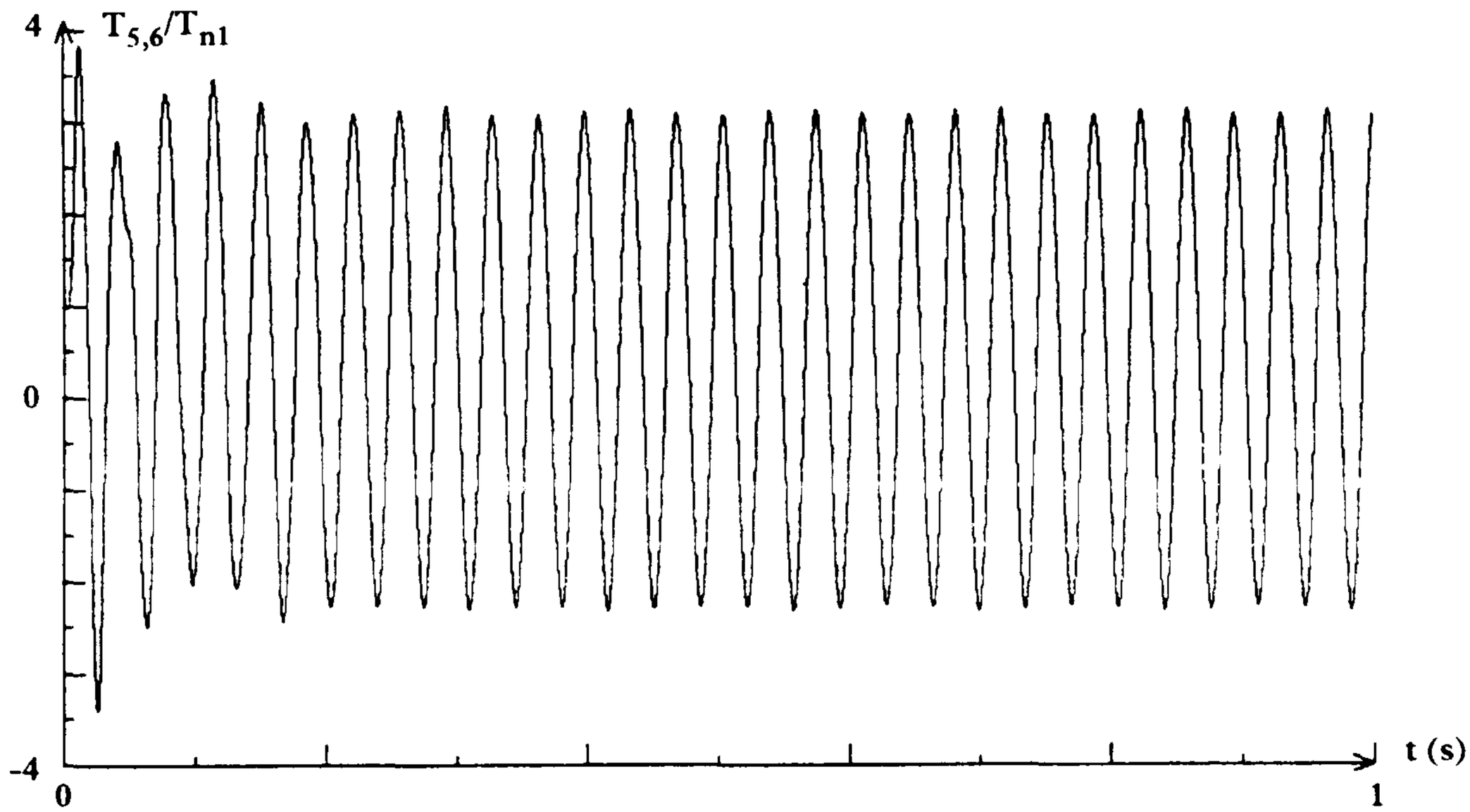

Figure 9.26. Short-circuit: $T_{5,6}/T_{n1}$ versus time

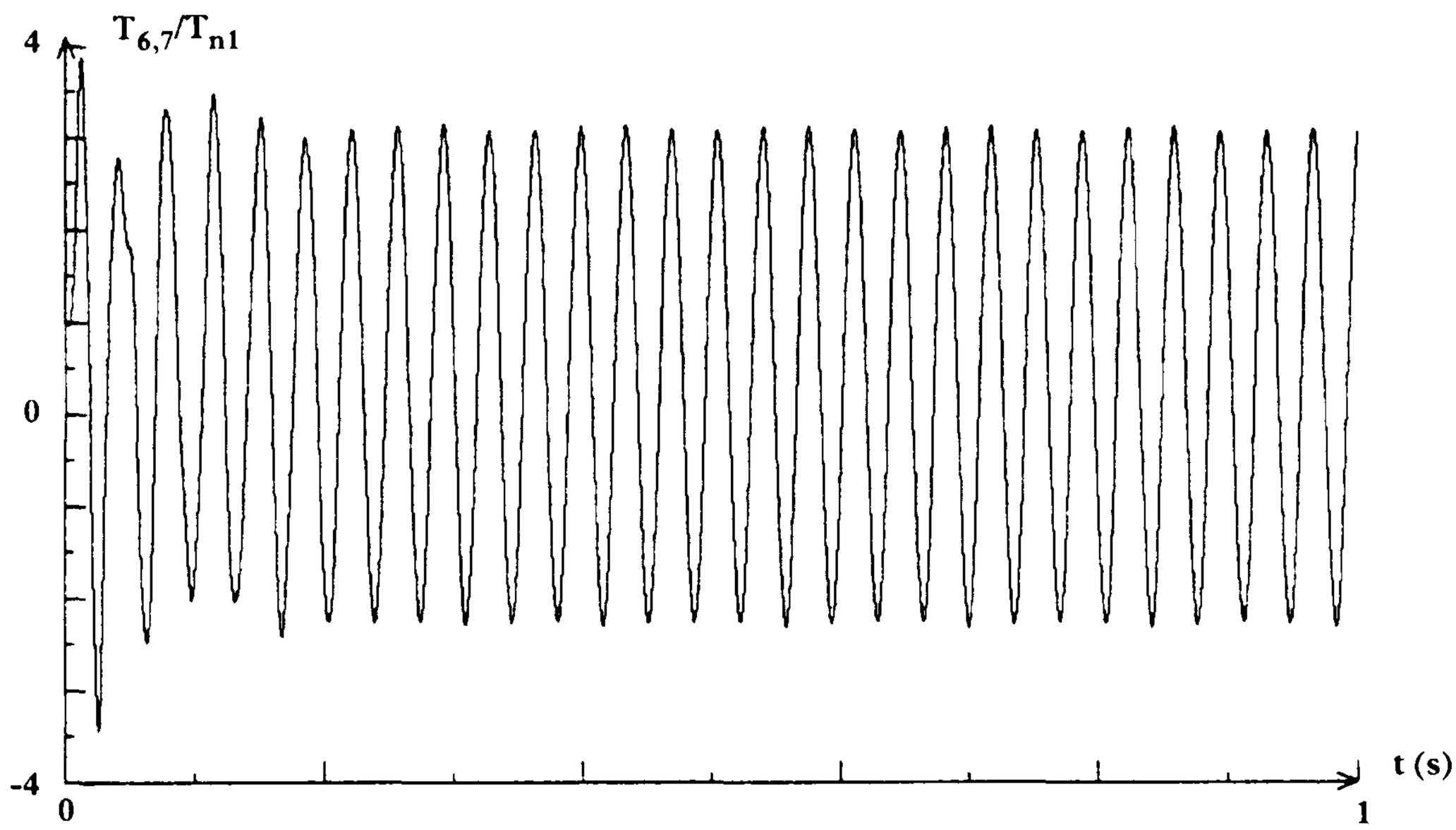

Figure 9.27. Short-circuit: $T_{6,7}/T_{n1}$ versus time

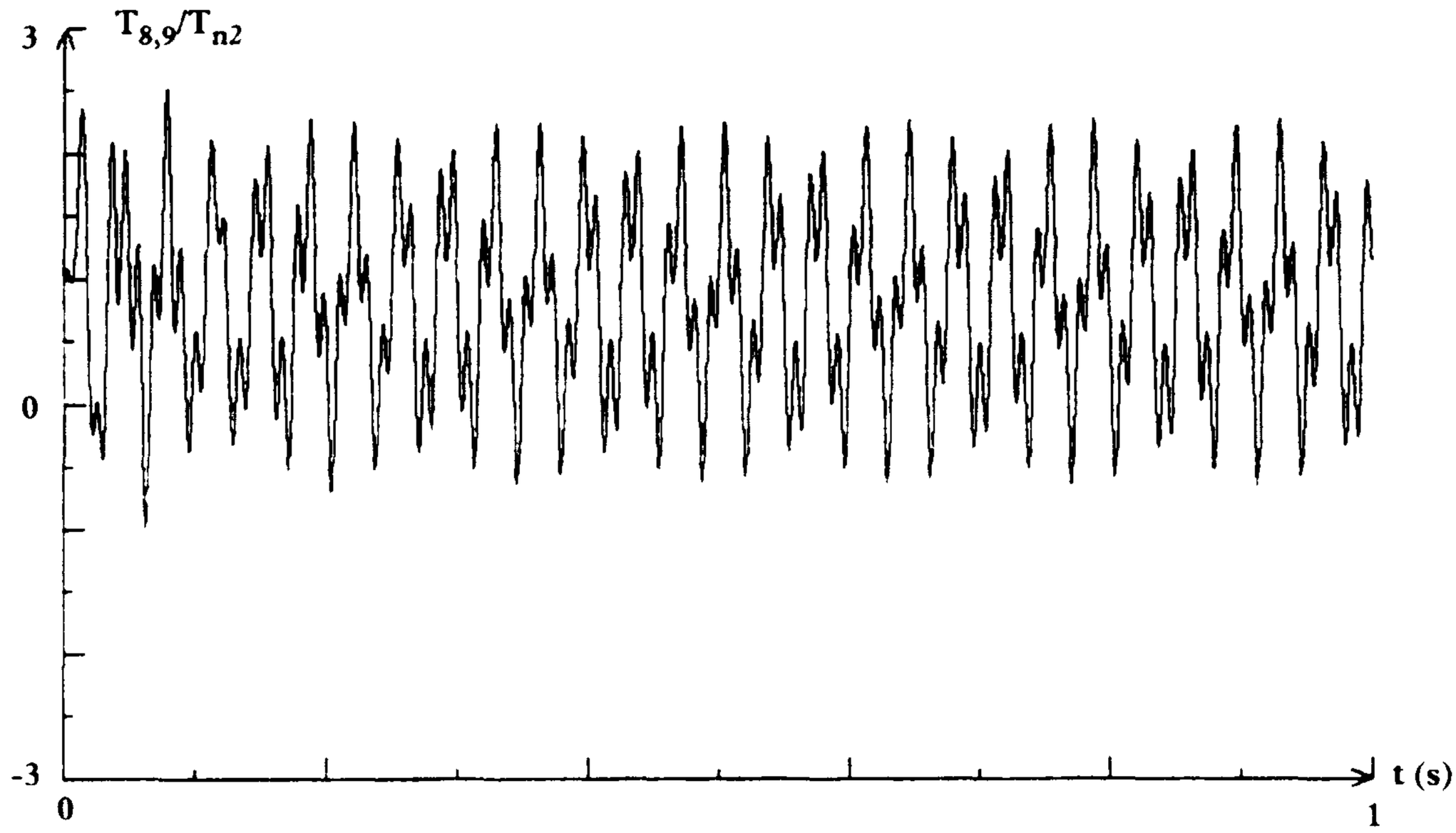

Figure 9.28. Short-circuit: $T_{8,9}/T_{n2}$ versus time

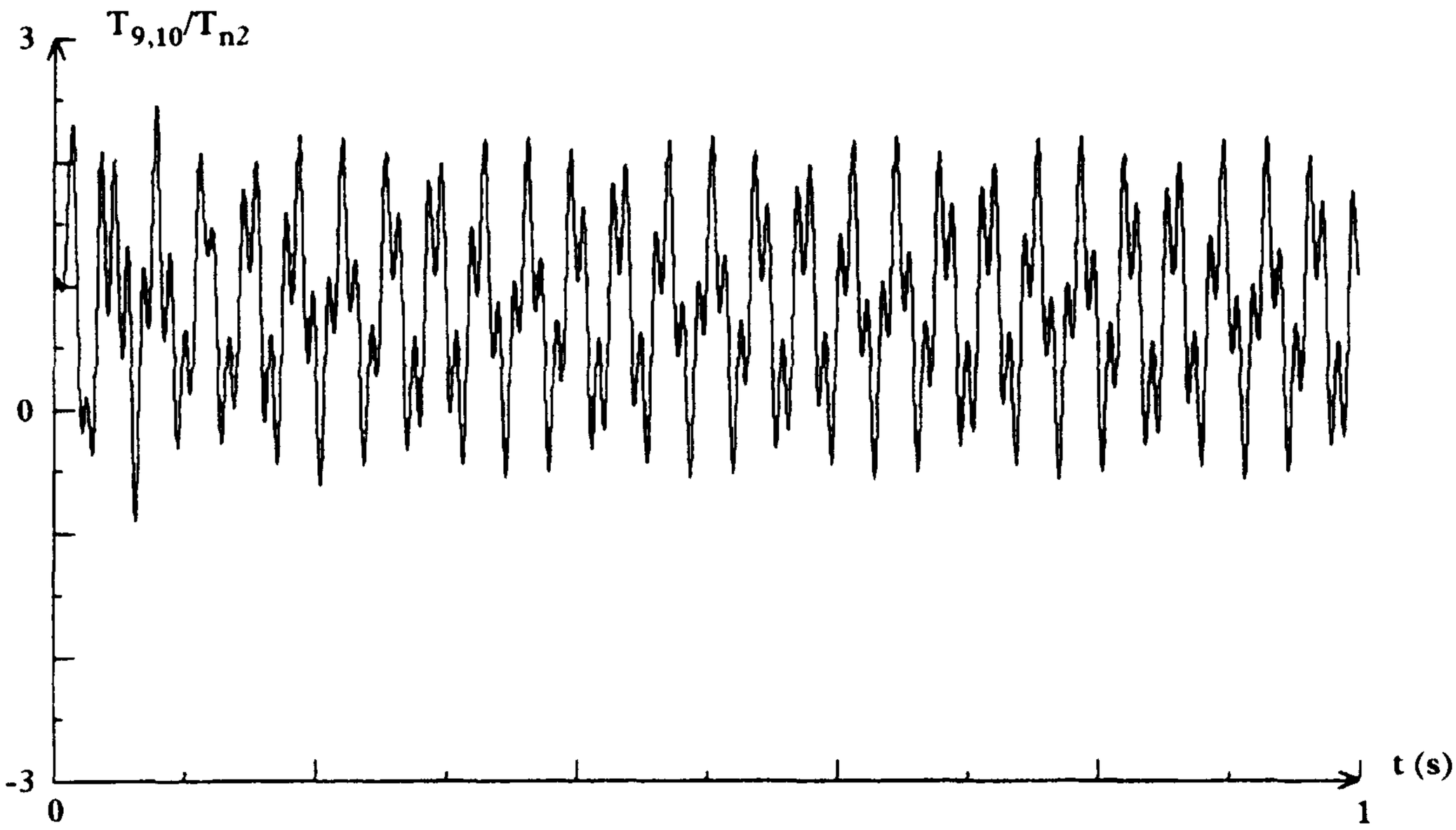

Figure 9.29. Short-circuit: $T_{9,10}/T_{n2}$ versus time

Conclusions

The highest torques occurring during start-up and short-circuit conditions are those due to the two-phase short-circuit. The shaft radius chosen is such that the low-speed shaft torque could reach $6T_{n1}$ and the high-speed shaft torque could reach $4T_{n2}$.

Other kinds of transient behavior could be of interest–passing through critical speeds, for example.

All these calculation results must be taken into account when considering the resistance of the shaft line to oligocyclic fatigue; and in the case of a turbogenerator it is possible to calculate the number of short-circuits the shaft line is able to withstand.

In steady-state conditions, torques which depend on the current frequency can be found; in the present case the frequency 12ω can exist. These torque values are generally low compared wih those caused during start-up and short-circuits, but must be considered for the classical fatigue resistance of shafts and couplings.

10

Miscellaneous Topics

This chapter looks at some situations that, though interesting, are not commonly considered at the design stage. First a simple model of an asymmetric rotor is studied. Then we deal with systems of equations containing periodic coefficients in the matrices. Finally we consider the influence of axial torque.

10.1 THE ASYMMETRIC SHAFT

A shaft can become asymmetric when a crack appears and grows, and it is obviously of interest to know the consequences [36, 44, 47, 52].

The simple model used here is shown in Figure 10.1. The model of the shaft is a concentrated mass m in M situated at a distance a from the rotation axis: O at rest, O_1 when the shaft rotates. The stiffness components of the shaft are k_u and k_v in the rotating reference frame, UV, fixed to the shaft. The stiffness components of the bearings are $k_x = k_y = k$ in the fixed reference frame, XY. The coordinates of O_1 are (u, v) and (x, y). Damping is not considered, and equations will be written in both the fixed and the rotating reference frames using

$$\begin{bmatrix} i \\ j \end{bmatrix} = \begin{bmatrix} \cos \Omega t & \sin \Omega t \\ -\sin \Omega t & \cos \Omega t \end{bmatrix} \begin{bmatrix} I \\ J \end{bmatrix} \tag{10.1}$$

where i, j, I and J are unit vectors, and Ω is the constant speed of rotation.

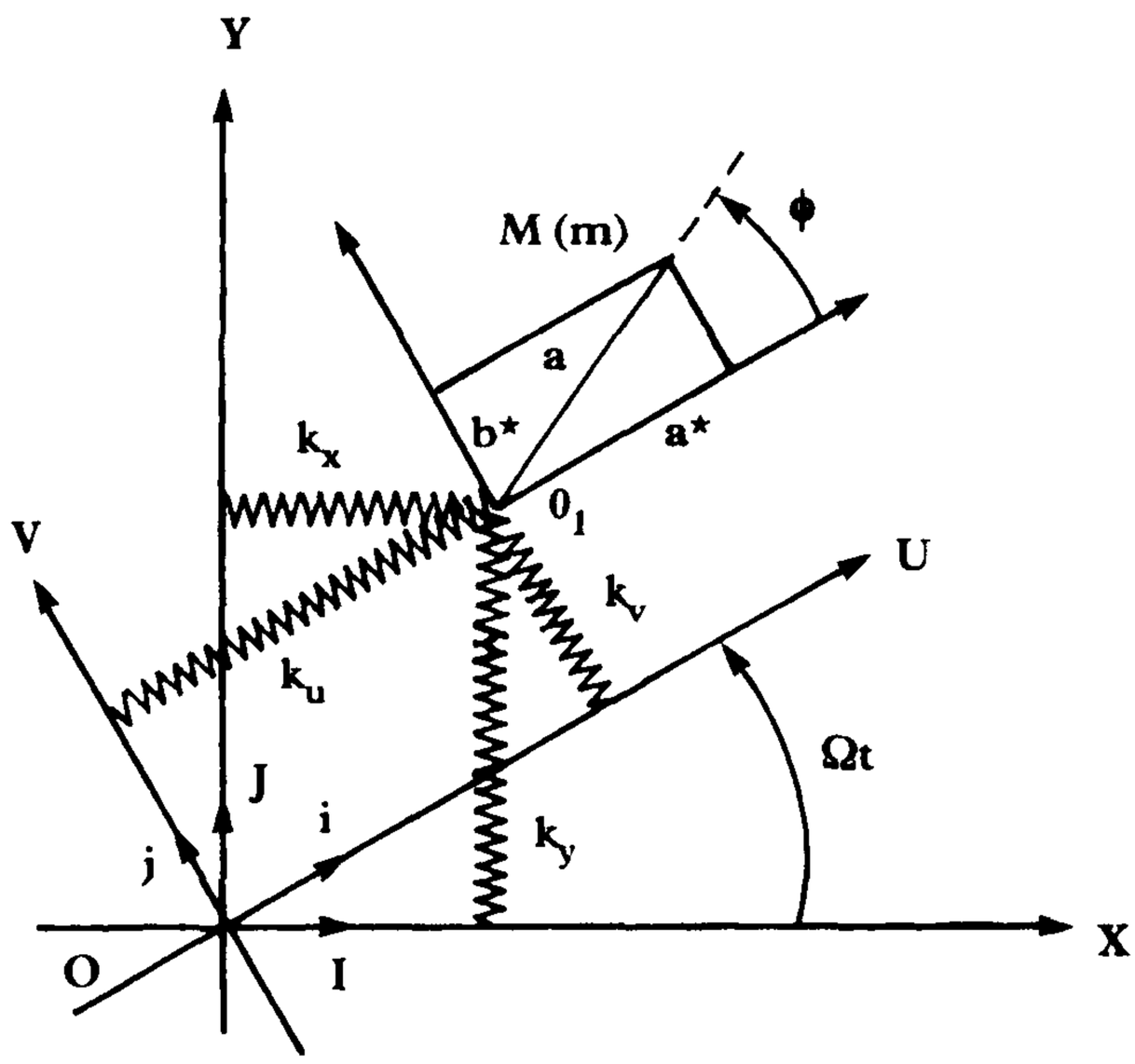

Figure 10.1. Simple model

10.1.1 Kinetic energy

The coordinates of M are expressed in the two reference frames, so that

$$OM = OO_1 + O_lM \tag{10.2}$$

$$= [x + a\cos(\Omega t + \varphi)]I + [y + a\sin(\Omega t + \varphi)]J \tag{10.3}$$

$$= (u + a^*)i + (v + b^*)j \tag{10.4}$$

The expression for the velocity V is

$$V = \frac{\mathrm{d}OM}{\mathrm{d}t} = [\dot{x} - a\Omega\sin(\Omega t + \varphi)]I + [\dot{y} + a\Omega\cos(\Omega t + \varphi)]J \tag{10.5}$$

$$= [\dot{u} - \Omega(v + b^*)]i + [\dot{v} + \Omega(u + a^*)]j \tag{10.6}$$

The expressions for the kinetic energy are

$$T = \frac{m}{2}[\dot{x}^2 + \dot{y}^2 + a^2\Omega^2 - 2a\Omega\dot{x}\sin(\Omega t + \varphi) + 2a\Omega\dot{y}\cos(\Omega t + \varphi)] \tag{10.7}$$

and

$$T = \frac{m}{2}(\dot{u}^2 + \dot{v}^2 + \Omega^2u^2 + \Omega^2v^2 + 2\Omega^2b^*v + 2\Omega^2a^*u + \Omega^2a^{*2} + \Omega^2b^{*2} - 2\Omega b^*\dot{u} + 2\Omega a^*\dot{v} - 2\Omega\dot{u}v + 2\Omega u\dot{v}). \tag{10.8}$$

Application of Lagrange's equations to (10.7) and (10.8) gives, in the fixed frame:

$$\frac{\mathrm{d}}{\mathrm{d}t}\left(\frac{\partial T}{\partial \dot{x}}\right) - \frac{\partial T}{\partial x} = m\ddot{x} - ma\Omega^2 \cos(\Omega t + \varphi) \tag{10.9}$$

$$\frac{\mathrm{d}}{\mathrm{d}t}\left(\frac{\partial T}{\partial \dot{y}}\right) - \frac{\partial T}{\partial y} = m\ddot{y} - ma\Omega^2 \sin(\Omega t + \varphi) \tag{10.10}$$

and in the rotating frame:

$$\frac{\mathrm{d}}{\mathrm{d}t}\left(\frac{\partial T}{\partial \dot{u}}\right) - \frac{\partial T}{\partial u} = m(\ddot{u} - 2\Omega\dot{v} - \Omega^2 u - \Omega^2 a^*) \tag{10.11}$$

$$\frac{\mathrm{d}}{\mathrm{d}t}\left(\frac{\partial T}{\partial \dot{v}}\right) - \frac{\partial T}{\partial v} = m(\ddot{v} + 2\Omega\dot{u} - \Omega^2 v - \Omega^2 b^*) \tag{10.12}$$

10.1.2 Forces

Gravity

$$F = -mgJ \tag{10.13}$$

$$= -mg \sin \Omega t i - mg \cos \Omega t j \tag{10.14}$$

Shaft stiffness

The force acting on the mass is

$$F = -k_u u i - k_v v j \tag{10.15}$$

and Equation (10.1) gives the force components in the fixed frame:

$$\begin{aligned} F = &- k_u(x \cos \Omega t + y \sin \Omega t)(\cos \Omega t I + \sin \Omega t J) \\ &- k_v(y \cos \Omega t - x \sin \Omega t)(\cos \Omega t J - \sin \Omega t I) \end{aligned} \tag{10.16}$$

$$\begin{aligned} = &- \tfrac{1}{2}[(k_u + k_v)x + (k_u - k_v)y \sin 2\Omega t + (k_u - k_v)x \cos 2\Omega t]I \\ &- \tfrac{1}{2}[(k_u + k_v)y + (k_u - k_v)x \sin 2\Omega t - (k_u - k_v)y \cos 2\Omega t]J \end{aligned} \tag{10.17}$$

Bearing stiffness

To avoid equations with periodic coefficients in the rotating frame, the bearings are assumed to be symmetric:

$$F = -kxI - kyJ \tag{10.18}$$

$$= -k(u\cos\Omega t - v\sin\Omega t)(\cos\Omega t i - \sin\Omega t j)$$
$$-k(u\sin\Omega t + v\cos\Omega t)(\sin\Omega t i + \cos\Omega t j) \tag{10.19}$$

$$= -kui - kvj \tag{10.20}$$

Equations

Let us introduce

$$k_1 = \frac{k_u + k_v}{2} + k$$
$$k_2 = \frac{k_u - k_v}{2} \tag{10.21}$$

The equations in the two reference frames are then, respectively,

$$\begin{bmatrix} m & 0 \\ 0 & m \end{bmatrix}\begin{bmatrix} \ddot{x} \\ \ddot{y} \end{bmatrix} + \begin{bmatrix} k_1 & 0 \\ 0 & k_1 \end{bmatrix}\begin{bmatrix} x \\ y \end{bmatrix} + \sin 2\Omega t\begin{bmatrix} 0 & k_2 \\ k_2 & 0 \end{bmatrix}\begin{bmatrix} x \\ y \end{bmatrix}$$
$$+\cos 2\Omega t\begin{bmatrix} k_2 & 0 \\ 0 & -k_2 \end{bmatrix}\begin{bmatrix} x \\ y \end{bmatrix} = \begin{bmatrix} 0 \\ -mg \end{bmatrix} + ma\Omega^2\begin{bmatrix} \cos(\Omega t + \varphi) \\ \sin(\Omega t + \varphi) \end{bmatrix} \tag{10.22}$$

and

$$\begin{bmatrix} m & 0 \\ 0 & m \end{bmatrix}\begin{bmatrix} \ddot{u} \\ \ddot{v} \end{bmatrix} + 2\Omega\begin{bmatrix} 0 & -m \\ m & 0 \end{bmatrix}\begin{bmatrix} \dot{u} \\ \dot{v} \end{bmatrix}$$
$$+\begin{bmatrix} k + k_u - m\Omega^2 & 0 \\ 0 & k + k_v - m\Omega^2 \end{bmatrix}\begin{bmatrix} u \\ v \end{bmatrix} = \begin{bmatrix} ma^*\Omega^2 \\ mb^*\Omega^2 \end{bmatrix} - mg\begin{bmatrix} \sin\Omega t \\ \cos\Omega t \end{bmatrix} \tag{10.23}$$

Equation (10.23) can now be solved.

Solution of equations: mass unbalance

The displacements due to unbalance are the steady-state solution of (10.23). Hence:

$$u = \frac{ma^* \Omega^2}{k + k_u - m\Omega^2} \tag{10.24}$$

$$v = \frac{mb^* \Omega^2}{k + k_v - m\Omega^2} \tag{10.25}$$

The critical speeds, supposing that $k_u < k_v$, are

$$\Omega_1 = \omega_u = \sqrt{\frac{k + k_u}{m}} \tag{10.26}$$

$$\Omega_2 = \omega_v = \sqrt{\frac{k + k_v}{m}} \tag{10.27}$$

Solution of equations: gravity

The gravity influence is obtained from (10.23), which can be written as

$$\ddot{u} - 2\Omega\dot{v} + (\omega_u^2 - \Omega^2)u = -g \sin \Omega t \tag{10.28}$$

$$\ddot{v} + 2\Omega\dot{u} + (\omega_v^2 - \Omega^2)v = -g \cos \Omega t \tag{10.29}$$

The displacements due to gravity are the steady-state solutions of (10.28) and (10.29), which can be written in the form

$$u = u_0 \sin \Omega t \tag{10.30}$$

$$v = v_0 \cos \Omega t \tag{10.31}$$

Hence:

$$u_0 = \frac{-g(\omega_v^2 - 4\Omega^2)}{\omega_u^2\omega_v^2 - 2\Omega^2(\omega_u^2 + \omega_v^2)} \tag{10.32}$$

$$v_0 = \frac{-g(\omega_u^2 - 4\Omega^2)}{\omega_u^2\omega_v^2 - 2\Omega^2(\omega_u^2 + \omega_v^2)} \tag{10.33}$$

A critical speed due to gravity appears at

$$\Omega^2 = \frac{\omega_u^2 \omega_v^2}{2(\omega_u^2 + \omega_v^2)} \tag{10.34}$$

Supposing now that

$$\omega_v = \omega_u + \varepsilon\omega_u = \omega_u(1 + \varepsilon) \tag{10.35}$$

Equation (10.34) becomes

$$\Omega^2 = \frac{\omega_u^4(1 + \varepsilon)^2}{2\omega_u^2[1 + (1 + \varepsilon)^2]} \tag{10.36}$$

$$\simeq [\omega_u^2(1 + \varepsilon)/4] \tag{10.37}$$

Then

$$\Omega \simeq (\omega_u + \omega_v)/4 \tag{10.38}$$

This critical speed, commonly referred to as a secondary critical speed due to gravity, is equal to roughly half the critical speed due to mass unbalance. This critical speed can be used to monitor the emergence of cracks in horizontal rotors.

Solution of equations: instability

The free motion shows a possible instability zone. Let us then consider Equation (10.23) for the case of free motion. It is written as

$$\ddot{u} - 2\Omega\dot{v} + (\omega_u^2 - \Omega^2)u = 0 \tag{10.39}$$

$$\ddot{v} + 2\Omega\dot{u} + (\omega_v^2 - \Omega^2)v = 0 \tag{10.40}$$

and solutions are sought in the form

$$u = u_0 e^{rt} \tag{10.41}$$

$$v = v_0 e^{rt} \tag{10.42}$$

The characteristic equation obtained is

$$r^4 + (\omega_u^2 + \omega_v^2 + 2\Omega^2)r^2 + (\omega_u^2 - \Omega^2)(\omega_v^2 - \Omega^2) = 0 \tag{10.43}$$

and the solutions are

$$2r_1^2 = -(\omega_u^2 + \omega_v^2 + 2\Omega^2) + \sqrt{(\omega_u^2 + \omega_v^2 + 2\Omega^2)^2 - 4(\omega_u^2 - \Omega^2)(\omega_v^2 - \Omega^2)} \tag{10.44}$$

$$2r_2^2 = -(\omega_u^2 + \omega_v^2 + 2\Omega^2) - \sqrt{(\omega_u^2 + \omega_v^2 + 2\Omega^2)^2 - 4(\omega_u^2 - \Omega^2)(\omega_v^2 - \Omega^2)} \tag{10.45}$$

The discriminant Δ is

$$\Delta = (\omega_u^2 + \omega_v^2 + 2\Omega^2)^2 - 4(\omega_u^2 - \Omega^2)(\omega_v^2 - \Omega^2) \tag{10.46}$$

$$= (\omega_u^2 - \omega_v^2)^2 + 8\Omega^2(\omega_u^2 + \omega_v^2) \tag{10.47}$$

Equation (10.47) shows that Δ is always a positive quantity, so r_1^2 and r_2^2 are real quantities. In addition, $(\omega_u^2 - \Omega^2)(\omega_v^2 - \Omega^2)$ can be a negative quantity; then r_1^2 is a positive quantity and can be written as

$$r_1^2 = a, \quad 0 < a \tag{10.48}$$

and hence

$$r_{1,1} = -\sqrt{a} \tag{10.49}$$

$$r_{1,2} = +\sqrt{a} \tag{10.50}$$

and the solution $\exp(t\sqrt{a})$ grows indefinitely with time. In conclusion, the system is unstable when

$$\omega_u < \Omega < \omega_v \tag{10.51}$$

10.2 EQUATIONS WITH PERIODIC COEFFICIENTS

Unfortunately matrices with coefficients which are a function of time are sometimes impossible to avoid; for example, in asymmetric shafts, such

as craked shafts with hydrodynamic bearings, when two shafts in parallel are connected by gears having a stiffness function of time, or in shafts subjected to parametric excitations [1, 15]. In this kind of rotor it is necessary to predict the zones of instabilities and the response to forces of excitation: mass unbalance and asynchronous force. This is quite difficult to achieve. Several methods have been proposed, including an infinite determinant method, a harmonic balance method [32], a Runge-Kutta-Fehlberg procedure [26], a Floquet transition matrix method [49, 58], and Chebyshev polymomials [50].

In this section the instability and unbalance response of rotors is examined [28, 29]. The zones of instability are found by a transfer matrix method and the unbalance response is predicted by means of a Newmark method. The methods have been tested in examples which give equations with periodic coefficients in one coordinate system and equations with constant coefficients in another system.

10.2.1 Instability

Let δ and $\dot{\delta}$ be respectively the displacement and velocity vectors of the system of order N, the period of which is T. The behavior at the instants t and $t + T$ is such that

$$X(t + T) = T_{\mathrm{F}} X(t) \tag{10.52}$$

with

$$X(t) = (\delta, \dot{\delta})^{\mathrm{T}} \tag{10.53}$$

and where T_{F} is a Floquet transition matrix over a period T.

It has been shown [6] that the $2N$ complex eigenvalues of the matrix T_{F} give the $2N$ conditions of stability: if each modulus of the $2N$ eigenvalues is less than unity, the system is stable.

The interest here is in solving the equations of free motion which are written as

$$M\ddot{\delta} + C(t)\dot{\delta} + K(t)\delta = 0 \tag{10.54}$$

where some terms of K and C are of period T.

To obtain the Floquet transition matrix T_F the period T is divided into n intervals of length $h = T/n$, in such a way that it is possible to consider that $C(t)$ and $K(t)$ are constant over each interval. Then the state transition matrix T_i can be calculated over the different intervals. This gives

$$\begin{aligned} X(h) &= T_0 X(0) \\ X(2h) &= T_1 X(h) \\ &\vdots \\ X(nh) &= T_{n-1} X((n-1)h) \end{aligned} \tag{10.55}$$

The Floquet transition matrix over one period is thus given by

$$X(T) = T_{n-1} \cdots T_1 T_0 X(0) \tag{10.56}$$

The state transition matrix can be obtained from an implicit formulation using the trapezöidal form of Newmark. Equilibrium is first written at time t_{i+1}:

$$M\ddot{\delta}_{i+1} + C_{i+1}\dot{\delta}_{i+1} + K_{i+1}\delta_{i+1} = 0 \tag{10.57}$$

Newmark expressions lead to

$$\dot{\delta}_{i+1} = -\dot{\delta}_i + \frac{2}{\Delta t}(\delta_{i+1} - \delta_i) \tag{10.58}$$

$$\ddot{\delta}_{i+1} = -\ddot{\delta}_i + \frac{4}{(\Delta t)^2}(\delta_{i+1} - \delta_i - \Delta t\dot{\delta}_i) \tag{10.59}$$

which gives

$$D\delta_{i+1} = M\left[\ddot{\delta}_i + \frac{4}{\Delta t}\dot{\delta}_i + \frac{4}{(\Delta t)^2}\delta_i\right] + C_{i+1}\left[\dot{\delta}_i + \frac{2}{\Delta t}\delta_i\right] \tag{10.60}$$

with

$$D = \frac{4M}{(\Delta t)^2} + \frac{2C_{i+1}}{\Delta t} + K_{i+1} \tag{10.61}$$

A square matrix of order $2N$ is obtained by writing equilibrium at time $t = t_i$:

$$\ddot{\delta}_i = -M^{-1}C\dot{\delta}_i - M^{-1}K_i\delta_t \tag{10.62}$$

If

$$E = D^{-1}\left(\frac{4M}{\Delta t} + C_{i+1} - C_i\right) \tag{10.63}$$

$$F = D^{-1}\left(\frac{4M}{(\Delta t)^2} + \frac{2C_{i+1}}{\Delta t} - K_i\right) \tag{10.64}$$

the matrix T_i becomes

$$T_i = \begin{bmatrix} F & E \\ \dfrac{2(F-I)}{\Delta t} & \dfrac{2E}{\Delta t} - I \end{bmatrix} \tag{10.65}$$

where I is the unit matrix.

10.2.2 Mass unbalance response

The unbalance response is the steady-state response of

$$M\ddot{\delta} + C(t)\dot{\delta} + K(t)\delta = F(t) \tag{10.66}$$

The system (10.66) is solved in the same way as for instability, with each period T divided into n intervals. In order to eliminate the transient solution, calculations have to be performed on a large number of periods; and the lower the damping, the higher has to be the number of periods to be considered. A Newmark procedure can be used again. Thus:

$$\begin{aligned} D\delta_{i+1} =& M\left(\ddot{\delta}_i + \frac{4}{\Delta t}\dot{\delta}_i + \frac{4}{(\Delta t)^2}\delta_i\right) \\ &+ C_{i+1}\left(\dot{\delta}_i + \frac{2}{\Delta t}\delta_i\right) + F_{i+1} \end{aligned} \tag{10.67}$$

The initial conditions chosen are

$$t = 0,\ \delta(0) = 0, \dot{\delta}(0) = 0, \ddot{\delta}(0) = M^{-1}F(0) \tag{10.68}$$

10.2.3 Applications

The system shown in Figure 10.1 has been used to test instability. The solution of Equation (10.22) was in very good agreement with the instability condition given in (10.51). The mass unbalance responses were also in quite good agreement.

Next the steam compressor rotor analyzed in Section 5.1 of [40] was used to check both instability and mass unbalance response. The model shown in Figure 10.2 now uses only four finite elements.

Data for the shaft

The shaft, which has a constant cross-section and is symmetrical, has an outside radius of 1.85×10^{-2} m and an inside radius of 0.5×10^{-2} m. Also, $L_1 = L_4 = 8 \times 10^{-2}$ m and $L_2 = L_3 = 7 \times 10^{-2}$ m.

Data for the bearings

Node 2:

$$K(\text{N/m}) = \begin{bmatrix} 0.796 & -0.119 \\ -0.594 & 1.1 \end{bmatrix} \times 10^8$$

$$C(\text{N/m/s}) = \begin{bmatrix} 0.84 & -0.32 \\ -0.32 & 1.26 \end{bmatrix} \times 10^4$$

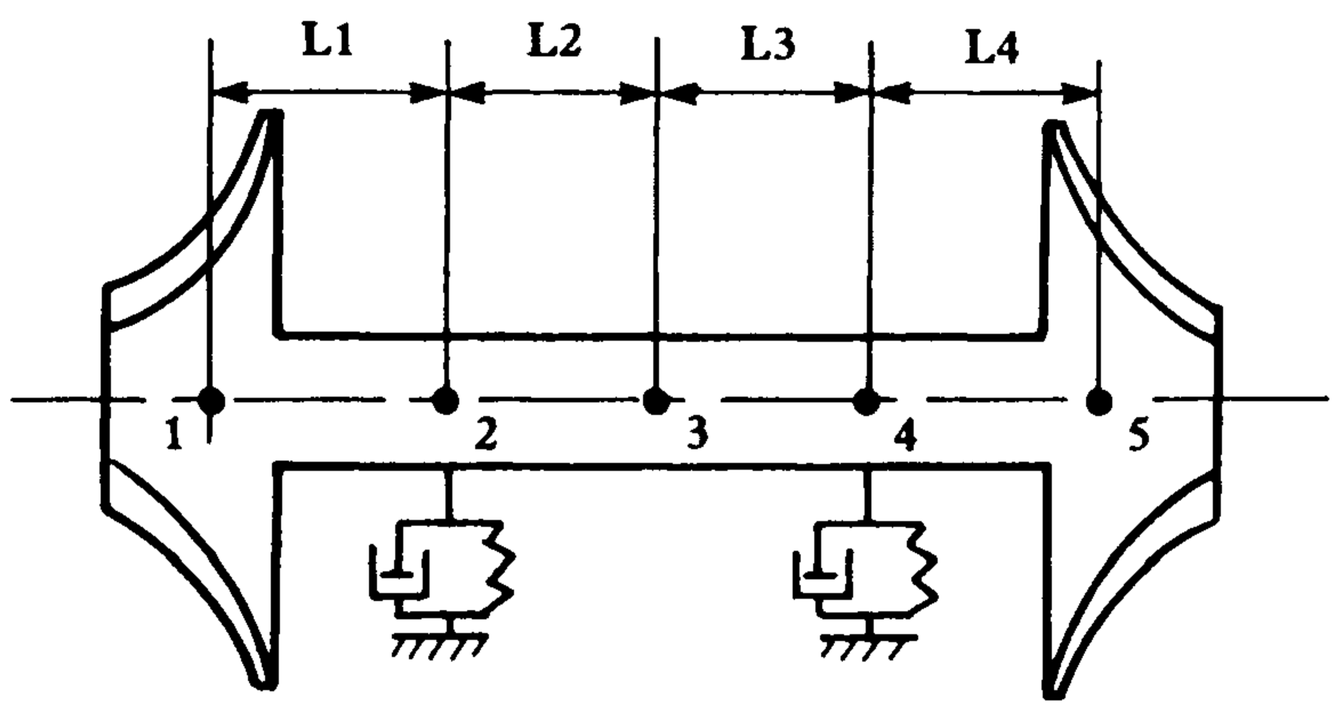

Figure 10.2. Steam compressor model

Node 4:

$$K(\text{N/m}) = \begin{bmatrix} 0.525 & -0.0229 \\ -0.385 & 0.71 \end{bmatrix} \times 10^8$$

$$C(\text{N/m/s}) = \begin{bmatrix} 0.61 & -0.16 \\ -0.16 & 0.85 \end{bmatrix} \times 10^4$$

Data for the disks

Two sets of data are given–one corresponding to steel disks (used to find instability zones) and the other to aluminum disks (used to find the response to mass unbalance).

Node 1, aluminium: $m_D = 1.26\,\text{kg}$

$$I_{Dx} = 0.125 \times 10^{-2}\,\text{kg m}^2;\ I_{Dy} = 0.249 \times 10^{-2}\,\text{kg m}^2$$

Node 1, steel: $m_D = 3.64\,\text{kg}$

$$I_{Dx} = 0.3611 \times 10^{-2}\,\text{kg m}^2;\ I_{Dy} = 0.7193 \times 10^{-2}\,\text{kg m}^2$$

Node 5, aluminium: $m_D = 1.134\,\text{kg}$

$$I_{Dx} = 0.11 \times 10^{-2}\,\text{kg m}^2;\ I_{Dy} = 0.22 \times 10^{-2}\,\text{kg m}^2$$

Node 5, steel: $m_D = 3.276\,\text{kg}$

$$I_{Dx} = 0.3178 \times 10^{-2}\,\text{kg m}^2;\ I_{Dy} = 0.6356 \times 10^{-2}\,\text{kg m}^2$$

Data for the masses

Two masses of 3 g mm each, in phase opposition, are situated on disks 1 and 2.

Results

Instability. It is found that for steel disks, the motion becomes unstable near 20 950 rpm when the calculations are performed in the fixed frame

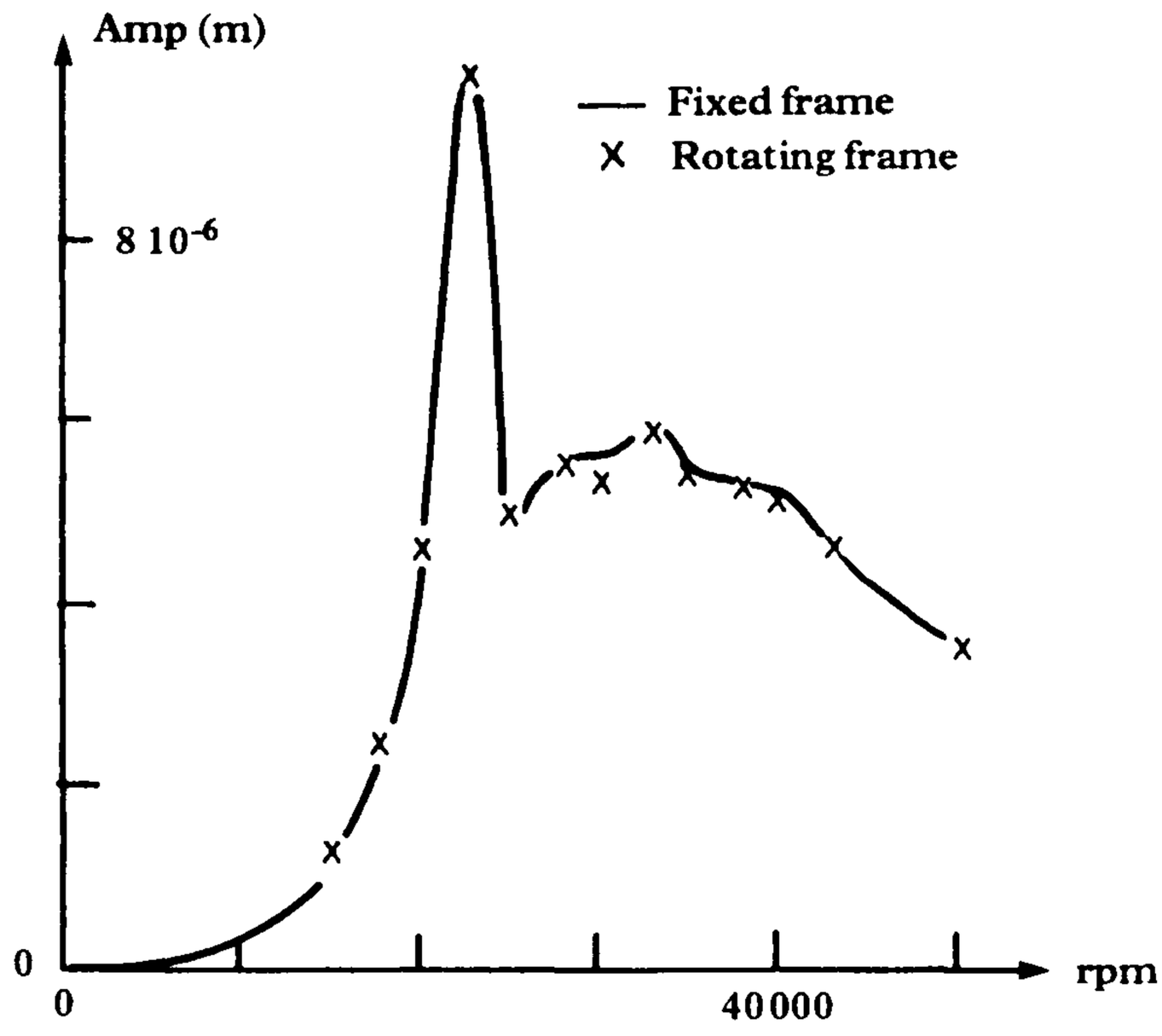

Figure 10.3. Mass unbalance response, node 1

and near 20 850 rpm when the calculations are performed in the rotating frame. Period T is divided in 60 intervals. The agreement is here very satisfactory.

Unbalance response. As shown by the results in Figure 10.3, the accuracy of the method is satisfactory. For the unbalance response, the main problem encountered is with low damping. It then takes a long time for the transient solution to disappear and the cost of the calculations may become prohibitive.

For practical applications more than a hundred degrees of freedom are frequently necessary. But as general periodic coefficients appear with a smaller number of degrees of freedom, a modal or a substructure method should be used to reduce the number of degrees of freedom of the system [27].

10.3 THE INFLUENCE OF AXIAL TORQUE

The influence of axial torque on bending can be significant. The equations of motion for a rotor in bending (no gyroscopic effect is included) subjected to secondary effects such as a constant axial torque have been given in [17], where it is shown that the stiffness of the shaft decreases as the axial torque increases. This effect is predominant over

the other secondary effects if the slenderness ratio $R/2L$ is lower than 0.0025. Experiments have been performed to show the influence of the combined constant and pulsating axial torque [13, 18, 57]. Simple models have shown the possibility of three kinds of instability which have also been observed in experiments [14, 54]. These instabilities occur when the axial torque frequency Ω equals:

- a natural frequency of the system $(\omega_1, \omega_2, \ldots)$
- twice a natural frequency of the system
- a combination of the natural frequencies of the system $((\omega_i + \omega_j)/k$ with i, j, k integers).

10.3.1 Shaft equations

Equations for the coupled system presented in Figure 10.4 are

$$\rho S \frac{\partial^2 w}{\partial t^2} + EI \frac{\partial^4 w}{\partial y^4} + T \frac{\partial^3 u}{\partial y^3} = 0 \tag{10.69}$$

$$\rho S \frac{\partial^2 u}{\partial t^2} + EI \frac{\partial^4 u}{\partial y^4} + T \frac{\partial^3 w}{\partial y^3} = 0 \tag{10.70}$$

with

$$T = T_0 + T_1 \cos \Omega t \tag{10.71}$$

Here no other external forces such as mass unbalance are taken into account. Equations (10.69) and (10.70) with (10.71) can be solved using

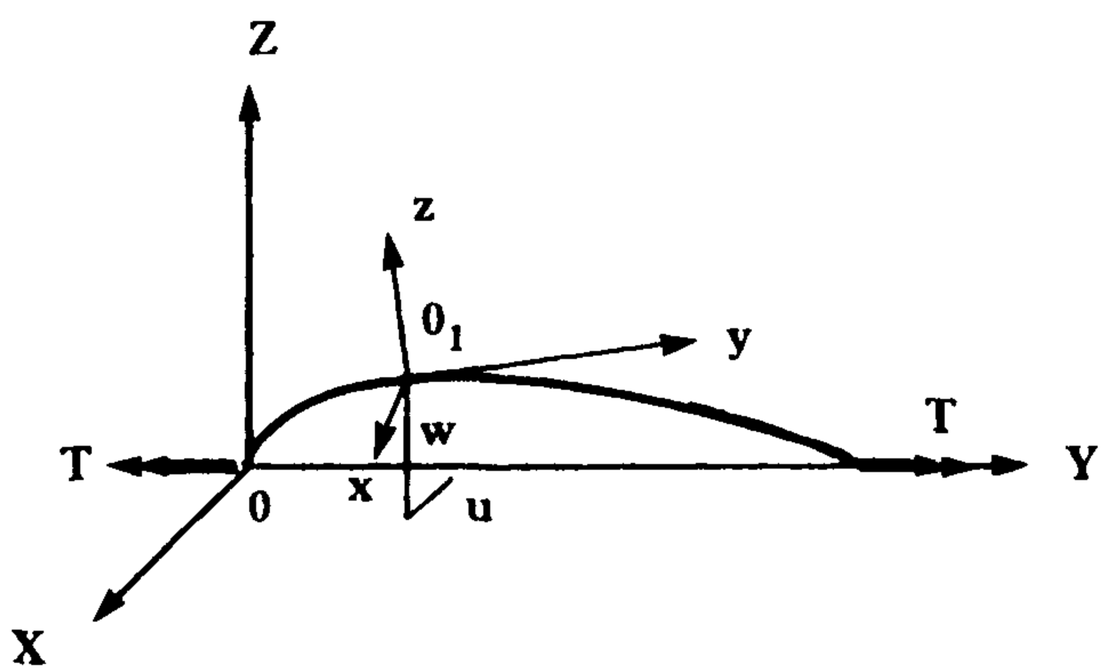

Figure 10.4. Beam reference axis

a simple Galerkin procedure which makes the phenomena easy to understand [13].

10.3.2 Finite element model

The virtual work of the torque components is calculated and a supplementary stiffness matrix K_T can be obtained [59]. Its expression for a constant cross-section element of length L is given below:

$$K_T = -(T_0 + T_1 \cos \Omega t) \begin{bmatrix} 0 & 0 & -1/L & 0 & 0 & 0 & 1/L & 0 \\ 0 & 0 & 0 & -1/L & 0 & 0 & 0 & 1/L \\ -1/L & 0 & 0 & -0.5 & 1/L & 0 & 0 & 0.5 \\ 0 & -1/L & 0.5 & 0 & 0 & 1/L & -0.5 & 0 \\ 0 & 0 & 1/L & 0 & 0 & 0 & -1/L & 0 \\ 0 & 0 & 0 & 1/L & 0 & 0 & 0 & -1/L \\ 1/L & 0 & 0 & -0.5 & -1/L & 0 & 0 & 0.5 \\ 0 & 1/L & 0.5 & 0 & 0 & -1/L & -0.5 & 0 \end{bmatrix} \tag{10.72}$$

where the nodal displacement vector is that defined by Equation (4.5) in Chapter 4. The influence of the constant axial torque is generally a second-order effect and is very easy to include in a rotordynamics computer program. The harmonic exciting torque can be significant in specific industrial applications and dangerous because of the instability zones. The prediction of the instability zones and of the unbalance response can be performed as in Section 10.2.

APPENDIX 1

Rayleigh–Ritz/Finite Element Methods

In order to demonstrate that the Rayleigh–Ritz procedure and the finite element results are close, the critical speeds due to mass unbalance (monorotor and multirotors) and asynchronous force response (monorotors) have been determined by the two methods.

Monorotors

The comparison is performed for asymmetric rotors. The results presented in Chapter 2, Figure 2.10, are compared in Table A1.1 to the results obtained with a three finite element regularly spaced model (the results obtained with six finite elements are the same).

The three lowest critical speeds obtained by the Rayleigh–Ritz procedure are satisfactory, since the differences are lower than 9 percent.

Multirotors

The comparison is performed for asymmetric rotors. The results presented in Chapter 3, are compared in Tables A1.2–A1.4 to the results obtained from finite elements (with 18 elements for shaft 1 and six for shaft 2) for $n = -5$ (see Figure 3.8), $n = -1$ (see Figure 3.9) and $n = 5$ (see Figure 3.10).

The three lowest critical speeds obtained by the Rayleigh–Ritz procedure are very satisfactory as the differences are lower than 3 percent.

Table A1.1. Critical speeds in rpm

	Mass unbalance		Asynchronous excitation	
Points	A	B	C	D
FE	2533	3122	4535	6448
RR	2642	3377	4938	7731
Diff. (%)	4.3	8.2	8.9	19.9

Table A1.2. Critical speeds in rpm for $n = -5$

Points	A	B	C	D
FE	2003	2295	9342	11 961
RR	1987	2308	9224	13 039
Diff. (%)	−0.8	0.6	−1.3	9.0

Table A1.3. Critical speeds in rpm for $n = -1$

Points	A, C	B, D
FE	9860	11 337
RR	9919	11 570
Diff. (%)	0.6	2.1%

Table A1.4. Critical speeds in rpm for $n = 5$

Points	A	B	C	D
FE	1954	2306	8355	14 318
RR	1956	2360	8299	17 916
Diff. (%)	0.1	2.3	−0.7	25.1

Comment

It must be emphasized that the Rayleigh–Ritz method does not necessarily give results as close as the finite element results; for example, if k_{zz} (in the monorotor and multirotors) were very high, one sine function for each displacement would not be sufficient.

APPENDIX 2

Downloading the Software

In this appendix, the procedure to obtain a free demo version of the SYSROTOR program via the Internet is presented. As this version is a demo version, restrictions are applied on the number of nodes (10) and the number of frequencies (4). However, all the capabilities described in the previous chapters are available. This program is written in FORTRAN and C languages but only binary files, data files and utility files are given freely.

System recommendations

The SYSROTOR demo version is intended to run only on PC computers. You need the following hardware:

- An IBM or 100 percent compatible system with an Intel 486 or Pentium processor
- Operating system: MS-DOS 4.01 or better
- An EGA, VGA or SVGA graphic card (a color display is preferable)
- A Hard disk with approximately 3 MB available disk space
- A Mouse (with serial adaptor)
- A 640K system memory is required for the demo version (with 490 K free). Windows can be used but is not essential (extended memory is not supported).

As in the full version, graphic printing is available. Supported plotter types are: Postscript, HP GL color or Bitmap.

Downloading the software through the Internet

To obtain the software package through the Internet you need to do the following FTP procedure:

- login as **anonymous** on the site: **lmst.insa-lyon.fr** or **134.214.80.41** (with TELNET,RLOGIN, etc.)
- type your own name (or E-mail address) in response to the password prompt.

Get the files README.TXT and ROTORZIP.EXE located in the **/pub/sysrotor** directory.

README.TXT is a text file which describes how to install the software and contains recent informations on the program.

A manual is also included in the self-expanding file ROTORZIP.EXE. This manual can be read with MS-WORD6.

Before using the software, you should be familiar with rotordynamics. Problems and suggestions can be reported to the authors at the following E-mail address:

lmst@lmst.insa-lyon.fr or by Fax:(**33**) **4 72 43 89 30**

The laboratory web site is **http://www.Insa-lyon.fr/Insa/Laboratoires/LMST**

Registered Trademarks

All product names mentioned in this manual are trademarks or registered trademarks of their respective manufacturers.

References

[1] Berlioz, A., Der Hagopian, J., Dufour, R., Draoui, E., Dynamic behavior of a drill-string: experimental investigations of lateral instabilities. *ASME J. Vib. Ac.*, **118**, July 1996.

[2] Berthier, P., Ferraris, G., Lalanne, M., Prediction of critical speeds, unbalance and nonsynchronous forced response of rotors. *53th Shock and Vib. Bull.*, 1983.

[3] Berthier, P., Ferraris, G., Lalanne, M., Prédiction due comportement dynamique des moteurs d'avion: vitesses critiques–effets de balourd. *J. Mec. Th. Appl.*, **5**, 1986.

[4] Berthier, P., Ferraris, G., Der Hagopian, J., Lalanne, M., Application d'une méthode pseudo-modale à la détermination du comportement dynamique des monorotors et des multirotors coaxiaux. *Proceedings 7th World IFToMM Congress*, Pergamon Press, 1987.

[5] Bigret, R., Vibration des machines tournantes et des structures. *Techniques et Documentation*, 1980.

[6] Bolotin, V. V., *The Dynamic Stability of Elastic Systems*. Holden Day, 1964.

[7] Borri, M., Mantegazza, M., Efficient solution of quadratic eigenproblem arising in dynamic analysis of structures. *Comp. Met. Appl. Mech. Eng.*, **12**, 1977.

[8] Childs, D., *Turbomachinery Rotordynamics*. Wiley, 1993.

[9] Delbez, A., Charlot, G., Ferraris, G., Lalanne, M., Dynamic behavior of a counter-rotating air turbine starter. ASME Paper 93 GT 55, 1993.

[10] Dimaragonas, A., Papetis, S., Analytical methods in rotordynamics. *Applied Sciences*, 1983.

[11] Dimaragonas, A., *Vibrations for Engineers*. Prentice-Hall, 1996.

[12] Dimentberg, F. M., *Flexural Vibrations of Rotating Shafts*. Butterworth, 1961.

[13] Dufour, R., Influence du couple axial sur le comportement dynamique des rotors flexibles. Thèse de 3° Cycle, Lyon, 1985.

[14] Dufour, R., Der Hagopian, J., Lalanne, M., Influence of an axial torque on the dynamic behavior of rotors in bending. *55th Shock and Vib. Bull.*, 1985.

[15] Dufour, R., Berlioz, A., Parametric instability of a beam due to axial excitations and to boundary conditions. To appear In: *ASME J. Vib. Ac.*, 1998.

[16] Ehrich, F., *Handbook on Rotordynamics*. McGraw-Hill, 1992.

[17] Eshleman, R. L., Eubanks, R. A., On the critical speeds of a continuous rotor. *ASME J. Eng. Ind.*, **89**, Nov. 1969.

[18] Eshleman, R. L., Eubanks, R. A., Effects of a axial torque on rotor response: an experimental investigation. ASME Paper 70-WA/DE-14, 1970.

[19] Ferraris, G., Maisonneuve, V., Lalanne, M., Prediction of the dynamic behavior of nonsymmetric coaxial co or counter-rotating rotors. *J. Sound Vib.*, **195**(4), 1996.

[20] Frêne, J., Nicolas, D., Degueurce, B., Berthe, D., Godet, M., *Lubrification Hydrodynamique: Paliers et Butées*. Edition Eyrolles, Collection EDF, **72**, 1990.

[21] Gash, R., Pfutzner, H., *Rotordynamik*. Springer-Verlag, 1975.

[22] Genta, G., *Vibrations of Structures and Machines. Practical Aspects*. Springer-Verlag, 1995.

[23] Geradin, M., Rixen, D., *Théorie des Vibrations. Application à la Dynamique des Structures*. Masson, 1993.

[24] Gjika, K., Dufour, R., Swider, P., Thouvenin, D., The dynamic behavior of a turbocharger rotor involving subassembly. *NAFEMS Int. Conf. Structural Dynamics Modelling, Analysis and Correlation*, 1993.

[25] Glasgow, D. A., Nelson, H. D., Stability analysis of rotor-bearings systems using component mode synthesis. *ASME J. Mech. Des.*, **102**, April 1980.

[26] Grabowski, B., The vibrational behavior of a turbine rotor containing a transverse crack. *ASME J. Mech. Des.*, **102**, Jan. 1980.

[27] Guilhen, P. M., Berthier, P., Ferraris, G., Lalanne, M., Dynamic behavior of dissymmetric rotor bearings modeled with a periodic coefficient large system. *NASA Conf. Pub.* 2488, Oct. 1987.

[28] Guilhen, P. M., Prédiction du comportement dynamique de rotors dans le cas d'équations à coefficients péeriodiques: Instabilité–Réponse aux balourds. Thèse de Doctorat, INSA, Lyon, 1988.

[29] Guilhen, P. M., Berthier, P., Ferraris, G., Lalanne, M., Instability and unbalance response of dissymmetric rotor bearing systems. *ASME J. Vib. Ac. Str. Rel. Des.*, **110**, July 1988.

[30] Gunther, E.J., Dynamic stability of rotor bearings systems. NASA Paper SP113, 1966.

[31] Imbert, J.F., *Analyse des Structures par Eléments Finis*. Cepadues Editions, 1979.

[32] Inagaki, T., Kanki, H., Shiraki, K., Response analysis of a general asymmetric rotor-bearing system. *ASME J. Mech. Des.*, **102**, Jan. 1980.

[33] Kassaï, A., Berthier, P., Der Hagopian, J., Ferraris, G., Lacroix, J., Lalanne, M., Dynamique des rotors linéaires: montée et descente en vitesse. Contract Report MRT, 1988.

[34] Kramer, E., *Dynamics of Rotors and Foundations*. Springer-Verlag, 1993.
[35] Lacroix, J., Comportement dynamique d'un rotor au passage des vitesses critiques. Thèse de Doctorat, INSA, Lyon, 1988.
[36] Lalanne, M., Quéau, J. P., Tran, D. M., Dynamique des rotors: vitesses critiques, instabilitiés. *Mécanique, Matériaux, Electricité*, March 1982.
[37] Lalanne, M., Berthier, P., Der Hagopian, J., *Mechanical Vibrations for Engineers*. Wiley 1983.
[38] Lalanne, M., Berthier, P., Der Hagopian, J., Ferraris, G., Lacroix, J., Vibrations non-linéaires de rotors de turbomachines. Contract Report DRET, 1985.
[39] Lalanne, M., Berthier P., Der Hagopian, J., *Mécanique des Vibrations Linéaires*. Masson, 1986.
[40] Lalanne, M., Ferraris, G., *Rotordynamics Prediction in Engineering*, first edition. Wiley, 1990.
[41] Lalanne, M., Ferraris, G., Dynamic behavior of symmetrical coaxial co and counter-rotating rotors. Application to a propfan engine. *Proceedings 4th IFToMM Rotordynamics Conference*, Vibration Institute, 1994.
[42] Lalanne, M., Ferraris, G., Dynamique des rotors en flexion. *Techniques de l'Ingénieur, traité Génie Mécanique*, **B5 110**, 1996.
[43] Lee, C. W., *Vibration Analysis of Rotors*. Pergamon Press, 1993.
[44] Loevy, R., Piarully, V., Dynamics of rotating shafts. *Shock and Vib. Monographs*, **4**, 1969.
[45] Morel, J., *Vibration des Machines et Diagnostic de leur Etat Mécanique*. Edition Eyrolles, Collection EDF, **77**, 1992.
[46] Nelson, H. D., McVaugh, J. M., The dynamics of rotor bearing systems using finite elements. *ASME J. Eng. Ind.*, **98**, May 1976.
[47] Rao, J.S., *Rotordynamics*. John Wiley Eastern, 1983.
[48] Rieger, N., Balancing of a rigid and flexible rotor. *Shock and Vib. Monographs*, **12**, 1986.
[49] Schmied, J., Kramer, E., Vibrational behavior of a rotor with a cross sectional crack. I Mech E Paper C279/84, 1984.
[50] Sinha, S. C., Pandiyan, R., Gibas, D. M., Dynamic analysis of rotor-bearing systems via Chebyshev polynomials. *ASME/ESDA Conf.* 1994, London.
[51] Someya, T., *Journal Bearings Data Book*. Springer-Verlag, 1988.
[52] Tondl, A., *Some Problems of Rotordynamics*. Chapman and Hall, 1965.
[53] Tran, D. M., Etude du comportement dynamique des rotors flexibles. Thèse D. I., Lyon, 1981.
[54] Unger, A., Brull, M. A., Parametric instability of a rotating shaft due to pulsating torque. *ASME J. App. Mech*, **48**, Dec. 1981.
[55] Vance, J. M., *Rotordynamics of Turbomachinery*, Wiley, 1988.
[56] Wilkinson, J. H., *The Algebraic Eigenvalue Problem*. Oxford University Press, 1965.

[57] Willems, N., Holzer, S. M., Critical speeds of rotating shaft subjected to axial loading and tangential torsion. *ASME J. Eng Ind.*, **87**, May 1967.
[58] Zhou, S., Rieger, N. F., Instability analysis procedure for three-level multi-bearing rotor foundation systems. NASA Conf. Pub. 2049, Dec. 1985.
[59] Zorzi, E. S., Nelson, H. D., The dynamics of rotor bearing systems with axial torque: a finite element approach. *ASME J. Mech. Des.*, **102**, Jan. 1980.